Interfacial Bonding in Metal-Matrix Composites Reinforced with Metal-Coated Diamonds

Dimitris-Peter Margaritis
(Dipl. Eng)

Thesis submitted to the University of Nottingham for the degree of Doctor of Philosophy
July 2002

Dedicated to the memory of my late grand father,
my mother and father, with all my love

Acknowledgments

I would like to express my sincere gratitude to Prof. J. V. Wood and Dr. P. H. Shipway of School of Mechanical, Materials, Manufacturing Engineering and Management, University of Nottingham, for their supervision of the work described in this thesis. I would also like to thank all of the technical staff in the department for their expertise in the use of analytical equipment and procedures. In particular, I would like to thank Mr. Keith Dinsdale for assisting in the use of mechanical testing apparatus and Differential Scanning Calorimeter and Dr. A. R. Kennedy for his helpful advices relating to methods of testing and evaluating the mechanical properties of diamond composites.

Acknowledgments are also due to Prof. T. W. Clyne of Department of Materials Science and Metallurgy, Cambridge University, for allowing to me to use their laboratory equipment for the non-destructive mechanical testing conducted in this thesis. Particular thanks goes to my friend and "old colleague" from Athens Technical University (NTUA) Dr. Athina Markaki for her valuable assistance and for helping me conducting the non-destructive mechanical tests.

Special thanks goes as well to Dr. James Sung, vice-president of Kinik Company, Tapei, Taiwan for the scientific discussions over the Internet on aspects of diamond crystal properties and reactivity.

Acknowledgments are due to NIMBUS Diamond Tool and Machine Company Ltd., Burgess Hill, West Sussex, UK for the supply of material and providing the facilities for the preparation of the diamond composites. Special thanks goes to the R&D director Dr. Monday Igharo for the fruitful co-operation as well as to the staff at the manufacturing plant for assisting me in the preparation of the diamond composite segments

I would like to take this opportunity to thank some very special and important people to me that with their own way, friendship and love helped me to go through the process of this PhD and be able to finally present this thesis. First of all I would like to thank my two Greek flatmates and friends Dr. Alexander Karantzalis and Mr. Nikos Kontogiannis for their boundless spirit that

lightened up my stay in the UK. Thanks for everything guys, I had the best time of my life. Special thanks goes to Mrs. Katianna Iglezou for her unlimited love that gave me a reason for wanting to finish this PhD. Finally and most importantly I would like to express my gratitude to my friend Dr. Mark Jones (Doctor Jones, "Indiana") one of the most talented persons I have ever met, a philosopher and excellent scientist. I find it hard to express in few words my gratitude for this man. Without his valuable assistance I could never have finished this thesis. Mark, I share the best memories with you and I look forward to share a JD with you "on the ground".

At last but not least, I would like to thank my family. My brother Alexander and especially my mother who made whatever possible to express and remind me almost every day that although I was far away I remained in her heart and with her phonecalls, letters and all those small gifts that I regularly received, I felt even closer to her than ever. Special thanks also goes to my family in Denmark who helped me a lot during the time of my military service and made it possible for me to effectively continue the writing-up of this thesis at my spare time.

Finally, I would like to express my gratitude and love to my father, my mentor, the most versatile and hard working engineer and businessman I have ever known, who inspired me to study for this PhD. I realise today how much I have gained from always choosing the hardest way as he has always suggested me to do. Thank you for everything dad, I hope one day to make you proud and be able to stand up at your highest levels.

Table of Contents

Abstract I

Chapter 1 : Introduction 1

1.1 Introduction - Definitions 1
1.2 State of the Art 3
1.3 Aim of the Research 5
1.4 Structure of the Thesis 6

Chapter 2 : Diamond 7

2.1 Introduction 7
2.1.1 Diamond Synthesis 8
2.2 Diamond Structure and Shape 9
2.3 Diamond Properties 10
2.3.1 Cleavage 10
2.3.2 Hardness 10
2.3.3 Strength of Diamond 11
2.3.3.1 Elastic Moduli 11
2.3.3.2 Toughness 11
2.3.4 Thermal Properties 12
2.3.5 Chemical Properties 13
2.3.6 Oxidation - Graphitisation 14

Chapter 3 : Impregnated Diamond Tools 16

3.1 Introduction 16
3.2 Production Methods 17
3.3 The Cutting Operation 19
3.4 The Role of Metal Matrix 20
3.4.1 Diamond Retention 20
3.4.1.1 Mechanical Retention 20
3.4.1.2 Chemical Retention 22
3.4.2 Wear Resistance 22
3.4.3 Fabrication Requirements 24
3.5 The Role of Diamond 25
3.5.1 Diamond Type 25
3.5.2 Diamond Size 26
3.5.3 Concentration 26
3.6 Metal-Matrices for Diamond Impregnated Tools 27

Chapter 4 : Coated Diamonds 30

4.1 Introduction 30
4.2 Characteristics and Properties of Coated Diamonds 33
4.2.1 Retention of Coated Diamonds 33
4.2.2 Graphitisation & Oxidation Resistance - Thermal Stability 34
4.2.3 Protection Against Fracture 36
4.2.4 Heat Conductivity 37
4.2.5 Wetting 37
4.3 Coating Requirements 37
4.4 Types of Coated Diamonds 43
4.4.1 Single Layer Coated Diamonds 43
4.4.2 Multiple Layered Metal Coated Diamonds 47
4.5 Deposition Techniques 51
4.5.1 Chemical Vapour Deposition (CVD) 52
4.5.2 Physical Vapour Deposition (PVD) 56
4.5.2.1 Vacuum Deposition / Evaporation (VD / VE) 56
4.5.2.2 Reactive Deposition / Evaporation (RD / RE) 59
4.5.2.3 Magnetron Sputtering 61
4.5.3 Immersion in Molten Salt Baths (IMBS) 62
4.5.4 Other Methods 63
4.5.5 Post and Posterior Deposition Treatments 63
4.6 Mechanical Properties of Coated Diamonds 64
4.6.1 Strength of Coated Diamonds 64
4.6.2 Coating Adhesion Strength 66

Chapter 5 : Interfaces in Diamond Metal-Matrix Composites 71

5.1 Introduction 71
5.2 Interphase Interfaces in Solids 72
5.2.1 Coherent Interfaces 72
5.2.2 Semi-coherent Interfaces 73
5.2.3 Incoherent Interfaces 73
5.3 Diffusion and Interface Migration 74
5.4 Types of Interfaces in Metal Matrix Composites (MMCs) 75
5.5 Types of Interface Bonding 76
5.5.1 Mechanical Bond 76
5.5.2 Dissolution Bond 77
5.5.3 Reaction Bond 78
5.5.4 Exchange Reaction Bond 79
5.5.5 Oxide Bond 79
5.5.6 Mixed Type Bond 79
5.6 Requirements of the Interface 80
5.6.1 Mechanical Requirements of the Interface 80
5.6.2 Physical-Chemical Requirements of the Interface 80
5.7 Interfacial Interactions in Diamond Composites 82
5.8 Wetting and Adhesion Strength of Diamond-Metal Interfaces 86
5.9 Reactivity and Solubility in Diamond-Metal Systems 87

Chapter 6 : Mechanical Properties and Performance of Diamond MMCs 89

6.1 Introduction 89
6.2 Particulate-Composites Mechanics 90

6.2.1 Elastic Behaviour 90
6.2.2 Plastic Deformation 92
6.3 Failure 93
6.3.1 Reinforcement Cracking 93
6.3.2 Void Formation 94
6.4 The role of the Interface 95
6.5 Mechanical Properties of Diamond MMCs 97
6.6 Performance of Coated-Diamond Reinforced MMCs 100

Chapter 7 : Experimental Procedures 102

7.1 Introduction and Aim of Experimental Work 102
7.2 Diamond Characterization & Diamond Reactivity 103
7.2.1 Tested Diamonds – Coated & Non-coated 103
7.2.1.1 Diamond Types 103
7.2.1.2 SEM Characterisation 103
7.2.1.3 X-ray Diffraction 104
7.2.2 Diamond Reactivity 105
7.2.2.1 Diamond Reactivity Experiment (DRE) 105
7.2.2.2 Differential Scanning Calorimetry (DSC) 106
7.2.2.3 Metal-Leaching Procedure 109
7.2.2.4 Graphite-Leaching Procedure 109
7.2.2.5 Diamond Retrieval Procedure 109
7.2.2.6 Diamond Weight Change Measurement Procedure 109
7.2.2.7 Microscopic Examination 110
7.2.2.7A Scanning Electron Microscopy (SEM) 110
7.2.2.7B Optical Microscopy (OM) 111
7.3 Properties of Coated-Diamond Composites 112
7.3.1 Introduction - Aim 112
7.3.2 Materials & Composite Preparation 113
7.3.2.1 Diamond Composites (segments) Composition 113
7.3.2.2 Production Methods 115
7.3.3 Test Methods 119
7.3.3.1 Density Measurement 119
7.3.3.2 Modulus of Elasticity Measurement (Young's Modulus) 119
7.3.3.3 3-Point Bending 121
7.3.3.4 Tensile Testing – Uniaxial Tension 123
7.3.3.5 SEM Examination 124
7.4 Coated-diamond Composites with Alloy Metal-Matrices 126
7.4.1 Introduction – Aim 126
7.4.2 Diamond Composites (segments) 126

Chapter 8 : Results Part-I 129
"Material Characterisation - Diamond Reactivity"

8.1 Introduction 129
8.2 Diamonds Characterisation 129
8.2.1 Non-coated diamonds 129
8.2.2 Coated diamonds 130
8.2.3 X-ray Diffraction 132
8.3 Diamond Reactivity Experiment 132
8.3.1 Diamond Weight Change Measurement 132
8.3.2 DSC Analysis 134
8.3.3 SEM 137

8.3.3.1 Plain Synthetic Diamonds 137
8.3.3.1A SYN-1 Diamonds (SDA100 30/40 US Mesh made by DB) 137
8.3.3.1B SYN-2 Diamonds (MBS960 50/60 US Mesh by GE) 137
8.3.3.1C SYN-3 Diamonds (SDA75 30/40 US Mesh made by DB) 138
8.3.3.2 Diamond - Cobalt Systems 139
8.3.3.2A SYN-1 heat-treated with Co-EF powder 139
8.3.3.2B SYN-1 heat-treated with Co (CoC) powder 140
8.3.3.2C SYN-2 heat-treated with Co-EF powder 140
8.3.3.2D SYN-2 heat-treated with Co-SMS powder 141
8.3.3.2E SYN-2 hot-pressed with Co-EF powder 142
8.3.3.3 Diamond – Copper Systems 143
8.3.3.3A SYN-1 heat-treated with Cu powder 143
8.3.3.3B SYN-2 heat-treated with Cu powder 143
8.3.3.3C SYN-2 hot-pressed with Cu powder 143
8.3.3.3D SYN-2 hot-pressed with $Cu_{85}Sn_{15}$ powder 144
8.3.3.4 Diamond – Nickel Systems 144
8.3.3.4A SYN-1 heat-treated with Ni powder 144
8.3.3.4B SYN-2 heat-treated with Ni powder 145
8.3.3.4C SYN-2 hot-pressed with Ni powder 146
8.3.3.5 Diamond – Iron Systems 147
8.3.3.5A SYN-1 heat-treated with Fe powder 147
8.3.3.5B SYN-2 heat-treated with Fe powder 148
8.3.3.5C SYN-2 hot-pressed with Fe powder 148
8.3.3.6 Diamond - Molybdenum Systems 149
8.3.3.6A SYN-1 heat-treated with Mo powder 149
8.3.3.6B SYN-2 heat-treated with Mo powder 149
8.3.3.6C SYN-2 hot-pressed with Mo powder 150
8.3.3.7 Diamond – Tungsten Systems 150
8.3.3.7A SYN-1 heat-treated with W powder 150
8.3.3.7B SYN-2 heat-treated with W powder 151
8.3.3.7C SYN-3 coated with W by PVD (Code CD13) 153
8.3.3.7D SYN-3 coated with W by PVD industrially heat-treated (Code CD23) 155
8.3.3.8 Diamond – Titanium Systems 155
8.3.3.8A SYN-1 heat-treated with Ti powder 155
8.3.3.8B SYN-2 heat-treated with Ti powder 155
8.3.3.8C SYN-1 coated with Ti by CVD (Code CD6) 156
8.3.3.8D SYN-1 coated with Ti by CVD (by DB) industrially heat-treated (Code CD18) 157
8.3.3.8E SYN-1 coated with Ti by PVD (Code CD8) 157
8.3.3.8F SYN-1 coated with Ti by PVD (by TC) industrially heat-treated (Code CD19) 158
8.3.3.9 Diamond – Chromium Systems 159
8.3.3.9A SYN-1 heat-treated with Cr powder 159
8.3.3.9B SYN-2 heat-treated with Cr powder 160
8.3.3.9C SYN-3 coated with Cr by PVD (Code CD9) 161
8.3.3.9D SYN-1 coated with Cr by CVD industrially heat-treated (Code CD20) 162
8.3.3.9E SYN-3 coated with C-enriched Cr [Cr(C)] by PVD (Code CD11) 162
8.3.3.9F SYN-3 coated with C-enriched Cr [Cr(C)] by PVD industrially heat-treated (Code CD21) 164
8.3.3.10 Diamond – Titanium / Chromium Systems 164
8.3.3.10A SYN-3 coated with Ti/Cr by PVD (Code CD12) 164
8.3.3.10B SYN-3 coated with Ti/Cr by PVD industrially heat-treated (Code CD22) 165
8.3.4 OM Analysis 166

Chapter 9 : Results Part-II 168

"Characterisation & Properties of Coated Diamond Composites"

9.1 Introduction 168
9.2 Density 168
9.3 Modulus of Elasticity (Young's Modulus) 170
9.4 3-point Bending 174
9.5 Tensile Testing 180
9.6 SEM Examination 183

9.6.1 Qualitative Fracture Surface Examination 183
9.6.1.1 FS-ed & HIP-ed segments – Fractured by 3-point Bending 183
9.6.1.1A Non-coated Diamonds (CD2, CD3, CD4, CD5) 183
9.6.1.1B Ti-coated Diamonds (CD6, CD7, CD8) 184
9.6.1.1C Cr-coated Diamonds (CD9, CD10) 185
9.6.1.1D Cr(C)-coated Diamonds (CD11) 185
9.6.1.1E Ti/Cr-coated Diamonds (CD12) 186
9.6.1.1F W-coated Diamonds (CD13, CD14) 186
9.6.1.2 Hot-Pressed segments (HP) – Fractured by 3-point Bending 188
9.6.1.2A Non-coated Diamonds (CD15, CD16, CD17) 188
9.6.1.2B Ti-coated Diamonds (CD18, CD19, CD32, CD33, CD39, CD40) 188
9.6.1.2C Cr-coated Diamonds (CD20, CD24, CD34, CD38, CD42, CD43) 191
9.6.1.2D Cr(C)-coated Diamonds (CD21, CD35) 193
9.6.1.2E Ti/Cr-coated Diamonds (CD22, CD36) 193
9.6.1.2F W-coated Diamonds (CD23, CD25, CD26, CD30, CD31, CD37, CD44, CD45) 194
9.6.1.2G Co-powder encapsulated Diamonds (CD28, CD29) 196
9.6.1.3 Tensile test segments (DBS) – Fractured by Uniaxial Tension 197
9.6.1.3A Non-coated Diamonds (DBS-2, DBS-3, DBS-4) 197
9.6.1.3B Ti-coated Diamonds (DBS-5, DBS-6, DBS-11, DBS12) 198
9.6.1.3C Cr-coated Diamonds (DBS-13, DBS-14, DBS-19, DBS20) 199
9.6.1.3D Cr(C)-coated Diamonds (DBS-15, DBS-16) 201
9.6.1.3E Ti/Cr-coated Diamonds (DBS-7, DBS-8) 201
9.6.1.3F W-coated Diamonds (DBS-9, DBS-10, DBS-17, DBS-18, DBS-21, DBS-22, DBS-25, DBS-26) 202
9.6.1.3G Co-powder encapsulated Diamonds (DBS-23, DBS-24) 206
9.6.2 Quantitative Fracture Surface Examination 206
9.6.2.1 FS-ed segments – Fractured by 3-point Bending 207
9.6.2.2 HIP-ed segments – Fractured by 3-point Bending 207
9.6.2.3 HP-ed segments – Fractured by 3-point Bending 208
9.6.2.4 Tensile Test (DBS) segments – Fractured by Uniaxial Tension 212

Chapter 10 : Results Part-III 215
"Coated-Diamond MMCs with Alloy Metal-Matrices"

10.1 Introduction 215
10.2 Density 215
10.3 Modulus of Elasticity (Young's Modulus) 217
10.4 3-point Bending 218
10.5 SEM Examination 221
10.5.1 Qualitative Fracture Surface Examination 221
10.5.1.1 MB-1 : Co + 15%wt. Ni, Co-powder encapsulated 30/40 mesh SYN-3 221
10.5.1.1A Non-coated 30/40 US mesh SYN-3 Diamonds (MB1-N) 221
10.5.1.1B Co-powder encapsulated (J) 30/40 US mesh SYN-3 Diamonds (MB1-C) 221
10.5.1.2 MB-2 : Co + 10%wt. W, Co-powder encapsulated 30/40 mesh SYN-3 222
10.5.1.2A Non-coated 30/40 US mesh SYN-3 Diamonds (MB2-N) 222
10.5.1.2B Co-powder encapsulated (J) 30/40 US mesh SYN-3 Diamonds (MB2-C) 222
10.5.1.3 MB-3 : Co + 10%wt. bronze 85/15, Cr-PVD 30/40 mesh SYN-3 222
10.5.1.3A Non-coated 30/40 US mesh SYN-3 Diamonds (MB3-N) 222
10.5.1.3B Cr-PVD (TC) 30/40 US mesh SYN-3 Diamonds (MB3-C) 223
10.5.1.4 MB-4 : Co + 10%wt. bronze 85/15, Cr(C)-PVD 30/40 mesh SYN-3 223
10.5.1.4A Non-coated 30/40 US mesh SYN-3 Diamonds (MB4-N) 223
10.5.1.4B Cr(C)-PVD (TC) 30/40 US mesh SYN-3 Diamonds (MB4-C) 223
10.5.1.5 MB-5 : Co + 20%wt. bronze 85/15, Ti-CVD 30/50 mesh SYN-1 224
10.5.1.5A Non-coated 30/50 US mesh SYN-1 Diamonds (MB5-N) 224
10.5.1.5B Ti-CVD (DB) 30/50 US mesh SYN-1 Diamonds (MB5-C) 224
10.5.1.6 MB-6 : Co + 20%wt. bronze 85/15, Ti-PVD 30/50 mesh SYN-1 225
10.5.1.6A Non-coated 30/50 US mesh SYN-1 Diamonds (MB6-N) 225
10.5.1.6B Ti-PVD (TC) 30/50 US mesh SYN-1 Diamonds (MB6-C) 225
10.5.1.7 MB-7 : Pre-alloyed Cu-Fe-Co + 20%wt. Fe, W-PVD 30/50 mesh SYN-1 225
10.5.1.7A Non-coated 30/50 US mesh SYN-1 Diamonds (MB7-N) 225

10.5.1.7B W-PVD (TC) 30/50 US mesh SYN-1 Diamonds (MB7-C) 226
10.5.1.8 MB-8 : Pre-alloyed Cu-Fe-Co + 20%wt. Fe, W-CVD 35/50 mesh SYN-1 226
10.5.1.8A Non-coated 30/50 US mesh SYN-1 Diamonds (MB8-N) 226
10.5.1.8B W-CVD (NC) 35/50 US mesh SYN-1 Diamonds (MB8-C) 227
10.5.1.9 MB-9 : Pre-alloyed Cu-Fe-Co + 20%wt. W, W-PVD 30/50 mesh SYN-1 229
10.5.1.9A Non-coated 30/50 US mesh SYN-1 Diamonds (MB9-N) 229
10.5.1.9B W-PVD (TC) 30/50 US mesh SYN-1 Diamonds (MB9-C) 230
10.5.1.10 MB-10 : Pre-alloyed Cu-Fe-Co + 20%wt. W, W-CVD 35/50 mesh SYN-1 230
10.5.1.10A Non-coated 30/50 US mesh SYN-1 Diamonds (MB10-N) 230
10.5.1.10B W-CVD (NC) 35/50 US mesh SYN-1 Diamonds (MB10-C) 230
10.5.2 Quantitative Fracture Surface Examination 231

Chapter 11 : Discussion 234

11.1 Introduction 234
11.2 Solid-State Interactions of Synthetic Diamonds with Metals 235
11.2.1 Interactions in Diamond / Metal Systems - Introduction 236
11.2.2 Interactions in Diamond – Metal Powder Systems 236
11.2.2.1 Mode of interaction between diamonds and metals 236
11.2.2.2 Morphological changes occurring to diamonds with heat-treatment with metals 240
11.2.2.2A Plain diamonds 240
11.2.2.2B Diamonds heat-treated with Co-powders 241
11.2.2.2C Diamonds heat-treated with Ni-powder 246
11.2.2.2D Diamonds heat-treated with Fe-powder 247
11.2.2.2E Diamonds heat-treated with Cu-powder 247
11.2.2.2F Diamonds heat-treated with Mo-powder 248
11.2.2.2G Diamonds heat-treated with W-powder 248
11.2.2.2H Diamonds heat-treated with Ti-powder 250
11.2.2.2I Diamonds heat-treated with Cr-powder 250
11.2.3 Interactions in Hot-Pressed Diamond – Metal Composites 251
11.2.4 Interactions in Metal-Coated Diamonds 253
11.2.4.1 Titanium coatings 253
11.2.4.1A Chemical-Vapour-Deposited (CVD) coating 253
11.2.4.1B Physical-Vapour-Deposited (PVD) coating 254
11.2.4.2 Chromium coatings 255
11.2.4.2A Standard chromium PVD-coating 255
11.2.4.2B Carbon-enriched chromium PVD-coating [Cr(C)] 256
11.2.4.3 Titanium/Chromium Dual coating 257
11.2.4.4 Tungsten coating 258
11.3 Interfacial Bonding in Coated-Diamond reinforced Co-matrix MMCs 260
11.3.1 Densification of the Coated-Diamond Composites 260
11.3.2 Mechanical Properties 261
11.3.2.1 Modulus of Elasticity (Young's modulus) 261
11.3.2.2 Transverse Rupture Strength (TRS) in 3-point Bending 262
11.3.2.3 Tensile Strength 264
11.3.3 Interfacial Bonding in Coated-Diamond / Cobalt Composites 265
11.3.3.1 Non-coated diamond systems 265
11.3.3.2 Co-powder encapsulated diamond systems 267
11.3.3.3 Ti-coated diamond systems 268
11.3.3.4 Cr-coated diamond systems 271
11.3.3.5 Cr-powder encapsulated diamond systems 274
11.3.3.6 Carbon-enriched Chromium-coated diamond systems 276
11.3.3.7 Ti/Cr-coated diamond systems 277
11.3.3.8 W-coated diamond systems 278
11.3.3.9 W-powder encapsulated diamond systems 283
11.4 Interfacial Bonding in Coated-Diamond reinforced Alloy-matrix MMCs 285
11.4.1 Densification of the Coated-Diamond Composites 285
11.4.2 Mechanical Properties 285

11.4.2.1 Modulus of Elasticity (Young's modulus) 285
11.4.2.2 Transverse Rupture Strength (TRS) in 3-point Bending 286
11.4.3 Interfacial Bonding in Coated-Diamond / Alloy-Metal Matrix Composites 286
11.4.3.1 MB-1 : Co + 15%wt. Ni, Co-powder encapsulated 30/40 mesh SYN-3 286
11.4.3.2 MB-2 : Co + 10%wt. W, Co-powder encapsulated 30/40 mesh SYN-3 287
11.4.3.3 MB-3 : Co + 10%wt. bronze 85/15, Cr-PVD 30/40 mesh SYN-3 288
11.4.3.4 MB-4 : Co + 10%wt. bronze 85/15, Cr(C)-PVD 30/40 mesh SYN-3 288
11.4.3.5 MB-5 : Co + 20%wt. bronze 85/15, Ti-CVD 30/50 mesh SYN-1 289
11.4.3.6 MB-6 : Co + 20%wt. bronze 85/15, Ti-PVD 30/50 mesh SYN-1 290
11.4.3.7 MB-7 : Pre-alloyed Cu-Fe-Co + 20%wt. Fe, W-PVD 30/50 mesh SYN-1 290
11.4.3.8 MB-8 : Pre-alloyed Cu-Fe-Co + 20%wt. Fe, W-CVD 35/50 mesh SYN-1 292
11.4.3.9 MB-9 : Pre-alloyed Cu-Fe-Co + 20%wt. W, W-PVD 30/50 mesh SYN-1 292
11.4.3.10 MB-10 : Pre-alloyed Cu-Fe-Co + 20%wt. W, W-CVD 35/50 mesh SYN-1 293
11.5 Summary 295
11.5.1 Part-I: Fundamental Study of Diamond-Metal Reactivity 295
11.5.2 Part-II: Characterisation of Coated-Diamond / Co-matrix MMCs 296
11.5.3 Part-III: Characterisation of Coated-Diamond / Alloy-matrix MMCs 300

Chapter 12 : Conclusions 304
12.1 Introduction 304
12.2 Interactions between Synthetic Diamonds and – Elemental Metals 304
12.3 Interfacial Bonding & Mechanical Properties of Coated-Diamond reinforced MMCs 306

Chapter 13 : Future Work 309

Appendix A 313

Appendix B : Wetting and Solubility Data 315

Appendix C : Models of Composite Mechanics 320

Appendix D 327

References 332

Abstract

Diamond reinforced metal-matrix composites (MMCs) are utilised for cutting, drilling, grinding and polishing a variety of materials, in many cases being the most efficient and economic choice. The increased cost of synthetic diamond abrasives has led to constant search for ways to extent diamond tool life. This has been realised by introducing chemical reactions at the interfaces in order to develop chemical bridges between diamonds and metals that prolong the retention of crystals at the operating surfaces of the tools. Alloying the matrix with carbide forming metals is a way to introduce interfacial reactivity, but involves problems with concentrating the alloying element at the interfacial region and may cause alteration of the wear resistance characteristics of the binder, which may be an undesirable effect. A recent development and alternative method to alloying is the coating of the diamonds with carbide forming metals, offering unique advantages. Although metal-coated diamonds are commercially available, the effectiveness of their usage and the understanding of interfacial phenomena occurring in composites reinforced with such abrasives still remain unexplored. The work carried out in this research has examined the interfacial bonding in diamond MMCs reinforced with metal-coated crystals.

The work described in this thesis included a preliminary study on diamond/metal reactivity serving the need to identify the mode and intensity at which synthetic diamonds and elemental metals interact at various conditions. This was achieved by examining the changes occurring to diamond surfaces when crystals were heated in the presence of various elemental metals. The latter were brought in contact with the diamonds either in the form of loose or hot-pressed metallic powders or in the form of thin metal coatings deposited onto the crystals by vapour deposition methods. Results showed that metals, depending on their electronic configuration, either catalyse the graphitisation of diamond surfaces and dissolve carbon or react at the diamond surfaces to form carbide crystallites. Dissolution of the diamond occurred by formation of oriented hexagonal/triangular and rectangular pits on octahedral {111} and cubic {100} surfaces respectively. Intensity of interactions strongly depended on heating temperature and time. Metal coatings were found to efficiently react with the diamonds only after annealing at temperatures of the order of 1000°C subsequent to the deposition.

The diamond impregnated MMCs investigated in this research were reinforced with various types of metal-coated and metal-powder encapsulated diamonds of the carbide forming metals of Ti, Cr and W. The tested composites included two types of metal-matrices that of standard plain cobalt as well as some selected alloyed matrices typically employed in practice. Interfacial bonding characterisation and assessment of the potential capability of the metal-coatings to offer enhanced diamond retention has been made by determining the mechanical properties of the composites and by conducting extensive microscopic analysis of the developed fracture surfaces.

The results suggested that incorporating metal-coated crystals could be beneficial in improving the diamond retention, provided that consolidation temperature is sufficiently high to favour diamond/metal reactions. Results showed improvements in mechanical properties to be achieved when reinforcing with the coated diamonds compared to non-coated grit. The characteristics of the interactions at the diamond surfaces in the composites conformed to the findings of the preliminary study on the fundamentals of diamond/metals interactions. Reactions on crystal surfaces took place at the locations where prior dissolution of the diamond had occurred. Metal coatings were found to provide excellent protection to the diamonds against catalysed dissolution by aggressive binders. Thin coatings suffered from loss of continuity in systems were the coating metal atoms were readily soluble in the metal-matrix. This was avoided with thicker coatings that also appeared to provide a supplementary mechanical effect in addition to the chemical bonding in improving the retention of the diamond crystals.

Encapsulation of diamond with carbide forming metals was a hybrid method between alloying the metal-matrix and coating the crystals. Although encapsulation provided sufficient levels of chemical interactions, it was shown that diamonds could not be efficiently protected from aggressive binders. In addition, composites impregnated with powder-encapsulated diamonds suffered from inadequate sintering of the carbide forming metal zones surrounding the crystals when consolidation was performed at relatively low temperatures, which was reflected in inferior mechanical properties.

1

Introduction

1.1 Introduction - Definitions

The term "diamond tools" refers to a wide range of tools that utilise the unique high hardness and strength of diamond in sawing, grinding, milling and drilling applications. These tools consist of a body/carrier to which the diamond abrasive medium is attached. This body is commonly a steel, other metal or alloy and is usually referred to as "core", "blank" or "hub". The abrasive medium can be in the form of large single crystal diamonds, polycrystalline synthetic diamond (PCD) blocks (inserts) or specially shaped masses in which the diamond grits are dispersed in a binder. The specially shaped masses that incorporate the diamonds are known as "segments" in the diamond tool industry, and the tools are then referred to "impregnated diamond tools". The binder in which the diamonds are randomly dispersed is usually referred to as the "bond", and is most commonly a metal or metal alloy and in that case, the segments fall into the category of metal matrix composites (MMCs). The segments are fastened on the carrier by brazing, laser welding, adhesive fixing or sintering.

Diamonds or PCD inserts can be fixed directly on to the core at the working surface. Diamond single crystals can be positioned by means of brazing or electroplating so that they form a single

layer that covers completely the working surface. Alternatively, a number of large single crystal diamonds or PCD inserts can be fixed by means of brazing, welding, adhesive fixing or sintering to specific positions on the surface of the tool, forming a particular pattern. This pattern must ensure even cutting and loading of the diamonds and cost effective operation. These tools are the so-called *"surface-set diamond tools"*.

Metal bonded impregnated diamond tools are readily employed in sawing, drilling and surface grinding in the stone, building and road construction industries. The formulation and consolidation of the segments is achieved in the vast majority, by powder metallurgy (P/M) techniques.

Apart from considerations concerning the quality, the characteristics and the chemistry of the involved materials and the fabrication procedures, the design of the diamond tools is important. It must ensure stability, even loading of the diamond abrasive, efficient cooling, allowance of effective flushing of the formed debris and good surface finishing of the workpiece. Various designs for both the segments and cores have been invented throughout the years, with varying degrees of sophistication.

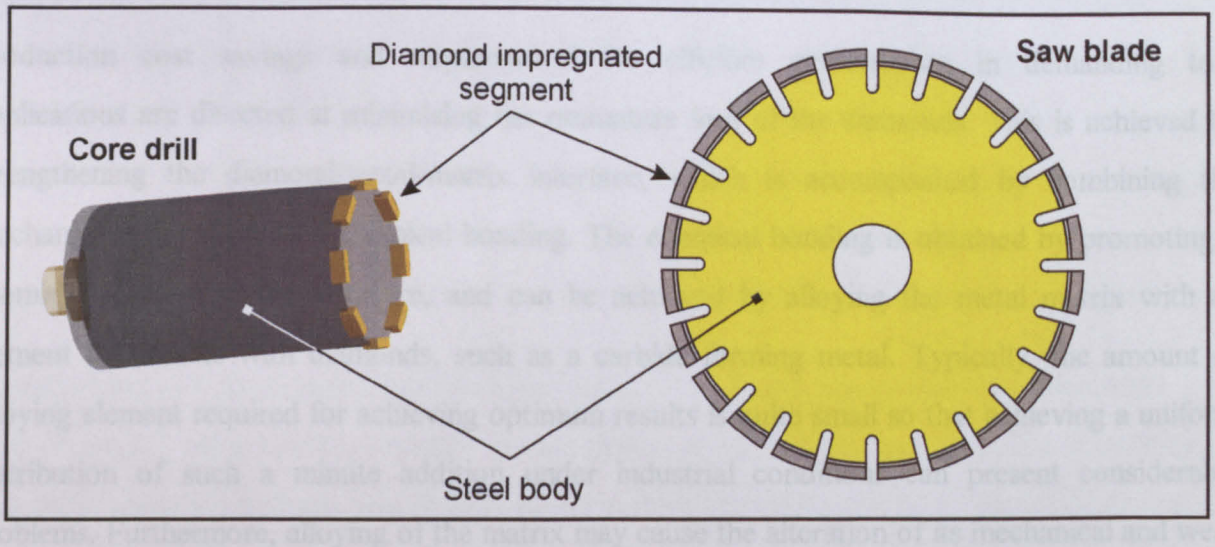

Figure 1-1 : Sketch illustrating typical metal bonded diamond impregnated cutting tools used in the construction and stone industries.

The research presented here, is concerned with metal bonded diamond impregnated cutting tools, which are used in the stone and construction industries.

1.2 State of the Art

During the tool service, gradual erosion of the matrix occurs, exposing the diamonds to the contacting operating surface, allowing them to perform the cutting action. There is a need to adjust the wear characteristics of the matrix according to the abrasiveness of the material that is being processed and the quality (strength) of the diamond which is employed, in order for the matrix to erode at an appropriate rate to allow the diamond particles to be revealed. Apart from an optimum rate of erosion, the matrix has the additional task of securing the diamonds in a firm position at the operating surface and allowing them to dislodge only after their useful life is ended. Mechanically enclosing diamonds in a metal matrix socket satisfies the above requirement only for a limited period after the time the diamond is first exposed at the surface, which is however much shorter than the capable useful life of diamond. Typically, when diamonds are exposed by more than 1/3 of their diameter, the surrounding metal is incapable of further providing a fast grip, and erosion becomes critical, resulting in premature loss of the grit [1]. Depending on the abrasiveness of the workpiece and the mechanical properties of the metal matrix, the mechanical retention of diamonds can be slightly prolonged, but diamond pull-out still occurs prematurely. It has been observed that the proportion of diamonds lost at an early stage can be as high as 80% [2].

Production cost savings and requirements for efficient performance in demanding tool applications are directed at minimising the premature loss of the diamonds. This is achieved by strengthening the diamond/metal-matrix interface, which is accomplished by combining the mechanical gripping with a chemical bonding. The chemical bonding is obtained by promoting a chemical reaction at the interface, and can be achieved by alloying the metal matrix with an element that reacts with diamonds, such as a carbide forming metal. Typically, the amount of alloying element required for achieving optimum results is quite small so that achieving a uniform distribution of such a minute addition under industrial conditions can present considerable problems. Furthermore, alloying of the matrix may cause the alteration of its mechanical and wear resistance properties. Two methods may be employed to overcome these difficulties, which are :

- sintering in the presence of a liquid phase in order to enhance the atomic mobility of the alloying elements, or
- using metal coated diamonds.

The liquid phase sintering process presents some potential technical difficulties. Specifically, when hot pressing, which is the most commonly employed production method of diamond tools, there is a danger of squeezing the liquid out of the graphite mould. In addition, liquid phase sintering

cannot eliminate the demand for alloying the metal matrix with a carbide forming element, which as stated above may alter its wear properties in a detrimental manner.

The second method involving metal-coated diamonds has no restrictions in production methods, so that both pressure-less or pressure assisted sintering can be applied. In addition, there is no need for matrix alloying, since the alloying element is concentrated exactly where it is needed, around the diamonds in the form of a metal coating. Hence, the application of metal-coated diamond particles in the production of impregnated diamond cutting tools has gained a great deal of research interest in recent years. The metal coatings of the carbide forming elements (i.e. Ti, Cr, W, Zr etc.) have been found to improve the bonding of the abrasive particles to the matrix material by generating a carbide layer at the diamond/metal-matrix interface [3].

Although research on metal-coated diamonds has been carried out, particularly in the last decade, there is still no considerable work published. The research has been mostly directed at the development of the coatings on the diamond crystals and the characterisation/identification of the formed coatings and any reaction products at the diamond/coating interface. Limited research deals with the adhesion/bonding strength at the diamond/coating interface. Examining the actual effect of the coated diamonds in their true operating environment, i.e. while incorporated in the bond, has not been given attention, and the limited available data are almost all restricted to the patent literature. In addition, in most cases qualitative or comparative data on the cutting ability or performance of diamond tools are given and only in few cases is this data presented quantitatively. Furthermore, there is a lack of published information as it pertains to the mechanical properties of coated diamond impregnated materials in relation to the cutting action.

Coated diamonds have been available commercially for many years. Tool manufacturers have been or are still using coated diamonds in their products without having a sufficient knowledge of how these abrasives operate, which prevents them from optimising the performance of their tools. Employing coated diamonds has been found to improve the cutting performance of diamond tools, but deterioration in cutting action has been observed in some cases.

1.3 Aim of the Research

The present status dictates that a better understanding of the coated diamonds technology is needed.

The direct way to establish whether the use of coated diamonds is beneficial would be by performing a series of drilling or cutting field tests. However, such kind of tests involve a lot of parameters with some of them being difficult to control, as for example the properties of material to be cut, the lubrication and removal of debris from the cutting zone. Additionally, any observed differences would be difficult to relate to microstructural characteristics of the diamond impregnated segments.

In this thesis, evaluation of coated diamonds is made by direct identification of the interfacial chemical bonding achieved in composites reinforced with these crystals. Assessment of interfacial bonding is realised by means of relating mechanical properties of diamond-reinforced segments with results from detailed microscopical analysis of fracture surfaces.

A necessary step before examining the interfacial phenomena in diamond composites was to understand the fundamental chemical phenomena that take place in simple two component systems, made of synthetic diamonds and elemental metals. Acquiring this basic knowledge would help the understanding and identification of chemical phenomena taking place in the more complex systems of the diamond composites. This comprised the first objective of this research.

Having established this basic knowledge, the second objective was to primary evaluate various metal-coated diamonds in simple composites having a binder composed of a single metal, which was selected to be cobalt because of it's wide use in diamond tool industry.

The third and final objective was to explore the potential of enhanced diamond composite properties with the use of selected metal-coated in more complex systems having alloy metal binders which is the typical case in commercial practice.

1.4 Structure of the Thesis

The first five chapters review the literature relevant to the coated diamond technology, the interfacial bonding aspects and the mechanical properties of MMCs with particular focus to diamond reinforced composites.

Chapters 2 and 3 present in brief the basics as concerning the characteristics of synthetic industrial diamond abrasives and the technology associated with the impregnated diamond composites.

Chapter 4 is dedicated to a detailed review of the metal-coated diamond technology. Description covers topics related to the various types of coated diamonds and deposition techniques and focuses on their main characteristics and properties as has reported.

The possible types of interfacial bonding in MMCs are reviewed in Chapter 5. The final sections of this chapter review published information on interfacial bonding in diamond composites accompanied by presentation of studies concerning wetting, solubility and reactivity in diamond-metal systems.

Chapter 6 is the final section of the literature review and describes in brief the principles of elastic and plastic behaviour of particulate MMCs relevant to the diamond composites. The final sections of this chapter review published information on mechanical properties of diamond composites.

The experimental work carried out during the course of this research is described in Chapter 7. The work is divided into three parts corresponding to the three main objectives of this project as addressed above.

The results gained from this work are described in three separate chapters, in line with the three experimental parts. Chapter 8 describes the results of the experimental work into identifying the fundamentals of diamond-to-metal reactivity. The following chapter presents the complete sets of results that concerned the study of interfacial bonding and mechanical properties of coated diamond reinforced cobalt. Chapter 10 gives the results for the examined systems with the alloyed metal matrices.

An extensive discussion of the results follows in Chapter 11, and conclusions to the work are drawn in Chapter 12. The final chapter, Chapter 13, highlights areas where further research on the subject may be carried out as evolved during the course of this research.

2

Diamond

2.1 Introduction

The principal superabrasives are found as phases in the boron-carbon-nitrogen-silicon family of materials [4] (Figure 2-1). Diamond is the hardest known material with second the cubic boron nitride (cBN). Diamond is either found in nature or is synthesised, while cBN does not occur in nature. Diamond found in earth is known as *natural diamond* while the man-made is referred as *synthetic diamond*. Diamonds can be additionally classified into two major categories of gem and industrial diamonds. Gem diamonds are commonly natural stones of attractive appearance used as jewellery. Industrial diamonds are the synthetic crystals and the natural stones that do not meet the standards of gem diamonds, because of colour, size or other imperfections. Industrial diamonds are attractive for their properties of unique hardness and strength or semiconductivity.

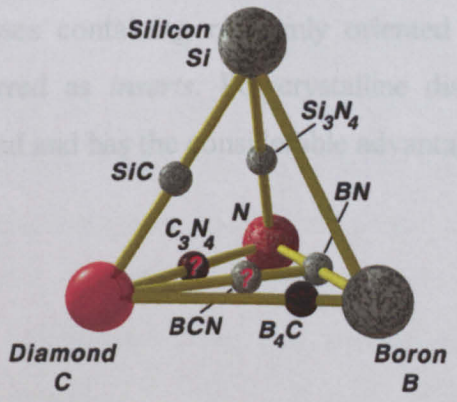

Figure 2-1 : The C-B-N-Si composition tetrahedron showing the principal known superhard materials [4].

2.1.1 Diamond Synthesis

Diamond was first synthesised in mid-1950's and late the same decade the first commercial synthetic industrial diamonds were made available. Diamond can be grown as an equilibrium phase at high pressures or grown metastably at subatmospheric pressures in the form of single crystals or thin films respectively [5]. The idea of the equilibrium growth synthesis is to transform the soft hexagonal crystal structure of graphite to the hard cubic form of diamond. This is achieved by subjecting graphite to extremely high pressures and temperatures [6]. The technique is the so-called *static synthesis*, alternatively known as the *high-pressure high-temperature synthesis* (HPHT). In practice, in order to minimise the demand for extremely high pressures and temperatures and in order to achieve acceptable graphite-to-diamond transformation rates, the graphite is catalysed by various molten metals or alloys (such as iron, nickel etc.) [7]. Catalysis takes place while graphite is subjected to high temperatures and high pressures in large special purpose presses [8]. Typically, the pressures are of the order of 60kbar (6GPa) and temperatures exceeding 1500°C. The HPHT synthesis is the technique used to produce the largest amount of commercially available industrial diamond. However, the resultant diamond contains inclusions from the metal catalysts, which degrade its strength as they increase in content [9]. The extremely high pressures required for the graphite-diamond transformation can be alternatively obtained by shock waves generated by explosive charges in the so-called *shock synthesis* [10]. This technique however, is only capable of producing very fine diamonds, which are normally utilised as seed crystals for the production of large diamonds or polycrystalline blocks with the HPHT synthesis [4].

Metastable synthesis involves the growth of diamond films at subatmospheric pressures from hydrocarbon gases in the presence of atomic hydrogen by vapour deposition techniques (plasma-assisted, chemical vapour deposition - CVD or physical vapour deposition - PVD) [5, 11].

Diamond fine crystallites, natural or synthetic, can be sintered into strong masses at high temperatures and high pressures to form *polycrystalline diamond* (PCD) [12]. Thus, large isotropic masses containing randomly oriented diamond crystals can be produced. These are typically referred as *inserts*. Polycrystalline diamond is almost as strong and hard as single crystal diamond and has the considerable advantage of being tougher than the latter.

2.2 Diamond Structure and Shape

The carbon atoms that make up diamond are tetrahedrally co-ordinated so that each carbon atom shares one of its outer four electrons with each of the four adjacent carbon atoms spaced symmetrically about it [13] (Figure 2-2a). The distance between the centres of any pair of atoms is about 0.154 nm [14]. Eight of the atoms are located at the corners of a cube (shown as blue spheres), six other atoms are situated at the centres of the cube faces (shown as light blue spheres) and four more carbon atoms are linked by four bonds to their neighbouring atoms another (shown as differently coloured spheres) (Figure 2-2b). This arrangement repeats itself all through the diamond. The atoms shown as blue spheres form a face-centred cubic (FCC) lattice. The atoms shown as differently coloured spheres lie also on the points of another FCC lattice similar and parallel to the first, but somewhat displaced from it. Thus, the complete diamond lattice may be described as consisting of two interpenetrating FCC lattices. The structure of graphite consists of a stacking arrangement of layers consisting of hexagonal rings [15] (Figure 2-2c). The conversion from graphite to diamond is accompanied by 26% decrease in volume [4].

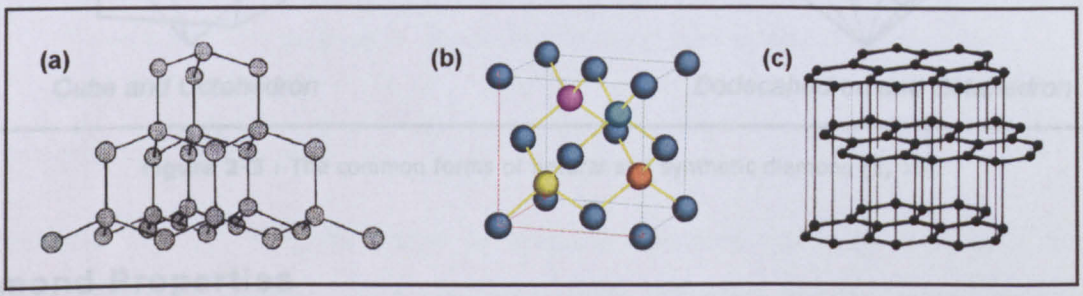

Figure 2-2 : Models of the diamond (a,b) and graphite (c) lattices [16].

The shape of the diamond crystal depends on which planes were favoured during growth. The growth usually takes place on low index planes such as {001}, {011}, {111} [17]. The octahedral form of diamond, for example, appears to be the result of equal outward growth on all eight {111} planes (Figure 2-3a). Different shapes may rise when growth is developed on {001} or {011} planes. The uniform growth on each of the six {001} planes would result in a crystal of cubic form (Figure 2-3b) while the growth on each of the twelve {011} planes results in a crystal of twelve sides known as dodecahedron (Figure 2-3c). Other crystal forms are possible when the growth has occurred on more than one family of planes (Figure 2-3d and f). Diamond is often found in the so-called *cubo-octahedral* form, which occurs when both octahedral and cubic faces are grown. Natural diamond generally grows predominantly in an octahedral habit, very occasionally of cubic habit and never in the dodecahedral form. On the other hand, synthetic diamonds are commonly either octahedrons or cubooctahedrons and only occasionally with dodecahedron facets.

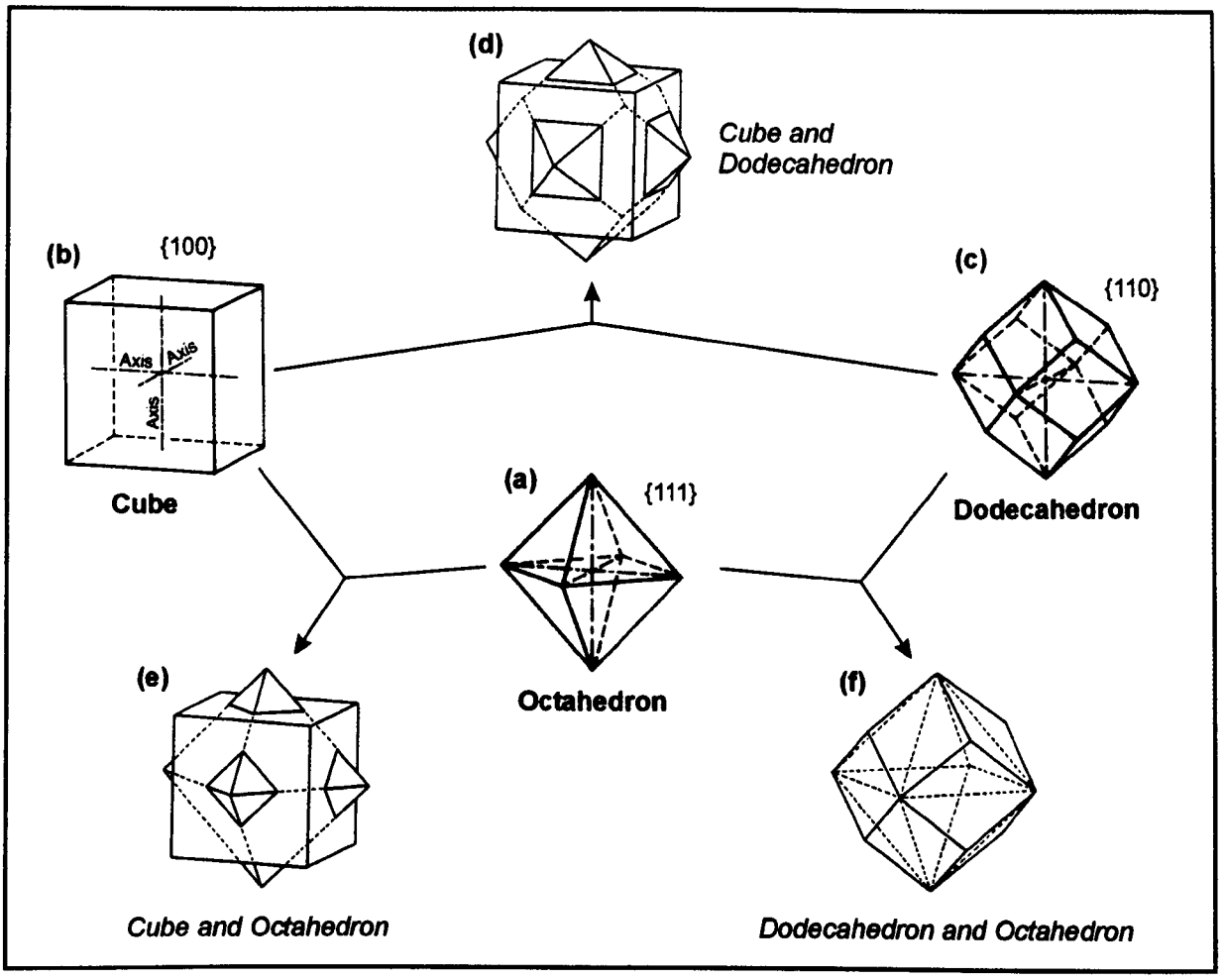

Figure 2-3 : The common forms of natural and synthetic diamond [1, 16].

2.3 Diamond Properties

Some of the most important physical, mechanical and thermal properties of industrial diamonds, as concerns their use in sawing, cutting and grinding applications, are briefly reviewed.

2.3.1 Cleavage

The dominant cleavage plane of diamond is the octahedral (111), which is defined by the faces of the octahedron [18]. Cleavage is important because it allows diamond to regenerate sharp edges during operation [16]. However, when sawing or cutting cleavage is not always a beneficial incident.

2.3.2 Hardness

Hardness is maybe the most important physical property of an abrasive. The Moh's scale of hardness is a relative scale based on the ability of materials to scratch each other. On this scale

diamond is the hardest known material possessing therefore the maximum value of 10 [4]. Aluminium oxide has a value of 9 with cBN's Moh's hardness lying somewhere in between. Knoop hardness is a measure of a material's ability to indent other materials. The larger the Knoop number the harder the material. Diamond has a Knoop number of about 7000 MPa while Al_2O_3 and cBN exhibit values of order of 2000 and 4700, respectively [4] (see Table 2-2 on page 12).

Diamond does not exhibit isotropic hardness. It is well established today that the hardness of diamonds depend on many factors such as the orientation, the diamond type, the impurity content, the load and shape of indenter [19]. Even the in-plane hardness of diamond surfaces varies with orientation, exhibiting *soft* and *hard* directions (Table 2-1).

	Knoop hardness number (GPa)					
	(001) plane		(110) plane		(111) plane	
	<100>	<110>	<001>	<110>	<110>	<112>
Diamond (type I)	98	83	108	88	56	63
Diamond (type II)	103	91	115	94	76	110

Table 2-1 : Knoop hardness of cubic diamond single crystals at room temperature [20].

2.3.3 Strength of Diamond

The small size and the irregular shape of synthetic diamonds crystals impose difficulties in directly measuring the strength. At room temperature, diamond behaves almost entirely as an ideal brittle material [21].

2.3.3.1 Elastic Moduli

Diamond like other crystals is not isotropic. Both Young's modulus and bulk modulus vary by about 10% with the crystallographic direction of the measurements [21]. Poisson's ratio varies greater than Young's and bulk modulus. Table 2-2 on page 12 includes the average values that are used in practice for calculations.

2.3.3.2 Toughness

Toughness is a measure of material's ability to absorb energy before undergoing brittle failure. For industrial diamonds intended to be used as abrasives, toughness is of great importance since cutting and sawing operations involve cyclic impacts of the crystals onto the material being processed. For mesh materials like industrial diamonds, the relative toughness can be determined

by subjecting a sieved quantity of the abrasive to an impact test [16, 21]. The toughness is then defined as the ratio of the quantities of the sieved on-size abrasive before and after the test. The higher this ratio, or the higher the percentage of remaining on-size quantity, the tougher is the material characterised. This type of test is often referred to as the *friability test* or *Friatest* in diamond tools industry.

The strength of synthetic diamonds decreases when crystals are heat-treated [22, 23]. This is mainly attributed to the metallic inclusions trapped in diamond during the HPHT metal-catalytic synthesis [24]. Thermal weakening of diamonds has been related to internal stresses arising from differential thermal expansivities between metal inclusions and diamond [5]. It has been recently argued that internal stresses arise because of the catalytic graphitisation than takes place around the metal inclusions [9, 25]. Since the volume occupied by graphite is considerably greater than of diamond, the void volume available for the metal inclusion to expand is limited or even annihilated, thus setting up internal stresses.

For the same grade of synthetic diamonds, finer crystals exhibit lower reduction in strength than larger crystals [23]. This can be explained by considering the fact that larger crystals will always have a higher possibility of containing internal defects compared to smaller crystals.

Natural diamonds are less sensitive to strength decreases with temperature increases, due to their higher internal purity.

2.3.4 Thermal Properties

The thermal conductivity of some near perfect diamond crystals can be as high as five (5) times that of copper at room temperature [16] (Table 2-2). Even less perfect crystals have high conductivity.

	Density	Knoop Hardness	Young's Modulus	Compressive strength	CTE	Thermal conductivity
	g/cm^3	GPa	GPa	GPa	$mm/mm/°C \times 10^{-6}$	W/m ·K
Diamond	3.52	70-100	1075	10	0.8	2100
Cubic Boron Nitride	3.48	45	662	7	5.6	1400
Silicon carbide	3.21	27	207	1.3	4.5	42
Alumina	3.92	25	308	3	8.6	33
Cement WC+6%Co	15	17		5.4	4.5	105

Table 2-2 : A selection of physical and mechanical and thermal properties of single crystal industrial diamond compared to PCD and other abrasives or hard materials [4].

2.3.5 Chemical Properties

Diamond is chemically resistant to liquid organic and inorganic acids at room temperatures as well as to alkalis and solvents [14]. However, diamond can be chemically etched by strong oxidizers such as sodium and potassium nitrates at temperatures of the order of 500°C [14, 26]. Several other compounds also attack diamond, including fluxes of sodium and potassium chlorates and molten hydroxides like NaOH.

At room temperatures, diamond surfaces are typically terminated with bonded heteroatoms, such as hydrogen, oxygen and fluorine [27]. Diamond surfaces can become reactive if conditions are such to cause desorption of the heteroatoms or if a very active reagent can access the diamond surfaces and displace them. Carbon oxides can begin to desorb at significant rates at temperatures as low as 350°C, but only at temperatures of the order of 700°C is oxygen completely removed. Temperatures of the order of 900-1000°C and 1200°C are necessary for removal of hydrogen and fluorine respectively [27].

Clean diamond surfaces are produced by cleavage at the tips of diamonds during machining [27]. It is due to these highly reactive clean surfaces generated during operation that machining of iron and other metals produces high wear rates to diamonds [28, 29, 30, 31]. However, clean surfaces are quickly contaminated. Unfortunately, during machining the operation of the diamonds is cyclic and therefore clean surfaces are constantly generated producing a continuous wear.

Under certain conditions, e.g. heat treatment or cleavage, the terminal carbon atoms on diamond surfaces can be freed from any heteroatom leaving unsaturated carbon bonds [28]. These bonds can rearrange themselves into new C-C bonds with partial double-bond (pi) character, reconstructing the diamond surfaces [27]. Reconstructed diamond surfaces are unreactive to most potential absorbates at room temperatures. Subsequent treatment of reconstructed surfaces can restore one of the diamond surface conditions described above [28].

Upon heating, diamond reacts with various metals such as iron, nickel, cobalt, tantalum, tungsten, titanium and others. Chapter 5 deals in detail with reactivity and solubility of diamond to various metals.

2.3.6 Oxidation - Graphitisation

Diamond at atmospheric pressure is the unstable form of carbon at all temperatures [10]. However, at normal conditions the transformation of diamond to graphite, which is the thermodynamically stable form of carbon, is very slow [32].

From early studies on diamond stability it was well established that diamond's back-conversion to graphite was accelerated by oxidative agents [33] or metals [32]. The temperature for the onset of transformation being considerably reduced compared to that for "true" uncatalysed graphitisation.

It has been reported that oxidation of diamond can begin at temperatures as low as of the order of 500 to 600°C and becomes significant at temperatures above 700°C [16]. Evans and Phaal [34] measured the rates of oxidation of low index diamond faces heated in a stream of oxygen. In the temperature range of 700-1000°C, oxidation was found to be proportional to the oxygen pressure with highest oxidation rate found for {111} surfaces followed by {110} and with {100} exhibiting the lowest rate. The activation energy for the diamond-oxygen reaction was measured to be 230 ± 10 $kJ \cdot mol^{-1}$. Oxidation of diamond by molecular oxygen has been suggested to occur by an initial adsorption of oxygen and subsequent desorption of CO or CO_2 leaving a graphite layer on diamond surface [35]. The process may involve two stages or at lower temperature occur directly as a single step. Upon formation of a graphite film on the diamond surfaces, oxidation rate is reduced, as graphite provides protection to the diamonds [28]. Such graphite crystallites formed on diamond surfaces exhibit a preferential orientation influenced by the symmetry of the diamond substrate [36].

Graphitisation of diamond is also catalysed by certain metals and alloys, such as nickel, iron and cobalt [32, 37-40]. Metals or alloys that are effective catalysts (solvents) for the HPHT synthesis are expected to catalyse as well the conversion of diamond back to graphite at low pressures, in the stability field of graphite [25]. It has been proposed that the rate-determining step for the catalysed graphitisation of diamond surfaces by metals is the detachment of single carbon atoms from the diamond surface into metal's interstices [32, 37, 38]. As has been addressed earlier in this chapter, catalysed graphitisation may also occur internally around the metallic inclusions inside the diamond crystals.

Uncatalysed graphitisation essentially occurs under ultra-high vacuum [32]. Under vacuum of 10^{-6} or better, diamond can be heated up to about 1450°C without undergoing any change for

certain periods of time [28, 41]. The rate of graphitisation has been found to follow an Arrhenius relationship of the form [42] :

$$\frac{dx}{dt} = C \cdot e^{-\Delta E/RT} \qquad \textbf{(Eq. 2-2)}$$

where ΔE is the activation energy of the transformation, C is a constant related to the number of active sites available for graphitisation at the diamond surface, T is the temperature, and R the gas constant. The activation energy (ΔE) has been found to vary for the various faces of the diamond crystal as follows:

$$\Delta E_{\{011\}} = 730 \pm 50 \text{ kJ mol}^{-1} \quad \text{and} \quad \Delta E_{\{111\}} = 1060 \pm 80 \text{ kJ mol}^{-1}$$

Evans T. [33] suggested that the low activation volumes calculated from the above determined activation energies indicated that the primary process for the graphitisation of diamond should be the detachment of single carbon atoms from the diamond surface. The relative ranking of low index diamond planes on their graphitisation rate was explained in terms of the number of C-C bonds joining adjacent layers for each plane. Carbon atoms in {011} surfaces are bonded with two C-C bonds to the layer below, while the atoms in successive {111} layers alternate between a situation where each atom is joined to the lower layer by one C-C and a situation where each atom is joined to the lower layer by three C-C bonds. According to this approach, graphitisation of {111} planes requires the breaking of three C-C bonds instead of the two C-C bonds for the {011} surfaces, thus explaining the larger activation energy of the former.

Fedoseev *et al.* [43] in their study on the surface graphitisation of diamonds have determined the thickness of graphite layer formed onto diamond crystals. It was shown that finer crystals were associated with thinner layers of graphite, which suggested that smaller diamonds are more resistant to graphitisation than larger crystals.

The rate of graphitisation is considerably reduced at pressures of the order of 5GPa [7, 42], which is not surprising if someone considers that graphite has a larger molar volume than diamond.

3

Impregnated Diamond Tools

3.1 Introduction

This chapter is concerned with the impregnated diamond tools utilised for sawing, cutting and drilling in the construction and stone industries. However, most of the principles discussed in the following sections can in general apply to all types of diamond tools. Depending on the chemistry of the binder, diamond tools can be classified into three main groups [4, 44]:

- *resin bonded* diamond tools, of either a thermosetting or thermoplastic resin,
- *vitrified bonded* diamond tools, or
- *metal bonded* diamond tools, which also include metal/ceramic bonded (cermet) and electroplated diamond tools.

A rough estimate of the market of superabrasives tools finds CBN tools to occupy 10 to 15% of the market while diamond tools account for the 85 to 95% [44]. The section occupied by each of the different diamond tool types in the diamond tool market is given schematically in Figure 3-1 on next page. The difference in the market share for the various types of tools, arise from the different fields of application with regard both to the material to be processed and to the processing task.

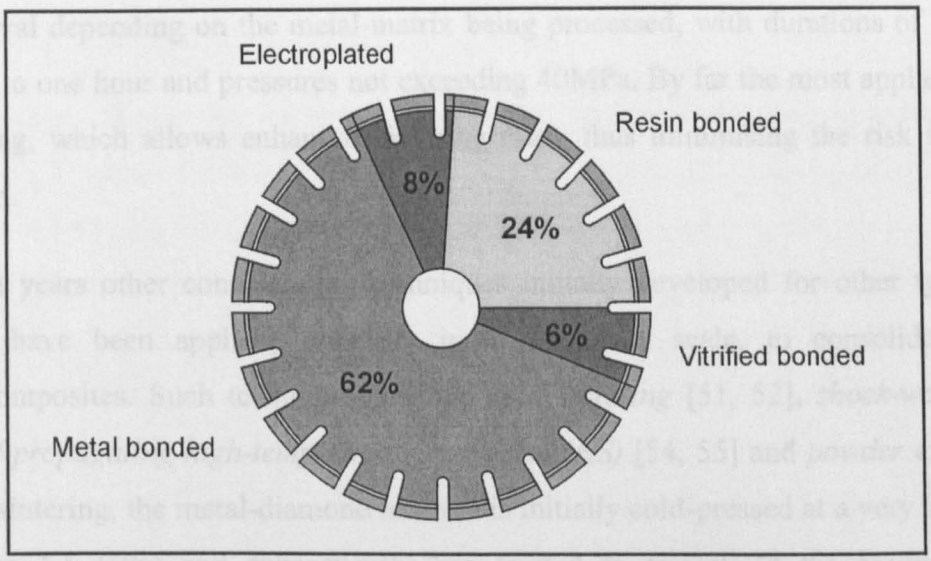

Figure 3-1 : Rough estimate of the market share for the various types of diamond tools [44].

The following paragraphs are concerned with the technology of the diamond-reinforced composites attached on metal-bonded diamond tools, which are widely employed in sawing and drilling applications in the stone and construction industries.

3.2 Production Methods

Diamond impregnated tools are constructed by a number of segments mounted on a carrier. The main part of the tools is the abrasive segments, which are essentially metal-matrix composites (MMCs), with diamond crystals being the reinforcement. Typically, the segment consolidation routes involve powder metallurgy (PM) production methods. The general guidelines of the steps involved in a typical production line include:

- preparation of the metal matrix powder - diamond mixture (alloying, blending, granulation, diamond coating or roughening, addition of lubricants and/or sintering additives etc.),
- shaping of segments by cold pressing,
- hot consolidation by pressure assisted or pressureless sintering treatment,
- segment quality control,
- mounting the segments on the blank (brazing, laser welding etc.),
- dressing the segments, final finishing of the tool and packing.

In commercial practice the consolidation of the diamond-metal powder mixture is typically achieved with sintering, infiltration, hot-pressing (HP) or hot-isostatic pressing (HIP) in inert, reducing atmospheres or vacuum [44-50]. Consolidation temperature typically range in the 500-

1150°C interval depending on the metal-matrix being processed, with durations of the order of few minutes to one hour and pressures not exceeding 40MPa. By far the most applied technique is hot-pressing, which allows enhanced sintering rates, thus minimising the risk for diamond graphitisation.

In the recent years other consolidation techniques initially developed for other types of P/M components have been applied, primarily in a laboratory scale, to consolidate diamond reinforced composites. Such techniques include *cold sintering* [51, 52], *shock-wave sintering* [53] and *self-propagating high-temperature synthesis (SHS)* [54, 55] and *powder extrusion* [56, 57]. In cold sintering, the metal-diamond mixture is initially cold-pressed at a very high pressure (of the order 3-5 GPa) and subsequently heat-treated to anneal. In the second technique, consolidation is achieved by utilising the frictional heat developed at particles contacts by the rapid plastic flow attributed to a travelling explosive wave generated by a detonator. In the SHS method, sintering is achieved by utilising the heat released by an exothermic reaction, which takes place between some of the metal-matrix constituents. The above techniques present some difficulties; mainly in controlling the heat generated and are still in the development stage. The steps that may be involved in a typical production line are graphically illustrated in the flow diagram given in Figure 3-2.

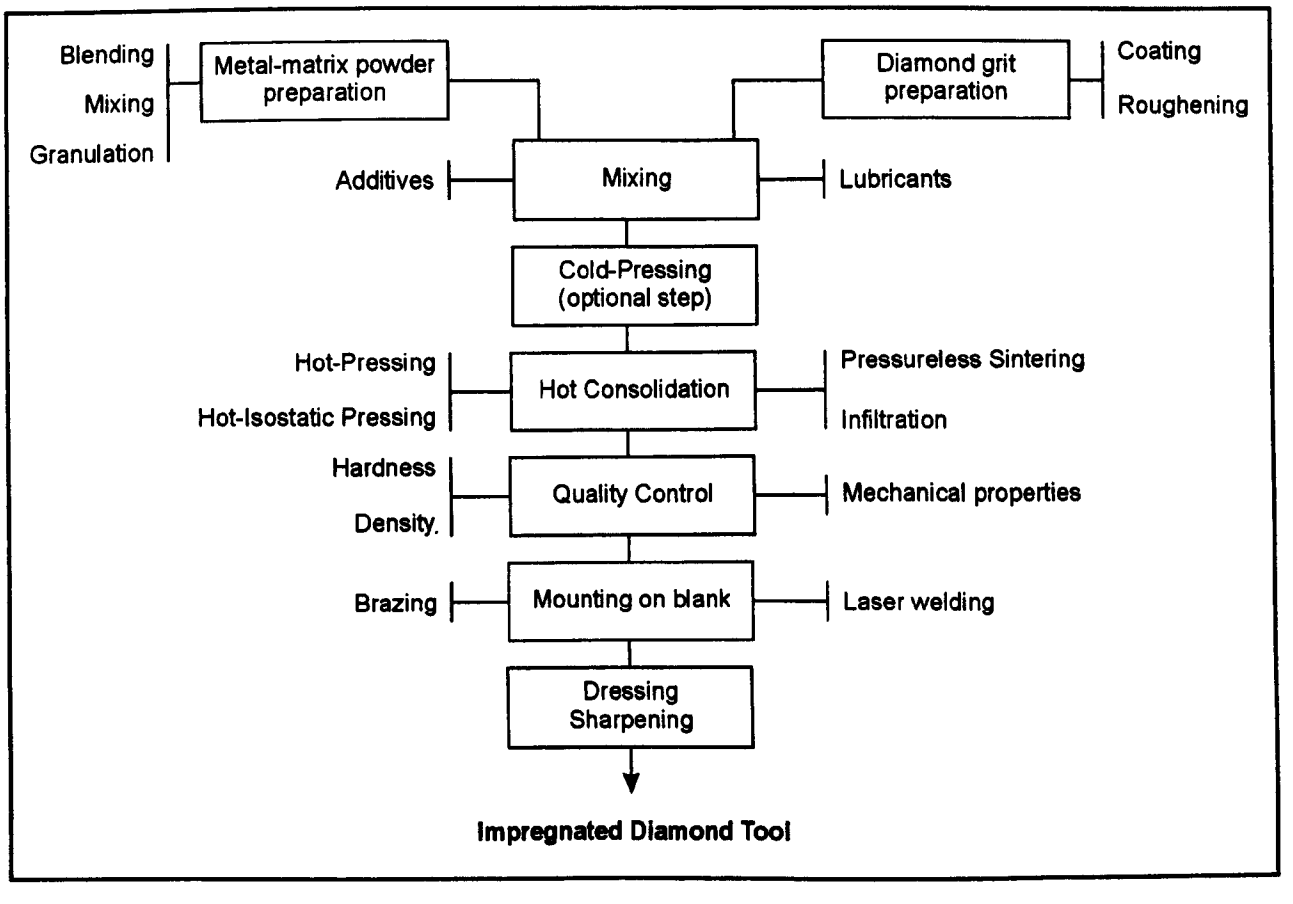

Figure 3-2 : Flow diagram illustrating typical production steps for impregnated diamond tool production.

3.3 The Cutting Operation

The operating faces of the diamond impregnated tool segments can be realised as surfaces of the metal-matrix from which diamond particles protrude and perform the cutting (Figure 3-3). Each exposed diamond while in rotating motion, is forced by the applied pressure to the diamond tool to penetrate the workpiece material surface. During this action, diamonds are subjected to wear and the debris that breaks away from the processed material is forced within the space between the diamond tool working surface and the workpiece area (known as *clearance*) causing the gradual erosion of the matrix. The metal-matrix wears faster at the front and sides of the diamond, while the abrasive volume protects the matrix behind the diamond thus, forming a tail (see Figure 3-3). The tail is the main source of supporting the diamond in place and withstands the longitudinal forces applied on diamond from the workpiece during cutting. As cutting proceeds, the protrusion of the operating diamonds gradually increases because the supporting matrix erodes, and at a point the surrounding metal matrix is inadequate to support the diamond, which is then lost. The dislodging of the diamond is known as *pull-out*. As the matrix erodes, some of the working diamonds chip, producing new cutting points, others are lost and some new diamonds are gradually uncovered from the removed matrix. This sequence of events lasts throughout the life of the tool and an equilibrium surface state of protruding diamonds is set up [1, 46]. At any time during the life of a segment, some of the exposed diamonds exhibit a different height of protrusion, so that not all uncovered diamonds are in contact with the workpiece performing the cutting [58]. It has been found [59], that only about 25% of the exposed diamonds are actually operating.

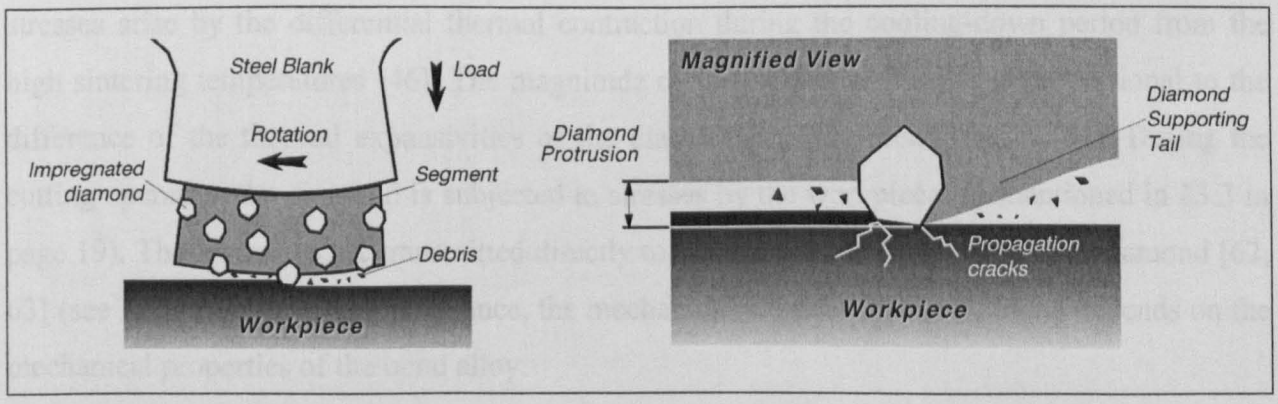

Figure 3-3 : The cutting action in an impregnated diamond segment. The formed debris erodes the metal matrix. The matrix wears faster at the front and sides of the abrasive crystal leaving a tail behind the diamond, which supports the crystal.

3.4 The Role of Metal Matrix

The two basic functions of the metal matrix are to hold the diamonds tight in place and position and to erode at a rate compatible with the diamond loss. Many factors are involved in the metal bond selection, with the following being dominant for the case of diamond impregnated segments [45] :

- diamond retention capacity,
- wear resistance, and
- segment fabrication requirements.

3.4.1 Diamond Retention

During operation, the matrix must withstand the turning moment to which the diamond particles are subjected. Diamonds must be secured in such a way that they are not prematurely pulled out, pushed-in deeper in the matrix, or moved around, while the tool is cutting. In the majority of diamond impregnated tools the diamond retention is primarily of mechanical character. Improvement of the retention can be achieved if the mechanical gripping is accompanied by a chemical bonding [60].

3.4.1.1 Mechanical Retention

Neglecting the physical nature of covering of the diamonds by the matrix, the mechanical bonding is enhanced by the tensile stresses induced in the matrix around the diamond. These stresses arise by the differential thermal contraction during the cooling-down period from the high sintering temperatures [46]. The magnitude of these internal stresses is proportional to the difference of the thermal expansivities of the diamond and the metal matrix [61]. During the cutting operation the diamond is subjected to stresses by the workpiece (as mentioned in §3.3 in page 19). These stresses are transmitted directly to the metal matrix tail behind the diamond [62, 63] (see Figure 3-3 on page 19). Hence, the mechanical retention of the diamond depends on the mechanical properties of the bond alloy.

It can be assumed that the best mechanical retention is achieved when there is no deformation of the matrix or when only reversible elastic deformation occurs [63]. Considering the case of a single loaded diamond (see Figure 3-4), it is clear that when the deformation is elastic, the supporting matrix will restore its initial shape as soon as the stresses cease so that the diamond grip will be re-established. However, if this deformation is plastic, the matrix does not reverse to

its shape after the stresses cease, so that the cavity in which the diamond is being secured becomes bigger. Subsequently, when the diamond is again under load the matrix might deform even more allowing the diamond to move inside the cavity. At a latter stage the socket will no longer be sufficiently tight to hold the diamond and consequently, diamond pull-out will occur.

The matrix will deform plastically and the mechanical retention will fail, only if the yield strength of the matrix is exceeded. The potential retentive properties of the matrix can be better assessed by its modulus of resilience than just from its yield strength value. The ability of the metal matrix to absorb elastically the induced stresses or to deform plastically is not only dependent on the level of stresses induced during the cutting action, but also depends on the shape of the diamond [62]. The angular shaped diamond crystals promote stress concentration, thus making the notch sensitivity of a metal matrix an important property that has to be considered when designing the matrix chemical composition [46].

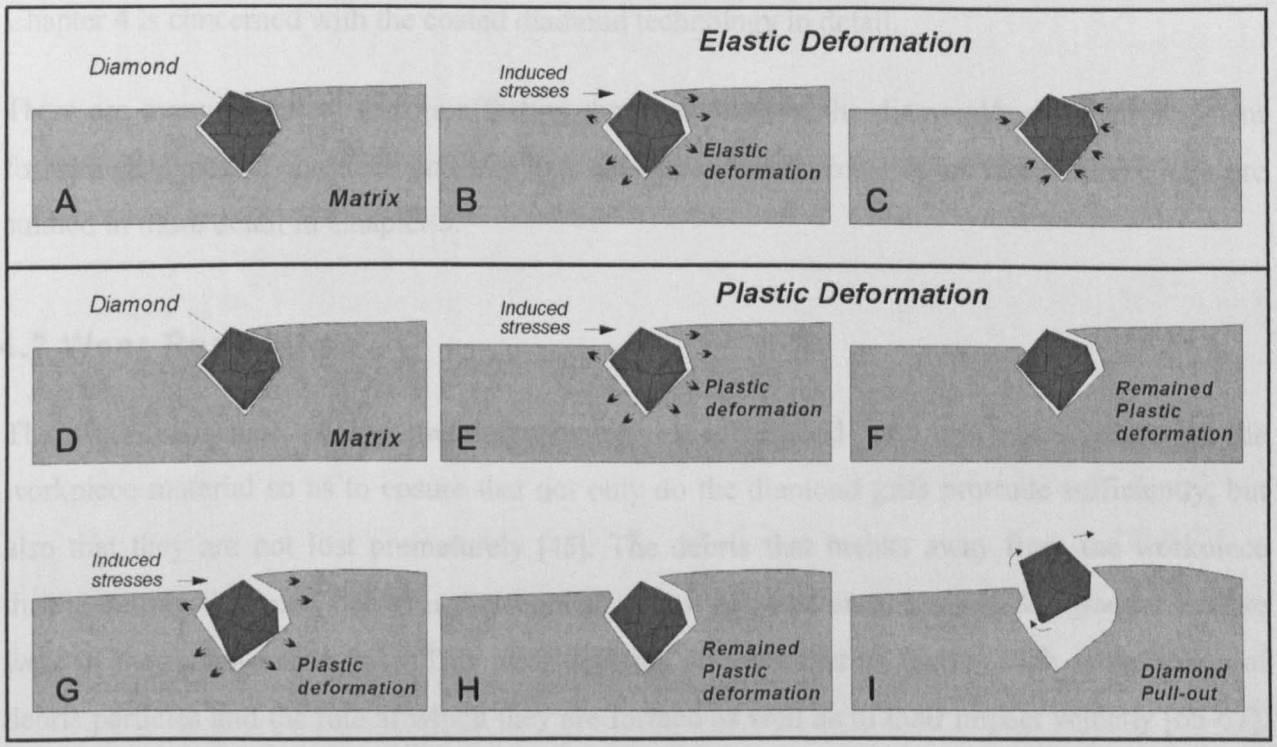

Figure 3-4 : The concepts of mechanical retention. The diamond is loaded and unloaded in a cyclic manner as the tool rotates. **Elastic deformation :** The embedded diamond (A) during cutting transmits the induced stresses to the matrix (B). The matrix is stretched elastically and when the stresses cease returns to its initial shape (C) restoring the grip. **Plastic deformation :** The embedded diamond (D) is loaded and transmits the induced stresses to the matrix (E). The stresses exceed the yield strength of the matrix and unloading finds the matrix plastically deformed (F). Subsequent loading (G) increases the amount of permanent deformation (H) and the diamond becomes unstable and might move and rotate in the cavity. After a few cycles of loading and unloading, the socket is substantially enlarged and the diamond pull-out occurs (I).

3.4.1.2 Chemical Retention

When diamond retention relies on mechanical means alone, it is found that the proportion of diamond particles lost due to inadequate bonding can be as high as 80% [2]. This impairs the life and the efficiency of the tool and from an economical point of view increases the cost of production. It is therefore necessary to strengthen the diamond/matrix interface in order to provide an additional anchoring factor to couple with the mechanical gripping of diamonds by the formed matrix sockets. Thus, the mechanical bonding is often combined with a chemical bonding of the diamonds to the metal matrix. This is achieved by atomic reaction at the diamond/matrix interfacial region [60]. The strengthening of the interface is realised by the formation of a thin carbide film at the interface. Hence, carbide-forming elements are introduced to the diamond/metal-matrix system. In practice, it is common to add small amounts of the carbide formers as alloying elements into the base metal-matrix alloy. Alternatively the diamond crystals can be coated with the carbide former element prior to their incorporation in the bond. Chapter 4 is concerned with the coated diamond technology in detail.

There are many chemical factors affecting the interaction in the diamond/metal-matrix system for various types of matrices and alloying elements. Some concepts of these interactions are studied in more detail in Chapter 5.

3.4.2 Wear Resistance

The wear resistance of the metal-matrix has to correspond with the abrasiveness of the workpiece material so as to ensure that not only do the diamond grits protrude sufficiently, but also that they are not lost prematurely [45]. The debris that breaks away from the workpiece during cutting is forced between the segment and workpiece area, causing the gradual erosive wear of the metal-matrix [64]. This wear depends on a number of factors such as the shape of debris particles and the rate at which they are formed as well as to their impact velocity [65-67]. These factors however do not necessarily coincide with the factors causing the wear of the diamond particles.

In many cases the factors responsible for the diamond and matrix wear operate inversely to each other [46]. When a hard and dense material is sawn, very little debris is formed and only as fine powder. Under such conditions, diamonds are strongly loaded and wear fast, whereas the erosive wear of the matrix is slow [68]. On the other hand, when cutting soft, open-textured and gritty materials, a great quantity of coarse debris is released. Such conditions cause little wear on the diamond but the erosion of the matrix is excessive. A "too soft" bond that wears faster than the

diamond increases the possibility of premature pull-out [69]. Inversely, an extremely wear resistant matrix wears much slower that the rate of diamond break-down, causing the segment surface to gradually decrease in protruding diamond points concentration, and to polish. This phenomenon is known as *glazing* [45, 46].

In designing diamond-impregnated segments, the wear of both the diamond and the matrix must be optimised for the particular material to be processed and the application task. A sufficiently fast matrix removal is needed to ensure that protruding diamonds are always available, but at the same time the matrix wear must be sufficiently slow to coincide with the diamond break-down, in order to utilise the abrasive grit during its total capable operation life, avoiding early pull-out [58]. The general rule for designing a diamond-impregnated tool appoints stronger diamonds (better quality, smaller size) and softer matrices (less wear resistant) as the material hardness increases, the abrasiveness decreases or the texture becomes more condensed [39, 70]. On the other hand, less demanding diamond quality (moderate strength, large crystal size) and hard wear resistant matrix must be used, as the hardness of the workpiece decreases, the abrasiveness increases, and the texture is more open. Figure A-1 in Appendix A illustrates in a graphical manner, the choice in segment parameters as a function of some general workpiece properties, according to the general designing rule presented above.

The bulk hardness and abrasion resistance of the metal-matrix are two properties that do not always coincide. This is attributed to the fact that during service the hardness of the metal-matrix at the vicinity of the operating surface is subjected to strain hardening [71]. A better correlation is typically found between wear resistance and hardness of strain-hardened worn surfaces of metal and alloys. The inability to always directly relate the bulk hardness with wear resistance is also demonstrated by various metals and alloys often used as binders in segments. It has been found, for example, that the wear resistance of some bronze alloys increases as their bulk hardness decreases [46] (Figure 3-5). Furthermore, wear resistance of metals and alloys used as matrices in impregnated diamond composites has been suggested to be related to the modulus of resilience and toughness [45, 46]. Tanaka *et al.* [72] have shown the wear volume and grinding efficiency of various metals alloys to linearly depend on the elastic and elastic-plastic failure energies obtained by 4-point bending.

In many cases, in order to modify the wear resistance of the matrix, additives (or fillers) can be introduced in the binder alloy [46]. These are typically metal carbides, oxides, graphite or carbon. By far, the most applied additives are tungsten and tungsten carbide due to their hardness and strength properties [69]. Aside from the incorporation of additives, the

modification of the relative abrasion resistance can be achieved by manipulating the shape of the starting powders, which make up the metal matrix [45]. Thus, multi-sized and irregularly shaped powders (e.g. dendritic, irregular) provide an interlocking effect, which makes the matrix more wear resistant than a matrix of the same chemistry but produced from equally sized and regularly shaped powders (e.g. spheroidal, nodular) [45, 69]. However, the increase in wear resistance by utilising multi-sized and irregular powders, is accompanied by the undesirable effects of poor flow and packing characteristics [73].

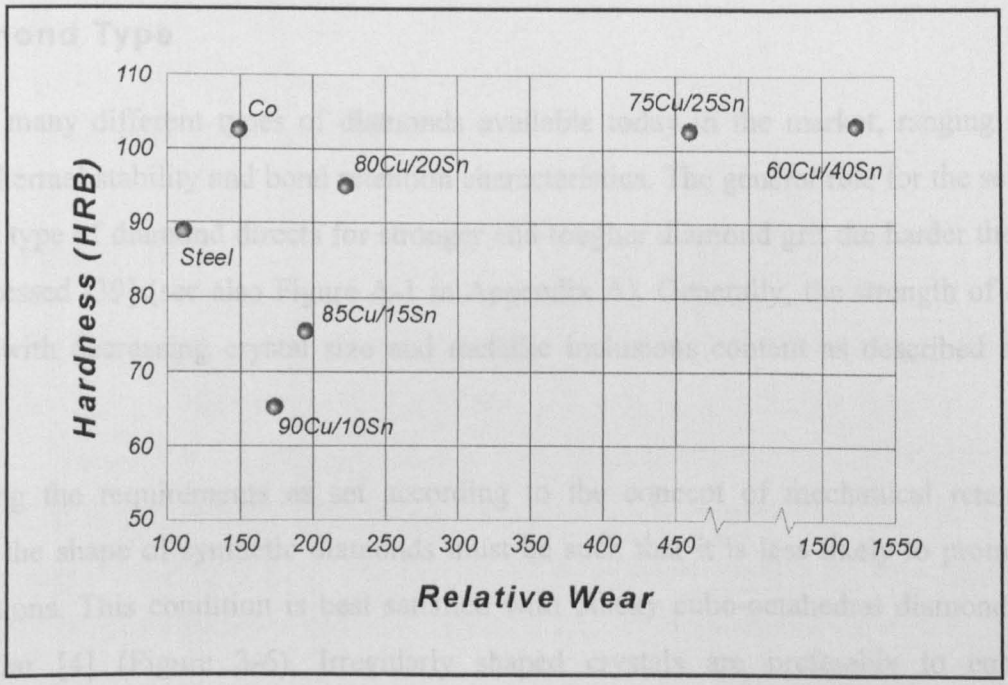

Figure 3-5 : The relationship between wear resistance and hardness of some bronze alloys, cobalt and steel. The results are relative to a wrought mild steel specimen [46].

3.4.3 Fabrication Requirements

All restrictions concerning the selection of the metal-matrix and the consolidation parameters arise from the need to protect the diamonds from catalysed graphitisation and dissolution by the metal-matrix as has been addressed in Chapter 2.

Consolidation temperatures typically do not exceed 1000°C. However, higher temperatures are necessary for sintering highly wear resistant binder containing tungsten or WC particles. In such cases, natural industrial diamonds are often chosen instead of the synthetic crystals, due to their increased thermal stability.

3.5 The Role of Diamond

The function of the diamond is to perform the cutting. The optimum grade of grit must be selected in order to fulfil the requirements as set from the given task and conditions of cutting, while simultaneously being the most cost-effective choice. The most significant parameters that must be taken in consideration when selecting the diamonds are the diamond type, the grit size and the concentration in the segment [45].

3.5.1 Diamond Type

There are many different types of diamonds available today in the market, ranging in shape, strength, thermal stability and bond retention characteristics. The general rule for the selection of the proper type of diamond directs for stronger and tougher diamond grit the harder the material to be processed [39] (see also Figure A-1 in Appendix A). Generally, the strength of diamonds increases with decreasing crystal size and metallic inclusions content as described already in Chapter 2.

Considering the requirements as set according to the concept of mechanical retention (see §3.4.1.1), the shape of synthetic diamonds must be such that it is less likely to promote stress concentrations. This condition is best satisfied with blocky cubo-octahedral diamonds that are less angular [4] (Figure 3-6). Irregularly shaped crystals are preferably to enhance the mechanical retention by an interlocking effect. From this point of view, natural diamonds increase interlocking effects, because of their many re-entrant surfaces [39, 45, 46].

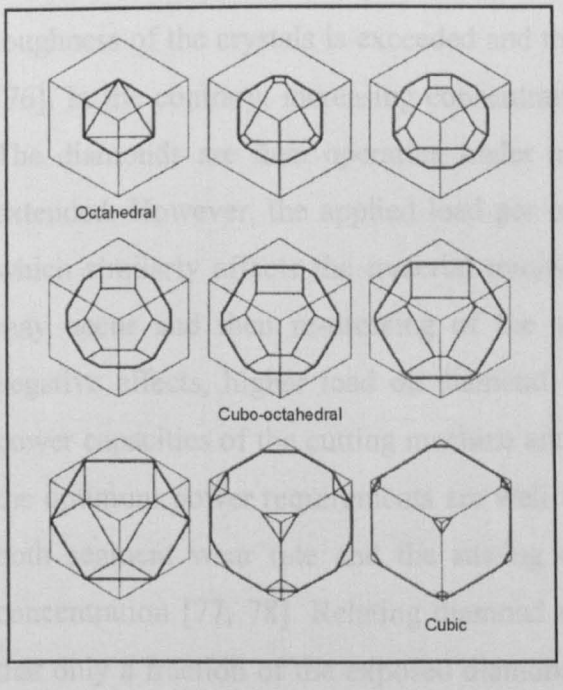

Figure 3-6 : The blocky cubo-octahedral diamond crystal is the shape that ensures the minimum stress concentration in the metal-matrix [74].

3.5.2 Diamond Size

When referring to diamond size the US mesh size scale is commonly used (see Table A-1 in Appendix A). Finer grit sizes are typically associated with higher strengths for diamonds belonging to the same quality grade. Crystal size also determines the maximum permitted protrusion height above the matrix surface during operation before the metal-matrix can no longer retain the diamonds [58]. This height influences the clearance of swarf from the cutting zone. If the load applied to the diamond is sufficiently high, larger sized crystals will penetrate deeper into the workpiece enhancing the cutting rate [75]. This however, will result in increased mechanical loading of the diamonds that may result in either excessive pull-out or extensive cleavage and fracture of the crystals [39, 45, 46, 59].

3.5.3 Concentration

On diamond tool industry concentration is referred to an unofficial standard where by definition concentration 100 is equivalent to 4.4 carats per cm^3 (or 25% by volume). All other dimensionless concentrations are proportional. The diamond concentration in conjunction with the diamond particle size, control the number of exposed cutting points per unit area available at the cutting face of the tool. The total number of available diamonds at the working zone is proportional to the concentration and inversely proportional to the mean particle size.

On decreasing the diamond concentration, the available cutting points decrease and the applied load on each individual diamond becomes higher thus increasing the amount of material removed per crystal. This condition is satisfied until a critical point where the strength and toughness of the crystals is exceeded and the grains start to shatter or are prematurely pulled-out [76]. In the contrary, increasing concentration increases the number of available cutting points. The diamonds are then operating under milder conditions and the overall life of the tool is extended. However, the applied load per crystal decreases thus reducing the penetration depth, which similarly affects the material removal rates. Under such conditions, diamond polishing may occur and then re-dressing of the segments is necessary. In order to overcome these negative effects, higher load on diamond is required, which in turn sets high demands in the power capacities of the cutting machine and increases the operational costs. In some cases where the optimum power requirements are well within the capabilities of a well-maintained machine, both segment wear rate and the sawing costs can be considerably reduced when increasing concentration [77, 78]. Relating diamond concentration and crystal size, it must be considered that only a fraction of the exposed diamonds is actually in action, as has been shown in a study

of the segment wear of diamond impregnated bits [59]. From the total number of exposed diamond crystals on the working surface of the segments, only the 25% of the protruding diamonds have the correct operational height.

3.6 Metal-Matrices for Diamond Impregnated Tools

Most of the binders employed in diamond-impregnated composites consist of mixtures of carefully selected metal powders to formulate alloys. The selection of the metal powders and consolidation method is made on the basis to achieve a set combination of properties which are primarily determined from the intended use of the diamond tool and the properties of the material to be processed. As previously addressed, some of the metal-matrix properties of designing importance are the mechanical strength (elastic and plastic behaviour), the chemical activity and wetting to the diamond, the wear resistance and thermal expansion.

The most commonly employed binders in the diamond tool industry are based on metals which are either relatively inert to diamond or exhibit variable degrees of carbon dissolution, such as cobalt (Co), copper (Cu), nickel (Ni) and iron (Fe). These base metals are commonly alloyed with small additions of carbide forming metals such as tungsten (W), titanium (Ti), chromium (Cr), molybdenum (Mo) in order to enhance chemical reactions with the diamonds. In addition to this alloying, hard filler particles may occasionally introduced into the binder in order to control the wear resistance as was described in a previous section.

Apart from the relative portions of the metal powders required to formulate the desired binder alloying composition, all P/M principles and criteria for powder selection are applicable. Thus, powder characteristics such as particle shape, size, specific surface, oxygen content etc. are considered with regard to ease of processing, enhanced packing and densification and effect to final properties of the sintered composite. Often, powders are granulated into aggregates in order to prevent segregation of the large diamond crystals, reduce the airborne susceptibilities of fine powders and to facilitate better flowing and packing especially in cases of automatic die feeding cold-presses.

The capability to influence the final properties of the matrix with such many parameters can theoretically give the ability to produce a variety of binders to suit all possible applications. In practice however, the existence of such many variables make it difficult to understand the clear effect of each individual variable to the final properties of the bond. Thus, although commonly complex and sophisticated binders are in use by the tool manufacturers, their formulation is

commonly based on empirical observations and rarely is scientifically established. Typical powder sizes range from sub-micron size up to mesh size powder (400 microns). Table 3-1 lists the most commonly employed metal powders for diamond MMCs together with their main characteristics.

Base Metal Matrix	**Main Characteristics**	**Application**
Cu , Sn (bronzes)	• CuSn liquid at most sintering temperatures • no carbide formation • insignificant carbon solubility • small amount of physical etching on diamond • no effect other than oxygen or other impurities	• less abrasive materials
Co , Ni	• solid at typical sintering temperatures (the pure metals) • poor carbide formation • significant carbon solubility (at higher temperatures) • variable diamond etching depending on processing	• very abrasive materials
Fe & alloys (partially substitutes of Co)	• solid at sintering temperatures • carbide formation (hard, unstable carbides) • surface reaction on diamond	• similar applications as Co, Ni base binders
Alloying Metal Powders		
Cr , Ti , Mo , W , Ta , V	• Carbide formers • improvement of diamonds retention • solid at sintering temperatures • very reactive metals	
Al , Ag , Zn	• insignificant or small carbide formation • used for liquid phase sintering	

Table 3-1 : Metal powders commonly employed in diamond MMCs [45, 46, 69, 79].

In modern diamond tool industry, cobalt and cobalt alloys seem to be the most suitable materials for diamond impregnated segments used for cutting and grinding hard and fine grained natural stones as granite and basalt [82]. Cobalt is a suitable binder for diamond tools since it does not react strongly with the abrasive grains. In fact, cobalt appears to have an almost ideal affinity for carbon ascertaining a good wetting of diamond [83]. Cobalt exhibits very good mechanical retention of diamond due to its exceptional combination of high yield strength and toughness. Its wear resistance seems to be suitable for most applications allowing similar wear rates as the abrasive grains. In addition, cobalt's wear resistance can be modified to a large extent by addition of alloying elements, thus expanding its field of applications.

Pure cobalt exists in either a hexagonal closed-packed (HCP, cobalt-ϵ) or face-centre cubic (FCC, cobalt-α) structure. The brittle HCP structure is stable at the lower temperatures, whereas the more ductile and tough FCC structure is stable at the higher temperatures. The allotropic

transformation takes place at a temperature of 417°C. In order to achieve the excellent combination of properties mentioned above, it must be ensured that the cobalt binder must have a large degree of the FCC structure. This can be achieved by introducing small alloying additions (up to 6 wt-%) of elements conserving the FCC structure, such as Fe, Ni, Mn, Ti, Al, Zr and Ta [82, 84]. Cobalt can be fully densified by means of P/M under relatively low temperatures and mild pressures giving products with excellent combination of high strength, ductility and wear resistance. Consolidation temperatures range from 750 to 950°C and pressures of up to 35MPa. The time at sintering temperature is of the order of few minutes and the total cycle of not more than 20 minutes. The advantageous combination of properties for the cobalt P/M materials, not readily attainable by other methods, is attributed to the drastic reduction in grain size as well as an excellent dispersion of fine pores and cobalt oxides [85-87]. Both these factors hinder the FCC to HCP allotropic phase transformation on cooling after consolidation, resulting in a large fraction of the metastable ductile FCC phase being retained at room temperature.

The recent trend in the diamond tool industry is to substitute cobalt with ternary or quaternary system alloys including iron (Fe), nickel (Ni) or copper (Cu) and containing only small amount of cobalt. Powder producers offer already such system alloys as pre-alloyed powders. It is claimed that these pre-alloyed powders exhibit superior properties compared to pure cobalt, and perform equally or better than pure cobalt products in sawing and grinding applications [88-91]. The main reason for substituting cobalt is its high and fluctuating price and uncertainty about supply as well as the latest findings that cobalt might be poisonous [92].

4

Coated Diamonds

4.1 Introduction

One of the primary functions of the metal-matrix of diamond MMC's, as addressed in the previous chapter, is to retain the diamond crystals at the operating surface of the diamond tool the maximum possible time in order to utilise them efficiently. Diamond retention by the metal-matrix can be improved when the mechanical captivity of the abrasive grit by the binder is combined with a chemical strengthening of the diamond-matrix interface. Such a combined physical and chemical bonding, will allow the diamonds to be retained for longer periods at the abrading surface, thus increasing the total operational life of each individual crystal of the tool. This will in turn increase the overall life of the diamond tool, while decreasing the specific consumption of diamonds. Since diamonds are the most expensive constituents of the tool, the previous benefits can then be realised as considerable cost savings for the diamond tool.

Pure mechanically enveloped diamonds cannot be retained at the abrading surface when the gradual erosion of the surrounding matrix exposes them by more than about the 1/3 of their diameter. If diamonds are additionally chemically bonded to the metal-matrix, higher levels of diamond protrusion from this threshold value can be achieved [93-95]. This ability for higher grit protrusion may allow achievement of higher cutting rates, freer cutting with lower load

requirements, power savings and reduce heat generation due to the more efficient access of the coolant [96].

Chemical strengthening of the diamond-matrix interface can be realised either by a reaction to form new compounds or by atom diffusion and solid solution formation. These phenomena can occur individually or can take place simultaneously. In the case of a reaction between the diamond and the matrix, one or more new compounds are formed at the interface. For each new compound forming at the interfacial region, two new interfaces are developed (i.e. the diamond-reaction product and the reaction product-matrix) Strengthening is provided when these interfaces are strong and the reaction product is stiff and tough. In the case of dissolution, carbon atoms originating from the diamond dissolve into the surrounding metal, thus forming a transitional zone of solid solutions at the interface. However, dissolution of carbon substantially consumes diamond, which is not a desirable effect. In addition the increased diffusion of carbon originating from the diamond may result in high concentration of Kirkendall vacancies in the diamond's near surface zones [97]. This will either weaken the exterior zones of the crystals, which may influence their performance during cutting or favour the local graphitisation with the same undesirable effect. In some cases a very limited diffusion of metal atoms into the diamond may also take place.

Strengthening and enhancing diamond retention is far more effective for the case of an interfacial reaction. As addressed in the previous chapter, in practice the metal-matrix is chosen to be relatively inert with respect to diamond. A chemically active binder would encourage excessive reaction or carbon dissolution, which would both consume diamond and degrade its properties. Typically, the matrix is chemically activated by the addition of small quantities of metals having a high affinity for carbon and which react readily with the diamond and form metal carbides. Such metals are the transition metals, known also as "carbide formers". If the binder is relatively aggressive to the diamond, it can be neutralised by adding elements chemically inert to diamond such as tin.

Typically, the required amount of alloying metal for optimum result is rather small, which makes achievement of a uniform distribution in the base metal difficult under industrial conditions. In addition, alloying alters the bulk matrix properties, which in the general case may not be a desirable effect [45]. It is obvious, that the ideal situation would be if the alloying element could be concentrated only in the near vicinity of each individual impregnated diamond particle.

This last statement constitutes the concept of metal coating the diamonds. This technology concerns the coating of the abrasive particles with one or more metals, chemically active to the diamond. By this way, the alloying elements, otherwise dispersed in the whole matrix, are now concentrated exactly where they are needed, in other words at the diamond-matrix interface. This technique ensures a better control over both the matrix properties and the interfacial chemical phenomena. In literature, coating of diamonds with metals may also be referred as "metallizing" or "gladding".

Metal gladding was first introduced to diamonds utilised in resin bonded grinding diamond tools, in 1966 [98]. The purpose for metallizing diamonds was not particularly to promote any chemical bonding between the abrasive grains and the resin, but to protect the resin from thermal degradation. Metal coating could act as a heat sink, slowing the transfer of heat generated at the diamond cutting points to the resin bond, thus delaying the onset of charring and degradation of the resin. The life of the abrasive wheel was extended. Additionally, it became possible to employ resin bonds that did not wet diamond, since gladding could alter the wetting characteristics of the abrasive grains. The rough surface of the metal gladding produced diamonds particles with irregular shape, which enhanced the mechanical retention due to interlocking effects. Additionally, the metal jacket formed around the diamonds was capable of retaining the diamond fragments as a unit, while the friable grits, typically used in grinding, were splitting off. By this way loosening and early loss of the diamonds could be avoided [98, 99]. These coatings, which are still widely employed in grinding applications, commonly consist of nickel or copper. Copper is preferred for dry grinding while nickel is suitable for wet operation [4]. Typically, such coatings are applied by electroplating techniques. The deposited metal can be in amounts up to 60%wt. of the total coated grit weight.

Since the invention of coated diamonds for resin bonded grinding tools research on exploiting the potential properties of such crystals and tools has taken place. This can be seen from the patent literature of the early 70's [100-103]. Coatings containing metals reactive to diamonds, not particularly intended for use in metal binders, have been reported in the patent literature as early as in 1972 [104]. Patents dealing in specific with chemically active metal coatings on diamonds, especially designed for metal bonds, were disclosed during 70's [105-109]. However, application of metal coatings to the larger, tougher and well blocky shaped crystals utilised in metal bonded tools for sawing and drilling, has been realised as a promising technology only much later in the mid 80's beginning of 90's [94, 110-113].

Even though research in the private industrial sector has been carried out the last decade, little detailed published information is available. In addition, most of the aspects of the coated diamond technology are yet not clear or fully understood, mainly due to the complexity of the phenomena taking place at the various interfaces during the deposition and during the consolidation of the diamond composites. Consequently, although metal-coated diamonds for impregnated metal bonded tools are available in the market for some years, their application remains limited. In general, the performance of tools impregnated with coated diamonds has been improved, but the potential benefits from the use of metallized grit have not yet been universally accepted, mainly due to some cases where a reduced cutting speed has been found [111].

The present chapter comprise an effort of enlightening the various aspects of diamond coating technology. This is done by gathering the available published information on the characteristics and properties of coated crystals and the deposition techniques employed to coat the diamonds. Where possible, the available data on the kinetics of coating deposition or reactivity of the coating is given. At various points in the following sections, the basic concepts of interfacial strengthening in coated-diamond MMCs are discussed. The final parts of this chapter review the mechanical properties of coated diamonds as reported in literature with particular emphasis on the adhesion strength of the deposited metal films with the diamond surfaces. A detailed examination of the interfacial phenomena in diamond composites as well as the background of chemical reactivity of various metals with diamond is given in Chapter 6.

4.2 Characteristics and Properties of Coated Diamonds

The use of the metal coating on diamonds serves the need of strengthening the otherwise weak interface between the diamond and the metal-matrix. However, by coating the diamonds, a series of additional benefits may be obtained, which may further improve the quality and performance of the tools. The sections that follow review some of these properties.

4.2.1 Retention of Coated Diamonds

In comparative cutting tests where the only variable in the tools was the presence of the coating film on the diamonds, coated diamonds have been found to increase the overall life of diamond tools by factors of 1.5-2 [114] or even 2-3 [115, 116] compared to non-coated diamonds. Other comparative laboratory cutting tests have shown up to tenfold increases of the grinding ratio of

segments impregnated with metal-coated diamonds [95]. These results provided evidence of increased retention of the coated diamonds.

Manukyan *et al.* [114, 117, 121] in a number of studies have reported a decrease in the consumption of the order of 33-47% of titanium, chromium and iron coated diamonds compared to non-coated grit to process the same volume of stone. Brauninger *et al.* [594] in a microscopic evaluation of worn segments have found that the diamond pull-out rate of coated diamonds was reduced to 29% compared to the 39% of the non-coated. Subjecting the worn segment surfaces to laser profilometry, they found that although the height of diamond protrusion of whole crystals was similar for both segments with non-coated and coated grit, there was a dramatic increase in the number of fractured coated diamonds that were retained on the surface. Additionally, the pull-out craters in the case of segments with coated diamonds were in average considerably shallower, which indicated that the worn crystals were lost at a much later stage. In cutting and drilling various materials, the tools impregnated with Ti- or Cr-coated diamonds achieved increases in life between 16-138% compared to non-coated abrasives.

Vander Sande *et al.* [3] examined a large number of fractured surfaces developed on segments reinforced with diamonds having a dual metal coating, the inner being of a carbide forming metal (Ti, Zr, or Hf) and the outer of a selected metal or alloy to chemically match with the metal-matrix. A large increase in the number of fractured diamonds retained in the matrix was found to be associated with the segments containing the coated diamonds. In a similar test, McEachron *et al.* [113] showed that retention of coated crystals could reach levels of increase of up to 60% compared to non-coated diamonds. These diamonds had either a single coating of Cr, or Ti or could be additionally coated with an outer coating of Ni or Co.

Hsieh *et al.* [95] examined the worn surfaces of segments reinforced with Ti-coated grit in comparison with standard segments incorporating non-coated diamonds. The authors found that not only did the pull-out sites drastically reduce in number with the use of coated abrasives, but also the Ti-coated diamonds appeared to protrude with more than one-half of their height.

4.2.2 Graphitisation & Oxidation Resistance - Thermal Stability

As already brought up in Chapter 2, diamonds are susceptible to considerable graphitisation and oxidation at temperatures above 700°C. The metal coating has been found to provide protection to the diamond against graphitisation, oxidation and strength degradation at high temperatures even when diamonds are heated in air [114, 116, 136, 152, 155]. The resistance of coated

diamonds to these degradation processes was found further improved in vacuum and inert atmospheres. Figures 4-1 and 4-2 and Table 4-1 present the superior oxidation and graphitisation resistance of various coated grits compared to non-coated, as have been reported in literature.

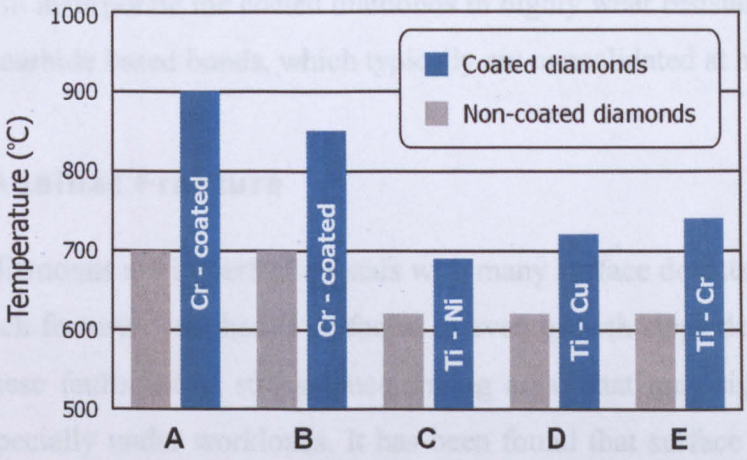

Figure 4-1 : The temperature of onset of oxidation in air for various coated diamonds. **(A)** Diamond: GE MBS* 970 40/45 US mesh [152], **(B)** Diamond: GE MBS* 50/60 US mesh, Coating: 1.8µm, 850°C for 2h Method: Immersion in molten salt bath [116], **(C),(D)** and **(E)** Diamond: unknown, Coating: <2.5µm Method: Thermodiffusion saturation process [114].

Coating	Temperature (°C)		Parameters	Reference
	Onset of oxidation	DTA maximum		
Uncoated	720	880	Diamond: AS15 (160/200 µm) Average thickness: 0.1 - 0.2 µm Method: CVD, 700-900°C	[136]
TiC	730	910		
NbC	790	970		
Mo_2C	660	900		
WC	780	910		
Cr_7C_3	710	910		
$(Mo, W)_2C$	800	920		
Non-coated	720	880	Diamond: AS15 (160/200 µm) Method: CVD, 800-1000°C	[155]
Mo-disilicide 0.05 µm	780	980		
Mo-disilicide 0.10 µm	760	920		
Mo-disilicide 0.15 µm	760	900		

Table 4-1 : Oxidation onset temperature for various coated and non-coated diamonds.

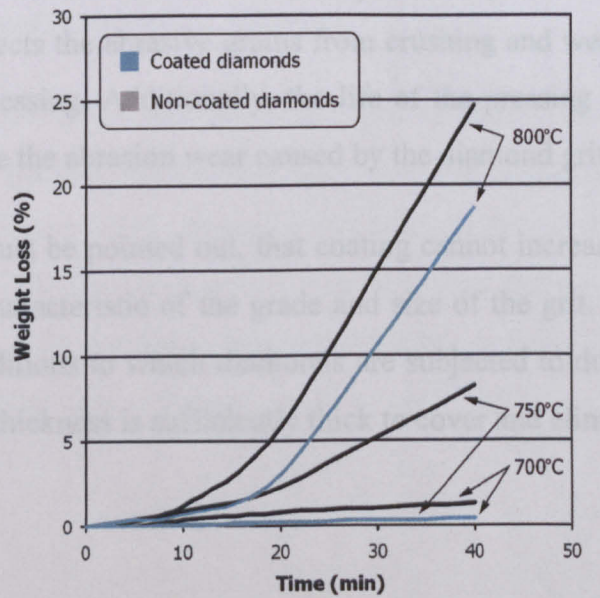

Figure 4-2 : Weight loss of non-coated and Cr-carbide coated diamonds when heated in air. The coatings were developed by immersion in molten salt baths [137].

The increased thermal stability of coated diamonds indicates that these crystals are less sensitive to high temperatures providing some potential benefits. For example, longer processing cycles and higher consolidation temperatures can be employed without risking diamond degradation. It is therefore possible to incorporate the coated diamonds in highly wear resistant matrices such as tungsten or tungsten carbide based bonds, which typically are consolidated at high temperatures.

4.2.3 Protection Against Fracture

Industrial synthetic diamonds are imperfect crystals with many surface defects. Such defects may be surface cracks, etch features, roughened surfaces, or even growth steps developed during the HTHP synthesis. These faults act as stress-concentrating areas that may significantly promote diamond fracture especially under workloads. It has been found that surface cracks may reduce diamonds strength by 34-49% while metallic inclusions by 13-43%, and in average defects can generally cause a 25-35% reduction in strength [114].

When depositing a metal coating on diamonds by diffusion controlled processes, the nucleation of the coating begins from the surface defective areas, which possess a higher energy. The growth of the coating gradually eliminates any surface irregularities caused by the defects. The further thickening of the coating is evenly developed for the total volume of the crystal. At the end of the process a metallic jacket forms enclosing the diamond. Thus, the initially rough and irregular crystal is transformed into a smooth and regular shaped crystal with flat planes. Hence, the coating can eliminate the stress raising defects induced by surface abnormalities. Manukyan *et al.* [114, 117] refers to this action of diffusional coatings as the "healing" of the diamonds. The strength of the metal jacket depends on the composition of the coating and the existence of any internal defects in the deposited layer. Another benefit is that the formed metal sleeve protects the abrasive grains from crushing and wearing during powder preparation, handling and processing. Additionally, the life of the pressing moulds and transporting media are prolonged since the abrasion wear caused by the diamond grit is minimised [114].

It must be pointed out, that coating cannot increase the inherent strength of the diamond, which is characteristic of the grade and size of the grit. Coating can only reduce the severity of stress conditions to which diamonds are subjected to during operation, and this is only the case when the thickness is sufficiently thick to cover and eliminate any surface irregularities.

4.2.4 Heat Conductivity

The thermal conductivity of diamond can be as high as five times than that of copper at room temperature. Metal and metal carbide coatings on diamonds may act as a barrier to slow down the heat transfer from the diamond cutting points to the bond. This is important in cases where the matrix is sensitive to high temperatures such as resin bonds or low melting point metal bonds.

4.2.5 Wetting

Metal or carbide coatings on diamonds may improve the wetting of diamonds by liquid metals. This is a very important parameter when production of the segments is done by melt infiltration [115, 118] or by sintering in the presence of a liquid phase or when diamonds are to be brazed as a single layer in diamond tools [119, 120]. The wetting of non-coated and coated diamonds by various metal and alloys is discussed in detail in the next chapter and a series of wetting data are given in Appendix B-1.

4.3 Coating Requirements

As discussed in the previous sections, the main purpose for coating diamonds is to improve the retention by chemically strengthening the diamond-matrix interface. It is obvious that the candidate elements for coating the diamonds are those metals exhibiting a substantial affinity for carbon. This affinity for carbon can be demonstrated either by a reaction to form stable carbides or by high levels of carbon atoms dissolution. As has been addressed in the introductory section of this chapter, excess carbon dissolution is not desirable since it is associated with consumption and weakening of the diamond.

It is for that reason that most of the research on coated-diamonds concerns metals that belong to the transition metals that are classified as reactive to carbon forming stable carbides. These metals are often referred to as "carbide formers". However, numerous researchers [114, 117, 121-125] have also studied the deposition and properties of metal-coated diamonds in which the metals do not form stable carbides but rather dissolve carbon, such as iron, nickel, cobalt and combinations of those.

Table 4-2 shows a section of the periodic table of elements listing the possible carbides that each element can form. The coloured gradient bars below Table 4-2 graphically illustrate the tendency of the listed elements to react with carbon or dissolve it.

III B	IV B	V B	VI B	VIII B			
Scandium	Titanium	Vanadium	Chromium	Manganese	Iron	Cobalt	Nickel
$Sc_{2-3}C$ ScC_2 Sc_2C_3	TiC	V_2C VC	$Cr_{23}C_6$ Cr_7C_3 Cr_3C_2	$Mn_{23}C_6$ Mn_3C Mn_5C_2 Mn_7C_3	Fe_3C	Co_3C Co_2C	Ni_3C
Yttrium	Zirconium	Niobium	Molybdenum	Technetium	Ruthenium	Rhodium	Palladium
Y_2C Y_2C_3 YC_2	ZrC	Nb_2C NbC	Mo_2C Mo_3C_2 MoC_{1-x}	TcC	Ru ×	Rh ×	Pd ×
Lanthanum	Hafnium	Tantalum	Tungsten	Rhenium	Osmium	Iridium	Platinum
LaC_2	HfC	Ta_2C TaC	W_2C W_3C_2 WC	ReC	OsC	Ir ×	Pt ×

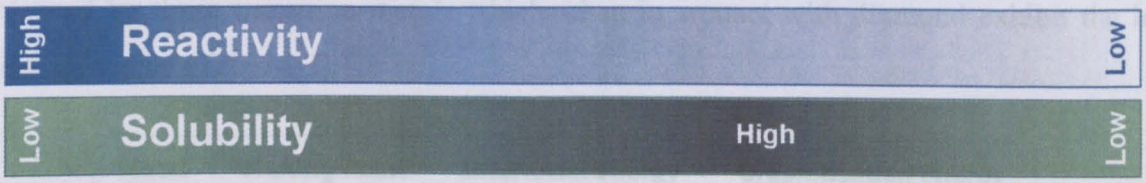

Table 4-2 : Section of the periodic table of elements, showing the carbide formation capability of transition metals. The (×) symbol indicates no carbide formation [126].

Carbon solubility tends to peak at the iron group metals [25]. The transition metals belonging to the VIII-B group primary dissolve carbon and typically form unstable carbides. The reactivity towards carbon with formation of stable carbides is increased as moving towards the III-B group elements. The reactivity and solubility tendency of the elements is associated with their electronic structure and is further discussed in Chapter 5.

As has been addressed in Chapter 2, at atmospheric conditions chemisorbed atoms such as hydrogen and oxygen cover diamond surfaces [127]. Therefore, adhesion of metals onto such surfaces involves weak van der Waals bonds [42, 128-130]. In order to achieve strong bonding to the diamonds, chemical and covalent interactions need to be established at the interface. Heating can prove efficient to remove the weakly bonded physisorbed atoms [27, 131], but the unsaturated carbon bonds rearrange into a reconstructed state, which is a relatively non-reactive surface condition. Thus, the ability of a metal to react with diamond depends firstly on whether the metal is able to remove the absorbed atoms and secondly on whether it is subsequently capable of disrupting the reconstructed carbon bonds [131]. The metals belonging to the VI-B

and V-B groups satisfy these requirements and have been reported to strongly adhere onto diamond surfaces [42, 127, 132, 133].

Manukyan *et al.* [114] state that the necessary condition for achievement of bonding between diamond and metal is the graphitisation of the diamond surface. Their proposed interaction mechanism involves an initial adsorption of the metal atoms, which will catalyse the formation of amorphous carbon at the interface. This amorphous carbon can then either react directly with the metal and form carbides or can be first crystallised into graphite and subsequently react with the metal. The composition of the interface will depend on the relative transition speeds of the above phenomena. Hence, if the transition speed of formation of graphite is faster than the speed of carbide formation, the interface will be composed primarily of graphite. The authors describe, similarly to the studies reviewed above, that the potential work of adhesion of a metal to diamond to depend on two parameters, the first being the van der Waals interaction energy and the second being the chemical interaction between the metal and diamond. The authors additionally suggest that since graphitisation is a necessary requirement, this process can be accelerated by those transition metals which when in contact with diamond exhibit the lowest interfacial energy (Table 4-3).

Metal	Melting Point (°C)	Interfacial Energy ($\times 10^7$ J·cm^{-2})	Graphitisation Energy (kcal·mol^{-1})
W	3442	5900	77.4
Mo	2623	6600	86.9
Ta	3020	6700	88.0
V	1910	7310	95.2
Cr	1857	7510	98.2
Ti	1662	7700	100.6
Fe	1536	7786	102.8
Mn	1246	8070	105.6
Co	1495	8155	106.6
Ni	1455	8377	109.4

Table 4-3 : Interfacial and graphitisation energy of various metals as suggested by Manukyan *et al.* [114].

Incorporating coated diamonds into diamond MMCs instead of non-coated crystals replaces the original diamond/metal-binder interface with two new interfaces, those of the diamond/coating and the coating/metal-binder. It is obvious that improved retention will be achieved only if both of these new interfaces are stronger than the original interface between the non-coated diamond and the metal-matrix.

Metal coatings deposited on diamonds typically will have a gradient composition. This is expected to arise from the fact that during deposition at high temperatures or during subsequent annealing or composite consolidation the metal atoms close to the diamond surface will react with it and simultaneously carbon atoms will dissolve at variable distances into the coating layer. Whichever the case and the relative intensities of these phenomena, the coating will have a different composition close to the diamond surface than at the exterior coating zones.

In order to achieve improved retention as described above, a strong adherence must be attained at the diamond/coating inner interface while the outer regions of the coating must have such a composition to allow adequate chemical interaction with the metal-matrix. It has been observed that in cases where coated diamonds have been deposited or annealed for extended times at high temperatures that the metal coating has substantially reacted with the carbon atoms originating from the diamond to form carbides [134, 135]. The coatings of such diamonds may lose the ability to subsequently bond to the metal-matrix [111].

For cases where more than one coating is applied onto diamonds, all the above requirements must be satisfied for each additional interface. Hence, the inner interface of each coating must adhere strongly to the underlying substrate while its outer zones must be chemically active with the material externally in contact.

Figure 4-3 illustrates the various interfaces present in diamond composites for the case of impregnation with single layer and multi-layer coated-diamonds.

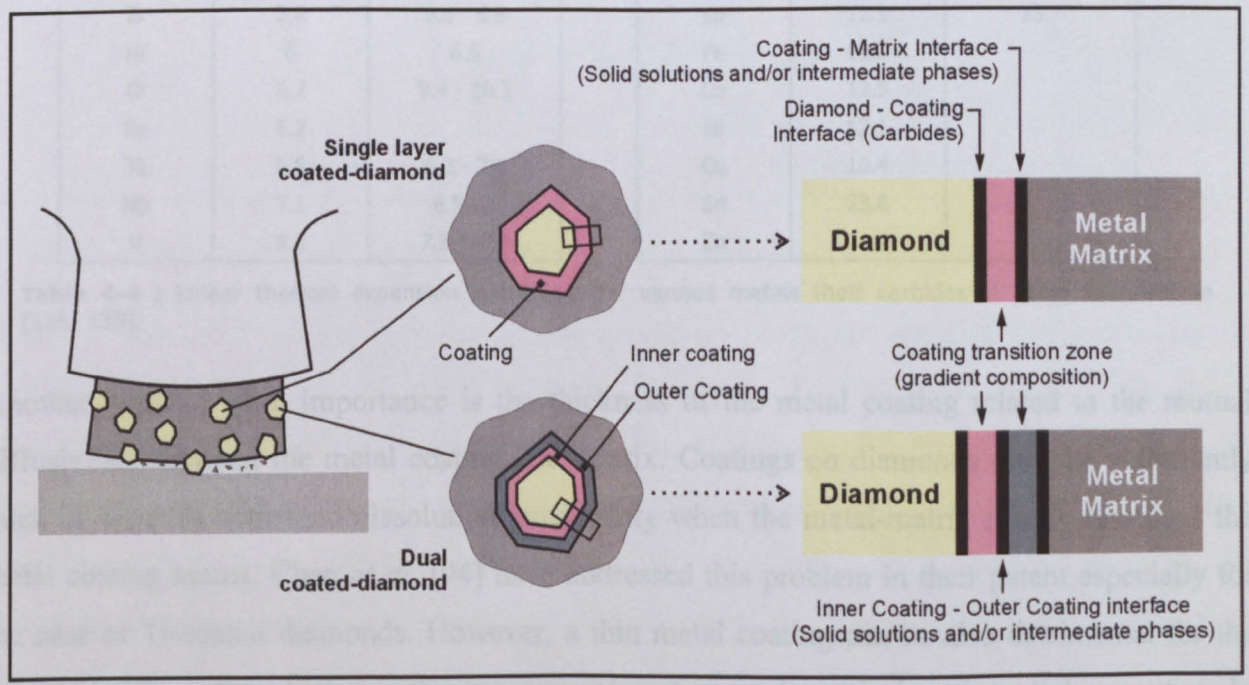

Figure 4-3 : The various interfaces developed in diamond composites when reinforced with single layer coated diamonds and dual layer coated diamonds.

In order to avoid diamond degradation during the high temperature consolidation, it is desirable that the formed metal coating provides a means of protection against oxidation. This ability of a coating depends not only on the inherent oxidation resistance of the deposited metal or compound, but also depends on the physical state of the coating. Thus, the integrity of the coating in terms of cracks, holes or porosity is important, since such defects provide paths for oxygen diffusion to the diamond surface [136, 137].

The quality of the coating relies greatly on the deposition technique and conditions. Whether the coating will retain its integrity after cooling down from the deposition temperature will additionally depend on the difference in thermal expansion between the diamond and the coating material. Diamond has a low thermal expansion coefficient (CTE). Large stresses may arise at the interfacial region from differential thermal contraction effects since coating typically will have a thermal expansion coefficient considerably higher than that of diamond. Such stresses may induce coating cracking or even partial peeling [120]. Table 4-4 lists the thermal expansion coefficients for diamond and various metal and their carbides. The refractory metals and their carbides exhibit closest CTE values to diamond. It is thus expected that their coatings will be associated with lower internal stresses after cooling down from deposition temperature [109].

	CTE ($\times 10^{-6}$ °C^{-1})	
	Metals	**Their Carbides**
Diamond	0.8	
W	4.4	4.2 - 5
Mo	4.9	4.9
Zr	5.8	6.6 - 6.8
Hf	6	6.6
Cr	6.2	9.4 - 10.3
Re	6.2	
Ta	6.5	6.3 - 7.4
Nb	7.1	6.5 - 7
V	8.3	7.2 ± 0.6

	CTE ($\times 10^{-6}$ °C^{-1})	
	Metals	**Their Carbides**
Ti	8.9	8.31 ± 0.68
Sc	10.2	11.4
Y	10.6	11.1
La	12.1	13.7
Fe	12.2	
Co	12.5	
Ni	13.1	
Cu	16.4	
Sn	23.8	
Zn	31.2	

Table 4-4 : Linear thermal expansion coefficient for various metals their carbides at room temperature [126, 138].

Another issue of great importance is the thickness of the metal coating related to the mutual diffusivities between the metal coating and matrix. Coatings on diamonds must be sufficiently thick in order to withstand dissolution particularly when the metal-matrix readily dissolves the metal coating atoms. Chen *et al.* [94] have addressed this problem in their patent especially for the case of Ti-coated diamonds. However, a thin metal coating can be also detrimental for the case when the metal coating is the one dissolving the metal-matrix in substantial quantities. In this case the metal atoms of the matrix can easily diffuse through the thin coating and access the

diamond/coating interface and disrupt the achieved bonding between the diamond and the metal-coating atoms [111]. In case the diffusing atoms belong to those metals exhibiting high solubility for carbon, catalysed graphitisation of diamond may additionally take place at the interface.

On the other hand thick coatings have an increased probability of containing internal defects and are typically more susceptible to cracking than thinner layers. For the extreme case of very thick coatings, alloying of the matrix may take place altering its bulk properties, which as has already been addressed may not be acceptable. However, relatively thick coatings can also exhibit an additional mechanical strengthening effect on the diamond retention aside to the chemical factor. This is particularly effective when the metal coating has a high strength, such as tungsten [109]. The thick coating can act as a stiff metal jacket that resists plastic deformation during the cyclic loading of the diamond in cutting operation. In addition, the coating can resist the erosive wear by the formed debris and provides protection to the face of the diamond crystal from the debris particle impingement [139]. Since the metal-matrix will gradually erode around the diamond, the thick coating will partially protrude from the surface of the metal-matrix and can thus be considered to partially participate in the cutting action. Simultaneously, this geometry with the coating protruding from the matrix will provide the necessary geometrical factors to prolong mechanical retention of the diamonds (Figure 4-4).

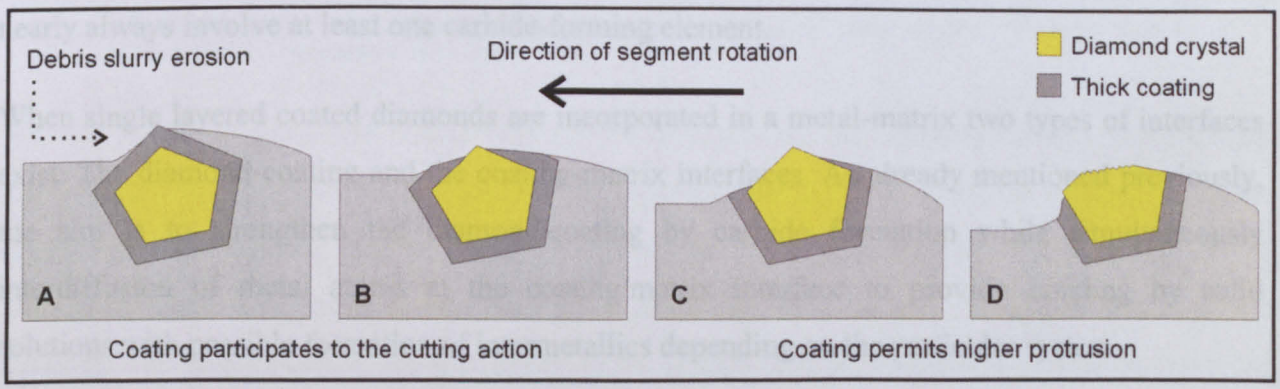

Figure 4-4 : Schematic representation of how thick coatings function during the cutting operation.

Provided that most of the requirements as presented above are satisfied and neglecting the additional costs involved, the metal to form the coating should be deposited at the lowest possible temperature and for the shortest possible duration in order to minimise the risk for diamond degradation. Qualitative coatings can be achieved when the deposition technique enables accelerated and effective mass transfer (i.e. metal transport to diamond surface). The deposited coatings can acquire an even thickness only if the process enables the access of the metal transport medium to all the diamond surfaces [114].

4.4 Types of Coated Diamonds

There are principally two approaches on how to fulfil the requirements needed to obtain a sufficient strengthening of both the diamond-coating and coating-matrix interfaces. According to these approaches coated diamonds can be classified into two types:

- coated diamonds having a single layer of one or more metallic components, or
- coated-diamonds with two or more metallic layers having distinct interfaces between them.

The first type is referred to as "single layer coated diamonds" and the second type as "multi-layer coated diamonds". The following paragraphs examine these two types in more detail.

4.4.1 Single Layer Coated Diamonds

These types of diamonds have a single layer of coating deposited on their surface. The layer may consist of: **(a)** one metal, **(b)** an alloy or **(c)** two or even three metals deposited simultaneously. Typically, strong carbide formers are used as single layer coated diamonds. When more than one metal are deposited at the same time, the coating that is produced has a complex chemistry, and such coatings are referred to as "multi-component" coatings. Alloy or multi-component systems nearly always involve at least one carbide-forming element.

When single layered coated diamonds are incorporated in a metal-matrix two types of interfaces exist. The diamond-coating and the coating-matrix interfaces. As already mentioned previously, the aim is to strengthen the diamond/coating by carbide formation while simultaneously interdiffusion of metal atoms at the coating/matrix interface to provide bonding by solid solutions with possible formation of intermetallics depending on the particular system.

Reaction at the diamond/coating interface may start during deposition, but often this is not the case. In the majority of cases a subsequent heat treatment of the coated grit is necessary to induce interfacial reactivity. In practice such a step may be avoided and interfacial reactivity may be allowed to occur during segment consolidation.

The coating of a single layer coated-diamond impregnated in the metal-matrix will have a variable composition attributed to the various degrees of atom diffusions. Some carbon atoms will react at the interfacial region forming carbides while others will diffuse through these reaction products and form C-solid solutions, with carbon atom concentration decreasing as moving away from the diamond surface.

At the outer zone of the coating mutual diffusion of coating and matrix metal atoms will occur. Depending on the relative diffusivities of each metal into the other, either the coating will dissolve faster into the metal-matrix or the metal-matrix atoms will diffuse into the coating and form solid solutions. In the first case the coating/matrix interface will move towards the diamond whereas in the second case will move away from it. It is desirable not to have too high mutual diffusivities in order to avoid the effects described in the previous section and to avoid the formation of voids either in the matrix or the coating due to the Kirkendall-Frenkel effect. The above described diffusion phenomena are schematically illustrated in Figure 4-5.

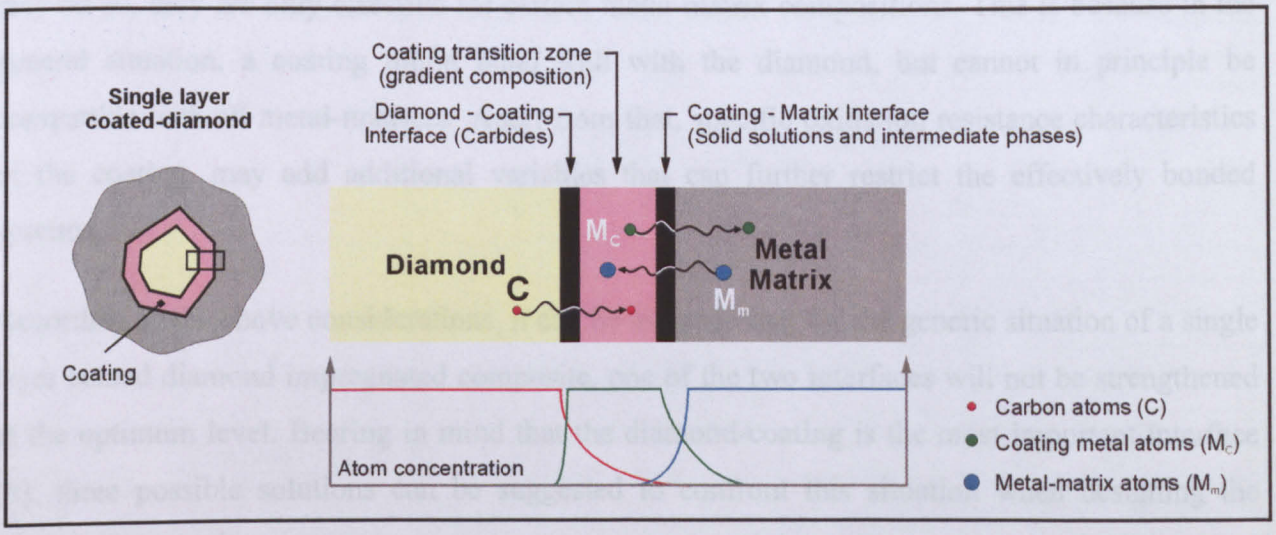

Figure 4-5 : Schematically illustrated diffusion phenomena taking place at the interfacial regions of diamond composites impregnated with single layer coated diamonds.

For a given metal coating to bond to the metal-matrix will not only depend on the relative mutual solubility as described above, but also on the degree of metal character of the coating. If excess carbide formation of the coating has occurred then less coating metal will be available to diffuse and at the same time carbides will reduce the ability of metal-matrix atoms to diffuse into the coating. The degree of carbide formation of the coating can be controlled by manipulating the deposition parameters, the segment consolidation conditions or by introducing a heat treatment of the coated grit subsequent to the deposition. Achieving the optimum degree of carbide formation is a difficult task and deviations from this condition may alter significantly the bonding ability of the coated particles. When carbide formation of the coating is insufficient the diamond-coating interface will be weak. On the other hand when the interactions are excessive, the coating will have insufficient amount of free metal atoms to allocate for bonding with the matrix. There is a minor possibility for carbon-based bonding at the coating-matrix interface if conditions are such to permit substantial diffusion of carbon atoms to take place. However, even if it is assumed that bonding at the outer interface may also be attributed to carbon activity, the

properties of such coated diamonds most probably will be deteriorated for the following two reasons:

- increased carbide content in the coating will increase the possibility of flaws and defects within the coating, and
- the excessive carbon diffusion, apart from consuming substantial diamond, it will cause the weakening of the abrasive crystal at the regions near the diamond-coating interface due to formation of vacancies (Kirkendall-Frenkel effect) [3, 97, 115, 140].

Single layer coated diamonds rarely satisfy all the set requirements at the optimum level and if they do so, they are only effective for certain metal-matrix compositions. This is because in the general situation, a coating might bond well with the diamond, but cannot in principle be compatible with all metal-matrices. Apart from that, specific oxidation resistance characteristics of the coating, may add additional variables that can further restrict the effectively bonded systems.

According to the above considerations, it can be assumed that for the generic situation of a single layer coated diamond impregnated composite, one of the two interfaces will not be strengthened at the optimum level. Bearing in mind that the diamond-coating is the most important interface [3], three possible solutions can be suggested to confront this situation when designing the diamond composite:

(I) select a coated diamond which adheres strongly to the diamond and optimise the poorly bonded coating-matrix interface by appropriately alloying the matrix, or

(II) compromise with a coated diamond which gives intermediate strength interfaces with both the diamond and the matrix, or finally

(III) select a multi-coated grit instead of a single layer coated diamond.

The first solution brings back the issues of alteration of the matrix properties something, which might not be acceptable. The multi-coated diamonds are examined in the following section.

Table 4-5 gives a comprehensive list of metals and alloy systems deposited as single layers on diamonds, as has been reported. Most employed metals are titanium (Ti) and chromium (Cr). Both exhibit a high activity to diamond and their carbides possess a high level of physical and mechanical properties. Their deposition is more economical and requires less complicated technologies and equipment compared to the refractory transition metals, such as W, Mo, Ta and V. However, their thermal expansion mismatch to diamond is larger than that of the refractory metals (see on page 41).

	Coating	Diamond		Metal-matrix / Notes - Characteristics	Reference
		Type	Size		
Single Metal Coating	Cr	MBS-960	25/80	Suitable for : Co, low Fe, Bronze and WC bonds	[114]
		AC15	16-200	80% Cu - 20% Sn	[114]
		AS40	250-315	80% Cu - 20% Sn	[117, 141]
		ASO	80-100	-	[127]
		AS15	-	-	[142]
		-	215-250	Ni - based matrix	[120]
		(APR)	50-63	-	[143]
		-	-	Cu , Al, Cu-Ni-Mn alloy	[115]
		-	-	-	[97, 110, 135, 137, 140, 144, 145]
	Co	-	-	-	[146]
	Fe	AC15	16-200	80% Cu - 20% Sn	[114]
		AS40	250-315	80% Cu - 20% Sn	[117]
		AS15	-	-	[121, 146]
	Mn	-	-	-	[110]
	Mo	AS6	80-100	-	[147-149]
		ASK-AS32	100-500	-	[150]
		-	60/170	Fe/Ni (12/5), Ni/Co/Cr/Fe (34/18/14/5), Fe/Si (63/2), Ti/Ni (37/6),Ti/Si (34/3), WC-10%Co	[105]
		-	-	Cu , Al, Cu-Ni-Mn alloy	[115]
		-	-	-	[97, 135, 140, 145]
	Nb	-	-	-	[115]
	Ni	-	-	-	[146, 151]
	Ta	-	-	-	[115]
	Ti	MBS-960	25/80	Suitable for : Co-bronze and Fe-based bonds	[152]
		AC15	16-200	80% Cu - 20% Sn	[114]
		AS40	250-315	80% Cu - 20% Sn	[117, 141]
		AS15-AS40	250-315	-	[142]
		(APR)	50-63	-	[143]
		-	60/170	Fe/Ni (12/5), Ni/Co/Cr/Fe (34/18/14/5), Fe/Si (63/2), Ti/Ni (37/6),Ti/Si (34/3), WC-10%Co	[105]
		MBS960	30/40/50	Fe, Fe + 11.3% Ni	[95]
		-	-	-	[97, 110, 135, 140, 145]
	V	-	-	Cu , Al, Cu-Ni-Mn alloy	[115]
		AS6	80-100	-	[135]
		-	-	-	[145, 153]
	W	EMBS SDA100	30/40	80% Bronze - 20% Cemented WC filler by HP-ing Coating thickness : 7.75 - 10 microns	[94]
		-	-	-	[97, 115, 135, 140, 145]
Multi-component Coating	Cr-Cu	-	-	-	[154]
	Cr-Ni	AS6	160-200	-	[144]
	Co - Ni	ASR-ASK	100-200	80%Cu-20%Sn	[123]
		-	-	Coating : 55-60% Co - 40-45% Ni	[151]
	Cu-Ga-Cr	-	-	Coating : Cu - 17.5% Ga	[97, 140]
	Cu-Ga-Ti	-	-	Coating : Cu - 17.5% Ga	[97, 140]
	Mo disilicide	AS15	125-160	-	[155]
	Mo-Ni	AS6	63-80	-	[156]
		-	-	-	[157, 158]
	Ni-Mn-Sn-Ti	ASV	50-63	Coating : 40%Ni-60%Mn , (40%Ni-60%Mn)+20%Sn , (40%Ni-60%Mn)+10%Ti , (40%Ni-60%Mn)+20%Sn 10%Ti	[159]
	Ti-Al	AC15	16-200	Reason for Al in coating : Al good compatibility with Ti	[114]
	Ti-Cr	AC15	16-200	Coating : 0-20% Cr	[114]
	Ti-Cr-Al	AC15	16-200	Coating : 16% Al - 20% Cr	[114]
	Ti-Cu	AC15 AS40	16-200 250-315	Cu-based bonds, 80%Cu-20%Sn Optimum results for coatings : 0-10% Cu	[114]
	Ti-Cu-Al	AC15	16-200	Cu-based bonds, Al good compatibility with Ti Optimum results : 3.6% Al - 4.5% Al	[114]
	Glass	-	-	Coatings contain oxides of : Si, Al, Ca, Mg, Li, Na, B & Fe	[125]

Table 4-5 : Listing of metals and alloys used as single layer coated diamonds as reported in literature.

4.4.2 Multiple Layered Metal Coated Diamonds

Multi-layer metal-coated diamonds have been developed in order to overcome the situation where a single layer metal coating cannot offer the optimum level of bonding to both the diamond and the matrix. The concept is to gradually modify the chemistry of the coating by layering a number of distinct metallic coatings on the diamond surface. The innermost layer of such coatings is selected to be compatible to the diamond while the outermost layer is suitably chosen to offer compatibility with the selected metal-matrix. Depending on whether these two coating materials are compatible with each other an additional number of intermediate layers may be included in order to achieve bonding between the layers. The number of intermediate metallic layers determines also the number of interfaces that are developed (Figure 4-6). The necessary condition for enhanced retention is that each of these interfaces has to be stronger than the original interface formed in the non-coated diamond-matrix system. The overall properties of a multi-layer coated- diamonds can be further engineered by incorporating layers with specific characteristics. For example, an oxidation resistant layer can be deposited in order to offer increased oxidation protection of inner layers and diamond [93, 94, 104, 111, 112]. Furthermore, a thick layer of a ductile metal can contribute effectively to raising the overall toughness of the coated diamond and enable the coating to absorb more efficiently induced stress such as those arising from differential thermal contractions [112].

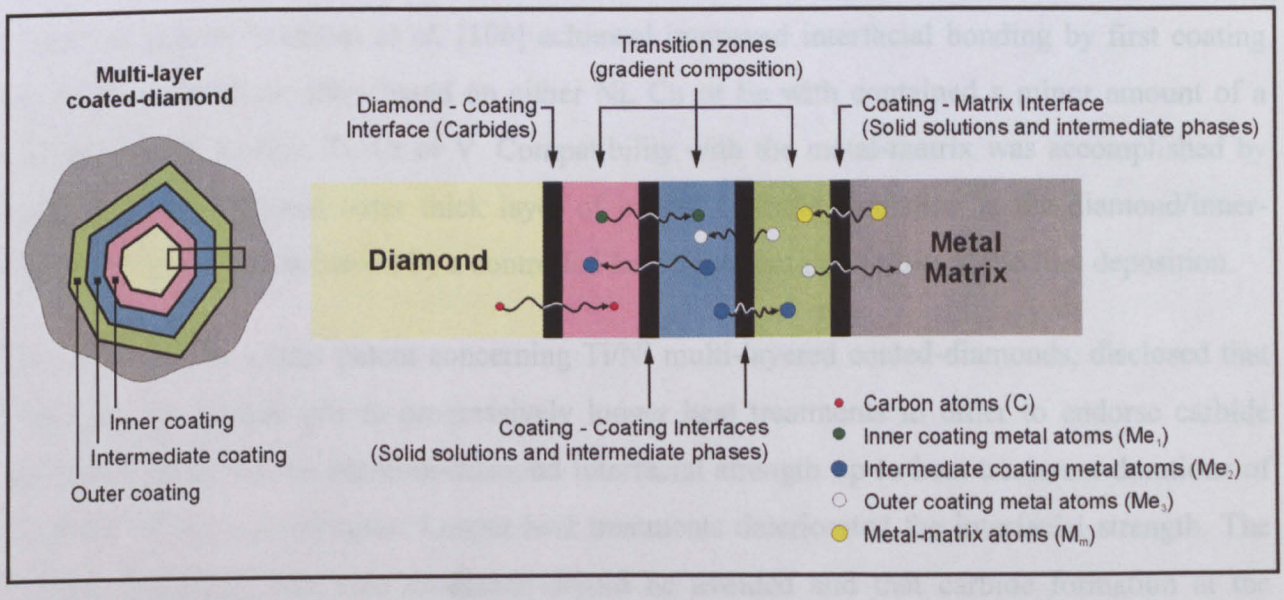

Figure 4-6 : Schematically illustrated diffusion phenomena taking place at the interfacial regions of diamond composites impregnated with multi-layered coated diamonds.

The advantages of multi-layer coatings are obvious. The ability of manipulating the properties of the coated grit provides a great degree of flexibility. Thus, when a certain coating has been found to adhere strongly to the diamond possible lack of compatibility with a particular metal-matrix

can be avoided by depositing suitable number of additional metallic layers until achievement of the optimum chemical composition to allow strong bonding to the metal-matrix. It can be said, that multi-layer coated diamond consists the concept of *"multi-purpose coated-diamonds"*. However, the various heating-cycles associated with each coating deposition typically involve high temperatures that are well within the range of diamond graphitisation and oxidation. Hence, although interfacial bonding may be improved, the inherent strength of the enclosed diamond may degrade in such an extent, that during operation the benefits from improved retention to be overbalanced by the decreased toughness of the crystal. For this reason, multi-layer coating of diamonds makes sense only for premium grade diamonds of high thermal stability and strength. In addition, multi-layering is an overall more complex process, which is accompanied by increased material, equipment and operational costs.

From the early years of the research on metal-coated diamonds intended for impregnation of diamond MMCs, Farkas [104] conceived the idea of multi-layering the diamonds for improved retention and oxidation resistance. With his patent disclosed a method by which initially a thin layer of titanium or zirconium was deposited onto the diamond in order to achieve a high cohesion bonding attributed to the formation of carbides. Subsequently, a second layer of an oxidation resistant metal, such as nickel or copper, was deposited in order to offer protection against oxidation to the inner titanium or zirconium coating.

In another patent, Nicholas *et al.* [106] achieved improved interfacial bonding by first coating the diamonds with an alloy based on either Ni, Cu or Fe with contained a minor amount of a carbide former, such as Ti, Cr or V. Compatibility with the metal-matrix was accomplished by depositing an additional outer thick layer of nickel. Carbide formation at the diamond/inner-coating interface was achieved by a controlled heat treatment that followed the first deposition.

Caveney [107] in a later patent concerning Ti/Ni multi-layered coated-diamonds, disclosed that subjecting the coated grit to progressively longer heat treatments in order to endorse carbide formation improved the titanium-diamond interfacial strength up to heat treatment durations of the order of 10 to 15 minutes. Longer heat treatments deteriorated the interfacial strength. The inventor suggested that heat treatment should be avoided and that carbide formation at the diamond-coating interface should be designed to occur during the segment consolidation.

Nicholas *et al.* [146] in a later patent, postulated that carbide formation at the diamond-coating interface is not a necessary condition and claimed that strong bonding could be achieved with metals capable of dissolving carbon without needing to form stable carbides. Such diamonds had

two Ni coatings the inner being deposited at a high temperature and the outer formed by electroless plating. Diamond tools utilising such coated diamond showed considerable reduction in wear compared to conventional tools impregnated with non-coated grit.

In another patent [160], a technique for producing diamond granules invented by Kimura [161] was employed to coat diamonds with an inner layer of a carbide former and an outer layer of second carbide former or another metal. The prerequisite condition for this invention was that the metal selected to form the outer layer should sinter at a temperature at least 50°C below the melting point of the inner metal coating. After depositing both coatings, the diamond pellets were heated at a sufficiently high temperature in order to cause the melting of the inner layer while the sintered outer layer sealed the liquid metal from escaping. Enhanced carbide formation at the diamond surface was accomplished due to liquid state of the carbide former.

Vander Sande *et al.* [3] reported dual coatings to have increased retention in Fe-, Ni-, Co-based matrices compared to single layered coated diamonds and to standard non-coated grit. The dual coatings comprised of an inner layer of a strong carbide former and the outer layer of a metal or alloy capable of forming extensive solid solutions and intermetallics to the selected metal-matrix. Lin *et al.* [162] studying the fracture behaviour of diamond composites, found that dual coated diamonds increased the toughness of the diamond composite compared to non-coated grit. Their diamonds consisted of an inner layer of a Ti-4%V-6%Al alloy and of an outer alloy of Cu-10%Ni capable of bonding to the Cu-40%Ni metal-matrix.

In a number of patents assigned in the last decade [93, 111-113], triple or even fivefold coatings on diamonds have been disclosed. McEachron [113] claimed improved retention achieved by triple coated diamonds having an inner layer of a carbide former and two outer layers of non-carbide forming metals. Combinations of Cr-Co and Cr-Ni gave the best retention and wear results. In another patent, Chen [111] disclosed triple coated diamonds of improved retention and oxidation resistance capability. Oxidation resistance of the coated grit was achieved by an intermediate layer of oxidation resistant carbide former. Horton *et al.* [112] engineered the mechanical properties of a multi-layered coated diamond by suitably selecting the coating metals in order to achieve a tough and stress absorbing coating capable of withstanding thermally induced cracking during cooling down. The inventors accomplished such coated grit, by layering a thin inner and outer coating of a carbide former with a low CTE, such as tungsten. A thick intermediate layer of a metal such as copper was included to enhance stress absorbance.

Table 4-6 lists the main characteristics of the multi-coated diamonds described above.

Ref.	Layer	Coating	Deposition Method / Temp. (°C) / Atm. / Time (h)	Heat Treatment T (°C) / t (min)	Thickness (%wt. or μm)		Option	Purpose - Requirements	Matrix Composition Method/°C/MPa/min
[104]	1st	Ti, Zr	MVD/850-900 (350-1000)/10^{-4} mmHg/0-0.25	-	5% vol. of UD		N	Carbide formation, bond to D	-
	2nd	Ni, Cu	Not Available	-			N	Oxidation resistance, Bond to 1st & MM	
[106]	1st	Alloys of: Ni, Cu, Fe with 0-30%wt. Ti, Cr, V	VE (SP)/ 500-(MP-50)/ He-Ar-H_2-N_2, 10^{-2}mmHg	-	1-2%		N	Carbide formation, bonding to diamond	-
	2nd	Ni, or Ni compatible metals	EP, ELP	-	20-55%		N	Bond to 1st & MM	
[107]	1st	Ti	VE	500°C / 10-30 min	<3%		N	Very little carbide formation, bond to D	Bronze (80/20) at 720 (700-850)°C or Co at T<1400°C
	2nd	Ni, (Fe, Co, Cu)	EP, ELP, (VE)/ 80-90/-/3-5%wt. per h	-	10-100%		N	Bond to 1st & MM	
[146]	1st	Ni, (Co, Fe)	VE/800/ He, Ar, H_2, N_2, >10^{-2} mmHg/2	-	1-2%		N	C-dissolution but no stable carbides	-
	2nd	Ni	ELP	-	20%		N		
[160]	1st	Ni, Co, Fe, Si or metals from IVB, VB, VIB groups	Diamond Granulation according to [161]	-	>20%		N	Carbide formation & be liquid at T	-
	2nd		Diamond Granulation according to [161]	-	>20%		N	Sinter 50°C below MP of 1st metal	
[3]	1st	Ti, Zr, Hf	Tumble plating	-	Not Available		N	Carbide formation, bond to D	Fe-/Ni-/Co- + WC HP/900-1100/5-60min
	2nd	Al, Si, Ni, Al-Cu-Mg, Al-Ni, Cr, Ni-Cr, Cr-Co, Al-Cu & Ni-Ti	Tumble plating	-	Not Available		N	Bond to 1st & MM	
[162]	1st	Ti-4%V-6%Al	VE/1100/vacuum/0.25	-	0.1-0.2		N	Carbide formation, bond to D	60%Cu-40%Ni HP/1140/13/15
	2nd	Cu-10%Ni		-	10-12		N	Bonding to 1st & MM	
[94]	1st	W, (Ta, Mo, Nb or alloys thereof)	CVD/700/12 Torr/1.25	Etching prior to CVD and/or HT	1-50	1-30	N	Carbide & oxidation resistant, bond to MM	80%Bronze-20%WC HP/815/24/-
	2nd	Cu, Ni, Ni-B	ELP/Ni-B solution(Niklad 752, pH6)/80/-		approx. 30		O	Bonding to 1st & MM	
[111]	1st	Cr, (Ti, Zr)	MVD (CVD)/720-920/>10^{-6} Torr, (Ar, H_2)/0.25-6	670°C / 60 min (Outgassing step prior to deposition)	0.05-5	0.05-0.30	N	Strong carbide formation, bond to D	Ni, (Co, Cu, Sn or their alloys) 70%(85Cu15Sn)/ 30Co, HP/790/35/3
	2nd	W, Ta, (Mo)	CVD/700/7 Torr/0.25-1.5		5-30	≤ 15	N	Carbide & oxidation resistant, bond to MM	
	3rd	Ni, (Co, Fe or alloys)	EP, ELP		0.5-100	≤ 20	O	Oxidation resistant, bond to 2nd & MM	
[112]	1st	W, Ti, Cr, (Ta, Mo)	CVD (MVD)/700/ He, Ar, H_2, WF_6/1	-	>3	10-20	N	Carbide formation, bond to D, low CTE	WC, Fe, Co, infiltrated by Cu-based alloys such as 55Cu-20Mn-25Sn
	2nd	Ni, (Pd, Pt, Co, Re, Fe)	EP/ Woods Ni Strike Solution/10min	-	1-3	2	O	Bond to 1st & 3rd layer	
	3rd	Cu (Ni, Ag or alloys)	EP/ Cu sulfate & sulfuric acid/2.5	-	20-50	30	N	Ductility to facilitate stress absorbing	
	4th	Ni, (Pd, Pt, Co, Re, Fe)	EP/ Woods Ni Strike Solution/10min	-	1-3	2	O	Bond to 3rd & outer layer	
	5th	W (Mo, Ta, Re)	CVD (MVD)/700	-	10-20	11	N	Oxidation resistant, bond to MM	
[93]	1st	Cr	MVD (IMSB)/600-700/10^{-6} Torr	-	0.05-5	0.05-0.3	N	Carbide formation, bond to D	Bronze or bronze alloys or Co-, Ni-based infiltrated by Cu-Zn-Ni
	2nd	TiN	MVD (CVD, PVD)/900/10^{-6} Torr/6	1000°C, N_2, 2h	0.1-10		N	Bond 1+3, protect 1st from CVD gas	
	3rd	W, Mo	CVD (PVD)/700/7 Torr/0.25-1.5	-	5-50	30	N	Bond to MM	
[113]	1st	Cr (other carbide former)	IMSB (CVD)/600-100/-/2	-	0.1-10	2-5	N	Carbide formation, bond to D	Ni-, Co-based or Co-bronze
	2nd	Ni, Co, (Fe or alloys)	ELP/ Hypophosphile solution	-	10-50 (25-35)%		N	Non-carbide former, bond 1st & MM	
	3rd	Co, Fe	EP	-	Not Available		O	Non-carbide former, bond 2nd & MM	

Table 4-6 : Details for various multi-layered coated diamonds for use in diamond MMCs as reported in literature. **NOMENCLATURE: Brackets ( )** denote alternative solutions or optional actions, **N** (Necessary), **O** (Optional), **UD** (Non-coated diamond), **D** (Diamond), **MM** (Metal-matrix), **HP** (Hot-Pressing), **CTE** (Coeff. of Thermal Expansion), **MP** (melting Point). **DEPOSITION METHODS: CVD** (Chemical Vapour Deposition), **PVD** (Physical Vapour Deposition), **MVD** (Metal Vapour Deposition), **ME** (Vacuum Evaporation), **IMSB** (Immersion in Molten Salt Baths),**EP** (Electrolytic plating), **ELP** (Electroless Plating). For details on deposition techniques please refer to the following section.

4.5 Deposition Techniques

Various techniques have been employed to deposit the metal films on diamonds. These include mainly vapour phase depositions but also immersions in molten baths. Vapour phase depositions include methods such as chemical vapour deposition (CVD), physical vacuum deposition/evaporation (VD or VE), reactive deposition/evaporation (RD or RE) and sputtering (SP). Immersion techniques include formation of metal coatings from molten salt baths (IMBS) or by electroplating.

Other techniques occasionally found in literature mainly involve methods of adhering fine metal powders on the surfaces of the diamonds to form granules. Although such metal-powder encapsulated diamonds may not be directly regarded as coated abrasives, their intended function is to concentrate a selected metal at the diamond interface. Since this is basically the same principle as that of coated diamonds, the techniques used to formulate such granules are treated here as "coating" methods.

Electrolytic and electroless plating are well-established techniques. Their employment in diamond coating [163] is made according to the known art and therefore they are not reviewed here.

The selection of the most appropriate deposition technique depends on the metal to be layered. For a given metal, apart from material, equipment and operational costs, the most suitable method is the one performed at the lowest possible temperature giving sufficiently fast deposition rates so that the desired thickness to be achieved at relatively short times. This is a necessary condition in order to minimise exposure of diamonds to high temperatures or aggressive environments. Other considerations concern the quality of the deposited metallic layer in terms of purity and internal structure of the resultant layer. Reactions taking place at the interface during deposition are considered beneficial if such to aid the adhesion of the coating. If the chemical bonding at the interface is not achieved during deposition, a post heat treatment of the coated diamonds may be required, or alternatively, necessary modifications to the segment consolidation cycle must be made to allow reactions at the diamond/coating interface [3, 94, 106]. Finally, the selected process and deposition equipment must ensure that all diamond crystals surfaces can be accessed at the same degree by the metal being deposited in order to produce continuous and even coatings.

The various deposition methods discussed above are reviewed in the following sections.

4.5.1 Chemical Vapour Deposition (CVD)

The CVD process can be defined as the deposition of a solid on a heated surface, via a chemical reaction from the vapour or gas phase [164]. It belongs to the vapour-transport processes that are atomistic in nature, which means that the deposition species are atoms, molecules or combination thereof [164]. One or more volatile inorganic, metal-organic, or organometallic precursors are transported in the vapour phase, often in a carrier gas, to the reactor chamber. They are then adsorbed on a heated substrate where they react with it or decompose and subsequently deposit as a solid film while the volatile reaction products are transported away from the reactor (Figure 4-7). Often, the carrier gases are inert, such as Ar or N_2 or reducing such as H_2 or are a mixture of those. The numerous reactions used in CVD include thermal decomposition (pyrolysis), reduction, hydrolysis, disproportionation, oxidation, carburization and nitridation. Various types of CVD technologies exist differing mainly on the energy source for the activating the chemical reaction. A large number of metals, carbides, nitrides, borides and oxides can be layered with CVD.

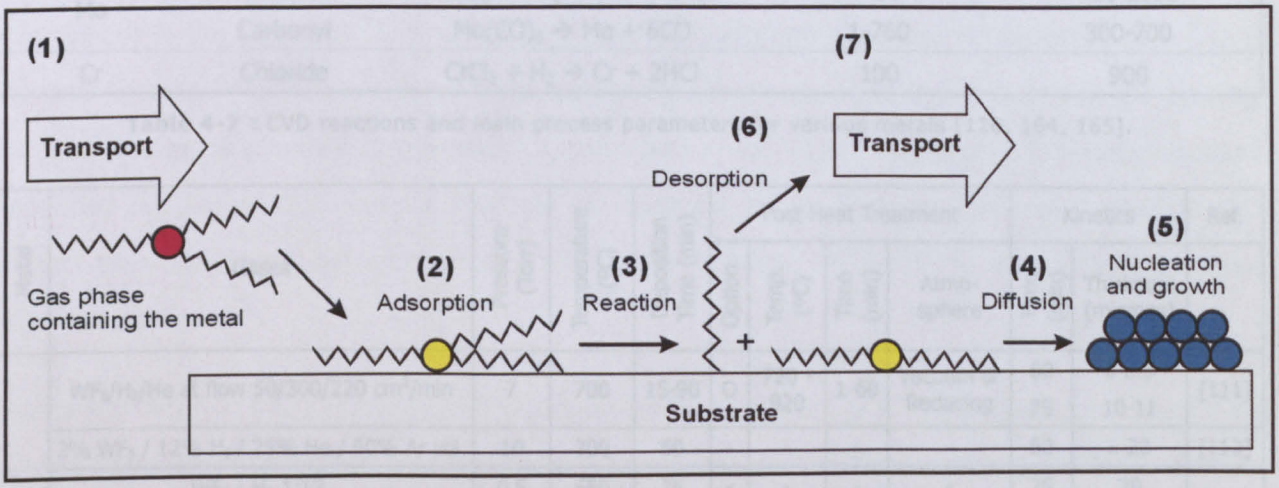

Figure 4-7 : Illustration showing the fundamental steps involved in the CVD [165].

The main advantages of the CVD are the ability to deposit in holes and recessed areas and the deposition of refractory metals at relatively low temperatures and at high rates compared to the other techniques. Main disadvantages are the increased cost and the necessity to operate in a closed system due to the corrosive and toxic reactants.

When metallizing diamond, CVD is the preferred method for the deposition of refractory metals such as tungsten (W), molybdenum (Mo), tantalum (Ta), zirconium (Zr) etc. Titanium and chromium are occasionally reported to be chemical vapour deposited [111, 120]. Tungsten is the metal most commonly deposited by CVD onto industrial diamonds. The deposition of tungsten is

achieved by decomposition of tungsten carbonyl ($W(CO)_6$) at 300-600°C or by hydrogen reduction of either tungsten hexachloride (WCl_6) or tungsten hexafluoride (WF_6) at 700-900°C.

The decomposition of the carbonyl results in coatings with minimal internal stresses from differential thermal contraction effects due to the lower temperatures involved. From the deposition methods involving reductions, the reduction of the halide (WF_6) is the preferred reaction since the hexafluoride is an easily vaporised liquid. However, implications result from the involved atmosphere, which is aggressive and toxic.

Some details for the CVD deposition of tungsten and other metals are listed in Table 4-7. Table 4-8 lists the process parameters for the CVD metallization of industrial diamonds as have been reported in literature.

Metal	Precursor	Reaction	Pressure (Torr)	Temperature (°C)
W	Halide	$WF_6 + 3H_2 \rightarrow W + 6HF$	10-760	300-700
	Chloride	$WCl_6 + 3H_2 \rightarrow W + 6HCl$	15-20	900-1300
Mo	Chloride	$MoCl_6 + 3H_2 \rightarrow Mo + 6HCl$	<20	400-1350
	Carbonyl	$Mo(CO)_6 \rightarrow Mo + 6CO$	1-760	300-700
Cr	Chloride	$CrCl_2 + H_2 \rightarrow Cr + 2HCl$	100	900

Table 4-7 : CVD reactions and main process parameters for various metals [120, 164, 165].

Metal	Gases	Pressure (Torr)	Temperature (°C)	Deposition Time (min)	Post Heat Treatment				Kinetics		Ref.
					Option	Temp. (°C)	Time (min)	Atmo-sphere	Time (min)	Thickness (microns)	
W	$WF_6/H_2/He$ at flow 50/300/220 cm^3/min	7	700	15-90	O	720 - 920	1-60	Vacuum or Reducing	60 75	6-8.5 10-11	[111]
	2% WF_6 / 12% H_2 / 25% He / 60% Ar vol.	10	700	60	-	-	-	-	60	≈ 20	[112]
	WF_6 : H_2 1:12,	0.5	650	75	-	-	-	-	75	20	[166]
	Flow rates: WF_6=32 and H_2=380 sccm	0.5	550	60	N	950	60	Reducing	60	16	
	Gases and flow rates as above. After CVD at T1 for t1 heat treated and then CVD at T2 for t2	0.5	T1:450 T2:650	t1:60 t2:60	N	990	30	Reducing		15	
Cr	$Cr + 2HCl \rightarrow CrCl_2 + H_2$ $CrCl_2 + H_2 \rightarrow Cr + 2HCl$ HCl 0.2 lt/min, Ar 5 lt/min, H_2 1lt/min Cr in form of granules	50	900 to 1000	15-60	O	720-920	1-60	Vacuum or Reducing	60 75	6-8.5 10-11	[111]
	$Cr + TiCl_4 \rightarrow CrCl_2 + TiCl_2$ $CrCl_2 + H_2 \rightarrow Cr + 2HCl$ Ar 2.5 lt/min, H_2 2.5 lt/min, $TiCl_4$ 2% in the Cr granules	100	900	60	-	-	-	-	-	-	[120]

Table 4-8 : CVD process parameters for depositing various metals onto diamond crystals [120, 164, 165].
NOMENCLATURE: N : Necessary step, **O** : Optional step, **T** : temperature, **t** : time.

Almost all reported tungsten CVD for coated diamonds is performed in a manner and reactor similar to the one disclosed in a patent by Wilder *et al.* [109]. The main design feature of the reactor is its tubular shape chamber that has a perforated bottom on which the diamonds are placed (Figure 4-8A on next page). The reacting gases enter the chamber from the bottom at sufficiently high flow rates in order to set the diamond crystals in a fluidised condition and thus allow their even coating.

Chattopadhyay *et al.* [120] have deposited chromium onto diamond crystals by a closed-reactor CVD process described by Hanni *et al.* [167]. The process parameters are given in Table 4-8 and a sketch of the reactor is illustrated in Figure 4-8B. The reactive gases (HCl, Cl_2 and $TiCl_4$) were carried in a stream either of Ar, H_2 or He or a mixture of those through a chamber containing the chromium granules, which was kept inside the reactor. The granules reacted with the gas and Cr was introduced to the vapour phase in the form of chloride, which was then transported to the diamonds where it was reduced to Cr by the H_2 gas (see Figure 4-8B).

Vesna *et al.* [168] have also reported the CVD deposition of chromium in a chromium iodide atmosphere at the temperature range of 700-1000°C to achieve thickness of the order of 0.1 to 2 microns (Figure 4-9). The authors found increasing chromium carbide formation in the coating with increasing deposition temperature. Grishachev *et al.* [155] employing the same method deposited molybdenum disilicide coatings on diamond grains from molybdenum chloride and silicon chloride gases at temperatures and times between 800-1000°C and 30-60 minutes respectively.

Manukyan *et al.* [117, 121, 122] and Oganyan [141, 142] used a CVD process they termed as *thermodiffusional saturation*, to deposit strongly adhered and uniform coatings of Ti, Cr, Fe and other metals in a specially designed reactor. The reactor comprised of a rotating tubular chamber, which was loaded with the charge of diamonds, the powder of the material to be deposited and ammonium chloride (NH_4Cl). At a temperature of about 350-400°C the ammonium chloride decompose and the gaseous products react with the metal powder charge introducing the metal to the vapour state in a chloride form. The latter was then reduced to atomic metal on the diamond surface. The authors reported that for the case of depositing Fe metal, intense reactions on the diamonds had taken place with formation of both carbides and carbon solid solutions. The authors claimed that because of the rotational movement of the chamber the gas streams in it were brought in a non-steady-state condition accelerating the removal of reaction products and brought diamonds in a suspended state, which ensured their uniform coating. (see Figure 4-8C).

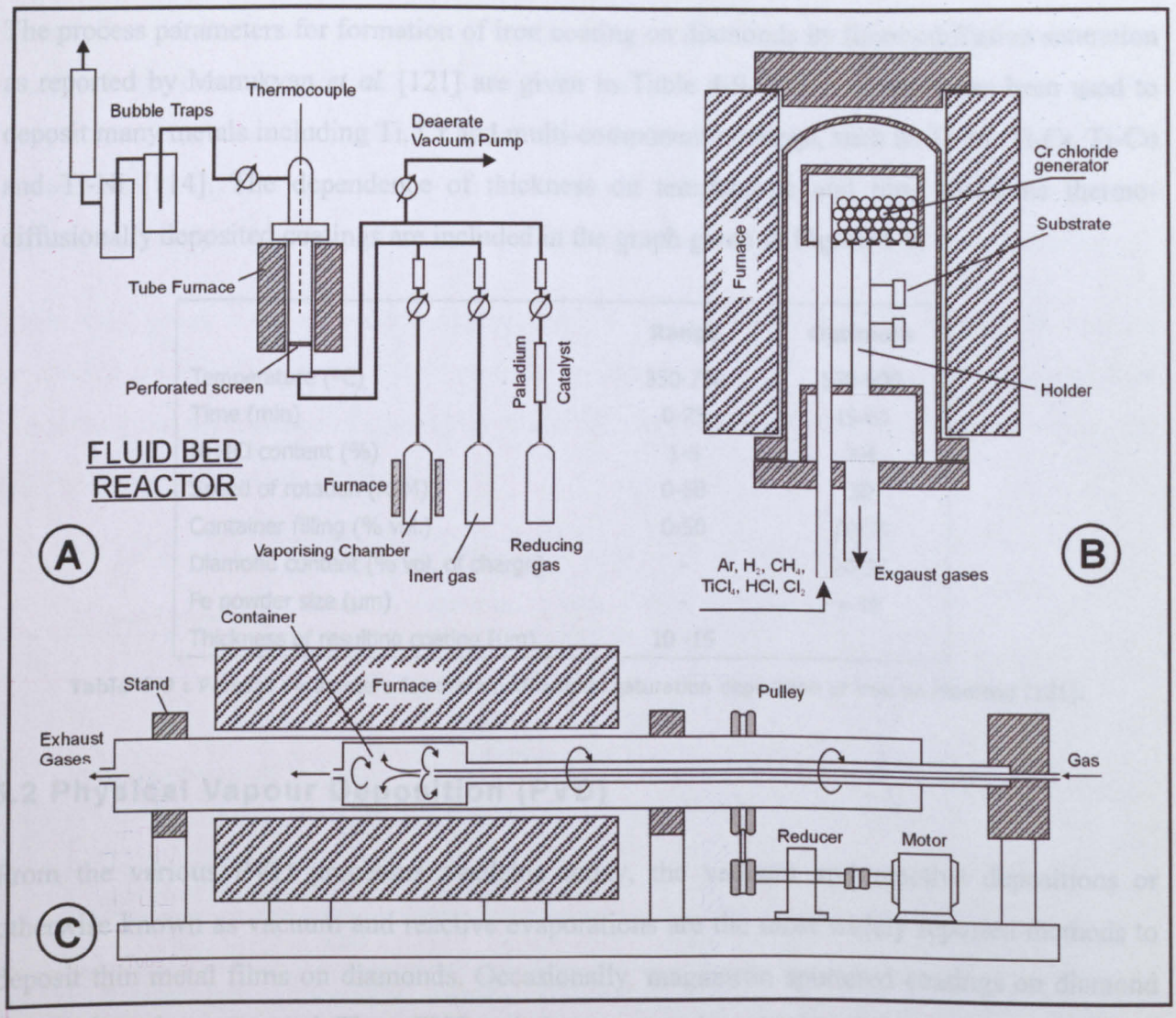

Figure 4-8 : CVD reactors used for diamond coating as reported in literature, **(A)** [109], **(B)** [167] and **(C)** [121].

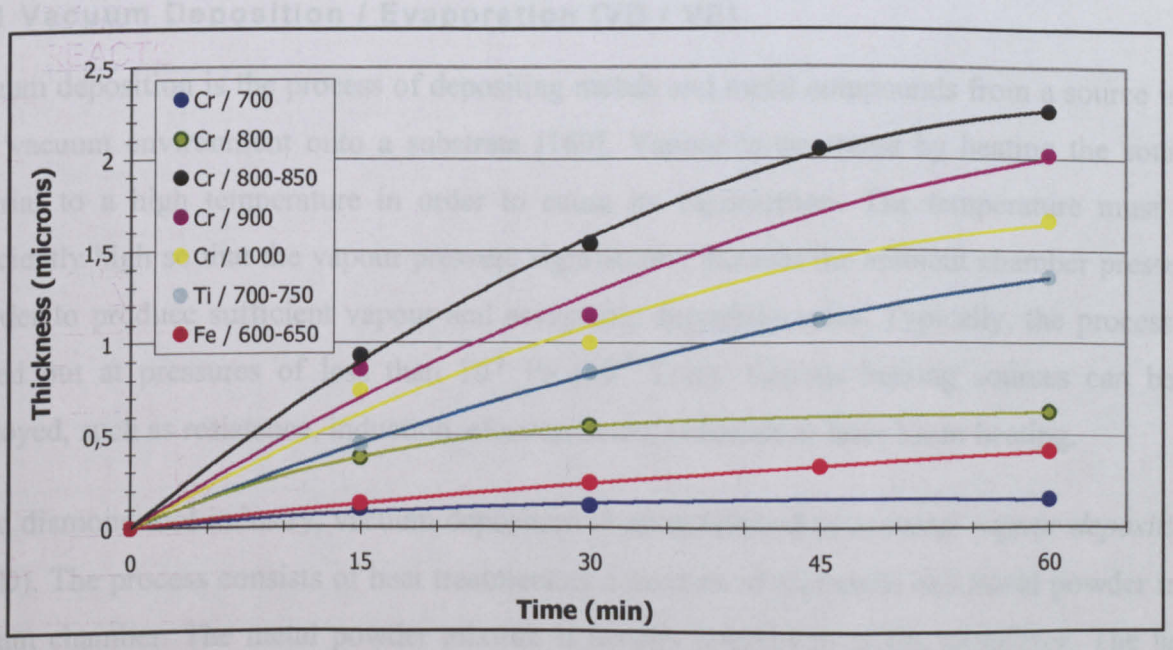

Figure 4-9 : Thickness of metal coatings deposited by CVD on diamonds as a function of temperature and time. [114, 117, 168].

The process parameters for formation of iron coating on diamonds by thermodiffusion saturation as reported by Manukyan *et al.* [121] are given in Table 4-9. This technique has been used to deposit many metals including Ti, Cr and multi-component coatings, such as Ti-Al, Ti-Cr, Ti-Cu and Ti-Ni [114]. The dependence of thickness on temperature and time for some thermo-diffusionally deposited coatings are included in the graph given in Figure 4-9.

	Range	Optimum
Temperature (°C)	350-750	550-600
Time (min)	0-75	45-60
NH4Cl content (%)	1-5	3-4
Speed of rotation (RPM)	0-50	30
Container filling (% vol.)	0-50	20-30
Diamond content (% vol. of charge)	-	20-25
Fe powder size (μm)	-	≈ 40
Thickness of resulting coating (μm)	10 -15	

Table 4-9 : Process parameters for thermodiffusional saturation deposition of iron on diamond [121].

4.5.2 Physical Vapour Deposition (PVD)

From the various PVD processes available today, the vacuum and reactive depositions or otherwise known as vacuum and reactive evaporations are the most widely reported methods to deposit thin metal films on diamonds. Occasionally, magnetron sputtered coatings on diamond crystals have been reported. These PVD techniques are reviewed in the following sections.

4.5.2.1 Vacuum Deposition / Evaporation (VD / VE)

Vacuum deposition is the process of depositing metals and metal compounds from a source in a high vacuum environment onto a substrate [169]. Vapour is generated by heating the source material to a high temperature in order to cause its vaporisation. The temperature must be sufficiently high so that the vapour pressure significantly exceeds the ambient chamber pressure in order to produce sufficient vapour and acceptable deposition rates. Typically, the process is carried out at pressures of less than 10^{-1} Pa (10^{-3} Torr). Various heating sources can been employed, such as resistance, induction, electron beam, radiation or laser beam heating.

In the diamond tool industry, vacuum deposition is often referred to as *metal vapour deposition* (MVD). The process consists of heat treatment of a mixture of diamonds and metal powder in a vacuum chamber. The metal powder mixture is usually referred to as the *metallizer*. The heat treatment temperature and time must be carefully selected in order to achieve the best combination of deposition rates and minimal risk of diamond degradation. This condition can not

be satisfied for the refractory metals (W, Ta, Mo, etc.), which exhibit relatively low vapour pressures at temperatures below 1000°C. Deposition of refractory metals would require temperatures and times in excess of 1000°C and 10 hours respectively. This is not permissible for the sensitive to high temperatures synthetic diamonds. Modifications of the vacuum evaporation method include heat treatment in a non-oxidising or inert atmosphere such as argon or hydrogen.

Table 4-10 gives a list of process parameters for various metal coatings formed by vacuum deposition on industrial diamonds as reported in literature. Table 4-11 gives some kinetics data concerning the dependence of coating thickness on temperature and time for some of the vacuum deposited metals listed in Table 4-10.

	Powder Source and Diamond-Powder Ratio	Temperature (°C)		Time		Post or Posterior to deposition Heat Treatments		Atmosphere	Ref.
		Range	Preferred	Range	Pref.				
Co	Ni	> 500	-	-	-	-	-	He, Ar, H_2, N_2 or vacuum>10^{-2} Torr	[146]
Cr	Cr	<1000	1000	< 1h	30min	-	-	Ar, Ne or vacuum>10^{-4} Torr	[110]
	10gr 30/40 SDA+100 and 10gr Cr 5µm	720-920	720	0.25-6h	6h	Prior Outgassing : 670°C, 1h Subseq. HT : 770-850°C, 1h		Vacuum>10^{-6} Torr or Ar, H_2	[111]
	Cr	≈ 1000	-	< 10h	-	-	-	-	[112]
	Cr (99.8% pure, Fe 0.1%) and diamond 500µm	720-920	720	0.25-6h	6h	-	-	Vacuum10^{-6} Torr or CH_4, Ar, H_2	[93]
Fe	Fe	> 500	-	-	-	-	-	He, Ar, H_2, N_2 or vacuum>10^{-2} Torr	[146]
Ti	Ti and TiH_2 (hydrite)	350-1000	850-900	>10min	10-15min	-	-	Non-oxidizing or vacuum>10^{-4} Torr	[104]
	Ti	> 500	-	-	-	-	-	-	[105] [107]
	70% vol.Ti + Diamond Ti : 74-88 (37-125µm)	<1000	700	<1h	30min	-	-	Ar, Ne or vacuum>10^{-4} Torr	[110]
	10gr 30/40 SDA+100 and 10gr Tir 5µm	720-920	-	0.25-6h	-	Prior Outgassing : 670°C, 1h Subseq. HT : 770-850°C, 1h		Vacuum>10^{-6} Torr or Ar, H_2	[111]
	Ti	≈ 1000	-	< 10h	-	-	-	-	[112]
	Ti-Diamond ratio 1:1 and 0.1ml HCl per 3gr of Ti Ti : 325mesh (44µm)	-	900	-	6h	Subsequent HT at 1000°C for 2h in N_2 to nitridate the outer region of coating		Vacuum 10^{-5} Torr	[93]
Ni + 1%Ti	-	> 500	800	30min-2h	30min	-	-	He, Ar, H_2, N_2 or vacuum>10^{-2} Torr	[106]
Ni	Ni	> 500	800	30min-16h	2h	-	-	He, Ar, H_2, N_2 or vacuum>10^{-2} Torr	[146]
Mn	Mn	< 1000	700	< 1h	30min	-	-	Ar, Ne or vacuum>10^{-4} Torr	[110]
Mo	Mo	> 500	-	-	-	-	-	-	[104]
V	V	≈ 1000	-	< 10h	-	-	-	-	[112]
Zr	Zr and ZrH_2 (hydrite)	350-1000	-	>10min	-	-	-	Non-oxidizing or vacuum>10-4 Torr	[104]
	10gr 30/40 SDA+100 and 10gr Zr 5µm	720-920	-	0.25-6h	-	Prior Outgassing : 670°C, 1h Subseq. HT : 770-850°C, 1h		Vacuum>10^{-6} Torr or Ar, H_2	[111]
	Zr	≈ 1000	-	< 10h	-	-	-	-	[112]

Table 4-10 : Metals and process parameters for metal vapour deposition (MVD) on industrial diamonds.

	Temperature (°C)	Time (h)	Atmosphere Type / Pressure (Torr)		Diamond Type & US mesh size	Metal Powder (mesh size)	Outgassing Temp. (°C)	Outgassing Time (h)	Coating Thickness (microns)	Ref.
Cr	720	4 - 6	Vacuum	10^{-6}	SDA100+	Nominal Diameter 5 µm	-	-	at least 0.05	[111]
	770	2	Vacuum	10^{-6}			-	-	0.1 - 0.4	
	820	2	Vacuum	10^{-6}	30/40 US mesh		-	-	0.3 - 0.5	
	870	2	Vacuum	10^{-6}			-	-	0.5 - 08	
	920	1	Vacuum	10^{-6}			-	-	1	
	720	6	Vacuum	10^{-6}	Nominal Diameter 500 µm		670	1	0.05 - 0.1	
	770	1	Vacuum	10^{-6}			670	1	0.05 - 0.1	
	820	0.5	Vacuum	10^{-6}			670	1	0.05 - 0.1	
	870	0.25	Vacuum	10^{-6}			670	1	0.05 - 0.1	
	720	6	Vacuum	10^{-6}	SDS 100s (30/40)		670	1	0.05 - 0.1	
	720	6	Vacuum	10^{-6}	MSD (30/40)		670	1	0.05 - 0.1	
	745	16	Vacuum	10^{-7}	200 µm		-	-	0.05 - 0.1	
	1000	0.5	Vacuum	10^{-4}	-	170/200	-	-	0.5	[110]
Ti	700	0.5	Vacuum	10^{-4}	-	170/200	-	-	0.5	
	900	6	Vacuum	10^{-5}	500 µm	325 (44 µm)	-	-	0.1	[93]
Mn	700	0.5	Vacuum	10^{-4}	-	170/200	-	-	0.5	[110]
Ni	800	0.5	Vacuum	10^{-2}	40/50	-	-	-	1-2%wt. gain	[106]
Ni+1%Ti	800	0.5	Vacuum	10^{-2}	40/50	-	-	-	1-2%wt. gain	

Table 4-11 : Thickness of metal coatings deposited by MVD on industrial diamonds as a function of temperature and time.

As can be seen from Table 4-11 for a given temperature and coating time, the deposited chromium coatings are thicker than the titanium, which is similar to CVD processes. From studying a large number of chromium MVD depositions, Chen *et al.* [111] established that if iron contamination in the chromium powder feedstock is greater than 0.2% longer duration or higher deposition temperatures will be required for depositing a given layer thickness The authors stated that the presence of other contaminations in the metal powder charge was expected to cause a similar decrease to deposition rate not only for the MVD of chromium but also for the MVD of other metals too. The authors found depositing onto smaller diamonds would have had the same effect.

The use of non-oxidising atmospheres such as Ar or H_2 instead of vacuum may also set requirements for higher MVD temperatures and times. This is possibly because of the collision of evaporating atoms with the gas molecules, which results in lowering their energy and in diverging them from their trajectories [169]. When the process is performed under vacuum, no deposition takes place during the initial period of the deposition. This is the time required for removal of moisture and other surface contamination by the vacuum pump. Thus, subjecting diamonds to the deposition temperature form the beginning of the process can cause unnecessary degradation to the diamonds without deposition taking place. It has been found [111], that an outgassing step at a temperature below that of the oxidation and graphitisation onset of diamond prior to exposing the grit to the deposition temperature may decrease the risk for excessive graphitisation. At the same time similar thickness is achieved as in deposition cycles without the outgassing step (Table 4-11).

4.5.2.2 Reactive Deposition / Evaporation (RD / RE)

Coating diamonds with reactive deposition (RE) is a rather similar process to vacuum deposition. The deposition may again be performed under vacuum, but the metallizer is a mixture of powders containing the pure metal as well as powders of the oxides of the same or other metal. The oxides evaporate or dissociate under the process conditions and contribute to the transfer of metal to the diamond surfaces, where they are reduced by reacting with the carbon and deposit the metal. The released oxygen returns in the gas phase in the form of carbon monoxide (CO) and is evacuated or reacts at the metallizer by reducing higher oxides to lower and lower oxides to metal. A group of Russian researchers have studied in detail the mechanism and kinetics of the reactive deposition of various carbide former metals and some of their alloys by means of X-Ray diffraction techniques and coating thickness measurements (see Table 4-12 and Figure 4-10).

Coating	Metallizer	Oxygen content	Reference
Cr	Cr powder	-	[97, 115, 135, 140, 143-145]
Ti	Oxidised Ti powder consisting of <Ti(O)>, TiO & TiO_2	15% wt.	[97, 115, 135, 140, 145, 170]
V	Vanadium powder oxidised in air consisting of V_2O_5 and <V(O)>	18% wt.	[115, 135, 145, 153,]
Mo	Oxidised Mo powder consisting of <Mo(O)>, MoO_2 & MoO_3	10% wt.	[97, 115, 118, 135, 140, 145, 147-149,158]
W	Oxidised W powder consisting of W & WO_3	10% wt.	[97, 140, 154]
Cr - Cu	Oxidised Cr and Cu powders	0 - 6.2% wt.	[125]
Cr - Ni	7-24% Ni in Cr	-	[144]
Mo - Ni	Mo and NiO powders	2-14.7% wt.	[157]

Table 4-12 : Metallizer compositions as has been reported in literature for reactive deposition of various carbide forming metals onto synthetic diamond crystals.

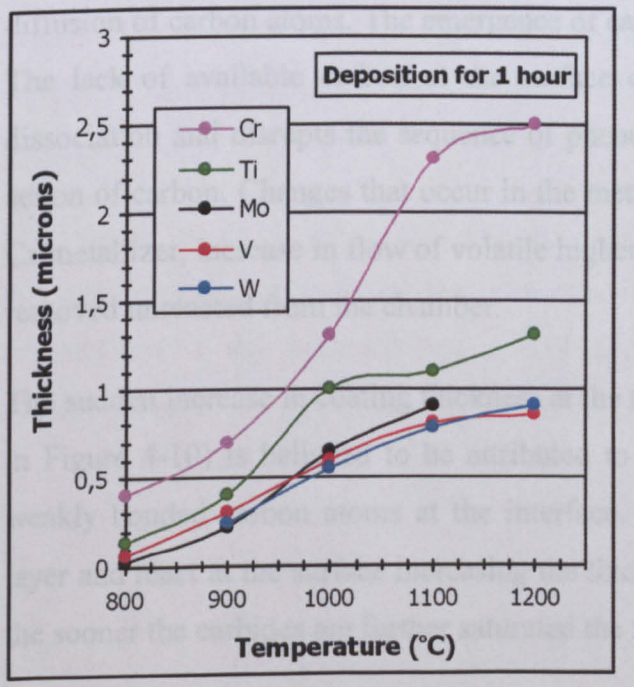

Figure 4-10 : Thickness of coating of carbide forming metals as a function of temperature. Coatings were deposited by reaction deposition (RD) for 1 hour [145].

According to the above studies, the mechanism for reaction deposited coatings of carbide forming metals on diamond can be summarised as follows [145].

During the initial stages of the process, metal is transported to the diamond surfaces by the gas phase and by solid-state diffusion at the diamond-powder metallizer contacting areas. The gas phase present at that moment in the chamber is the result of evaporation of metal (Cr) or oxides (MoO_3, V_2O_5, WO_3). Additionally, gas may result from the dissociation of oxides to metal and oxygen or by disproportionation of lower oxides to higher ones when heating is conducted at the higher temperatures in the presence of a reducing agent and a vacuum.

Metal on the diamond is generated by the reduction of the oxide transporters at the diamond surface and is additionally brought there by diffusion from the metal powders in contact the diamond crystals. Metal atoms react with the available carbon atoms on diamond surfaces. Carbon monoxide released by the reduction is either carrier away by the evacuating pump or can react with the metallizer, or reduce evaporated oxide gases or reduce metal oxides in the solid powder mixture.

After a continuous layer has formed on the diamond the further thickening of the coating is controlled by the diffusion of carbon though this layer. At the same time the carbon content in the coating increase and lower carbides (Cr_7C_3, V_2C, W_2C) start to convert to higher carbides (Cr_3C_2, VC, WC), or carbides are saturated by filling the carbon vacancies of their defective lattice (α-Mo_2C, TiC, VC). As the coating continues to grow, the formed carbides retard further diffusion of carbon atoms. The emergence of carbon atoms at the surface of the grits is hindered. The lack of available carbon at the surface of the diamonds leads to a reduction of oxide dissociation and disrupts the sequence of phenomena and reactions resulting from the reducing action of carbon. Changes that occur in the metallizer involve for example, carbide formation in Cr-metallizer, increase in flow of volatile higher oxides of Mo-, V- and W-metallizers, which are removed unreacted from the chamber.

The sudden increase in coating thickness at the temperature range of 1000-1100°C (see Cr and Ti in Figure 4-10) is believed to be attributed to the graphitisation of diamond, which generates weakly bonded carbon atoms at the interface. The latter can then diffuse through the coating layer and react at the surface increasing the thickness. The sooner the metallizer is depleted, and the sooner the carbides are further saturated the faster is the thickening rate again decreased.

4.5.2.3 Magnetron Sputtering

Sputtering is a coating technique, which uses ion beam or plasma discharges to produce a flux of atoms from a target material, by bombardment with energetic ions of an inert gas. A negative bias is applied to the target, which acts as the cathode of the electric discharge, and the positive ions from the plasma strike the target. The coating material is thus passed into the vapour phase by momentum transfer, which is a mechanical process, as opposed to chemical or thermal processes described earlier. Because of this mechanical character virtually any material is a candidate coating [171]. Among the advantages of sputtering techniques is the ease of depositing refractory metals at low-temperatures, which is of particular importance for the coating of diamond crystals.

One of the variations of the numerous available sputtering configurations is magnetron sputtering, in which permanent magnets, placed behind the target material, produce a magnetic field which confines the plasma above the substrate. As the electrons that sustain the plasma discharge are confined, a high degree of ionization is possible, leading to higher sputtering rates and the ability to carry out deposition at lower pressures.

There are only few reports on the use of magnetron sputtering to deposit chromium [172] titanium, molybdenum [134, 173] and TiN [174] coatings onto synthetic diamond crystals.

Zhu *et al.* [172] formed 150 nm thick Cr-coatings onto synthetic diamonds using magnetron sputtering with dc mode in an Ar atmosphere achieving deposition rates of the order of 0.3 nm/sec. The authors found interface diffusion and reaction to form Cr_2C_3 to take place during deposition of the Cr-layer. Increasing the deposition power was found to intensify these phenomena.

Novikov *et al.* [134] using the magnetron sputtering with a specific power of 95 $W \cdot cm^{-2}$ deposited titanium and molybdenum coatings on diamond crystals. Carbide formation was detected with X-ray diffraction for the Ti-coatings, but not for the molybdenum, which only showed to carbidise after subsequent annealing at temperatures in excess of 300°C.

4.5.3 Immersion in Molten Salt Baths (IMBS)

Several patents exist claiming development of coatings on industrial diamonds by immersion techniques in various molten salt baths [113, 116, 175]. The temperature of the molten bath varied in the range of 700-1000°C and deposition duration was from one to several hours. According to these patents, the molten salt bath may be a fluoride-containing chloride bath, with the chloride bath comprising of at least one chloride of an alkali metal or alkali earth metal. The fluoride can be either a fluoride of an alkali metal or of an alkali earth metal. A molten iodide or molten fluoride bath may substitute the molten chloride bath. The metal to be deposited was introduced to the liquid bath in the form of powder, which could either be powder of the elemental metal or powders of oxides, halides, or alloys containing the metal or could even be mixtures of all those types. The abrasive particles were held in a wire mesh bucket.

Coating growth in thickness was controlled by carbon diffusion. The following graph gives the thickness of coating for various carbide-forming elements formed by immersion in molten salt baths. The adhesion of coatings was evaluated by the percentage of coating peeling-off when milling the coated grains with carbide balls. As can be seen from the graph, unlike the other processes, titanium coatings were found thicker than chromium for a given deposition. However, their adhesion was found to be inferior. Best combination of thickness and bonding strength was found for V, Zr and Nb.

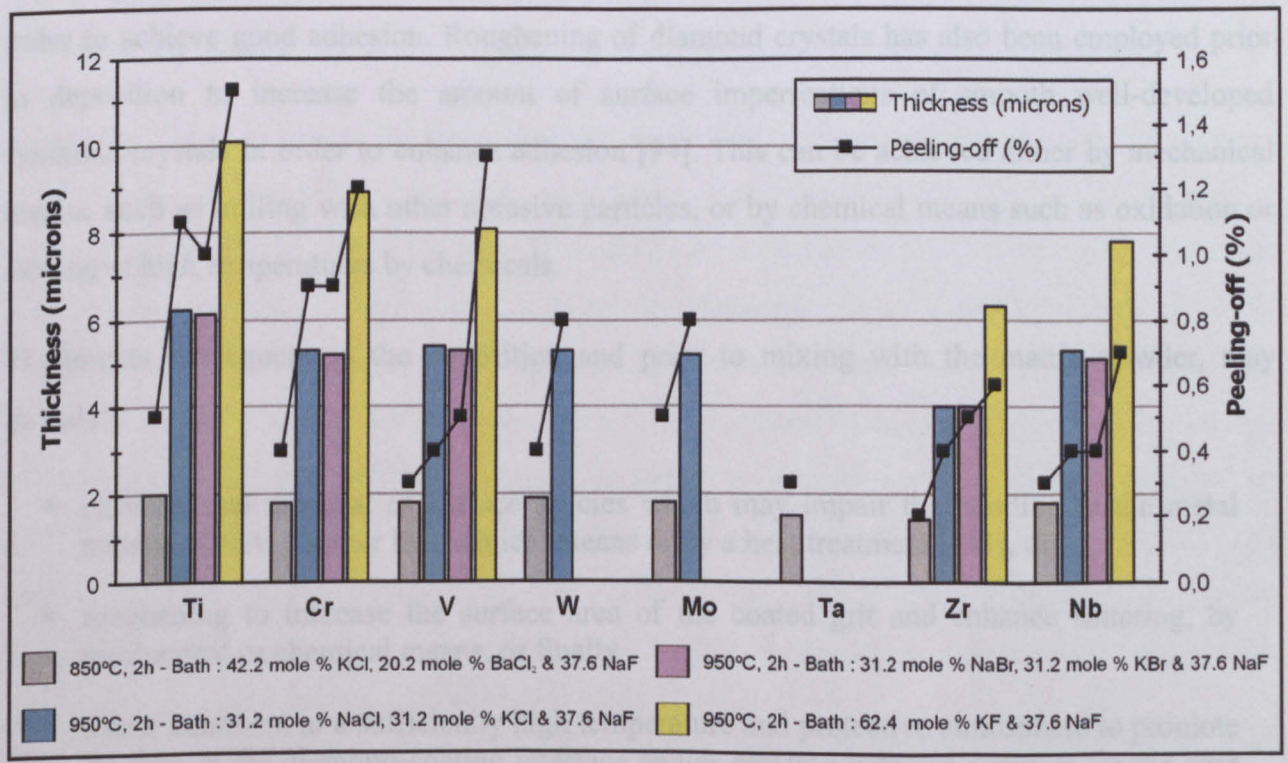

Figure 4-11 : Thickness of metal carbide forming metals deposited by immersion in molten salt baths. The adhesion of coatings with diamond is given by the % peeling-off when milling with carbide balls at 150 RPM for 15 min. Diamond: MBS 50/60 US mesh (General Electric) [116].

4.5.4 Other Methods

Kimura [161] discloses in his patent a method of forming metal-powder diamond granules. According to this method, a slurry of the metal powder with a solution is initially prepared. An agglomerating binder dissolved in an organic solvent composes the solution. Agitating the slurry brings the metal powder in homogeneous suspension in the slurry. The slurry is then sprayed onto a fluidised suspension of diamond particles by an atomising nozzle within a fluid bed granulator. A constant flow of warm gas entering the chamber from beneath maintains the grit in the fluid bed condition and ensures fast drying. Progressively, diamonds are encapsulated in uniform spherical metal envelope. Kimura claims that unlike other granulation techniques, his invention ensures that each granule will contain only one abrasive crystal. The diamond granules may subsequently heat-treated to achieve a chemical bonding at the interface [94].

Minyong *et al.* [108] disclose in their patent a method of mechanically covering the diamond crystal surfaces with metal. They achieved this by milling diamond particles with the metal, with the latter smearing onto the abrasive crystals. Subsequent firing the granules accomplishes the chemical bonding.

4.5.5 Post and Posterior Deposition Treatments

Cleaning and removal of contamination from diamond surfaces is almost always necessary in order to achieve good adhesion. Roughening of diamond crystals has also been employed prior to deposition to increase the amount of surface imperfections of smooth well-developed synthetic crystals in order to enhance adhesion [94]. This can be achieved either by mechanical means, such as milling with other abrasive particles, or by chemical means such as oxidation or etching at high temperatures by chemicals.

Treatments subsequent to the deposition and prior to mixing with the matrix powder, may include:

- cleaning and removal of surface species which may impair the bonding to the metal matrix, achieved either by chemical means or by a heat treatment [111], or
- roughening to increase the surface area of the coated grit and enhance sintering, by mechanical or chemical means, or finally
- a heat treatment at a sufficiently high temperature and protective atmosphere to promote reaction at the diamond-coating interface and/or reaction between coatings for the case of multi-coated diamonds.

4.6 Mechanical Properties of Coated Diamonds

There are basically two aspects when referring to the mechanical properties of coated diamonds. The first refers to the strength of the coated crystals and the second refers to the strength of the diamond-coating interface. The latter is the so-called "adhesion strength".

4.6.1 Strength of Coated Diamonds

The strength of industrial diamond refers to its ability to resist fracture. As already pointed out, coating of the diamond cannot increase the inherent strength of the crystal (§4.2.3). In fact, crystals having been exposed to a deposition treatment typically show reduced strength compared to the original non-coated grit. The magnitude of this decrease reflects the degree of diamond degradation due to the exposure at the deposition conditions.

The strength of diamonds can be measured by a standardised test known as the "friability test", as already mentioned in §2.3.3.2. The test measures the ability of a predetermined amount of a given mesh size diamond crystals to resist fracture when shaken together with a number of small carbide balls. After milling for a specified period, the grit is screened with a sieve of a mesh size corresponding to that of the tested diamonds. Screening separates the broken diamond pieces from the non-fractured grit. The weight percentage of the remaining diamond on the sieve is defined as the friability index (FI). The closer the index is to unity, the stronger and tougher is the diamond characterised.

Chen *et al.* [111] measured the friability index of dual Cr/W-coated diamonds after the coatings were chemically removed. The inner chromium layer was deposited by MVD at various temperatures and times, while the outer W coating was deposited by CVD at constant conditions. The dependence of the friability index with temperature for this study is given in Figure 4-12. As can be seen from the graph, increasing the deposition temperature effectively increased the thickness of the coating, but the strength of the diamond was considerably decreased for temperatures exceeding 800°C. An outgassing step at a lower temperature to allow removal of adsorbed species proved to be beneficial for avoiding the diamond strength reduction. The authors claimed that since outgassing was performed at a lower temperature the duration the crystals were exposed to temperatures above 700°C during deposition, which are associated with accelerated diamond degradation, was effectively reduced.

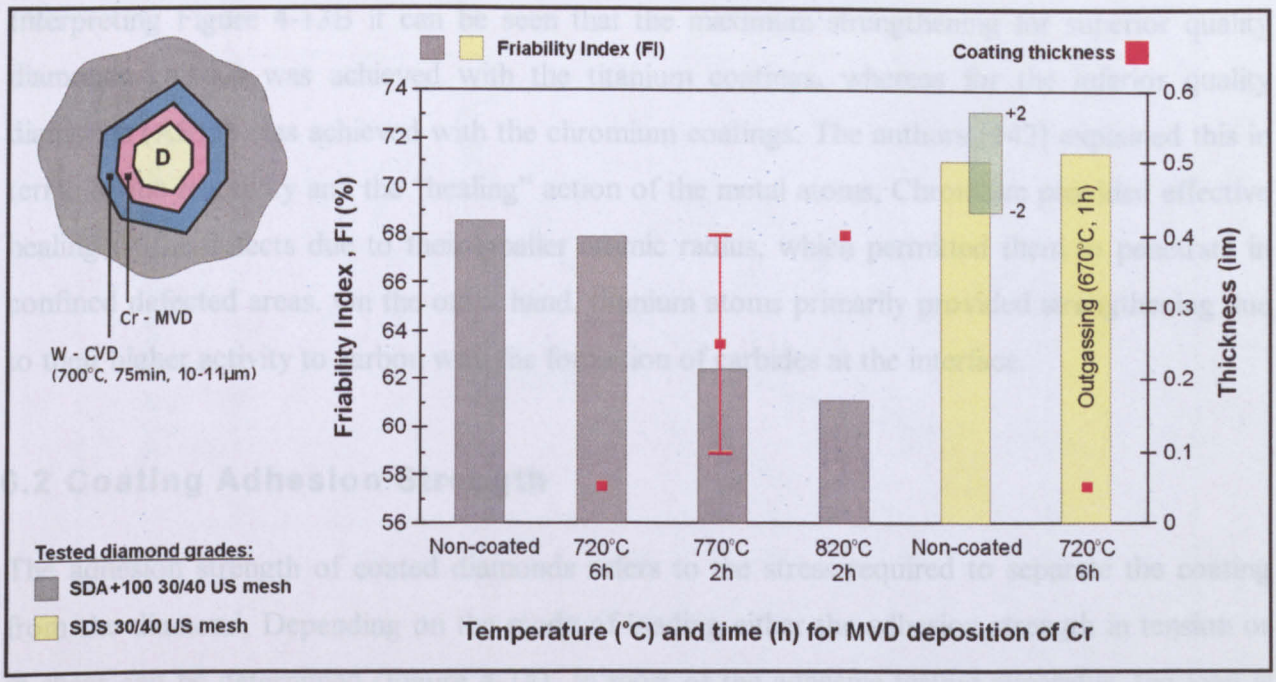

Figure 4-12 : Friability index dependence on temperature and time for dual coated Cr/W diamonds [111].

Manukyan *et al.* [121] measured the force required to fracture coated diamonds in a specially developed device. The coatings were deposited by thermo-diffusion saturation process. The diamonds were tested without having their coating removed. The results of these mechanical tests are graphically presented in Figure 4-13. The coated diamonds were found to withstand higher loads than the equivalent non-coated grit. The authors claimed this to be attributed to "healing" of the diamond surface defects by the metal layers, which effectively reduced the stress raising points on the crystals.

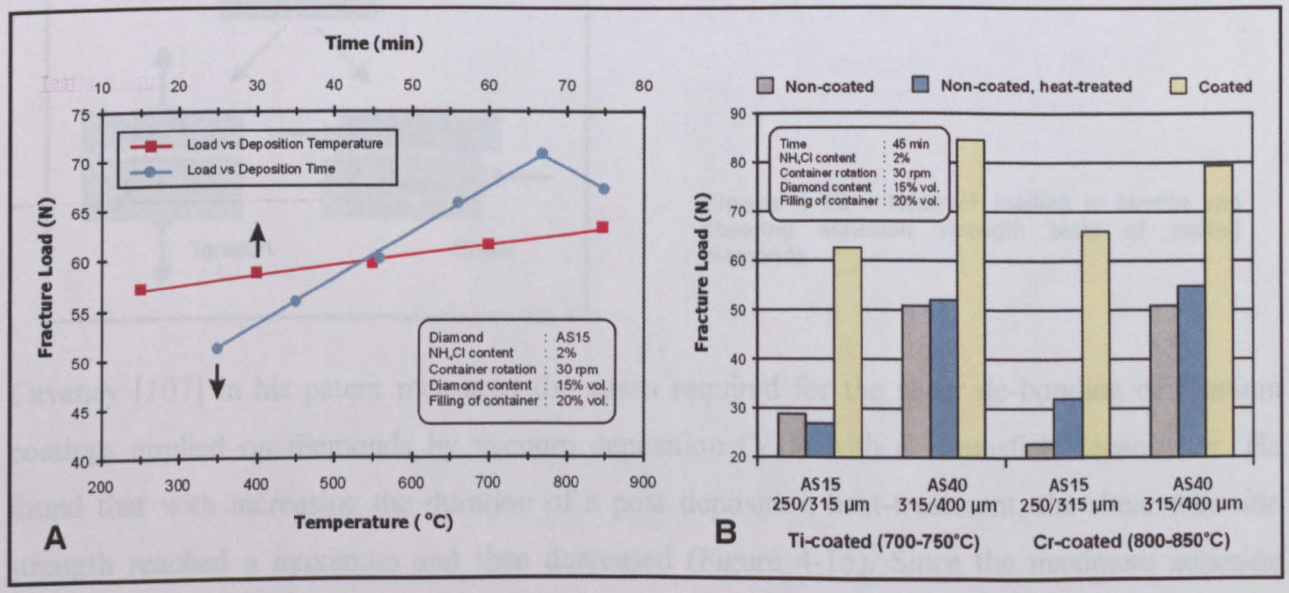

Figure 4-13 : (A) Fracture load of iron coated diamonds as a function of temperature (for 45min deposition) and as a function of time (T=550-600°C) [121]. **(B)** Load required to fracture two grades of synthetic diamond at their original condition), Non-coated (at their original condition), Heat-Treated Non-coaed (the non-coated after heat treatment at a temperature as high as that of the deposition) & Coated (after coating with Ti or Cr by thermodiffusion saturation) [142]. The AS40 is a better quality synthetic diamond with less-amount of defects than AS15.

Interpreting Figure 4-13B it can be seen that the maximum strengthening for superior quality diamonds (AS40) was achieved with the titanium coatings, whereas for the inferior quality diamonds (AS15) was achieved with the chromium coatings. The authors [142] explained this in terms of the reactivity and the "healing" action of the metal atoms. Chromium provided effective healing of the defects due to their smaller atomic radius, which permitted them to penetrate in confined defected areas. On the other hand, titanium atoms primarily provided strengthening due to their higher activity to carbon with the formation of carbides at the interface.

4.6.2 Coating Adhesion Strength

The adhesion strength of coated diamonds refers to the stress required to separate the coating from the diamond. Depending on the mode of loading either the adhesion strength in tension or in shear can be determined (Figure 4-14). In most of the adhesive testing apparatus, the load is applied by a pair of special rods attached on both diamond and coating [97]. The fixing of the rods is primarily achieved by brazing. Special care must be given that the load is applied in an exactly normal or parallel direction to the coating-diamond interface when testing the adhesion strength in tension or shear respectively. The adhesion of coatings on diamonds can also be assessed by determining the weight loss caused by coating peeling-off after diamonds have been ball milled with carbides [116].

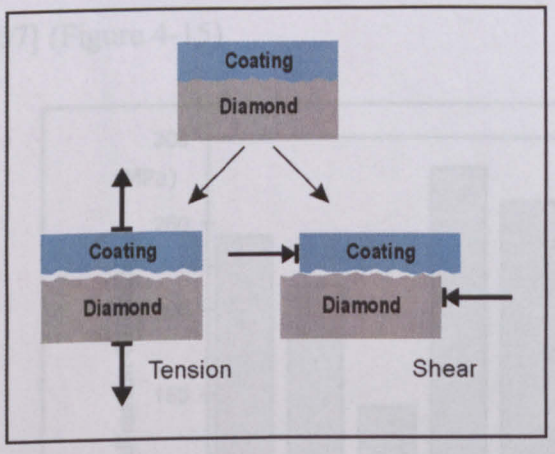

Figure 4-14 : Mode of loading in tensile and shearing adhesion strength tests of coated diamonds.

Caveney [107] in his patent measured the stress required for the shear de-bonding of titanium coatings applied on diamonds by vacuum deposition (VD) with a Hounsfield tensometer. He found that with increasing the duration of a post deposition heat-treatment, the shear adhesion strength reached a maximum and then decreased (Figure 4-15). Since the maximum adhesion strength was found for 15 minutes heating, the inventor claimed that a heat treatment should be avoided, and instead a suitable modification to the composite consolidation route should be made in order to allow carbide formation to take place.

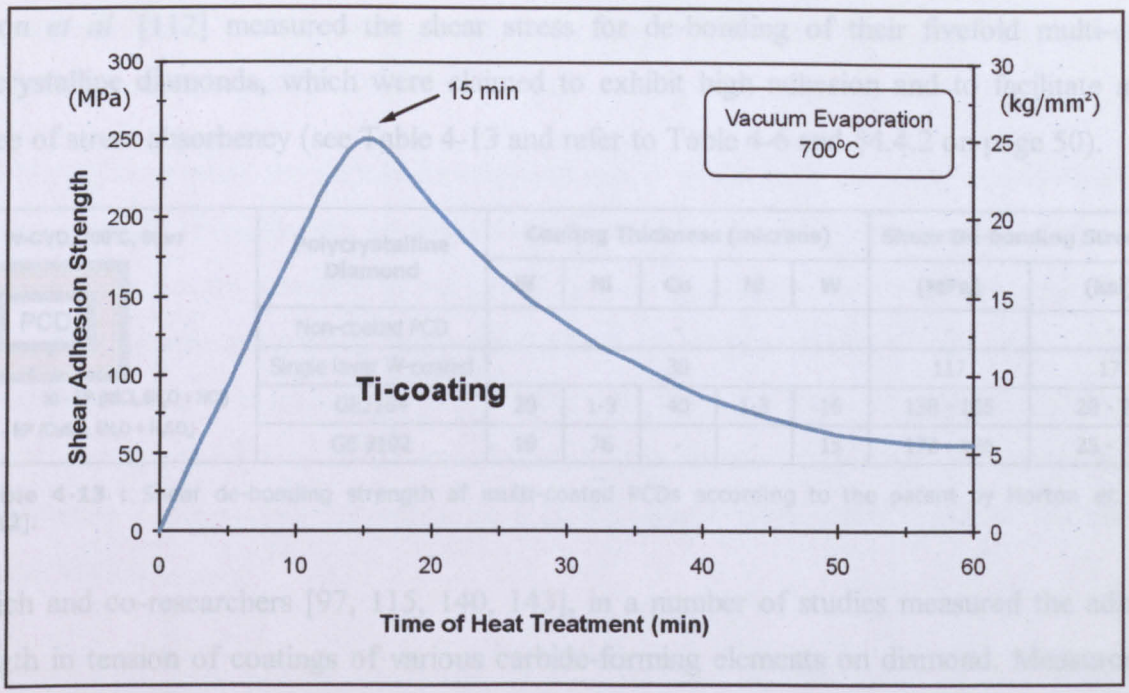

Figure 4-15 : Interfacial shear strength of titanium coated diamonds as a function of the duration of the Vacuum Deposition at 700°C [107].

Nicholas *et al.* [106, 146] using the same apparatus as Caveney [107], measured the shear adhesive strength for various diamonds coated with Ni, Ni-alloys and Cu-alloys (Figure 4-16). The coatings were layered by vacuum deposition and the coated diamonds were subsequently heat treated for various times. The shear adhesion strength was found to depend on time of heat treatment in similar manner to what was found for the Ti-coated diamonds tested by Canveney [107] (Figure 4-15).

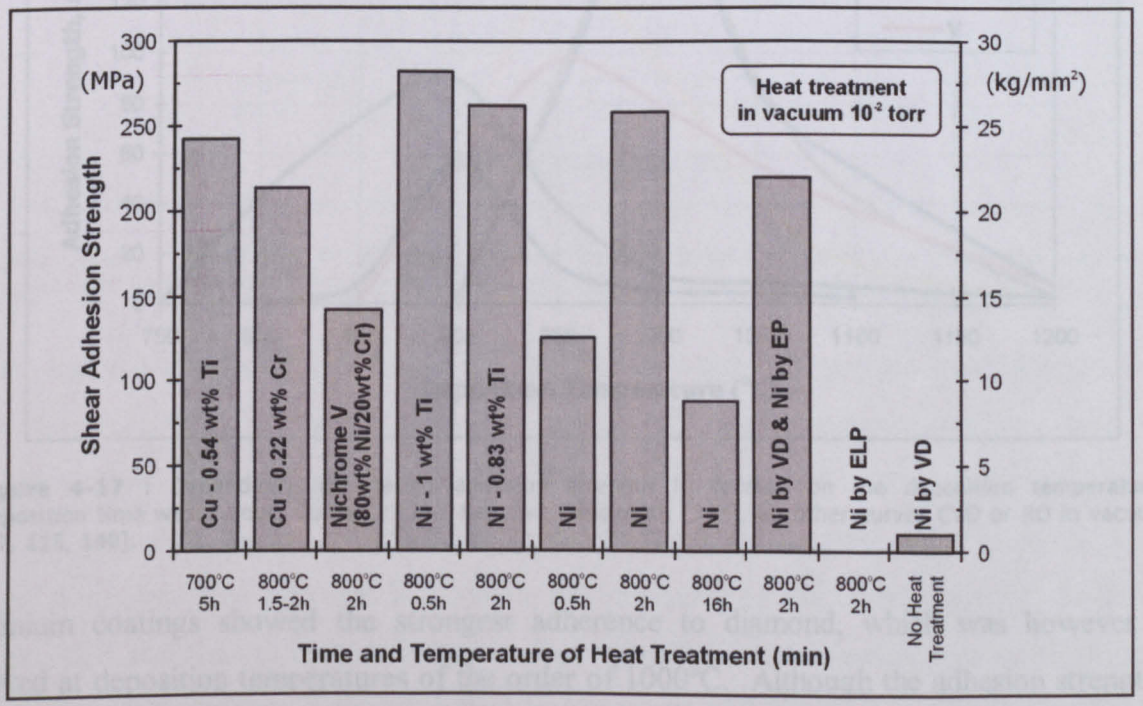

Figure 4-16 : Interfacial shear strength of Ni, Ni-alloys and Cu-alloys on diamonds as a function of the duration a heat treatment that followed the Vacuum Deposition at 700-800°C [106, 146].

Horton *et al.* [112] measured the shear stress for de-bonding of their fivefold multi-coated polycrystalline diamonds, which were claimed to exhibit high adhesion and to facilitate a high degree of stress absorbency (see Table 4-13 and refer to Table 4-6 and §4.4.2 on page 50).

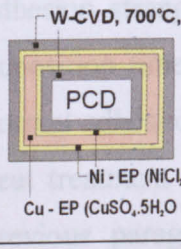

Polycrystalline Diamond	Coating Thickness (microns)					Shear De-bonding Strength	
	W	Ni	Cu	Ni	W	(MPa)	(ksi)
Non-coated PCD	-					-	-
Single layer W-coated	30					117	17
GE2164	20	1-3	40	1-3	16	138 - 165	20 - 24
GE 2102	19	76	-	-	15	172 - 186	25 - 27

Table 4-13 : Shear de-bonding strength of multi-coated PCDs according to the patent by Horton *et. al.* [112].

Naidich and co-researchers [97, 115, 140, 143], in a number of studies measured the adhesion strength in tension of coatings of various carbide-forming elements on diamond. Measurements were carried out with a specially designed apparatus, which was claimed to ensure strict normal loading of the coating in respect to the diamond-coating interface. The measured adhesion strengths as a function of the deposition temperature are given in Figure 4-17.

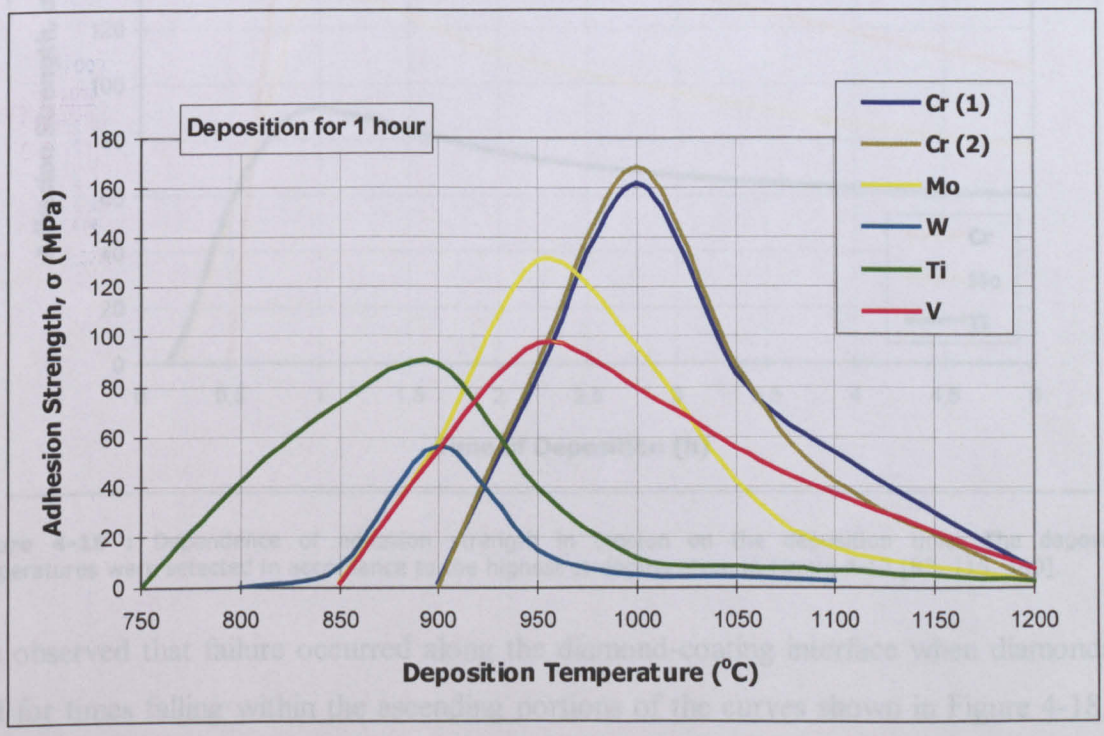

Figure 4-17 : Dependence of coating adhesion strength in tension on the deposition temperature. Deposition time was 1 hour. Curve Cr (1) : Reactive Deposition [143], all other curves CVD or RD in vacuum [97, 115, 140].

Chromium coatings showed the strongest adherence to diamond, which was however only achieved at deposition temperatures of the order of 1000°C. Although the adhesion strengths of titanium and tungsten were lower, their maximum strengths were achieved at a considerably

lower temperature. In fact, titanium showed measurable increases in adhesion strength at deposition temperatures as low as 750°C.

After having established the deposition temperatures at which each metal showed the maximum adhesion strength, Naidich and co-researchers [97, 115, 140, 143] examined the influence of deposition time on the adhesion strength. Figure 4-18 graphically illustrates the dependence of normal adhesion strength on deposition time. The mode of dependence of adhesion strength on heat treatment time was found to coincide with what has been found by other researchers (see previous paragraphs) [106, 107, 146]. Strength was found to increase up to a maximum corresponding to deposition durations of 1 hour. Longer times were found to decrease the adhesion strength.

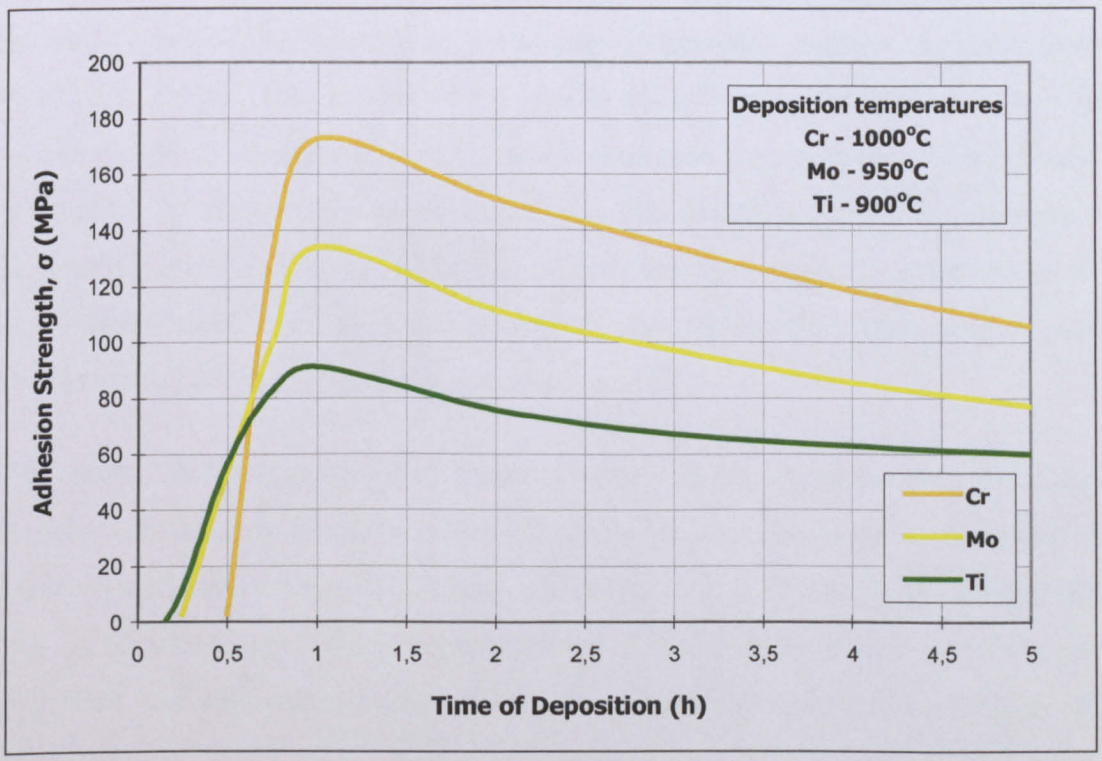

Figure 4-18 : Dependence of adhesion strength in tension on the deposition time. The deposition temperatures were selected in accordance to the highest strengths given in Figure 4-17 [97, 115, 140].

It was observed that failure occurred along the diamond-coating interface when diamonds were coated for times falling within the ascending portions of the curves shown in Figure 4-18, while for longer times (descending parts of the curves) the fracturing took place within the bulk diamond. According to the authors, this indicated that after reaching the maximum point of strength the subsequent decrease in strength was attributed to the combined effect of diamond graphitisation and the increased number of Kirkendall-Frenkel vacancies. The latter originated from excess carbon atom diffusion below and near to the interface within the crystal, thus weakening the diamond.

Oki *et al.* [116] in their patent, measured the coating peeling-off for diamonds coated with various carbide forming elements. The coatings were deposited by immersion in molten salts baths at 850°C and 950°C for durations of one and two hours. The amount of peeling-off was found to depend on the composition of the salts and the temperature (see Figure 4-11 on p.62). Based on the values, the various carbide formers can be ranked according to the increasing percent of peeling-off, which is equivalent to ranking them according to decrease in adhesion strength. The resultant ranking is:

(Zr, Nb) → **V** → **Ta** → **(Cr, W)** → **Mo** → **Ti**

Low % peeling-off
High adhesion

High % peeling-off
Poor adhesion

5

Interfaces in Diamond Metal-Matrix Composites

5.1 Introduction

In the vast majority of diamond metal-matrix composites consolidation is achieved in the solid state by powder metallurgical means. For that reason, the introductory sections of this present chapter present some of the fundamental aspects of interfaces developed between two different solid phases. The discussion is then carried on to interfaces developed in MMCs, covering aspects such as possible type of interfaces, the required properties of interfaces for enhanced composite performance and the types of interfacial bonding. Where possible, the general discussion will be correlated to the interfacial systems found in diamond MMCs with particular attention to those systems reinforced with coated-grit. For reasons of simplicity, wherever coated diamonds are being discussed, focus will be given on single layered coated-grit. This does not prevent the understanding of the involved phenomena for multi-layered coated-diamonds, since these latter systems only differ in the number of interfaces being concerned, but the principles of interactions between those interfaces being the same as for the single-layered coated diamonds.

The final sections of this chapter discuss the wetting of diamonds by molten metals and alloys, as well as the reactivity and solubility of metals with respect to diamond and carbon.

5.2 Interphase Interfaces in Solids

The interface in a solid-solid system separates two different phases that can have different crystal structures and/or compositions. Depending on the atomic structure at the interfacial boundary the interfaces can be divided into three classes: *coherent*, *semi-coherent* and *incoherent* [176].

5.2.1 Coherent Interfaces

Coherence between two solids arises if the continuity of atomic bonding at the interfacial boundary is not disturbed. This is the case when the lattice of the two adjoining crystal match perfectly at the interface plane (Figure 5-1). For the general case of crystals of different structure and apart from considerations of chemical species, the interfacial coherence will require the existence of at least one plane in each crystal in which the atomic configuration is identical. So, when the two crystals are oriented in a particular way so that the contact is achieved between such planes, the atomic configuration will not alter when moving across the interfacial boundary. In the special case of two adjoining phases of the same crystal structure and lattice parameter, the above requirement is satisfied for all the planes and coherence at the interface will be achieved for a much wider range of crystal orientations. The difference in composition of the two phases adds an additional variance in the system, which is the interatomic distance of the two lattices. Maintaining coherence is possible according to what was stated above, only if one or both of the lattices are strained in order to achieve the matching of the contacting planes (Figure 5-1C). The lattice distortions are known as *coherency strains*.

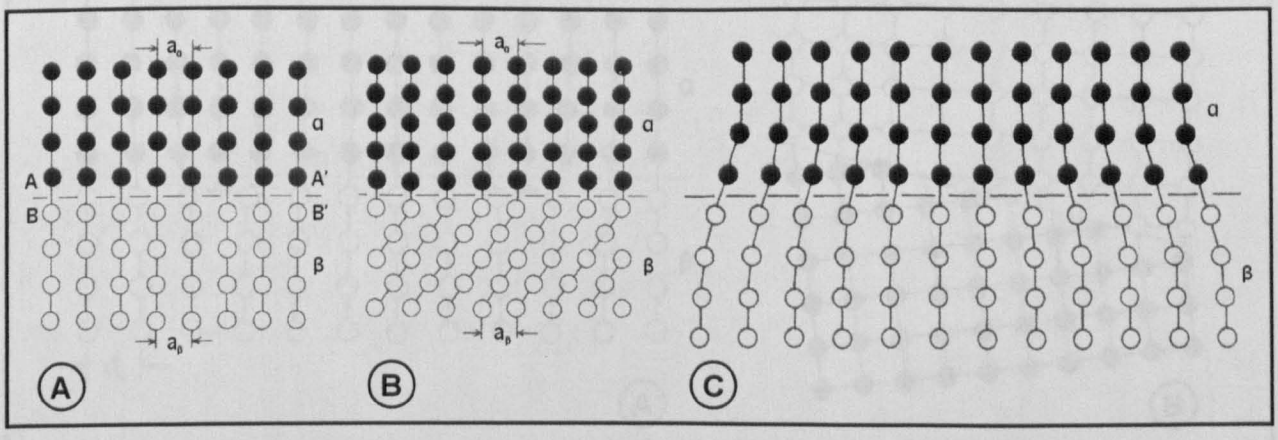

Figure 5-1 : Coherent interfaces. **(A)** Each crystal has a different chemical composition but same crystal structure. **(B)** The two phases have different lattices. **(C)** The two crystals have a slight mismatch in interatomic spacing, which leads to coherency strains in the adjoining lattices [176].

5.2.2 Semi-coherent Interfaces

The strains associated with a coherent interface raise the total energy of the system. When the atomic misfit is large or when the interfacial area is wide, the amount of such an energy raise is not thermodynamically permitted. Strains have to be locally relaxed in order to reduce the total energy. Thus, an excessively strained coherent interface is replaced by a semi-coherent interface in which the disregistry is periodically taken up by misfit dislocations (Figure 5-2A). The matching in the interface is almost perfect except of the areas around a dislocation where the structure is highly distorted and the lattice planes are discontinuous. The dislocation spacing in the boundary area diminishes as the misfit (δ) between the two lattices increases ($\delta=\{d_\beta-d_\alpha\}/d_\alpha$). When $\delta>0.25$, the dislocations occurrence is approximately every four interplanar spacings. The regions of poor fit in the dislocation neighbourhood overlap each other and the interface can no longer be retained coherent and becomes incoherent.

5.2.3 Incoherent Interfaces

Incoherent interfaces result when the interfacial plane has a very different atomic configuration in the two adjoining phases eliminating any possibility of good matching across the interfacial boundary (Figure 5-2B). This is either due to the different patterns of atoms of the two contacting planes or the interatomic distances differ by more than 25%, as was mentioned in the previous paragraph.

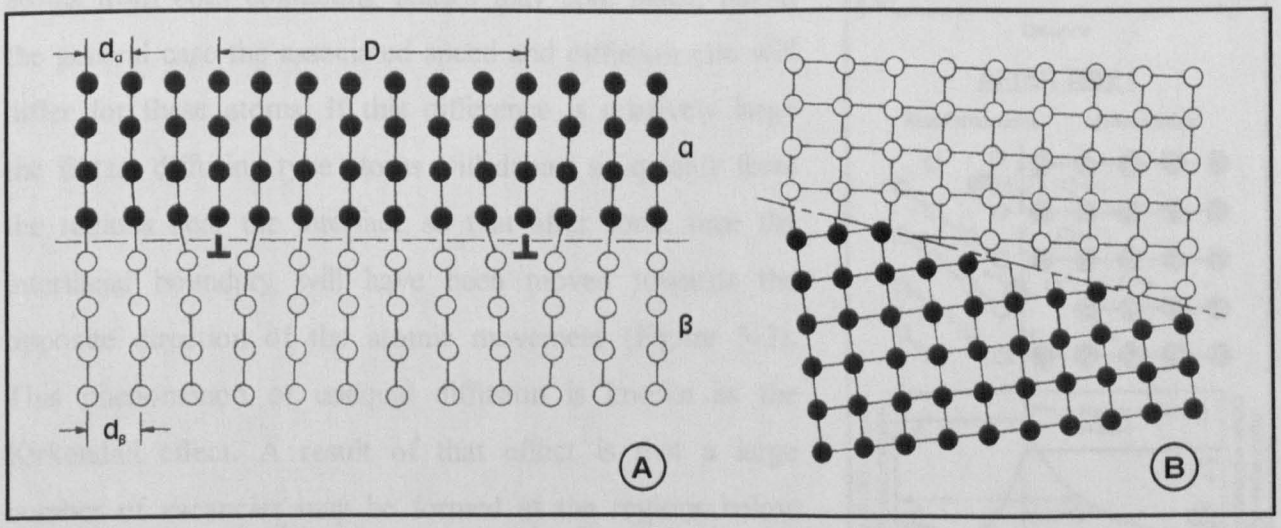

Figure 5-2 : (A) Semi-coherent interface. The misfit parallel to the interface is accommodated by a series of edge dislocations. **(B) Incoherent interface.** The large misfit in interatomic distance cannot allow any degree of coherence [176].

5.3 Diffusion and Interface Migration

Diffusion is the process of movement of atoms within a material driven by the need to eliminate atomic concentration differences [177]. Atoms supplied with sufficient energy (thermal energy) find paths through which they are easier diffused either by squeezing into interstitial sites (interstitial diffusion) or by gradually occupying available vacancy sites in crystals (vacancy diffusion). The preferable way, by which diffusion will take place, depends on a number of factors such as the temperature, the size of the diffusing atom, the crystal structure in which diffusion takes place and others. The diffusion of an atom from a position A to a position B across a distance Δx is termed *steady-state diffusion* if the concentration of the diffusing atom is constant at both A and B positions as time elapses. However, in the majority of real situations, the concentration will vary with time and the diffusion is then termed as *non-steady state* [177].

In MMCs the non-steady state type diffusion is taking place where the reinforcement and matrix come in contact. Diffusion rate will be fast at the initial stages of contact, but as time elapses the decrease in concentration gradient across the interfacial region will slow down the flow of atoms. In addition, in case of reactive systems the formation of a compound at the interface will act as a barrier and the atomic movement will be further impeded. Diffusion of atoms from both contacting phases may take place, but in the general case the associated speed and diffusion rate will differ for these atoms. If this difference is relatively large the fastest diffusing type atoms will depart so quickly from the regions near the interface so that after some time the interfacial boundary will have been moved towards the opposite direction of the atomic movement (Figure 5-3). This phenomenon of unequal diffusion is known as the Kirkendall effect. A result of that effect is that a large number of vacancies may be formed at the regions below the interface, because of the massive departure of atoms to the other side. This concentration of voids may weaken the strength of the phase at the areas close to the interface.

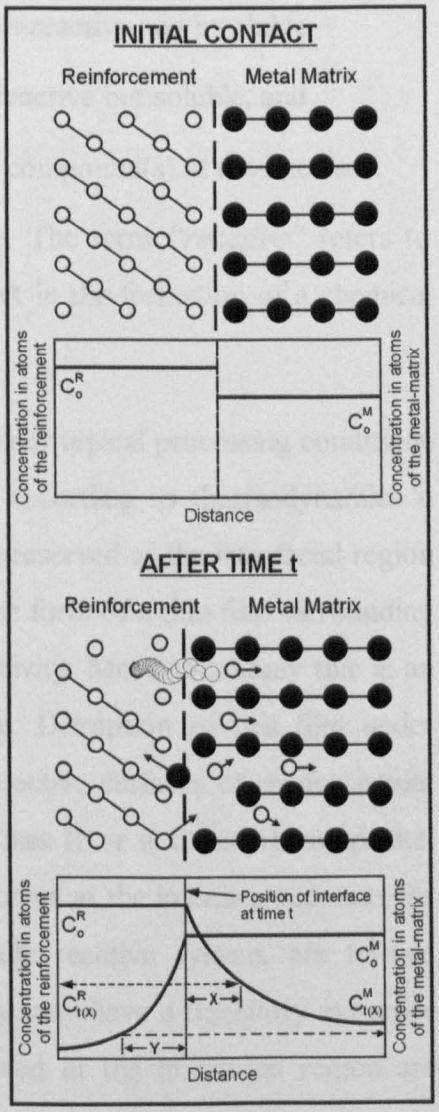

Figure 5-3 : Diffusion and migration of the interface in a MMC.

5.4 Types of Interfaces in Metal Matrix Composites (MMCs)

The interface in a composite material can be defined as follows [178]:

> *An interface is the region of significantly changed chemical composition that constitutes the bond between the matrix and reinforcement for transfer of loads between these members of the composite structure.*

The term *"significantly changed chemical composition"* in the definition excludes random fluctuations of composition and specifies only the systematic changes caused by thermodynamically required effects such as solution, segregation, adsorption and reaction.

Metal matrix composite can be classified into three groups based on the type of chemical reaction occurring between the reinforcing inclusion and the metal matrix at the interface:

- **Class I :** The reinforcement and the matrix are mutually non-reactive and insoluble,
- **Class II :** The reinforcement and matrix are mutually non-reactive but soluble, and
- **Class III :** The reinforcement and the matrix react to form compound(s) at the interface.

Absolute definition between the classes is not always possible. The term *"reactive"* refers to those systems that the interactions at the interfacial region result in the formation of a chemical compound or compounds.

There is another group of composites not listed above, which under typical processing conditions appears free of any interaction between the constituents, but according to thermodynamics it should react. Reaction is inhibited by the presence of a barrier preserved at the interfacial region between the reinforcement and the matrix. Such a barrier has the form of a thin film surrounding the reinforcement and is responsible for the apparent non-reactivity. Most commonly this is an oxide layer, but can also be contamination or even porosity. Disruption of this film under suitable manufacturing conditions will expose the other wise reactive surfaces of reinforcement and matrix to each other, and the system becomes either a Class II or a Class III composite. Composites such as the one described above, where a film preserved at the interface accounts for the apparent non-reactivity of an otherwise thermodynamically reactive system, are termed **pseudo-Class I** composites. Both Class II and Class III systems may have a transitory existence as pseudo-Class I systems until the pre-existing films preserved at the interfacial region are dissipated.

Classification of diamond composites with the above considerations would characterise for example a diamond/bronze (rich in tin) system as Class I, a diamond/cobalt system as a Class II and a diamond/cobalt-based bond alloyed with a carbide former as a Class III composite. A system in which coated diamonds are employed can be classified as pseudo-Class I system if the metal coating has been oxidised and a continuous oxide film prevents the underlying metal of the coating to come in contact with the matrix.

5.5 Types of Interface Bonding

Depending on the interactions occurring at the interfacial region the bonding in metal matrix composites can be classified according to six bond types: mechanical, dissolution, reaction, exchange reaction, oxide or mixed type [179].

5.5.1 Mechanical Bond

Mechanical bond is the bond achieved when no chemical sources of bonding are present in the composite system. Total absence of a chemical source of bonding can never be obtained because weak van de Waals forces will always be present. Hence, mechanical bond can be more precisely defined as the bonding in which the mechanical nature interactions predominate. Mechanical bonding can arise from interlocking effects when irregularly shaped reinforcements with rough surfaces are incorporated in the matrix (Figure 5-4). Additionally, adhesion may also arise from the frictional effects caused by the contraction of the matrix on the reinforcement, which sets the latter under compressive stresses [180]. A primarily mechanically bonded interface is characterised by a low strength, which is only associated with loading parallel to the interface, while the strength in transverse loading is almost absent. The weak mechanically bonded interface is reflected to inferior properties of the composite.

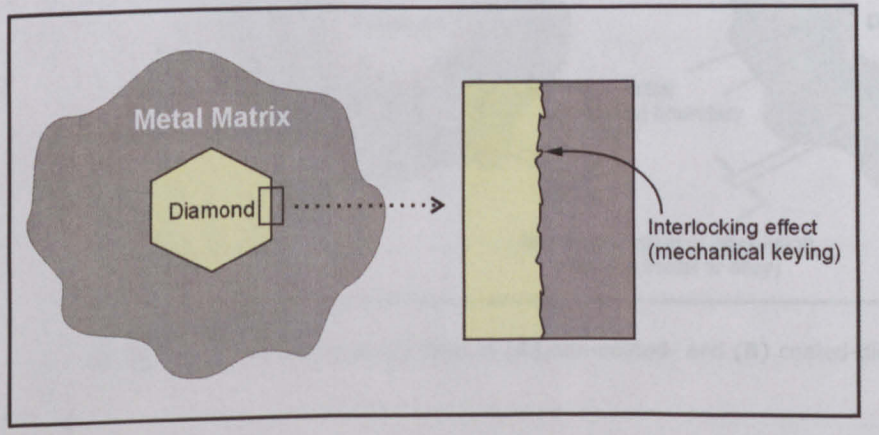

Figure 5-4 : Mechanical bonding at the diamond-metal matrix interface.

In most of the conventional diamond composites the mechanical bond is the primary source of bonding the stiff diamond crystals to the metal matrix. The main reason for mechanical bonding being so widely encountered is that it proves to be the easiest way to retain diamond integrity and protection from excessive reaction or dissolution, which may cause partial loss of crystal strength. The mode of diamond loading during the diamond tool operation induces minimal amount of transverse stresses in respect to the working surface of the tool in which the diamond crystal is partially embedded. This will allow the mechanical bonding to operate until the surrounding metal matrix is incapable of providing a mechanical gripping which can withstand the induced forces that tend to pull the diamond out of its socket. Finite element analysis studies have shown that failure of mechanical bonding is associated with the exposure of a crystal corner at the front side of the diamond [62].

5.5.2 Dissolution Bond

This type of bonding occurs when the matrix dissolves the reinforcement and/or the matrix is as well dissolved in the reinforcement, but when no compounds are formed. The interface will be a transitional zone of gradually altered concentration in diffusing atoms (Figure 5-5). As moving across the interface from the reinforcement towards the matrix the concentration in reinforcement atoms will decrease, whereas the concentration of matrix atoms will increase. The compositional profile across the interface and the position of the interface at a given time after the two constituents were first brought in contact will depend on the relative rates of diffusion of the atoms as described in §5.3 (see also Figure 5-3 on page 74).

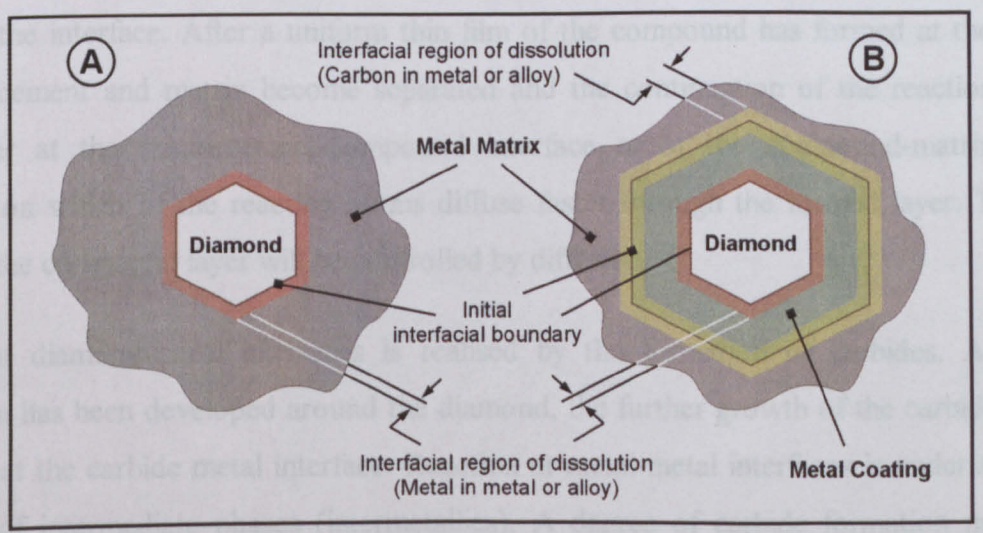

Figure 5-5 : Bonding by dissolution in **(A)** non-coated- and **(B)** coated-diamond metal-matrix composites.

In diamond composites dissolution bonding takes place at the interfacial region when the metal-matrix dissolves carbon without forming stable carbides. For example, such a matrix is cobalt, which although it can form stable carbides it primarily dissolves carbon. Carbon atoms, due to their smaller atomic radius, are much more mobile than the metal-matrix atoms and diffuse considerably faster in the matrix. Even if it is possible for metal atoms to diffuse in diamond, the diffusion rate will be much lower than that for carbon atoms. Thus, the diamond-matrix interface is migrating towards the diamond side. Conditions of prolonged and accelerated carbon diffusion, apart from excess diamond consumption, will cause the Kirkendall effect and can weaken the crystal (see §5.3).

In the case of coated-diamonds incorporated in a metal-matrix, the diamond-coating interface will behave as the diamond-matrix interface of the non-coated-diamond composites, only if the metal of the coating is capable of dissolving carbon and not reacting with it. The coating-matrix interface may bond according to the dissolution bonding depending on the compatibility of the two metals (or alloys) in contact. The dissolution may be mutual. If the coating metal can dissolve in the matrix, it is desirable that this dissolution is little in order to avoid consumption of the layered metal and dissipation of the coating. Considerations on selected materials and consolidation parameters should also be directed into avoiding diffusion of metal-matrix atoms at the diamond/coating interface where they can disrupt the achieved bonding.

5.5.3 Reaction Bond

This bonding occurs when the matrix reacts with the reinforcement and a new compound is formed at the interface. After a uniform thin film of the compound has formed at the interface, the reinforcement and matrix become separated and the continuation of the reaction will take place either at the reinforcement-compound interface or at the compound-matrix interface depending on which of the reacting atoms diffuse faster through the formed layer. The further growth of the compound layer will be controlled by diffusion.

Reaction at diamond-metal interfaces is realised by the formation of carbides. After a thin carbide film has been developed around the diamond, the further growth of the carbide layer will take place at the carbide metal interface. Reaction at metal-metal interfaces is understood as the formation of intermediate phases (intermetallics). A degree of carbide formation may be also accommodated if the outermost metal is a carbide former and if carbon diffusion is sufficient to penetrate the inner metallic or compound layer. Metal-metal interfaces are developed between the coating and metal-matrix and between the various metal layers in multi-layered coated grits.

5.5.4 Exchange Reaction Bond

This is a special case of the reaction bonding in which the overall reaction can be represented by two sequential reactions, although these two reactions may be indistinguishable on a practical basis. The term *exchange reaction* describes the adjustment of equilibrium between two phases in a system containing three or more constituents. For example, an exchange reaction bonding occurs when a second element in the matrix begins to exchange lattice sites with elements in the reaction product. In diamond composites, exchange reaction bonding might take place between a multi-component matrix alloy and a diamond-coating which might also be of multi-component type. Additionally, such interactions can also occur between the various layers of multi-coated diamonds.

5.5.5 Oxide Bond

The term *oxide bond* refers primarily to those composites containing an oxide as the reinforcement or to the systems in which bonding is achieved between oxide layers. The particular importance of this type of bond for the diamond composites is that many of the metal powders or even metal-coated diamonds might have thin oxide layers on their surfaces. Conventional diamond tool production, which involves not such strict oxidation protective atmospheres, might not be sufficient to cause total removal of the oxide layers. Thus, the interaction of diamond with the metal(s) will be affected and the bonding potential of the system might alter dramatically in respect to thermodynamic predictions. As has been seen from other composite systems (e.g. alumina composites) direct bonding between oxides is possible and depends on factors such as the mutual oxygen solubility of the contacting species. Even in systems of that kind, it is not clear whether the reaction is achieved by some sort of bonding, involving oxides, or the reaction is the result of oxide film dissipation due to processing conditions which subsequently allow the direct contact of reinforcement and matrix. Whichever the case, the bonding in presence of oxides is particularly important for metal-coated-diamond composites. The potential of a metal coating to be able to bond by oxide type bonding with the binder is necessary in order to use beneficially the coated grit under standard conditions.

5.5.6 Mixed Type Bond

This type of bonding will occur in pseudo-Class I systems during the breakdown from a Class I to either a Class II or Class III composite. It also refers to systems in which reactivity and solubility are simultaneously taking place, both at considerable extent.

5.6 Requirements of the Interface

The primary function of any interface in a composite is to transfer load between the reinforcement and the matrix [181]. This may be considered as a mechanical requirement and must be satisfied for all types of loading and last throughout the life of the composite. The latter condition demand the interface to be stable in respect of time and operational conditions and constitutes a physical-chemical requirement of the interface.

5.6.1 Mechanical Requirements of the Interface

The ideal situation for load transferring requires a mechanics continuum across the interfacial zone, which in other words means a perfect bond between adjacent component members of the composite [182]. This would require that atomic structure of the components on both sides of the interface to be coherent across the interface and that a uniform and constant interfacial strength exist all over. However, as will be discussed below, achievement of mechanics continuum is difficult due to the nature of chemical discontinuum across the interface.

5.6.2 Physical-Chemical Requirements of the Interface

One of the most demanding requirements in achieving a high performance metal-matrix composite (MMC) is attaining a stable interface. There are five basic sources of instability in a MMC [179].

The first form of instability may arise from dissolution and re-precipitation effects similar to those causing instability and overaging in precipitation hardened alloys. The driving force for this type of instability is the interfacial surface energy that is reduced as the surface area of interfaces is reduced. Dissolution without subsequent re-precipitation constitutes the second type of instability. The principal disadvantage of dissolution is partial loss of the reinforcement. Imbalance of atomic diffusion may lead to the formation of voids (Kirkendall effect) and make the interfacial region prone to unstable behaviour.

The third type of instability arises from continued reaction at the interface in a reactive Class III system. The magnitude of induced instability of a continued reaction is larger than the case of simple solution. The source of instability is attributed to the mechanical properties of the layer formed at the interface. In the case of a diamond composite with a reaction product at the interface, the strength of the reaction zone (interfacial compound) (σ_i) will be lower than that of

diamond (σ_D) (Figure 5-5A). Since in the general case the reaction compound is a brittle phase the strain-to-fracture will be lower than that of diamond. The cracks formed in the interfacial layer at this strain will determine the subsequent mechanical behavior of the composite (Figure 5-6B). Achievement of good bonding in composite with brittle interfaces requires that the interfacial layer remain below a critical thickness. When the interface layer is a solid solution, there will be enough ductility and in most cases the fracture is expected to initiate within the diamond.

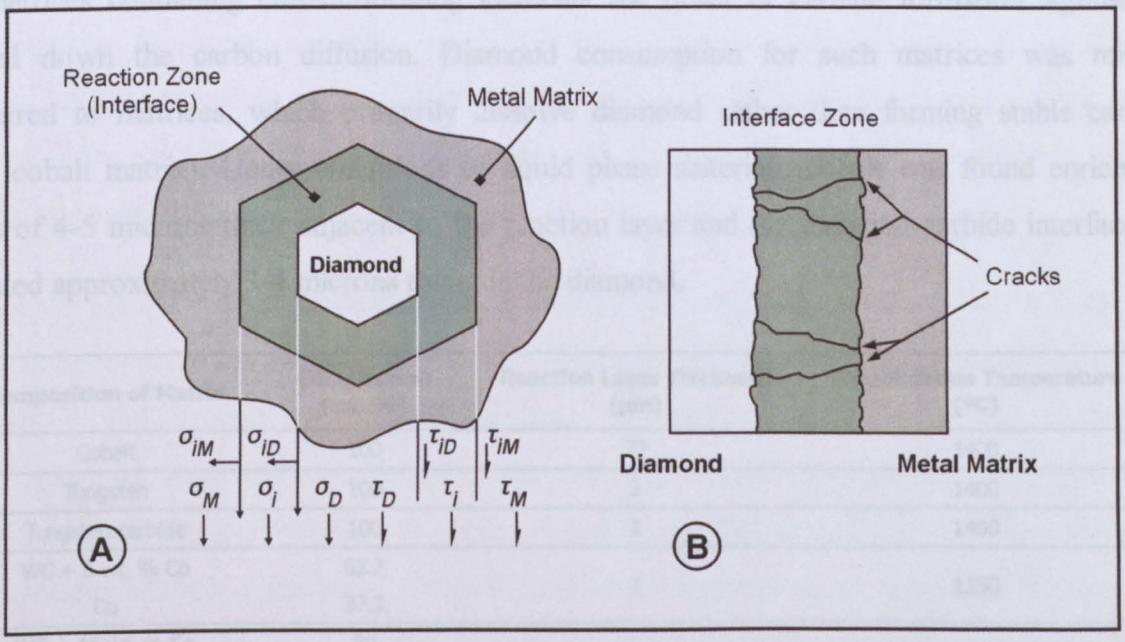

Figure 5-6 : (A) Definition of some strengths for a Class-III diamond composite. **(B)** Cracks in the interfacial reaction zone.

The fourth source of unstable behaviour might be an exchange reaction. Instability arises from variation in concentration of atoms in the vicinity of the compound-matrix interface, caused by the exchange reaction.

The final type of instability is due to breakdown of a pseudo-stable interface (pseudo Class I systems). This type of instability involves a change in the interface occurring under unpredictable conditions. The dissipation of the film causing the non-reactivity (e.g. oxide) allows chemical reaction to begin. The mechanism of breakdown in the general case is complex involving mechanical rupture, dissolution or spheroidization. The process of breakdown will in the general situation occur at local sites, which is the reason of imbalance. Otherwise, the breakdown phenomenon is a beneficial event for the bonding in the composite.

5.7 Interfacial Interactions in Diamond Composites

A limited number of reported work is available in which special attention is given to the interfacial region in diamond reinforced composites from a chemical perspective.

Bronshtein *et al.* [183] have studied the reaction of defect-free natural diamond with various hard metals alloys, commonly used as metal matrices, in terms of measuring the thickness of the interfacial reaction or dissolution zone. Their results, which are given in Table 5-1, indicated that for matrices containing carbide-forming elements the onset of carbide formation significantly slowed down the carbon diffusion. Diamond consumption for such matrices was minimal compared to matrices, which primarily dissolve diamond rather than forming stable carbides (pure cobalt matrix). Under conditions of liquid phase sintering, cobalt was found enriched in zones of 4-5 microns thick adjacent to the reaction layer and the diamond-carbide interface had migrated approximately 3-4 microns towards the diamond.

Composition of Matrix	Composition (wt. %)	Reaction Layer Thickness (μm)	Consolidation Temperature (°C)
Cobalt	100	27	1400
Tungsten	100	3	1400
Tungsten carbide	100	2	1400
WC + 6 wt. % Co	62.7	1	1150
Cu	37.3		
WC + 15 wt. % Co	80	1	1150
Co	8		
Cu	12		
WC + 6 wt. % Co	100	4	1400

Table 5-1 : Reaction layer thickness between natural diamond and various hard metal alloys [183].

Naidich *et al.* [184] having establish in prior work [185] that diamond behaves similarly to graphite in wetting, studied the reaction kinetics of graphite wetted by a copper-chromium alloy (Cu-1.1wt.%Cr). It was found that increasing contact time and temperature increased the thickness of the reaction layer, with temperature being more effective than time. Kinetics was found not to be carbon diffusion controlled, but rather controlled by the interfacial reaction.

Molinari *et al.* [186], have found that when hot-pressing diamond in a pure cobalt matrix both graphite and an interstitial Co-C solid solution are present at the interfacial region. As the authors report, fracture in such composites occurred in the matrix, thus indicating a strong diamond-cobalt interface. Alloying cobalt with small amounts of tin (Sn) inhibited both the formation of graphite and Co-C solid solution. The ductile fcc α-Co phase was found to be preserved at the areas close to the diamonds, while the bulk matrix was constituted by the

thermodynamically stable hcp ε-Co phase. This was attributed to the different conditions applying at the diamond-interfacial zones caused either by overheating of the matrix in the vicinity of the electrical resistive diamonds or by the highly strained field near the rigid diamond crystals. The presence of tin in matrix has the effect of arresting oxygen by forming tin-oxides thus inhibiting the graphitization of the diamond leaving no carbon available for Co-C solid solution formation. Examination of the interface by Auger electron spectroscopy (AES), revealed that cobalt carbides were formed and remained stable during cooling down. According to the authors, this confirmed that graphitisation during consolidation is not attributed to the decomposition of formed carbides, but is the result of direct transformation at the diamond surface due to temperature and oxidation. In the case of pure cobalt matrix small amount of Co-carbides were identified at zones considerably far from the diamonds. The alloying with tin reduced the carbide contents to traces.

Levin *et al.* [187], studied the bonding of Nichrome (Ni-20wt.%Cr) and Co-20 wt.% W alloys to diamond under solid state processing. Consolidation was achieved by cold-sintering, which was followed by a heat treatment in either vacuum, a non-oxidizing or reducing (H_2) atmosphere. With both alloys stable carbides formed at the interface. Reaction kinetics was controlled by the supply of carbide forming elements to the interfacial zone. The reaction products were formed by rapid surface diffusion at the initial stages of contact during the cold-pressing step. The presence of the carbide layers already formed during the cold-sintering step, acted as a barrier for further diffusion during the subsequent heat treatment, leaving practically unchanged the thickness of the reaction zone. Mechanical testing showed that the formation of the carbides was beneficial for the strength of the composites. Fracture occurred in the intermediate layer-matrix interface when the thickness of the reaction zone was below 3 microns. For thickness exceeding 5 microns the fracture path went mainly along the diamond-intermediate layer interface. As part of the study, it was revealed that annealing in a hydrogen atmosphere prevented any reaction from taking place.

This effect of hydrogen has also been reported by Naidich [115], who reported that annealing of Mo-coated diamonds in the presence of hydrogen results in loss of adhesion strength between the coating and the diamond due to the disruption of the interfacial bonding. In the same study, Cr-coated diamonds annealed in the same atmosphere were not affected by the presence of hydrogen. According to the author, the hydrogen penetrated through the coating layer and reached the coating-diamond interface where it disrupted the metal-carbon bonds. Molybdenum-

carbon bonds were preferably disrupted because of the lower affinity of carbon for molybdenum compared to that for hydrogen and chromium.

Scott *et al.* [129] investigated the wetting and bonding of copper alloyed with small amount of Cr, Ti or V. Similarly to work of others, it was found that the transition elements migrated to the interface and formed carbides. It was found that the optimum alloying concentration for achieving the highest bonding strength was below that needed to induce wetting. This observation coupled with measurements of interfacial carbide layer thickness, led the authors to the conclusion that higher concentration of carbide formers result in more intense carbidisation leading to interfacial strength reductions. The authors proposed a model for the nucleation and growth of the carbide layer. According to this model, initially and after the first contact is achieved, islands of carbide nucleate at favoured sites on diamond surface. While bonded to both the underlying diamond and the overlying metal matrix, these islands are then grown epitaxially and are strengthened. At this stage the carbides form a chemical bridge between the diamond and the metal alloy. Increasing the concentration of the reactive element in the alloy increases the size and rate of formation of the carbide nuclei, and as these grow they contact each other and form a continuous layer at the interface. After this point has been reached, the interface is unable to provide any further strengthening probably due to the presence of flaws or porosity in the thick brittle carbide layers. The average thickness of the carbide layer to form a continuous layer covering the diamond was approximately 0.1μm. Similarly to other studies, it was found that with intensification of carbide formation the fracture path migrated from the carbide-matrix interface to the diamond-carbide interface.

The same group of researchers in a later article [188], examined the bonding to diamond of Cu- and Ni-based alloys with Cr, Ti and V additions under solid state processing. Somewhat similar results as those obtained under liquid state bonding were achieved. Addition of carbide formers was found rather beneficial for the copper alloys although the achieved bonding strengths were lower than that obtained with the liquid alloys. Alloying of nickel gave also an enhanced bonding strength, but the increase was much smaller compared to that obtained for copper alloys. Bonding strength increased with processing time and temperature. According to the observations and their proposed *carbide islands* model described above, the authors estimated that the carbide islands will coalesce to form a continuous layer when they reach a thickness of about 0.01 microns. This thickness is smaller compared to when contacting with the liquid phase. This observation and the fact that processing takes place at lower temperatures, led the authors to the

assumption that under solid state processing there seams to exist more interfacial carbide nucleation sites available, so that the islands join to form the layer when they are still thin.

Lin *et al.* [189] studied the significant changes in bonding achieved when incorporating 15wt.%Ti in a bronze (88Cu-12Sn wt.%) matrix alloy. In consistency with the work of others, Ti was found to migrate from the bulk matrix areas to the diamond-matrix interface. Carbide was formed at the interface in a thickness of about 3-5 microns. The titanium reached its alloy concentration at distances of the order of 40 microns. While titanium was enriched as approaching diamond the other matrix constituents were accordingly depleted.

Duda [151] examined by EDAX analysis the element distribution of diamond composites having diamonds coated with either a Ni- or a composite Co-Ni layer. When such diamonds were incorporated in bronze alloys with additions of SiC fillers and small amounts of Al and Zn, the Ni- or Co-Ni-C solid solutions were formed at the interfacial region at a zone of thickness of about 5-10 μm. A small amount of the other elements was found to have been diffused in the interfacial zone, and the author suggested that probably complex intermetallics were formed with Cu and Ni being the base elements of such phases.

Akuyz *et al.* [190] studied the interfacial bonding in Co-based matrices alloyed with variable amounts of chromium. Chromium was found to segregate at the interface with possible carbide formation. Enhanced interfacial bonding was associated with increased chromium content as indicated by the increased number of cleaved crystals found on examined fractured surfaces. For alloying additions exceeding 10%wt. there was no significant change in interfacial bonding.

There are several other reported studies [191-194] on characterization of diamond composites, in which the binder consisted of a relatively inert metal or alloy activated by variable additions of a carbide-forming element. In all these studies, the carbide-forming element was found to migrate towards the diamond surfaces, where it preferentially formed carbides at variable degrees. Similarly, to the other studies presented above, an enhancement of interfacial strength was found with increasing the carbide forming element additions up to a level beyond which either no significant change was evident or even reduction of composite properties were observed attributed to the effect of excessive reactivity.

5.8 Wetting and Adhesion Strength of Diamond-Metal Interfaces

Wetting of diamond by liquid metals and alloys is very important when consolidation of the diamond composites is to be achieved either by liquid phase sintering or by the infiltration of porous diamond-containing compacts with a liquid metal binder. In practice, solid state sintering is the dominating processing method, which does not involve any liquid phase. However, wetting data may provide a means of qualitatively predicting the diffusion intensity of systems at the solid-state processing temperatures [195].

Wetting of a solid by a liquid metal can be represented by a liquid droplet resting on a flat solid surface. The wettability is assessed by the contact angle (θ) and the work of adhesion (W_α). The contact angle is the angle formed at the edges of the liquid meniscus with the solid substrate and the work of adhesion is the thermodynamic value, which characterize the energy of the interface bond [196]. These two factors are related with the well-known Young-Dupre equation:

$$W_\alpha = \gamma_{LG} \cdot (1 + \cos\theta) \qquad \textbf{(Eq. 5-1)}$$

where, W_α is the work of adhesion (erg/cm^2), γ_{LG} is liquid/gas interfacial energy (erg/cm^2) and θ is the contact angle (degrees) (Figure 5-7).

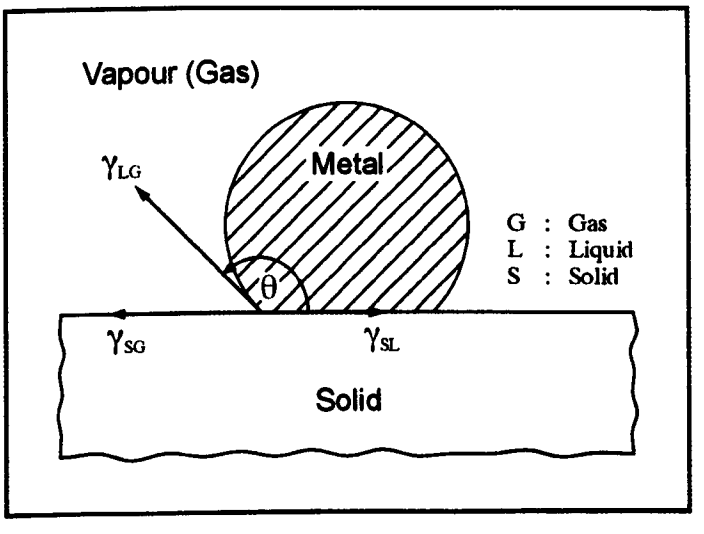

Figure 5-7 : Graphical representation of wetting.

High wettability of diamond is expected for those elements that enter into substantially intensive chemical interaction with carbon i.e. they form carbides, dissolve carbon and diffuse inside the solid phase [197]. Diamond and graphite differ very little energetically with their reaction intensities being similar. This is expected to reflect similar metal wettability for these two forms. This statement has been confirmed experimentally and permitted the substitution of inexpensive graphite for diamond in many trial studies [185]. Metals inert to carbon do not wet diamond and

their bonding energy (work of adhesion) is low, ranging in the 70-300 $mJ \cdot m^{-2}$ ($erg \cdot cm^{-2}$) interval. Alloying inert metals with small amount of carbide forming elements causes wetting of diamond. Adhesion energy of such alloys as well as for carbide-forming or strong carbon dissolving elements ranges from 2000 to 3000 $mJ \cdot m^{-2}$. Elements forming covalent bonds with carbon (such as Si, Ge, Al and B) wet the diamond, but their work of adhesion (1000-1200 $mJ \cdot m^{-2}$) is somewhat inferior compared to that for reactive transition metals.

Appendix B-1 contains a listing in a tabular manner of the contact angle, the work of adhesion and measured bonding strengths of various metals and alloys to diamond and graphite.

5.9 Reactivity and Solubility in Diamond-Metal Systems

The behavior of metals with respect to solubility or reactivity with carbon can be explained from their electronic structure. Transition metals tend to react with carbon by overlapping their *d*-orbitals with carbon's *p*-orbitals [25]. The reactivity of a metal towards carbon is specifically determined by its number of electron vacancies in *d*-orbitals [25, 185]. Therefore, the reactivity of transition metals generally decreases as moving from III-B towards II-B groups on the periodic table. This increase in reactivity is also demonstrated by the increased friction coefficient as the number of *3d* vacancies increases (Table 5-2).

Higher friction coefficient means that a greater amount of heat is generated during machining of metals. Cutting at high temperatures can trigger the chemical wear of diamond by oxidation, dissolution, graphitization or carbide formation [29, 30]. This is one of the reasons why diamond is not suitable for machining transition metals with high number of *d*-vacancies.

Metal	Vacant 4s and 3d orbitals	Friction Coefficient
Sc	9	1.0
Ti	8	0.8
V	7	0.7
Cr *	6	0.6
Mn	5	(0.6)
Fe	4	0.5
Co	3	0.5
Ni	2	(0.5)
Cu *	1	(0.4)
Zn **	0	(0.3)

Table 5-2 : Friction coefficients between *3d* transition metals and diamond [25].

( ) Projected value

* with vacant s-orbital and half-full d-orbitals

** with full s- and d-orbitals

The increasing reactivity between metal and carbon is also reflected in increasing solubility of carbon in metal. However, this trend of increasing solubility with increasing number of *d*-vacancies peaks at the iron group metals and then starts to decrease while reactivity is still

increasing. This is the result of excessive reaction between the metals and carbon. By exceeding a threshold value of dissolved carbon atoms in the metal, the carbon atoms start to loose mobility and eventually are engaged into the structure of the metal carbide. The increasing reactivity between a metal and carbon can also be seen by the maximum carbon-to-metal (C/M) ratio of stable carbides the element forms (Table 5-3).

Ratio	Ia	IIa	IIIb	IVb	Vb	VIb	VIIb	VIIIb			Ib	IIb
	K	**Ca**	**Sc**	**Ti**	**V**	**Cr**	**Mn**	**Fe**	**Co**	**Ni**	**Cu**	**Zn**
C/M	>3/1	2/1	2/1	1/1	1/1	2/3	3/7	1/3	1/3	1/3	0/1	0/1
N/M	-	-	1/1	1/1	1/1	1/1	2/3	2/3	2/3	2/3	0/1	0/1
H/M	-	-	2/1	2/1	2/1	2/1	1/1	1/1	1/1	1/1	0/1	0/1
	Rb	**Sr**	**Y**	**Zr**	**Nb**	**Mo**	**(Tc)**	**Ru**	**Rh**	**Pd**	**Ag**	**Cd**
C/M	>3/1	2/1	2/1	1/1	1/1	2/3	1/2	0/1	0/1	0/1	0/1	0/1
N/M	-	-	1/1	1/1	1/1	1/1	1/1	0/1	0/1	0/1	0/1	0/1
H/M	-	-	3/1	2/1	2/1	1/1	1/1	1/1	1/1	1/1	0/1	0/1
	Cs	**Ba**	**La**	**Hf**	**Ta**	**W**	**Re**	**Os**	**Ir**	**Pt**	**Au**	**Hg**
C/M	>3/1	2/1	2/1	1/1	1/1	1/1	1/1	1/1	0/1	0/1	0/1	0/1
N/M	-	-	1/1	1/1	1/1	1/1	1/2	0/1	0/1	0/1	0/1	0/1
H/M	-	-	3/1	2/1	-	-	1/1	-	-	-	-	-

Table 5-3 : Maximum atomic ratios of stable carbides, nitrides and hydrides for transition metals. (C/M) : Carbon/metal ration, (N/M) : Nitrogen/metal ratio, and (H/M) : Hydrogen/metal ration [25].

The type and intensity of interaction of metals with carbon atoms is in parallel lines to their interaction with nitrogen, oxygen and hydrogen atoms. Hence, a transition metal with a higher number of *d*-vacancies (such as Ti) is more easily oxidized during sintering or brazing, which sets stringent requirements for environmental control during high temperature processing. Indication of the reactivity of metals to carbon can also be drawn from the higher melting points of their carbides. Ellingham diagrams for carbides can also provide a comparative means to assess the thermodynamic tendency for a metal to react with carbon, with larger negative values of free enthalpies of formation (ΔG) to indicate more stable-carbides (see Appendix B-2).

If there are not sufficient *d*-vacancies, the reactivity of the transition metal toward carbon is not strong enough to form carbides. Carbon atoms are not tied up in fixed places, but form free-moving solutes. However, the amount of such solutes depends on the reactivity of the metals. Thus, elements with no vacancies in *d*-orbitals, e.g. Cu, Ag or Zn, can dissolve only a trace amount of carbon. On the other hand, elements with many vacancies, e.g. Sc, Ti or V will readily form stable carbides. Only metals with moderate amounts of vacancies in *d*-orbitals, e.g. Fe, Co or Ni, can dissolve a substantial amount of carbon. Appendix B-3 contains a listing of the eutectic solubilities of carbon in solid and liquid metals as well as the estimated carbon solubilities for solid and liquid metals at a temperature of 1000°C.

6

Mechanical Properties and Performance of Diamond MMCs

6.1 Introduction

Diamond MMCs for cutting and sawing applications are composed of a dispersion of diamonds in a metal-matrix. This kind of material could be classified as belonging to the category of the discontinuous composites having a particulate type of reinforcement. However, diamond composites form a special category of particulate MMCs, because of the characteristics of the diamond-reinforcement. Diamond crystals have an angular shape, are very large and extremely stiff. In typical particulate MMCs, the reinforcement size rarely exceeds the size of 50-100 μm, whereas in diamond composites for sawing, cutting or drilling typically crystals range in sizes of 20/80 US mesh (approx. 150-900 μm). Only diamond composites for fine grinding or polishing utilize smaller grit that fall within the reinforcement size range of common particulate MMCs.

In the first part of this chapter a brief discussion about basic mechanics and failure mode of particulate MMCs will be given with special attention to large and rigid particle reinforcement, which best describes the situation of diamond MMCs. The discussion will then be carried on reported mechanical properties of diamond MMCs, followed by a presentation of data related to mechanical properties and wear performance of coated-diamond MMCs.

6.2 Particulate-Composites Mechanics

Central to an understanding of the mechanical behaviour of a composite is the concept of load sharing between the matrix and the reinforcing phase [198]. In any type of composite material there is a requirement for some sort of load transfer between the composite constituents in order for the composite structure to operate. Composite materials are inherently inhomogeneous, in terms of both elastic and inelastic properties. As a consequence, on applying a load a non-uniform distribution of stress is set-up within the composite.

Particulate composites can be divided into two broad categories depending on their deformation behaviour under load. Thus, particulate composites can be divided into composites in which the dispersed reinforcement particle can deform under load, and composites in which the dispersoid does not deform under load [199]. In the former composites, if conditions for load transfer across the interface are satisfied (see later section), the dispersed particles can contribute substantially to the overall strength of the composites. In such composites, the bonded reinforcement to the matrix constrains the deformation of the latter when the composite structure is loaded. Improvement of the mechanical properties of the composite is realised as increased strength in tension or compression as compared to the non-reinforced matrix, which is however accompanied by a decrease in ductility (elongation-to-fracture).

In particulate composites in which the dispersed reinforcement does not deform under load, the particulate phase remains essentially rigid, imparting strength to the composite, but drastically lowering the ductility below that of the matrix phase alone. In this class of composites the duty of the reinforcement may not primarily be the strengthening of the matrix, but to improve other properties such as wear resistance, oxidation resistance etc. Diamond composites belong to this group of materials, since the diamond particles are rigid and remain elastically strained under loading conditions.

Thus, the discussion that follows will be restricted only to composites with non-deformable particulate reinforcement.

6.2.1 Elastic Behaviour

Throughout the years, much effort has been devoted to understanding and predicting the distribution of stresses within a loaded composite in order to determine its elastic response. Apart from experimentally establishing the elastic properties of composites (Young's modulus, proof stress, ductility etc.) numerous models have been put forward to predict the stress distributions in

composites, most commonly such models giving prediction of the modulus of elasticity (Young's modulus).

When the composite is loaded, the matrix is restricted from deforming in the same manner it would if it was alone. This restriction of matrix deformation imposed by the presence of the rigid particles results in a hydrostatic state of stress generated in the matrix. The magnitude of the restrain is unknown and complex, but it is a function of the elastic properties of the composite constituents (Young's modulus and Poisson's ratio). Variation in hydrostatic constrain will vary from point to point in the composite arising from constructional variations in the composite, such as spatial distribution of reinforcement, size of reinforcement, shape of interfaces etc. The greater disparity in stiffness between reinforcement and matrix in non-deformable particle-reinforced MMCs prevents the hydrostatic stress-state to reach the levels obtained in composites with deformable particles.

One of the basic and fundamental expressions of the elastic modulus in composite materials mechanics is the *rule-of-mixtures*, which results from modelling the situation in a composite where both reinforcement and matrix are equally strained [200]. The elastic modulus of a two phase non-deformable particle reinforced MMCs will be below the value predicted by the rule-of-mixtures and above the value which results when modelling the situation of equally stressed composite constituents [199]. The bounds of the elastic modulus are given by the expression:

$$\underbrace{\frac{E_m \cdot E_p}{V_m \cdot E_p + V_p \cdot E_m}}_{\text{Lower bound}} \leq E_C \leq \underbrace{V_m \cdot E_m + V_p \cdot E_p}_{\text{Upper bound}}$$

Lower bound
Equal stress situation
(Reuss Model)

Upper bound
Equal strain situation
Rule-of-Mixtures (Voigt model)

where, E is the Young's modulus and V the volume fraction of each phase ($V_m = 1\text{-}V_p$) with the subscripts c, m and p denoting the composite, matrix and particle respectively. According to Hashin and Shtrikman [201] the upper and lower bounds of non-deformable particle reinforced MMCs can be predicted with even more stringent elastic modulus bounds than the ones given above (see Appendix C.2). A variety of other expressions for the elastic modulus, some even empirical or semi-empirical, have been suggested, with that of Halpin and Tsai [202] and Cohen and Ishai [203] being frequently used for relatively fast and simple calculations (see Appendix C.3 & C.4). Most of the models involve mathematical approximations while some being rather limited in terms of properties that can be predicted, while others are computationally daunting. The Eshelby method is a useful model for predicting a wide range of composite properties with a rigorous mathematical approach. Although the originally derived equations are based on an

ellipsoidal particle shape the equations can be fairly easily transformed to suit other reinforcement shapes [204].

6.2.2 Plastic Deformation

Since the stiff reinforcement remains elastic as the composite is loaded, the plastic behaviour of the MMCs will depend on factors governing the plasticity of the matrix. These factors can broadly be divided into two areas; those affecting the stress state of the matrix, and those, which alter the flow properties of the matrix [205].

The stress-state in the matrix varies greatly from point to point and is more severe at the sharp corners of irregular shaped particles, such as the edges of the angular synthetic diamond crystals. Even for low applied stresses to the composite, matrix stress peaks at such regions and might exceed the inherent matrix yield stress, while, at the same time, the average matrix stress is far below the inherent yield stress of the matrix. It has been found experimentally, that although premature micro-yielding occurs at rather low applied stresses, the global yielding of the composite will take place only when the average stress in the matrix is sufficiently high [205].

Internal stresses in a composite arise also by differential thermal contraction. The large disparity in the coefficients of thermal expansion (CTE) of matrix and reinforcement can lead to the build up of substantial residual stresses on cooling from the fabrication temperature [205]. Especially in the case of diamond composites, such residual stresses are significant due to the very small CTE of diamond compared to that of most metal and alloys. After cooling, the diamond particles are set in compression by the matrix, whereas the latter is left in a net residual tension. These internal stresses effectively pre-stress the matrix and therefore both composite behaviour in tension and compression are affected.

Microstructural effects arising from the presence of particles in the metal-matrix often modify the behaviour of the matrix and thereby the properties of the composite. Such effects might be dislocation strengthening and grain size refinement (for composites fabricated by cast methods).

The elongation of composites reinforced with non-deformable particles such as diamonds, is less than a few percent and therefore these composites are classified as brittle materials with low impact strength. The inability of the particulate reinforcement to be deformed under load results in a dependence of mechanical properties on volume concentration of the reinforcement and thus

the mean free matrix separation*. During deformation of the composite the developed stresses can temporarily or locally be relaxed. This requires a suitable mechanism of relaxation to exist, and that the process to be accompanied by decrease in the system free energy. Relaxation processes can be: particle cracking, interfacial debonding or sliding, matrix cavitation, dislocation motion and rearrangement, recrystallisation, diffusion and structural transformation [205]. The first three processes are catastrophic and therefore will cause the failure of the composite.

6.3 Failure

In particulate MMCs, fracture is thought to occur primarily by the formation and link-up of voids within the matrix formed at or near the particle/matrix interface [206]. Particle cracking has been observed for some particle/metal-matrix systems (e.g. SiC/Al-matrix), but in general a damage process of that kind has little likelihood to occur at such a scale to govern the composite failure.

6.3.1 Reinforcement Cracking

As mentioned above, particle cracking for the general situation cannot be solely responsible for the composite failure. The requirement for particle fracture to occur is achievement of interfacial bonding, which permits load transfer from the matrix to the reinforcement. Weak bonding is associated with absence of load transfer and thus void formation will occur with no particle-cracking taking place. If the stress-state in the reinforcement as induced by the load transfer is sufficient to cause particle cracking, the composite will be weakened because of the cracked particle acting as a void. This is because of a fracture particle being unable to carry significant levels of stress when the matrix is subject to loading. The fractured particle will resemble a flaw in the composite structure and thus, the loss of strength of the composite imposed by the particle cracking will depend on the relative size of this flaw.

It is known from composite mechanics, that the reinforcement stress is approximately independent of the particle size [206]. This suggests that reinforcement fracture will preferentially occur for larger particles due to the increased likelihood of larger particles to contain a sufficiently large flaw capable of promoting their fracture. If particle fracture was independent of particle size and was only a matter of load transfer, then it would be expected that smaller particles would tend to fail preferentially, since greater load transfer could take place

* The mean free matrix path (mfp) is a measure of how close the reinforcing particles are located in the composite and is given by : (mfp) = (2·d / 3·Vp) (1-Vp) , where *d* is the average particle diameter and *Vp* the volume fraction of particles.

across their increased surface area for a given reinforcement volume. The above considerations assign that judgement of degree of interfacial bonding by considering the evidence of particle cracking is valid only for comparisons between composites, when: ***(a)*** the reinforcement-matrix systems are the same; ***(b)*** the particle size is restricted to a specific narrow size range; ***(c)*** the quality of reinforcement is approximately given and constant; and ***(d)*** the reinforcement volume fraction is the same.

6.3.2 Void Formation

Void formation is associated with the ductile failure of a particulate MMC. The nucleation of cavities will preferentially take place at or in the immediate vicinity of the particle-matrix interface where high levels of hydrostatic stresses are encountered, i.e. interfaces perpendicular to the tensile axis. The severe stress-state at these areas is attributed to the high levels of triaxial constraint and the increased matrix work-hardening, which result from both localisation of the applied plastic strain and from differential thermal contraction effects [206]. After voids or cavities have originated in the composite structure the further plastic deformation will cause the gradual growth of the voids and possibly the nucleation of new voids. Finally, these voids will link-up and the composite will fail (Figure 6-1).

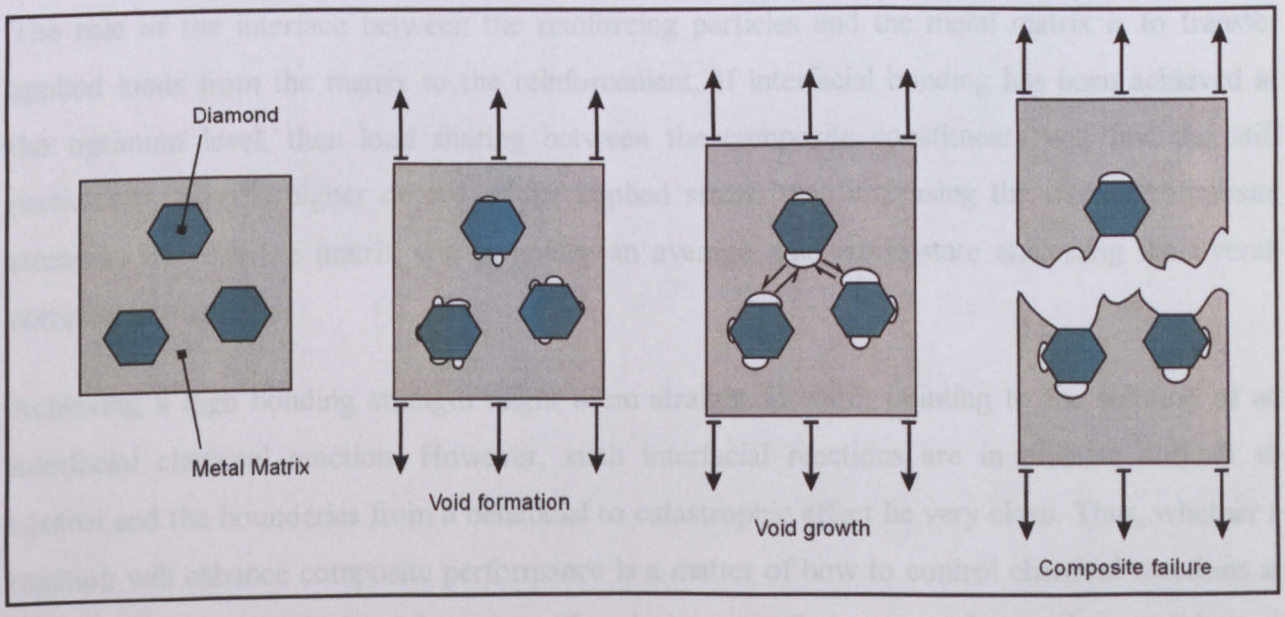

Figure 6-1 : A schematic representation of nucleation and link-up of voids to cause failure shown for a diamond reinforced metal-matrix composite.

For composites that are strongly bonded at the interfaces, voids might originate in the bulk matrix. In such cases it is expected that there must be a critical hydrostatic stress characteristic of the metal-matrix which when exceeded will allow the onset of void nucleation within the matrix. For weakly bonded composites it is probable for a critical normal or radial stress to exist, which

would determine the beginning of interfacial de-bonding. Because of difficulties in interfacial testing such values of critical stresses for void formation are not readily available and when existent are characterised by a lack in reliability. However, useful estimates of the void growth as a function of local stress for a given overall composite strain rate can be obtained. Some factors which tend to encourage the formation of voids are [206]: ***(a)*** large particle size, ***(b)*** high matrix flow stress, ***(c)*** large imposed plastic strain; ***(d)*** particle clustering; ***(e)*** low adhesion work; ***(f)*** particles located on grain boundaries (for small size particles); ***(f)*** large particle surface normal to loading axis; ***(g)*** matrix with small grain size and ***(h)*** weak interfacial bonding.

The degree of bonding at the interfacial region is of great importance and will strongly affect the composite behaviour. The shape of the reinforcement also plays a significant role in the void nucleation process. Angular particles will give rise to high local stresses, which however can be relieved by local microplastic flow. In contrast, spherical particles are associated with high hydrostatic stresses, which are much more prone to induce voiding. However, comparing the net effect of particle shape finds spherical particles to be associated with the lowest rates of void nucleation and growth [207].

6.4 The role of the Interface

The role of the interface between the reinforcing particles and the metal matrix is to transfer applied loads from the matrix to the reinforcement. If interfacial bonding has been achieved at the optimum level, then load sharing between the composite constituents will find the stiff particles to carry a higher degree of the applied stress, thus increasing the overall composite strength, whereas the matrix will be under an average mild stress-state enhancing the overall composite toughness.

Achieving a high bonding strength might seem straight forward, pointing to the solution of an interfacial chemical reaction. However, such interfacial reactions are in practise difficult to control and the boundaries from a beneficial to catastrophic effect lie very close. Thus, whether a reaction will enhance composite performance is a matter of how to control chemical reactions at the interfacial zone, which might occur either during manufacture or under service conditions at high temperature. In knowledge of these difficulties, it has been common practice to apply diffusion barrier coatings on the reinforcement to inhibit interfacial chemical reactions in composite reactive systems (e.g. TiB_2 coatings on SiC reinforcements incorporated in a Ti matrix) [181]. Interfacial reactions have been found to deteriorate the composite properties either by the formation of a thick brittle reaction product at the interfacial region and/or by the attack of

the reinforcement. However, there are numerous composite systems where interfacial reactions have been found beneficial, provided that the reaction layer thickness remains at low levels. Such systems are the diamond composites where many experimental results address the positive effects of an interfacial reaction, as has been reviewed analytically in Chapter 4. In addition, single or multiple layers have been deposited on reinforcements not for inhibiting reactions, but to promote interfacial bonding in non-reactive systems, or in order to manipulate the reaction intensities between reinforcement and matrix, or even to provide additional characteristics to the interfacial zone, such as stress absorbency, oxidation resistance etc. (see Chapter 4).

Although a strong bond is usually desirable, there are instances where a weak bond can become beneficial for the overall composite toughness since inelastic processes taking place at the interfacial zone can promote crack deflection. Inelastic processes at the interfacial region can arise from differential thermal contraction and from prior plastic flow of the matrix, as well as by the application of an external load. Inelastic interfacial phenomena can activate a variety of processes at the reinforcement-matrix boundary as illustrated in Figure 6-2.

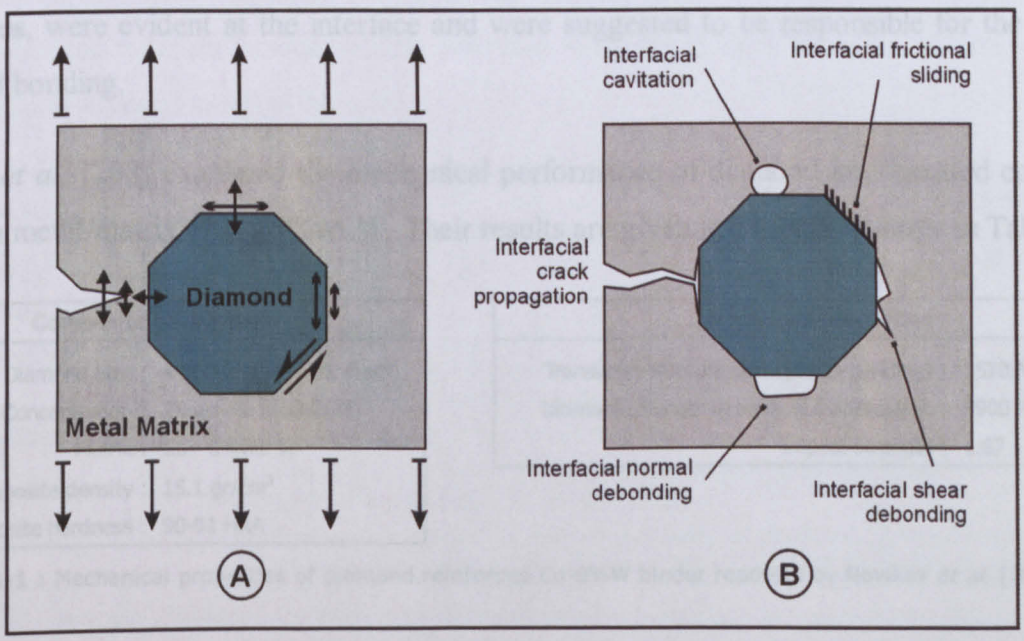

Figure 6-2 : Schematic illustration of stresses **(a)** near the interface in a diamond composite arising from an applied load and from differential thermal contraction, and **(b)** the various inelastic interfacial processes they initiate.

6.5 Mechanical Properties of Diamond MMCs

This section reviews reported mechanical properties for diamond-impregnated composites with particular attention to systems having either reactive alloying elements incorporated in the matrix or containing metal-coated diamonds.

Gutmanas *et al.* [51] prepared cylindrical diamond composites by cold-sintering followed by a subsequent heat treatment and obtained the stress-strain curves after loading the samples in a specially designed shear testing device. All tested matrices contained alloying elements reactive to diamond. Tested matrices included pure tantalum, Inconel 600 (76Ni-15.8Cr-7.2Fe) and stainless steel 830L (46Fe-29Ni-20Cr-3Cu-2Mo). The best results were obtained for samples cold sintered at the highest pressure of 3.5 GPa (35kbar) and subsequently annealed at 950°C in a nitrogen atmosphere. Composites having a tantalum binder gave the highest strengths when consolidation was made at the above optimum conditions. From microscopical examination of fracture surfaces, the authors observed high strengths to be associated with increased number of cleaved diamond crystals. In such samples, layers of a reaction product, which were assumed to be carbides, were evident at the interface and were suggested to be responsible for the achieved interfacial bonding.

Novikov *et al.* [208] examined the mechanical performance of diamond impregnated composites that had a metal-matrix of Co-6%wt.W. Their results are given in a tabular manner in Table 6-1.

Composite parameters	
Diamond Size :	≈ 500μm (≈ 35 US mesh)
Diamond Concentration :	25 vol. % (100 CON)
Matrix :	Co - 6%wt. W
Composite density :	15.1 gr/cm^3
Composite hardness :	90-91 HRA

Measured properties	
Transverse Rupture Strength (in bending) :	1570 MPa
Ultimate Strength in uniaxial compression :	3900 MPa
Impact Strength :	1.67 × 10^4 J/m^2

Table 6-1 : Mechanical properties of diamond reinforced Co-6%W binder reported by Novikov *et al.* [208].

The authors based on solubility data claimed that initially cobalt at the interface dissolves carbon that originates from the diamond. Such dissolution continues until the zones of cobalt around the diamonds saturate in diffused carbon. Unable cobalt to further dissolve carbon, graphite will start forming at the interface. The onset of graphite formation was associated with the deterioration of interfacial strength. The authors suggested that in order to avoid the undesirable graphite growth at the interface, the interaction zone containing the dissolved carbon should not exceed 4-5 microns in thickness. If these conditions were satisfied, then enhanced composite performance was achieved. Examination of fractured surfaces after a fracture toughness test showed that the

matrix efficiently held the diamonds. The authors also determined that with increasing diamond concentration, the strength and fracture toughness decreased, but in all cases remained greater than the non-diamond reinforced reference samples. The authors concluded that the bonded diamonds offered considerable enhancement in toughness since the crack, which caused composite failure, was effectively deflected along the interfacial paths.

Levin and Gutmanas [107] examined a number of composites having natural, synthetic diamond grit or large diamond plaques reinforcement incorporated in a matrix of either pure or alloyed nickel or Co-based with W additions. The composites had the diamond reinforcement forming a single layer located at their middle. The fabrication process involved an initial cold pressing at 0.8 GPa followed by annealing of the compacts in various atmospheres and times. A subsequent cold sintering at a higher pressure and heat treatment was performed for some of the composites. The authors found that carbide-forming elements migrated towards the interface where they reacted with diamond to form carbides at the interfacial zone. Both bending and tensile strength of the composites were improved by the achievement of these interfacial reactions (Table 6-2). When the reaction zone remained below a thickness of 3 microns the preferred fracture path went through the reaction product-matrix interface while for thicker zones the fracture occurred at the diamond-reaction product boundary.

Mechanical Property	Consolidation steps	**Ni**	**Ni – 20 wt.% Cr**		**Co – 20 wt.% W**	
		With diamond	No diamond	With diamond	No diamond	With diamond
Bending Strength, TRS, (MPa)	1 + 2	-	-	150	-	200
Bending Strength, TRS, (MPa)	1 + 2 + 3 + 4	-	1200	600	1500	1100
Tensile Strength, MPa (Step 1+2)	1+2	250	-	500	-	320

Diamond	:	Natural EMB 16/20 , Synthetic SDA100 30/40 US mesh or plaques
Diamond Concentration	:	Single layer occupying 20% of intermediate cross-section
Matrix	:	**(A)** Pure Ni 1-2 μm, **(B)** Pre-alloyed Nichrome (Ni-20wt.%Cr) -325 mesh, **(C)** Co-20wt.%W with Co : 1-2 μm, W : ≈ 1 μm.
Composite consolidation steps	:	**(1)** Cold pressing 0.8 GPa, **(2)** Annealling at 900°C or 1000°C for 30, 40 or 60 min, **(3)** Cold sintering 3 GPa, **(4)** Heat treatment 900-1000-1100°C for 30 min, 1h or 3h.

Table 6-2 : Strength in bending and tension of diamond composites obtained by cold sintering [107].

Bronshtein *et al.* [209] studied in detail the mechanical performance of diamond composites with tungsten carbide based binders with 6 and 8 wt.% cobalt alloying additions. The authors, among other properties, established experimentally the Young modulus by a dynamic non-destructive method, the ultimate bending strength and fracture toughness K_{IC}. These properties were also calculated with the equations suggested by Majstrenko [210] in an earlier theoretical study on predicting diamond composite strength and fracture properties. The complete set of the experimentally obtained and calculated values are given in Table 6-3. The authors concluded that diamond size practically did not affect the Young's modulus, which was however not the case

for the bending strength. Calculated values predicted fairly well the Young's modulus and fracture toughness, but not the bending strength. The authors postulated that this large different arose from stress concentrations existent at the tensile stressed side of the bended specimens attributed to the existence of the angular diamonds. In order to incorporate this effect, the experimentally obtained bending strengths, were accordingly corrected and it was then found to be closely approached by the predicted values.

Metal-Matrix	Diamond Size μm	CTE $10^{-6}\cdot K^{-1}$		Young's modulus E_C (GPa)		Bend strength σ_C (MPa)			Fracture toughness K_{IC} (MPa·m$^{-1/2}$)	
		Measured	Calculated	Measured	Calculated	Measured	Corrected	Calculated	Measured	Calculated
Co + 6wt.% W	No diamond	6.19	-	635 ± 36	-	1600 ± 19	1600	-	10.1 ± 1.5	-
	200/250	5.99	5.54	630 ± 25	669	490 ± 5	833	650	9.1 ± 1.1	10.2
	500/630	5.69	5.54	640 ± 36	626	380 ± 7	684	580	10.0 ± 1.7	9.7
WC + 8wt.%Co	No diamond	6.22	-	648 ± 8	-	1930 ± 23	1930	-	13.6	-
	200/250	4.82	5.55	630 ± 24	658	460 ± 6	782	708	11.2 ± 1.4	12.8
	500/630	5.30	5.55	640 ± 12	618	360 ± 4	648	536	11.6 ± 1.4	12.3

Table 6-3 : Experimentally and theoretically calculated values of diamond composites obtained by Bronshtein *et al.* [209]. Calculated values were computed from equations proposed by Majstrenko [210].

Lin and Queeney [162] investigated the effect of diamond coating on the fracture resistance of notched cylindrical diamond composites in three-point bending. The authors established that the presence of the coating promoted interfacial bonding, which showed a significant effect in increasing fracture resistance compared to composites, which exhibited no interfacial activity (Table 6-4 on next page). The authors also measured the adhesion strength in tension of coated and non-coated diamonds brazed onto the matrix alloy. The non-coated diamonds displayed no measurable tensile strength, whereas the coated diamonds exhibited an interfacial tensile strength being approximately the 1/5 of the inherent tensile strength of the matrix alloy. According to the authors, this indicated that incorporation of the coated diamonds in the matrix alloy had caused the deterioration in composite strength, but because a certain degree of load transfer had taken place at the interface, the magnitude of composite strength reduction was much lesser compared to specimens with the non-coated grit.

Composite parameters	
Diamond Size	: 20/30 US mesh (600/850 μm) or 80/100 US mesh (150/180 μm)
Diamond Concentration	: 25 vol. % (100 CON)
Matrix	: Cu – 40 vol.% Ni
Diamond coating	: Inner : Ti-4V-6Al, 0.1-0.2 μm, Vacuum Deposition-1100°C-15 min Outer : Cu-10%Ni, 10-12 μm, Vacuum Deposition-1100°C-15 min

Fracture Resistance K_{IC} (MPa·m$^{-1/2}$)	
Matrix	: 26.15
Composite	: 17.10
With coated diamonds	: 21.40

Table 6-4 : Fracture resistance of composites incorporating with coated and non-coated diamonds as reported by Lin and Queeney [162].

Chen and Sung [111] tested a number of composites incorporated with multi-layered coated diamonds prepared according to their patented method. The tensile test specimens were prepared having only a single layer of diamonds arranged normal to the tensile axis and located at the middle of the gauge length. The diamonds (SDA100+ 30/40 US mesh) had an inner coating of Cr deposited by MVD and an outer coating of W layered by CVD. The matrix was a 80wt.% bronze (85Cu-15Sn) and 20wt.% W alloy and consolidation was achieved by means of hot-pressing (815°C / 24MPa / 3min). The tensile strength varied from approximately 103 to 169 MPa. Tensile strength was found to depend on the deposition temperature and time of the MVD chromium, with the highest values attained for a deposition at 770°C for 2 hours, which corresponded to a 0.1-0.4 micron chromium layer thickness. In all cases the tungsten layer had a constant thickness of about 10-11 microns. The tensile strength for composites reinforced with non-coated diamonds gave almost no measurable strength. Additional details about the coated diamonds and methods used in this study were given in Table 4-6.

The same inventors in a later patent [94] prepared samples in the same manner as above but with coated diamonds having an inner W-layer of 10 microns deposited by the same CVD technique and an outer layer of nickel, 30 microns thick, deposited by electroless plating. The tensile strength was found to be of the order of 138 MPa, but when the diamonds were mechanically etched prior to the CVD of tungsten the strength reached the value of 241 MPa, indicating that chemical but also mechanical factors contributed to the load transfer.

6.6 Performance of Coated-Diamond Reinforced MMCs

As discussed extensively in Chapter 4, there exist numerous published articles reporting enhanced diamond retention due to interfacial bonding achieved by either carbide forming alloying elements in the matrix or by using specially engineered metal coated diamonds.

Hsieh *et al.* [95] examined the effects of incorporating Ti-coated diamonds in iron and Fe-11.3 wt.% Ni matrices. The increased retention of the coated diamonds was clearly evident as demonstrated by the increased protrusion and the almost absence of pull-out sites as seen from worn surfaces inspected by SEM. Cutting tests on granite showed segments incorporated with the Ti-coated diamonds to show up to ten-fold reductions in wear.

Manukyan *et al.* [114] have shown the average life of tools to be improved up to 35-40% with the use of coated diamonds. Table 6-5 presents the list of data from their field trials showing the lower diamond consumption associated with the coated grit.

Diamond wheels in cutting of Glass Ceramic

Diamond coating	Matrix	Specific Consumption of diamonds
Titanium	80%Cu-20%Sn	0.08 mg/cm^3
Uncoated		0.17 mg/cm^3
Iron	80%Cu-20%Sn	0.11 mg/cm^3
Uncoated		0.19 mg/cm^3

Test conditions :
Microhardness of workpiece = 8/12 x 10^3 MPa, Forward force = 25 N, Peripheral speed = 26 m/s, Feed rate = 30 mm/min,

Cutting Tuff

Diamond coating	Specific Consumption of diamonds	Comparative estimation
Titanium	0.08 x 10^{-6} crt/mm^3	1.87
Chromium	0.09 x 10^{-6} crt/mm^3	1.66
Iron	0.10 x 10^{-6} crt/mm^3	1.50
Uncoated	0.15 x 10^{-6} crt/mm^3	1.00

Diamonds : AC 15 400-500 microns

Diamond wheels in cutting granite

Diamond coating	Quantity of Granite processed, (cm^3)	Consumption of wheels, G	Specific Consumption of diamonds
Titanium	18.8214	177	5.26 x 10^{-5} gr/cm^3
Uncoated	18.8214	344	9.95 x 10^{-5} gr/cm^3

Test conditions : Type of wheel : AOCK 500mm, Rotational speed = 540 RPM, Feed rate = 600 mm/min

Table 6-5 : Results of commercial testing of diamond tools incorporating coated diamonds [114, 117].

Chen and Sung [111] conducted a number of wear tests with diamond blades having segments incorporating multi-layered coated diamonds prepared according to their patent (see also previous section §6.5 and Table 4-6). The test consisted of sawing slabs of cured concrete at a fixed depth. All slabs were prepared under strict and identical conditions in order to ensure constant concrete properties. Both the wear and the speed of cut were determined for various combinations of diamonds incorporated in bronze-cobalt matrix. The wear of the saw blades was determined by the loss in segment height. The use of coated grit was found to significantly reduce tool wear. The best results in terms of low wear, were exhibited by the blades with segments containing coated diamonds having their inner chromium layer deposited by MVD at 770°C. This was in line with the mechanical properties presented in the previous section (§6.5), since the same type of composites gave the highest tensile strengths. Comparing the worn surfaces of tool segments showed that almost twice as much diamond from the coated grit was retained. However, non-coated diamonds allowed higher cutting speeds to be achieved. The authors explained this behaviour in terms of probable deterioration of diamonds by the various coating heat treatments, which might have caused diamonds to become more friable than the original non-coated grit. It was thus assumed that during sawing the more friable coated grit gave a larger number of cutting points so that under the constant applied pressure on the tool, each individual diamond point received a lesser fraction of the load as compared to the less friable non-coated grit. Under such mild loading conditions the coated grit could not perform at equal rates as the non-coated, thus the total cutting speed of the tool was essentially reduced.

7

Experimental Procedures

7.1 Introduction and Aim of Experimental Work

The experimental work described in this thesis is essentially divided into three areas.

The first part (§7.2) includes the characterisation of the tested coated and non-coated diamond crystals and additionally covers the work carried out to investigate the changes occurring to diamond crystals when heated at high temperatures with and without the presence of various metals. Two types of systems were examined. These were systems of plain non-coated diamonds in contact with various elemental metallic powders and systems of metal-coated diamonds.

The second part (§7.3) covers an in-depth analysis of mechanical properties of coated-diamond reinforced MMCs. The aim of this series of tests was to establish which of the commercially available coated diamonds were potentially capable of providing enhanced composite properties under standard industrial conditions.

The third and final part (§7.4) was a further stage of the previous experimental step. The goal was to explore the potential of achieving enhanced and optimised composite properties of selected coated diamonds incorporated in specially engineered alloy metal matrices.

7.2 Diamond Characterization & Diamond Reactivity

The diamonds tested in this research included both metal-coated and non-coated crystals. All the employed diamonds are available commercially. Diamond characterisation involved primarily SEM examination to establish the morphology and surface status of the crystals. SEM was also employed in defining the condition and the approximate thickness of the deposited metal coatings. Supplementary X-ray diffraction (XRD) was employed to identify the coating composition.

7.2.1 Tested Diamonds – Coated & Non-coated

7.2.1.1 Diamond Types

Three types of synthetic diamonds were used and are listed in the table below.

Designation	US Mesh Size	Source	Grade
SYN-1	30/40 or 40/50	De Beers Industrial Diamonds (DB)	SDA100
SYN-2	50/60	General Electric Superabrasives (GE)	MBS960
SYN-3	30/40 or 40/50	De Beers Industrial Diamonds (DB)	SDA75

Table 7-1 : List of the synthetic diamonds used in this research.

Table 7-2 on next page lists the various types of coated diamonds tested in this research. In addition to the type of metal coating the table gives a short description of the deposition method as has been disclosed by the manufacturers or is available in literature.

7.2.1.2 SEM Characterisation

SEM examination was performed with a JEOL 6400 WINSEM scanning electron microscope equipped with a NORAN energy dispersive X-ray EDAX analysis instrument. In addition to crystal characterisation, SEM examination at high magnifications also served to determine the thickness and morphology of the various metal coatings. Thickness was estimated from crystal locations where the metal coating had partially fractured or peeled-off enabling positioning of the coating cross-section perpendicular to the scanning electron beam. A minimum of three measurements was taken for each type of coated diamond. For some of the metal-powder coated diamonds it was impossible to measure a thickness with the above-described method. In those cases, the thickness was calculated from weight/volume measurements according to a simple model given in Appendix D-1.

Coating Type	Diamond Crystal Substrate	Manufacturer	Deposition Method	Description
Co - powder	SYN-3	Fuji Paudal Kabushiki Kaisha (J)	PC	Diamond granulated with fine Co powder. The technique is described in Ref. [161] (see also §4.5.5).
Cr	SYN-1 & SYN-3	Teer Coatings (TC)	PVD	Process: Closed field unbalanced magnetron sputter ion plating (Process parameters were not disclosed).
Cr - powder	SYN-1	Nimbus Diamond Tool (NDT)	PC	Chromium powder coating granulation. Process steps : (a) Mixing of diamonds with metal powder and organic substance, (b) sieving, (c) baking, and (d) milling
Cr(C)	SYN-3	Teer Coatings (TC)	PVD	Chromium enriched with free carbon. Process : Closed field unbalanced magnetron sputter ion plating (Process parameters were not disclosed).
Ti	SYN-1	De Beers (DB)	CVD	Chemical Vapour Deposition of Ti. Details of the process were not disclosed.
Ti	SYN-1 & SYN-3	Teer Coatings (TC)	PVD	Process : Closed field unbalanced magnetron sputter ion plating (Process parameters were not disclosed).
Ti/Cr	SYN-3	Teer Coatings (TC)	PVD	Multi-component coating co-deposition of Titanium and Chromium. Process : Closed field unbalanced magnetron sputter ion plating (Process parameters were not disclosed).
W	SYN-3	Teer Coatings (TC)	PVD	Process : Closed field unbalanced magnetron sputter ion plating (Process parameters were not disclosed).
W	SYN-1	Norton Company (NC)	CVD	Tungsten Chemical Vapour Deposition. Process is described in Ref. [109] and process parameters can be found in Ref. [111, 112]. Additionally refer to §4.5.2 and Table 4-6.
W - powder	SYN-1	Van Moppes (VM)	PC	Tungsten powder encapsulation. Process steps and parameters were not disclosed.

Table 7-2 : The various types of coated diamonds examined in this research. **CVD** : Chemical vapour deposition, **PVD** : Physical Vapour Deposition, **PC** : Powder encapsulation / granulation.

7.2.1.3 X-ray Diffraction

X-ray diffraction was performed with a Siemens Kristalloflex diffractometer (D500) employing Cu Ka radiation (λ=1.5406Å) with a Ni filter, operating at 40kV and 50mA. Diamonds were placed in the rectangular groove of a specially machined aluminium holder (Figure 7-1). The groove had a depth of approximately 0.5 mm and diamonds were attached in it with the aid of a two-face sticker tab. Typical testing involved the collection of diffraction data from 15 to 135 degrees at increments of 0.05 deg./5-secs. The resulting spectra were analysed with the aid of the Siemens Diffrac-AT (Version 3) software that allows determination of peak position and intensities. The JCPDS-ICDD database was used as the reference for material identification.

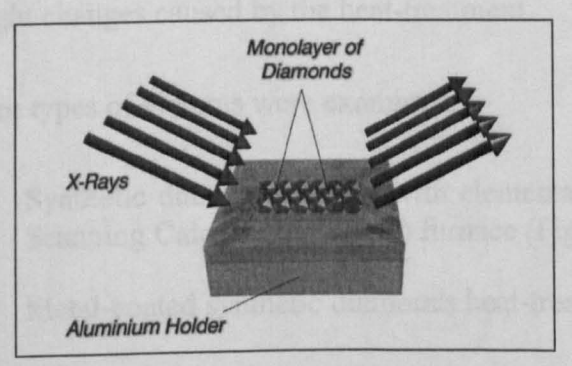

Figure 7-1 : X-ray diffraction test set-up.

7.2.2 Diamond Reactivity

The examination of the solid-state reactivity of bulk diamond crystals with metals is a difficult task for two main reasons. First, the high hardness of diamond makes sample preparation for most of the available techniques difficult or even impossible, and secondly, diamond composites typically involve alloy metal-matrices with interfacial regions of complex reactivity. It is obvious that establishing an understanding of the interaction between synthetic diamonds and metals involved in typical diamond-metal composite systems, could provide useful knowledge and assist in identifying the net effect of each metal on the diamond. This knowledge could then be a powerful tool in the understanding of reactivity in the complex diamond-composite systems that are of interest in practice.

With these considerations in mind, a testing method was designed based on a series of experiments aiming to establish the fundamentals of chemical reactivity/interaction of various metals with diamond. This testing method will be referred to as the "Diamond Reactivity Experiment (DRE)", throughout the remainder of this work.

The present section of this chapter describes the materials and methods related to the DRE. Complementary descriptions and details of individual procedures employed in the DRE and not completely described in the text that follows is given in Appendix D.

7.2.2.1 Diamond Reactivity Experiment (DRE)

The DRE was built-up by a sequence of experimental procedures, where initially a weighed quantity of synthetic diamonds was heat-treated in the presence of a given metal. Diamonds were subsequently separated from the metallic environment by a metal leaching process. An additional leaching process followed in order to dissolve any graphite that might have formed on the diamond surfaces. Diamonds were microscopically analysed following both the metal-leaching and the final graphite-leaching steps. For a series of systems supplementary diamond weighing and crystal counting were made at certain points of the DRE in order to establish the diamond weight changes caused by the heat-treatment.

Three types of systems were examined:

- Synthetic diamonds mixed with elemental metal powders heat-treated in a Differential Scanning Calorimetric (DSC) furnace (Figure 7-3 A),
- Metal-coated synthetic diamonds heat-treated in the DSC furnace (Figure 7-3 C), and

- Synthetic diamonds mixed with elemental metal powders and consolidated into disc shaped metal-matrix composites (segments) by a standard hot-pressing (HP) sintering treatment (Figure 7-3 B).

The diagrams given in Figure 7-3 on the next page outline graphically the 3 parts of the DRE as applied to the 3 types of systems investigated.

The same three types of synthetic diamonds as listed in Table 7-1 were employed for the DRE experiment. Table 7-3 on page 108 lists the metal powders that were employed and Table 7-5 on page 108 gives the details of the metal coated diamonds tested with the DRE.

7.2.2.2 Differential Scanning Calorimetry (DSC)

A Netzsch 404 DTA/DSC was employed for heat-treating the diamonds/metal-powder mixtures and the metal-coated diamonds (refer also to Figure 7-3 on page 107). In all situations samples were heated with the same time-temperature program in a constant flow of argon (Figure 7-2). Data were acquired by an electronic data collector and were forwarded to a computer allowing subsequent peak analysis and drawing of the temperature-heat flow curves.

Performing the heat-treatment in the DSC furnace served a dual purpose. The compact high temperature DSC furnace allowed the heating in a controlled inert atmosphere and at the same time permitted the monitoring of metal-diamond interactions.

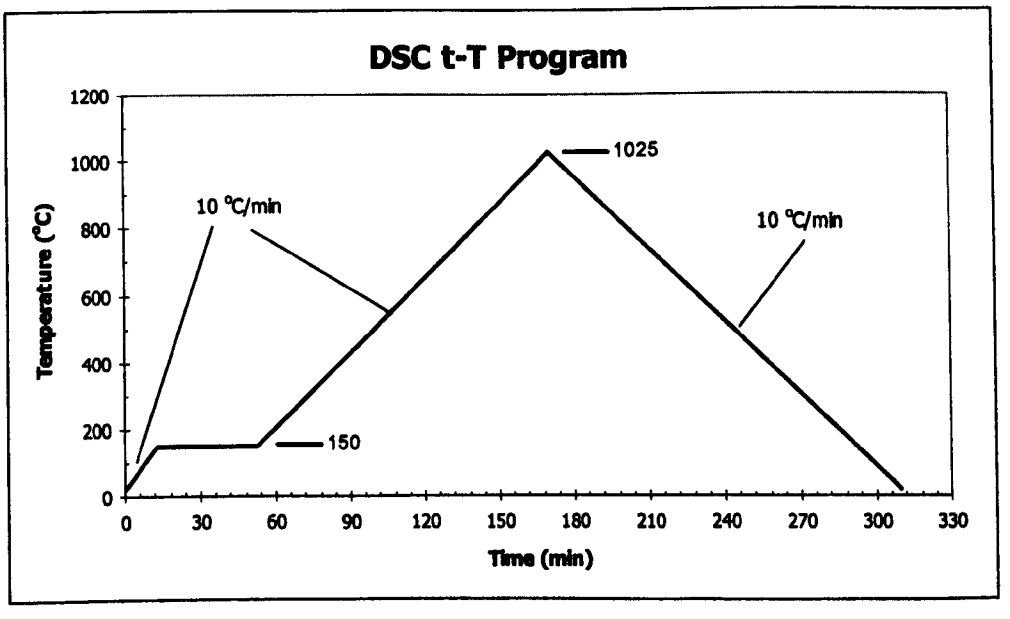

Figure 7-2 : The time-temperature program for the DSC heat-treatments involved in the DRE.

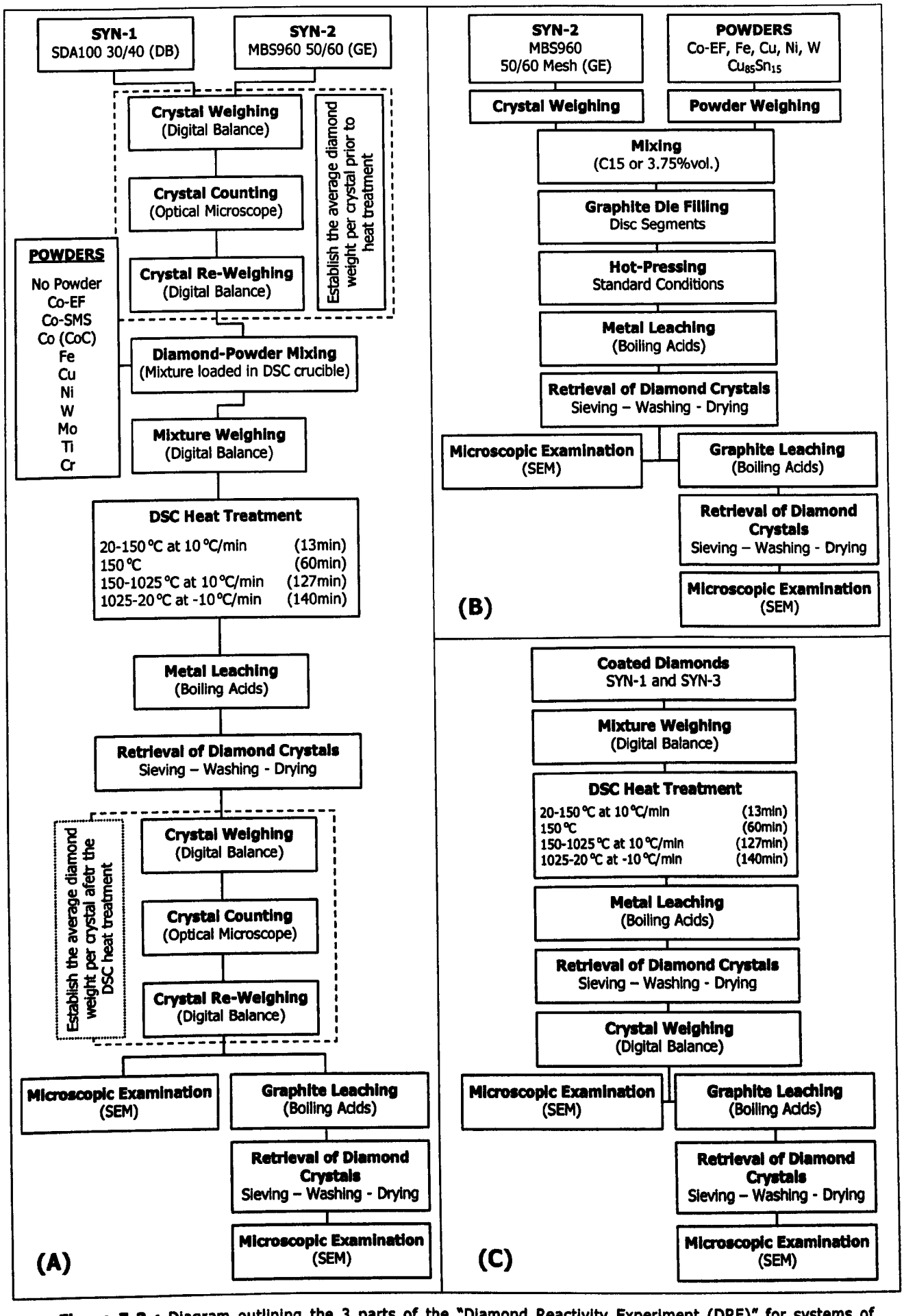

Figure 7-3 : Diagram outlining the 3 parts of the "Diamond Reactivity Experiment (DRE)" for systems of **(A)** metal-powders and diamonds, **(B)** hot-pressed diamond-metal composites and **(C)** metal-coated diamonds.

Metal Powder	Producer or Supplier	Grade – Powder Specifications
Co-EF	Union Miniere (Belgium)	Extra fine grade, 1.2-1.5 μm Fisher SSS
Co-SMS	Union Miniere (Belgium)	Submicron Size Grade, 0.8 μm Fisher SSS
Co (COC)	Eurotungstene Poudres (France)	COC, 1.6 ± 0.15 μm Fisher SSS
Fe	Union Miniere (Belgium)	Extra fine grade
Cu	Union Miniere (Belgium)	Extra fine grade
Ni	Union Miniere (Belgium)	Extra fine grade
W	Union Miniere (Belgium)	Extra fine grade
Mo	Union Miniere (Belgium)	Extra fine grade
Ti	Nimbus Diamond Tools (UK)	Extra fine grade
Cr	Nimbus Diamond Tools (UK)	-45 μm

Table 7-3 : List of the metal powders used in the various metal-diamond systems tested with the DRE.

Disc Segment Designation	Metal Matrix	Diamond Type	Diamond Concentration
HP-1	Co-EF	SYN-2 (MBS960 50/60 US Mesh GE)	C15 (3.15 %vol.)
HP-2	Fe	SYN-2	C15
HP-3	Cu	SYN-2	C15
HP-4	Ni	SYN-2	C15
HP-5	Mo	SYN-2	C15
HP-6	$Cu_{85}Sn_{15}$	SYN-2	C15

Table 7-4 : Composition of the disc shaped composites (segments) tested with the DRE. Consolidation was made by hot-pressing in graphite moulds at 850°C for 3 minutes at a pressure of 350 bar.

Coated Diamond Designation	Diamond Type	Diamond Size (US Mesh)	Metal Coating	Coating Deposition Method	Coating Manufacturer
CD2	SYN-3	30/40	Non-coated	-	-
CD3	SYN-3	40/50	Non-coated	-	-
CD4	SYN-1	30/40	Non-coated	-	-
CD5	SYN-1	40/50	Non-coated	-	-
CD6	SYN-1	30/40	Ti	CVD	De Beers
CD7	SYN-1	40/50	Ti	CVD	De Beers
CD8	SYN-1	30/40	Ti	PVD	Teer Coatings
CD9	SYN-3	30/40	Cr	PVD	Teer Coatings
CD10	SYN-3	40/50	Cr	PVD	Teer Coatings
CD11	SYN-3	30/40	Cr(C)	PVD	Teer Coatings
CD12	SYN-3	30/40	Ti/Cr	PVD	Teer Coatings
CD13	SYN-3	30/40	W	PVD	Teer Coatings
CD14	SYN-3	40/50	W	PVD	Teer Coatings

Table 7-5 : Details for the metal coated diamonds tested by the DRE.

7.2.2.3 Metal-Leaching Procedure

After the heat-treatment of the diamond-metal systems, diamonds were separated from their metallic environment by a leaching procedure. Metallic environment in this sense refers to the sintered metal powders (part A of the DRE), the hot-pressed segments (part B of the DRE) or the metal-coating of the coated grit (part C of the DRE). Metals were dissolved in boiling acid solutions. Sufficient leaching times were allowed in order to ensure complete dissolution of the metals. However, even for systems strongly reactive in leaching, a minimum of 1 hour leaching duration was endorsed. Leaching was only terminated when the signs of metal dissolution disappeared, in other words when the gas bubbles production at diamond surfaces ended. A full description of the metal leaching procedure is given in Appendix D-2.

7.2.2.4 Graphite-Leaching Procedure

Retrieved diamonds were subjected to an additional leaching step subsequently to the metal leaching, with the aim of removing any graphite that might have formed on the diamond surfaces during the heat-treatment. Graphite removal was achieved by treating the previously metal leached diamonds in a hot chromic acid bath. Crystals were immersed into the hot bath for at least 30 minutes before they were retrieved. Further details of the graphite leaching procedure are given in Appendix D-3.

7.2.2.5 Diamond Retrieval Procedure

Following each leaching step, diamond crystals were retrieved from the metal-acid solutions. The procedure involved initially the dilution of the acid with water. The solutions were then poured through a sieving column made of a 250 μm and a 100 μm mesh sieves. The sieves were then positioned in a stream of hot air in such a way to allow the drying of the oversize, which was comprised of the retrieved diamond crystals and occasionally contained small metal fragments that were not fully dissolved. In these cases, the metal fragments were carefully separated with the aid of vacuum tweezers under the light of a stereoscope. Diamonds were afterwards ultrasonically washed in a bath of acetone and then sieved, dried and retrieved in a similar manner as described above.

7.2.2.6 Diamond Weight Change Measurement Procedure

A series of diamond weight measurements were carried out in order to establish whether any crystal weight change occurred on the diamonds heat-treated with metal powders (part A of the DRE, see Figure 7-3). This was achieved by determining the average crystal weight prior to the

heat-treatment in the DSC furnace and after the retrieval from the metal leaching. The weight change was computed according to the following expression:

$$\overline{D} = \overline{D}_B - \overline{D}_A = \frac{WD_B}{\eta_B} - \frac{WD_A}{\eta_A} \qquad \textbf{(Equation 7-1)}$$

where, $\overline{D}$ is the calculated weight change in mgr based on the average diamond crystal weight values, $\overline{D}_B$ is the average crystal weight in mgr prior to the heat-treatment, $\overline{D}_A$ is the average crystal weight in mgr after the heat-treatment, WD_B is the weight in mgr of the tested quantity of diamond prior to the heat-treatment, WD_A is the crystal weight in mgr of the retrieved quantity of diamonds after the heat-treatment, and η_B and η_A are the numbers of counted crystals of the weighted diamond quantities prior and after the heat-treatment respectively.

Prior to mixing with the powder, a quantity of fresh diamonds was accurately weighed with a high precision digital balance (WD_B). The number of crystals comprising the weighed quantity was determined by counting the crystals with the aid of the magnifying lens of a stereoscope (η_B). An additional weighing was performed to ensure that there was no loss of crystals during the counting procedure. A similar sequence of weighing and crystal counting was employed for the retrieved diamonds after the metal leaching that followed the heat-treatment of the powder-diamond mixture.

7.2.2.7 Microscopic Examination

Microscopic examination of the tested diamonds was the most important aspect of the DRE. It was mainly based on Scanning Electron Microscopy supplemented by general Optical Microscopy.

7.2.2.7A Scanning Electron Microscopy (SEM)

Diamonds were examined at 3 stages of the DRE (refer to Figure 7-3 on page 107):

- in the "as received condition", in other words before the thermal treatment,
- after the thermal treatment and after metal leaching, and
- after the final graphite leaching step.

Analysis was performed either with a Phillips XL30 SEM or an environmental Phillips Field Emission Gun SEM (FEG-ESEM) operating in a high vacuum mode and equipped with an energy dispersive X-ray facility (EDAX-LEAP™ Detector with super ultra thin window). Both

Secondary (SE) and Backscattered (BSE) electron imaging modes were employed. Examination was carried out at a beam voltage of 10kV and a working distance of 10 mm unless otherwise stated. Crystals were spread on a self-adhesive carbon tab and were gold coated prior to examination. A minimum of 6 micrographs were taken for each sample, including representative images of a diamond crystal at a low magnification and micrographs of octahedral and cubic diamond faces at a magnification of x2000 in both SE and BSE modes. Additional micrographs were taken in those cases where specific surface features were detected.

7.2.2.7B Optical Microscopy (OM)

An optical microscope was primarily employed for the diamond crystal counting required for the diamond weight change measurements as described previously. However, in addition to this function the optical microscope was utilised to identify the colouring and the light reflection of diamond crystals after the various treatments.

7.3 Properties of Coated-Diamond Composites

7.3.1 Introduction - Aim

The series of experimental actions comprising the 2nd part of the experimental work of this research was aimed at determining the effect that metal-coating of diamond has on the mechanical properties of diamond reinforced composites (referred to as "segments"). The idea behind this objective is that improved mechanical properties are directly related to increased diamond tool performance by prolonged tool life and/or better cutting rates. In order to explore the true potential of beneficial usage of coated diamonds in industrial applications the raw material was selected from industrially available sources and the composite (segment) manufacturing methods followed common diamond tool production practice. In order to assure that any observed variation in the composite mechanical properties could be ascribed to the effect of the metal-coating and the coating-diamond interfacial bonding, it was necessary to keep as many as possible production parameters constant. Thus, parameters such as the metal-matrix composition, the diamond concentration and consolidation thermal treatment were kept the same for all tested composites. The diagram in Figure 7-4 outlines the experimental actions comprising the second experimental part of this research.

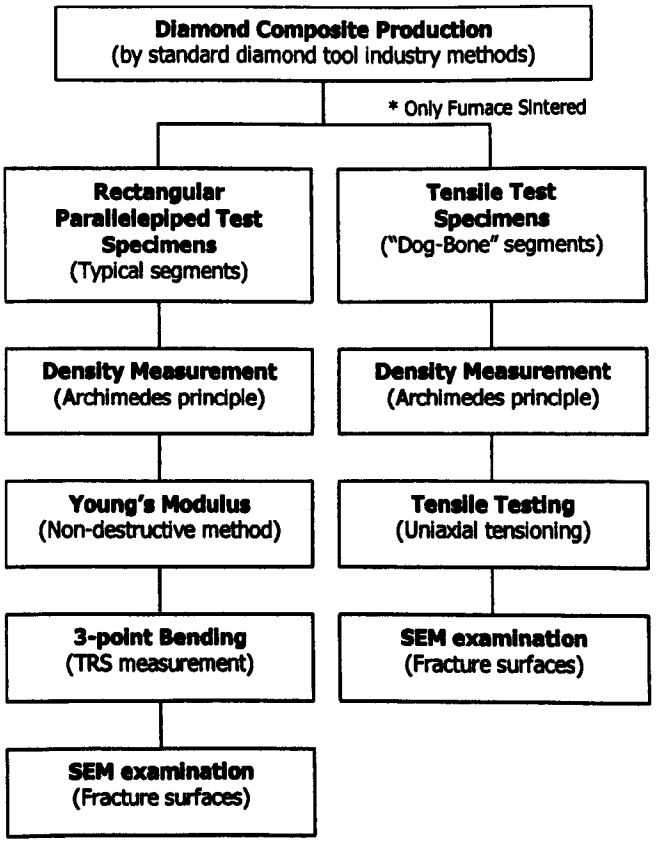

Figure 7-4 : Flow chart diagram outlining the experimental steps performed under the second experimental part of this research.

7.3.2 Materials & Composite Preparation

All types of raw materials that were used are commercially available. The preparation and consolidation of the diamond composites was performed by the author at the production facilities of *Nimbus Diamond Tool and Machine Company Ltd.*, at Burgess Hill, West Sussex, England.

7.3.2.1 Diamond Composites (segments) Composition

A series of selected types of both metal-coated and non-coated synthetic diamonds were incorporated into a standard metal matrix of cobalt, which is by far the most common metal used in the diamond tool industry. Table 7-6 lists some of the properties of the plain cobalt powder used as the metal-matrix of the diamond composites.

Powder type	:	Cobalt COC (min Cobalt 99.7%)
Source	:	Eurotungstene Poudres (France)
Fisher grain size	:	1.60 ± 0.15 μm
Oxygen content	:	Typical 0.5% (max 0.8%)

Table 7-6 : Details of the cobalt powder used as the metal-matrix for the diamond composites.

Both the coated and non-coated synthetic diamonds that were employed to formulate the diamond composites were from those also involved in the first experimental part and are listed in Table 7-3 (see page 108) and Table 7-5 (see page 108).

Composites were consolidated according to standard diamond tool manufacturing processes into rectangular parallelepiped specimens and into shapes to suit tensile testing ("dog-bone" type segments). A total of 59 sets of rectangular parallelepiped and 26 sets of "dog-bone" segments were prepared. Each set of the rectangular parallelepiped type segments comprised of 5 specimens whereas "dog-bone" type segments sets consisted of 3 samples. Specimens without diamond reinforcement and composites impregnated with plain non-coated diamonds were manufactured as well as those with the metal-coating in order to be used as a reference material for comparisons. Diamond concentration was 35* (8.75% vol.) for all rectangular parallelepiped segments and 25 (6.25% vol.) for the "dog-bone" specimens. Table 7-7 and Table 7-8 in the following pages list the parameters of the tested specimens.

* In diamond tool industry concentration is referred upon an unofficial standard where by definition concentration 100 equals to 4.4 carats per cm^3 (or 25% by volume).

	Segment Set Code	Number of Samples	Diamond Condition	Diamond Heat Treatment	Manufacturer	Coating Method	Diamond Size Range (US mesh)	Diamond Type	Reference Non-coated Segment	Reference Non-Heat Treated Segment
Sintered (FS)	CD 1 - FS	1-5	Blank (No diamond impregnation) - Reference segments						-	-
	CD 2 - FS	1-5	Non-coated	-	DB	-	30/40	SYN-3	-	-
	CD 3 - FS	1-5	Non-coated	-	DB	-	40/50	SYN-3	-	-
	CD 4 - FS	1-5	Non-coated	-	DB	-	30/40	SYN-1	-	-
	CD 5 - FS	1-5	Non-coated	-	DB	-	40/50	SYN-1	-	-
	CD 6 - FS	1-5	Ti - coated	-	DB	CVD	30/40	SYN-1	CD4	-
	CD 7 - FS	1-5	Ti - coated	-	DB	CVD	40/50	SYN-1	CD5	-
	CD 8 - FS	1-5	Ti - coated	-	TC	PVD	30/40	SYN-3	CD2	-
	CD 9 - FS	1-5	Cr - coated	-	TC	PVD	30/40	SYN-3	CD2	-
	CD 10 - FS	1-5	Cr - coated	-	TC	PVD	40/50	SYN-3	CD3	-
	CD 11 - FS	1-5	Cr(C) - coated	-	TC	PVD	30/40	SYN-3	CD2	-
	CD 12 - FS	1-5	Ti/Cr - coated	-	TC	PVD	30/40	SYN-3	CD2	-
	CD 13 - FS	1-5	W - coated	-	TC	PVD	30/40	SYN-3	CD2	-
	CD 14 - FS	1-5	W - coated	-	TC	PVD	40/50	SYN-3	CD3	-
Hot Isostatic Pressed (HIP)	CD 1 - HIP	6-10	Blank (No diamond impregnation) - Reference segments						-	-
	CD 2 - HIP	6-10	Non-coated	-	DB	-	30/40	SYN-3	-	-
	CD 3 - HIP	6-10	Non-coated	-	DB	-	40/50	SYN-3	-	-
	CD 4 - HIP	6-10	Non-coated	-	DB	-	30/40	SYN-1	-	-
	CD 5 - HIP	6-10	Non-coated	-	DB	-	40/50	SYN-1	-	-
	CD 6 - HIP	6-10	Ti - coated	-	DB	CVD	30/40	SYN-1	CD4	-
	CD 7 - HIP	6-10	Ti - coated	-	DB	CVD	40/50	SYN-1	CD5	
	CD 8 - HIP	6-10	Ti - coated	-	TC	PVD	30/40	SYN-3	CD2	-
	CD 9 - HIP	6-10	Cr - coated	-	TC	PVD	30/40	SYN-3	CD2	-
	CD 10 - HIP	6-10	Cr - coated	-	TC	PVD	40/50	SYN-3	CD3	-
	CD 11 - HIP	6-10	Cr(C) - coated	-	TC	PVD	30/40	SYN-3	CD2	-
	CD 12 - HIP	6-10	Ti/Cr - coated	-	TC	PVD	30/40	SYN-3	CD2	-
	CD 13 - HIP	6-10	W - coated	-	TC	PVD	30/40	SYN-3	CD2	-
	CD 14 - HIP	6-10	W - coated	-	TC	PVD	40/50	SYN-3	CD3	-
Hot Pressed (HP)	CD 15 - HP	1-10	Non-coated	-	DB	-	30/50	SYN-1	-	-
	CD 16 - HP	1-10	Non-coated	-	DB	-	30/50	SYN-3	-	-
	CD 17 - HP	1-5	Non-coated	-	DB	-	30/40	SYN-3	-	-
	CD 18 - HP	1-5	Ti - coated	HT	DB	CVD	30/50	SYN-1	CD15	CD32
	CD 19 - HP	1-5	Ti - coated	HT	TC	PVD	30/50	SYN-1	CD15	CD33
	CD 20 - HP	1-5	Cr - coated	HT	TC	PVD	30/50	SYN-1	CD15	CD34
	CD 21 - HP	1-5	Cr (C) - coated	HT	TC	PVD	30/40	SYN-3	CD17, CD41	CD35
	CD 22 - HP	1-5	Ti/Cr - coated	HT	TC	PVD	30/40	SYN-3	CD17, CD41	CD36
	CD 23 - HP	1-5	W - coated	HT	TC	PVD	30/50	SYN-1	CD15	CD37
	CD 24 - HP	1-5	Cr - coated	-	NDT	PC	30/50	SYN-1	CD15	-
	CD 25 - HP	1-5	W - coated	-	VM	PC	30/50	SYN-1	CD15	-
	CD 26 - HP	1-5	W - coated	HT	VM	PC	30/50	SYN-1	CD15	CD25
	CD 27 - HP	1-5	Blank (No diamond impregnation) - Reference segments						-	-
	CD 28 - HP	1-5	Co - coated	-	J	PC	30/40	SYN-3	CD17, CD41	-
	CD 29 - HP	1-5	Co - coated	HT	J	PC	30/40	SYN-3	CD17, CD41	CD28
	CD 30 - HP	1-5	W - coated	-	NC	CVD	35/50	SYN-1	CD15	-
	CD 31 - HP	1-5	W - coated	HT	NC	CVD	35/50	SYN-1	CD15	-
	CD 32 - HP	1-5	Ti - coated	-	DB	CVD	30/50	SYN-1	CD15	-
	CD 33 - HP	1-5	Ti - coated	-	TC	PVD	30/50	SYN-1	CD15	-
	CD 34 - HP	1-5	Cr - coated	-	TC	PVD	30/50	SYN-1	CD15	-
	CD 35 - HP	1-5	Cr (C) - coated	-	TC	PVD	30/40	SYN-3	CD17, CD41	-
	CD 36 - HP	1-5	Ti/Cr - coated	-	TC	PVD	30/40	SYN-3	CD17, CD41	-
	CD 37 - HP	1-5	W - coated	-	TC	PVD	30/50	SYN-1	CD15	-
	CD 38 - HP	1-5	Cr - coated	HT	NDT	PC	30/50	SYN-1	CD15	CD24
	CD 39 - HP	1-5	Ti - coated	-	TC	PVD	30/40	SYN-3	CD17, CD41	-
	CD 40 - HP	1-5	Ti - coated	HT	TC	PVD	30/40	SYN-3	CD17, CD41	CD39
	CD 41 - HP	1-5	Non-coated	-	DB	-	30/40	SYN-3	-	-
	CD 42 - HP	1-5	Cr - coated	-	TC	PVD	30/40	SYN-3	CD17, CD41	-
	CD 43 - HP	1-5	Cr - coated	HT	TC	PVD	30/40	SYN-3	CD17, CD41	CD42
	CD 44 - HP	1-5	W - coated	-	TC	PVD	30/40	SYN-3	CD17, CD41	-
	CD 45 - HP	1-5	W - coated	HT	TC	PVD	30/40	SYN-3	CD17, CD41	CD44

Nomenclature :

HT : Diamond Heat treatment at 500°C, 20min, in $10H_2$ / $90N_2$ atmosphere Diamond Type : **SYN-1** is superior quality **SYN-3** produced by De Beers

Metal coating deposition methods : **CVD** : Chemical Vapour Deposition, **PVD** : Physical Vapour Deposition, **PC** : Powder Coating / Encapsulation

Manufacturers of Coated Diamonds : **DB** : De Beers, **NDT** : Nimbus Diamond Tool, **NC** : Norton Company, **TC** : Teer Coatings, **VM** : Van Moppes, **J** : Fuji Paudal Kabushiki Kaisha

Table 7-7 : Complete listing of the parameters for the rectangular parallelepiped segments.

	"Dog-Bone" Segment Set Code	Number of Samples	Diamond Condition	Diamond Heat Treatment	Manufacturer	Coating Method	Diamond Size Range (US mesh)	Diamond Type	Reference Non-coated Segment	Reference Non-Heat Treated Segment	Equivalent Segment
Furnace Sintering (FS)	DBS 1	1-3	No diamond content – Reference sample						-	-	CD1, CD27
	DBS 2	1-3	Non-coated	-	DB	-	30/40	SYN-3	-	-	CD2, CD17
	DBS 3	1-3	Non-coated	-	DB	-	40/50	SYN-3	-	-	CD5
	DBS 4	1-3	Non-coated	-	DB	-	30/50	SYN-1	-	-	CD15
	DBS 5	1-3	Ti - coated	-	TC	PVD	30/40	SYN-3	DBS2	-	CD8, CD39
	DBS 6	1-3	Ti - coated	HT	TC	PVD	30/40	SYN-3	DBS2	DBS5	CD40
	DBS 7	1-3	Ti/Cr - coated	-	TC	PVD	30/40	SYN-3	DBS2	-	CD12, CD36
	DBS 8	1-3	Ti/Cr - coated	HT	TC	PVD	30/40	SYN-3	DBS2	DBS7	CD22
	DBS 9	1-3	W - coated	-	TC	PVD	30/40	SYN-3	DBS2	-	CD13, CD44
	DBS 10	1-3	W - coated	HT	TC	PVD	30/40	SYN-3	DBS2	DBS9	CD45
	DBS 11	1-3	Ti - coated	-	DB	CVD	30/50	SYN-1	DBS4	-	CD32
	DBS 12	1-6	Ti - coated	HT	DB	CVD	30/50	SYN-1	DBS4	DBS11	CD18
	DBS 13	1-6	Cr - coated	-	TC	PVD	30/50	SYN-1	DBS4	-	CD33
	DBS 14	1-3	Cr - coated	HT	TC	PVD	30/50	SYN-1	DBS4	DBS13	CD19
	DBS 15	1-3	Cr (C) - coated	-	TC	PVD	30/40	SYN-3	DBS2	-	CD11, CD35
	DBS 16	1-3	Cr (C) - coated	HT	TC	PVD	30/40	SYN-3	DBS2	DBS15	CD21
	DBS 17	1-3	W - coated	-	TC	PVD	30/50	SYN-1	DBS4	-	CD37
	DBS 18	1-3	W - coated	HT	TC	PVD	30/50	SYN-1	DBS4	DBS17	CD23
	DBS 19	1-3	Cr - coated	-	NDT	PC	30/50	SYN-1	DBS4	-	CD24
	DBS 20	1-6	Cr - coated	HT	NDT	PC	30/50	SYN-1	DBS4	DBS19	CD38
	DBS 21	1-6	W - coated	-	VM	PC	30/50	SYN-1	DBS4	-	CD25
	DBS 22	1-3	W - coated	HT	VM	PC	30/50	SYN-1	DBS4	DBS21	CD26
	DBS 23	1-3	Co - coated	-	J	PC	30/40	SYN-3	DBS2	-	CD28
	DBS 24	1-3	Co - coated	HT	J	PC	30/40	SYN-3	DBS2	DBS23	CD29
	DBS 25	1-3	W - coated	-	NC	CVD	35/50	SYN-1	DBS4	-	CD30
	DBS 26	1-6	W - coated	HT	NC	CVD	35/50	SYN-1	DBS4	DBS25	CD31

Nomenclature :

HT : Diamond Heat treatment at 500°C, 20min, in $10H_2$/ $90N_2$ atmosphere Diamond Type : **SYN-1** is superior quality **SYN-3** produced by De Beers

Metal coating deposition methods : **CVD** : Chemical Vapour Deposition, **PVD** : Physical Vapour Deposition, **PC** : Powder Coating / Encapsulation

Manufacturers of Coated Diamonds : **DB** : De Beers, **NDT** : Nimbus Diamond Tool, **NC** : Norton Company, **TC** : Teer Coatings, **VM** : Van Moppes, **J** : Fuji Paudal Kabushiki Kaisha

Table 7-8 : Complete listing of the parameters for the tensile test type ("dog-bone") segments.

7.3.2.2 Production Methods

The segment formulation was achieved by powder metallurgy (PM) techniques, which involved the weighing and mixing of metallic powders and diamonds, the cold compaction of the powder mixture into green compacts and finally the hot consolidation to dense segments. Firstly, the exact weights of granulated fine cobalt matrix powder, diamond grit and lubricant, were calculated according to the cold press mould dimensions, the desired green compact dimensions and the diamond concentration in the segment. When calculating the required amount for the coated diamonds, the weight of the metal coating had to be taken into account so as to ensure that the weighted amount of coated grit would contain the actually required quantity of diamonds. For the diamonds that had a very thin coating, the coating was neglected and the calculation was similar to that for the non-coated diamonds. However, for diamonds with a thick

coating and especially for metals with a high density such as tungsten, the coating had to be taken into account. Thus, the initially calculated weight of diamond was adjusted by multiplying by a suitable factor, so that the final weight of coated grit contained the actual desired amount of diamond.

The appropriate amounts of diamond grit, cobalt powder and zinc stearate lubricant $\{Zn(C_{18}H_{35}O_2)\}$ were weighed separately and were then mixed in a tubular mixer for sufficient time to achieve a homogeneous mixture. The powder mixture was then loaded in the pressing die and was uniaxially cold compacted in a hydraulic press to form the green compacts. All rectangular parallelepiped segments were cold compacted using a load of 1000 lbs (approx. 4.5 kN) whereas a higher load of 2800 lbs (approx. 12.5 kN) was required for the larger "dog-bone" type specimens.

The segments were then hot consolidated by three different methods:

- furnace sintering (FS),
- furnace sintering followed by container-less hot-isostatic-pressing (HIP), and
- uniaxial hot-pressing (HP).

Furnace sintering (FS) took place in a mesh belt furnace. The sintering treatment was done under a protective and slightly reducing atmosphere of a gas mixture of a 10/90 hydrogen and nitrogen ratio. The travelling speed of the belt was appropriately adjusted so that the segments were dewaxed at the first semi-hot sections of the furnace and remained at the hot zone of the furnace for the desired time required for sintering. Sintering in the mesh belt furnace was employed to produce the tensile test segments and a batch of 14 sets of rectangular parallelepiped segments.

In the case of the tensile test segments the dewaxing of the compacts took place in a separate mesh belt furnace of smaller size, but sintering to achieve densification took place in the same furnace as the one used for sintering the rectangular parallelepiped segments.

The diagrams in Figure 7-5 give the time-temperature cycles for the sintering treatments.

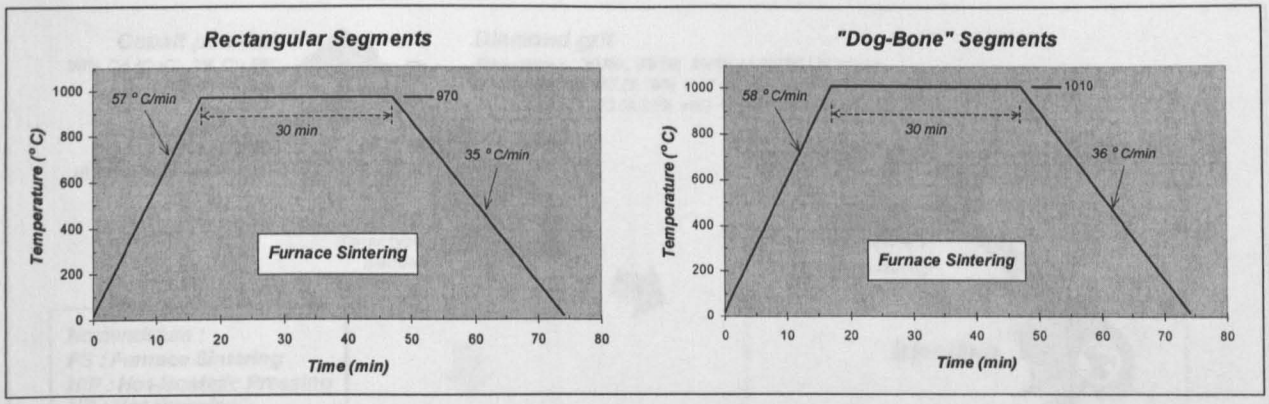

Figure 7-5 : The heating cycles of the furnace sintering heat treatments.

The **hot-isostatic pressing (HIP)** production route involved initially the sintering of the green rectangular segments in a mesh belt furnace with the same heating cycle as described in the previous paragraph. The sintered segments were then loaded in a HIP vessel without the use of any type of encapsulation (container-less HIP). The segments were hot-isostatically pressed at 850°C for 30 minutes under a pressure of 100MPa.

Hot-pressing (HP) was performed in a semi-automatic HP unit. The rectangular cold pressed green segments were loaded in batches of five in special graphite assembled moulds and were uniaxially hot pressed. Die wall lubricant was used to coat the punch faces and mould cavity walls to prevent diffusion bonding between the pressing tools and the compacts. A dewaxing step was included in the heating cycle. Pressure was applied from the beginning of the cycle and was only released when the temperature dropped below 400°C during cooling down. Figure 7-6 gives the details for the hot-pressings heating cycle.

Figure 7-7 on next page presents in a graphical manner the various steps and details for both the rectangular and "dog-bone" shaped segments production routes.

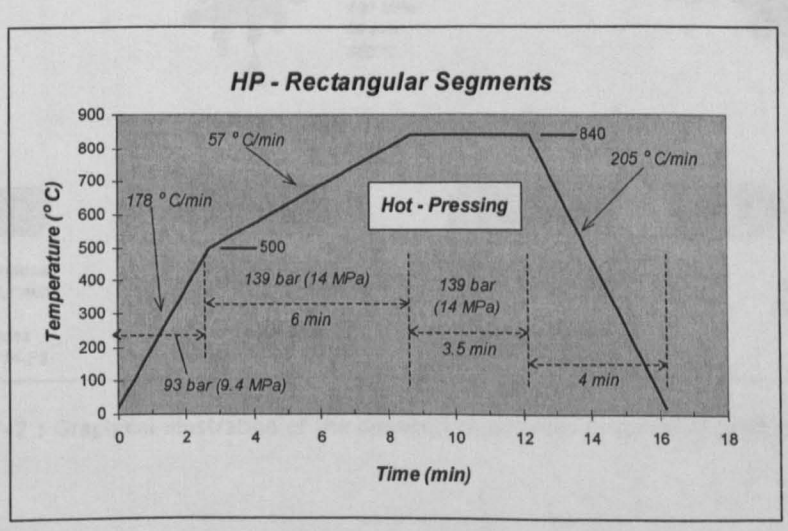

Figure 7-6 : The heating cycles of the hot-pressing (HP).

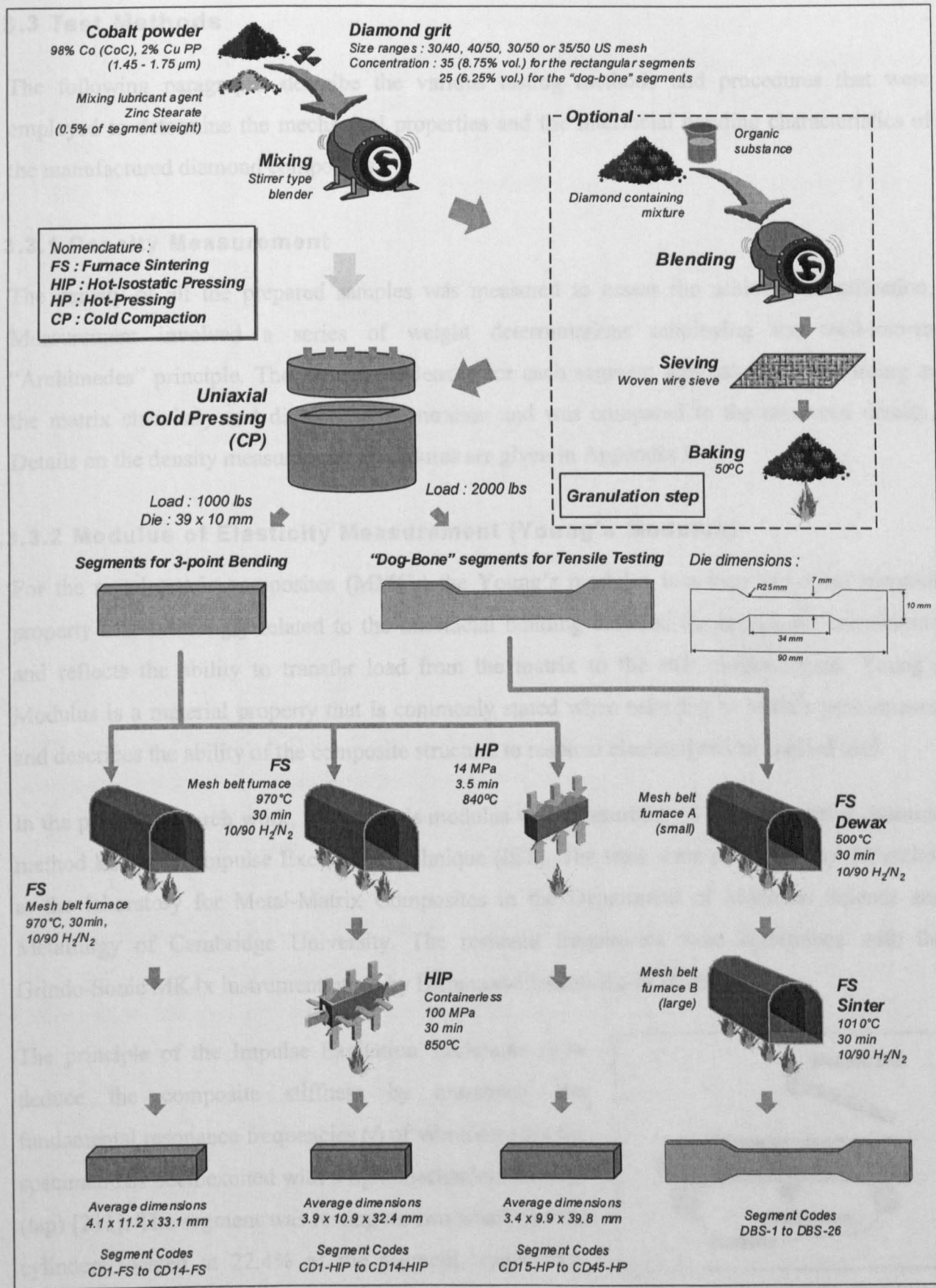

Figure 7-7 : Graphical illustration of the diamond composites (segments) production methods.

7.3.3 Test Methods

The following paragraphs describe the various testing methods and procedures that were employed to determine the mechanical properties and the interfacial bonding characteristics of the manufactured diamond composites.

7.3.3.1 Density Measurement

The density of all the prepared samples was measured to assess the achieved densification. Measurement involved a series of weight determinations employing the well-known "Archimedes" principle. The theoretical density for each segment was calculated according to the matrix chemistry and diamond concentration and was compared to the measured density. Details on the density measurement procedures are given in Appendix D-4.

7.3.3.2 Modulus of Elasticity Measurement (Young's Modulus)

For the metal-matrix composites (MMCs) the Young's modulus is a very important material property that is strongly related to the interfacial bonding between the composite constituents and reflects the ability to transfer load from the matrix to the stiff reinforcement. Young's Modulus is a material property that is commonly stated when referring to MMCs performance and describes the ability of the composite structure to respond elastically to an applied load.

In the present research work, the Young's modulus was measured by a non-destructive dynamic method known as Impulse Excitation Technique (IET). The tests were performed by the author at the laboratory for Metal-Matrix Composites in the Department of Materials Science and Metallurgy of Cambridge University. The resonant frequencies were determined with the Grindo-Sonic MK4x instrument made by Lemmens-Elektronika in Belgium.

The principle of the Impulse Excitation Technique is to deduce the composite stiffness by measuring the fundamental resonance frequencies (f) of vibration after the specimen has been excited with a light mechanical impulse (tap) [211]. The segment was resting on two small parallel cylinders located at 22.4% of the segment length from either end (see Figure 7-8). After positioning, the segment was excited by striking it with a small metallic ball. The transducer located at the bottom centre of the segment

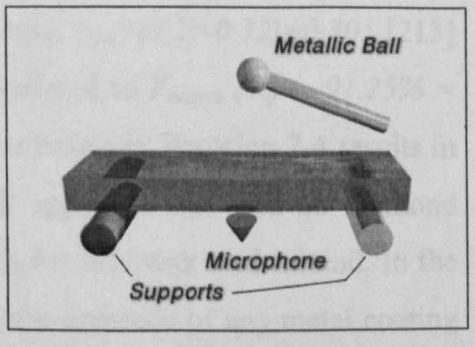

Figure 7-8 : The experimental set-up of the IET. The small steel ball causes the segment to vibrate in the fundamental flexural mode and the microphone detects the resulting vibrations.

picked up the mechanical vibration. The microprocessor analysed the signal and finally after a couple of seconds displayed a reading on the MK4x instrument panel, which corresponded to the duration of two periods (R) of the fundamental vibration expressed in microseconds (μs). This procedure was repeated three times for each segment in order to certify the consistency of the readings. The Young's Modulus (E) for a prismatic specimen of rectangular cross-section is given by the following formula [212] :

$$E = 0.94642 \cdot \frac{\rho \cdot L^4 \cdot f^2}{h^2} \cdot T \cdot 10^{-12} \quad (GPa) \qquad \textbf{(Equation 7-2)}$$

where, ρ is the density of the segment (g/cm^3), L and h is the segment length and height respectively (mm), f is the resonant frequency (Hz) and is related to the instrument reading (R), $f = 2 \cdot 10^6 / R$. T is a dimensionless shape factor, which depend on segment length (L), width (b) and Poisson's ratio according to the following expression [212]:

$$T = 1 + 6.585 \cdot \left(1 + 0.0752\nu + 0.8109\nu^2\right) \cdot \left(\frac{h}{L}\right)^2 - 0.868 \cdot \left(\frac{h}{L}\right)^4 - \frac{8.340 \cdot \left(1 + 0.2023\nu + 2.173\nu^2\right) \cdot \left(\frac{h}{L}\right)^4}{1 + 6.338 \cdot \left(1 + 0.14081\nu + 1.536\nu^2\right) \cdot \left(\frac{h}{L}\right)^2} \qquad \textbf{(Equation 7-3)}$$

where, ν is the Poisson's ratio of the composite. The Rule-of-Mixtures was employed to calculate the Poisson's ratio of the composites and was expressed as:

$$\nu_{segment} = V_{matrix}(\%) \cdot \nu_{matrix} + V_{diamond}(\%) \cdot \nu_{diamond} \qquad \textbf{(Equation 7-4)}$$

where, $V_{diamond}$ $(\%)$ and V_{matrix} $(\%)$ are the volume fraction of the segment occupied by the matrix and the diamonds respectively (V_{matrix} $(\%)$ + $V_{diamond}$ $(\%) = 100$). The Poisson's ratio for the cobalt matrix and the diamond were selected to be the average of values found in the literature. Thus, the values that were used in the calculation were: $\nu_{Co} = (0.29\text{-}0.32) = 0.305$ [213] and $\nu_{diamond} = 0.2$ [21]. The diamond concentration of 35 is translated to V_{matrix} $(\%) = 91.25\% = 0.9125$ and $V_{diamond}$ $(\%) = 8.75\% = 0.0875$. Inserting the above values in Equation 7-4 results in a Poisson' ration of 0.29 for the composite. For the blank segments that had no diamond impregnation the Poisson's ratio of the plain cobalt matrix ($\nu_{Co} = 0.305$) was used instead. In the calculation of the Poisson's ratio of the diamond composites the presence of any metal coating on the diamond crystals was neglected.

The Young's modulus of a composite containing 30/40 US mesh size diamonds was calculated from the equations of Hashin-Shtrikman [201], Tsai-Halpin [202] and Cohen-Ishai [203], which

provide a theoretical prediction of the modulus of elasticity for composite structures (for details see Appendix C). The calculated values were compared to the experimentally obtained ones in order to evaluate whether these relatively simple models can be successfully applied in predicting modulus of elasticity of diamond MMCs.

7.3.3.3 3-Point Bending

The 3-point bending of the rectangular parallelepiped specimens was made with a Mayes Universal Testing apparatus according to the British Standard BS EN 23327 [214] applicable to brittle materials, which determines the Transverse Rupture Strength (TRS). The standard designates two types of test specimens with dimensions as given in Table 7-9. The manufactured diamond composites had dimensions closer to those of the type A test specimen as designated by the BS standard. For that reason the 3-point bending test was designed according to the specifications for type A specimens as is stated in the standard.

The distance between the 6 mm diameter WC rollers that were used, was modified to keep approximately the same specimen length/span aspect ratio as for the type A standard test specimen (see Table 7-10 and Figure 7-9).

Test Specimen	Dimensions (mm)			Rollers Span (mm)
	Length	Width	Height	
Type A	35 ± 1	5 ± 0.25	5 ± 0.25	30 ± 0.5
Type B	20 ± 1	6.5 ± 0.25	5.25 ± 0.25	14.5 ± 0.5

Table 7-9 : The specifications for the test specimens and span between the rollers according to BS EN 23327 [214].

Test Segments	Average Dimensions (mm)			Rollers Span (mm)	
	Length	Width	Height	Calculated	Used
Sintered	33.1	11.2	4.1	28	28
HIP-ed	32.4	10.9	3.9	27.4	27.2
HP-ed	39.8	9.9	3.4	34.8	34.7 & 35.12

Table 7-10 : The average dimensions of the as-manufactured segments tested in 3-point bending and the distance of the supports that was used in each case so that to keep the Length to Span ratio equal to what is designated in the BS EN 23327 [214].

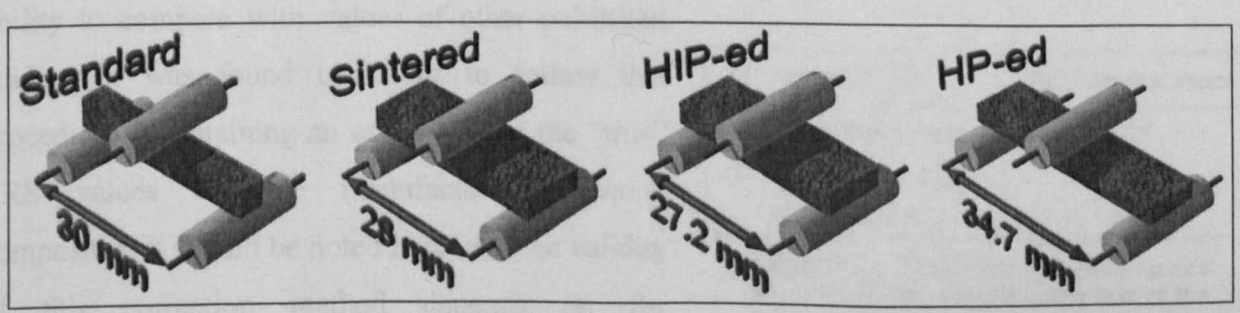

Figure 7-9 : The 3-point bending configuration showing the used distance of the supports for each case.

The transverse rupture strength (TRS) in 3-point bending is calculated according to the following equation [214]:

$$TRS = \frac{3FL}{2bh^2} \qquad \textbf{(Equation 7-5)}$$

where, F is the applied load at failure (N), L is the distance between the supports (mm), b is the specimen width (mm) and h is the specimen height (mm) (see Figure 7-10). The calculated TRS is given in units of MPa. All five segments from each set were tested in bending.

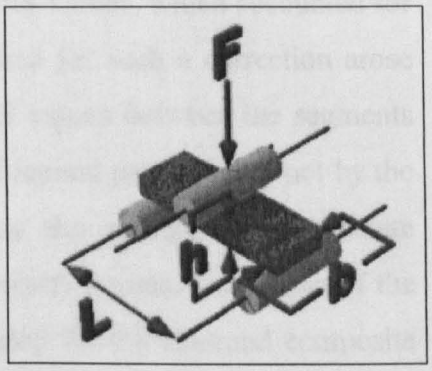

Figure 7-10 : The parameters involved in the TRS calculation.

The width (b) and height (h) used in the computations were the average values of measurements taken at three locations in each segment and were obtained by a point micrometer.

Since dimensions of tested specimens did not exactly comply with the BS EN 23327, the calculated TRS values had to be corrected. Bars made of WC 11%Co cemented carbide were machined to the dimensions of the type A standard specimen and to the average dimensions of each of the three (3) types of tested diamond composites (sintered, HIP-ed and HP-ed). A total of 20 bars were used to produce 4 sets of 5 specimens of each type. Specimens were subjected to 3-point bending according to the testing conditions that were applied for each of the three (3) types of diamond composites whereas the specimens machined to type A standard dimensions were tested exactly as directed by the BS EN 23327. With this procedure, it was possible to measure the deviation of the measured TRS values of the diamond composites from the BS standard TRS values, in other words from the TRS values that would have yielded if the test specimens have had the dimensions of type A test pieces as designated by the BS EN 233227.

Table 7-11 gives the TRS correction factors as resulted from the previously described procedure. Whether or not the dimensions of the test specimens are according to the standard test pieces does not affect the comparison of values of the tested samples. However, in order to have the ability to compare with values of other published studies, it was found necessary to follow this procedure for obtaining an estimation of the "true" TRS values for the manufactured diamond composites. It should be noted here, that the validity of this correction method depends on the

Segment Type	TRS Correction Factor
Furnace Sintered (FS)	1.25
Hot-Isostatic Pressed (HIP)	0.98
Hot Pressed (HP)	0.90

Table 7-11 : The TRS correction factors as computed from the bending test of the WC+11%Co cemented carbides

consistency of quality of the tested cemented carbide, something, which was however not certified.

As is known, the shape and amount of porosity influences the strength of materials [215]. Since the density of the manufactured diamond impregnated segments varied in a relatively wide range, it was necessary to eliminate the scatter in the measured TRS values, which accounted for the variation of the porosity levels in the composites. The demand for such a correction arose from the need to ensure that any variation in the measured TRS values between the segments could be accounted for by the effect of the metal-coating of the diamond particles and not by the porosity. Theoretical analysis studies [216] have shown that the strength of particulate composites is a linear function of porosity content in the low porosity regime. Correction of the TRS values was based on the theoretical density as was calculated for the diamond composite composition. The correction was done by adding to each measured TRS a certain positive value, which corresponded to the percentage of porosity in the segment compared to the 100% theoretical density. For example, the TRS of a segment with a relative density of 90% of theoretical (10% porosity) should increase by 10%. From this point forward in the thesis, this correction procedure will be referred to as *normalisation for porosity*. In this procedure it was assumed that the shape of the porosity in all the segment types was identical and had no additional effect in bending strength reduction and that only the net amount of porosity was critical.

7.3.3.4 Tensile Testing – Uniaxial Tension

The "dog-bone" shaped specimens produced with the furnace-sintering route (see Figure 7-7 and Table 7-8) were tested in uniaxial tension. Following sintering the average gauge length of the segments was 29 mm and with an average cross-sectional area of 6 mm × 4.3 mm. The samples were loaded on a Mayes tensile test machine fitted with a 100 kN load cell equipped with wedge grips (see Figure 7-11). Load-displacement curves obtained on a chart recorder were used to calculate the ultimate tensile strength (UTS), ductility and proof stress (0.2%) of the segments.

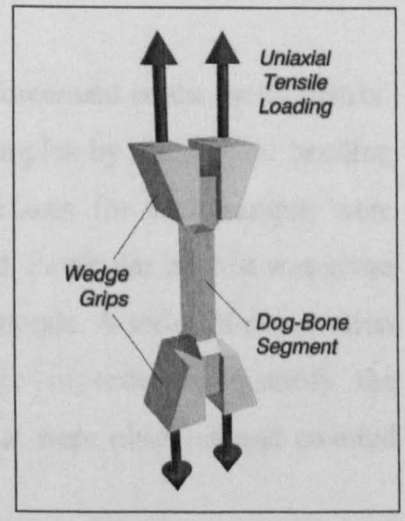

Figure 7-11 : Uniaxial tensile test set-up configuration.

7.3.3.5 SEM Examination

SEM work was performed with 3 different microscopes, a JEOL 6400 WINSEM microscope equipped with a NORAN EDAX analysis system, a Phillips XL30 SEM and a Phillips Field-Emission Gun SEM (FEG-ESEM) operating at a high vacuum mode and equipped with an ultra thin window EDAX detector. The JEOL microscope was used mainly for the examination of fractured surfaces at low magnification, because of its particular sample stage design, which offered the best possibility of loading at the same time both the positive and negative fractured surfaces for each sample (Figure 7-12). The FEG-ESEM was used for high-resolution imaging and EDAX analysis, whereas the XL30 on all other circumstances.

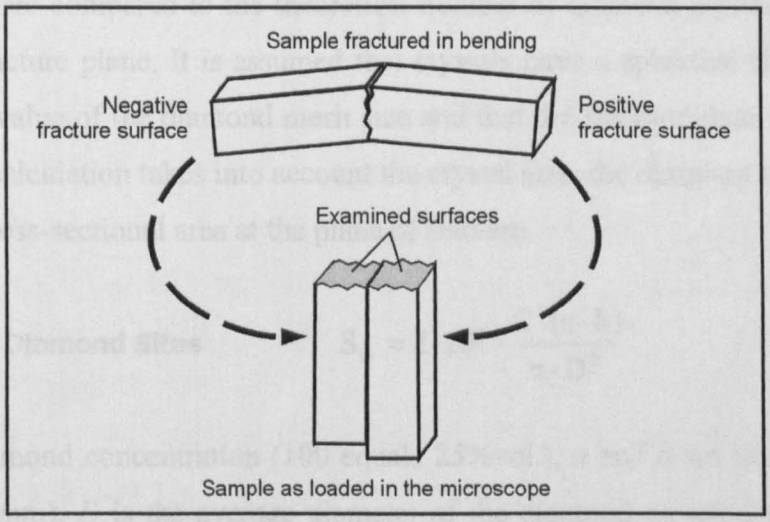

Figure 7-12 : Sketch showing how the two developed fracture surfaces for each sample were assembled in order to be examined simultaneously in the SEM.

SEM was employed to examine the bonding of the diamond reinforcement to the metal-matrix. Analysis was made on the fracture surfaces after breaking the samples by the 3-point bending and tensile testing. Both the positive and negative fracture surfaces for each sample were analysed. One specimen from each set of composites was examined. Particular interest was given to the interfacial regions and to the surface morphology of the diamonds. A series of observation features were counted and classified for each fracture surface in order to quantify the examination results. Table 7-12 on next page lists the features that were observed and counted for the SEM fracture surface analysis.

Based on the counted observation features, the number of lost diamonds (L) and the total number of crystal sites found at the fracture surfaces has been calculated for each segment according to the following expressions:

Lost Diamonds

$$L = \frac{\overbrace{\sum_{i=1,2,3}^{i} (DP)_i}^{\text{SurfaceA}} + \overbrace{\sum_{i=1,2,3}^{i} (DP)_i}^{\text{SurfaceB}} - (PO)_A - (PO)_B}{2} \qquad \textbf{(Equation 7-6)}$$

Total No. of Diamond Sites

$$S = \overbrace{\sum_{i=1,2,3}^{i} (DP)_i}^{\text{SurfaceA}} + (PO)_A \qquad \textbf{(Equation 7-7)}$$

where, $(DP)_i$ is the number of diamond crystals protruding at i-level with i=1,2 or 3, and (PO) the number of pull-out sites.

Obtained values were compared to the theoretical number of diamond crystals (S_N) expected to be found at the fracture plane. It is assumed that crystals have a spherical shape with diameter being the average value of the diamond mesh size and that the fracture plane cuts the crystals at their middle. The calculation takes into account the crystal size, the diamond concentration in the segment and the cross-sectional area at the plane of fracture.

Theoretical No. of Diamond Sites

$$S_N = 2 \cdot 10^4 \cdot \frac{C \cdot (a \cdot b)}{\pi \cdot D^2} \qquad \textbf{(Equation 7-8)}$$

where C is the diamond concentration (100 equals 25%vol.), a and b are the dimensions of the fracture plane (in mm), D is the average diameter of the diamond as calculated from the mesh size (in μm).

Observation Feature	Scale	Values / Levels
Diamond Protrusion (DP)	3	(3) Much, (2) Medium, (1) Little
Fractured Diamond (FD)	3	(6) Much, (5) Medium, (4) Little
Diamond Fragment remained in Pull-Out Crater (DF)	3	(9) Large, (8) Medium, (7) Small
Degree of Diamond Surface Modification (due to graphitization, reaction, dissolution etc.) (SM)	3	(12) High, (11) Medium, (10) Low
Signs of Reaction at the Interfacial Region (IR)	3	(15) Many Signs, (14) Few Signs, (13) No Signs
Metal-Matrix remains on diamond surfaces (MR)	3	(18) Much, (17) Medium, (16) Little
Cleaved Diamond (CL)	1	(19) Cleaved Diamond
Cracked Diamond (CR)	1	(20) Cracked Diamond
Pull-Out Crater (PO)	1	(•) Pull-Out
Lost Diamond (L)	1	(□) Lost Diamond
Lost Diamond Fragment from Pull-out crater (LF)	1	(■) Reacted Pull-Out

Table 7-12 : List of the features that were counted and observed for the SEM Fracture Surfaces Analysis. Note that the numbers and symbols in brackets denote the labelling method on the SEM micrographs.

7.4 Coated-diamond Composites with Alloy Metal-Matrices

7.4.1 Introduction – Aim

The series of experiments described under the above experimental procedures (§7.3) examined the mechanical properties and bonding of composites made of metal-coated diamonds incorporated in a standard matrix of cobalt. As already explained, the aim was to evaluate the various coated –diamonds. This required impregnating them in the same metal-matrix (standard cobalt matrix) in order to measure the net effect of the metallic coating. However, this restricted optimising the coating-matrix interface (2^{nd} interface) because the various metals used as coatings do not have the same degree of affinity for cobalt.

In order to explore the true potential of coated diamonds it is necessary to incorporate the coated diamonds in metal-matrices that are chemically compatible with each particular metal of the coating. For that reason in this 3^{rd} part of the experimental work a selection of the coated diamonds were incorporated in to alloyed metal-matrices of various compositions in order to achieve chemical bonding at the coating-matrix interface.

The criteria for selecting the matrices were primarily based on published data. Firstly, metal-matrix alloy components potentially compatible with each metallic coating were selected. Exact composition was then determined by adjusting to suit the alloys used in practice in the diamond tool industry.

7.4.2 Diamond Composites (segments)

All types of raw materials that were employed are commercially available. The preparation and consolidation of the diamond composites was made by the author at the production facilities of *Nimbus Diamond Tool and Machine Company Ltd.*, at Burgess Hill, West Sussex, England.

Both coated and non-coated diamonds that were employed were among those tested in the previous experimental sections (7.2 and 7.3). Rectangular parallelepiped composites were consolidated with the hot-pressing route as described in paragraph 7.3.2.2 on page 115. Maximum sintering temperature was selected appropriately to suit matrix composition. For all hot-pressing heating cycles, duration at maximum sintering temperature (dwell time) was kept constant at 3.5 min. Diamond concentration was 35 (8.75% vol.) and was the same for all composites. For each metal-matrix composition a series of reference segments were

manufactured in addition to the coated diamond impregnated composites. These included segments of plain metal-matrix with no diamond reinforcement and segments impregnated with non-coated diamonds.

The table below lists the type, main characteristics and origin of the powders that were employed to formulate the alloyed matrices.

Powder	**Trade Name** (Product Code)	**Particle Size** (FSSS)	**% Oxygen** Typical (Maximum)	**Manufacturer**
Bronze 85/15	$Cu_{85}Sn_{15}$ (PAA8515EP30)	-325 Mesh	*	MBC Metal Powders (UK)
Cobalt Extra Fine	Co-EF (00098)	1.5 µm	0.13 (0.6)	OMG Kokkola Chemical Oy (Finland)
Iron Carbonyl type	Fe (CN) (Fe 2000)	4-6 µm	< 0.2	Eurotungstene Poudres (France)
Next 100 Pre-alloyed Fe-Co-Cu	Next 100 **	< 1 µm	*	Eurotungstene Poudres (France)
Nickel	Ni (99.95%)	*	*	Ronald Britton & Company (UK)
Tungsten	WP30 (AW 2118)	2.5 ± 0.4 µm	*	Eurotungstene Poudres (France)

Table 7-13 : Listing of main details of the various powders used to formulate the tested alloyed metal-matrices. * Data not available. ** Composition not disclosed. EDAX analysis has shown Fe-Cu-Cu 28.6/25.2/46.2 %wt.

Table 7-14 on next page lists the complete set of parameters of the rectangular parallelepiped segments with the alloyed matrices that were manufactured and tested.

Same test methods as those used in experimental part-II (section 7.3) were employed for evaluating the mechanical properties and interfacial bonding of the composites.

Segment Set Code		Diamond Condition	Manufacturer of Coating	Coating Method	Diamond Size Range (US mesh)	Diamond Type	Metal-Matrix Composition (%wt.)	Sintering Temperature (°C)	Reference Blank Segment	Reference Segment with Non-coated Diamonds
MB-1	**MB1-B**	Blank segment - No diamond content – Reference Sample					Co + 15%wt. Ni	870	-	-
	MB1-N	Non-coated	-	-	30/40	SYN-3	Co + 15%wt. Ni	870	MB1-B	-
	MB1-C	Co-coated	J	PC	30/40	SYN-3	Co + 15%wt. Ni	870	MB1-B	MB1-N
MB-2	**MB2-B**	Blank segment - No diamond content – Reference Sample					Co + 10%wt. W	850	-	-
	MB2-N	Non-coated	-	-	30/40	SYN-3	Co + 10%wt. W	850	MB2-B	-
	MB2-C	Co-coated	J	PC	30/40	SYN-3	Co + 10%wt. W	850	MB2-B	MB2-N
MB-3	**MB3-B**	Blank segment - No diamond content – Reference Sample					Co + 10%wt. bronze 85/15	850	-	-
	MB3-N	Non-coated	-	-	30/40	SYN-3	Co + 10%wt. bronze 85/15	850	MB3-B MB4-B	-
	MB3-C	Cr-coated	TC	PVD	30/40	SYN-3	Co + 10%wt. bronze 85/15	850	MB3-B MB4-B	MB3-N MB4-N
MB-4	**MB4-B**	Blank segment - No diamond content – Reference Sample					Co + 10%wt. bronze 85/15	850	-	-
	MB4-N	Non-coated	-	-	30/40	SYN-3	Co + 10%wt. bronze 85/15	850	MB3-B MB4-B	-
	MB4-C	Cr(C)-coated	TC	PVD	30/40	SYN-3	Co + 10%wt. bronze 85/15	850	MB3-B MB4-B	MB3-N MB4-N
MB-5	**MB5-B**	Blank segment - No diamond content – Reference Sample					Co + 20%wt. bronze 85/15	870	-	-
	MB5-N	Non-coated	-	-	30/50	SYN-1	Co + 20%wt. bronze 85/15	870	MB5-B MB6-B	-
	MB5-C	Ti-coated	DB	CVD	30/50	SYN-1	Co + 20%wt. bronze 85/15	870	MB5-B MB6-B	MB5-N MB6-N
MB-6	**MB6-B**	Blank segment - No diamond content – Reference Sample					Co + 20%wt. bronze 85/15	870	-	-
	MB6-N	Non-coated	-	-	30/50	SYN-1	Co + 20%wt. bronze 85/15	870	MB5-B MB6-B	-
	MB6-C	Ti-coated	TC	PVD	30/50	SYN-1	Co + 20%wt. bronze 85/15	870	MB5-B MB6-B	MB5-N MB6-N
MB-7	**MB7-B**	Blank segment - No diamond content – Reference Sample					NEXT100 + 20%wt. Fe (CN)	820	-	-
	MB7-N	Non-coated	-	-	30/50	SYN-1	NEXT100 + 20%wt. Fe (CN)	820	MB7-B MB8-B	-
	MB7-C	W-coated	TC	PVD	30/50	SYN-1	NEXT100 + 20%wt. Fe (CN)	820	MB7-B MB8-B	MB7-N MB8-N
MB-8	**MB8-B**	Blank segment - No diamond content – Reference Sample					NEXT100 + 20%wt. Fe (CN)	820	-	-
	MB8-N	Non-coated	-	-	35/50	SYN-1	NEXT100 + 20%wt. Fe (CN)	820	MB7-B MB8-B	-
	MB8-C	w-coated	NC	CVD	35/50	SYN-1	NEXT100 + 20%wt. Fe (CN)	820	MB7-B MB8-B	MB7-N MB8-N
MB-9	**MB9-B**	Blank segment - No diamond content – Reference Sample					NEXT100 + 20%wt. W	880	-	-
	MB9-N	Non-coated	-	-	30/50	SYN-1	NEXT100 + 20%wt. W	880	MB9-B MB10-B	-
	MB9-C	W-coated	TC	PVD	30/50	SYN-1	NEXT100 + 20%wt. W	880	MB9-B MB10-B	MB9-N MB10-N
MB-10	**MB10-B**	Blank segment - No diamond content – Reference Sample					NEXT100 + 20%wt. W	880	-	-
	MB10-N	Non-coated	-	-	35/50	SYN-1	NEXT100 + 20%wt. W	880	MB9-B MB10-B	-
	MB10-C	w-coated	NC	CVD	35/50	SYN-1	NEXT100 + 20%wt. W	880	MB9-B MB10-B	MB9-N MB10-N

Nomenclature :

Diamond Type : **SYN-1** is superior quality **SYN-3** produced by De Beers

Metal coating deposition methods : **CVD** : Chemical Vapour Deposition, **PVD** : Physical Vapour Deposition, **PC** : Powder Coating / Encapsulation

Manufacturers of Coated Diamonds : **DB** : De Beers, **NC** : Norton Company, **TC** : Teer Coatings, **J** : Fuji Paudal Kabushiki Kaisha

Table 7-14 : Listing of parameters for the rectangular parallelepiped segments with alloyed metal matrices.

8

Results • Part-I

"Material Characterisation - Diamond Reactivity"

8.1 Introduction

This chapter presents the results of the series of experiments included in the first part of the experimental work of this thesis (Section 7.2). The work was carried out to characterise the raw material and to investigate the fundamentals of chemical reactivity/interactions of metals with bulk diamond crystals.

8.2 Diamonds Characterisation

8.2.1 Non-coated diamonds

All three different types of tested synthetic diamonds were cubo-octahedrons with either the octahedral or the cubic faces predominating. In the "as received" condition, crystals had sharp edges with smooth and flat surfaces. The SYN-1 & SYN-2 types were of superior quality compared to SYN-3 as could be visually judged from the amount of crystal defects, such as surface cavities, fractured areas and other imperfections. The main type of crystal defect was

large cavities located at the centre of the SYN-3 diamonds (Figure 8-1). Further SEM work on non-coated diamonds can be found in the section 8.3.3.1 presenting the results from the DRE.

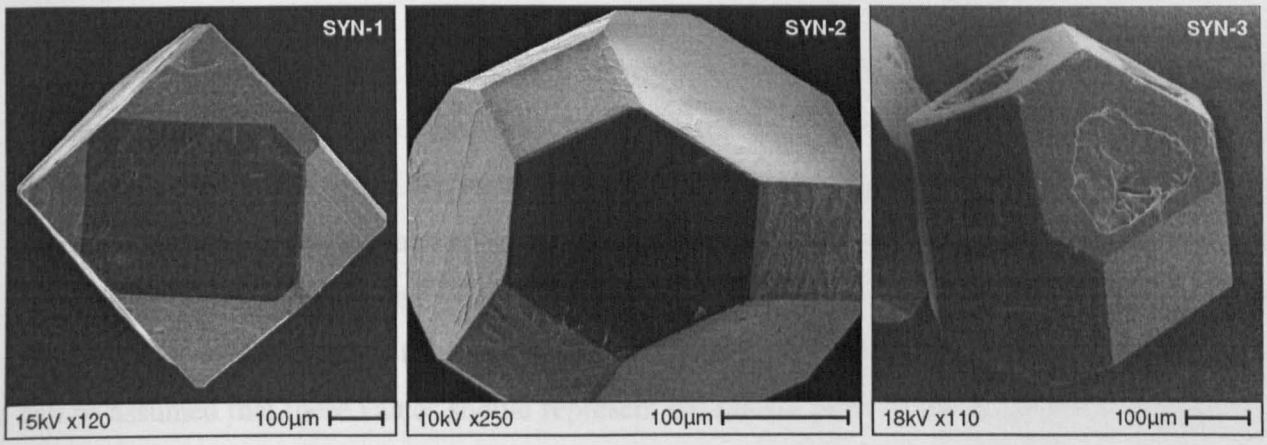

Figure 8-1 : SEM micrographs of the "as received" non-coated synthetic diamond crystals. **SYN-1:** SDA100 (De Beers), **SYN-2:** MBS960 (General Electric Superabrasives), **SYN-3:** SDA85 (De Beers).

8.2.2 Coated diamonds

SEM examination of the "as received" coated diamonds revealed that many of them had partially fractured and peeled-off coating layers. Stripped diamond surfaces appeared to have retained the flat and smooth morphology observed for the "as received" non-coated crystals. Layered vapour deposited coatings exhibited a dense columnar structure.

SEM analysis also served in determining the thickness of the various coatings (Figure 8-2). The results on coating thickness are presented in Figure 8-3. Calculated thickness for the powder-encapsulated crystals for which the SEM measurement was not feasible are listed in Table 8-1.

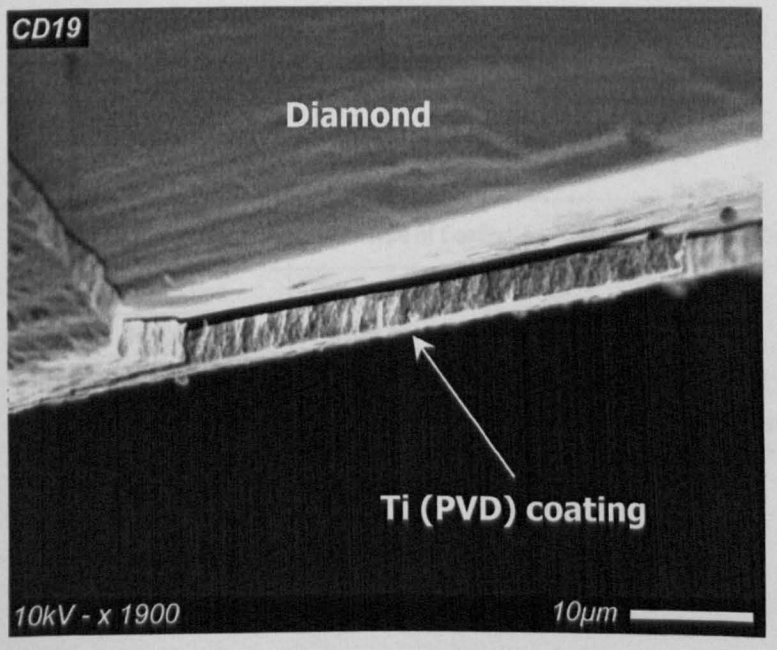

Figure 8-2 : SEM micrograph showing a site on a PVD Ti-coated synthetic diamond that permits measurement of the coating layer thickness.

All vapour deposited coatings had a thickness of the order of few microns. In areas where coatings had fractured or were partially removed, interfacial fissures could be seen separating the coatings from the diamond surfaces.

The cracking and fracturing of coatings is typically related to internal stresses arising from thermal expansion mismatches between the deposited layer and the substrate. In such coated systems, the internal stresses are expected to increase as the thickness of the coating increases. Considering the above, it can be assumed that fracturing of the metal coatings on diamond crystals occurred preferentially at locations where the deposited layer was thicker. Since measurement of the coating thickness was performed from cross-sections of fractured layers it can be assumed that these values should represent the thicker parts of the deposited coatings.

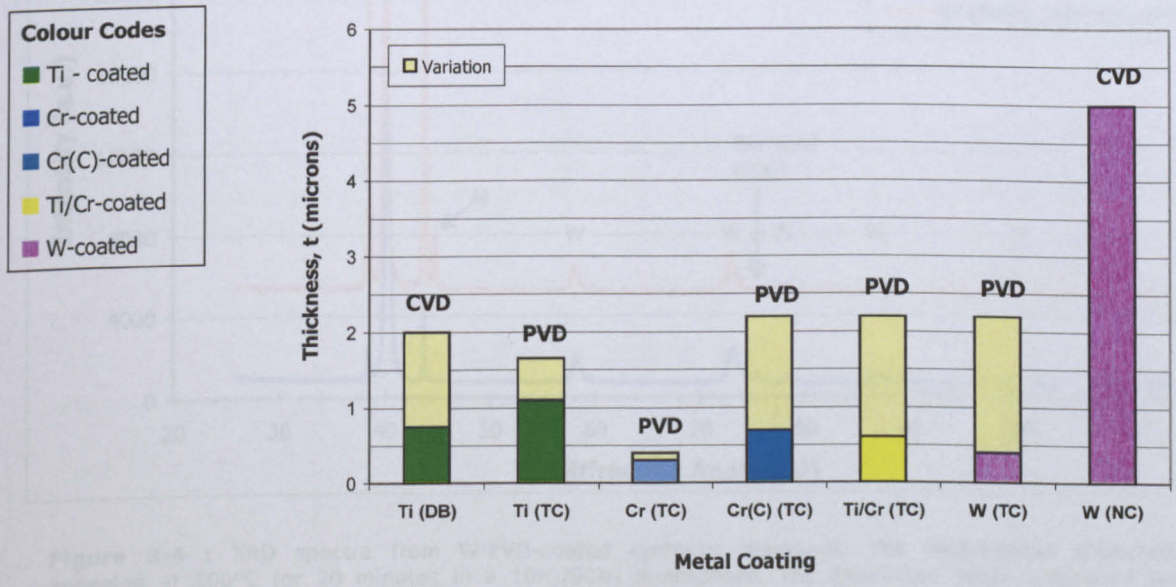

Figure 8-3 : Thickness of the metal-coating for the various examined coated-diamonds. (Manufacturer codes : DB-De Beers, TC-Teer Coatings & NC-Norton Company).

Diamond Condition	Type of Coating	Manufacturer / Source	Calculated Thickness of Metal Coating
Cr - coated	Powder encapsulation (PC)	NDT	53.6 μm
W - coated	Powder encapsulation (PC)	VM	11.9 μm
Co - coated	Powder encapsulation (PC)	J	18.4 μm

Table 8-1 : Calculated average thickness of the metal jacket of the metal-powder encapsulated diamonds. Refer to Appendix D-1 for calculation details. (Manufacturer codes : NDT-Nimbus Diamond Tools, VM-Van Moppes & J-Fuji Paudal Kabushiki Kaisha).

8.2.3 X-ray Diffraction

All obtained spectra confirmed the diamond structure and contained the characteristic diamond peak at 2θ angle 43.917° (JCPDS-ICDD standard No. 6-675), which corresponds to the octahedral (111) planes. In all the cases of tested coated diamonds that included both the diamonds in the "as received" condition after the deposition process, but also the heat-treated grit (500°C, 20 min, 10/90 H_2/N_2), the obtained diffraction spectra did not reveal the presence of any formed compound such as carbides. The spectra contained only the diamond peaks and those corresponding to the deposited metal. This is for example shown in Figure 8-4 with the XRD spectra obtained for both the "as received" and heat-treated W-PVD-coated diamonds.

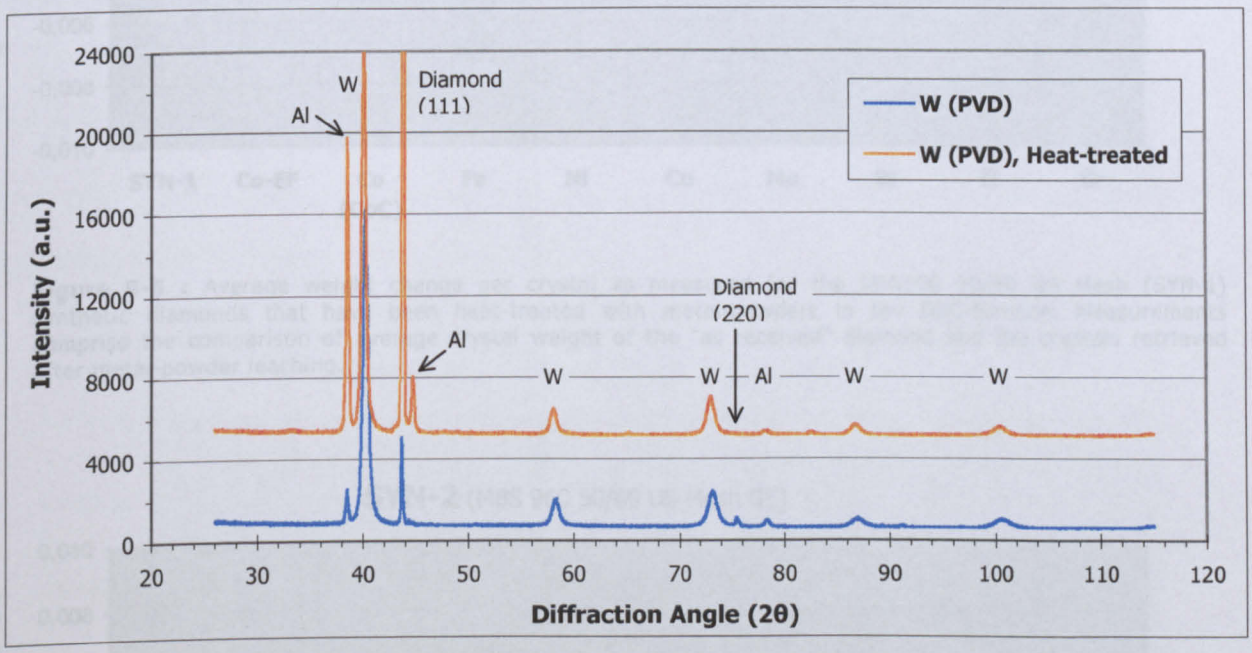

Figure 8-4 : XRD spectra from W-PVD-coated synthetic diamonds. The heat-treated diamonds were annealed at 500°C for 20 minutes in a $10H_2/90N_2$ atmosphere. The aluminium peaks originated from the aluminium holder containing the monolayer of diamonds (see Figure 7-1).

8.3 Diamond Reactivity Experiment

8.3.1 Diamond Weight Change Measurement

The measured average crystal weight changes for diamonds mixed with metal powders and heat-treated in the DSC furnace are given in Figure 8-5 and Figure 8-6 for SYN-1 and SYN-2 diamonds respectively.

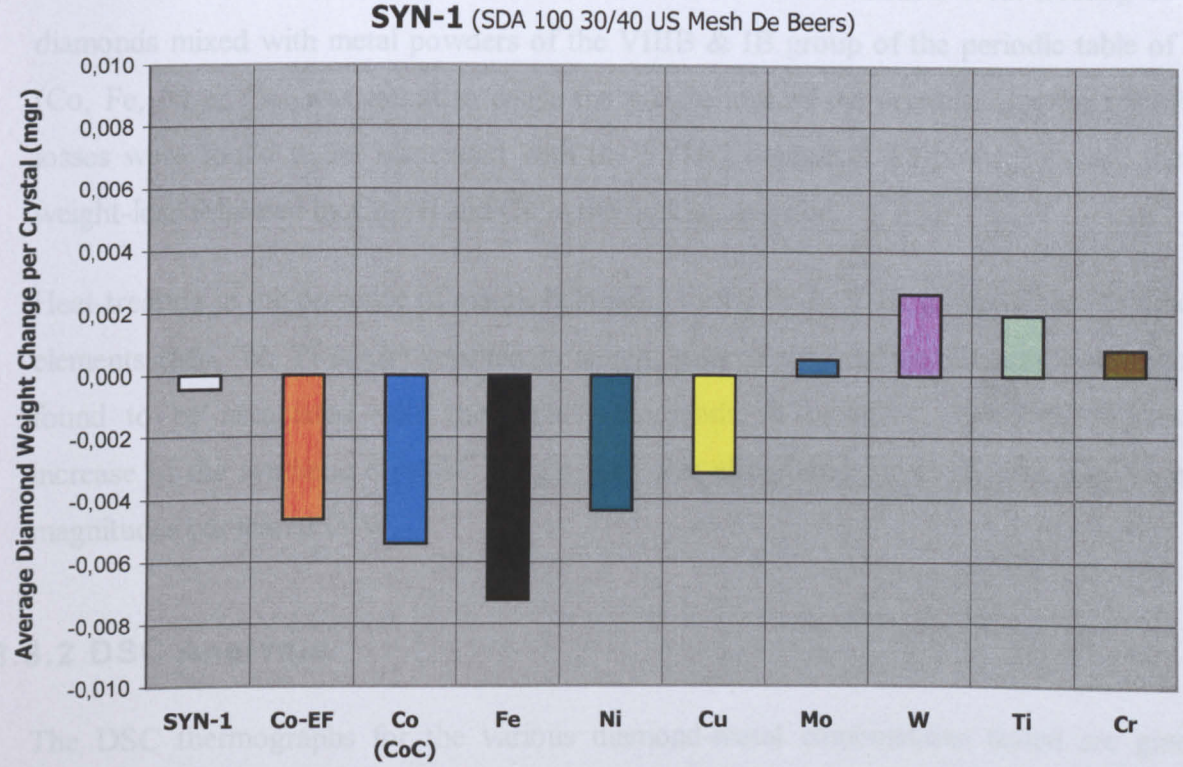

Figure 8-5 : Average weight change per crystal as measured for the SDA100 30/40 US Mesh (SYN-1) synthetic diamonds that have been heat-treated with metal-powders in the DSC-furnace. Measurements comprise the comparison of average crystal weight of the "as received" diamond and the crystals retrieved after metal-powder leaching.

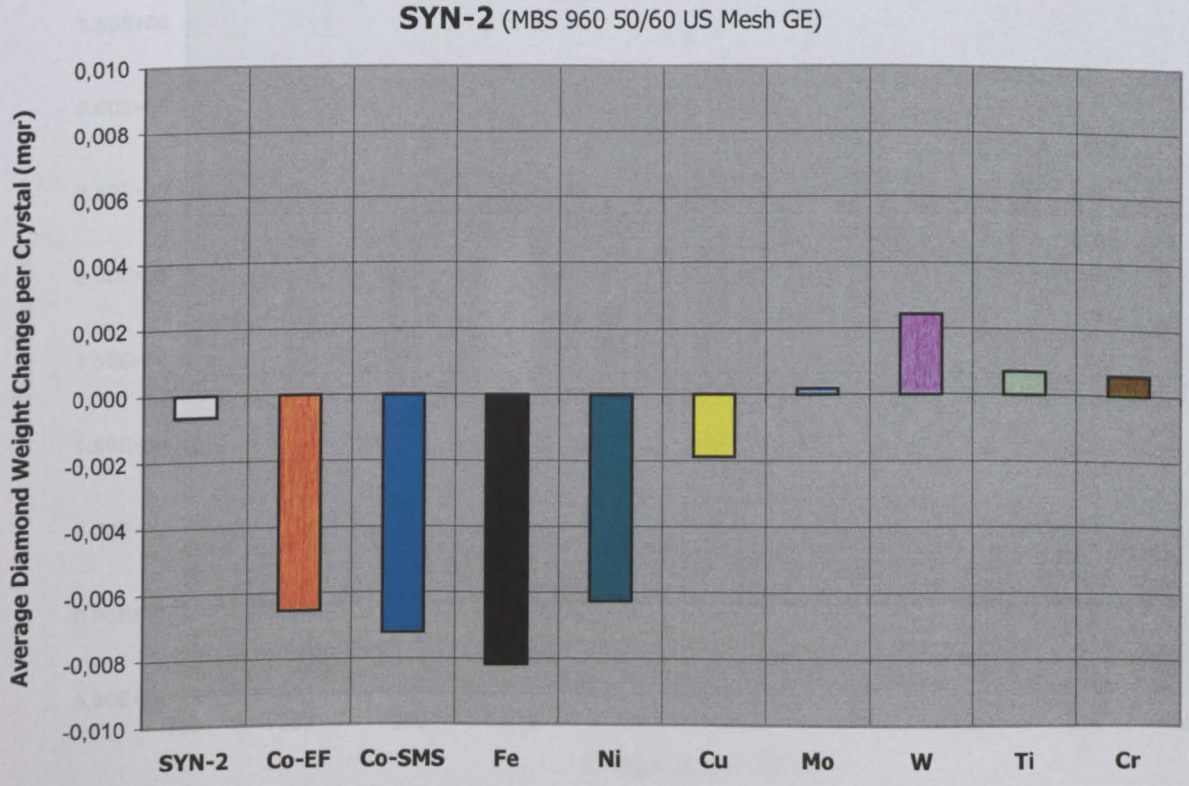

Figure 8-6 : Average weight change per crystal as measured for MBS960 50/60 US Mesh (SYN-2) synthetic diamonds that have been heat-treated with metal-powders in the DSC-furnace. Measurements comprise the comparison of average crystal weight of the "as received" diamond and the crystals retrieved after metal powder leaching.

Similar behaviour was found for both SYN-1 and SYN-2 diamonds. Heat-treating of synthetic diamonds mixed with metal powders of the VIIIB & IB group of the periodic table of elements (Co, Fe, Ni & Cu) was found to cause the weight loss of the crystals. Greater relative weight losses were found to be associated with the SYN-2 diamonds. Fe-powder caused the greatest weight-loss followed by Co, Ni and Cu in the ranking as listed.

Heat-treating in the presence of metals belonging to the IV to VIIB group of the periodic table of elements (Mo, W, Ti & Cr) resulted in weight gain of the crystals. Greater weight gains were found to be associated with the SYN-1 diamonds. W-powders yielded the highest weight increase of the synthetic crystals. Weight gain was also found for Cr, Ti and Mo but at smaller magnitudes compared to W.

8.3.2 DSC Analysis

The DSC thermographs for the various diamond-metal combinations tested are given in the following series of figures.

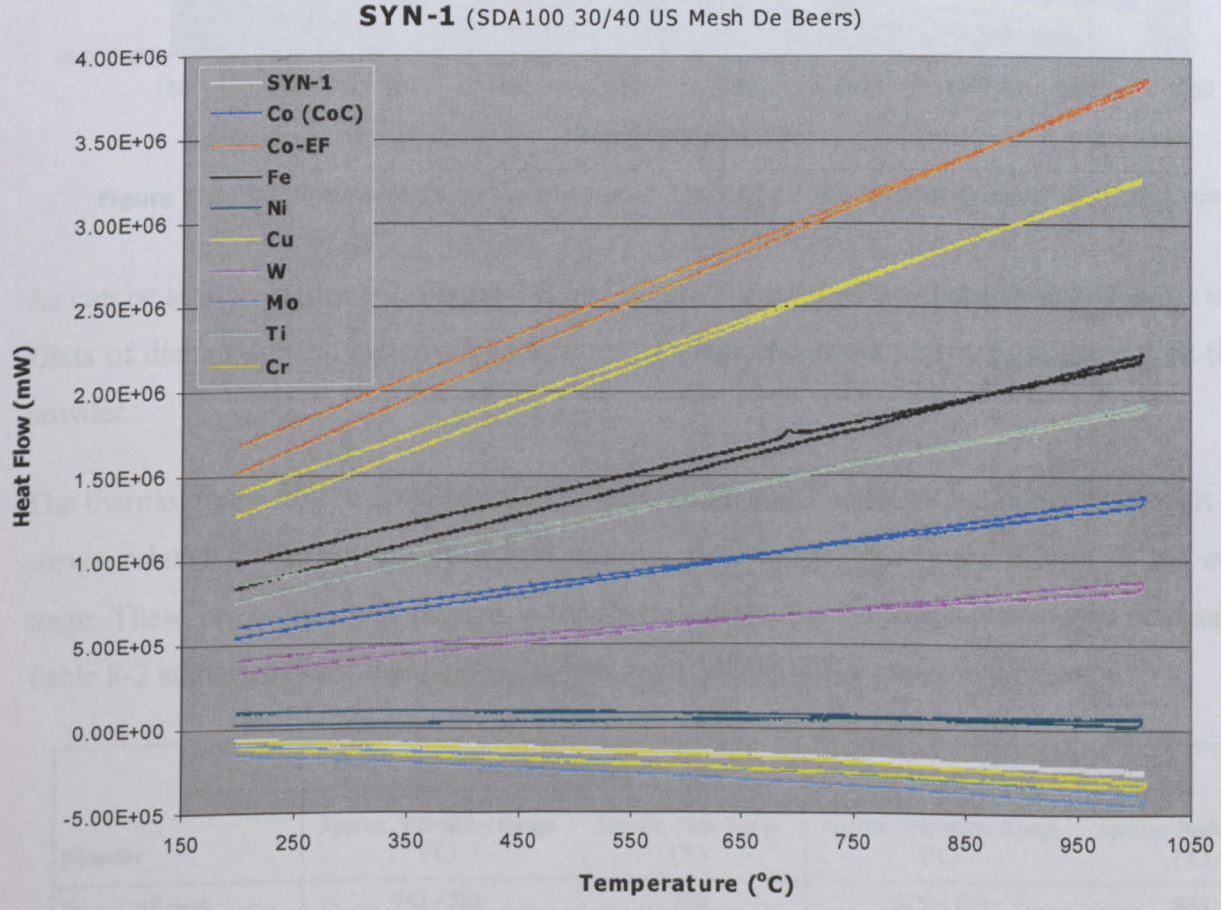

Figure 8-7 : DSC thermographs for the mixtures of SYN-1 type diamonds with elemental metal powders.

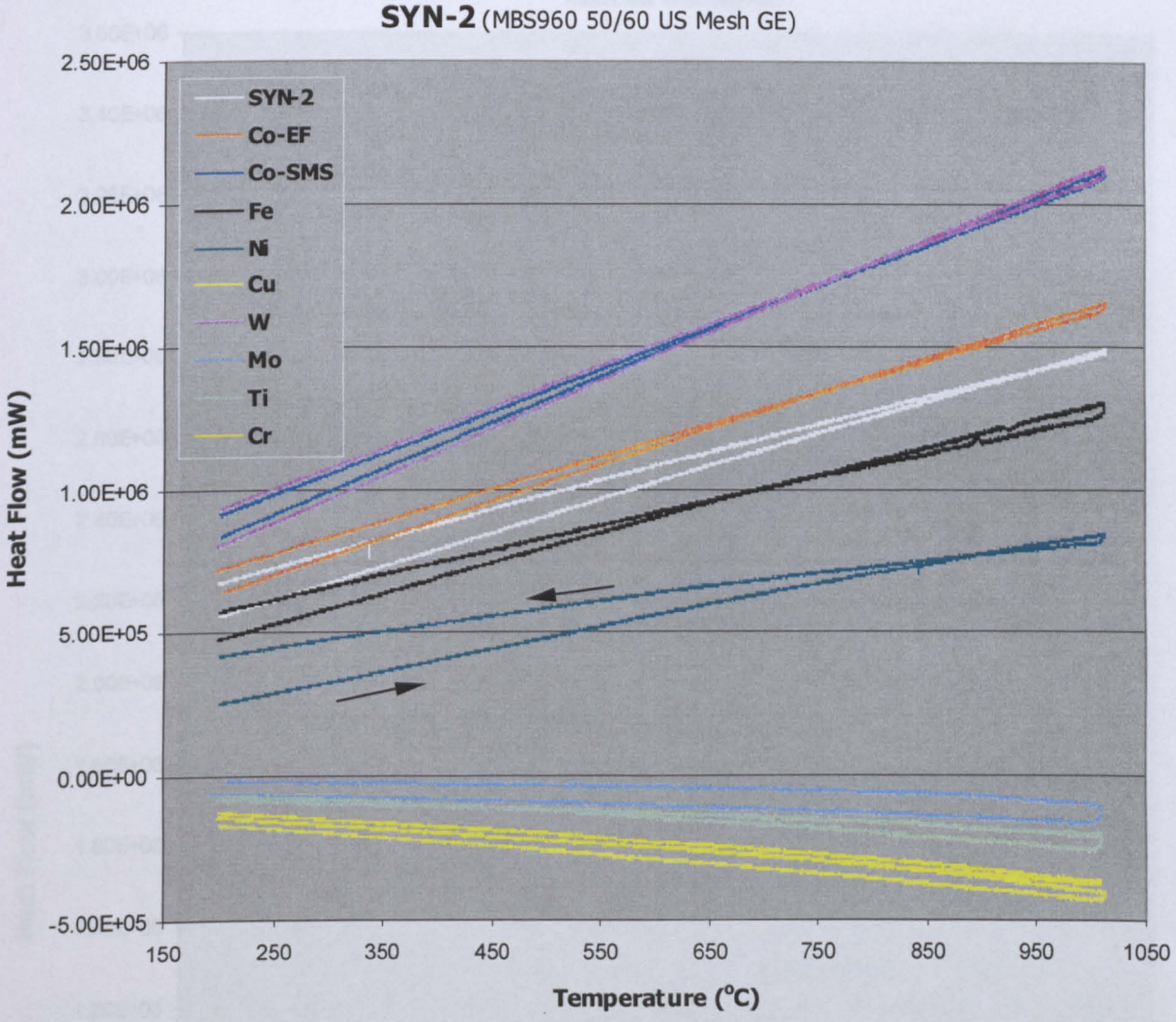

Figure 8-8 : DSC thermographs for the mixtures of SYN-2 type diamonds with elemental metal powders.

As can be seen in Figure 8-7, Figure 8-8 and Figure 8-9 none of the thermographs for the various kinds of diamond-metal systems exhibited any distinguished peaks apart from those with the Fe-powder.

The thermographs for the 2 diamond-Fe systems contained 2 endothermic peaks in the part of the curves related to the heating cycle and accordingly 2 exothermic peaks related to the cooling stage. These peaks were not present in the thermographs for the tested plain synthetic diamonds. Table 8-2 summarises list the various temperatures related to the monitored peaks.

Powder		Heating Curve		Cooling Curve	
		Approx. Transition Range (°C)	Approx. Peak Temp. (°C)	Approx. Transition Range (°C)	Approx. Peak Temp. (°C)
Fe	1st peak	743 - 781	768	675 – 705	688
	2nd peak	916 - 929	922	878 – 895	889

Table 8-2 : Transition temperatures for the detected peaks for the Diamond/Fe-powder systems.

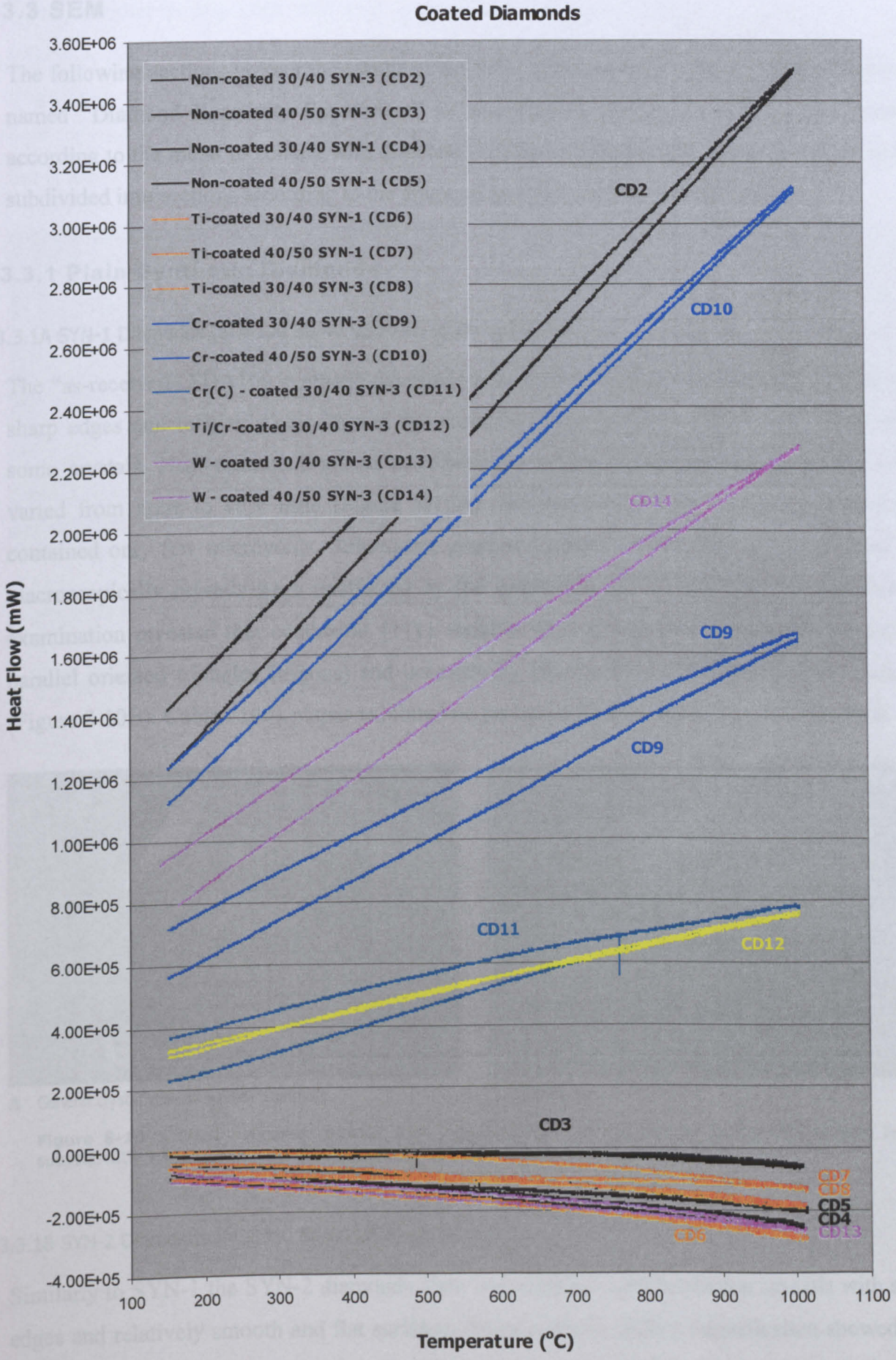

Figure 8-9 : DSC thermographs for the metal-coated diamonds.

8.3.3 SEM

The following sections present the results of the SEM work performed as part of the experiment named "Diamond Reactivity Experiment" as described in Chapter 7. Results are presented according to the metal in contact with diamond. Within each paragraph, observations are further subdivided into sections according to the diamond type and metal-diamond system.

8.3.3.1 Plain Synthetic Diamonds

8.3.3.1A SYN-1 Diamonds (SDA100 30/40 US Mesh made by DB)

The "as-received" SDA100 synthetic diamonds were well-defined cubo-octahedral crystals with sharp edges and relatively smooth and flat surfaces. Large surface cavities could be found in some crystals. Heat treatment caused no distinctive large-scale change. Edge sharpness loss varied from none to very little (Figure 8-10A). Surfaces retained their relative flatness and contained only few microvoids. Subsequent graphite leaching of the diamonds confirmed that macroscopically crystals were unaffected by the heat-treatment. However, high magnification examination revealed that octahedral {111} surfaces were etched by a network of intersecting parallel oriented triangles (trigons) and occasionally other polygonal shapes such as hexagons (Figure 8-10B). Cubic {100} planes exhibited no particular change from their original status.

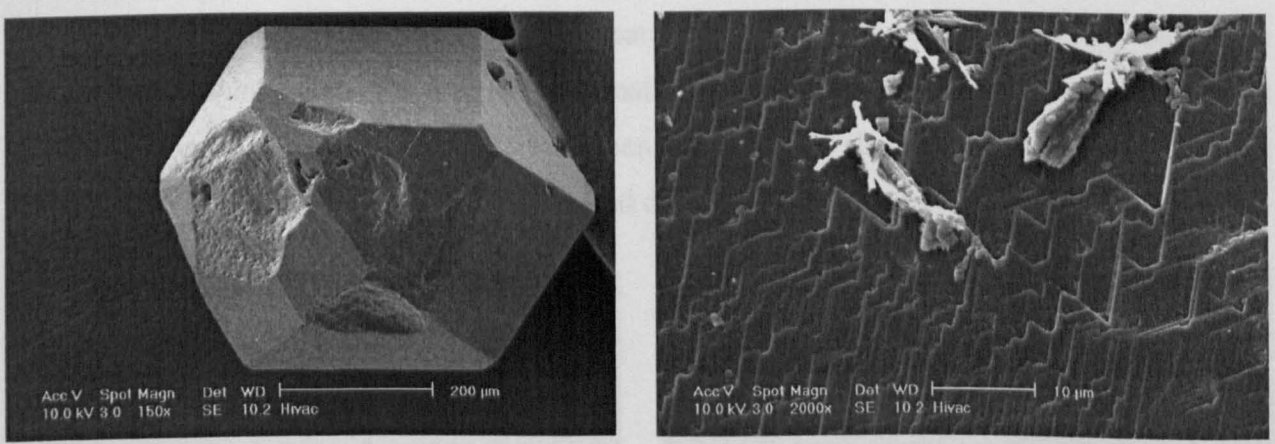

A General crystal view after heat-treatment.

B Octahedral (111) surface.

Figure 8-10 : SYN-1 diamonds (SDA100 30/40 US Mesh by DB) heat-treated in the DSC furnace and subsequently subjected to a leaching process for graphite removal.

8.3.3.1B SYN-2 Diamonds (MBS960 50/60 US Mesh by GE)

Similarly to SYN-1 the SYN-2 diamonds were well-defined cubo-octahedral crystals with sharp edges and relatively smooth and flat surfaces. Examination at higher magnification showed that surfaces contained planar irregularly shaped features that appeared visually to protrude from an underlying flat surface. This was more pronounced for the cubic {100} surfaces. Crystals

examined after having been subjected to the DSC treatment appeared almost identical to the originals. No major degradation features could be identified macroscopically. However, high magnification imaging revealed that cubic {100} planes contained a network of numerous small voids giving a slightly spongy appearance to the surface (Figure 8-11A). Similar etch features but at lower concentration were also found on the octahedral {111} surfaces (Figure 8-11B).

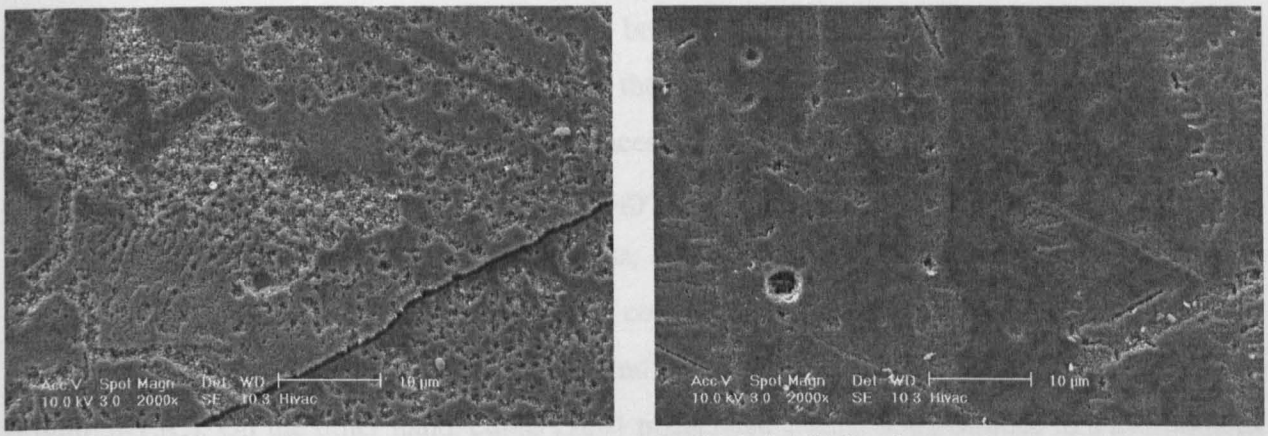

A Cubic (100) surface. **B** Octahedral (111) surface.

Figure 8-11 : Status of the surfaces of SYN-2 diamonds (MBS960 50/60 US Mesh by GE) after heat-treatment in the DSC furnace and subsequent leaching for graphite removal.

8.3.3.1C SYN-3 Diamonds (SDA75 30/40 US Mesh made by DB)

The "as received" SYN-3 diamonds were predominantly cubo-octahedral with macroscopically flat surfaces and sharp edges. Heat-treatment caused no obvious and macroscopically detectable crystal shape change. However, careful examination at higher magnification revealed octahedral {111} surfaces to contain numerous small oriented pyramidal shaped cavities, (Figure 8-12A). Cubic planes had a general irregular etching and did not contain pyramidal voids (Figure 8-12B).

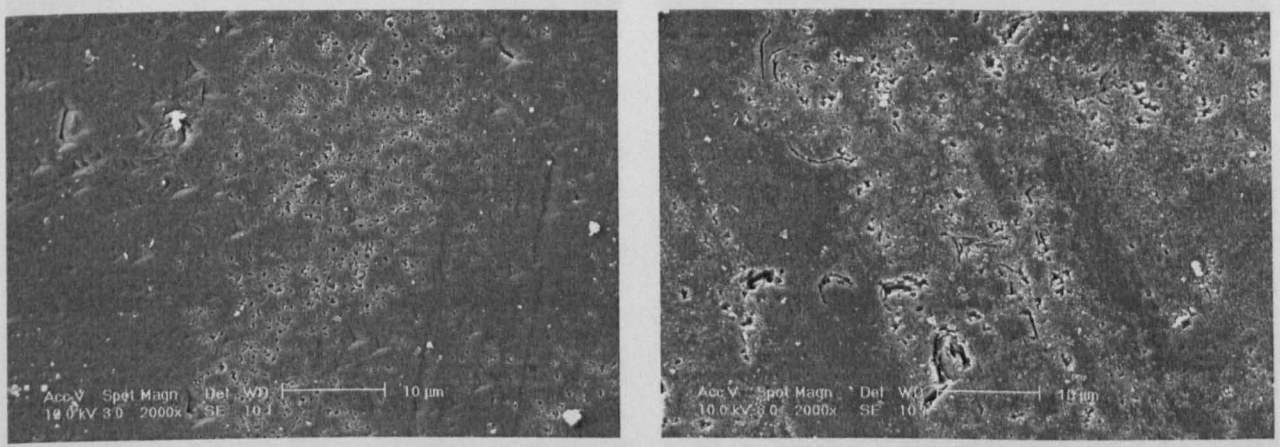

A Cubic (100) surface. **B** Octahedral (111) surface.

Figure 8-12 : Status of the surfaces of SYN-3 diamonds (MBS960 50/60 US Mesh by GE) after heat-treatment in the DSC furnace.

8.3.3.2 Diamond - Cobalt Systems

8.3.3.2A SYN-1 heat-treated with Co-EF powder

SYN-1 diamonds heat-treated with Co-EF powders were macroscopically uniformly etched, with a slightly overall spongy appearance and partial loss of edge sharpness (Figure 8-13A). Octahedral {111} planes contained hexagonal depressions, which occasionally intersected (Figure 8-13B). Larger cavities appeared to be rather irregularly etched. The flat diamond substrate could be distinguished in between the various features and at the bottoms of the depressions (Figure 8-13B). Cubic {100} surfaces looked rather spongy containing irregular and small sized cavities. The macroscopically spongy appearance of the crystals was preserved even after the subsequent graphite leaching process, however some flat and smooth regions were revealed. Octahedral {111} surfaces clearly contained hexagonal depressions as previously described, but the irregular morphologies found earlier in the larger cavities had disappeared (Figure 8-13C). On the other hand, cubic {100} planes had changed appearance to a morphology that was constructed of a large number of truncated pyramidal depressions of variable depth, being parallel oriented to each other and having either square or rectangular cross-sections (Figure 8-13D). A flat substrate could still be distinguished at the bottom of the hollow features.

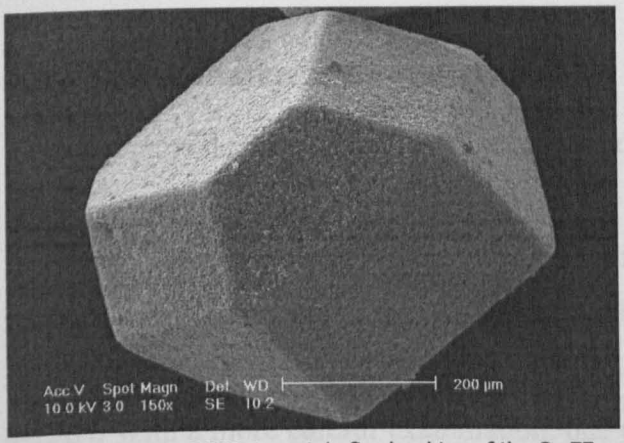

A General view of SYN-1 crystal after leaching of the Co-EF.

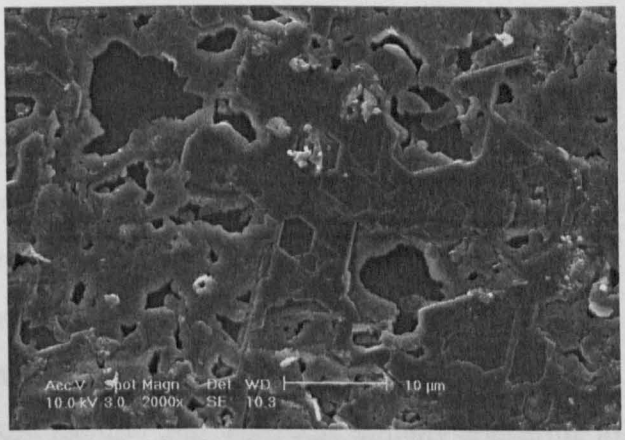

B Octahedral (111) surface after leaching of the Co-EF.

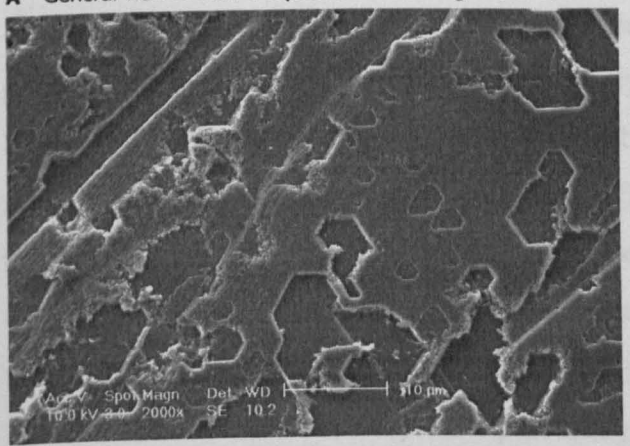

C Octahedral (111) surface after graphite leaching.

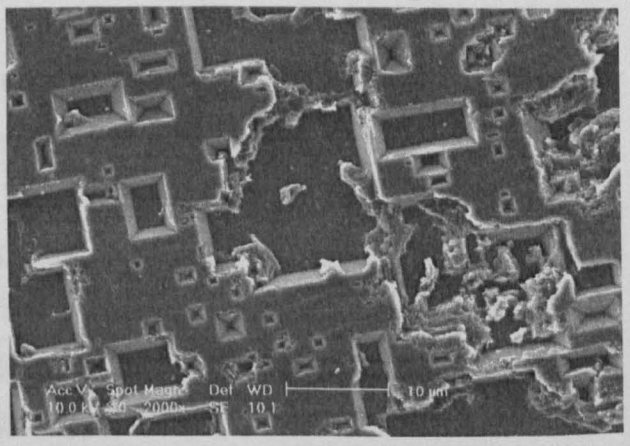

D Cubic (100) surface after graphite leaching.

Figure 8-13 : Various SEM micrographs of SYN-1 diamonds heat-treated with Co-EF powder.

8.3.3.2B SYN-1 heat-treated with Co (CoC) powder

Heat-treatment of SYN-1 diamonds with the Co (CoC) grade powder produced similar surface features as those observed for the SYN-1 crystals heated with the Co-EF. However, the etched cavities were easier distinguished at low magnification (Figure 8-14A). It could be said that the concentration of etch features was reduced compared to the case with the Co-EF. High magnification examination confirmed that etch patterns were present at lower surface concentrations (Figure 8-14B).

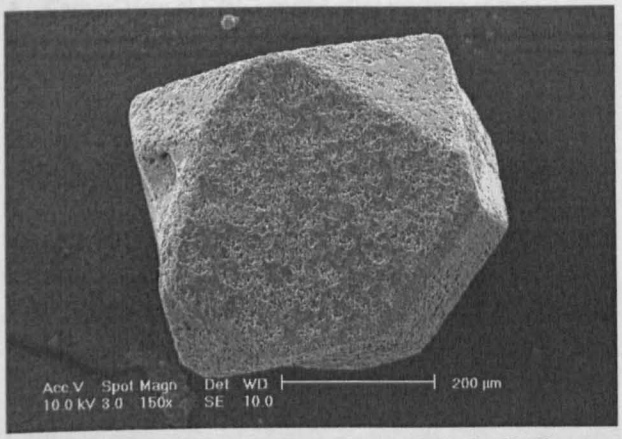

A General view of SYN-1 after leaching of the Co (CoC).

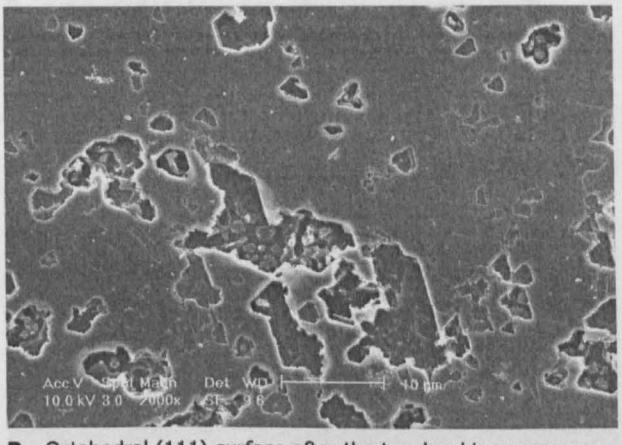

B Octahedral (111) surface after the two leaching processes.

Figure 8-14 : Various SEM micrographs of SYN-1 diamonds heat-treated with Co-(CoC) powder.

8.3.3.2C SYN-2 heat-treated with Co-EF powder

SYN-2 diamonds appeared more severely attacked by the Co-EF environment compared to the SYN-1 crystals. SYN-2 diamonds had been considerably rounded and greater loss of edge sharpness had taken place (Figure 8-15A). At first sight, surfaces appeared to have been etched randomly and with a rather irregular pattern. However, it could be recognized that flat diamond surfaces existed beneath the irregular features that had formed on the crystal surfaces (Figure 8-15B). With a more careful examination, one could identify that what was initially appearing to be random etching, was in fact a formed network of intersecting hexagonal or pyramidal geometries, like those found in the previously described diamond-cobalt systems, for which however their sharp boundaries have been lost probably due to an extended or more intensive surface attacking process (Figure 8-15B & C). This loss of etch pit sharpness produced the macroscopically observed random and irregular pattern. Subsequent graphite leaching revealed the triangular and hexagonal patterns associated with the octahedral {111} surfaces and the truncated pyramidal depressions on the cubic {100} surfaces, similarly to what has been found for the other diamond-cobalt systems previously described.

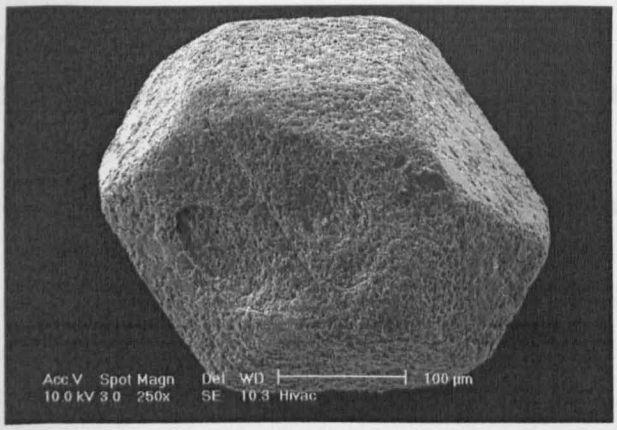

A General view of SYN-2 crystal after leaching of the Co-EF.

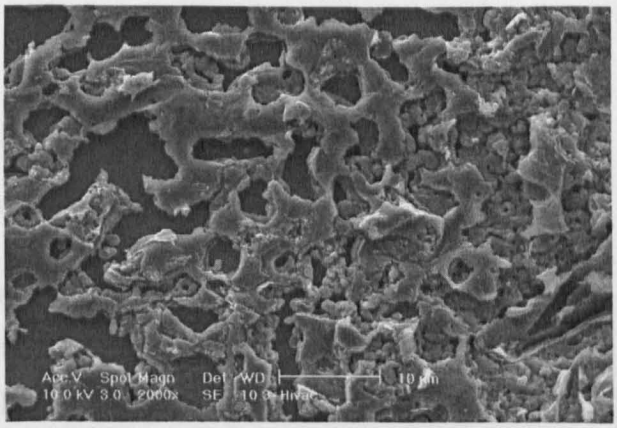

B Octahedral (111) surface after leaching of the Co-EF.

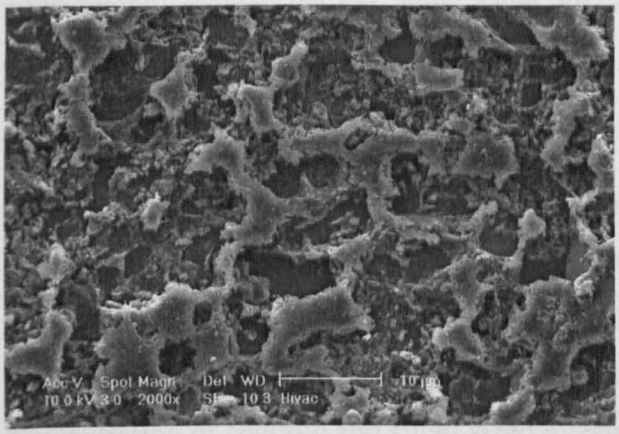

C Cubic (100) surface after leaching of the Co-EF.

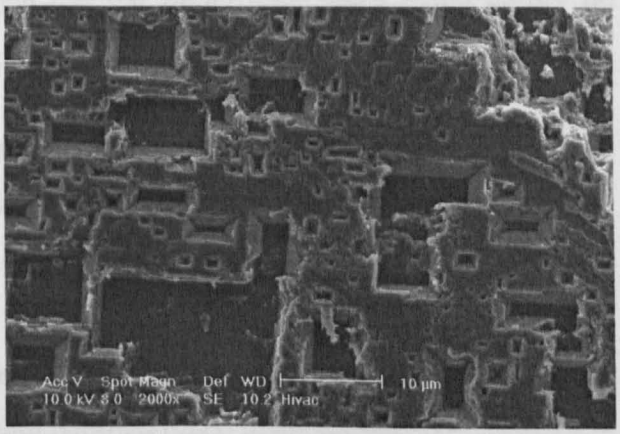

D Cubic (100) surface after the final graphite leaching.

Figure 8-15 : Various SEM micrographs of SYN-2 diamonds heat-treated with Co-EF powder.

8.3.3.2D SYN-2 heat-treated with Co-SMS powder

Co-SMS powder caused similar morphologies on SYN-2 diamond surfaces as those observed in the previous system with the Co-EF. Crystals were attacked to a slightly greater extent than when treated with the Co-EF powder (Figure 8-16A). Trigon, hexagonal and truncated pyramidal etch geometries were clearly present and formed on octahedral and cubic faces respectively (Figure 8-16B).

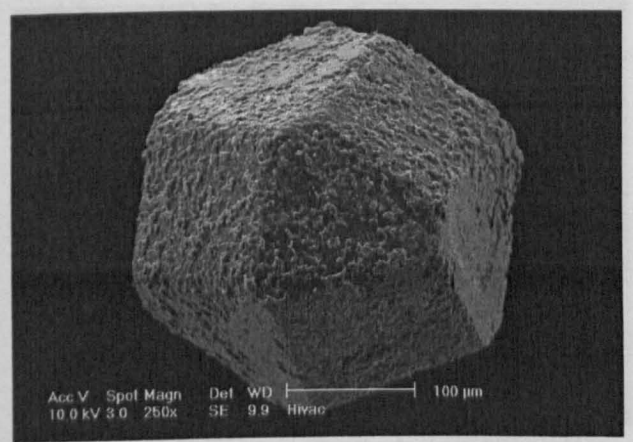

A General view of SYN-2 crystal after leaching of the Co-SMS.

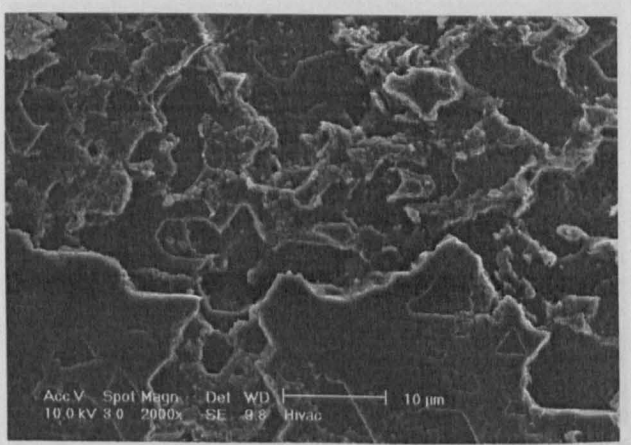

B Octahedral (111) surface after the final graphite leaching.

Figure 8-16 : Various SEM micrographs of SYN-2 diamonds heat-treated with Co-SMS powder.

8.3.3.2E SYN-2 hot-pressed with Co-EF powder

SYN-2 diamonds hot-pressed in Co-EF had also undergone surface attack and shape modification, which was however considerably smaller in extent than what was seen for all other systems of diamond-Co-powders heat-treated in the DSC furnace (Figure 8-17A).

Both octahedral {111} and the cubic {100} surfaces had a different morphology, which instead of geometrical depressions were composed of numerous spherical and rounded features appearing to be attached on a flat substrate. The density of these rounded structures was considerably greater for the cubic faces for which the flat underlying plane could hardly be distinguished (Figure 8-17B).

After graphite leaching, the rounded features almost disappeared from the diamond surfaces. Octahedral {111} planes were rather flat containing shallow depressions that made up a pattern that appeared to have been formed from numerous intersecting hexagons (Figure 8-17C). Cubic {100} surfaces were clearly modified more than the octahedral ones. Careful observation could reveal that the etch pattern resembled a surface that could possibly be formed by a high concentration of shallow and small sized intersecting parallelepiped depressions.

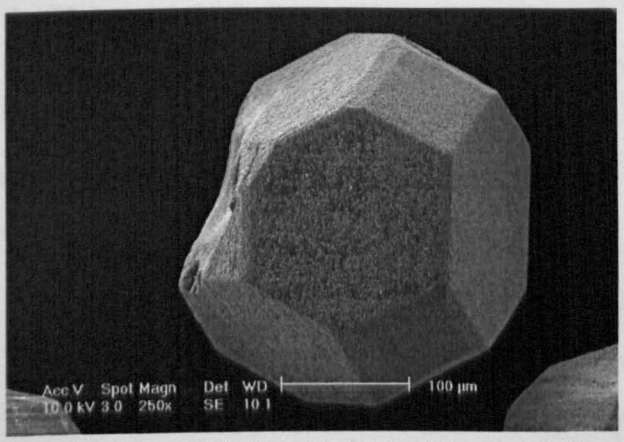

A General view of SYN-2 crystal after leaching of the Co-EF.

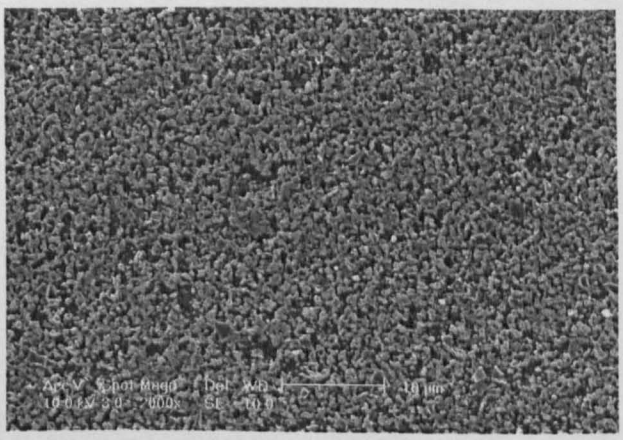

B Cubic (100) surface after leaching of the Co-EF.

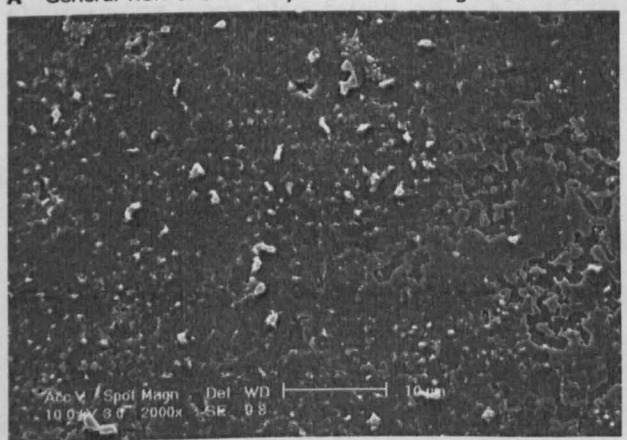

C Octahedral (111) surface after the final graphite leaching.

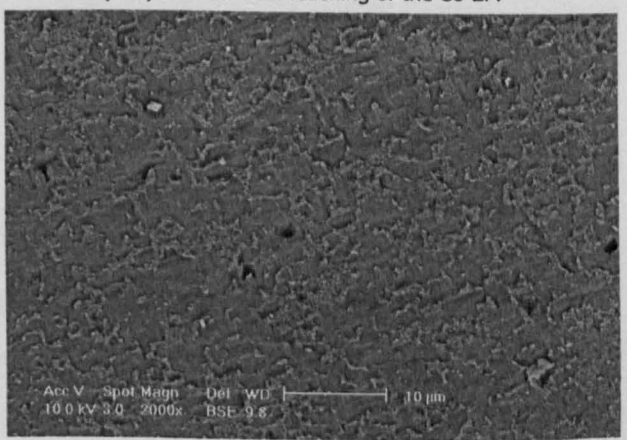

D Cubic (100) surface after the final graphite leaching (BSE mode).

Figure 8-17 : Various SEM micrographs of SYN-2 diamonds hot-pressed with Co-EF powder.

8.3.3.3 Diamond – Copper Systems

8.3.3.3A SYN-1 heat-treated with Cu powder

SYN-1 diamonds heat-treated with Cu-powders appeared macroscopically slightly etched with little loss of edge sharpness compared to diamonds treated with cobalt (Figure 8-18A). Octahedral {111} surfaces remained relatively flat and smooth containing few oriented triangular (trigons) depressions (Figure 8-18B). Cubic {100} faces were planar, but contained numerous protruding irregularly shaped islets. The latter were removed by subsequent graphite leaching leaving a relatively flat surface, which only contained few shallow depressions.

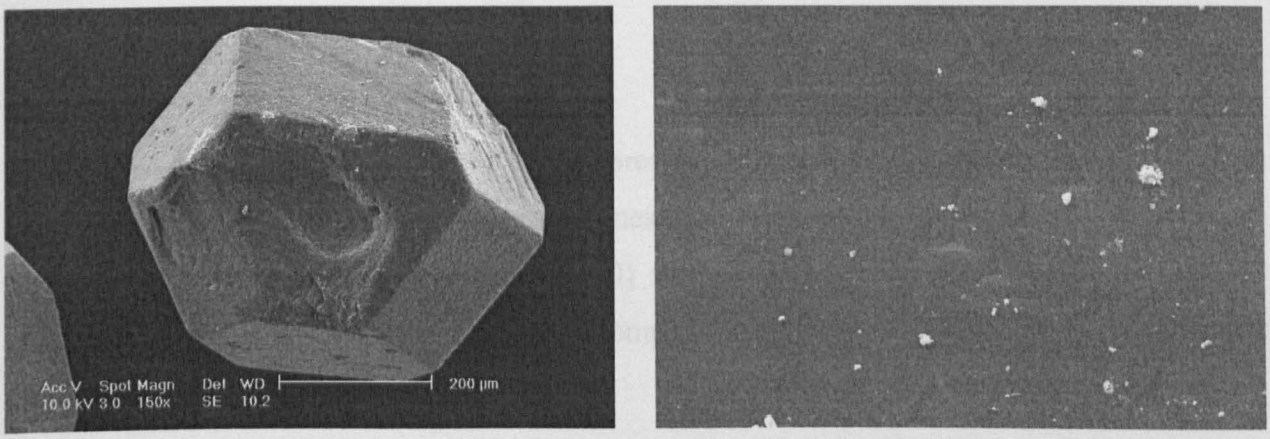

A SYN-1 crystal after the final graphite leaching. **B** Octahedral (111) surface after leaching of Cu.

Figure 8-18 : Various SEM micrographs of SYN-1 diamonds heat-treated with Cu powder.

8.3.3.3B SYN-2 heat-treated with Cu powder

Heat-treatment of SYN-2 diamonds with Cu-powder resulted in similar surface morphologies on the crystal as was found for the SYN-1 and described previously (Figure 8-19A). Etch trigons were found on octahedral {111} faces and were relatively larger and deeper. They were visually observable at relatively low magnifications compared to those observed on the SYN-1 diamonds. Depressions were also found on cubic {100} faces being relatively slightly more pronounced than those found on the SYN-1 diamonds (Figure 8-19B).

8.3.3.3C SYN-2 hot-pressed with Cu powder

SYN-2 diamonds retrieved from the hot-pressed Cu-matrix segment had almost intact surfaces, retaining the well-defined cubo-octahedral shape of the original diamonds (Figure 8-20A). Octahedral {111} faces contained few etch trigons, whereas square and parallelepiped shallow depressions of small size could be detected on the cubic {100} planes.

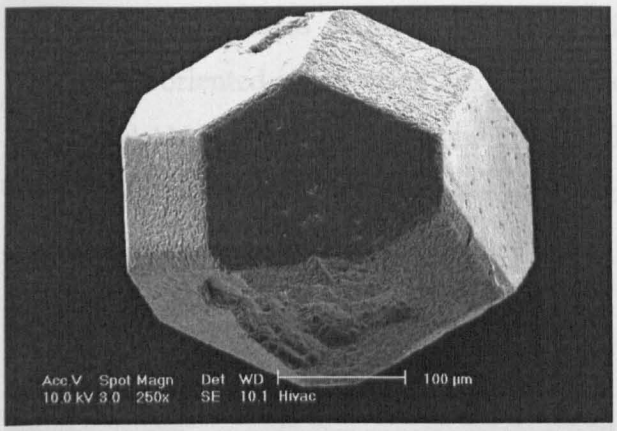

A SYN-2 crystal after the final graphite leaching.

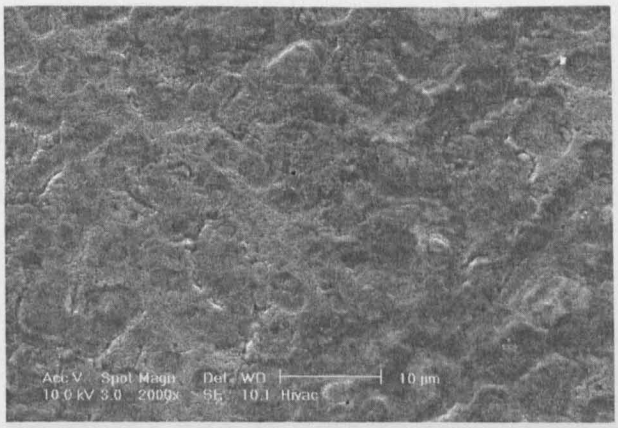

B Cubic (100) surface after final graphite leaching.

Figure 8-19 : Various SEM micrographs of SYN-2 diamonds heat-treated with Cu powder.

8.3.3.3D SYN-2 hot-pressed with $Cu_{85}Sn_{15}$ powder

The SYN-2 diamonds retrieved from the hot-pressed bronze matrix segment showed almost no signs of diamond shape change or edge sharpness loss (Figure 8-20B). Octahedral {111} faces were relatively clean and smooth. Cubic {100} surfaces gave the impression of being slightly modified in comparison with the {111}, but compared to the previously described systems were practically intact.

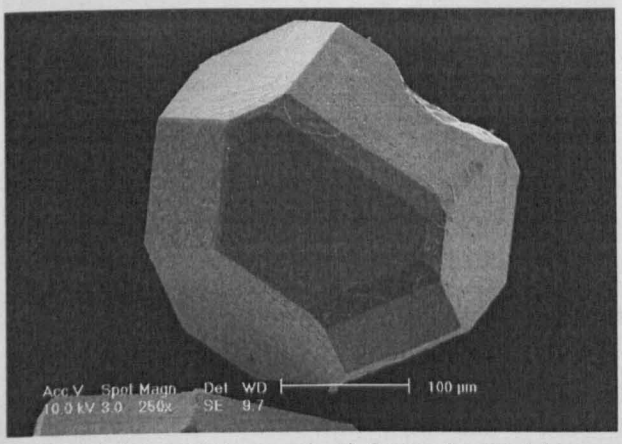

A SYN-2 diamond hot-pressed with Cu-powder. Crystal is shown after retrieval from the final graphite leaching.

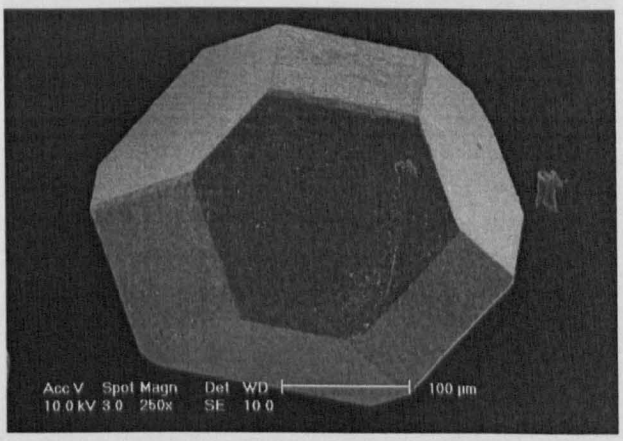

B SYN-2 diamond hot-pressed with 85/15 bronze. Crystal is shown after retrieval from the final graphite leaching.

Figure 8-20 : Various SEM micrographs of SYN-2 diamonds hot-pressed with Cu and bronze 85/15 powder.

8.3.3.4 Diamond – Nickel Systems

8.3.3.4A SYN-1 heat-treated with Ni powder

SYN-1 diamonds heat-treated with Ni-powders appeared macroscopically considerably etched with surfaces containing distinct cavities (Figure 8-21A). Compared with diamonds treated in cobalt powders, the overall crystal shape retained the cubo-octahedral form without rounding and only slight loss of edge sharpness. However, etch features were larger and deeper than those

developed on diamond surfaces in contact with both Co- and Cu-powders (Figure 8-21B). A network of oriented intersecting hexagonal and truncated pyramidal depressions had formed on octahedral {111} (Figure 8-21C) and cubic {100} surfaces respectively (Figure 8-21D). Low and high magnification examination revealed that cubic {100} faces were attacked to a greater extent than the octahedral {111} faces.

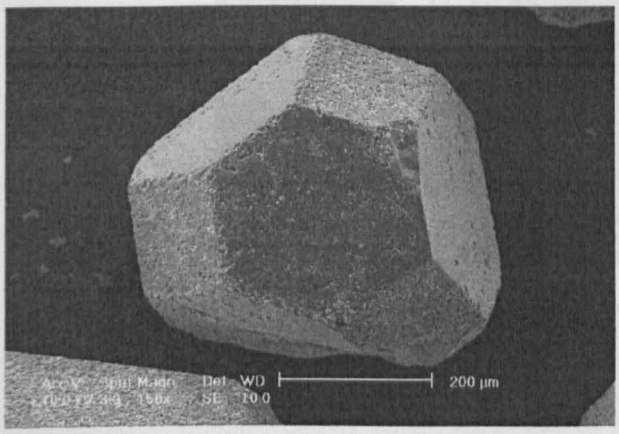

A General view of SYN-1 crystal after leaching of the Ni.

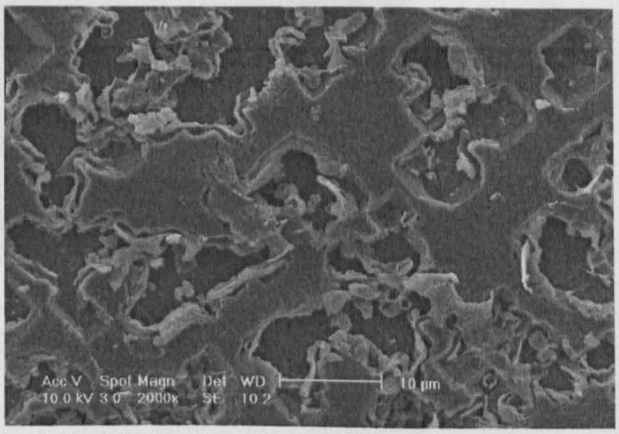

B Cubic (100) surface after leaching of the Ni.

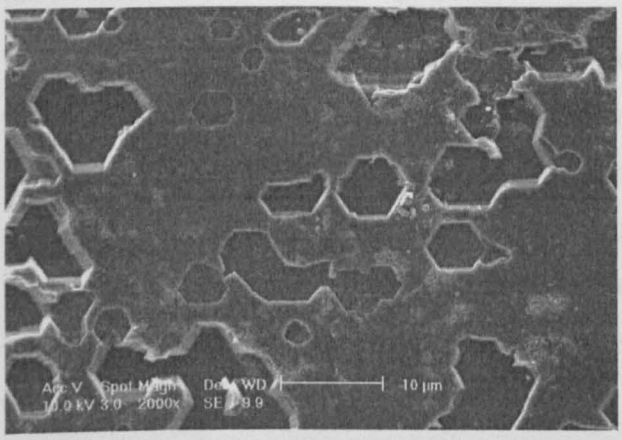

C Octahedral (111) surface after the final graphite leaching.

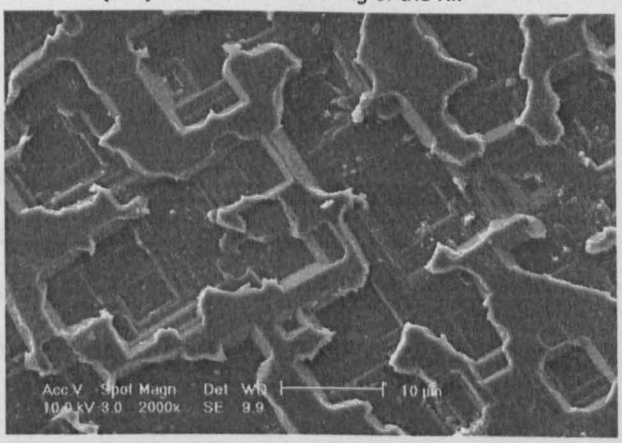

D Cubic (100) surface after the final graphite leaching.

Figure 8-21 : Various SEM micrographs of SYN-1 diamonds heat-treated with Ni powder.

8.3.3.4B SYN-2 heat-treated with Ni powder

SEM observations of SYN-2 crystals heat-treated with Ni-powders were similar to those found for the SYN-1 diamonds as described in the previous paragraph. However, the degree of SYN-2 surface attack was greater than that for the SYN-1 (see Figure 8-22). The difference between the etching of octahedral and cubic faces was not so clear as in the case of the SYN-1 diamonds. The cubic {100} faces were distorted slightly more than the octahedral {111} ones.

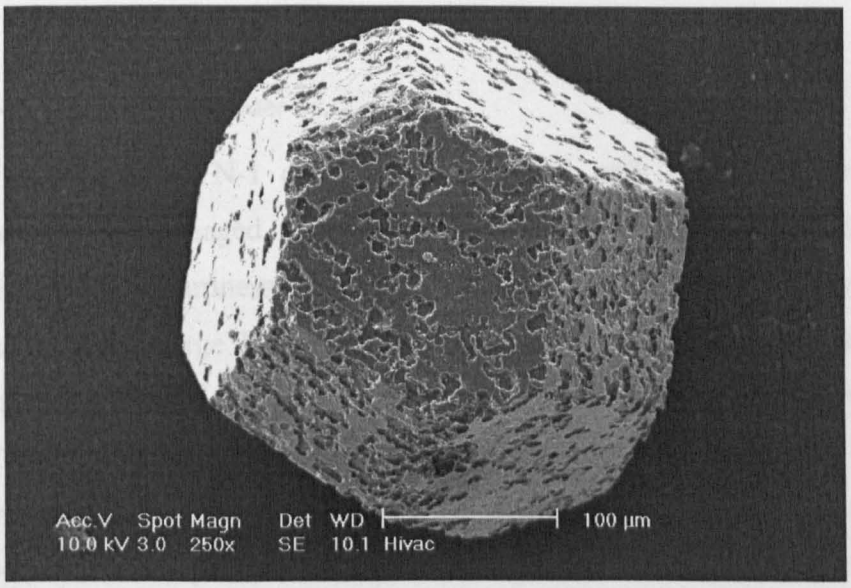

Figure 8-22 : SYN-2 diamond (MBS960 50/60 US Mesh by GE) initially heat-treated with Ni-powders in the DSC furnace and subsequently subjected to a Ni-leaching process.

8.3.3.4C SYN-2 hot-pressed with Ni powder

Surfaces of SYN-2 diamonds retrieved from the hot-pressed Ni-matrix segment were damaged at considerably lesser levels than those crystals heat-treated with Ni-powders in the DSC furnace. Hexagonal and truncated pyramidal etch cavities were present on octahedral {111} and cubic {100} faces respectively. The size and depth of the formed depressions was smaller than those found on the previously described diamond-nickel systems. Generally, it could be said that the overall appearance of the diamonds showed a finer scale attack than the one that took place during DSC treatment.

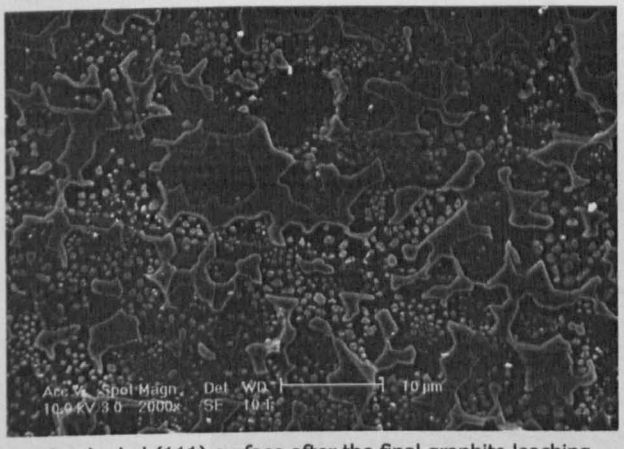

A Octahedral (111) surface after the final graphite leaching.

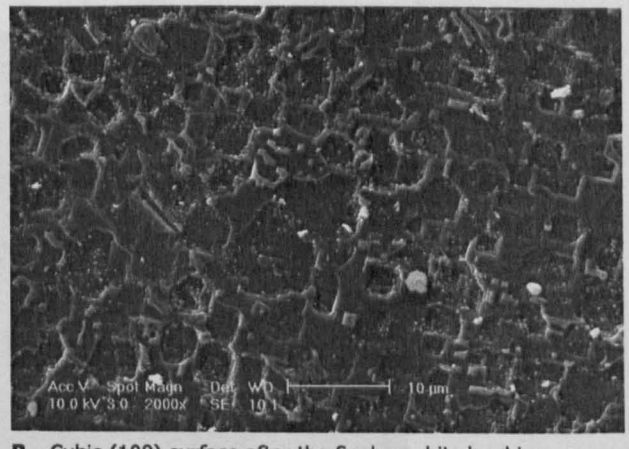

B Cubic (100) surface after the final graphite leaching.

Figure 8-23 : SEM micrographs of surfaces of SYN-2 diamonds hot-pressed with Ni powder.

8.3.3.5 Diamond – Iron Systems

8.3.3.5A SYN-1 heat-treated with Fe powder

The SEM examination of SYN-1 diamonds heat-treated with Fe-powder revealed that the crystals had been greatly damaged. Crystals had acquired a spongy surface morphology with considerable loss of edge sharpness (Figure 8-24A). Etch cavities were clearly visible even at very low magnifications. Large hexagonal depressions had formed on the octahedral {111} surfaces, which had however fully or partially lost their original angular shape and edge sharpness. In other words, the remaining area, the depression bottoms and walls, had been etched by numerous smaller sized hexagonal depressions, giving a macroscopically finer scale spongy look (Figure 8-24C). Cubic {100} faces had been attacked similarly to the octahedral {111} faces, but instead of the hexagonal depressions the etching geometry was truncated pyramids as had been seen before (Figure 8-24B). The overall degree of etching appeared to be slightly greater for the cubic {100} faces compared to the octahedral {111} ones.

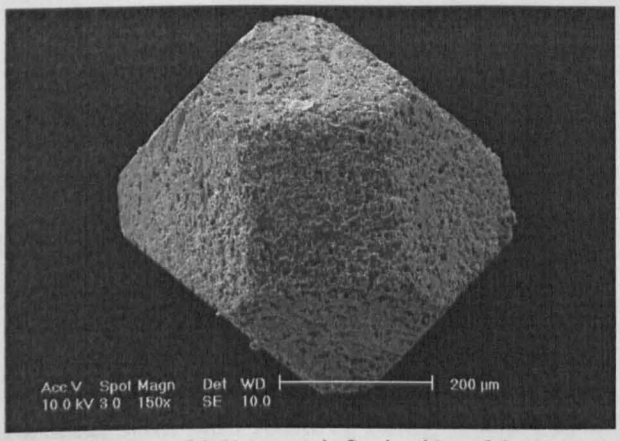

A General view of SYN-1 crystal after leaching of the Fe.

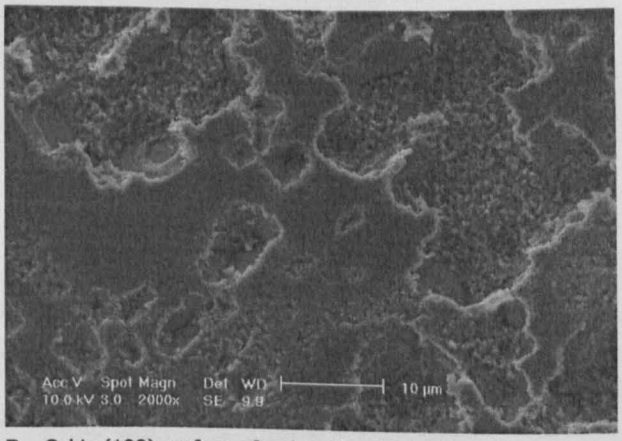

B Cubic (100) surface after leaching of the Fe.

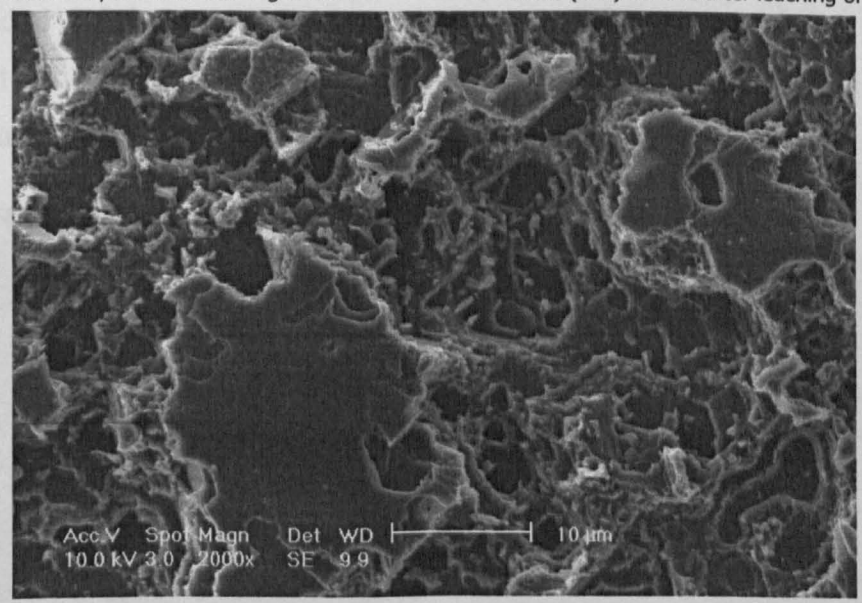

C Octahedral (111) surface after the final graphite leaching.

Figure 8-24 : Various SEM micrographs of SYN-1 diamonds heat-treated with loose Fe powders.

8.3.3.5B SYN-2 heat-treated with Fe powder

SYN-2 diamonds were etched by the Fe-powder in the same way as the SYN-1 crystals as described above. The only difference was that the degree of etching for the SYN-2 was greater compared to SYN-1 diamonds (Figure 8-25).

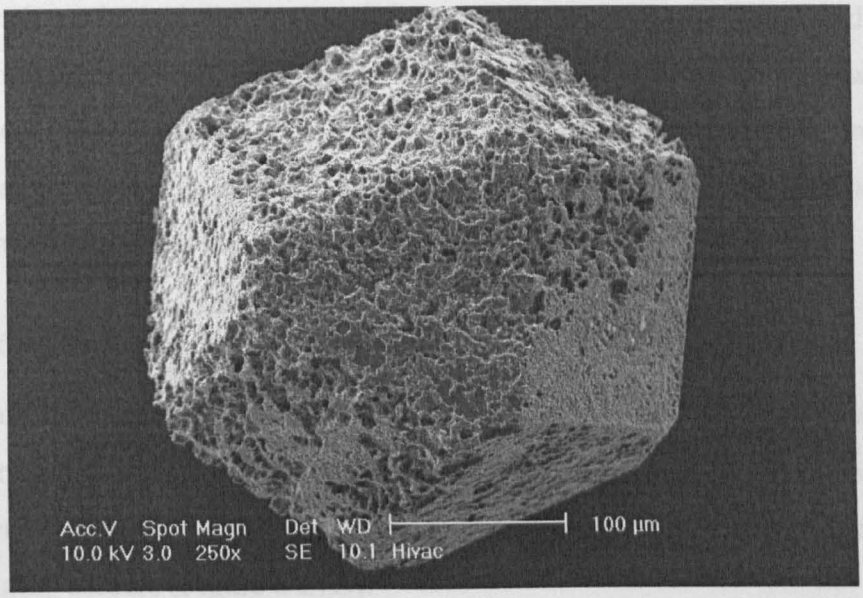

Figure 8-25 : SYN-2 diamond (MBS960 50/60 US Mesh by GE) initially heat-treated with Fe-powders in the DSC furnace and subsequently subjected to a Fe-leaching process.

8.3.3.5C SYN-2 hot-pressed with Fe powder

SYN-2 diamonds retrieved from the hot-pressed segment with the Fe-matrix had been etched at considerably lesser levels than the diamonds heat-treated with the loose Fe-powders in the DSC furnace, with etch features being smaller and shallower. Hexagonal etch features had developed on the octahedral {111} faces whereas cubic {100} surfaces were etched at a very fine scale, being difficult to identify whether or not this pattern arose from numerous intersecting small truncated pyramidal depressions.

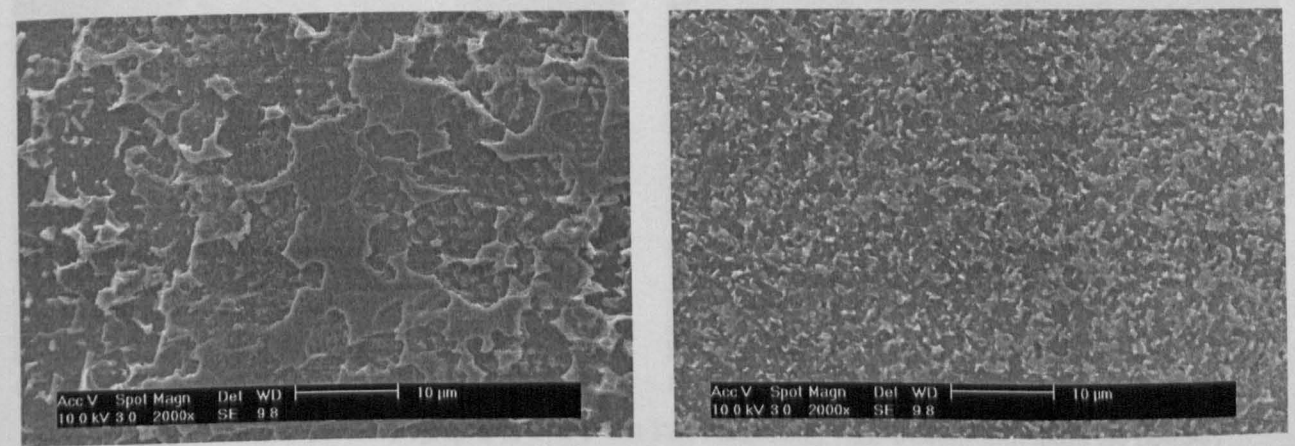

A Octahedral (111) surface after the final graphite leaching. **B** Cubic (100) surface after the final graphite leaching.

Figure 8-26 : SEM micrographs of surfaces of SYN-2 diamonds hot-pressed with Fe powders.

8.3.3.6 Diamond - Molybdenum Systems

8.3.3.6A SYN-1 heat-treated with Mo powder

SEM examination of SYN-1 diamonds that had been heat-treated with Mo-powders revealed that the abrasive grains were macroscopically almost unaffected (Figure 8-27A). Observation at lower magnifications showed diamond surfaces to retained their smoothness and flatness, while crystal edges remained sharp. Inspection at higher magnification in backscattering mode revealed that both the octahedral {111} and cubic {100} faces contained numerous very small rounded contrasting islets (Figure 8-27B). These were particularly concentrated at specific areas such as larger surface cavities.

8.3.3.6B SYN-2 heat-treated with Mo powder

Similarly to SYN-1 diamonds, the SYN-2 crystals seemed unaffected by the heat-treating with the Mo-powders when examined at low magnification (Figure 8-27C). Backscattered imaging revealed a spread concentration of contrasting features such as bright white islets and irregular planar areas of grey colours (Figure 8-27D).

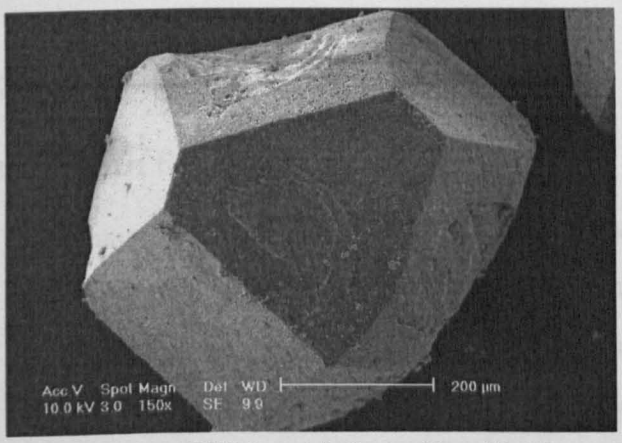

A General view of SYN-1 crystal after leaching of the Mo.

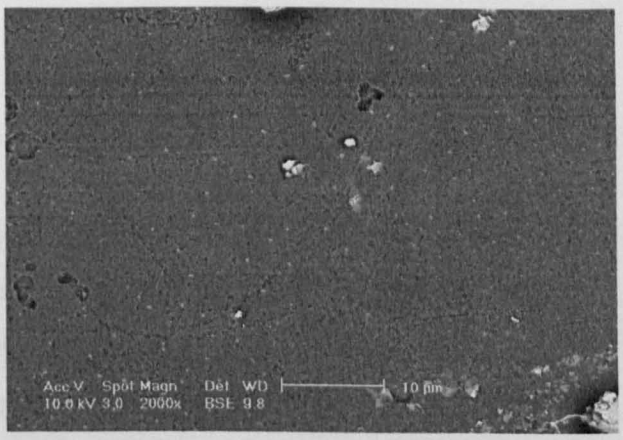

B Octahedral (111) surface of SYN-1 after the leaching of Mo.

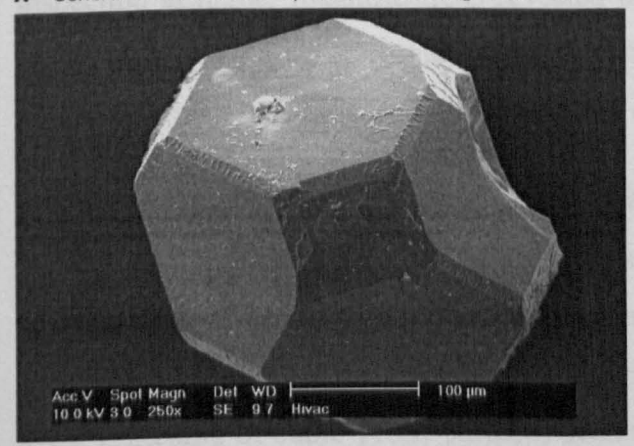

C General view of SYN-2 crystal after final graphite leaching.

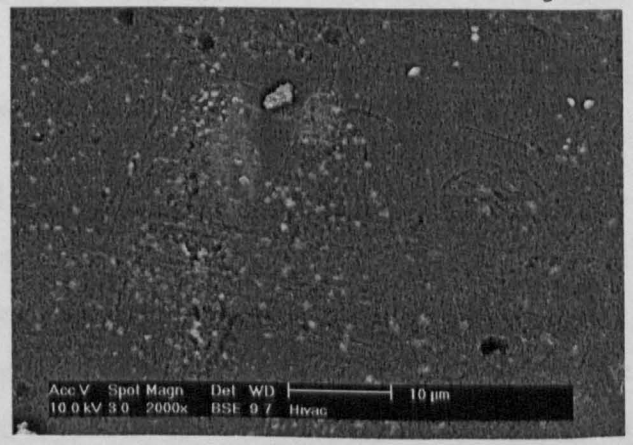

D Cubic (100) surface of SYN-2 after the leaching of Mo.

Figure 8-27 : Various SEM micrographs of SYN-1 and SYN-2 diamonds heat-treated with loose Mo powder.

8.3.3.6C SYN-2 hot-pressed with Mo powder

SYN-2 diamonds retrieved from the hot-pressed segment with the Mo-matrix appeared to be unaffected by the sintering process in the metallic environment (Figure 8-28A). Octahedral {111} faces had developed a few small etch trigons as well as a few rounded cavities (Figure 8-28B). Cubic {100} faces contained a pattern of planar features evenly protruding from the underlying surface similar to what was found on the original SYN-2 crystals.

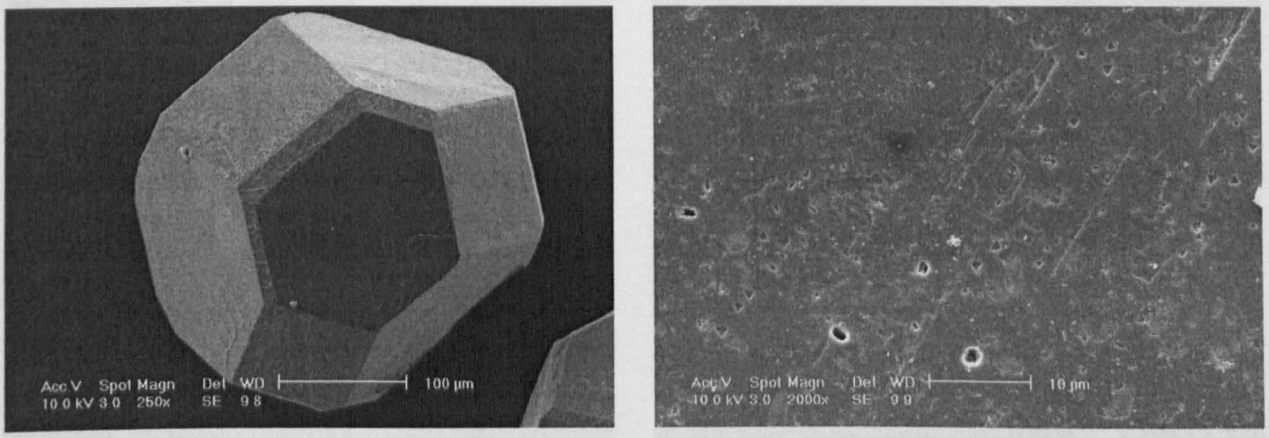

A General view of SYN-2 crystal after final graphite.

B Octahedral (111) surface of SYN-2 after the leaching of Mo.

Figure 8-28 : Various SEM micrographs of SYN-1 diamonds hot-pressed with Mo powder.

8.3.3.7 Diamond – Tungsten Systems

8.3.3.7A SYN-1 heat-treated with W powder

Low magnification SEM examination of SYN-1 diamonds that had been initially heat-treated with W-powders and subsequently exposed to the W-metal leaching revealed a white contrasting layer to have been developed on diamond surfaces (Figure 8-29A). The layer almost fully covered the crystals apart from the edges, where coverage was not entire (Figure 8-29A & B). Inspection at higher magnifications revealed that both octahedral {111} and cubic {100} faces where covered by a dense formation of platelets. The platelets seemed to have grown in groups, randomly grown outwards from the underlying diamond surface. (Figure 8-29C & D).

Subsequent graphite leaching removed almost all the platelets from the SYN-1 diamonds (Figure 8-29E). The uncovered diamond surfaces were macroscopically smooth and the edges retained the sharpness of the original crystals. Examination at higher magnifications revealed octahedral (111) faces to contain traces of a network of intersecting hexagonal shallow depressions (Figure 8-29F). Etching of cubic {100} surfaces occurred also at a very fine scale but it was difficult to distinguish whether the observed pattern arose from very small and shallow truncated pyramids.

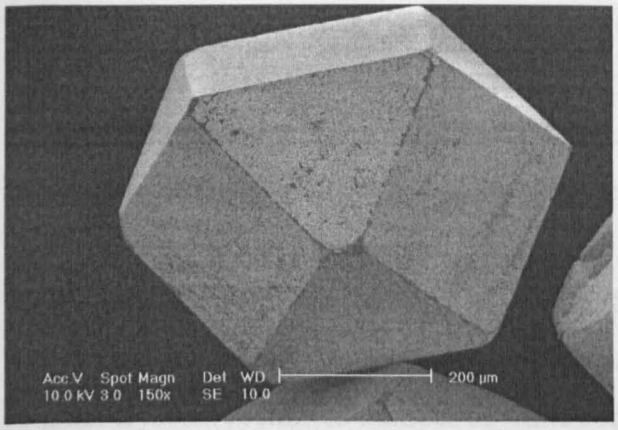

A General view of SYN-1 crystal after leaching of the W.

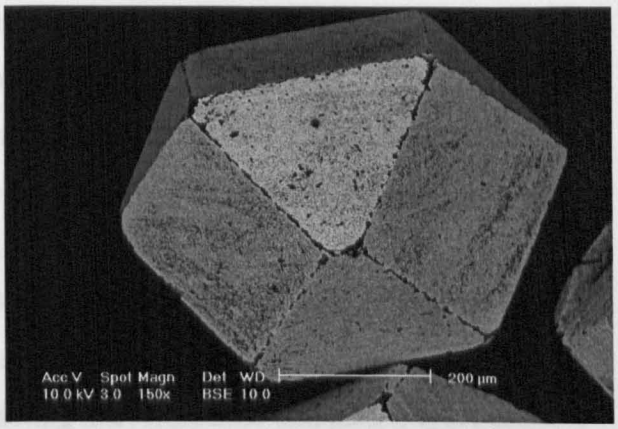

B Micrograph A, view in BSE mode.

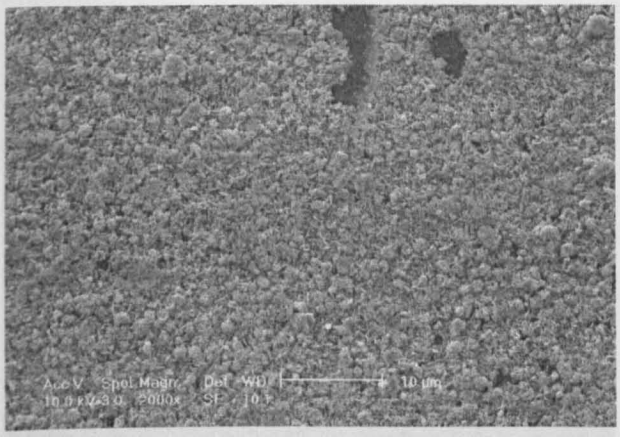

C Octahedral (111) surface of SYN-2 after the leaching of W (Magnification 2000x).

D Cubic (100) surface of SYN-2 after the leaching of Mo (Magnification 20000x).

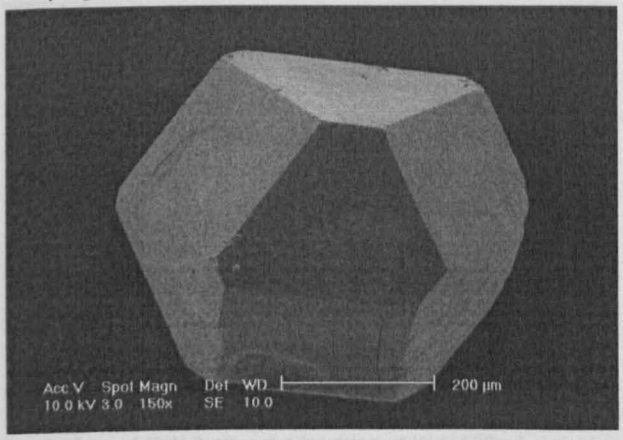

E General view of SYN-1 crystal after final graphite leaching.

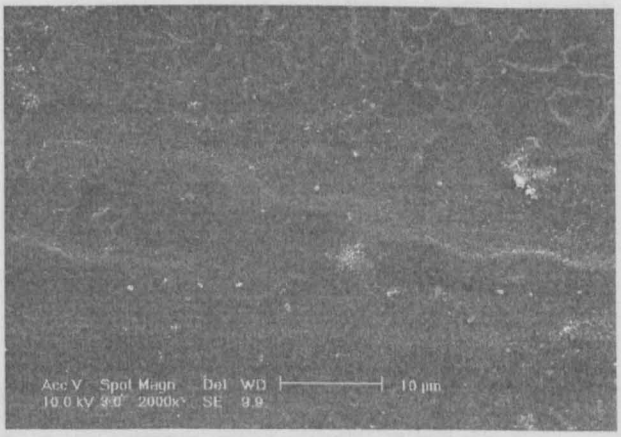

F Octahedral (111) surface after final graphite leaching.

Figure 8-29 : SYN-1 diamond (SDA100 30/40 US Mesh by DB) initially heat-treated with W-powders in the DSC furnace and subsequently subjected to a W-leaching process.

8.3.3.7B SYN-2 heat-treated with W powder

Platelets identical to those observed on the SYN-1 diamonds as described in the previous paragraph were also found on the SYN-2 diamond surfaces (Figure 8-30A to D). However, the crystals were not entirely covered, as was the case for the SYN-1. Cubic {100} faces were covered to a greater extent compared to the octahedral {111} planes (Figure 8-30A & B).

Subsequent graphite leaching removed the majority of the platelets leaving crystals with relatively smooth surfaces and sharp edges. Some platelets appeared to withstand the final leaching, and were preferentially located at crystal defected areas, such as large cavities and surface irregularities. Octahedral {111} surfaces clearly had acquired an etch pattern formed by a network of intersecting hexagonal depressions occasionally containing few rounded cavities but also some small white contrasting islets (Fig. 8-30E). Cubic {100} surfaces contained dendritic planar features evenly protruding from the underlying surface similar to those found on the original crystals. A limited number of white contrasting islet were also detected (Figure 8-30F).

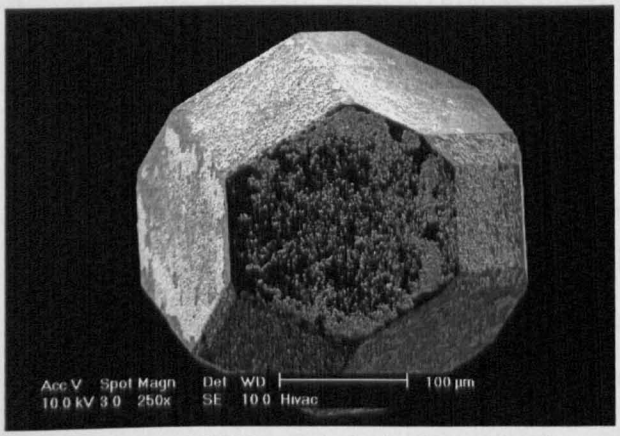

A General view of SYN-2 crystal after leaching of the W.

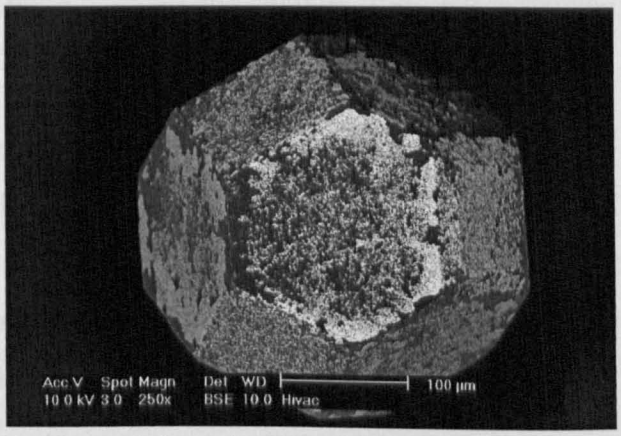

B Micrograph A, view in BSE mode.

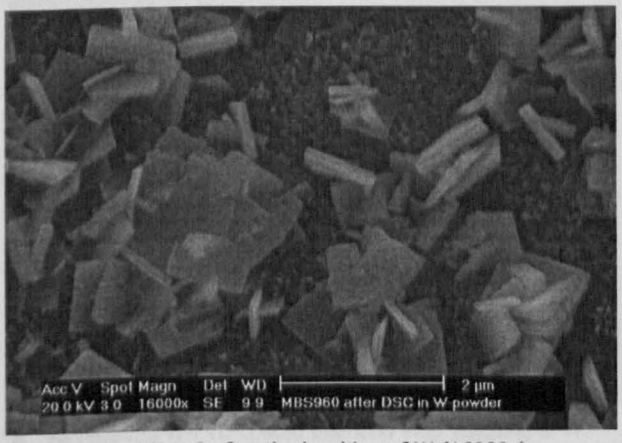

C Surface of SYN-2 after the leaching of W (16000x).

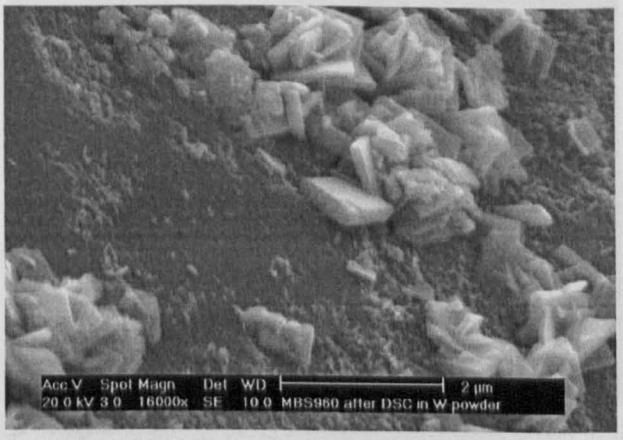

D Surface of SYN-2 after the leaching of W (16000x).

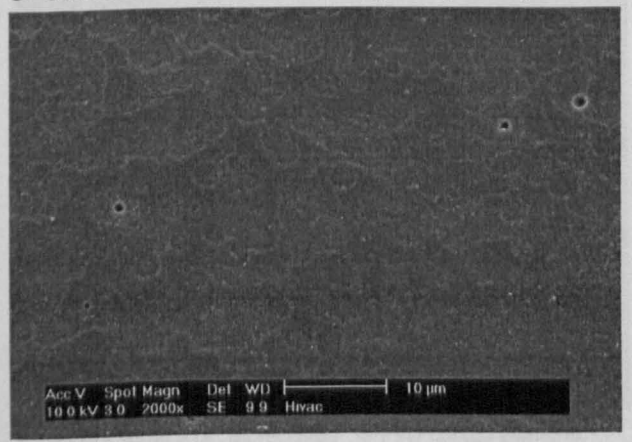

E Octahedral (111) surface after final graphite leaching.

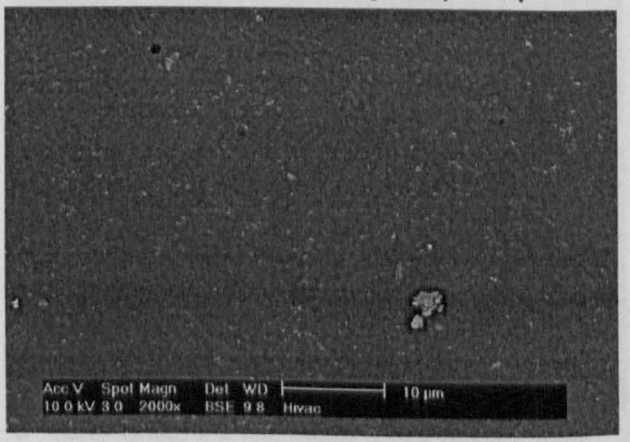

F Cubic (100) surface of SYN-2 after final graphite leaching (BSE mode).

Figure 8-30 : Various SEM micrographs of SYN-2 diamonds heat-treated with loose W powder.

8.3.3.7C SYN-3 coated with W by PVD (Code CD13)

SEM examination revealed that a continuous coating layer was not present on the surfaces of the W-PVD-coated SYN-3 diamonds (Figure 8-31A). Platelets identical to those described above were found in crystal defected areas (Figure 8-31B). Occasionally, pieces of a dense coating could be found on flat faces and the layer appeared to include some form of platelet structure. Subjecting the crystals to W-leaching followed by graphite leaching, caused almost the total removal of all contrasting structures. The octahedral {111} surfaces appeared smooth, but contained numerous grey elongated and irregular features, which seemed to be incorporated in the underlying diamond surface (Figure 8-31C). Traces of small and shallow truncated pyramidal etch depressions could be identified on cubic {100} faces as well as small grey contrasting islets.

No particularly different observations could be made for the coated crystals that had been heat-treated in the DSC furnace and subsequently W-leached compared to the "as received" crystals. Subsequent graphite leaching of these crystals showed that diamonds were practically intact macroscopically. Octahedral {111} faces contained numerous small and shallow cavities. Cubic {100} faces were also etched similarly, but at reduced level.

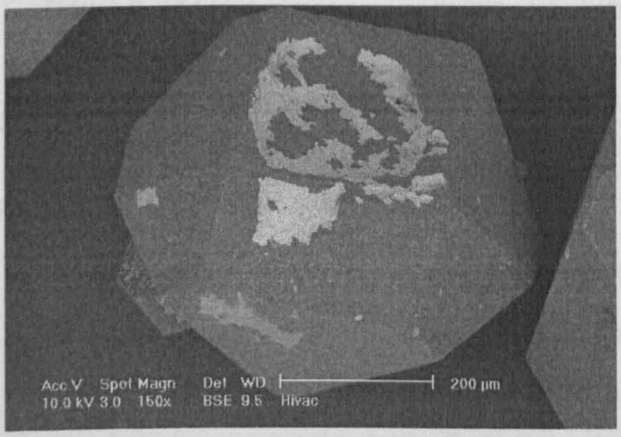

A As received W-PVD-coated diamond after leaching of W.

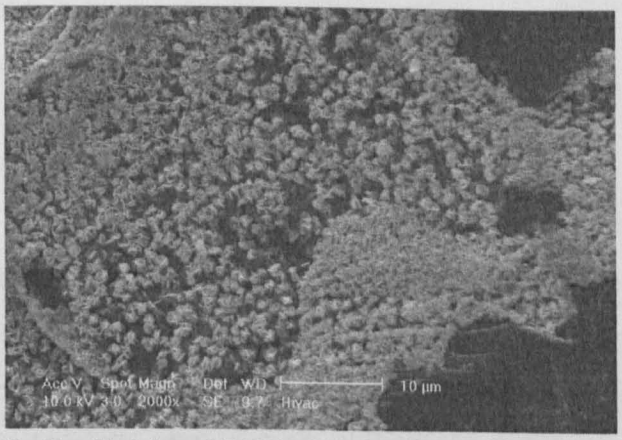

B Magnified view of (111) surface of crystal shown in A.

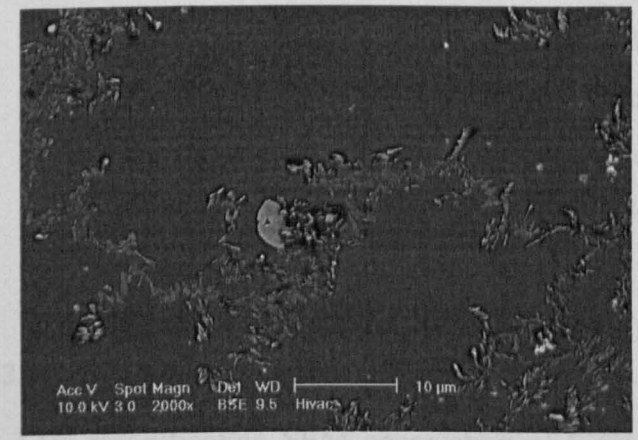

C {111} surface of "as received" W-PVD-coated diamond after final graphite leaching (BSE mode).

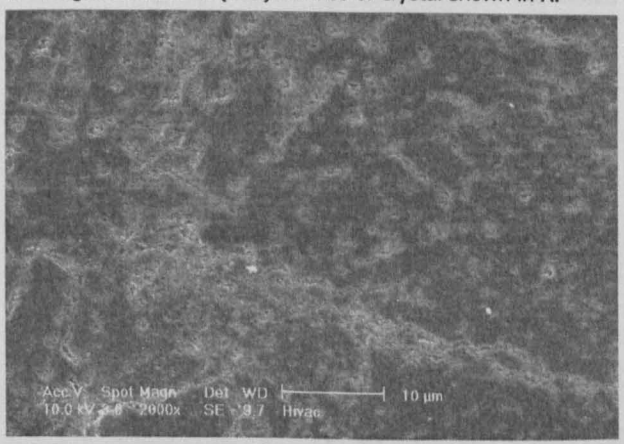

D {111} surface of a heat-treated W-PVD-coated diamond after the final graphite leaching process.

Figure 8-31 : SEM micrographs of W-PVD-coated (CD13) diamonds at various stages of the DRE.

8.3.3.7D SYN-3 coated with W by PVD industrially heat-treated (Code CD23)

The leaching process for metal removal resulted in considerable dissolution of the coating for the W-PVD-coated SYN-3 diamonds that had been annealed at 500°C for 20min in a reducing $10H_2/90N_2$ atmosphere (Figure 8-32A). The coating that withstood the leaching appeared to be dense but was extensively cracked (Figure 8-32B). Subsequent leaching in chromic acid removed the majority of this dense coating and only few contrasting features were evident on diamond surfaces. The stripped diamond surfaces showed signs of very limited etching.

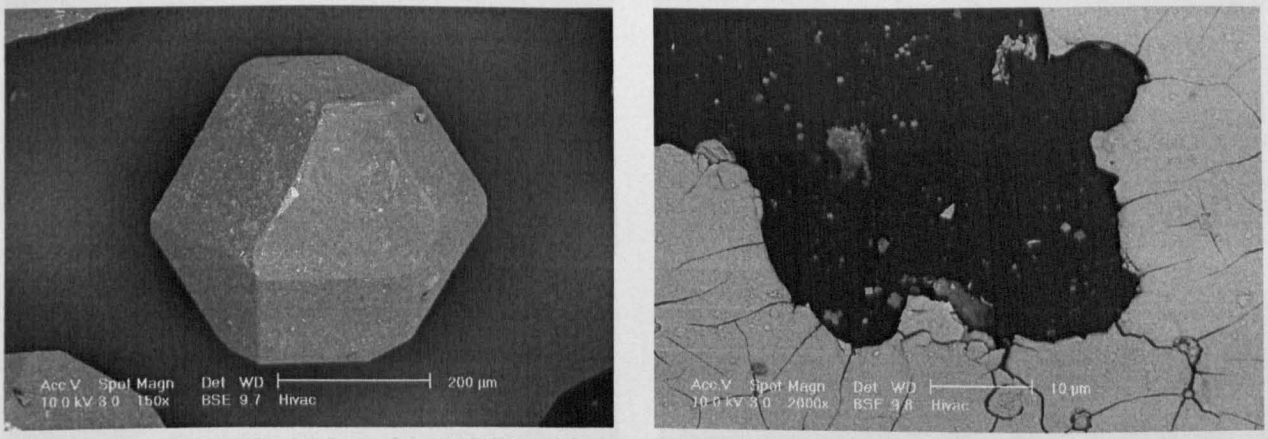

A General crystal view after leaching of the W (BSE mode). **B** (100) surface after leaching of the W (BSE mode).

Figure 8-32 : SEM micrographs of W-PVD-coated (CD23) heat-treated at 500°C / 20min. / $10H_2$-$90N_2$.

8.3.3.8 Diamond – Titanium Systems

8.3.3.8A SYN-1 heat-treated with Ti powder

SEM examination of SYN-1 crystals that had been heat-treated with Ti-powders revealed that a thick coating had been formed on the diamond surfaces (Figure 8-33A). The coating partially covered the grains and was heavily cracked along the surface (Figure 8-33B). The underlying diamond surfaces contained small shallow depressions. Graphite leaching resulted in the total removal of the coating. It was then revealed that octahedral {111} faces had a surface pattern, which was built-up by a large number of intersecting shallow depressions (Figure 8-33C). Because of their small size, it was difficult to distinguish whether these formed cavities were intersecting hexagonal or triangular etch pits. Cubic {100} faces had an overall fine scale etching by very small etch pits (Figure 8-33D).

8.3.3.8B SYN-2 heat-treated with Ti powder

Low magnification SEM observation of SYN-2 crystals heat-treated with Ti-powders showed that grains did not undergo any type of macroscopically visible shape change or surface etching. Backscattered imaging demonstrated an even coverage of small contrasting islets (Figure

8-34B). Their surface concentration appeared to increase in large diamond crystal defect areas. Examination of faces at high magnification revealed that the majority of contrasting islets had the form of platelets, partially emerging form the underlying diamond substrate appearing to be growing outwards and in random directions (Figure 8-34B).

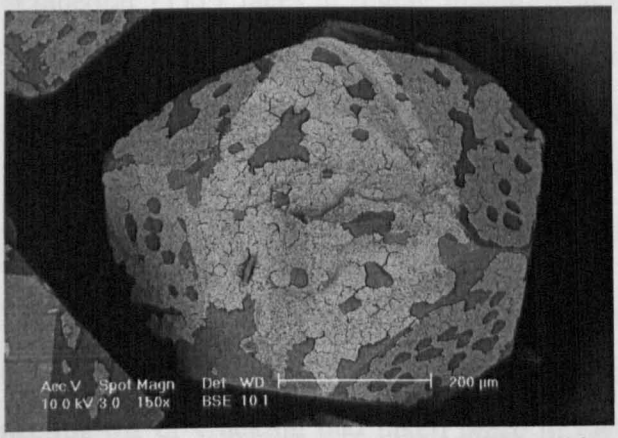

A Aspect of a SYN-1 crystal after leaching of Ti (BSE mode).

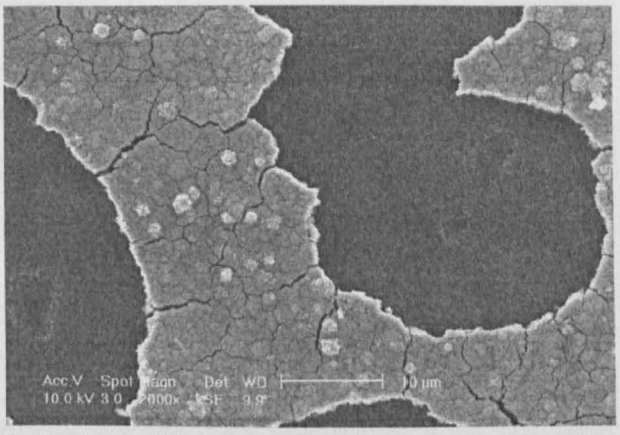

B Octahedral (111) surface of crystal shown in A (SE mode).

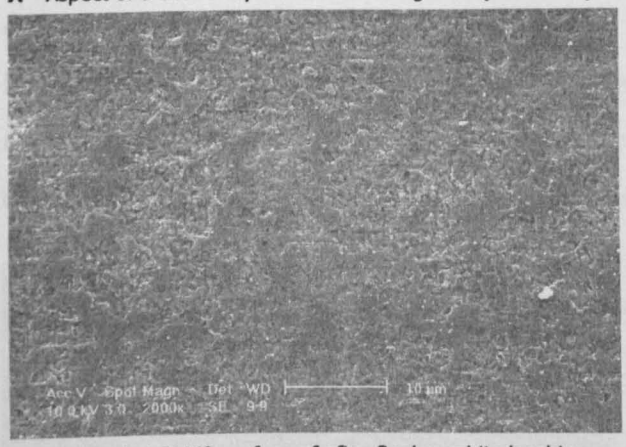

C Octahedral {111} surface of after final graphite leaching.

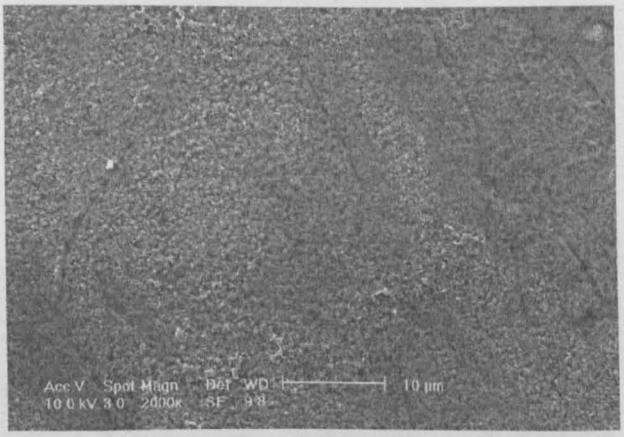

D Cubic {100} surface of after final graphite leaching.

Figure 8-33 : SEM micrographs of SYN-1 diamond heat-treated with loose Ti-powder.

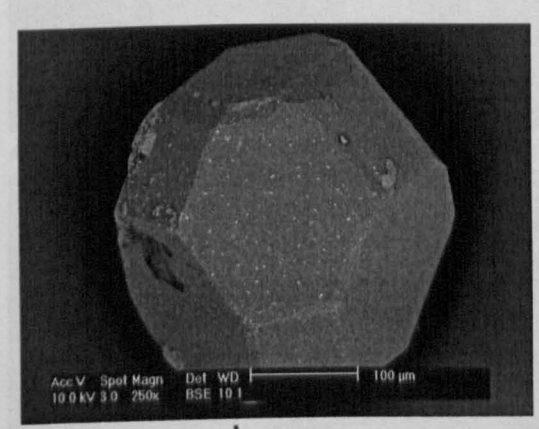

A

Magnified view of (111) surface

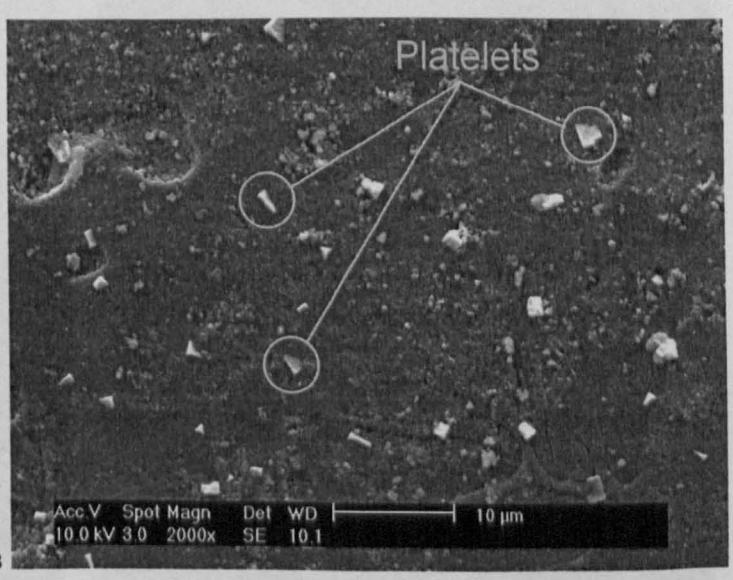

B

Figure 8-34 : SYN-2 diamond (MBS960 50/60 US Mesh by GE) initially heat-treated with Ti-powders in the DSC furnace and subsequently subjected to a Ti-leaching process. Some of formed platelets as described in the text are pointed out by the cycles.

8.3.3.8C SYN-1 coated with Ti by CVD (Code CD6)

SEM examination showed that metal leaching of the CVD Ti-coated SYN-1 diamonds resulted in total dissolution of the Ti-coating (Figure 8-35A). This demonstrated that the diamonds had not undergone any macroscopically significant change during the CVD deposition. Inspection of octahedral {111} faces at higher magnifications revealed the presence of numerous imprints of etch trigons that seemed evenly spread (Figure 8-35B). Cubic {100} faces were also etched but to a comparably lesser extent and without signs of any particular geometrical etch pits. Further graphite leaching of the "as received" Ti-coated diamonds did not change the appearance of crystals as described previously. Few contrasting platelet features could be found on surfaces.

Following heat-treating of the diamonds in the DSC furnace, the Ti-coating remained almost entirely attached to the crystals even after the Ti-leaching process. A small degree of coating peeling-off or cracking had taken place in the parts of the coating that covered large diamond defective areas (Figure 8-35C). The coating in these locations was brighter as seen in the backscattered imaging mode of the SEM (Figure 8-35D). Examination at higher magnifications, revealed that the coating was dense with only few cracks. In areas where peeling-off had occurred, the underlying diamond surface appeared almost intact.

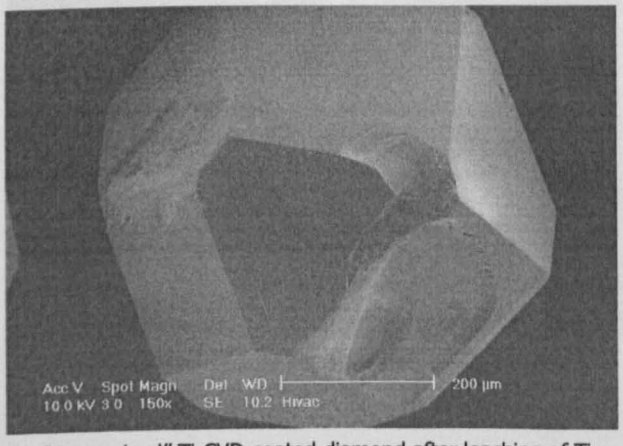

A "As received" Ti-CVD-coated diamond after leaching of Ti.

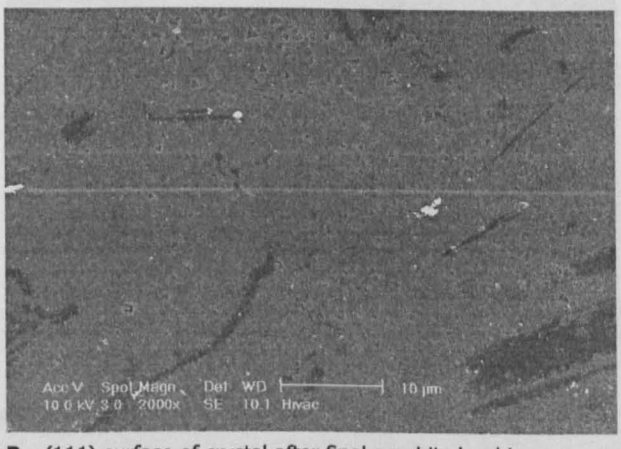

B (111) surface of crystal after final graphite leaching.

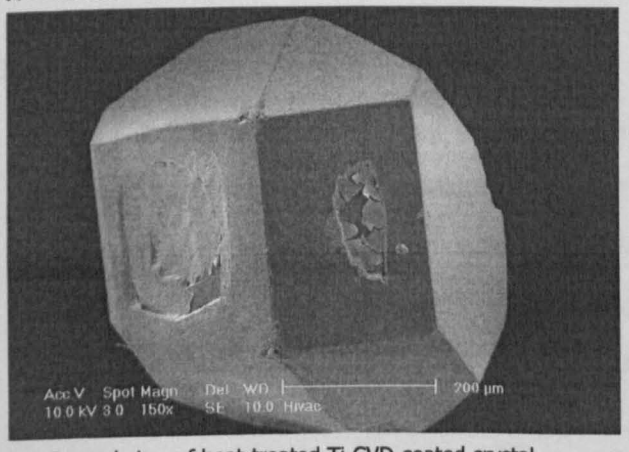

C General view of heat-treated Ti-CVD-coated crystal.

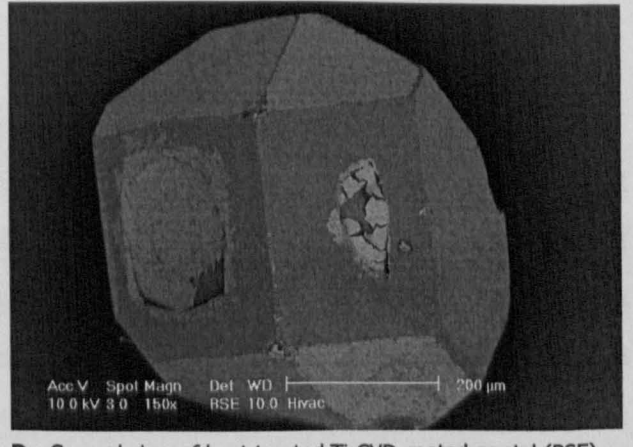

D General view of heat-treated Ti-CVD-coated crystal (BSE).

Figure 8-35 : SEM micrographs of Ti-CVD-coated (CD6) diamonds at various stages of the DRE.

8.3.3.8D SYN-1 coated with Ti by CVD (by DB) industrially heat-treated (Code CD18)

SEM examination showed that metal leaching of the CVD Ti-coated SYN-1 diamonds that had been heat-treated under industrial conditions at 500°C for 20min in a $10H_2/90N_2$ atmosphere resulted in broad peeling of the Ti-coating (Figure 8-36A). Coating was preserved to a higher extent on octahedral {111} than on the cubic {100} faces. White contrasting islets were visible even at low magnifications. Overall crystal shape and edge sharpness did not change compared to the original non-coated SYN-1 diamonds. A high concentration of features such as small islets and larger spheres were observed on octahedral {111} surfaces. Backscattered imaging showed islets to contrast as bright white spots whereas the larger spheres left imprints of black cycles (Figure 8-36B). Cubic {100} planes also contained small contrasting islets but the concentration was lower than what observed for the octahedral {111} faces. No spherical features were observed. Subsequent graphite leaching caused the entire removal of the Ti-coating. Crystals had smooth faces and sharp edges similarly to the original non-coated SYN-1 diamonds. Examination at high magnifications showed octahedral {111} faces to be smooth with few small contrasting islets, whereas cubic {100} faces contained few shallow depressions.

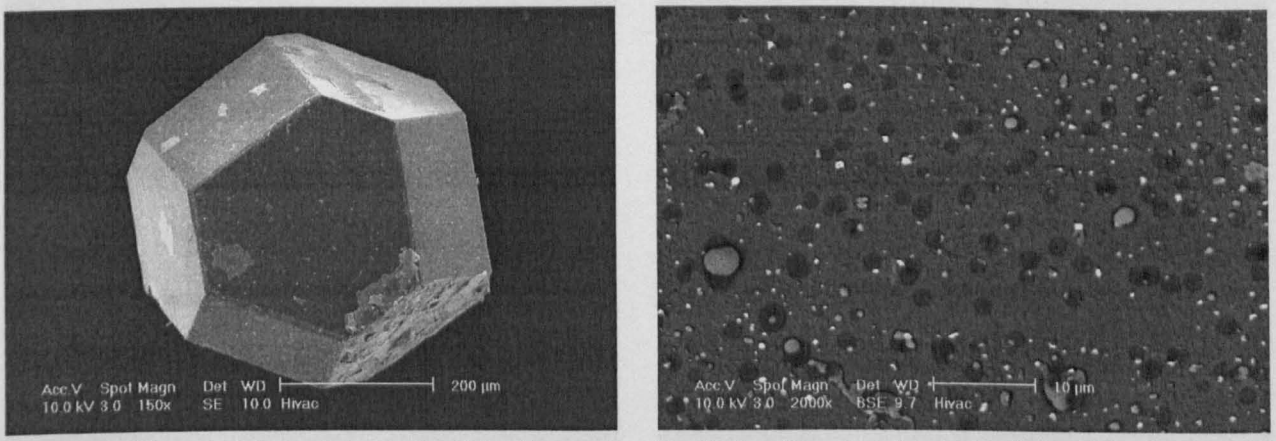

A CD18 Ti-CVD-coated diamond shown after Ti-leaching. **B** (111) surface of crystal after final graphite leaching.

Figure 8-36 : Micrographs of Ti-CVD-coated (CD18) diamonds heat-treated at 500°C / 20min. / $10H_2$-$90N_2$.

8.3.3.8E SYN-1 coated with Ti by PVD (Code CD8)

SEM examination showed that metal leaching of the "as received" PVD Ti-coated SYN-1 diamonds resulted in total dissolution of the Ti-coating (Figure 8-37A). Diamonds had not undergone any macroscopically significant change during the PVD deposition. Inspection of octahedral {111} faces at higher magnifications revealed a stepped morphology containing numerous small white contrasting islets (Figure 8-37B). Cubic {100} faces appeared almost intact.

Diamonds heat-treated in the DSC furnace were found to be partially covered by the coating layer. The coating appeared to preferentially remain attached at the large scale defected areas of the crystals (Figure 8-37C). Examination at higher magnifications, revealed that the coating was dense but contained some cracks (Figure 8-37D). In areas where peeling-off had occurred, the underlying diamond surface appeared almost intact. Further graphite leaching revealed numerous platelets emerging from octahedral {111} faces. Hexagonal contrasting prints were visible on diamond surfaces in areas in between the platelets (see Figure 8-38 on page 159). Cubic {100} planes also contained numerous contrasting features, but they were rather rounded and small in size compared to those found on {111}.

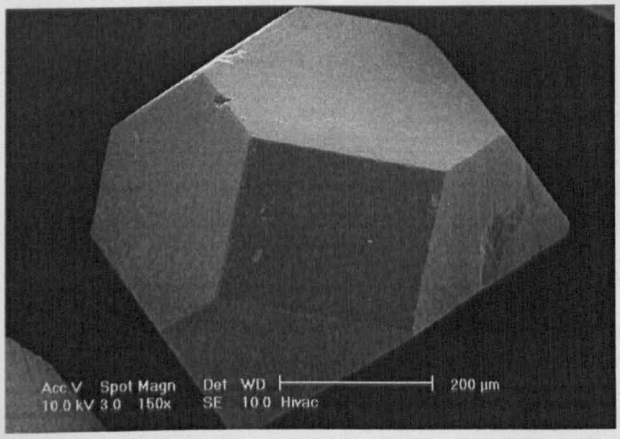

A "As received" Ti-PVD-coated diamond after leaching of Ti.

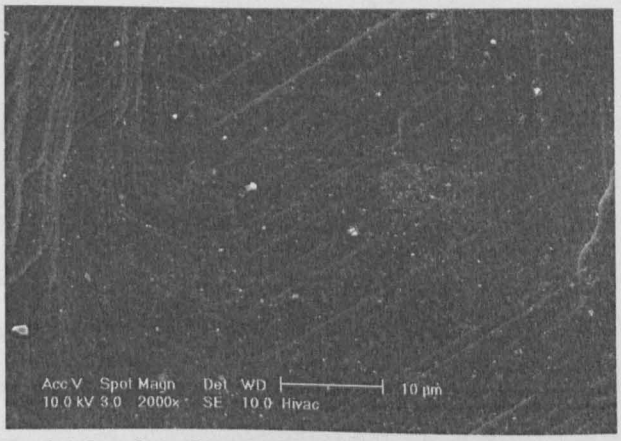

B (111) surface of crystal after leaching of Ti.

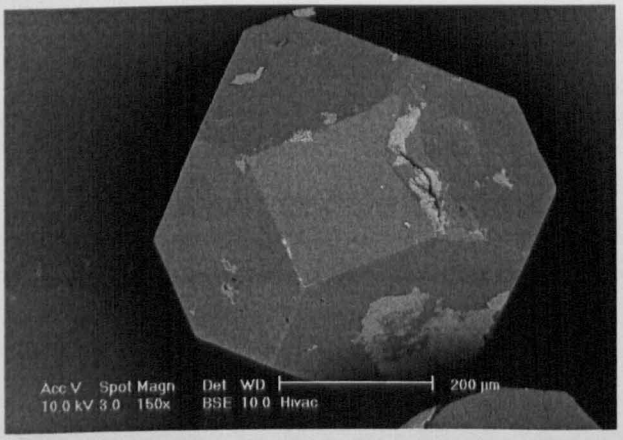

C General view of heat-treated Ti-PVD-coated crystal (BSE).

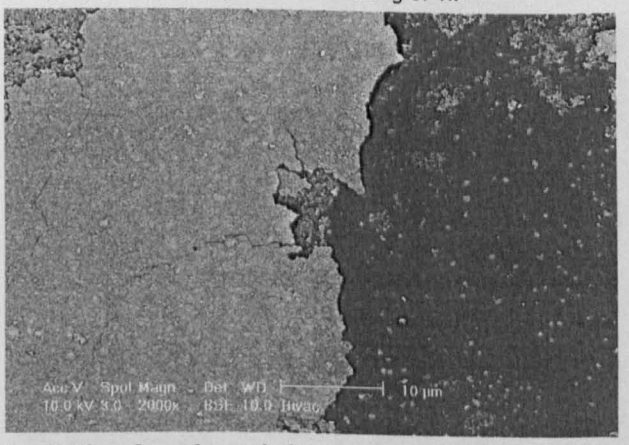

D (111) surface of crystal after leaching of Ti (BSE mode).

Figure 8-37 : SEM micrographs of Ti-PVD-coated (CD8) diamonds at various stages of the DRE.

8.3.3.8F SYN-1 coated with Ti by PVD (by TC) industrially heat-treated (Code CD19)

SYN-1 diamonds PVD coated with titanium by the TC manufacturer appeared to have lost a great part of the coating after the Ti-metal leaching that followed the heat treatment at 500°C for 20min in a $10H_2/90N_2$ atmosphere (Figure 8-39A). Octahedral {111} faces contained numerous contrasting features such as small grey islets and white cubic structures. The latter appeared as

black traces when viewed in BSE mode. Cubic {100} faces contained a large number of white contrasting platelets that appeared as lightly emerging from the diamond surface (Figure 8-39B).

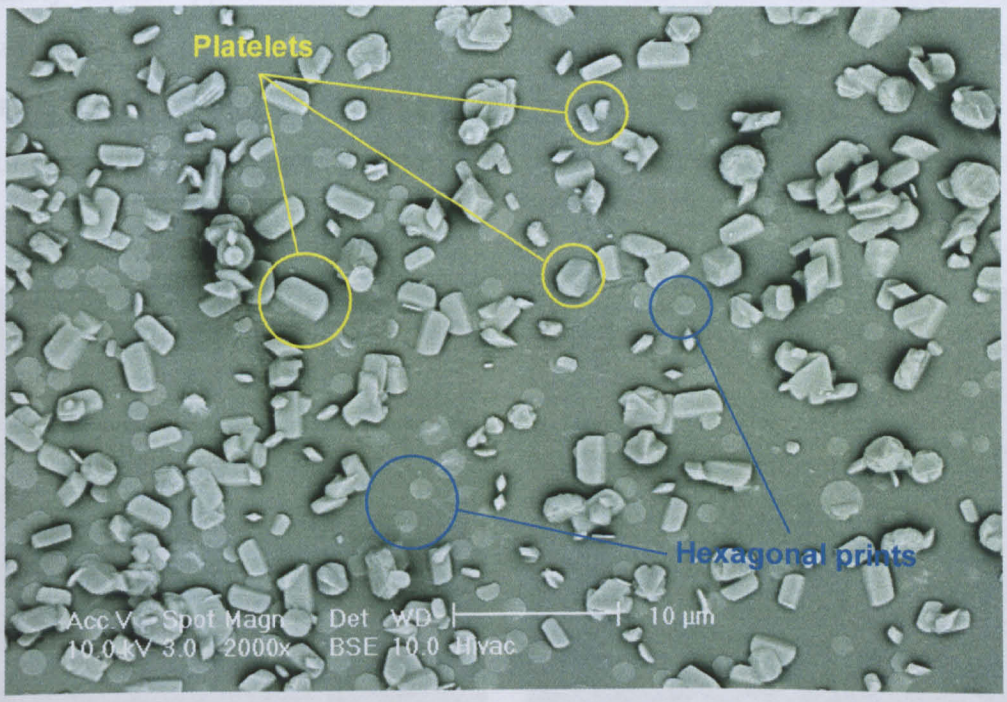

Figure 8-38 : Backscattered SEM micrograph of an octahedral (111) face of a PVD Ti-coated SYN-1 diamond (SDA100 30/40 US Mesh by DB) initially heat-treated in the DSC furnace and subsequently subjected to metal and graphite leaching processes. Some of formed platelets and the contrasting hexagonal prints as described in the text are pointed out by cycles.

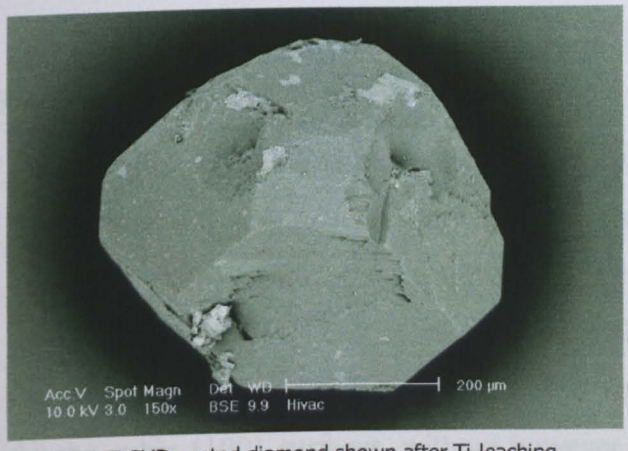

A CD19 Ti-PVD-coated diamond shown after Ti-leaching.

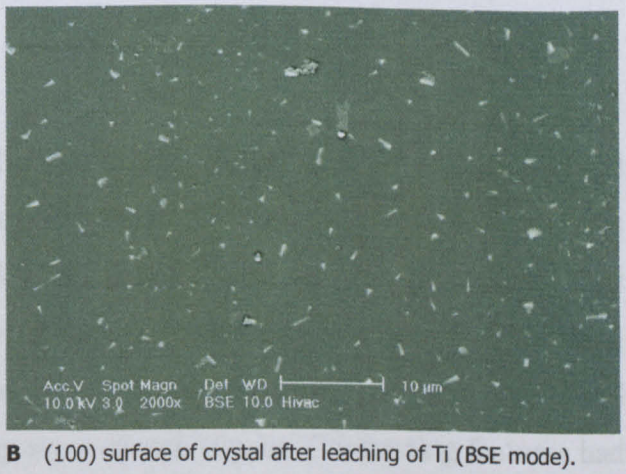

B (100) surface of crystal after leaching of Ti (BSE mode).

Figure 8-39 : Micrographs of Ti-PVD-coated (CD19) diamonds heat-treated at 500°C / 20min. / $10H_2$-$90N_2$.

8.3.3.9 Diamond – Chromium Systems

8.3.3.9A SYN-1 heat-treated with Cr powder

SEM examination of SYN-1 crystals that had been heat-treated with Cr-powders revealed that a product had formed on diamond surfaces. This product took the form of a coating in which a large number of intersecting stripes dividing it into numerous pieces, creating thus an appearance

that resembled a crazed surface (Figure 8-40B). The stripes were non-reacted diamond surfaces. The formed coating had a spongy surface morphology. Areas where coating had either peeled off or not entirely formed appeared to contrast as grey coloured regions when viewed in BSE mode of the microscope. Cubic {100} faces appeared to have a greater concentration of the formed coating product (Figure 8-40A). Further graphite leaching of the diamonds resulted in the entire removal of the formed coating described above. Crystal faces were left with fine scale etched morphology.

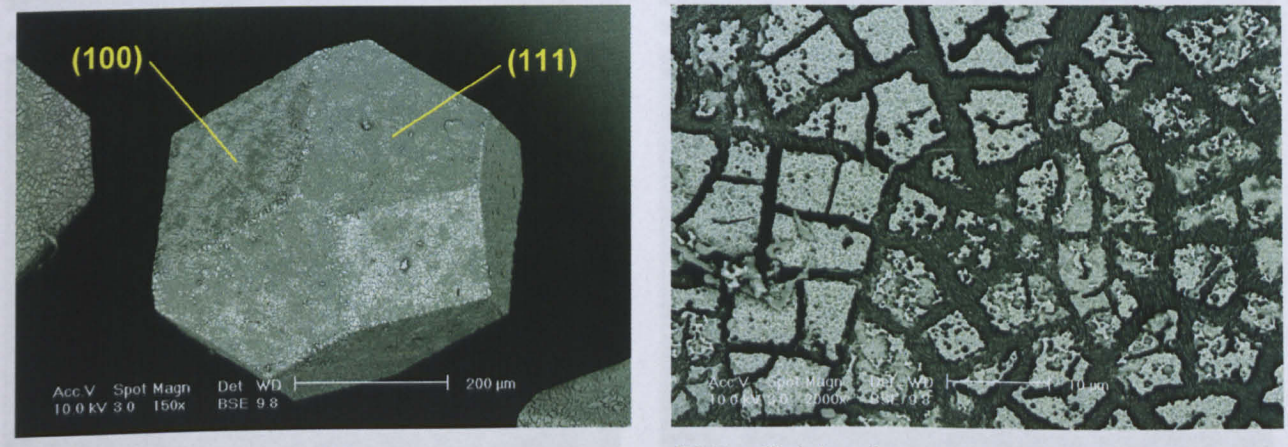

(A) View of diamond crystal in BSE mode.

(B) Magnified view of an octahedral (111) face in BSE mode.

Figure 8-40 : SYN-1 diamond (SDA100 30/40 US Mesh by DB) initially heat-treated with Cr-powders in the DSC furnace and subsequently subjected to a Cr-leaching process. A product appears to have formed on the diamond surfaces, in the form of a coating layer that is divided into pieces by numerous intersecting non-reacted diamond stripes.

8.3.3.9B SYN-2 heat-treated with Cr powder

Low magnification SEM examination of SYN-2 crystals heat-treated with Cr-powder showed that grains did not undergo any type of shape change. It was clearly visible that surfaces contained some contrasting features (Figure 8-41A). Examination at higher magnifications revealed octahedral {111} faces to be etched at a fine scale and contained small contrasting features (Figure 8-41B). Small etch trigons could be found. Similar appearance was also found for the cubic {100} surfaces, without however any signs of etch trigons. Contrasting features had a platelet shape and seemed to emerge from the diamond surfaces (Figure 8-41C). The concentration of contrasting features was higher for the cubic {100} compared to octahedral {111} faces. Further graphite leaching of the diamonds entirely removed all types of contrasting features. Octahedral {111} faces contained shallow etch cavities, which seemed to be triangular or hexagonal depressions that had lost their edge sharpness. Similarly, cubic {100} faces contained a series of etch depressions without any special geometrical form. Generally, the overall appearance of the grains resembled that of the original "as received" SYN-2 diamonds.

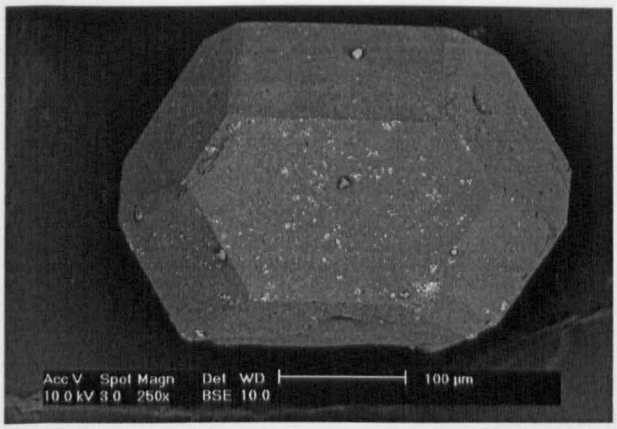

A General view of SYN-2 crystal after leaching of Cr (BSE).

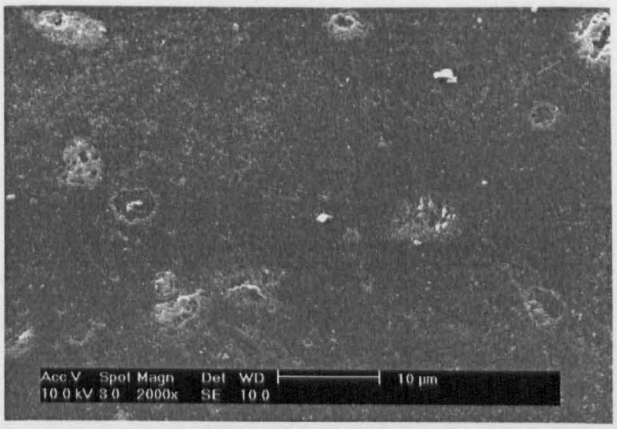

B Octahedral (111) diamond surface after leaching of Cr.

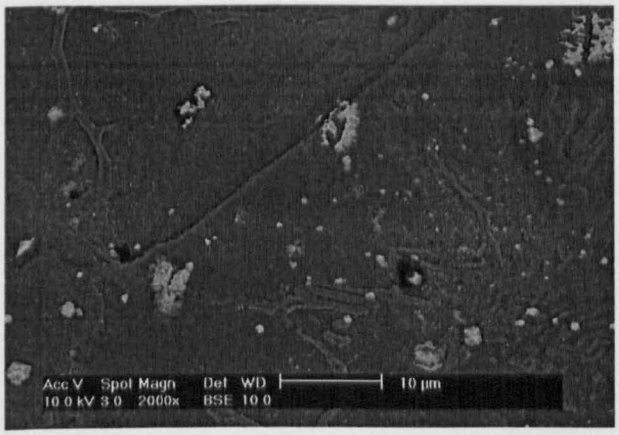

C Cubic (100) diamond surface after leaching of Cr (BSE).

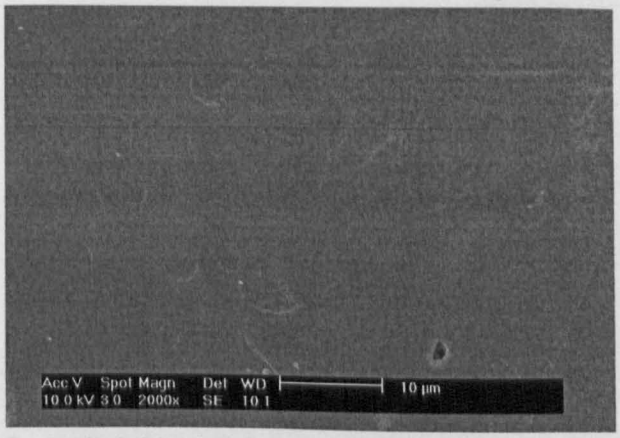

D Octahedral (111) surface after final graphite leaching.

Figure 8-41 : SEM micrographs of SYN-2 diamonds heat-treated with loose Cr powder.

8.3.3.9C SYN-3 coated with Cr by PVD (Code CD9)

SEM examination showed that parts of the PVD Cr-coating remained attached on the SYN-3 diamonds after the Cr-metal leaching process. The coating was preferentially retained at the diamond defected areas (Figure 8-42A). Inspection at higher magnifications revealed diamond faces to be slightly etched and containing some small contrasting features. These were however entirely removed by the subsequent graphite leaching, which returned the diamonds to their original non-coated state.

Heat-treating the diamonds in the DSC furnace resulted in the removal of virtually none of the Cr-coating even after the Cr-leaching process (Figure 8-42B). The degree of coverage was found to be higher for the octahedral {111} faces than the cubic {100}. Examination at higher magnifications revealed a dense coating, which was partially cracked but to a lower extent compared to the Ti-coatings (Figure 8-42C). With a careful inspection a series of small contrasting islets could be identified on coating surfaces. Especially on cubic {100} faces uncovered diamond areas were found to contain some small platelets appearing to emerge from the surface, even after the subsequent graphite leaching (Figure 8-42D).

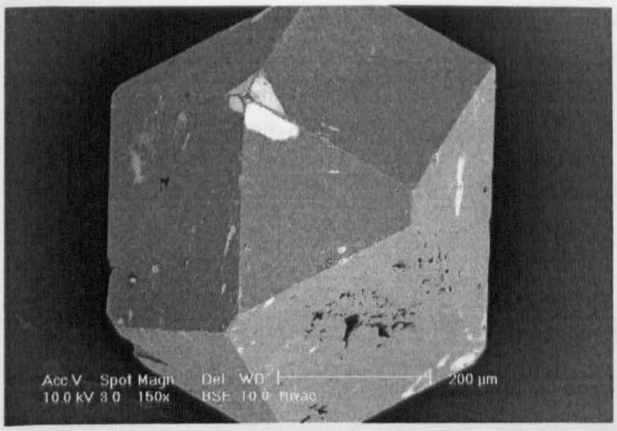

A "As received" diamond after leaching of Cr (BSE mode).

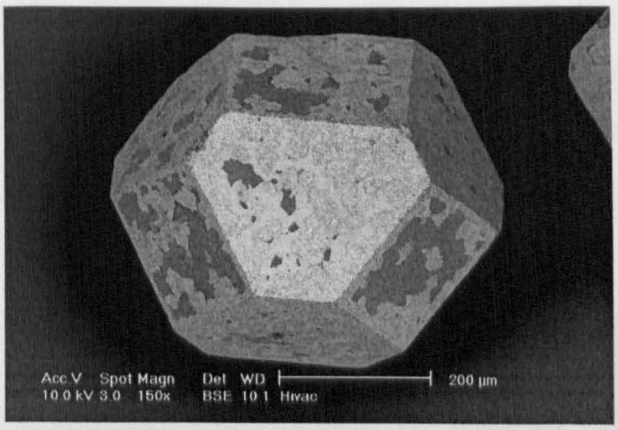

B Heat-treated Cr-PVD-coated diamond after leaching of Cr.

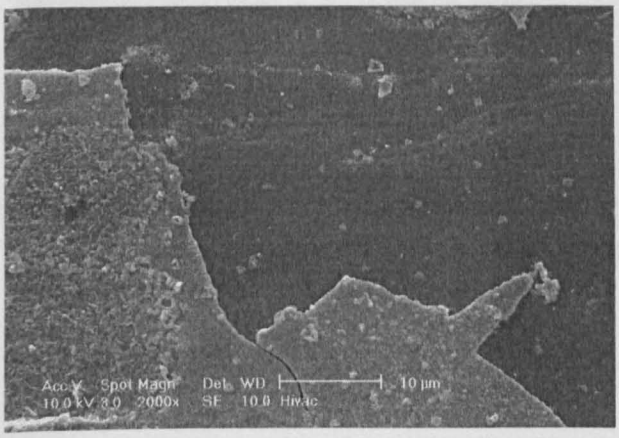

C Cubic (100) diamond surface of diamond shown in B.

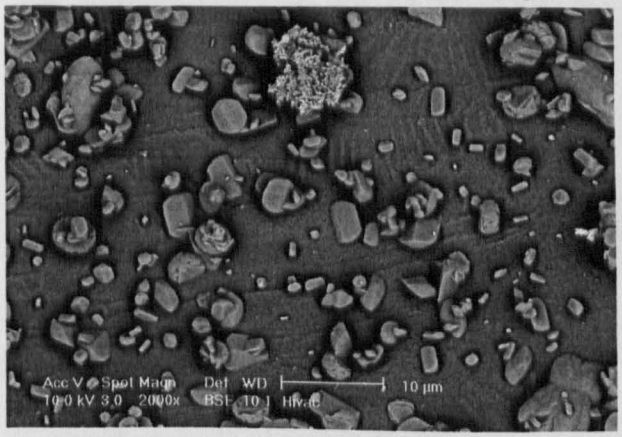

D (100) surface of heat-treated crystal after graphite leach.

Figure 8-42 : SEM micrographs of Cr-PVD-coated (CD9) diamonds at various stages of the DRE.

8.3.3.9D SYN-1 coated with Cr by CVD industrially heat-treated (Code CD20)

SYN-1 diamonds CVD coated with chromium appeared to have lost a considerable part of the coating after the Cr-metal leaching that followed the heat treatment at 500°C for 20min in $10H_2/90N_2$ atmosphere (Figure 8-43A). Coating was extensively cracked and diamond uncovered areas contained numerous contrasting islets that seemed to be small platelets emerging from the crystal faces (Figure 8-43B). Cubic {100} faces additionally contained some large spherical prints of grey contrasting colour. Subsequent graphite leaching removed almost entirely the contrasting features and revealed diamond faces to be slightly etched.

8.3.3.9E SYN-3 coated with C-enriched Cr [Cr(C)] by PVD (Code CD11)

Metal and subsequent graphite leaching of the "as received" Cr(C)-coated SYN-3 diamonds resulted in the complete removal of the PVD deposited layer (Figure 8-44A). SEM examination of the crystals showed that the diamonds were unaffected by the PVD coating process and had retained the smooth surfaces and the sharp edges of the original SYN-3 crystals. On the contrary, when the Cr(C)-coated diamonds were initially heat-treated in the DSC furnace, the metal leaching did not dissolve the coating. Instead, it remained entirely attached on the surfaces

forming a shell enclosing the crystals (Figure 8-44B). SEM examination at higher magnification revealed that the coating was dense and continuous with only very few cracks (Figure 8-44C). In areas where peeling-off had occurred, the underlying diamond surface seemed to have changed containing a number of ripples and appearing in grey contrast when viewing in BSE mode (Figure 8-44D).

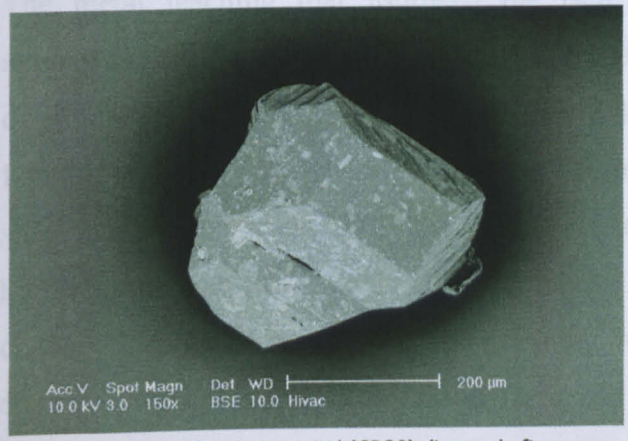

A General view of Cr-PVD-coated (CD20) diamond after leaching of Cr (BSE mode).

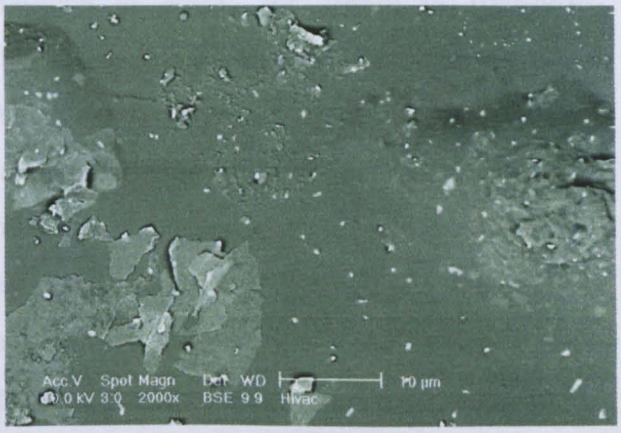

B Octahedral (111) surface of Cr-PVD-coated (CD20) diamond after leaching of Cr (BSE mode).

Figure 8-43 : Micrographs of Cr-PVD-coated (CD20) diamonds heat-treated at 500°C / 20min. / $10H_2$-$90N_2$.

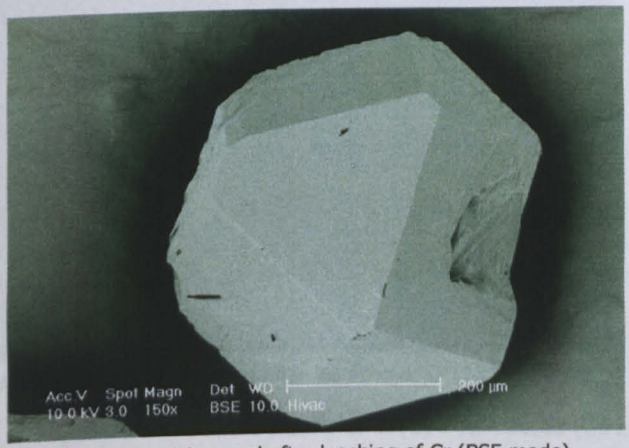

A "As received" diamond after leaching of Cr (BSE mode).

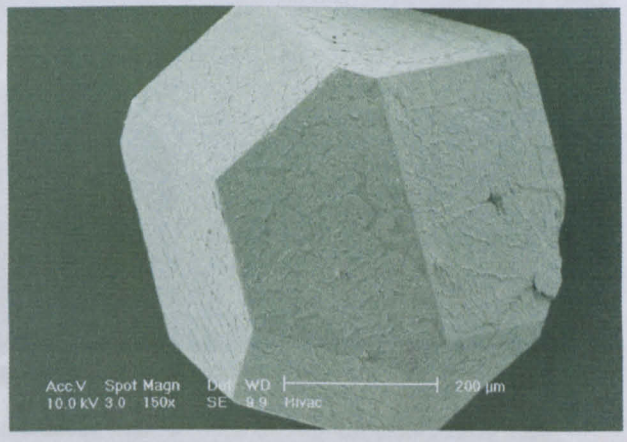

B Heat-treated Cr(C)-PVD-coated diamond after Cr-leaching.

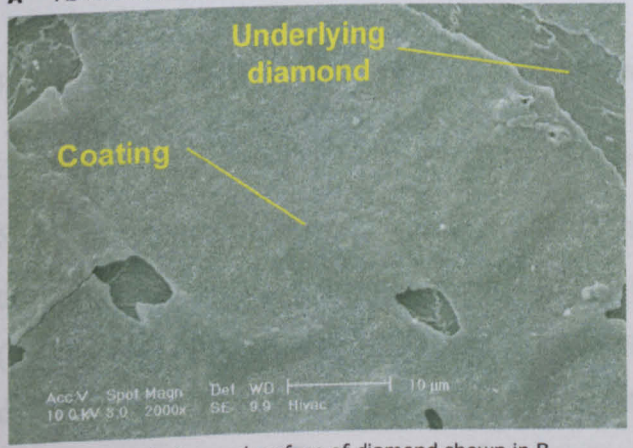

C Cubic (100) diamond surface of diamond shown in B.

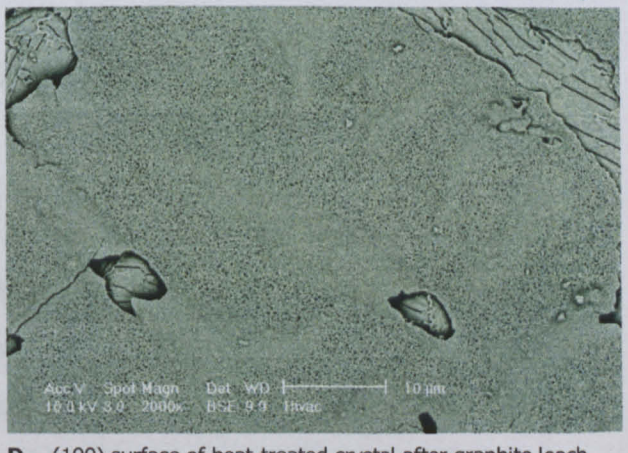

D (100) surface of heat-treated crystal after graphite leach.

Figure 8-44 : SEM micrographs of Cr(C)-PVD-coated (CD11) diamonds at various stages of the DRE.

Subsequent graphite leaching caused the entire removal of the coating. Macroscopically, crystals did not undergo any shape change. However, diamond surfaces had acquired a morphology constructed of ripples.

8.3.3.9F SYN-3 coated with C-enriched Cr [Cr(C)] by PVD industrially heat-treated (Code CD21)

The metal leaching that followed the heat treatment at 500°C for 20min in $10H_2/90N_2$ atmosphere of the SYN-3 diamonds PVD coated with C-enriched chromium resulted in the loss of almost the entire deposited layer (Figure 8-45A). Macroscopically diamonds retained surface flatness and edge sharpness. SEM examination revealed diamond faces to contain numerous small contrasting features (Figure 8-45B). It seemed that the concentration of these islets was higher in the octahedral {111} than the cubic {100} faces. Subsequent graphite leaching did not change the appearance of crystals. Coating remains were still present. Contrasting features appeared well attached on diamond faces and appeared to have been grown from the crystal surfaces.

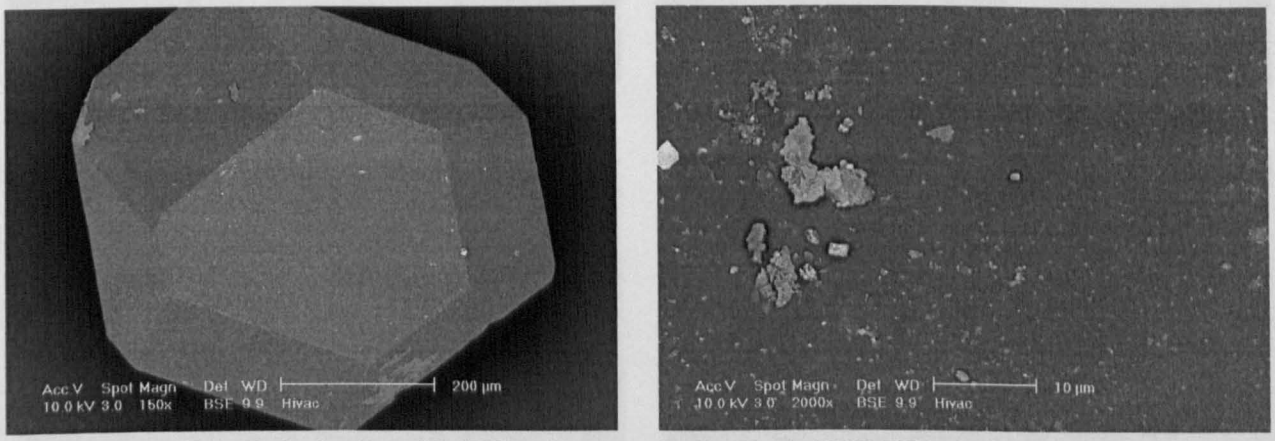

A "As received" diamond after leaching of Cr (BSE mode). **B** Heat-treated Cr(C)-PVD-coated diamond after Cr-leaching.

Figure 8-45 : Micrographs of Cr(C)-PVD-coated (CD21) diamonds heat-treated at 500°C/20min./$10H_2$-$90N_2$.

8.3.3.10 Diamond – Titanium / Chromium Systems

8.3.3.10A SYN-3 coated with Ti/Cr by PVD (Code CD12)

SEM examination showed that metal leaching of the "as received" SYN-3 diamonds co-deposited with titanium and chromium by PVD resulted in almost total dissolution of the coating (Figure 8-46A). The diamonds had not undergone any macroscopically significant changes during the PVD deposition retaining surface flatness and edge sharpness. Inspection of diamond faces at higher magnifications revealed traces of etching which seemed to be slightly higher for the cubic {100} faces. Further graphite leaching of the "as received" Ti/Cr-coated diamonds did not change the appearance of crystals as described previously.

Heat-treating the diamonds in the DSC furnace resulted in the Ti/Cr-coating remaining partially attached on the crystals following the metal leaching process (Figure 8-46B). Examination at higher magnification revealed that the coating was dense with only few cracks (Figure 8-46C). Uncovered diamond surfaces appeared intact. The morphology of the coating was found to be varying in different locations on the cubic {100} faces. Instead of a dense layer it had the form of a spongy film that seemed however, strongly attached to the underlying surface (Figure 8-46D). Subsequent graphite leaching caused the entire removal of the coating leaving crystals with only a few tiny contrasting features.

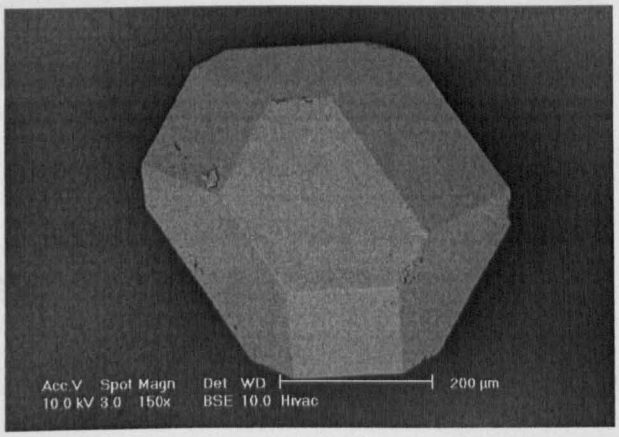

A "As received" coated crystal after leaching of Cr & Ti (BSE).

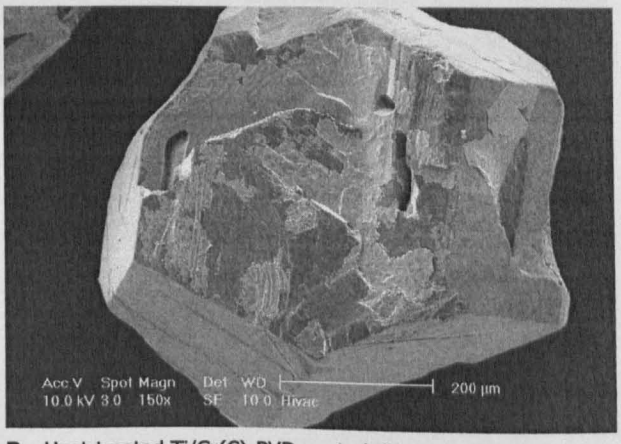

B Heat-treated Ti/Cr(C)-PVD-coated diamond after Cr-leaching.

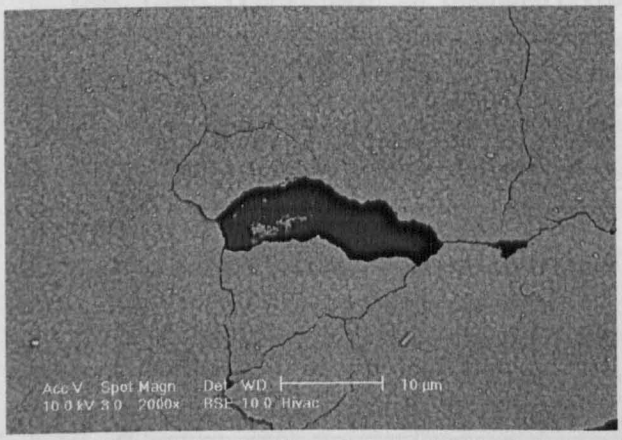

C Cubic (100) diamond surface of diamond shown in B.

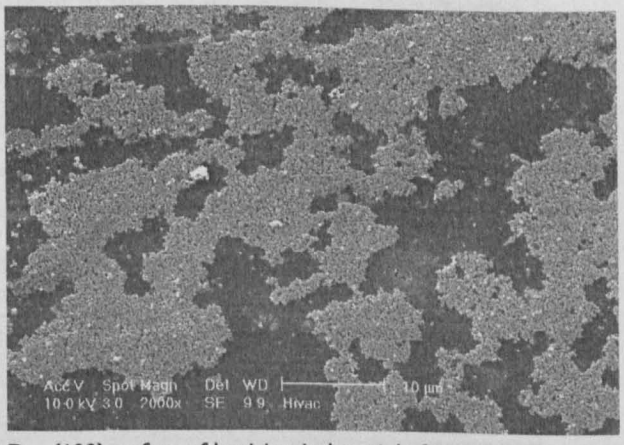

D (100) surface of heat-treated crystal after graphite leach.

Figure 8-46 : SEM micrographs of Ti/Cr-PVD-coated (CD12) diamonds at various stages of the DRE.

8.3.3.10B SYN-3 coated with Ti/Cr by PVD industrially heat-treated (Code CD22)

SYN-3 diamonds co-deposited with titanium and chromium by PVD appeared to have lost a considerable part of the coating after the metal leaching that followed the industrial heat treatment (Figure 8-47A). Macroscopically diamonds had retained their shape with flat surfaces and sharp edges. Some contrasting features were found on diamond faces. Examination at high magnification revealed that these features were small platelets appearing to be growing from

diamond surfaces (Figure 8-47B). Subsequent graphite leaching removed entirely all the contrasting features leaving diamonds in a state similar to the original crystals.

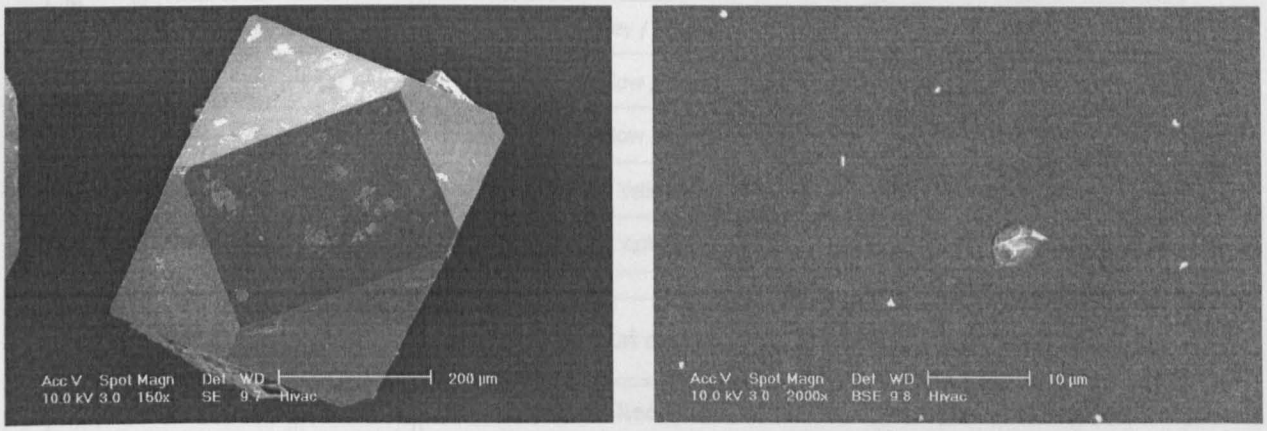

A "As received" coated crystal after leaching of Cr & Ti. **B** Octahedral (111) surface after leaching of Cr & Ti.

Figure 8-47 : Micrographs of Ti/Cr-PVD-coated (CD22) diamonds heat-treated at 500°C/20min./10H_2-90N_2.

8.3.4 OM Analysis

The results of the optical microscope examination are given in the following tables.

DSC Heat Treatment		Diamond crystal colour in Optical Microscope / Stereoscope	
Diamond – Metal Powder System		After Metal Leaching	After Graphite Leaching
SYN-1 diamonds + Metal Powder Systems	Plain SYN-1 diamonds	Very bright yellow	Very bright yellow (as previously)
	Co-EF powder	Grey/Black – Appears coated	Yellow – Coating removed
	Co (CoC) powder	Grey – Appears coated	Yellow – Coating removed
	Cu powder	Grey – Non coated	Yellow
	Ni powder	Grey/Gold – Non coated	Yellow
	Fe powder	Grey – Appears coated	Yellow – Coating removed
	Mo powder	Yellow – Black spots	Yellow – Spots removed
	W powder	Yellow – Non coated	Yellow
	Ti powder	Yellow – White spots	Yellow – Spots removed
	Cr powder	Silver/Grey – Appears coated	Yellow – Coating removed
SYN-2 diamonds + Metal Powder Systems	Plain SYN-2 diamonds	Very bright yellow	Very bright yellow (as previously)
	Co-EF powder	Grey – Appears coated	Yellow – Coating removed
	Co-SMS powder	Grey/Gold – Non coated	Yellow – Coating removed
	Cu powder	Yellow – Non coated	Yellow
	Ni powder	Yellow – Non coated	Yellow
	Fe powder	Grey – Appears coated	Yellow – Coating removed
	Mo powder	Yellow – Non coated	Yellow
	W powder	Yellow – Non coated	Yellow
	Ti powder	Yellow – Non coated	Yellow
	Cr powder	Gold – Partially coated	Yellow – Coating removed

Table 8-3 : Optical microscope examination results.

Hot-Pressed Segments		After Metal Leaching	After Graphite Leaching
SYN-2 diamonds Hot-Pressed with Metal Powder	HP1 : SYN-2 + Co-EF	Grey / Black	Yellow
	HP2 : SYN –2+ Fe	Grey / Black	Yellow
	HP3 : SYN-2 + Cu	Yellow / Grey	Yellow
	HP4 : SYN-2 + Ni	Yellow / Grey	Yellow
	HP5 : SYN-2 + Mo	Yellow	Yellow
	HP6 : SYN-2 + $Cu_{85}Sn_{15}$	Yellow	Yellow

Coated Diamonds		Diamond crystal colour in Optical Microscope / Stereoscope				
Diamond – Metal Powder System		As Received			DSC Heat Treated	
		Original	After Metal Leach	After Graphite Leach	After Metal Leach	After Graphite Leach
DSC Heat-Treated	CD2 : Plain SYN-3	Yellow	Yellow	Yellow	Yellow	Yellow
	CD6 : Ti-(CVD) SYN-1	Silver	Yellow	Yellow	Yellow / White	Yellow
	CD8 : Ti-(PVD) SYN-1	Silver	Yellow	Yellow	Yellow / White	Yellow
	CD9 : Cr-(PVD) SYN-3	Grey	Yellow	Yellow	Black / Grey	Yellow
	CD11 : Cr(C)-(PVD) SYN-3	Silver / Grey	Yellow	Yellow	Grey	Yellow
	CD12 : Ti/Cr-(PVD) SYN-3	Grey	Yellow	Yellow	Grey / Yellow	Yellow
	CD13 : W-(PVD) SYN-3	Silver	Yellow	Yellow	Yellow	Yellow
Industrially Heat-Treated (500°C, 20min, $10H_2/90N_2$)	CD18 : Ti-(CVD/DB) SYN-1	Grey / Yellow	Yellow & Some clustering	Yellow		
	CD19 : Ti-(PVD/TC) SYN-1	Grey / Yellow	Yellow & Some clustering	Yellow		
	CD20 : Cr-(PVD) SYN-1	Grey / Yellow	Yellow	Yellow		
	CD21 : Cr(C)-(PVD) SYN-3	Blue	Yellow	Yellow		
	CD22 : Ti/Cr-(PVD) SYN-3	Blue	Yelllow	Yellow		
	CD23 : W-(PVD) SYN-3	Blue	Yellow	Yellow		

Table 8-4 : Optical microscope examination results.

Table 8-3 shows that the diamonds crystals appeared grey or black under the light of the optical microscope after their heat-treatment with Co, Ni, Fe and Cu. These metals were those found to cause diamond weight loss. The Mo, W, Ti and Cr did not cause the darkening of the crystals. Similar observations were made for diamond retrieved from the hot-pressed specimens (Table 8-4). Almost all "as received" and industrially heat-treated coated diamonds were yellow at all stages of the DRE. Colour changes were evident for the DSC heat-treated coated diamonds, but crystals were not blackened as was seen with Co, Fe and Ni. In all cases the final graphite leaching process restored in most of the cases the yellow colour, which is characteristic of such industrial diamonds.

9

Results • Part-II

"Characterisation & Properties of Coated-Diamond Composites"

9.1 Introduction

This chapter presents the results of the series of experiments included in the second part of the experimental work of this thesis as described in Chapter 7. The work was carried out to characterise interfacial bonding and determine the main mechanical properties of P/M composites made of a cobalt metal-matrix impregnated with coated diamonds.

9.2 Density

Measured Archimedes densities compared to the calculated theoretical density are given in the three graphs of Figure 9-1 on the following page. The three plots correspond to the three different composite consolidation methods employed.

The pressure assisted manufacturing routes (HIP & HP) yielded segments of higher densities compared to those produced by furnace sintering under atmospheric pressure. Hot-pressed segments exhibited the highest densities accompanied with the smallest variation.

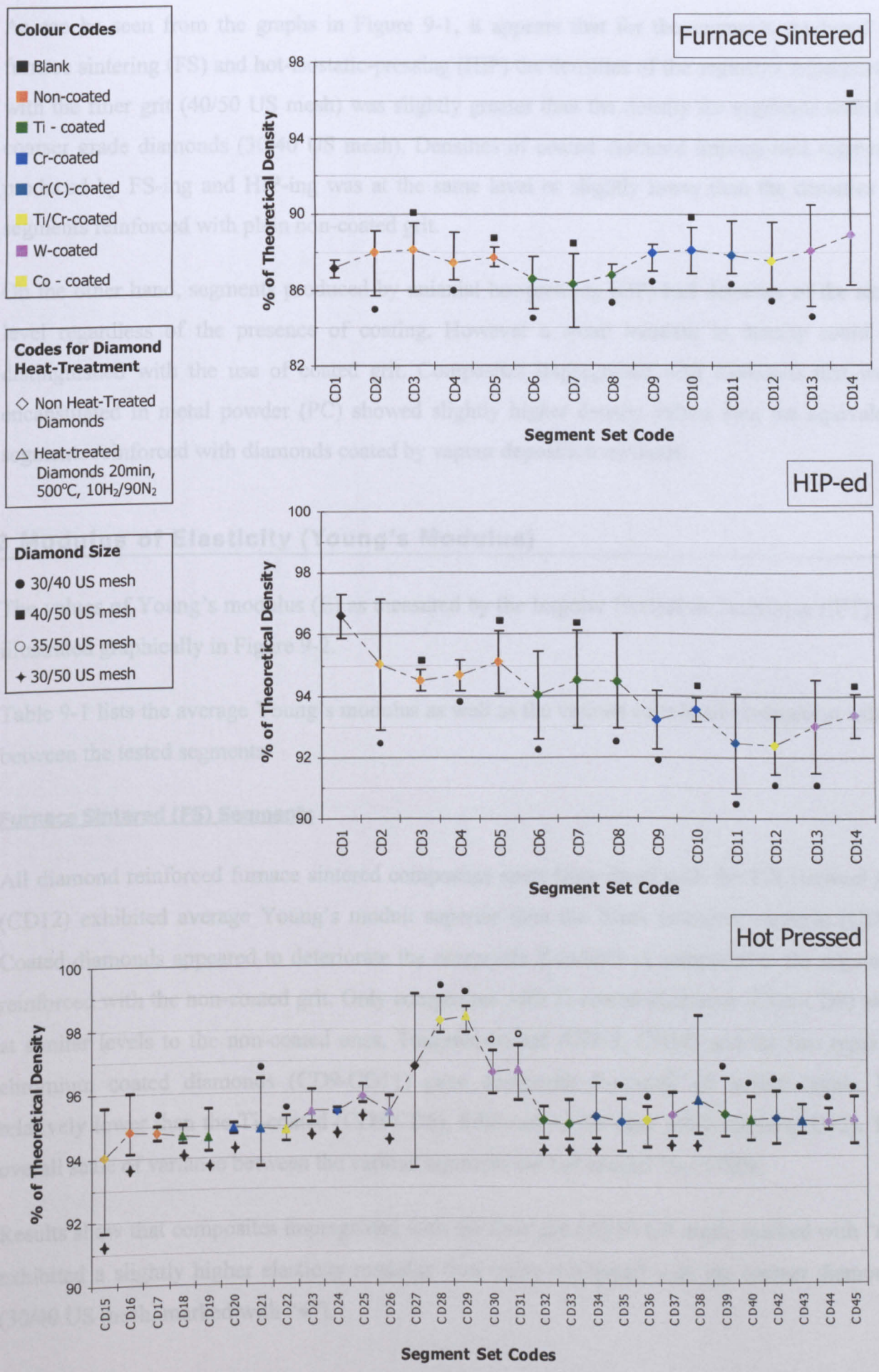

Figure 9-1 : Density of the rectangular parallelepiped segments compared to calculated theoretical density.

As can be seen from the graphs in Figure 9-1, it appears that for the segments produced by furnace sintering (FS) and hot-isostatic-pressing (HIP) the densities of the segments impregnated with the finer grit (40/50 US mesh) was slightly greater than the density for segments with the coarser grade diamonds (30/40 US mesh). Densities of coated diamond impregnated segments produced by FS-ing and HIP-ing was at the same level or slightly lower than the densities of segments reinforced with plain non-coated grit.

On the other hand, segments produced by uniaxial hot-pressing (HP) had densities of the same level regardless of the presence of coating. However a small increase in density could be distinguished with the use of coated grit. Composites impregnated with diamonds that were encapsulated in metal powder (PC) showed slightly higher density values than the equivalent segments reinforced with diamonds coated by vapour deposition methods.

9.3 Modulus of Elasticity (Young's Modulus)

The values of Young's modulus (E) as measured by the Impulse Excitation Technique (IET) are illustrated graphically in Figure 9-2.

Table 9-1 lists the average Young's modulus as well as the various calculated comparison values between the tested segments.

Furnace Sintered (FS) Segments

All diamond reinforced furnace sintered composites apart from those with the Ti/Cr-coated grit (CD12) exhibited average Young's moduli superior than the blank reference segment (CD1). Coated diamonds appeared to deteriorate the composite E-moduli as compared to the segments reinforced with the non-coated grit. Only composites with Ti-coated diamonds (CD6-CD8) were at similar levels to the non-coated ones. Tungsten-coated (CD13, CD14) and the two types of chromium coated diamonds (CD9-CD11) gave composite E-moduli of similar levels, but relatively lower than the Ti-coated (CD6-CD8), followed by the dual Ti/Cr-coated (CD12). The overall scale of variance between the various segments did not exceed 10-15 GPa.

Results show that composites impregnated with the finer grit (40/50 US mesh, marked with "■") exhibited a slightly higher elasticity modulus than those reinforced with the coarser diamonds (30/40 US mesh, marked with "●").

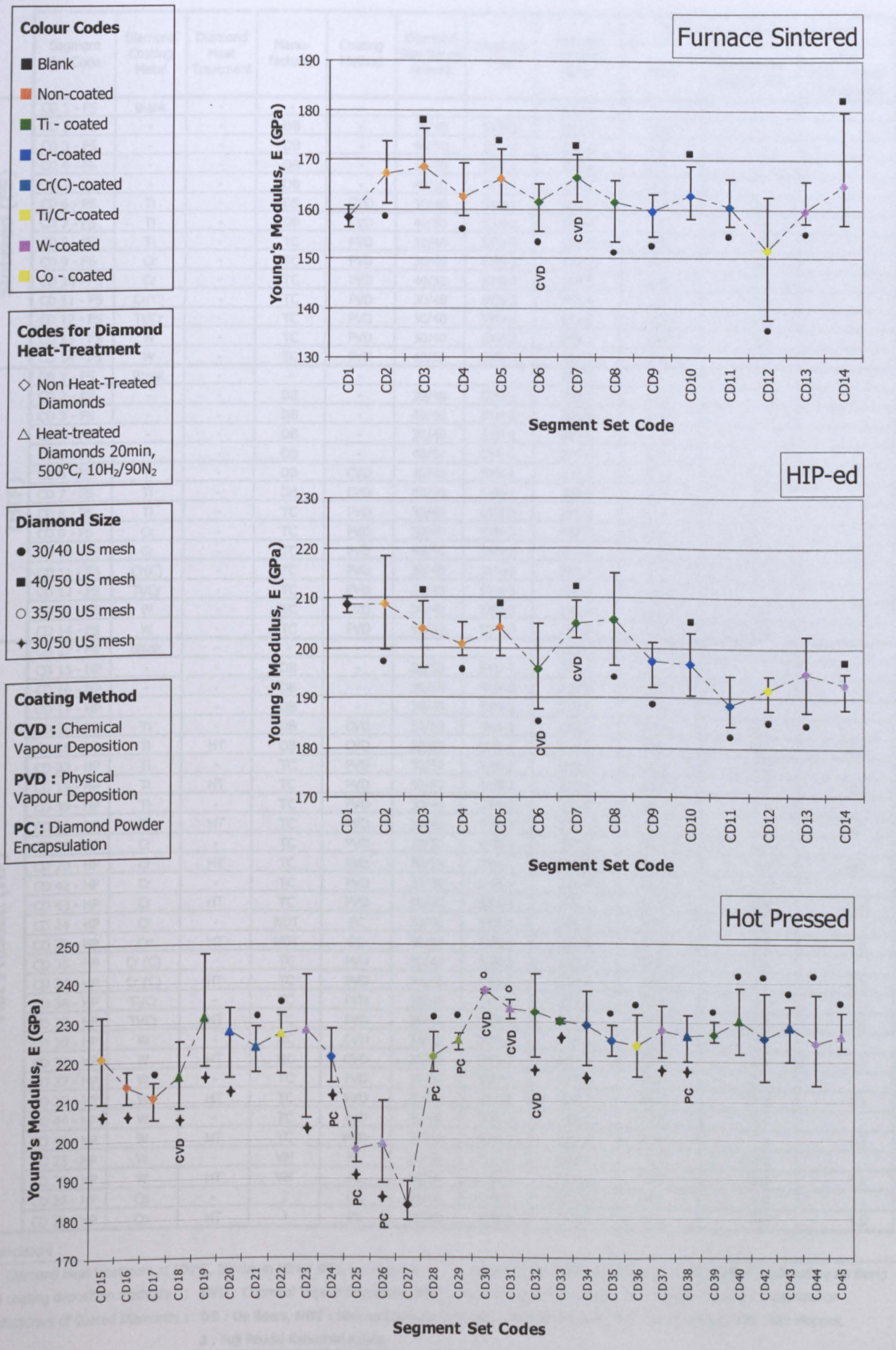

Figure 9-2 : Young's modulus of the rectangular parallelepiped segments obtained by the Impulse Excitation Technique (IET). *Coating method not denoted by symbol refers to PVD.

	Segment Set Code	Diamond Coating Metal	Diamond Heat Treatment	Manu-facturer	Coating Method	Diamond Size Range (mesh)	Diamond Type	Average E modulus (GPa)	% change compared to reference		
									Blank	Non-coated Impregnated	Non Heat-Treated Impregnated
Sintered (FS)	CD 1 - FS	Blank	-	-	-	-	-	158.4	-	-	-
	CD 2 - FS	-	-	DB	-	30/40	SYN-3	167.0	5.4	-	-
	CD 3 - FS	-	-	DB	-	40/50	SYN-3	168.4	6.3	-	-
	CD 4 - FS	-	-	DB	-	30/40	SYN-1	162.4	2.5	-	-
	CD 5 - FS	-	-	DB	-	40/50	SYN-1	166.1	4.9	-	-
	CD 6 - FS	Ti	-	DB	CVD	30/40	SYN-1	161.4	1.9	-0.7	-
	CD 7 - FS	Ti	-	DB	CVD	40/50	SYN-1	166.4	5.0	0.1	-
	CD 8 - FS	Ti	-	TC	PVD	30/40	SYN-3	161.5	1.9	-3.3	-
	CD 9 - FS	Cr	-	TC	PVD	30/40	SYN-3	159.6	0.7	-4.5	-
	CD 10 - FS	Cr	-	TC	PVD	40/50	SYN-3	162.6	2.6	-3.5	-
	CD 11 - FS	Cr(C)	-	TC	PVD	30/40	SYN-3	160.4	1.2	-4.0	-
	CD 12 - FS	Ti/Cr	-	TC	PVD	30/40	SYN-3	151.6	-4.3	-9.2	-
	CD 13 - FS	W	-	TC	PVD	30/40	SYN-3	159.7	0.8	-4.4	-
	CD 14 - FS	W	-	TC	PVD	40/50	SYN-3	164.7	4.0	-2.2	-
Hot Isostatic Pressed (HIP)	CD 1 - FS	Blank	-	-	-	-	-	208.7	-	-	-
	CD 2 - FS	-	-	DB	-	30/40	SYN-3	208.7	0.0	-	-
	CD 3 - FS	-	-	DB	-	40/50	SYN-3	203.9	-2.3	-	-
	CD 4 - FS	-	-	DB	-	30/40	SYN-1	200.6	-3.9	-	-
	CD 5 - FS	-	-	DB	-	40/50	SYN-1	204.0	-2.2	-	-
	CD 6 - FS	Ti	-	DB	CVD	30/40	SYN-1	195.6	-6.3	-2.5	-
	CD 7 - FS	Ti	-	DB	CVD	40/50	SYN-1	204.8	-1.9	0.4	-
	CD 8 - FS	Ti	-	TC	PVD	30/40	SYN-3	205.6	-1.5	-1.5	-
	CD 9 - FS	Cr	-	TC	PVD	30/40	SYN-3	197.2	-5.5	-5.5	-
	CD 10 - FS	Cr	-	TC	PVD	40/50	SYN-3	196.7	-5.8	-3.5	-
	CD 11 - FS	Cr(C)	-	TC	PVD	30/40	SYN-3	188.5	-9.7	-9.7	-
	CD 12 - FS	Ti/Cr	-	TC	PVD	30/40	SYN-3	191.4	-8.3	-8.2	-
	CD 13 - FS	W	-	TC	PVD	30/40	SYN-3	194.8	-6.7	-6.6	-
	CD 14 - FS	W	-	TC	PVD	40/50	SYN-3	192.7	-7.7	-5.5	-
Hot Pressed (HP)	CD 27 - HP	Blank	-	-	-	-	-	183.4	-	-	-
	CD 15 - HP	-	-	DB	-	30/50	SYN-1	221.1	20.5	-	-
	CD 16 - HP	-	-	DB	-	30/50	SYN-3	213.8	16.6	-	-
	CD 17 - HP	-	-	DB	-	30/40	SYN-3	210.9	15.0	-	-
	CD 32 - HP	Ti	-	DB	CVD	30/50	SYN-1	232.4	26.7	5.1	-
	CD 18 - HP	Ti	HT	DB	CVD	30/50	SYN-1	216.5	18.0	-2.1	-6.9
	CD 33 - HP	Ti	-	TC	PVD	30/50	SYN-1	230.3	25.6	4.2	-
	CD 19 - HP	Ti	HT	TC	PVD	30/50	SYN-1	231.6	26.3	4.7	0.6
	CD 39 - HP	Ti	-	TC	PVD	30/40	SYN-3	226.8	23.7	7.5	-
	CD 40 - HP	Ti	HT	TC	PVD	30/40	SYN-3	230.6	25.7	9.3	1.7
	CD 34 - HP	Cr	-	TC	PVD	30/50	SYN-1	229.3	25.0	3.7	-
	CD 20 - HP	Cr	HT	TC	PVD	30/50	SYN-1	227.8	24.2	3.0	-0.6
	CD 42 - HP	Cr	-	TC	PVD	30/40	SYN-3	225.8	23.1	7.1	-
	CD 43 - HP	Cr	HT	TC	PVD	30/40	SYN-3	229.1	24.9	8.6	1.4
	CD 24 - HP	Cr	-	NDT	PC	30/50	SYN-1	221.5	20.8	0.2	-
	CD 38 - HP	Cr	HT	NDT	PC	30/50	SYN-1	226.6	23.6	2.5	2.3
	CD 35 - HP	Cr (C)	-	TC	PVD	30/40	SYN-3	225.2	22.8	6.8	-
	CD 21 - HP	Cr (C)	HT	TC	PVD	30/40	SYN-3	223.8	22.0	6.1	-0.6
	CD 36 - HP	Ti/Cr	-	TC	PVD	30/40	SYN-3	223.9	22.1	6.1	-
	CD 22 - HP	Ti/Cr	HT	TC	PVD	30/40	SYN-3	227.4	24.0	7.8	1.6
	CD 30 - HP	W	-	NC	CVD	35/50	SYN-1	238.0	29.8	7.7	-
	CD 31 - HP	W	HT	NC	CVD	35/50	SYN-1	233.5	27.3	5.6	-1.9
	CD 37 - HP	W	-	TC	PVD	30/50	SYN-1	227.9	24.3	3.1	-
	CD 23 - HP	W	HT	TC	PVD	30/50	SYN-1	228.2	24.4	3.2	0.1
	CD 44 - HP	W	-	TC	PVD	30/40	SYN-3	224.6	22.5	6.5	-
	CD 45 - HP	W	HT	TC	PVD	30/40	SYN-3	226.6	23.6	7.4	0.9
	CD 25 - HP	W	-	VM	PC	30/50	SYN-1	197.8	7.8	-10.5	-
	CD 26 - HP	W	HT	VM	PC	30/50	SYN-1	199.4	8.7	-9.8	0.8
	CD 28 - HP	Co	-	J	PC	30/40	SYN-3	221.5	20.8	5.0	-
	CD 29 - HP	Co	HT	J	PC	30/40	SYN-3	225.8	23.1	7.0	1.9

Nomenclature :

HT : Diamond Heat treatment at 500°C, 20min, in $10H_2$ / $90N_2$ atmosphere Diamond Type : **SYN-1** is superior quality **SYN-3** produced by De Beers

Metal coating deposition methods : **CVD** : Chemical Vapour Deposition, **PVD** : Physical Vapour Deposition, **PC** : Powder Coating / Encapsulation

Manufacturers of Coated Diamonds : **DB** : De Beers, **NDT** : Nimbus Diamond Tool, **NC** : Norton Company, **TC** : Teer Coatings, **VM** : Van Moppes, **J** : Fuji Paudal Kabushiki Kaisha

Table 9-1 : Average Young's modulus of tested rectangular parallelepiped segments. Table also lists the calculated comparison values for the various diamond conditions.

Hot-Isostatic-Pressed (HIP) Segments

The moduli for the HIP-ed segments were higher than the FS-ed, approximately 30 to 40 GPa. However, in contrast to FS-ed segments, where the composite modulus was higher than the blank segments, the HIP-ed composites exhibited average Young's modulus which was inferior to that of the blank segments. However, coated-diamonds appeared to deteriorate composite E-modulus as compared to the segments impregnated with the non-coated grit (CD2-CD5), with only the Ti-coated diamonds (CD6-CD8) giving composite modulus of similar levels to the latter. Obtained ranking of the composites is similar to that found for the FS-ed with only the Ti/Cr-coated (CD12) impregnated to have improved in position to similar levels as the W-coated diamond reinforced (CD13, CD14).

Hot-Pressed (HP) Segments

Hot-pressing yielded the composites with the highest Young's modulus. Diamond reinforcement improved the composite modulus up to levels reaching 25-30% increase. Coated diamonds (CD18-CD45) provided composites with higher modulus than the corresponding segments impregnated with the non-coated grit (CD15-CD17). Only the W-encapsulated (CD25, CD26) exhibited considerable decrease in modulus. The 30/40-mesh grit (marked with "•") appeared to improve relatively at higher levels the composite modulus compared to the wider reinforcement fraction of the 30/50-mesh (marked with "✦").

Interpreting the results for the hot-pressed composites the following comments can be made as regarding the effect of the heat-treatment of the coated grit prior to consolidation. Comparing for the Ti-coated diamonds (see Table 9-1), one could identify that heat-treatment of the diamonds provided small levels of modulus improvement, which only applied for the composites with the PVD-coated grit, with greater increase observed for the SYN-3 diamonds. The same behaviour was exhibited for the segments with the Cr-coated diamonds (see Table 9-1). When encapsulating the diamonds in either Cr-powder (CD38) or Co-powder (CD29) the heat treatment provided, on average, an increase in E-modulus of the order of 2.3% and 1.9% respectively, compared to the segments with the non-heat-treated diamond-granules (CD24 and CD28). Heat-treatment provided no positive effect for the diamonds with the Cr(C)-coatings (CD21, CD35) and the W-CVD-coatings (CD30, CD31). However, heat treatment was found to have a slightly beneficial effect for the diamonds with the Ti/Cr-coating (CD22-CD36) and those with the W-PVD-coatings (CD23-CD37, CD44-CD45) (see Table 9-1).

The highest moduli were measured for composites reinforced with the W-CVD-coated diamonds (CD30, CD31). Encapsulating diamonds in Co-powder (CD28-CD29) gave composites with superior Young's modulus compared to the segments with the non-coated diamonds (CD17), although the composition of the segments remained practically the same.

9.4 3-point Bending

The measured values of the Transverse Rupture Strength (TRS) as obtained by the 3-point bending are illustrated graphically in Figure 9-3 on the page 176. Table 9-2 lists the average TRS as well as the various calculated comparison values between the tested segments. Figure 9-4 and Table 9-3 give the 3-point bending results in the same manner but after the originally obtained TRS values have been corrected according to the Standard Test Size Specimen A and normalised for porosity as has been described in Chapter 7.

Furnace Sintered (FS) Segments

All diamond reinforced furnace sintered segments exhibited lower strengths than the blank cobalt segments. The TRS values of the diamond impregnated segments varied between 650 and 713 MPa (Figure 9-3).

Best results were obtained for the segments reinforced with the Ti-coated diamonds (CD6-CD8), followed by those with the non-coated grit (CD2-CD5). The rest of the segments with the coated abrasives performed on average slightly lower than the composites incorporated with the non-coated crystals.

Hot-Isostatic-Pressed (HIP) Segments

Similarly to FS-ed segments, all diamond reinforced HIP-ed specimens had lower bending strengths than the blank cobalt reference. Composites impregnated with the finer grit (40/50 mesh) exhibited slightly higher average TRS values than those with the coarser diamonds (30/40 mesh). The measured TRS values were higher than those of the FS-ed segments when comparing the same coating. However, following correcting and normalising for porosity this trend was reversed.

Similar to the case for FS-ed specimens, the Ti-coated impregnated segments (CD6-CD8) were the strongest together with the non-coated diamond reinforced composites (CD2-CD5).

Hot-Pressed (HP) Segments

Measured bending strengths of the hot-pressed (HP-ed) segments were higher than those of the FS-ed and the HIP-ed. Diamond reinforced composites exhibited lower average TRS values than the reference blank, but the difference was reduced considerably compared to the FS-ed and the HIP-ed segments. For some samples the measured TRS was even higher than the average value of the blank. Composites impregnated with coated grit exhibited higher bending strengths relatively to the composites with the non-coated abrasives (Table 9-2 and Table 9-3).

Examining the results for the composites impregnated with Ti-coated diamonds (Table 9-2 and Table 9-3), one can identify that there was practically no difference between the obtained TRS values for the CVD and PVD coated SYN-1 diamonds (CD18-19 & CD32-33). Heat treatment of the grit was only beneficial in the case of the SYN-3 diamonds (CD40). The composites impregnated with the coarser SYN-3 quality grit (CD39-40) gave the best average bending performance compared to the other Ti-coated specimens, although the difference was relatively small.

As for the composites with the Ti-coated diamonds (Table 9-2 and Table 9-3), the segments produced with the 30/40 SYN-3 Cr-coated grit (CD42-43) had superior TRS than that with the 30/50 SYN-1 type (CD20 & 34). Bending properties of the composites impregnated with the Cr-powder encapsulated diamonds (CD24 & 38) were slightly inferior to those involving the PVD grit. Diamond heat-treatment was found to deteriorate the performance of those composites involving diamonds with chromium containing coatings apart from those with the dual Ti/Cr-coating (CD 22 & 36).

Composites impregnated with the various W-coated diamonds exhibited relatively high bending strengths. In particular, the CVD-coated (CD30-31) diamonds gave high levels of composite strength. The grade with the W-powder encapsulated diamonds (CD25-26) reached the level of the PVD-coated grit (CD23 & 37).

The highest average TRS values were obtained for the segments impregnated with Co-powder encapsulated diamonds (CD28-29), which reached the levels of the blank reference samples. Heat-treatment of the encapsulated grit did not provide considerable increase in composite bending strength.

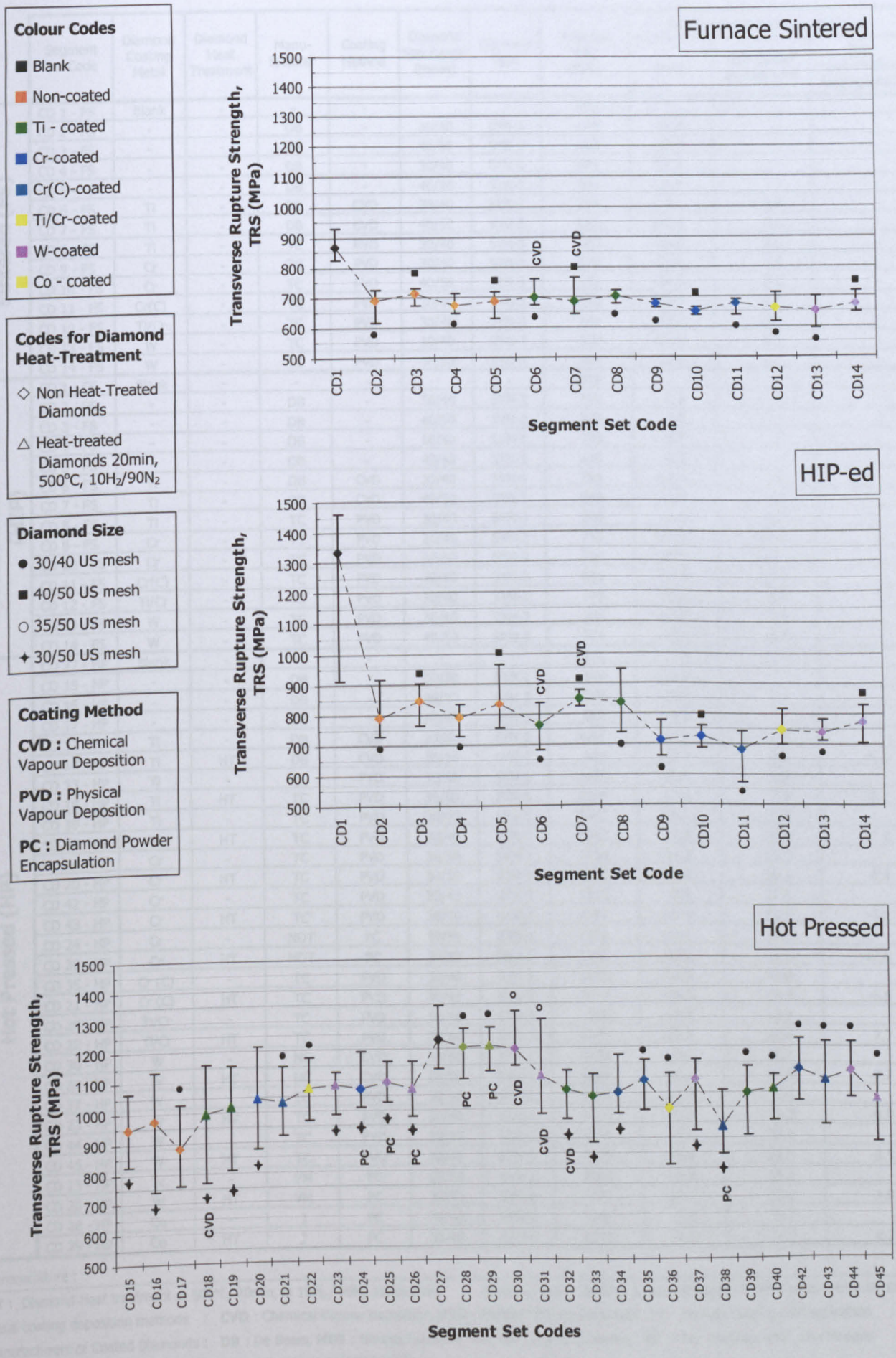

Figure 9-3 : Transverse Rupture Strength (TRS) of the rectangular parallelepiped segments obtained by the 3-point bending. *Coating method not denoted by symbol refers to PVD.

	Segment Set Code	Diamond Coating Metal	Diamond Heat Treatment	Manu-facturer	Coating Method	Diamond Size Range (mesh)	Diamond Type	Average TRS (MPa)	% change compared to reference		
									Blank	Non-coated Impregnated	Non Heat-Treated Impregnated
Sintered (FS)	CD 1 - FS	Blank	-	-	-	-	-	866	-	-	-
	CD 2 - FS	-	-	DB	-	30/40	SYN-3	689	-20.4	-	-
	CD 3 - FS	-	-	DB	-	40/50	SYN-3	713	-17.7	-	-
	CD 4 - FS	-	-	DB	-	30/40	SYN-1	675	-22.1	-	-
	CD 5 - FS	-	-	DB	-	40/50	SYN-1	684	-21.0	-	-
	CD 6 - FS	Ti	-	DB	CVD	30/40	SYN-1	701	-19.1	3.9	-
	CD 7 - FS	Ti	-	DB	CVD	40/50	SYN-1	685	-20.9	0.2	-
	CD 8 - FS	Ti	-	TC	PVD	30/40	SYN-3	703	-18.8	2.0	-
	CD 9 - FS	Cr	-	TC	PVD	30/40	SYN-3	679	-21.6	-1.4	-
	CD 10 - FS	Cr	-	TC	PVD	40/50	SYN-3	650	-25.0	-8.8	-
	CD 11 - FS	Cr(C)	-	TC	PVD	30/40	SYN-3	676	-22.0	-2.0	-
	CD 12 - FS	Ti/Cr	-	TC	PVD	30/40	SYN-3	661	-23.7	-4.1	-
	CD 13 - FS	W	-	TC	PVD	30/40	SYN-3	650	-24.9	-5.7	-
	CD 14 - FS	W	-	TC	PVD	40/50	SYN-3	672	-22.4	-5.7	-
Hot Isostatic Pressed (HIP)	CD 1 - FS	Blank	-	-	-	-	-	1336	-	-	-
	CD 2 - FS	-	-	DB	-	30/40	SYN-3	792	-8.6	-	-
	CD 3 - FS	-	-	DB	-	40/50	SYN-3	845	-2.5	-	-
	CD 4 - FS	-	-	DB	-	30/40	SYN-1	790	-8.8	-	-
	CD 5 - FS	-	-	DB	-	40/50	SYN-1	835	-3.6	-	-
	CD 6 - FS	Ti	-	DB	CVD	30/40	SYN-1	764	-11.8	-3.2	-
	CD 7 - FS	Ti	-	DB	CVD	40/50	SYN-1	849	-1.9	1.7	-
	CD 8 - FS	Ti	-	TC	PVD	30/40	SYN-3	840	-3.0	6.0	-
	CD 9 - FS	Cr	-	TC	PVD	30/40	SYN-3	712	-17.7	-10.0	-
	CD 10 - FS	Cr	-	TC	PVD	40/50	SYN-3	726	-16.2	-14.1	-
	CD 11 - FS	Cr(C)	-	TC	PVD	30/40	SYN-3	681	-21.3	-14.0	-
	CD 12 - FS	Ti/Cr	-	TC	PVD	30/40	SYN-3	747	-13.8	-5.7	-
	CD 13 - FS	W	-	TC	PVD	30/40	SYN-3	736	-15.0	-7.1	-
	CD 14 - FS	W	-	TC	PVD	40/50	SYN-3	774	-10.6	-8.4	-
Hot Pressed (HP)	CD 27 - HP	Blank	-	-	-	-	-	1233	-	-	-
	CD 15 - HP	-	-	DB	-	30/50	SYN-1	948	-23.2	-	-
	CD 16 - HP	-	-	DB	-	30/50	SYN-3	974	-21.0	-	-
	CD 17 - HP	-	-	DB	-	30/40	SYN-3	882	-28.5	-	-
	CD 32 - HP	Ti	-	DB	CVD	30/50	SYN-1	1061	-14.0	11.9	-
	CD 18 - HP	Ti	HT	DB	CVD	30/50	SYN-1	994	-19.4	4.9	-6.3
	CD 33 - HP	Ti	-	TC	PVD	30/50	SYN-1	1039	-15.8	9.6	-
	CD 19 - HP	Ti	HT	TC	PVD	30/50	SYN-1	1016	-17.6	7.3	-2.1
	CD 39 - HP	Ti	-	TC	PVD	30/40	SYN-3	1047	-15.1	18.7	-
	CD 40 - HP	Ti	HT	TC	PVD	30/40	SYN-3	1062	-13.9	20.4	1.4
	CD 34 - HP	Cr	-	TC	PVD	30/50	SYN-1	1054	-14.5	11.3	-
	CD 20 - HP	Cr	HT	TC	PVD	30/50	SYN-1	1045	-15.2	10.3	-0.9
	CD 42 - HP	Cr	-	TC	PVD	30/40	SYN-3	1125	-8.8	27.5	-
	CD 43 - HP	Cr	HT	TC	PVD	30/40	SYN-3	1093	-11.4	23.9	-2.9
	CD 24 - HP	Cr	-	NDT	PC	30/50	SYN-1	1071	-13.1	13.0	-
	CD 38 - HP	Cr	HT	NDT	PC	30/50	SYN-1	936	-24.1	-1.2	-12.6
	CD 35 - HP	Cr (C)	-	TC	PVD	30/40	SYN-3	1094	-11.3	24.0	-
	CD 21 - HP	Cr (C)	HT	TC	PVD	30/40	SYN-3	1032	-16.3	17.0	-5.6
	CD 36 - HP	Ti/Cr	-	TC	PVD	30/40	SYN-3	996	-19.2	12.9	-
	CD 22 - HP	Ti/Cr	HT	TC	PVD	30/40	SYN-3	1073	-13.0	21.6	7.7
	CD 30 - HP	W	-	NC	CVD	35/50	SYN-1	1195	-3.1	26.1	-
	CD 31 - HP	W	HT	NC	CVD	35/50	SYN-1	1109	-10.1	17.0	-7.2
	CD 37 - HP	W	-	TC	PVD	30/50	SYN-1	1093	-11.4	15.3	-
	CD 23 - HP	W	HT	TC	PVD	30/50	SYN-1	1083	-12.2	14.3	-0.9
	CD 44 - HP	W	-	TC	PVD	30/40	SYN-3	1124	-8.9	27.4	-
	CD 45 - HP	W	HT	TC	PVD	30/40	SYN-3	1029	-16.6	16.6	-8.5
	CD 25 - HP	W	-	VM	PC	30/50	SYN-1	1093	-11.4	15.3	-
	CD 26 - HP	W	HT	VM	PC	30/50	SYN-1	1072	-13.1	13.1	-1.9
	CD 28 - HP	Co	-	J	PC	30/40	SYN-3	1206	-2.2	36.7	-
	CD 29 - HP	Co	HT	J	PC	30/40	SYN-3	1209	-2.0	37.0	0.2

Nomenclature :

HT : Diamond Heat treatment at 500°C, 20min, in $10H_2$ / $90N_2$ atmosphere Diamond Type : **SYN-1** is superior quality **SYN-3** produced by De Beers

Metal coating deposition methods : **CVD** : Chemical Vapour Deposition, **PVD** : Physical Vapour Deposition, **PC** : Powder Coating / Encapsulation

Manufacturers of Coated Diamonds : **DB** : De Beers, **NDT** : Nimbus Diamond Tool, **NC** : Norton Company, **TC** : Teer Coatings, **VM** : Van Moppes, **J** : Fuji Paudal Kabushiki Kaisha

Table 9-2 : Average Transverse Rupture Strength (TRS) of tested rectangular parallelepiped segments. Table also lists the calculated comparison values for the various diamond conditions.

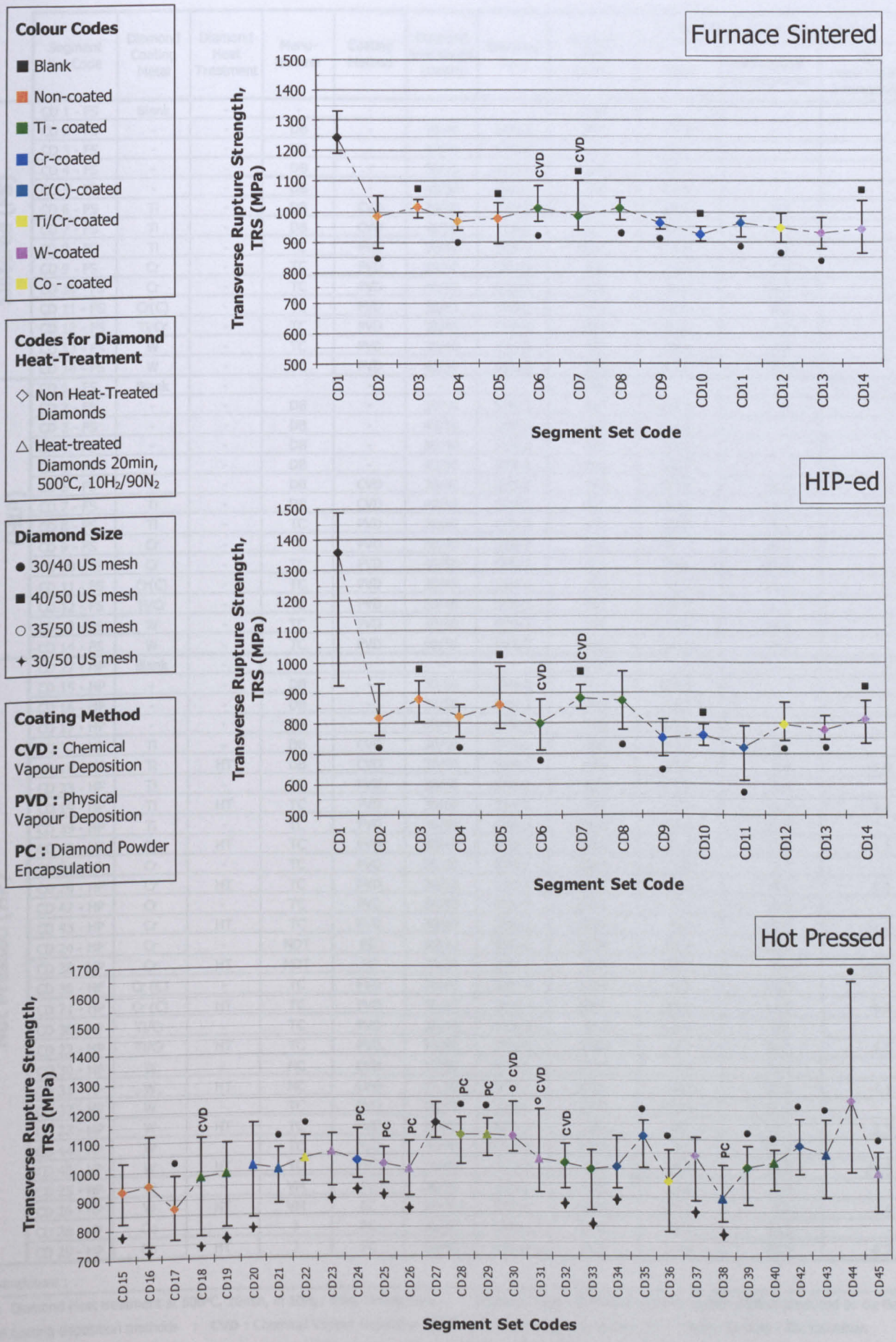

Figure 9-4 : Transverse Rupture Strength (TRS) of the rectangular parallelepiped segments obtained by the 3-point bending. The values are normalised for porosity and corrected to standard test specimen size. *Coating method not denoted by symbol refers to PVD.

	Segment Set Code	Diamond Coating Metal	Diamond Heat Treatment	Manu-facturer	Coating Method	Diamond Size Range (mesh)	Diamond Type	Average TRS (MPa)	% change compared to reference		
									Blank	Non-coated Impregnated	Non Heat-Treated Impregnated
Sintered (FS)	CD 1 - FS	Blank	-	-	-	-	-	1243	-	-	-
	CD 2 - FS	-	-	DB	-	30/40	SYN-3	983	-20.9	-	-
	CD 3 - FS	-	-	DB	-	40/50	SYN-3	1014	-18.4	-	-
	CD 4 - FS	-	-	DB	-	30/40	SYN-1	968	-22.1	-	-
	CD 5 - FS	-	-	DB	-	40/50	SYN-1	976	-21.4	-	-
	CD 6 - FS	Ti	-	DB	CVD	30/40	SYN-1	1011	-18.6	4.5	-
	CD 7 - FS	Ti	-	DB	CVD	40/50	SYN-1	987	-20.6	1.1	-
	CD 8 - FS	Ti	-	TC	PVD	30/40	SYN-3	1012	-18.6	2.9	-
	CD 9 - FS	Cr	-	TC	PVD	30/40	SYN-3	963	-22.5	-2.0	-
	CD 10 - FS	Cr	-	TC	PVD	40/50	SYN-3	926	-25.5	-8.6	-
	CD 11 - FS	Cr(C)	-	TC	PVD	30/40	SYN-3	962	-22.6	-2.2	-
	CD 12 - FS	Ti/Cr	-	TC	PVD	30/40	SYN-3	944	-24.1	-4.0	-
	CD 13 - FS	W	-	TC	PVD	30/40	SYN-3	930	-25.1	-5.4	-
	CD 14 - FS	W	-	TC	PVD	40/50	SYN-3	943	-24.1	-7.0	-
Hot Isostatic Pressed (HIP)	CD 1 - FS	Blank	-	-	-	-	-	1356	-	-	-
	CD 2 - FS	-	-	DB	-	30/40	SYN-3	817	-34.3	-	-
	CD 3 - FS	-	-	DB	-	40/50	SYN-3	877	-29.4	-	-
	CD 4 - FS	-	-	DB	-	30/40	SYN-1	819	-34.1	-	-
	CD 5 - FS	-	-	DB	-	40/50	SYN-1	861	-30.7	-	-
	CD 6 - FS	Ti	-	DB	CVD	30/40	SYN-1	797	-35.8	-2.6	-
	CD 7 - FS	Ti	-	DB	CVD	40/50	SYN-1	882	-29.0	2.4	-
	CD 8 - FS	Ti	-	TC	PVD	30/40	SYN-3	871	-29.9	6.7	-
	CD 9 - FS	Cr	-	TC	PVD	30/40	SYN-3	750	-39.7	-8.2	-
	CD 10 - FS	Cr	-	TC	PVD	40/50	SYN-3	761	-38.8	-13.2	-
	CD 11 - FS	Cr(C)	-	TC	PVD	30/40	SYN-3	723	-41.9	-11.5	-
	CD 12 - FS	Ti/Cr	-	TC	PVD	30/40	SYN-3	793	-36.2	-2.9	-
	CD 13 - FS	W	-	TC	PVD	30/40	SYN-3	776	-37.5	-4.9	-
	CD 14 - FS	W	-	TC	PVD	40/50	SYN-3	813	-34.6	-7.2	-
Hot Pressed (HP)	CD 27 - HP	Blank	-	-	-	-	-	1160	-	-	-
	CD 15 - HP	-	-	DB	-	30/50	SYN-1	934	-19.5	-	-
	CD 16 - HP	-	-	DB	-	30/50	SYN-3	949	-18.2	-	-
	CD 17 - HP	-	-	DB	-	30/40	SYN-3	869	-25.1	-	-
	CD 32 - HP	Ti	-	DB	CVD	30/50	SYN-1	1020	-12.1	9.2	-
	CD 18 - HP	Ti	HT	DB	CVD	30/50	SYN-1	980	-15.5	4.9	-3.9
	CD 33 - HP	Ti	-	TC	PVD	30/50	SYN-1	998	-14.0	6.8	-
	CD 19 - HP	Ti	HT	TC	PVD	30/50	SYN-1	992	-14.5	6.2	-0.6
	CD 39 - HP	Ti	-	TC	PVD	30/40	SYN-3	1002	-13.6	15.2	-
	CD 40 - HP	Ti	HT	TC	PVD	30/40	SYN-3	1019	-12.2	17.2	1.7
	CD 34 - HP	Cr	-	TC	PVD	30/50	SYN-1	1007	-13.2	7.7	-
	CD 20 - HP	Cr	HT	TC	PVD	30/50	SYN-1	1022	-11.9	9.4	1.5
	CD 42 - HP	Cr	-	TC	PVD	30/40	SYN-3	1076	-7.3	23.8	-
	CD 43 - HP	Cr	HT	TC	PVD	30/40	SYN-3	1047	-9.7	20.5	-2.7
	CD 24 - HP	Cr	-	NDT	PC	30/50	SYN-1	1034	-10.9	10.7	-
	CD 38 - HP	Cr	HT	NDT	PC	30/50	SYN-1	896	-22.7	-4.1	-13.3
	CD 35 - HP	Cr (C)	-	TC	PVD	30/40	SYN-3	1114	-4.0	28.2	-
	CD 21 - HP	Cr (C)	HT	TC	PVD	30/40	SYN-3	1007	-13.2	15.8	-9.6
	CD 36 - HP	Ti/Cr	-	TC	PVD	30/40	SYN-3	953	-17.9	9.6	-
	CD 22 - HP	Ti/Cr	HT	TC	PVD	30/40	SYN-3	1043	-10.1	20.0	9.5
	CD 30 - HP	W	-	NC	CVD	35/50	SYN-1	1114	-4.0	19.2	-
	CD 31 - HP	W	HT	NC	CVD	35/50	SYN-1	1035	-10.8	10.8	-7.1
	CD 37 - HP	W	-	TC	PVD	30/50	SYN-1	1042	-10.2	11.5	-
	CD 23 - HP	W	HT	TC	PVD	30/50	SYN-1	1066	-8.1	14.1	2.3
	CD 44 - HP	W	-	TC	PVD	30/40	SYN-3	1232	6.2	41.7	-
	CD 45 - HP	W	HT	TC	PVD	30/40	SYN-3	982	-15.3	13.0	-20.3
	CD 25 - HP	W	-	VM	PC	30/50	SYN-1	1018	-12.2	9.0	-
	CD 26 - HP	W	HT	VM	PC	30/50	SYN-1	1003	-13.6	7.3	-1.6
	CD 28 - HP	Co	-	J	PC	30/40	SYN-3	1117	-3.7	28.5	-
	CD 29 - HP	Co	HT	J	PC	30/40	SYN-3	1115	-3.9	28.3	-0.2

Nomenclature :

HT : Diamond Heat treatment at 500°C, 20min, in $10H_2$ / $90N_2$ atmosphere Diamond Type : **SYN-1** is superior quality **SYN-3** produced by De Beers

Metal coating deposition methods : **CVD** : Chemical Vapour Deposition, **PVD** : Physical Vapour Deposition, **PC** : Powder Coating / Encapsulation

Manufacturers of Coated Diamonds : **DB** : De Beers, **NDT** : Nimbus, **NC** : Norton Co., **TC** : Teer, **VM** : Van Moppes, **J** : Fuji Paudal Kabushiki Kaisha

Table 9-3 : Average Transverse Rupture Strength (TRS) of tested rectangular parallelepiped segments. The values are normalised for porosity and corrected to standard test specimen size. Table also lists the calculated comparison values for the various diamond conditions.

9.5 Tensile Testing

Results obtained from the tensile testing are given graphically in Figure 9-5 (page 181). Table 9-4 lists the calculated average tensile properties derived from the tests as well as the computed comparison values between the various composites.

All diamond reinforced segments exhibited lower tensile strength and ductility compared to the blank reference samples. Proof strength of the reinforced segments was found to be at the same levels or even exceeding that of the blank reference.

Segment Set Code	Diamond Coating Metal	Heat Treatment	Manufacturer	Coating Method	Diamond Size Range (mesh)	Diamond Type	UTS				Elongation				Proof Strength 0.2%			
							Average (MPa)	% change compared to reference			Average (%)	% change compared to reference			Average (MPa)	% change compared to reference		
								Blank	Non coated	Non HT		Blank	Non coated	Non HT		Blank	Non coated	Non HT
DBS-1	Blank	-	-	-	-	-	553	-	-	-	10.11	-	-	-	268	-	-	-
DBS-2	-	-	DB	-	30/40	SYN-3	312	-43.5	-	-	1.49	-85.3	-	-	222	-17.1	-	-
DBS-3	-	-	DB	-	40/50	SYN-3	302	-45.4	-	-	1.53	-84.9	-	-	219	-18.3	-	-
DBS-4	-	-	DB	-	30/50	SYN-1	288	-47.9	-	-	1.56	-84.6	-	-	217	-19.2	-	-
DBS-11	Ti	-	DB	CVD	30/50	SYN-1	276	-50.0	-4.0	-	1.07	-89.4	-31.3	-	213	-20.7	-1.8	-
DBS-12	Ti	HT	DB	CVD	30/50	SYN-1	370	-33.0	28.6	34.0	2.02	-80.0	29.5	88.4	260	-2.9	20.2	22.4
DBS-5	Ti	-	TC	PVD	30/40	SYN-3	298	-46.2	-4.7	-	1.08	-89.3	-27.2	-	227	-15.4	2.0	-
DBS-6	Ti	HT	TC	PVD	30/40	SYN-3	321	-41.9	2.9	7.9	1.82	-82.0	22.5	68.2	226	-15.7	1.7	-0.3
DBS-13	Cr	-	TC	PVD	30/50	SYN-1	390	-29.5	35.3	-	2.59	-74.4	66.1	-	276	2.7	27.2	-
DBS-14	Cr	HT	TC	PVD	30/50	SYN-1	353	-36.1	22.6	-9.4	1.42	-86.0	-9.2	-45.3	278	3.6	28.2	0.8
DBS-19	Cr	-	NDT	PC	30/50	SYN-1	382	-30.9	32.7	-	2.06	-79.6	32.3	-	285	6.2	31.4	-
DBS-20	Cr	HT	NDT	PC	30/50	SYN-1	409	-26.1	42.0	7.0	3.69	-63.5	136.5	78.7	268	-0.1	23.7	-5.9
DBS-15	Cr(C)	-	TC	PVD	30/40	SYN-3	364	-34.2	16.6	-	2.08	-79.4	39.9	-	263	-2.1	18.0	-
DBS-16	Cr(C)	HT	TC	PVD	30/40	SYN-3	351	-36.6	12.4	-3.6	1.55	-84.7	4.3	-25.4	269	0.3	20.9	2.5
DBS-7	Ti/Cr	-	TC	PVD	30/40	SYN-3	329	-40.5	5.4	-	1.43	-85.8	-3.6	-	261	-2.8	17.2	-
DBS-8	Ti/Cr	HT	TC	PVD	30/40	SYN-3	313	-43.3	0.4	-4.7	1.49	-85.2	0.4	4.1	238	-11.3	6.9	-8.8
DBS-25	W	-	NC	CVD	35/50	SYN-1	342	-38.2	18.7	-	1.43	-85.8	-8.3	-	267	-0.6	23.1	-
DBS-26	W	HT	NC	CVD	35/50	SYN-1	388	-29.9	34.7	13.5	3.82	-62.2	144.8	166.9	239	-10.9	10.3	-10.4
DBS-17	W	-	TC	PVD	30/50	SYN-1	329	-40.5	14.4	-	2.22	-78.0	42.3	-	230	-14.4	6.0	-
DBS-18	W	HT	TC	PVD	30/50	SYN-1	320	-42.2	11.0	-2.9	1.59	-84.3	1.9	-28.4	244	-9.2	12.5	6.0
DBS-9	W	-	TC	PVD	30/40	SYN-3	334	-39.6	7.1	-	1.09	-89.2	-26.4	-	274	2.2	23.2	-
DBS-10	W	HT	TC	PVD	30/40	SYN-3	283	-48.8	-9.4	-15.4	1.21	-88.0	-18.5	10.8	207	-22.7	-6.8	-24.3
DBS-21	W	-	VM	PC	30/50	SYN-1	385	-30.3	33.9	-	3.89	-61.5	149.5	-	229	-14.6	5.7	-
DBS-22	W	HT	VM	PC	30/50	SYN-1	356	-35.6	23.6	-7.7	2.83	-72.0	81.7	-27.2	226	-15.6	4.5	-1.1
DBS-23	Co	-	J	PC	30/40	SYN-3	434	-21.5	39.1	-	3.98	-60.7	167.4	-	260	-3.0	17.0	-
DBS-24	Co	HT	J	PC	30/40	SYN-3	404	-26.9	29.5	-6.9	2.22	-78.0	49.3	-44.2	305	13.6	37.0	17.1

Nomenclature :

HT : Diamond Heat treatment at 500°C, 20min, in $10H_2$ / $90N_2$ atmosphere Diamond Type : **SYN-1** is superior quality **SYN-3** produced by De Beers

Metal coating deposition methods : **CVD** : Chemical Vapour Deposition, **PVD** : Physical Vapour Deposition, **PC** : Powder Coating / Encapsulation

Manufacturers of Coated Diamonds : **DB** : De Beers, **NDT** : Nimbus, **NC** : Norton Co., **TC** : Teer, **VM** : Van Moppes, **J** : Fuji Paudal Kabushiki Kaisha

Table 9-4 : Average values of tensile test results for the tested "dog-bone" segments. Table also lists the calculated comparison values for the various diamond conditions.

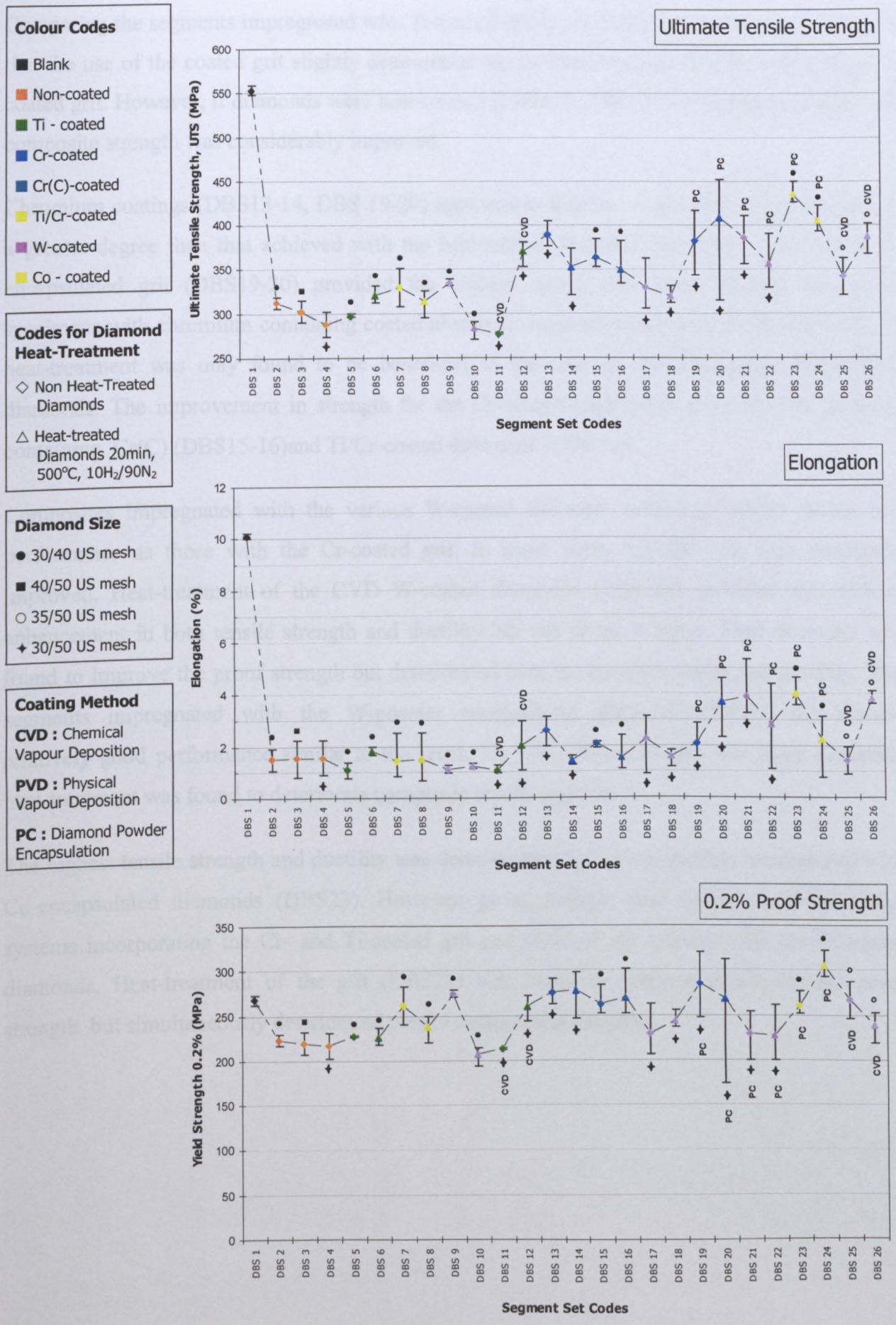

Figure 9-5 : Results of the tensile testing of the "dog-bone" shaped segments. *Coating method not denoted by symbol refers to PVD.

Comparing the segments impregnated with Ti-coated diamonds (DBS5 & DBS11) it can be seen that the use of the coated grit slightly deteriorated the performance when compared to the non-coated grit. However, if diamonds were heat-treated (DBS6 & DBS12) the situation changed and composite strength was considerably improved.

Chromium coatings (DBS13-14, DBS 19-20) appeared to improve composite tensile strength to a greater degree than that achieved with the heat-treated Ti-coated diamonds. The Cr-powder encapsulated grit (DBS19-20) provided the highest tensile and proof strength among all specimens with chromium containing coated abrasives. Regarding tensile strength and ductility, heat-treatment was only found to be beneficial in the case of the Cr-powder encapsulated diamonds. The improvement in strength for the Cr-coated composites was followed by those containing Cr(C) (DBS15-16)and Ti/Cr-coated diamonds (DBS7-8).

Composites impregnated with the various W-coated diamonds exhibited similar tensile test performance as those with the Cr-coated grit. In some cases ductility was also drastically improved. Heat-treatment of the CVD W-coated diamonds (DBS-26) provided considerable enhancement in both tensile strength and ductility but not in proof stress. Heat treatment was found to improve the proof strength but deteriorated both the tensile strength and ductility. The segments impregnated with the W-powder encapsulated diamonds (DSB21-22) showed relatively good performance similar to the levels for CVD W-coated grit. For these diamonds heat-treatment was found to deteriorate composite tensile response.

The highest tensile strength and ductility was demonstrated by the composites impregnated with Co-encapsulated diamonds (DBS23). However, proof strength was inferior to most of the systems incorporating the Cr- and Ti-coated grit and some of the systems with the W-coated diamonds. Heat-treatment of the grit (DBS24) was found to improve drastically the proof strength, but simultaneously deteriorated tensile strength and ductility.

9.6 SEM Examination

This section presents the results of the SEM examination of the fractured surfaces produced by the mechanical testing.

9.6.1 Qualitative Fracture Surface Examination

9.6.1.1 FS-ed & HIP-ed segments – Fractured by 3-point Bending

Results presented here concern the microscopic analysis of the fractured surfaces produced after fracturing the segments by 3-point bending. Observations for both the furnace sintered (FS) and the hot-isostatically pressed (HIP) segments were similar and therefore are presented combined in this single thematic section.

9.6.1.1A Non-coated Diamonds (CD2, CD3, CD4, CD5)

Non-coated diamonds exposed on fracture surfaces appeared with a slightly altered surface morphology, produced by fine scale etching (Figure 9-6 and Figure 9-7 on the next page).

The finer grit (40/50 mesh) (Figure 9-6B and Figure 9-7B) seemed to have been modified to a relatively larger degree than the coarser grade (30/40 mesh) (Figure 9-6A and Figure 9-7A). The degree of etching was also higher for the diamonds incorporated in the segments consolidated by the HIP route. Fissures were clearly evident at the diamond-cobalt interfaces.

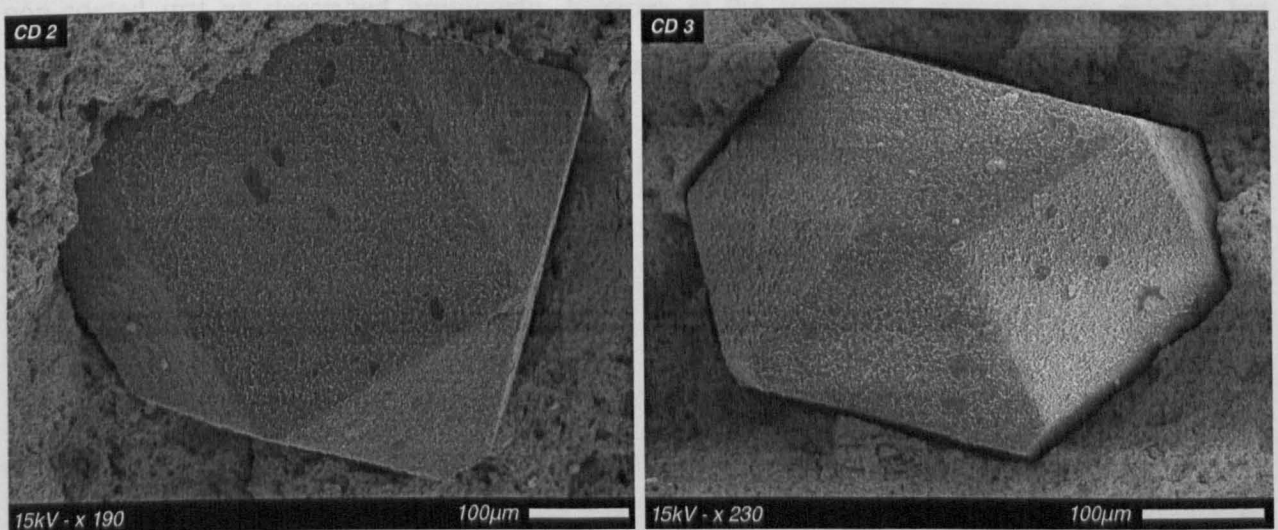

(A) CD 2 Non-coated 30/40 US-mesh SYN-3 (DB)

(B) CD 3 Non-coated 40/50 US-mesh SYN-3 (DB)

Figure 9-6 : SEM micrographs showing sections of fracture surfaces of segments produced by the HIP route and impregnated with the SYN-3 type of non-coated diamond.

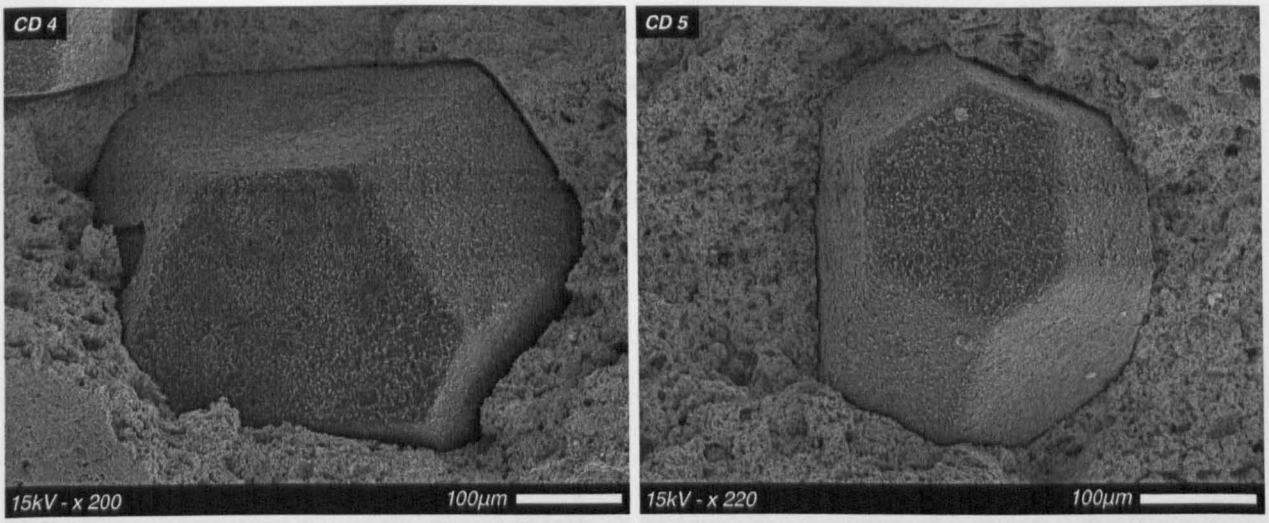

(A) CD 4 Non-coated 30/40 US-mesh SYN-1 (DB) **(B)** CD 5 Non-coated 40/50 US-mesh SYN-1 (DB)

Figure 9-7 : SEM micrographs showing sections of fracture surfaces of segments produced by the HIP route and impregnated with the SYN-1 type of non-coated diamond.

9.6.1.1B Ti-coated Diamonds (CD6, CD7, CD8)

Examination of fracture surfaces of segments impregnated with the SYN-1 Ti-coated diamonds (CD6, CD7) revealed that interfacial de-bonding occurred either at the Ti-coating/diamond or the Ti-coating/Co-matrix interface. Coating was either detached from the surfaces of the grit and remained in the pull-out craters (Figure 9-8A) or remained attached on the surfaces, partially fractured, but retaining the plate-layered morphology produced by the CVD (Figure 9-8B). Diamond surfaces stripped from the coating were macroscopically smooth and flat retaining edge sharpness and contained considerably lower concentration of etch features compared to the non-coated grit as described previously. Fissures at the interfacial regions were evident but appeared to be slightly narrower compared to those found for the non-coated diamonds.

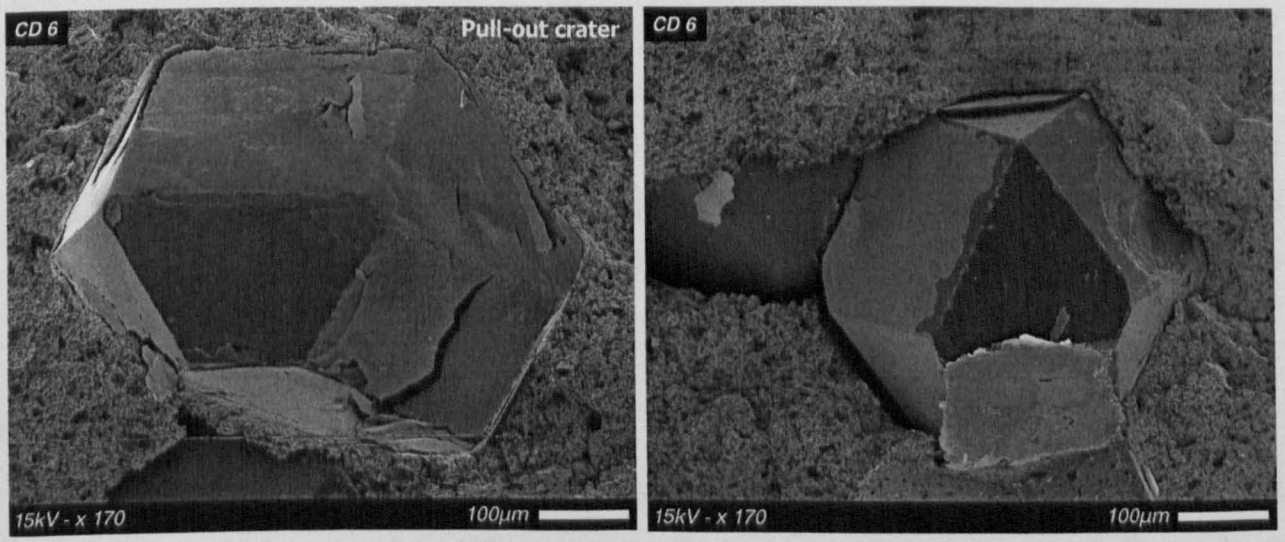

(A) CD 6 Ti-CVD-coated 30/40 US-mesh SYN-1 (DB) **(B)** CD 6 Ti-CVD-coated 30/40 US-mesh SYN-1 (DB)

Figure 9-8 : SEM micrographs showing sections of fracture surfaces of segments produced by the HIP route and impregnated with the Ti-CVD-coated diamonds (Ti-CVD, 30/40 mesh, SYN-1, DB).

The situation was generally similar for the segments with the Ti-coated SYN-3 diamonds (CD8). However, the titanium appeared to have interacted with the diamonds to a greater extent compared to the SYN-1 grade. Coating-diamond interaction appeared to have been slightly higher for the cubic {100} surfaces of the grit. (Figure 9-9A). Sites of good contact between the abrasive crystals and the Co-matrix were found (Figure 9-9B).

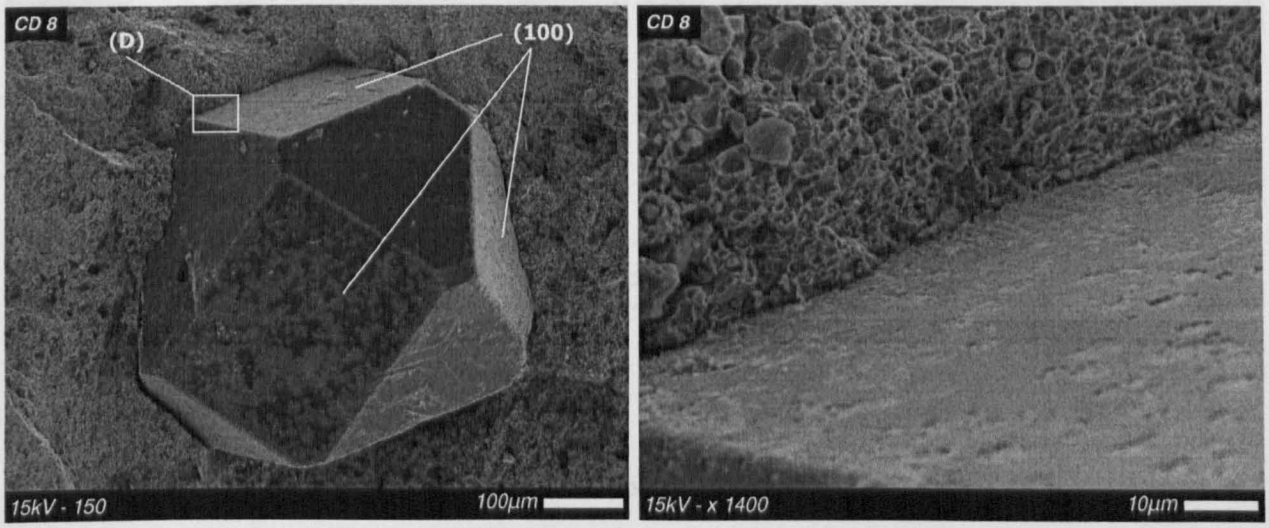

(A) CD 8 Ti-coated 30/40 US-mesh SYN-3 (PVD, DB) **(B)** CD 8 Ti-coated 30/40 US-mesh SYN-3 (PVD, DB)

Figure 9-9 : SEM micrographs showing sections of fracture surfaces of segments produced by the HIP route and impregnated with the Ti-PVD-coated diamonds (Ti-PVD, 30/40 mesh, SYN-3, DB).

9.6.1.1C Cr-coated Diamonds (CD9, CD10)

Examination of fracture surfaces of segments impregnated with the SYN-3 Cr-coated (PVD) diamonds (CD9, CD10) revealed that the coating preferentially remained intact in diamond pull-out sites (Figure 9-10A on next page). In most cases the Cr-coating shells retained the diamond shape with minimal degree of fracturing or cracking. The diamond surfaces that had lost their Cr-coating retained their smoothness and edge sharpness with very low levels of any type of diamond surface etching or interaction features as compared to Ti-coated grit. However, observation at higher magnifications revealed the presence of rectangular depressions whose bases had a rough irregular morphology constructed of small protruding features. These depressions were preferentially formed near diamond surface edges and on cubic {100} faces (Figure 9-10B on next page).

9.6.1.1D Cr(C)-coated Diamonds (CD11)

Observations of fracture surfaces of composites impregnated with the Cr(C)-coated diamonds were similar to what was found for the case of segments with the Cr-coated diamonds as described in the previous paragraph.

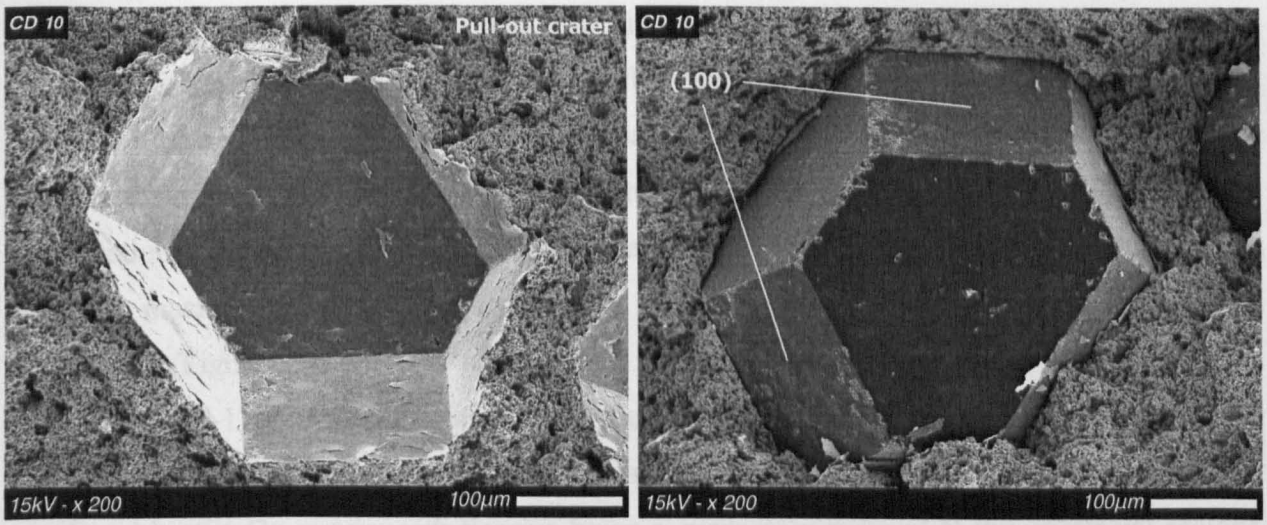

(A) CD 10 Cr-coated 40/50 US-mesh SYN-3 (PVD, TC) **(B)** CD 10 Cr-coated 40/50 US-mesh SYN-3 (PVD, TC)

Figure 9-10 : SEM micrographs showing sections of fracture surfaces of segments produced by the HIP route and impregnated with the Cr-PVD-coated diamonds.

9.6.1.1E Ti/Cr-coated Diamonds (CD12)

No particular preference of adhering to the cobalt matrix or remaining attached on diamond surfaces could be identified for the dual Ti/Cr-coated. Interfacial fissures were present in the majority of interfacial regions. Evidence of interaction phenomena could be found on diamond surfaces such as fine cobalt matrix remains and etch features. Etch trigons oriented parallel to the edges of octahedral faces were found on diamond surfaces (Figure 9-11).

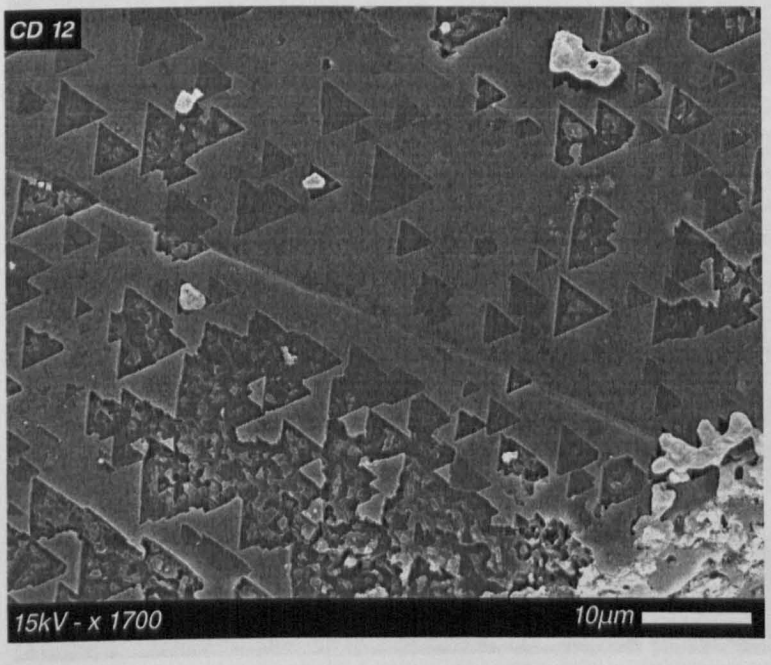

Figure 9-11 : SEM micrograph showing oriented etch trigons found on the octahedral (111) surface of a diamond exposed on the fracture surface of a segment impregnated with the Ti/Cr-coated diamonds.

9.6.1.1F W-coated Diamonds (CD13, CD14)

Examination of fracture surfaces of the segments impregnated with the PVD W-coated grit revealed that the degree of interactions between the diamonds and the metallic constituents of the

composite was considerably greater than any other system previously described (Figure 9-12A). A distinctive pattern constructed by bands of flat unaffected diamond surfaces had formed on diamond surfaces. The area in between these bands appeared to have been etched and was the region were metallic remains could be found attached on the diamond surfaces (Figure 9-12B). Examination at high magnifications revealed that the area in between the diamond bands, which appeared macroscopically irregularly etched, was constructed from intersecting hexagonal depressions (Figure 9-12B). This band pattern was more pronounced on the octahedral {111} faces (Figure 9-12C), whereas cubic {100} surfaces appeared to have been etched at greater extent and contained larger quantities of metallic remains. Diamonds appeared to be tightly enveloped by the Co-matrix with fissures being considerably reduced at the interfacial regions. Areas of good interfacial contact were abundantly found (Figure 9-12D).

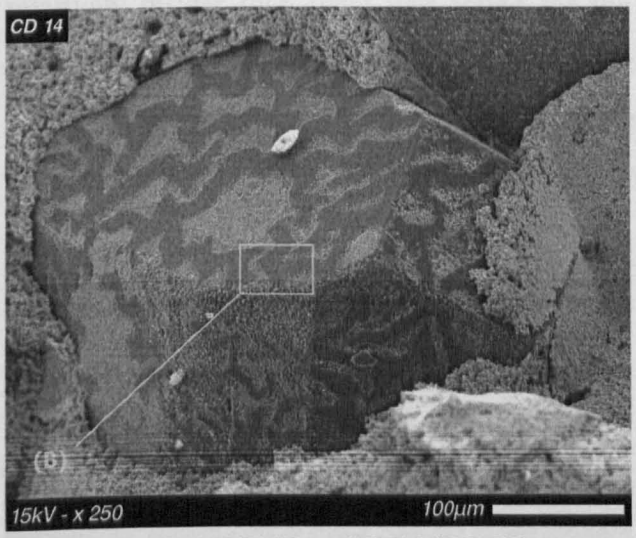

(A) CD 14 W-coated 40/50 US-mesh SYN-3 (PVD, TC)

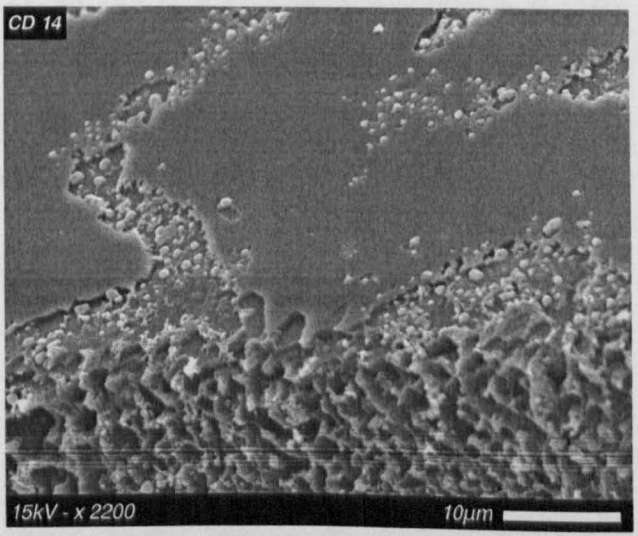

(B) CD 14 W-coated 40/50 US-mesh SYN-3 (PVD, TC)

(C) CD 14 W-coated 40/50 US-mesh SYN-3 (PVD, TC)

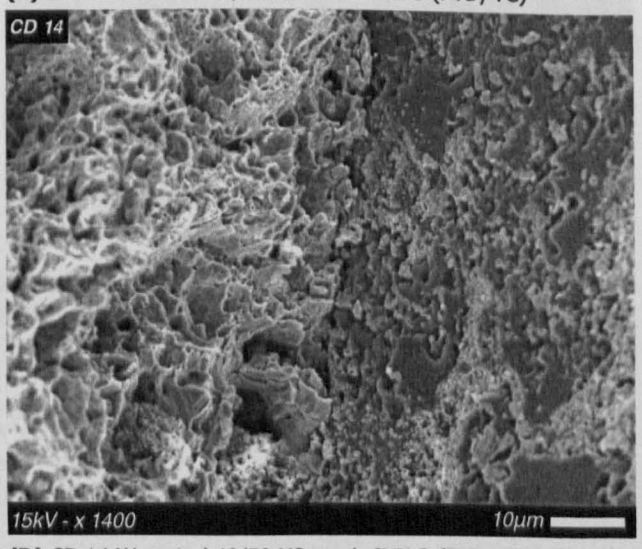

(D) CD 14 W-coated 40/50 US-mesh SYN-3 (PVD, TC)

Figure 9-12 : SEM micrographs showing sections of fracture surfaces of segments produced by the HIP route and impregnated with the various grades of W-coated diamonds.

9.6.1.2 Hot-Pressed segments (HP) – Fractured by 3-point Bending

Results presented here concern the microscopic analysis of the fractured surfaces of hot-pressed segments produced by 3-point bending.

9.6.1.2A Non-coated Diamonds (CD15, CD16, CD17)

Non-coated diamonds exposed on fracture surfaces appeared almost unchanged compared to the as received abrasive crystals (Figure 9-13). Dissolution etching was considerably reduced compared to the sintered (FS-ed) and hot-isostatically-pressed (HIP-ed) segments. In particular, the SYN-1 quality diamonds (CD15) appeared almost unaffected by the hot-pressing treatment, retaining clean and smooth surfaces and sharp crystal edges (Figure 9-13A). The surfaces of the SYN-3 diamonds revealed that crystals had undergone fine scale etching, which was however relatively milder than what was found for the FS-ed and HIP-ed composites (Figure 9-13B). Cubic {100} surfaces appeared to be slightly more prone to surface etching than the octahedral {111} faces. Interfacial fissures were narrower than those found for the FS-ed and HIP-ed segments giving the impression that diamonds were held tighter in the Co-matrix sockets.

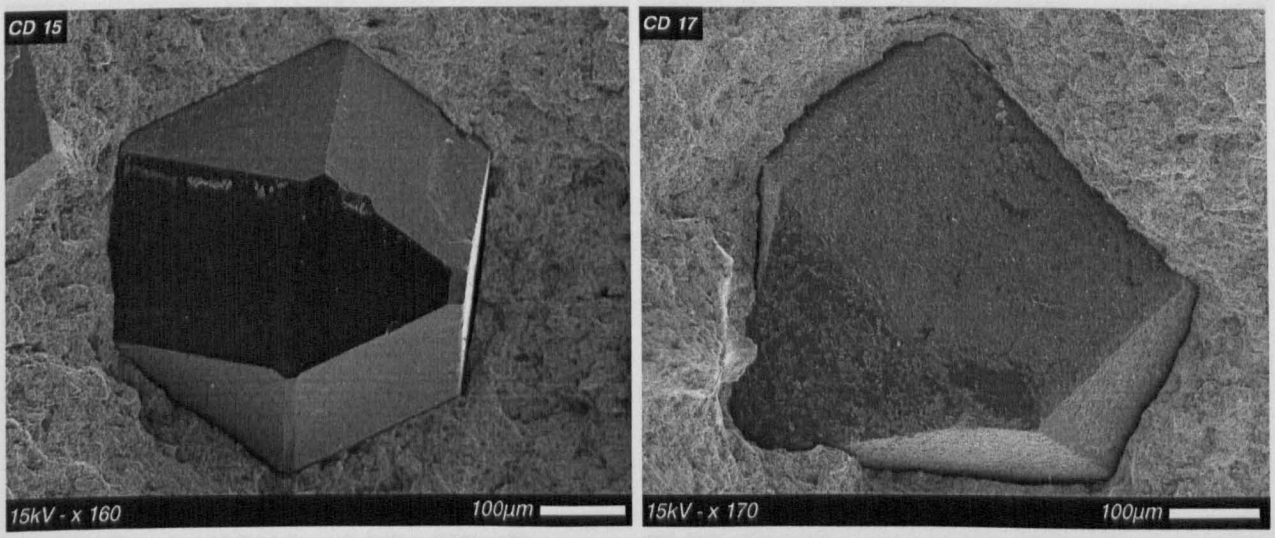

(A) CD 15 Non-coated 30/50 US-mesh SYN-1 (DB) **(B)** CD 17 Non-coated 30/40 US-mesh SYN-3 (DB)

Figure 9-13 : SEM micrographs showing sections of fracture surfaces of segments produced by the HP route and impregnated with the various grades of non-coated diamonds.

9.6.1.2B Ti-coated Diamonds (CD18, CD19, CD32, CD33, CD39, CD40)

CVD (DB) SYN-1 30/50 US mesh (CD32, CD18)

SEM examination revealed that the majority of diamond pull-out craters were covered by the Ti-coatings indicating a preference of the coating to remain attached to cobalt (Figure 9-14A). There were however instances where parts of the Ti-coating remained on diamonds with the fracture occurring either at the Co-Ti interface or within the coating itself (Figure 9-14B to D).

Surfaces of diamonds stripped from the coating were clean and smooth with minimal amount of etch pits. Heat-treatment of the diamond crystals prior to hot-pressing was found to have no particular effect on the interfacial bonding of the composite (CD18) apart from increasing the amount of diamond etching. EDAX analysis performed at the interfacial regions revealed segregation of oxygen at both the diamond/Ti and the Ti/Co interfaces.

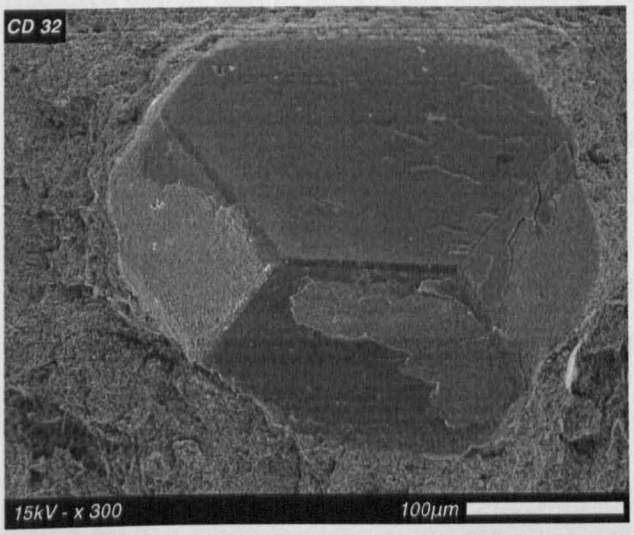

(A) CD 32 Ti-coated 30/50 US-mesh SYN-1 (CVD, DB)

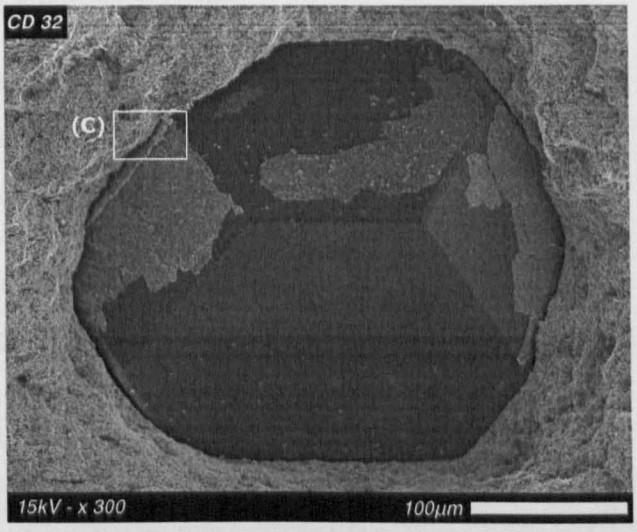

(B) CD 32 Ti-coated 30/50 US-mesh SYN-1 (CVD, DB)

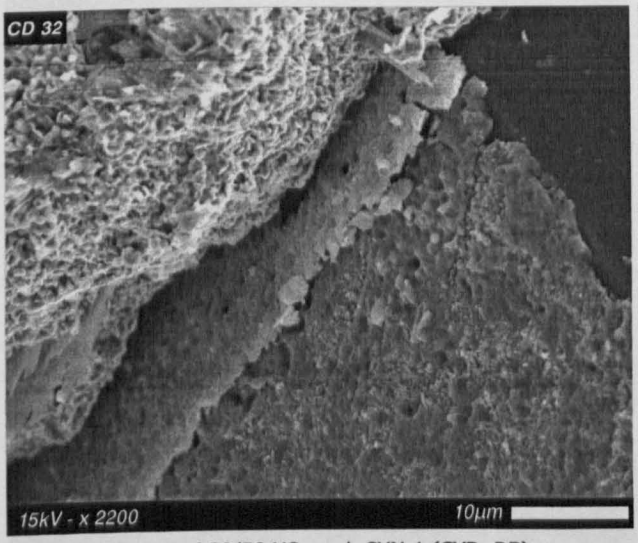

(C) CD 32 Ti-coated 30/50 US-mesh SYN-1 (CVD, DB)

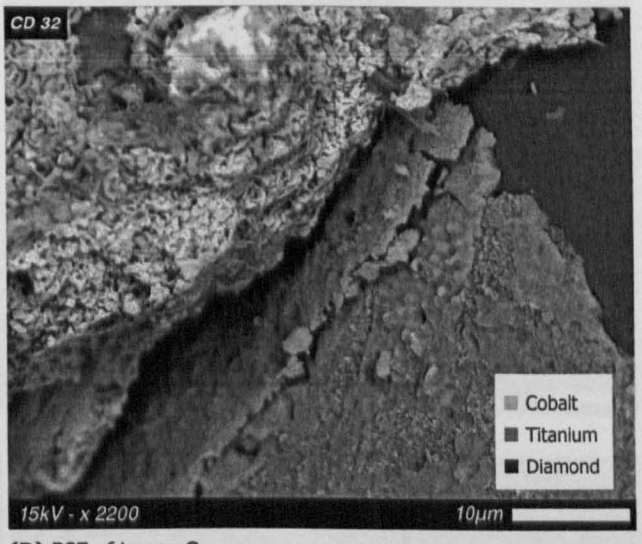

(D) BSE of image C

Figure 9-14 : SEM micrographs showing sections of fracture surfaces of segments produced by the HP route and impregnated with the CVD Ti-coated SYN-1 30/50 US mesh diamonds (DB).

PVD (TC) SYN-1 30/50 US mesh (CD33, CD19) & SYN-3 30/40 (CD39, CD40)

The examination of segments impregnated with the diamonds coated with titanium deposited by PVD showed clearly that the titanium coating was very well bonded to the cobalt matrix. There were many interfacial sites where additionally the diamond to titanium bonding appeared to have been achieved. The degree of diamond-to-metal interaction was clearly higher than that found for the CVD Ti-coated diamonds. Fracture had occurred primarily at the diamond-titanium interface but there were many sites where fracture also took place at the cobalt-titanium interface

or within the bulk of the titanium coatings (Figure 9-15A and Figure 9-15B). The reaction products that had formed at the interface were dense but also contained cracks. These had formed a network of cracks that travelled along the interface intersecting with the numerous smaller cracks perpendicular to the interfacial plane (Figure 9-15C and Figure 9-15D). The reaction layer thickness was approximately 10-12 microns. Spherical features were found in the fractured cobalt matrix zones that surrounded the diamond crystals.

Heat-treatment of the diamond crystals prior to hot-pressing did not produce any observable differences compared to the segments with the non heat-treated Ti-coated diamonds, apart from the presence of etch trigons on surfaces of the SYN-3 diamonds.

Macroscopic examination of the fracture surface of the CD39 segment showed clearly the effect of the bonded diamonds in that the crack that caused the rupture in bending was deflected (Figure 9-16).

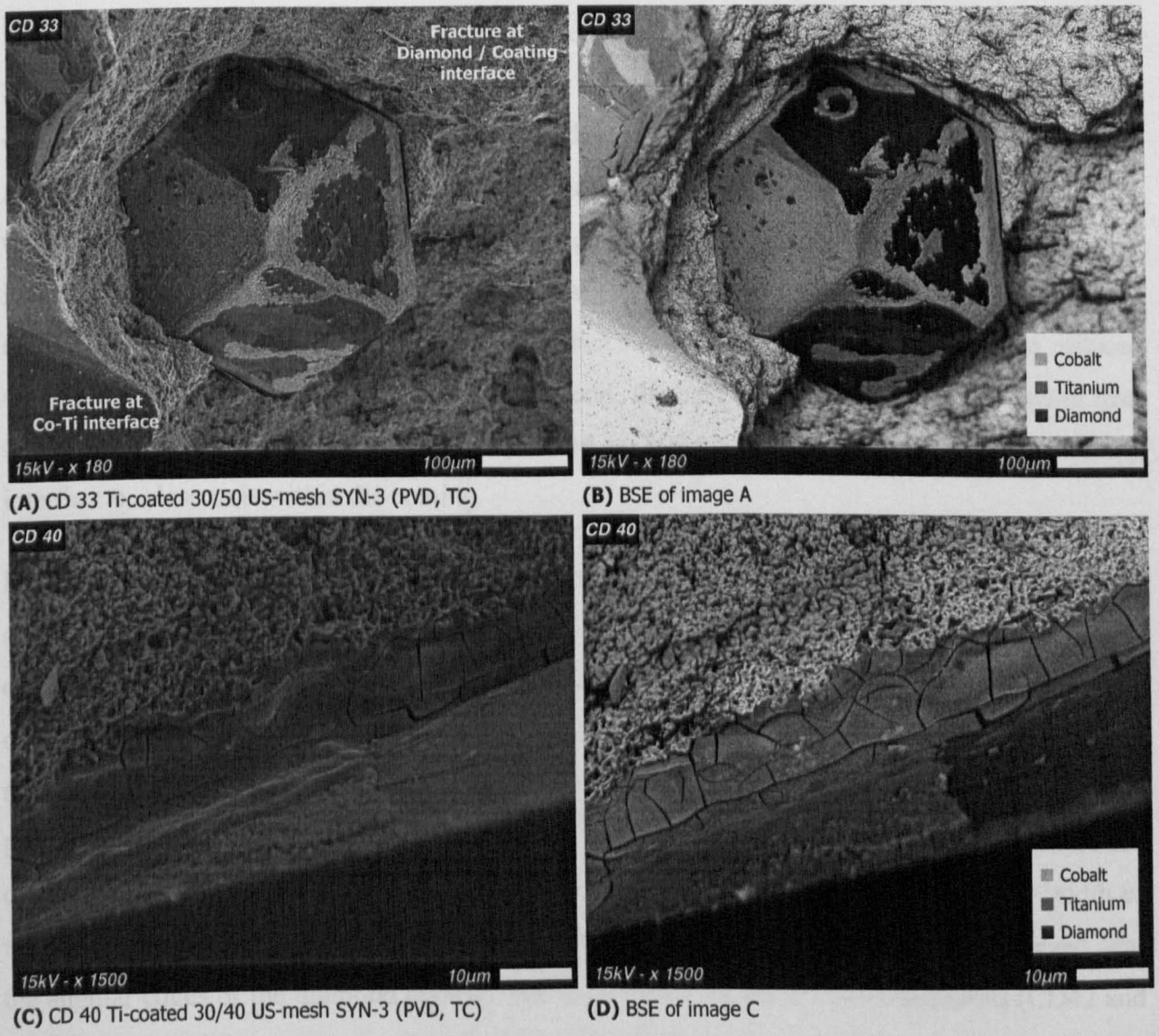

(A) CD 33 Ti-coated 30/50 US-mesh SYN-3 (PVD, TC)

(B) BSE of image A

(C) CD 40 Ti-coated 30/40 US-mesh SYN-3 (PVD, TC)

(D) BSE of image C

Figure 9-15 : SEM micrographs showing sections of fracture surfaces of segments produced by the HP route and impregnated with the PVD Ti-coated SYN-3 diamonds (TC).

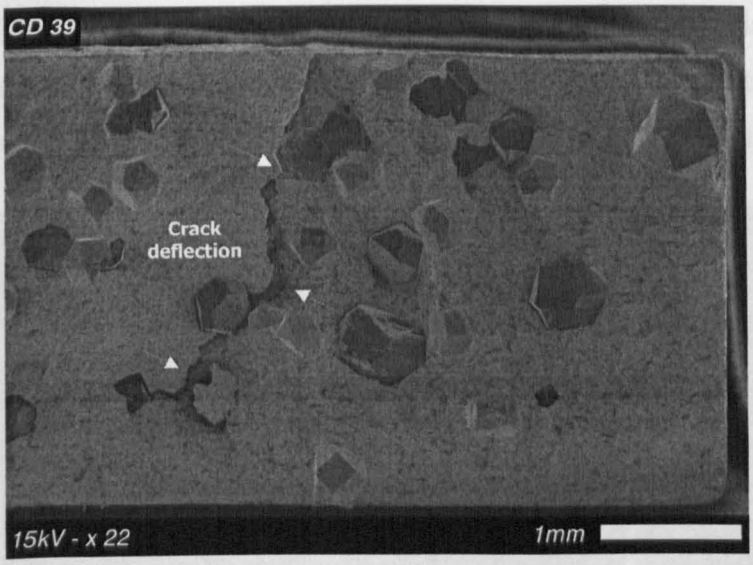

Figure 9-16 : SEM micrographs showing section of the fracture surface of segment produced by the HP route and impregnated with the PVD Ti-coated SYN-3 30/40 mesh diamonds (TC).

9.6.1.2C Cr-coated Diamonds (CD20, CD24, CD34, CD38, CD42, CD43)

PVD (TC) SYN-1 30/50 mesh (CD34, CD20) & SYN-3 30/40 mesh (CD42, CD43)

Inspection of fracture surfaces of segments impregnated with the PVD Cr-coated diamonds revealed that the chromium coatings were bonded well with the cobalt matrix. A dense reaction product was formed at the interfacial regions (Figure 9-17A). Reaction zones were thicker compared to what was found for the Ti-coated grit, approaching 40-50 microns at particular sites. The formed reaction product contained cracks the majority of which were located closer to the diamond (Figure 9-17B). Other smaller cracks lay at directions perpendicular to the interfacial plane. The concentration of cracks was reduced as the cobalt-chromium interface was approached. EDAX analysis of the reaction product showed that the carbon content was reduced when moving towards the cobalt-matrix. In general, the concentration of cracks was lower than that for the Ti-coated diamonds. Failure occurred preferentially parallel at the diamond-coating interface or close to it within the coating.

It is interesting to note that although thick reaction layers were formed at the interfacial region of some of the diamonds, for other diamonds this reaction zone was much thinner and for many others such a reaction layer did not exist at all. It appeared that reaction was promoted for some of the diamonds preferentially to others. Macroscopic examination of the fracture surface at low magnification revealed that reaction was promoted at the interfaces of the larger crystals. This phenomenon was dramatically enhanced for the diamonds that were located in areas where the diamond concentration parallel to the hot-pressing direction (in other words across the width of the segment) was high. Additionally, increased thickness of the reaction zone was observed near the angular edges of the diamond crystals. For some of the 30/40 US mesh diamonds (CD42 and CD43) dendritic features protruding from the diamond surfaces were found (Figure 9-17C).

These were preferentially located on the cubic {100} diamond faces. EDAX analysis showed that these dendrites were 95-98% carbon. Heat-treatment of the diamonds prior to hot-pressing was found to slightly increase crack density in the reaction product layers.

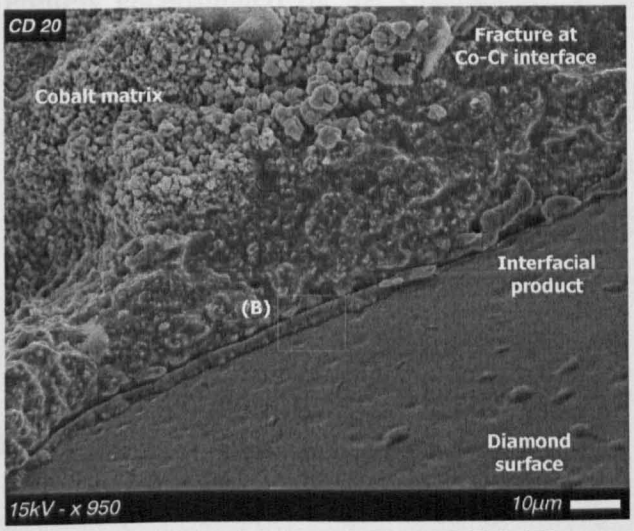

(A) CD 20 Cr-coated 30/50 US-mesh SYN-1 HT (PVD, TC)

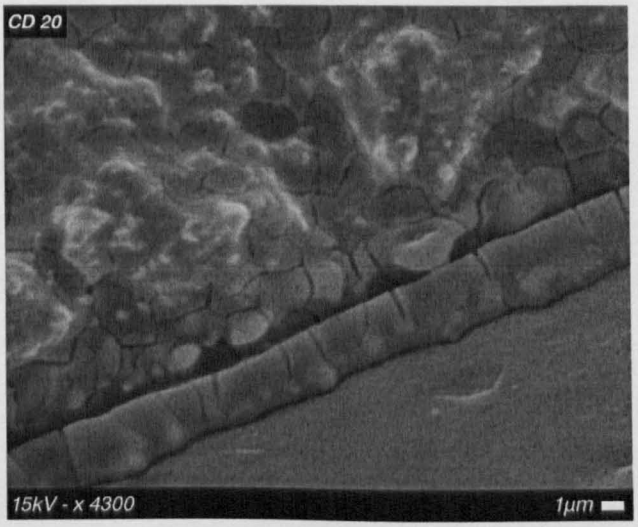

(B) Magnified section of image A

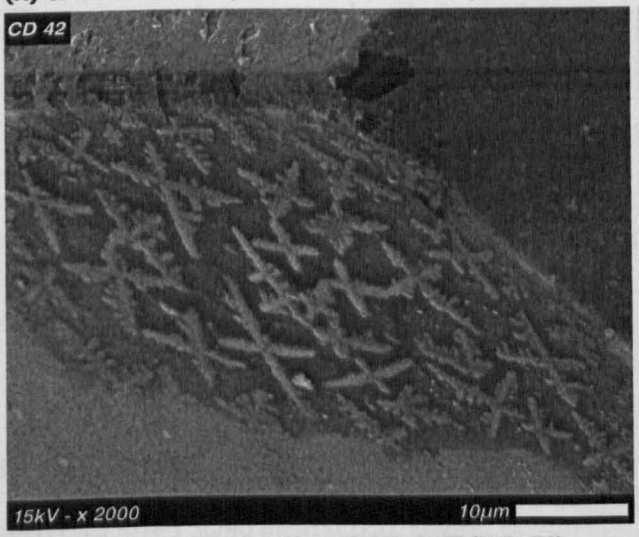

(C) CD 42 Cr-coated 30/40 US-mesh SYN-3 HT (PVD, TC)

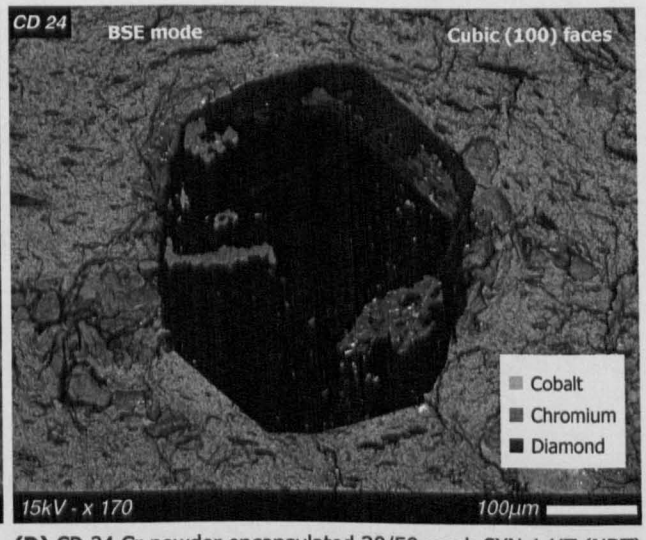

(D) CD 24 Cr-powder encapsulated 30/50 mesh SYN-1 HT (NDT)

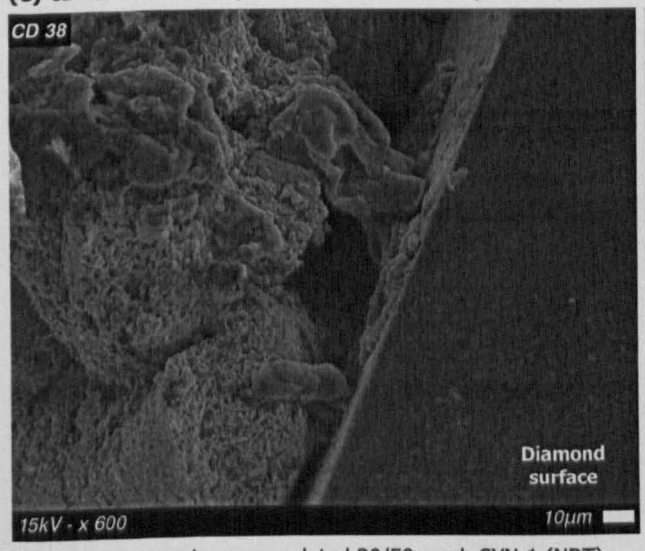

(E) CD 24 Cr-powder encapsulated 30/50 mesh SYN-1 (NDT)

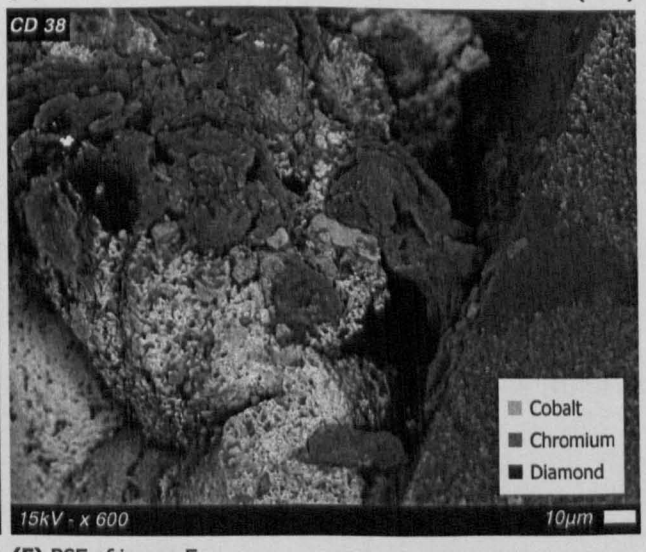

(F) BSE of image E

Figure 9-17 : SEM micrographs showing sections of fracture surfaces of segments produced by the HP route and impregnated with the various Cr-coated diamonds.

PC (NDT) SYN-1 30/50 mesh (CD24, CD38)

Chromium granules could easily be distinguished around diamond crystals on the fracture surfaces of segments impregnated with the Cr-powder encapsulated grit. Diamonds were not entirely encapsulated by the Cr-granules, which could be found even at significant distances from the diamonds. Examination revealed that reaction took place for the chromium granules that retained contact with the diamonds during hot-pressing (Figure 9-17E & F). Cubic {100} diamond faces were found to be slightly more reactive than the octahedral {111} surfaces (Figure 9-17D). Fragments from partially fractured diamonds remained attached at the bottom of pull-out craters. Composite rupture occurred preferably through the chromium zone or at the diamond-metal interface.

9.6.1.2D Cr(C)-coated Diamonds (CD21, CD35)

PVD (TC) SYN-3 30/40 mesh (CD35, CD21)

The segments impregnated with the carbon enriched Cr(C)-coated diamonds exhibited a different behaviour from what was observed for the other chromium coated diamonds. A distinctive reaction product layer was not formed and coatings appeared to remain non-reactive with respect to both the cobalt-matrix and the diamonds. However, coatings preferentially remained almost entirely on the diamond surfaces. Diamond surfaces stripped from the coating were smooth and relatively clean from any etch features or nuclei of reaction products. Crystal edge sharpness was equivalent to that of the original grains.

9.6.1.2E Ti/Cr-coated Diamonds (CD22, CD36)

PVD (TC) SYN-3 30/40 mesh (CD36, CD22)

Inspection of fracture surfaces of composites reinforced with the Ti/Cr-coated diamonds revealed that coating preferentially bonded to the cobalt-matrix. However, sites where the coating remained attached on diamonds could be found as well as locations where cobalt fragments adhered on diamond surfaces. A limited number of interfacial sites where a reaction product similar to that observed for the Ti- and Cr-coated diamonds was found. EDAX analysis indicated that chromium preferentially migrated towards the cobalt matrix whereas titanium followed the opposite direction towards the diamonds. Diamond surfaces stripped from the coating show a small degree of etching.

9.6.1.2F W-coated Diamonds (CD23, CD25, CD26, CD30, CD31, CD37, CD44, CD45)

CVD (NC) SYN-1 35/50 mesh (CD30, CD31)

Examination of the fracture surfaces of segments impregnated with CVD W-coated grit revealed that the thick W-coating layers bonded excellently to the cobalt-matrix (Figure 9-18). Tungsten appeared to have formed rigid jackets enclosing the diamonds. There were numerous diamonds that retained their dense W-coating with almost no signs of coating fracture. Stripped diamond surfaces were relatively free from any signs of etching. Heat-treatment of the CVD W-coated diamonds prior to hot-pressing was found to slightly improve the bonding of the coating to the crystals. Fracture surfaces contained a relatively high number of fractured crystals and diamond fragments remained attached in pull-out craters. In general, it could be said that composite failure in 3-point bending preferentially occurred at the diamond-tungsten coating interface.

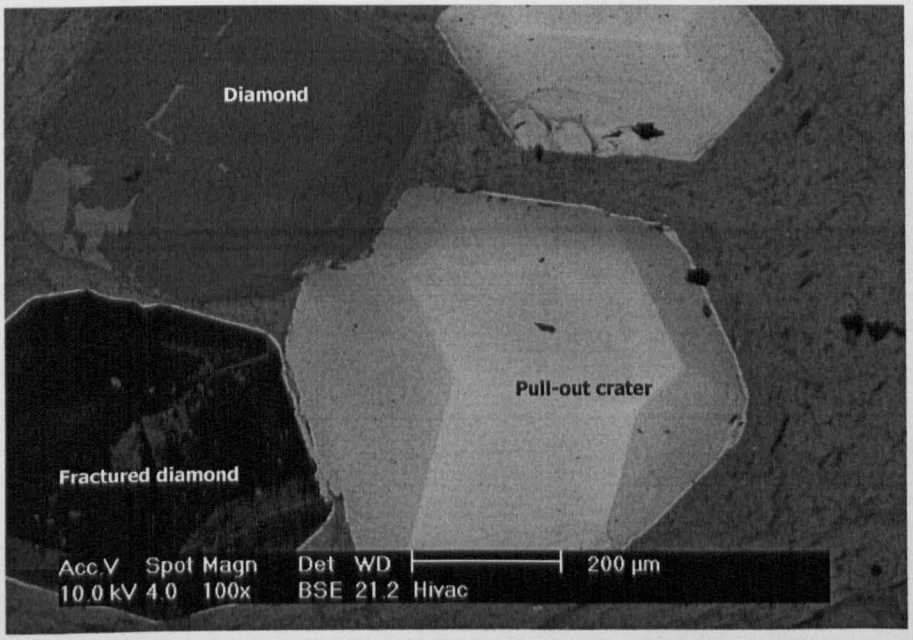

(A) CD 30 W-coated 35/50 US mesh SYN-1 (CVD, NC), BSE mode

□ Tungsten
■ Cobalt
■ Diamond

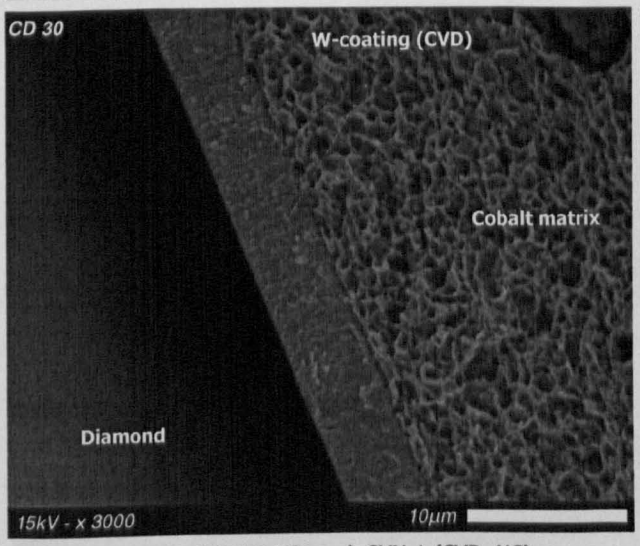

(B) CD 30 W-coated 35/50 US mesh SYN-1 (CVD, NC)

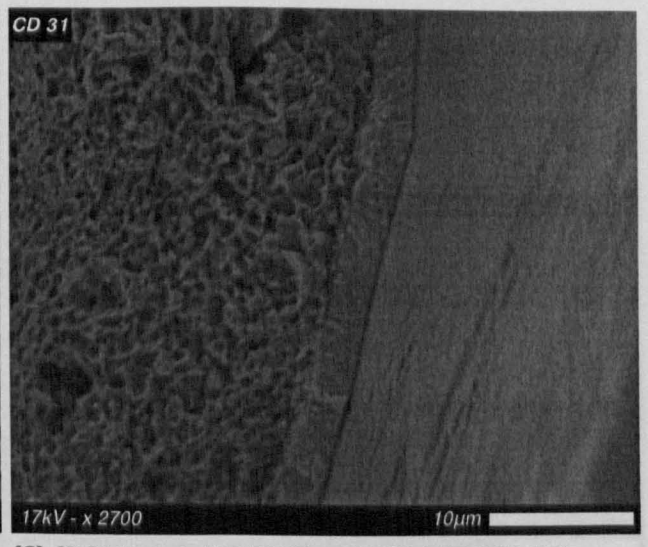

(C) CD 31 W-coated 35/50 US mesh SYN-1 HT (CVD, NC)

Figure 9-18 : SEM micrographs showing sections of fracture surfaces of segments produced by the HP route and impregnated with the CVD W-coated SYN-1 35/50 US mesh diamonds (NC).

PVD (TC) SYN-1 30/50 mesh (CD37, CD23) & SYN-3 30/40 mesh (CD44, CD45)

SEM inspection revealed that the PVD W-coatings bonded excellently to the cobalt matrix similarly to the CVD W-coated grit, as described previously. At numerous interfacial locations it appeared that tungsten had reacted with both the cobalt and the diamond (Figure 9-19A & B). The reaction product contained cracks, which were smaller in size and at considerably lower levels of concentrations than those found in the cases of both the Ti- and Cr-coated crystals (Figure 9-19C). Cracks were preferentially located near to the diamonds. At areas where bonding of the W-coating had been achieved to both the cobalt matrix and the diamond, a considerable extent of the fracture causing composite failure had gone through the cobalt-tungsten interface on the cobalt side (Figure 9-19D). Examination at high magnification revealed the presence of a closed-packed network of platelets growing from the diamond surface towards the cobalt, indicating the formation of carbide (Figure 9-19D). Diamonds stripped from the coating retained overall smooth surfaces, free from extensive etching and with sharp edges (Figure 9-19A).

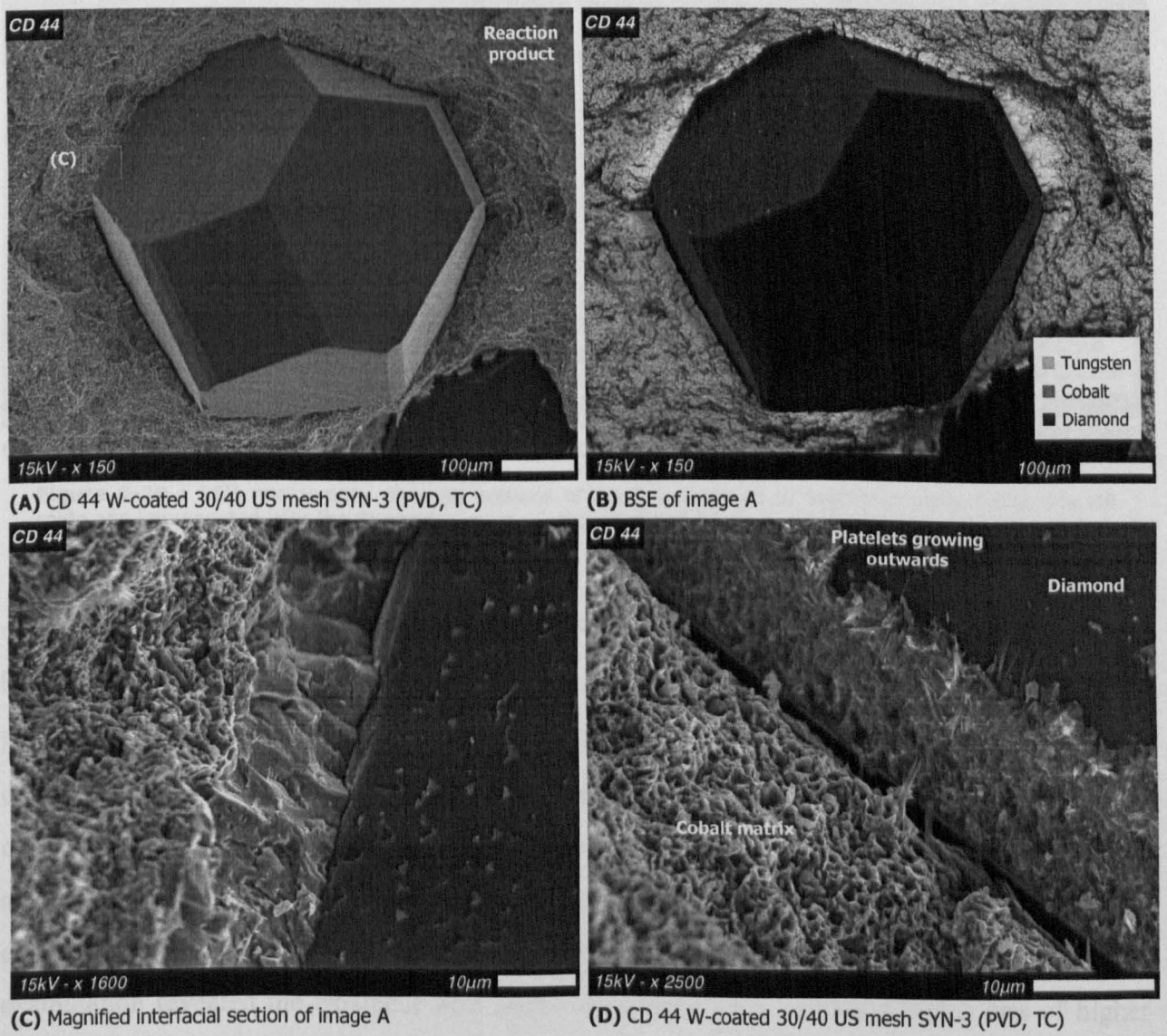

(A) CD 44 W-coated 30/40 US mesh SYN-3 (PVD, TC)

(B) BSE of image A

(C) Magnified interfacial section of image A

(D) CD 44 W-coated 30/40 US mesh SYN-3 (PVD, TC)

Figure 9-19 : SEM micrographs showing sections of fracture surfaces of segments produced by the HP route and impregnated with the PVD W-coated SYN-3 diamonds (TC).

PC (VM) SYN-1 30/50 mesh (CD25, CD26)

Examination of the fracture surfaces of segments impregnated with the W-powder encapsulated revealed that the diamonds were entirely surrounded by a zone of W-powder (Figure 9-20). A high degree of tungsten remains were found on the surfaces of exposed diamonds, providing evidence of diamond-tungsten reaction. Heat treatment of the W-granulated diamonds prior to hot-pressing was found to slightly increase the concentration of tungsten fragments found on diamond surfaces. However, the general appearance of the interfacial regions indicated that the tungsten powder was preferentially bonded to the cobalt and remained in the majority in the formed pull-out craters. A continuous crack that followed the shape of the tungsten-cobalt interface had formed indicating that failure occurred primarily within the W-zone but very near to the W-Co interface (Figure 9-20). Exposed diamonds retained the angular edges and flat surfaces with a minimal degree of etching.

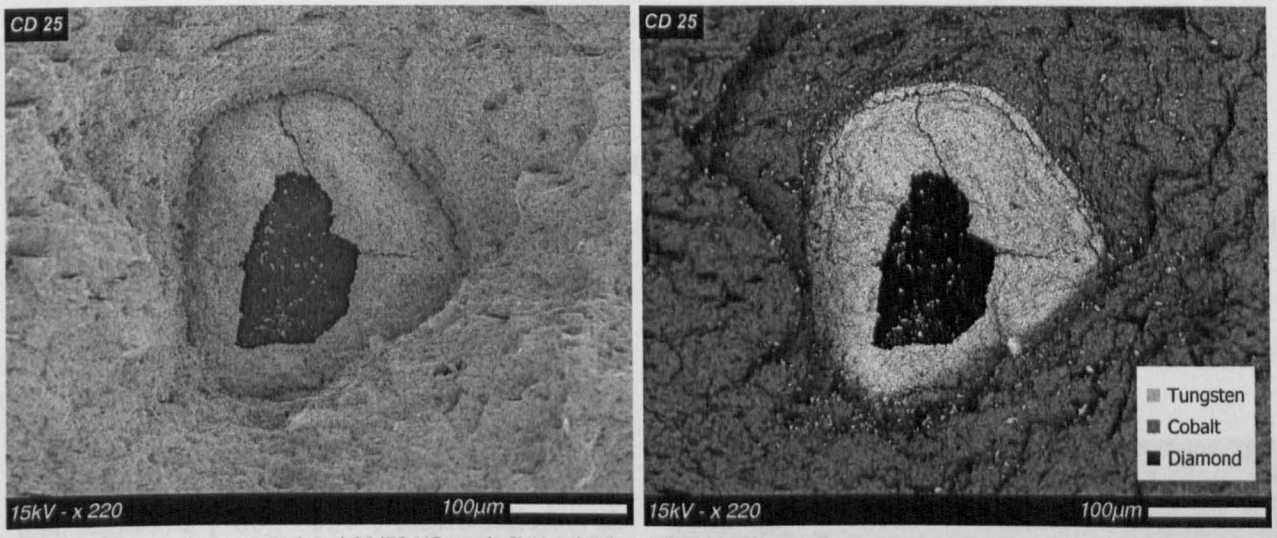

(A) CD 25 W-powder encapsulated 30/50 US mesh SYN-1 (VM) **(B)** BSE of image A

Figure 9-20 : SEM micrographs showing sections of fracture surfaces of segments produced by the HP route and impregnated with the W-powder encapsulated diamonds (VM).

9.6.1.2G Co-powder encapsulated Diamonds (CD28, CD29)

PC (J) SYN-3 30/40 mesh (CD28, CD29)

Inspection of the fracture surfaces of segments impregnated with the Co-powder encapsulated diamonds revealed that the abrasive crystals were enveloped in the matrix similarly to that observed for the segments reinforced with the non-coated grit. Diamond surfaces remained smooth and clean with only the previously heat-treated crystals showing a small degree of etching. This was particularly noticeable for the cubic {100} faces (Figure 9-21A). Careful examination revealed the existence of a zone surrounding each diamond which was of higher density when compared to the bulk Co-matrix. This zone appeared to form a thick metal jacket

tightly enclosing each crystal (Figure 9-21B). The interfacial fissures between the diamonds and cobalt were considerably narrower than those found in the segments with the non-coated grit.

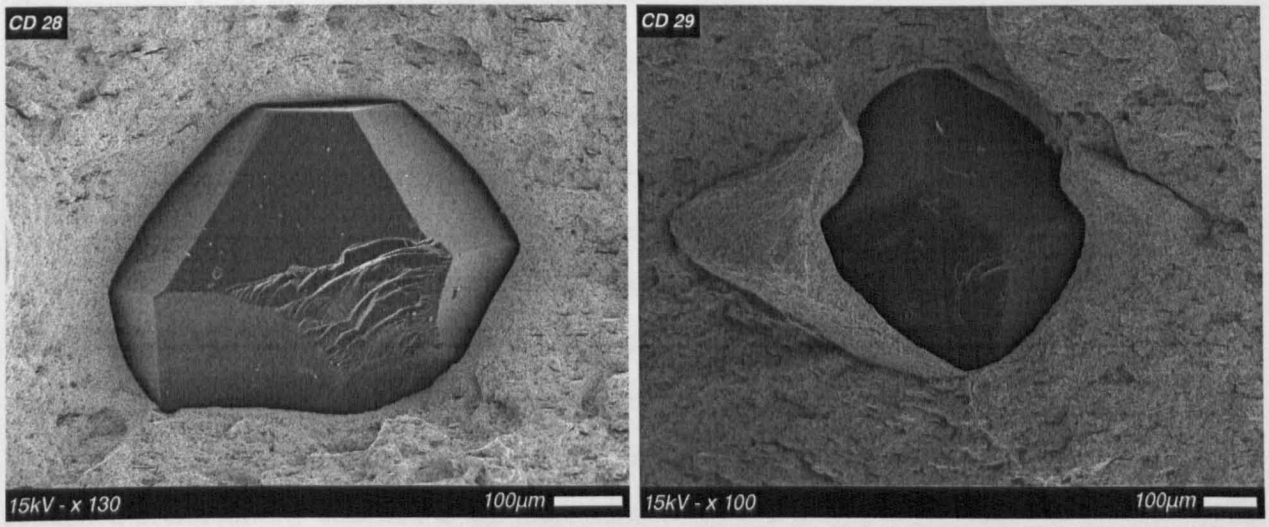

(A) CD 28 Co-powder encapsulated 30/40 US mesh SYN-3 (J) **(B)** CD 29 Co-powder encapsulated 30/40 US mesh SYN-3 HT (J)

Figure 9-21 : SEM micrographs showing sections of fracture surfaces of segments produced by the HP route and impregnated with the Co-powder encapsulated diamonds (J).

9.6.1.3 Tensile test segments (DBS) – Fractured by Uniaxial Tension

Results presented here concern the microscopic analysis of the fractured surfaces of sintered segments produced by uniaxial tensile testing.

9.6.1.3A Non-coated Diamonds (DBS-2, DBS-3, DBS-4)

Appearance of fracture surfaces of the tensile test segments ("dog-bone") impregnated with the various types of non-coated grit were similar to those of the FS-ed and HIP-ed segments reinforced with non-coated diamonds and tested by 3-point bending. Exposed diamond surfaces provided evidence that dissolution etching had taken place at a fine scale (Figure 9-22). The finer grit (40/50 mesh) seemed to have been etched at a relatively larger degree than the coarser grade (30/40 mesh). Interfacial fissures were clearly evident at the diamond-cobalt interfaces.

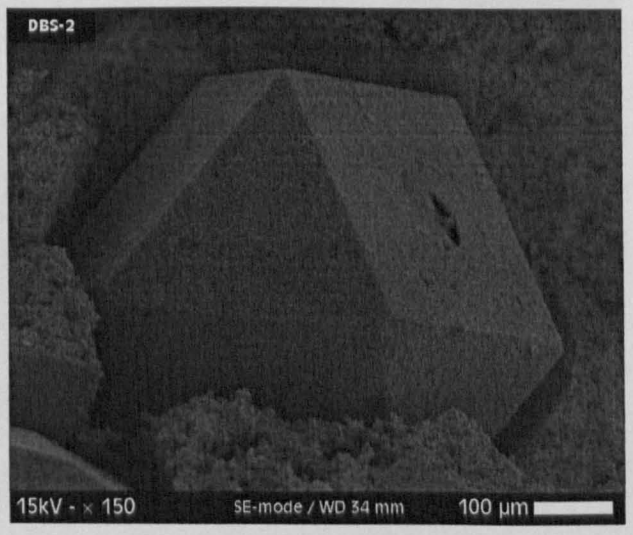

Figure 9-22 : SEM micrograph showing an exposed diamond on a fracture surface of a "dog-bone" segment impregnated with the SYN-3 30/40 US mesh non-coated diamonds.

9.6.1.3B Ti-coated Diamonds (DBS-5, DBS-6, DBS-11, DBS12)

CVD (DB) SYN-1 30/50 US mesh (DBS-11, DBS-12)

The examination of the fracture surfaces of the "dog-bone" segments impregnated with the CVD Ti-coated diamonds revealed that chemical interactions had occurred at the interfacial regions. Compared with the corresponding sintered segments tested by 3-point bending, it could be said that reactivity was slightly increased. Crystal edges were the preferential sites of reaction in addition to crystal defect areas such as fractured sites or other surface imperfections developed during crystal growth (Figure 9-23A). The interfacial reaction product was composed of planar whiskers that gave an overall appearance of a woven texture (Figure 9-23B). EDAX analysis of diamond surfaces that appeared etched, revealed the presence of titanium and cobalt, but also considerable levels of oxygen. The microscopic inspection revealed that the titanium coatings remained preferentially attached to the diamonds rather than in the cobalt pull-out craters. On the other hand, fragments of cobalt were found attached on the exposed diamond surfaces. These observations provided evidence that the cracks causing failure had preferentially followed the coating-cobalt interface within the cobalt side. Heat-treatment of the Ti-coated diamonds prior to consolidation sintering of the composite was found not to have any particular effect.

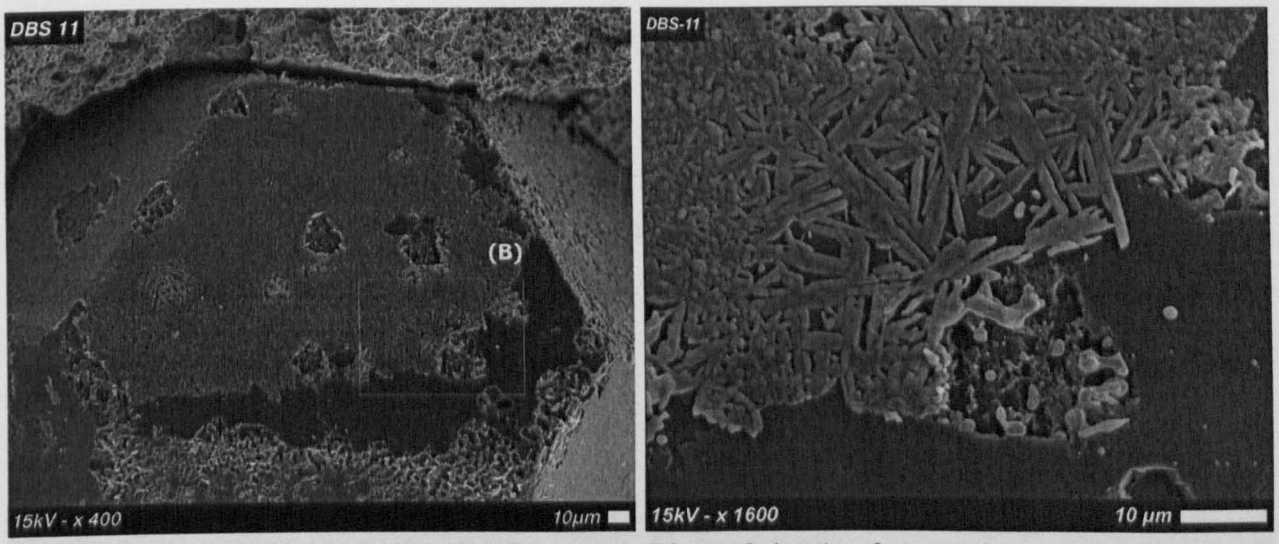

(A) DBS-11 Ti-coated 30/50 US mesh SYN-1 (CVD, DB) **(B)** Magnified section of micrograph A.

Figure 9-23 : SEM micrographs showing an exposed diamond on a fracture surface of "dog-bone" segment impregnated with the CVD Ti-coated 30/50 US mesh SYN-1 diamonds (DB).

PVD (TC) SYN-3 30/40 US mesh (DBS-5, DBS-6)

The examination of the fracture surfaces of the "dog-bone" segments impregnated with the PVD Ti-coated diamonds revealed that interactions between the diamonds and the metal constituents of the composite had occurred (Figure 9-24A). Fragments of the PVD Ti-coating layers were found attached on only a few diamond surfaces. The majority of the exposed diamond surfaces

contained a large quantity of etch features, primarily etch trigons. Almost every such etch feature contained a spheroidal cobalt fragment attached at the centre of each etched cavity (Figure 9-24B). Heat-treatment of the Ti-coated diamonds prior to consolidation sintering of the composite was found not to have any particular effect.

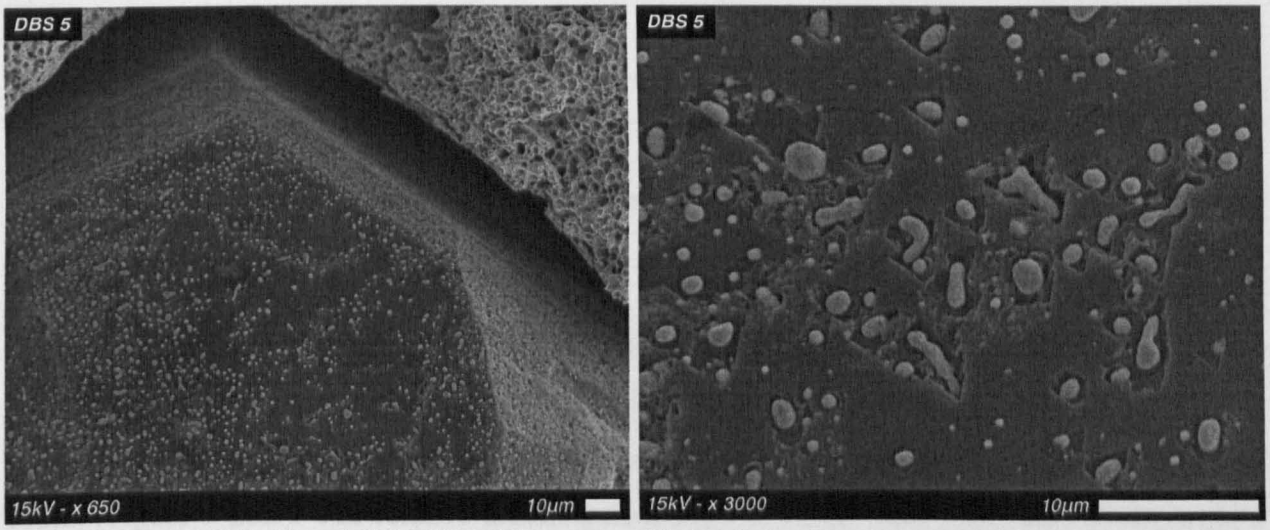

(A) DBS-5 Ti-coated 30/40 US mesh SYN-3 (PVD, TC) **(B)** Magnified section of micrograph A.

Figure 9-24 : SEM micrographs showing an exposed diamond on a fracture surface of "dog-bone" segment impregnated with the PVD Ti-coated 30/40 US mesh SYN-3 diamonds (TC).

9.6.1.3C Cr-coated Diamonds (DBS-13, DBS-14, DBS-19, DBS20)

PVD (TC) SYN-1 30/50 US mesh (DBS-13, DBS-14)

The inspection of the fracture surfaces of "dog-bone" segments impregnated with the PVD Cr-coated diamonds revealed that many of the exposed diamonds had retained the Cr-coating to a large extent (Figure 9-25).

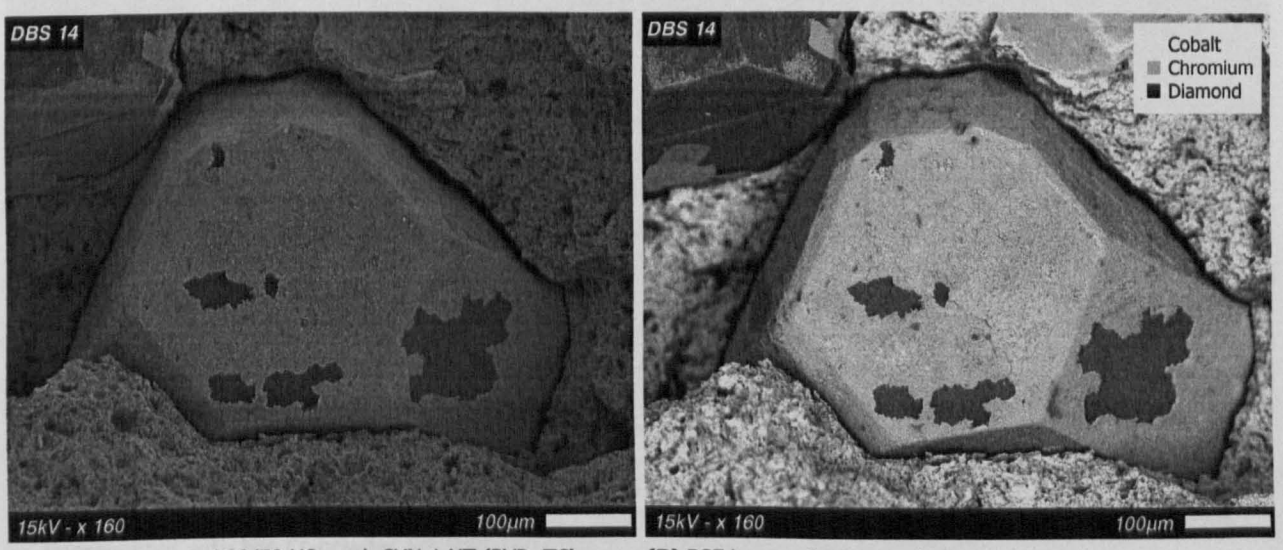

(A) DBS-14 Cr-coated 30/50 US mesh SYN-1 HT (PVD, TC) **(B)** BSE image of micrograph A.

Figure 9-25 : SEM micrographs showing an exposed diamond on a fracture surface of "dog-bone" segment impregnated with the PVD Cr-coated 30/50 US mesh SYN-1 diamonds (TC).

Fragments of cobalt were found attached on exposed diamond surfaces. Diamond surfaces stripped from the Cr-coating were relatively smooth and clean. The heat treatment of the coated grit prior to the consolidation increased the amount of the coating found to be retained on to the diamond surfaces (Figure 9-25).

PC (NDT) SYN-1 30/50 US mesh (DBS-19, DBS-20)

SEM examination of fracture surfaces of the "dog-bone" segments impregnated with the Cr-powder encapsulated diamonds showed that a pattern of shallow craters were formed on the exposed diamond surfaces, which appeared to be the imprint of the chromium powders (Figure 9-26).

This pattern revealed the sites where contact of the chromium powders and diamond surfaces had taken place. Each crater contained a relatively large knoll, which as the EDAX analysis showed was composed mainly of chromium and carbon with small percentages of oxygen and cobalt (Figure 9-26B). The relative atomic percentages in carbon and chromium atoms suggest that possibly chromium carbides with high carbon content were formed as well as chromium oxides. The chromium to carbon atomic ratio varied in the range of 0.6 to 0.77.

In general, reactivity appeared to be greater than that observed for the segments impregnated with PVD Cr-coated diamonds. Many sites of very good interfacial contact between diamonds and cobalt were found. Additionally, a large amount of cobalt fragments were found on the diamond surfaces.

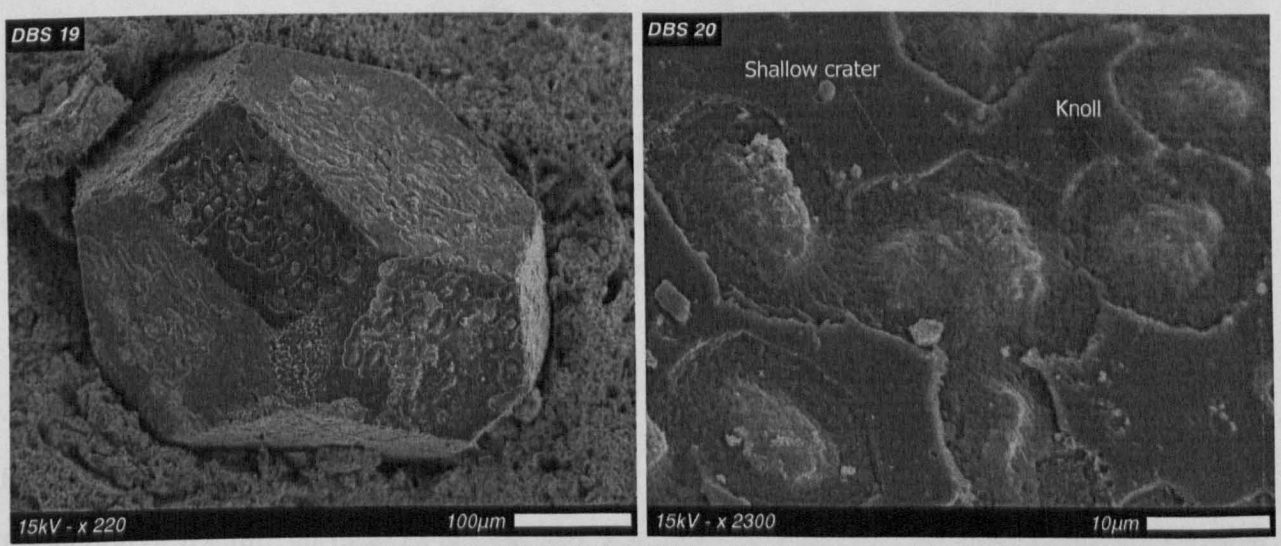

(A) DBS-19 Cr-powder encapsulated 30/50 mesh SYN-1 (NDT) **(B)** DBS-19 Cr-pdr encapsulated 30/50 mesh SYN-1 HT (NDT)

Figure 9-26 : SEM micrographs showing an exposed diamond on a fracture surface of "dog-bone" segment impregnated with the Cr-powder encapsulated 30/50 US mesh SYN-1 diamonds (NDT).

9.6.1.3D Cr(C)-coated Diamonds (DBS-15, DBS-16)

PVD (TC) SYN-3 30/40 mesh (DBS-15, DBS-16)

The inspection of the fracture surfaces of "dog-bone" segments impregnated with the PVD carbon-enriched-chromium coated diamonds showed that the mode of interactions between the composite constituents and the abrasive grit was similar to that found for the PVD Cr-coated segments as described previously. However, the intensity of the interactions was relatively milder compared to the other chromium-coated diamonds.

Cobalt remains were found on diamond surfaces. Some of the stripped diamond surfaces contained etch trigons that had spheroidal cobalt fragments attached to their centre (Figure 9-27B), giving surface morphologies similar to what was found for the PVD Ti-coated diamonds (see §9.6.1.3B on page 198). However, the concentration of the etch features with the cobalt fragments was much lower than what was found for titanium. Heat treatment of the coated grit prior to the consolidation slightly increased the extent of Cr(C)-coatings retained on the diamond surfaces.

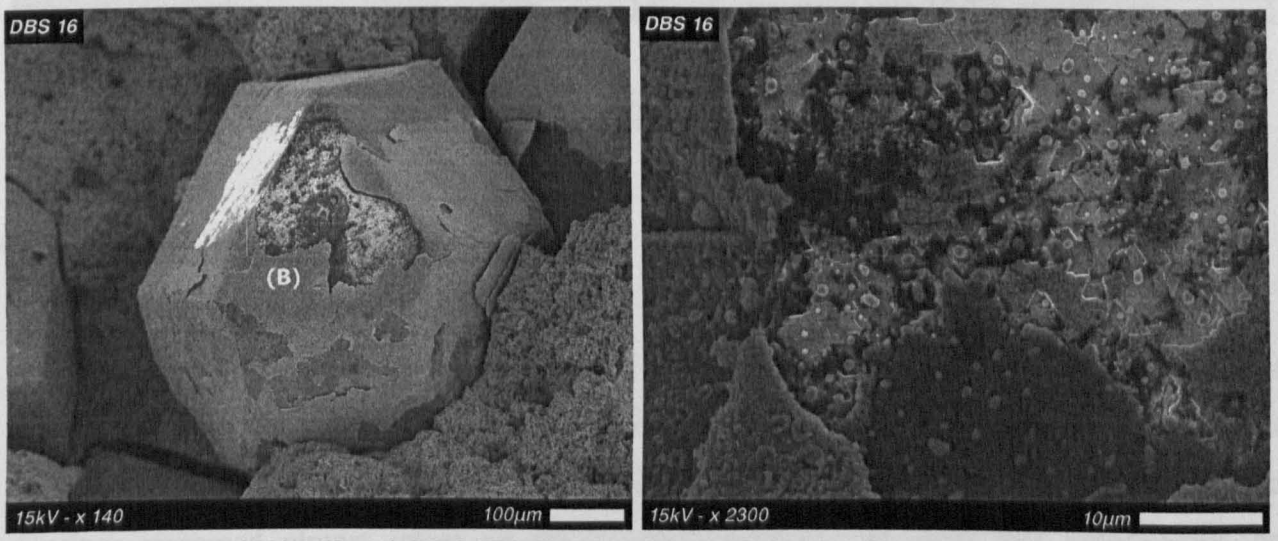

(A) DBS-16 Cr(C)-coated 30/40 US mesh SYN-3 HT (PVD, TC) **(B)** Magnified section of micrograph A.

Figure 9-27 : SEM micrographs showing an exposed diamond on a fracture surface of "dog-bone" segment impregnated with the PVD Cr(C)-coated 30/40 US mesh SYN-3 diamonds (TC).

9.6.1.3E Ti/Cr-coated Diamonds (DBS-7, DBS-8)

PVD (TC) SYN-3 30/40 mesh (DBS-7, DBS-8)

Inspection of fracture surfaces of composites reinforced with the Ti/Cr-coated diamonds revealed that coatings preferentially remained attached to the diamond surfaces (Figure 9-28A). Microscopic examination and EDAX analysis showed that the interfacial areas close to the diamond surfaces were rich in titanium. Titanium-rich fragments were preferentially found on

diamond surfaces (Figure 9-28B). However, the mean composition of the coating as calculated from EDAX data was richer in chromium. The chromium to titanium atomic percentage ratio varied from about 2 to 4.7. High levels of oxygen were detected in the coating. The majority of stripped diamond surfaces were relatively smooth and clean, indicating that the diamond deterioration processes remained at a low level. The degree of diamond attack increased slightly when diamonds were heat-treated prior to sintering.

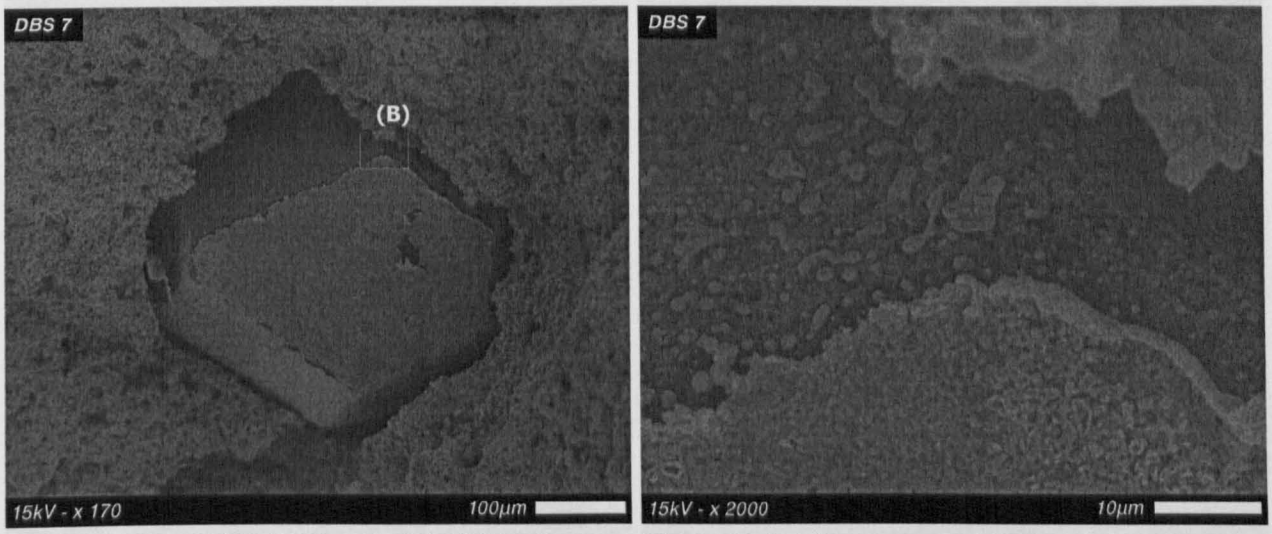

(A) DBS-7 Ti/Cr-coated 30/40 US mesh SYN-3 (PVD, TC) **(B)** Magnified section of micrograph A.

Figure 9-28 : SEM micrographs showing an exposed diamond on a fracture surface of "dog-bone" segment impregnated with the PVD Ti/Cr-coated 30/40 US mesh SYN-3 diamonds (TC).

9.6.1.3F W-coated Diamonds (DBS-9, DBS-10, DBS-17, DBS-18, DBS-21, DBS-22, DBS-25, DBS-26)

CVD (NC) SYN-1 35/50 mesh (DBS-25, DBS-26)

The examination of the "dog-bone" segments impregnated with the CVD W-coated diamonds revealed that the thick CVD coating was perfectly bonded to the cobalt matrix similarly to what was found for the hot-pressed rectangular segments. There were quite a few instances where the coatings remained almost intact on the diamond surfaces indicating that occasionally the diamond-tungsten bonding was stronger than the tungsten-cobalt one (Figure 9-29A). However, the cases where failure had taken place at the tungsten coating-diamond interfaces were clearly dominant (Figure 9-29B). Inspection at high magnifications revealed that the diamond deterioration processes had been almost avoided since the stripped diamond surfaces were quite smooth, planar and clean. Heat treatment of the diamonds prior to sintering seemed to increase the number of interfacial sites of good bonding of the diamonds with both the coating and the matrix. Furthermore, the number of fractured diamond crystals was also increased in the segments impregnated with the heat-treated diamonds.

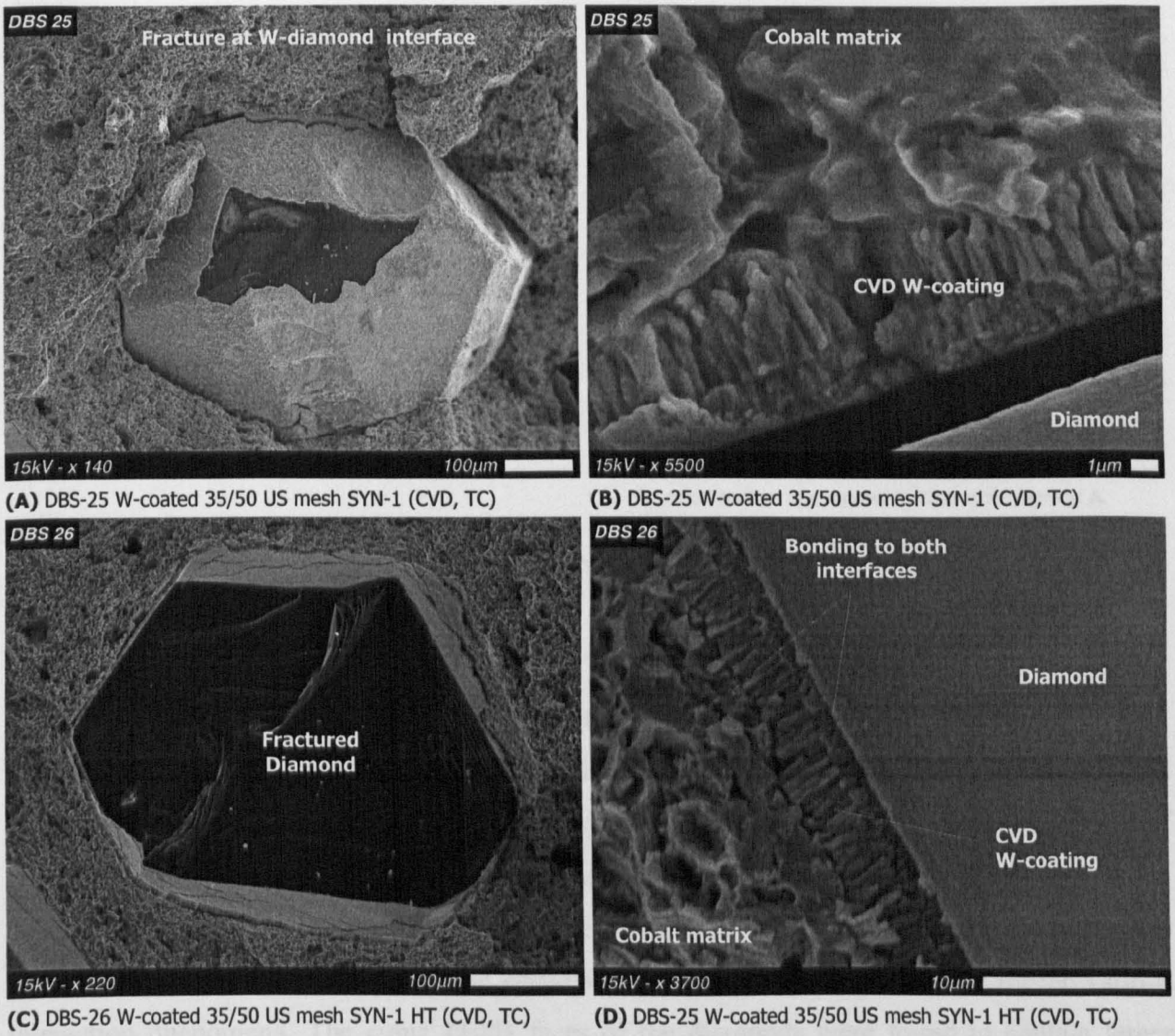

(A) DBS-25 W-coated 35/50 US mesh SYN-1 (CVD, TC)

(B) DBS-25 W-coated 35/50 US mesh SYN-1 (CVD, TC)

(C) DBS-26 W-coated 35/50 US mesh SYN-1 HT (CVD, TC)

(D) DBS-25 W-coated 35/50 US mesh SYN-1 HT (CVD, TC)

Figure 9-29 : SEM micrographs showing an exposed diamond on a fracture surface of "dog-bone" segment impregnated with the CVD W-coated 35/50 US mesh SYN-1 diamonds (NC).

PVD (TC) SYN-1 30/50 mesh (DBS-17, DBS-18) & SUN-3 30/40 mesh (DBS-9, DBS-10)

The inspection of the "dog-bone" segments impregnated with the PVD W-coated diamonds did not show any W-coating in the form of a layer attached on either the exposed diamond surfaces or the developed pull-out craters. Examination at high magnifications revealed that diamond surfaces contained a high concentration of metallic features (Figure 9-30). EDAX verified the presence of both W and Co on the diamonds. In the space between the metallic areas the diamonds had undergone a degree of etching resulting in the formation of a network of trigon pits. The quantity of tungsten and cobalt remains found on diamond surfaces was greater for the coarser and inferior quality synthetic diamond grade (30/40 US mesh SYN-3). In addition, the number of fractured diamonds was higher for the segments impregnated with the 30/40 US mesh SYN-3 grit and on average the interfacial fissures were narrower compared to the samples with the 30/50 US mesh SYN-1 crystals.

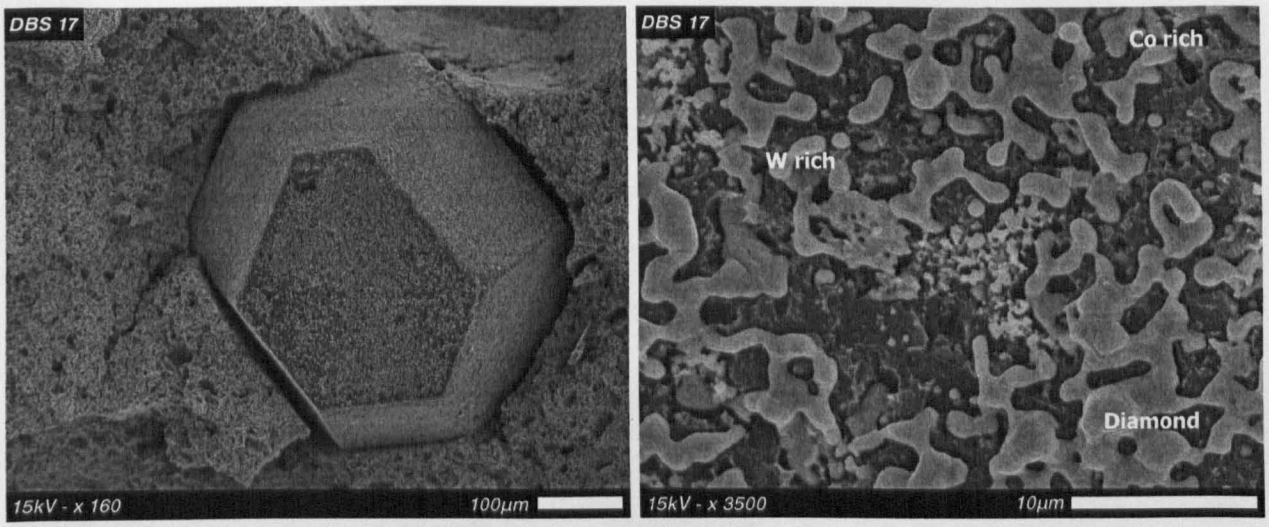

(A) DBS-17 W-coated 30/50 US mesh SYN-1 (PVD, TC)

(B) Magnified section of diamond surface of micrograph A.

Figure 9-30 : SEM micrographs showing an exposed diamond on a fracture surface of "dog-bone" segment impregnated with the various types of PVD W-coated (TC).

PC (VM) SYN-1 30/50 mesh (DBS-21, DBS-22)

The observations made for the fracture surfaces of the "dog-bone" segments impregnated with the W-powder encapsulated grit were quite similar to those made for the equivalent hot-pressed rectangular segments. A zone of tungsten powder surrounded the diamond crystals. Fragments of W-powder were evident on crystal surfaces (Figure 9-31). Heat treatment of the W-granulated diamonds prior to sintering appeared to increase the amount of powder remained attached to the grit surfaces. The edges of the diamond crystals seemed to be the preferred sites for the various interaction phenomena. The cubic {100} faces of the diamonds were found to contain larger amounts of attached powder.

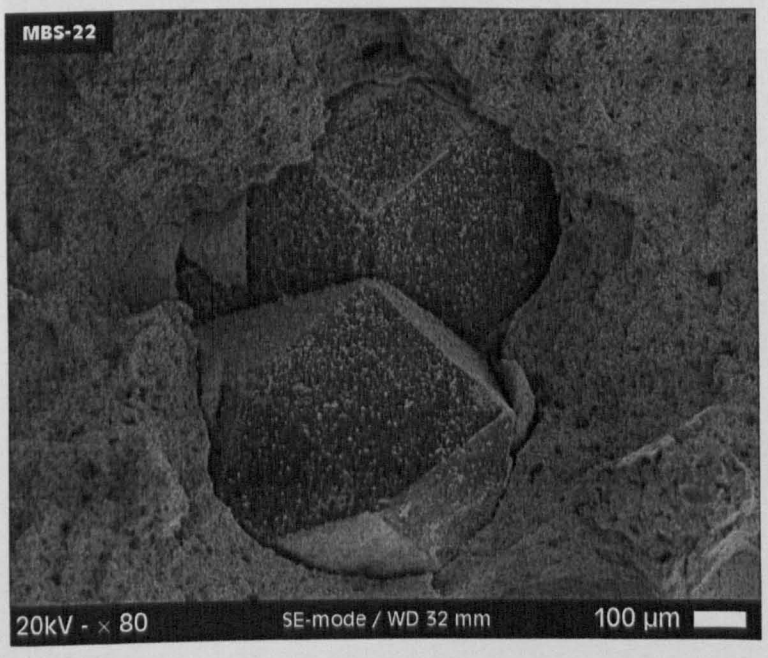

Figure 9-31 : SEM micrograph showing an exposed diamond on a fracture surface of a "dog-bone" segment impregnated with the W-powder encapsulated diamonds (VM).

Closer inspection at the uncovered diamond surfaces revealed that the shallow etch pits contained a fine textured material. EDAX analysis revealed this material to possess a high W/C ratio (Figure 9-32). This material seemed to have grown from within the attacked diamond surface, appearing to be strongly bonded to the latter. Large sintered cobalt powder blocks were also occasionally found attached on diamond surfaces, but did not look as strongly adhered to the diamonds as the material within the shallow etch craters.

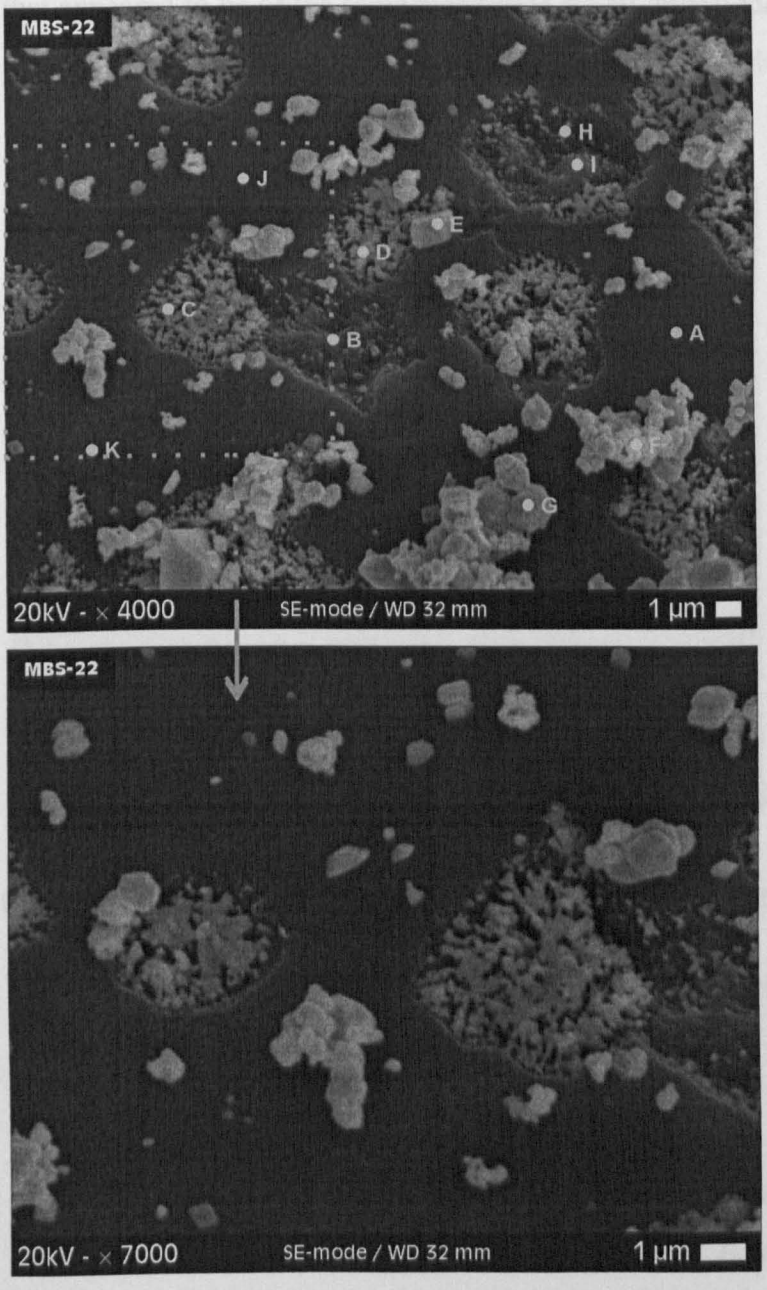

Quantitative EDAX analysis			
Position	Element	wt. %	W/C ratio
A	C	93,84	0,03
	Co	2,90	
	W	3,26	
B	C	91,93	0,05
	Co	3,76	
	W	4,31	
C	C	40,08	1,24
	Co	10,20	
	W	49,72	
D	C	35,21	1,52
	Co	11,30	
	W	53,49	
E	C	88,20	0,11
	Co	2,11	
	W	9,69	
F	C	47,29	1,03
	Co	3,81	
	W	48,90	
G	C	29,40	2,27
	Co	3,84	
	W	66,76	
H	C	88,21	0,08
	Co	4,53	
	W	7,26	
I	C	52,79	0,72
	Co	9,22	
	W	37,99	
J	C	54,95	0,73
	Co	5,09	
	W	39,97	
K	C	93,37	0,03
	Co	3,58	
	W	3,05	

Figure 9-32 : SEM micrographs from segments sintered at 1010°C for 30 minutes containing the W-powder encapsulated diamonds. The results of EDAX analysis carried out at various points on the diamond surfaces are also shown.

9.6.1.3G Co-powder encapsulated Diamonds (DBS-23, DBS-24)

PC (J) SYN-3 30/40 mesh (DBS-23, DBS-24)

Inspection of the fracture surfaces of the segments impregnated with the Co-powder encapsulated diamonds, revealed that the abrasive crystals were enveloped in the matrix in a similar manner to that found for the rectangular parallelepiped segments. Interfacial fissures were relatively narrow. Examination showed that diamonds had undergone a fine scale etching that appeared to be of the same magnitude for all crystal faces (Figure 9-33). A distinctive denser zone of cobalt surrounding the diamonds could not be detected as in the case of the hot-pressed segments.

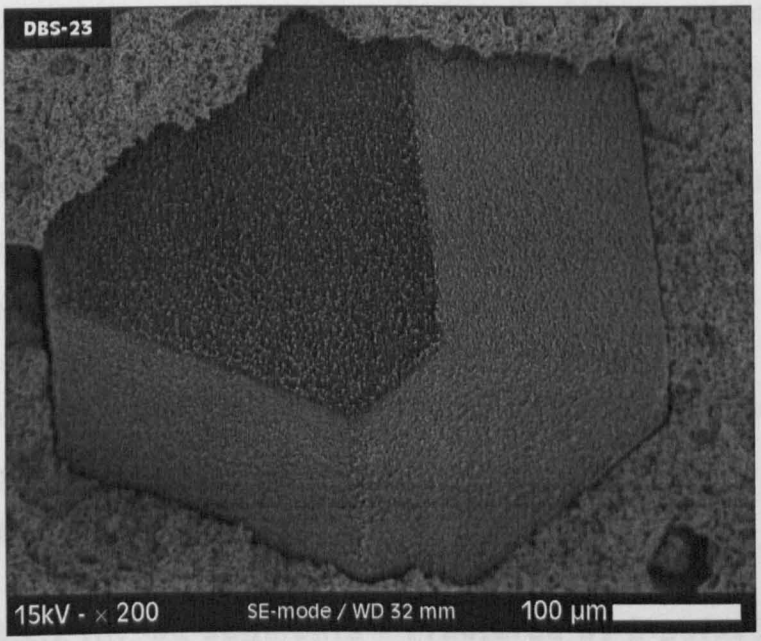

Figure 9-33 : SEM micrograph showing an exposed diamond on a fracture surface of "dog-bone" segment impregnated with the Co-powder encapsulated diamonds (J).

9.6.2 Quantitative Fracture Surface Examination

The graphs and tables on the following pages present some selected counted observation features resulting from the quantitative SEM analysis method, which was applied to the examined fracture surfaces as described in Chapter 7.

Based on composite materials theory, it is expected that enhanced mechanical properties and interfacial bonding of composite constituents can be related to a low number of lost diamonds (L) from the fracture surface, a low total number of diamonds (S) intersected by the fracture plane and finally a high number of fractured crystals. Interpretation of results at this stage is made according to these basic statements.

In the text that follows, and for any comparisons being made, a composite will be considered to show "enhanced performance" if it exhibits a combination of a lower number of lost diamonds

(L), a reduced number of exposed crystals at the fracture surface (S) and a high number of fractured crystals. The factors of "lost diamonds" and "fractured crystals" are directly associated with interfacial bonding and are thus assumed to be slightly more important than the total number of exposed crystals (S), which may also depend on other parameters related to how effectively the diamonds were distributed in the composite mass.

9.6.2.1 FS-ed segments – Fractured by 3-point Bending

The presentation of results included in this paragraph considers Figure 9-34 and Table 9-5.

A general overview of the results, indicated that the SYN-3 grade diamonds provided enhanced composite performance compared to the SYN-1. A comparison of segments with the same diamond grade and size, showed that the non-coated 30/40 mesh SYN-1 (CD-4) increased performance compared to the Ti-CVD (CD-6). However for the SYN-1 40/50 mesh this trend was reversed (CD5 & CD7). The comparison for the 30/40 SYN-3 grade segments was generally inconclusive. It appeared that non-coated diamonds were performing better than the coated grades. The only clear result was that the Cr(C)-coated yielded the worse performance. The situation for the 40/50 mesh size was however different. The segment with the W-PVD-coated diamonds (CD14) clearly performed better than the equivalent composite with the non-coated grit (CD-3). The comparison of the 40/50-mesh Cr-PVD with the equivalent non-coated grade (CD-3) was rather inconclusive.

9.6.2.2 HIP-ed segments – Fractured by 3-point Bending

The presentation of results included in this paragraph considers Figure 9-34 and Table 9-5.

Similarly to FS-ed segments, the samples reinforced with the SYN-3 grade diamonds appeared to perform relatively better than the SYN-1. Among the segments with SYN-1 diamonds, the non-coated grades were found to give better results than the Ti-CVD-coated. However, for the SYN-3 diamonds, the various coated grades were at the same levels or even better than the non-coated. It could be said that W-coated seemed to distinguish from the other coated types. The segment incorporating the Cr-PVD (CD-10) gave the worse results among the composites impregnated with 40/50-mesh SYN-3 type diamonds.

9.6.2.3 HP-ed segments – Fractured by 3-point Bending

The presentation of results included in this paragraph considers Figure 9-35 and Table 9-5.

Two different types of diamonds were used to impregnate the hot-pressed segments and therefore results presented below are divided accordingly.

Comparison for 30/50 US mesh SYN-1 diamonds:

Comparing in between the non-coated 30/50 mesh diamonds, the composite with the SYN-1 grade (CD-15) performed better than that with the SYN-3 grade (CD-16). The segment with the Ti-CVD-coated grit (CD-32) was slightly reduced in performance than the equivalent non-coated system (CD-15). However, this situation was improved when the composite incorporated the heat-treated grit (CD18). Performance was then found to be at similar levels with the segment having non-coated diamonds (CD-15). The Ti-PVD-coated grit (CD19 & 33) performed slightly better than the non-coated (CD-15). However, this was not the case the Cr-PVD-coated diamonds (CD20 & 34), which were associated with reduced performance. The segment with the Cr-powder encapsulated grit (CD24 & 38) showed slightly better performance than those using the Cr-PVD-coated type (CD20 & 34), but were still slightly inferior to the non-coated (CD15).

The W-CVD diamonds (CD30-31) exhibited the best combination of counted values. The rest of the W-coated diamonds varied in performance to levels similar to those found for the Cr-PVD-coated diamonds. For all the PVD-coated diamonds, the heat-treatment of the coated grit prior to consolidation appeared to be have a small but noticeable beneficial effect. However, for the CVD and powder encapsulated types the heat-treatment effect was inconclusive.

Comparison for 30/40 US mesh SYN-3 diamonds:

The situation for the 30/40 SYN-3 grade was different to that of the SYN-1 type. For these segments, the majority of coated grades provided composite properties at equal or greater levels than the non-coated references. Apart from the Ti-PVD (CD39-40) and Cr-PVD (CD42-43) grades, all other types gave a better combination of counted features.

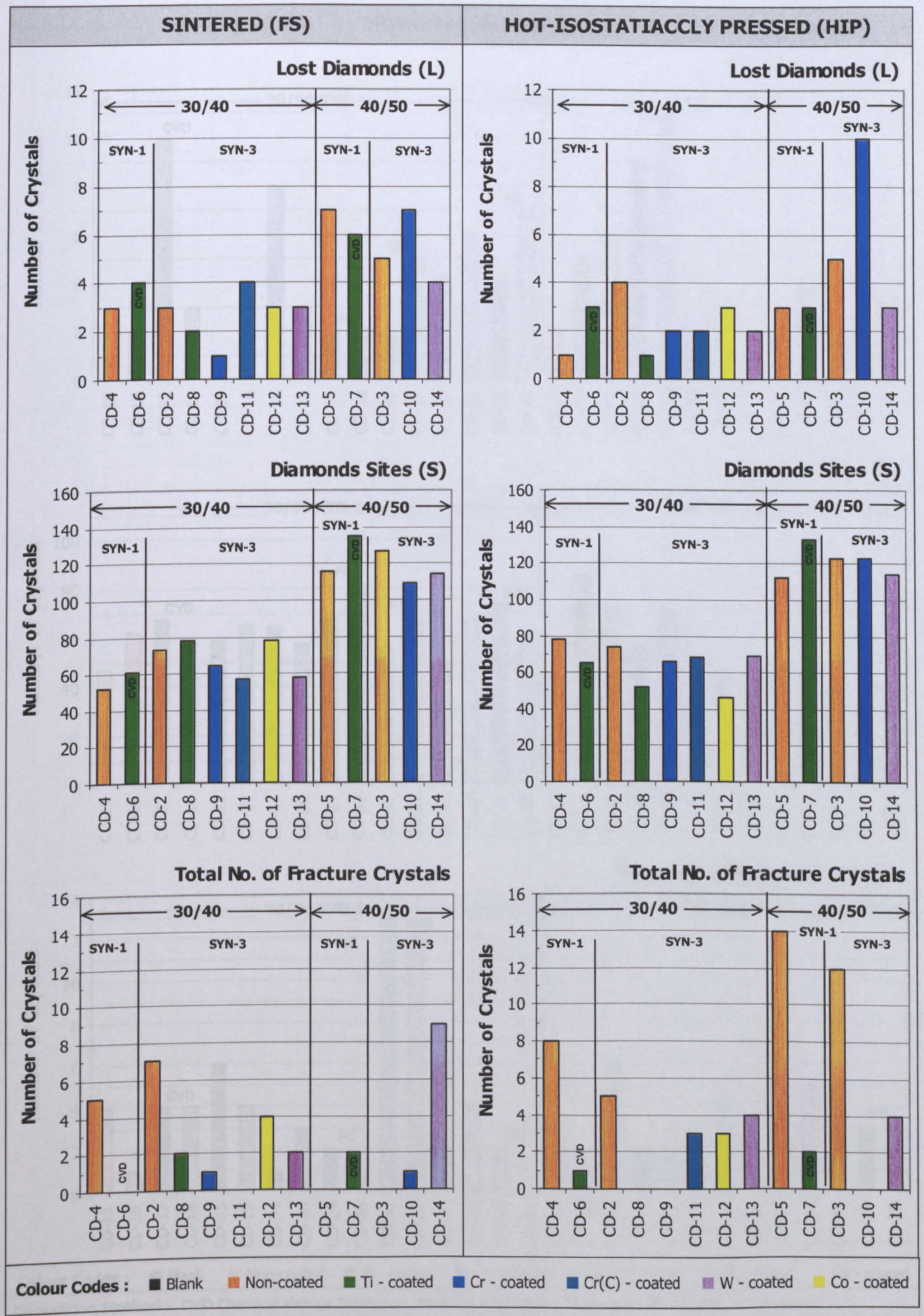

Figure 9-34 : Listing of selected counted observation features as resulted from the quantitative SEM analysis method applied to the fracture surfaces of the 3-point bended Sintered (FS) and Hot-Istostatic-Pressed (HIP) segments.

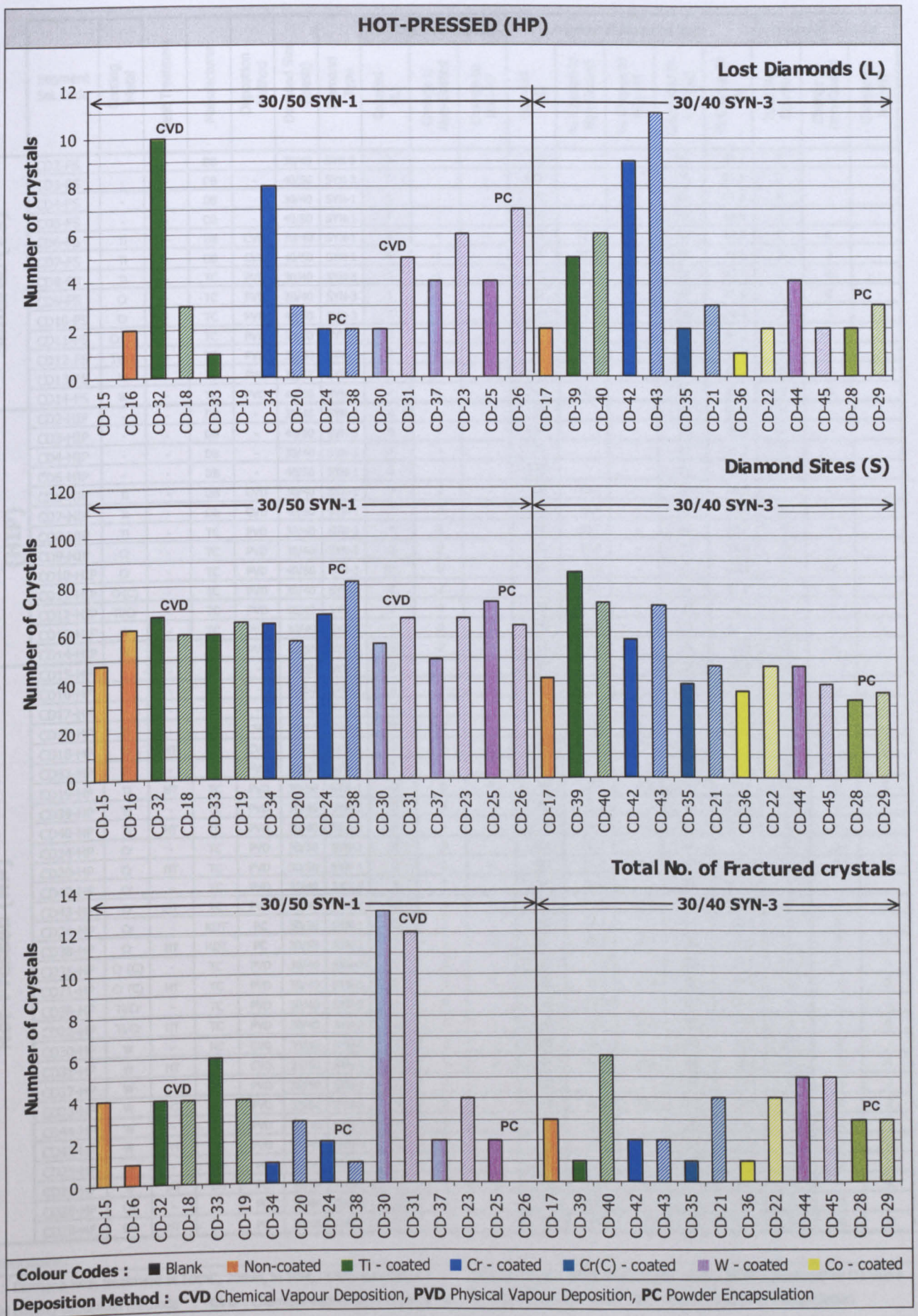

Figure 9-35 : Listing of selected counted observation features as resulted from the quantitative SEM analysis method applied to the fracture surfaces of the 3-point bended Hot-Pressed (HP) segments. The striped coloured bars represent the segments impregnated with diamonds that have been heat-treated at 500°C for 20 min in $10H_2/90N_2$ atmosphere. If not otherwise marked, deposition method is PVD.

	Segment Set Code	Coating Metal	Heat Treatment	Manufacturer	Deposition Method	Diamond Size (mesh)	Diamond Type	Lost Diamond Crystals			Number of Diamond Sites					Fractured Crystals		
								Counted (L)	Change to Non-Coated	Change to Non-HT	Counted (S)	% Change to Non-Coated	% Change to Non-HT	Calculated th. No. (S_N)	% Change to S_N	Total No. Counted	Change to Non-Coated	Change to Non-HT
Sintered (FS)	CD2-FS	-	-	DB	-	30/40	SYN-3	3	-	-	73	-	-	50	45.7	7	-	-
	CD3-FS	-	-	DB	-	40/50	SYN-3	5	-	-	127	-	-	78	63.5	0	-	-
	CD4-FS	-	-	DB	-	30/40	SYN-1	3	-	-	52	-	-	40	31.5	5	-	-
	CD5-FS	-	-	DB	-	40/50	SYN-1	7	-	-	115	-	-	79	45.8	0	-	-
	CD6-FS	Ti	-	DB	CVD	30/40	SYN-1	4	1	-	61	17.3	-	40	53.9	0	-5	-
	CD7-FS	Ti	-	DB	CVD	40/50	SYN-1	6	-1	-	135	17.4	-	78	73.5	2	2	-
	CD8-FS	Ti	-	TC	PVD	30/40	SYN-3	2	-1	-	78	6.8	-	39	97.6	2	-5	-
	CD9-FS	Cr	-	TC	PVD	30/40	SYN-3	1	-2	-	64	-12.3	-	40	61.9	1	-6	-
	CD10-FS	Cr	-	TC	PVD	40/50	SYN-3	7	2	-	109	-14.2	-	79	38.4	1	1	-
	CD11-FS	Cr(C)	-	TC	PVD	30/40	SYN-3	4	1	-	57	-21.9	-	40	43.3	0	-7	-
	CD12-FS	Ti/Cr	-	TC	PVD	30/40	SYN-3	3	0	-	78	6.8	-	52	48.8	4	-3	-
	CD13-FS	W	-	TC	PVD	30/40	SYN-3	3	0	-	58	-20.5	-	40	44.4	2	-5	-
	CD14-FS	W	-	TC	PVD	40/50	SYN-3	4	-1	-	114	-10.2	-	79	43.4	9	9	-
Hot-Isostatic Pressed (HIP)	CD2-HIP	-	-	DB	-	30/40	SYN-3	4	-	-	74	-	-	46	60.2	5	-	-
	CD3-HIP	-	-	DB	-	40/50	SYN-3	5	-	-	123	-	-	73	68.8	12	-	-
	CD4-HIP	-	-	DB	-	30/40	SYN-1	1	-	-	78	-	-	37	111.5	8	-	-
	CD5-HIP	-	-	DB	-	40/50	SYN-1	3	-	-	112	-	-	73	54.3	14	-	-
	CD6-HIP	Ti	-	DB	CVD	30/40	SYN-1	3	2	-	65	-16.7	-	37	74.2	1	-7	-
	CD7-HIP	Ti	-	DB	CVD	40/50	SYN-1	3	0	-	133	18.8	-	72	84.3	2	-12	-
	CD8-HIP	Ti	-	TC	PVD	30/40	SYN-3	1	-3	-	52	-29.7	-	36	44.7	0	-5	-
	CD9-HIP	Cr	-	TC	PVD	30/40	SYN-3	2	-2	-	66	-10.8	-	37	78.9	0	-5	-
	CD10-HIP	Cr	-	TC	PVD	40/50	SYN-3	10	5	-	123	0.0	-	73	68.2	0	-12	-
	CD11-HIP	Cr(C)	-	TC	PVD	30/40	SYN-3	2	-2	-	68	-8.1	-	37	81.8	3	-2	-
	CD12-HIP	Ti/Cr	-	TC	PVD	30/40	SYN-3	3	-1	-	46	-37.8	-	48	-4.6	3	-2	-
	CD13-HIP	W	-	TC	PVD	30/40	SYN-3	2	-2	-	69	-6.8	-	37	87.1	4	-1	-
	CD14-HIP	W	-	TC	PVD	40/50	SYN-3	3	-2	-	114	-7.3	-	74	54.3	4	-8	-
Hot-Pressed (HP)	CD15-HP	-	-	DB	-	30/50	SYN-1	0	-	-	47	-	-	37	25.9	4	-	-
	CD16-HP	-	-	DB	-	30/50	SYN-3	2	-	-	62	-	-	38	61.4	1	-	-
	CD17-HP	-	-	DB	-	30/40	SYN-3	2	-	-	41	-	-	29	39.9	3	-	-
	CD32-HP	Ti	-	DB	CVD	30/50	SYN-1	10	10	-	67	42.6	-	37	82.8	4	0	-
	CD18-HP	Ti	HT	DB	CVD	30/50	SYN-1	3	3	-7	60	27.7	-10.4	38	58.7	4	0	0
	CD33-HP	Ti	-	TC	PVD	30/50	SYN-1	1	1	-	60	27.7	-	37	63.6	6	2	-
	CD19-HP	Ti	HT	TC	PVD	30/50	SYN-1	0	0	-1	65	38.3	8.3	37	74.1	4	0	-2
	CD39-HP	Ti	-	TC	PVD	30/40	SYN-3	5	3	-	85	107.3	-	28	203.6	1	-2	-
	CD40-HP	Ti	HT	TC	PVD	30/40	SYN-3	6	4	1	72	75.6	-15.3	28	153.9	6	3	5
	CD34-HP	Cr	-	TC	PVD	30/50	SYN-1	8	8	-	64	36.2	-	36	76.9	1	-3	-
	CD20-HP	Cr	HT	TC	PVD	30/50	SYN-1	3	3	-5	57	21.3	-10.9	37	55.9	3	-1	2
	CD42-HP	Cr	-	TC	PVD	30/40	SYN-3	9	7	-	57	39.0	-	28	102.8	2	-1	-
	CD43-HP	Cr	HT	TC	PVD	30/40	SYN-3	11	9	2	71	73.2	24.6	28	151.0	2	-1	0
	CD24-HP	Cr	-	NDT	PC	30/50	SYN-1	2	2	-	68	44.7	-	37	84.8	2	-2	-
	CD38-HP	Cr	HT	NDT	PC	30/50	SYN-1	2	2	0	81	72.3	19.1	36	122.0	1	-3	-1
	CD35-HP	Cr (C)	-	TC	PVD	30/40	SYN-3	2	0	-	39	-4.9	-	28	37.5	1	-2	-
	CD21-HP	Cr (C)	HT	TC	PVD	30/40	SYN-3	3	1	1	46	12.2	17.9	29	60.7	4	1	3
	CD36-HP	Ti/Cr	-	TC	PVD	30/40	SYN-3	1	-1	-	36	-12.2	-	28	27.0	1	-2	-
	CD22-HP	Ti/Cr	HT	TC	PVD	30/40	SYN-3	2	0	1	46	12.2	27.8	29	60.6	4	1	3
	CD30-HP	W	-	NC	CVD	35/50	SYN-1	2	2	-	56	19.1	-	45	23.7	13	9	-
	CD31-HP	W	HT	NC	CVD	35/50	SYN-1	5	5	3	66	40.4	17.9	45	46.4	12	8	-1
	CD37-HP	W	-	TC	PVD	30/50	SYN-1	4	4	-	49	4.3	-	37	33.7	2	-2	-
	CD23-HP	W	HT	TC	PVD	30/50	SYN-1	6	6	2	66	40.4	34.7	38	74.0	4	0	2
	CD44-HP	W	-	TC	PVD	30/40	SYN-3	4	2	-	46	12.2	-	28	62.7	5	2	-
	CD45-HP	W	HT	TC	PVD	30/40	SYN-3	2	0	-2	39	-4.9	-15.2	28	37.5	5	2	0
	CD25-HP	W	-	VM	PC	30/50	SYN-1	4	4	-	73	55.3	-	36	100.2	2	-2	-
	CD26-HP	W	HT	VM	PC	30/50	SYN-1	7	7	3	63	34.0	-13.7	37	70.4	0	-4	-2
	CD28-HP	Co	-	J	PC	30/40	SYN-3	2	0	-	32	-22.0	-	28	15.9	3	0	-
	CD29-HP	Co	HT	J	PC	30/40	SYN-3	3	1	1	35	-14.6	9.4	28	23.2	3	0	0

Nomenclature :

HT : Diamond Heat treatment at 500°C, 20min, in $10H_2$ / $90N_2$ atmosphere Diamond Type : **SYN-1** is superior quality **SYN-3** produced by De Beers

Metal coating deposition methods : **CVD** : Chemical Vapour Deposition, **PVD** : Physical Vapour Deposition, **PC** : Powder Coating / Encapsulation

Manufacturers of Coated Diamonds : **DB** : De Beers, **NDT** : Nimbus Diamond Tool, **NC** : Norton Company, **TC** : Teer Coatings, **VM** : Van Moppes, **J** : Fuji Paudal Kabushiki Kaisha

Table 9-5 : Listing of counted and calculated values of selected observation features as resulted from the quantitative SEM analysis method applied to the fracture surfaces of the 3-point bended segments.

9.6.2.4 Tensile Test (DBS) segments – Fractured by Uniaxial Tension

The presentation of results included in this paragraph considers Figure 9-36 and Table 9-6.

Two different types of diamonds were used to impregnate the sintered segments and therefore results presented below are divided accordingly.

Comparison for 30/50 US mesh SYN-1 diamonds:

Comparing for the 30/50 SYN-1 finds the non-coated (DBS-4) and the W-powder encapsulated (DBS21-22) grades to give the worse segment performance. The Ti-CVD (DBS11) and Cr-PVD (DBS13) exhibited similar intermediate performance. The heat-treatment of those coated diamonds prior to sintering provided no positive effect (DBS12 & DBS14). The CVD (DBS25-26) and PVD (DBS17-18) W-coated grit provided the best composite performance. For those W-coated diamonds the heat-treatment was found to act considerably beneficially.

Comparison for 30/40 US mesh SYN-3 diamonds:

Comparing for the 30/40 mesh SYN-3 grade diamonds finds the non-coated grit (DBS-2) to show the worse performance. The Ti-PVD (DBS5-6) and the Ti/Cr-PVD (DBS7-8) coated diamonds provided similar levels of performance, whereas the Cr(C)-PVD (DBS15-16) gave the best combination of measured values among all segments impregnated with the 30/40 mesh SYN-3 diamonds. The W-PVD (DBS9-10) and Co-PC (DBS23-24) followed the Cr(C)-PVD in performance. The heat-treatment of the coated grit prior to sintering was found to have beneficial effect only for the W-PVD (DBS10) and Co-PC (DBS24) coated diamonds.

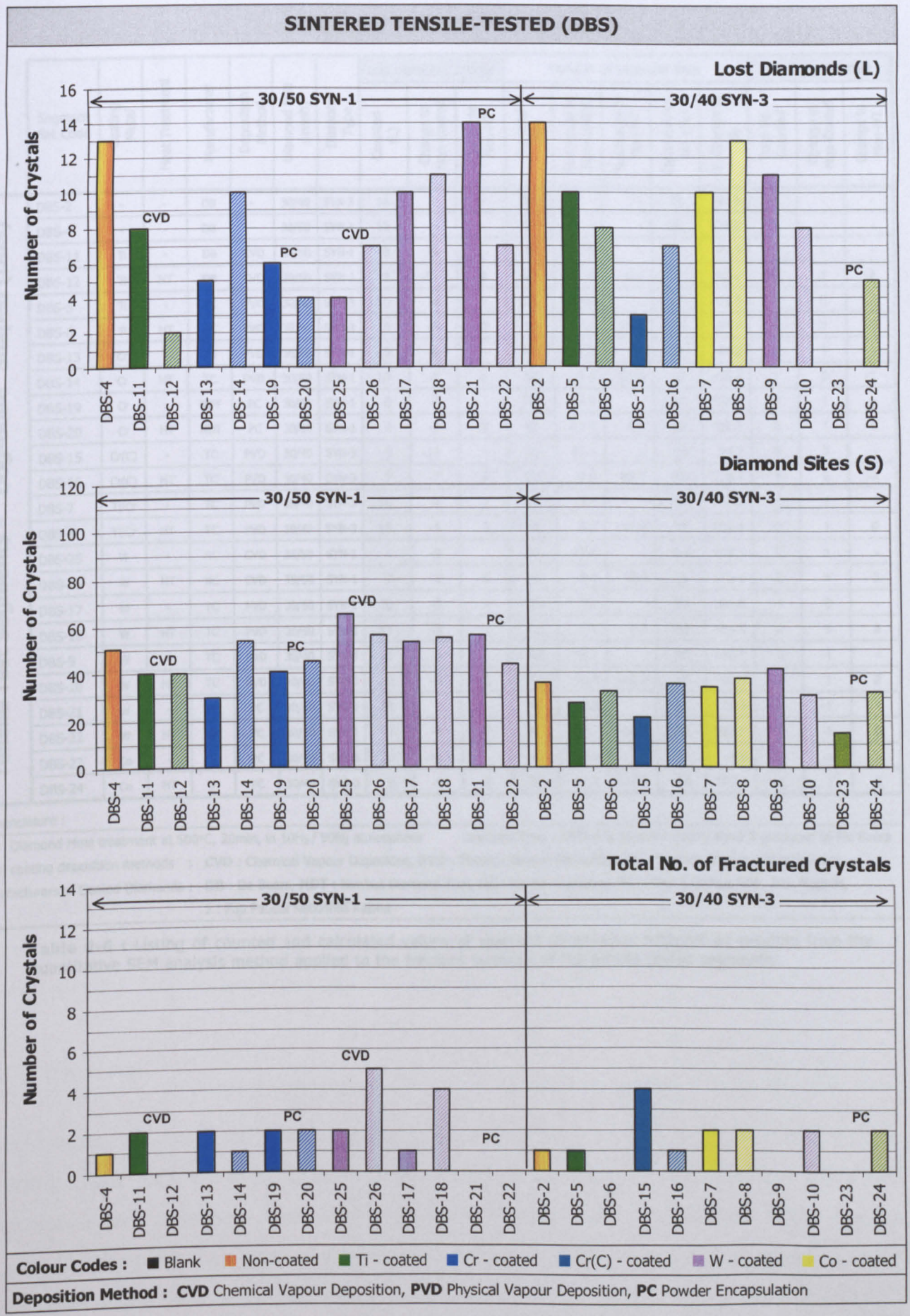

Figure 9-36 : Listing of selected counted observation features as resulted from the quantitative SEM analysis method applied to the fracture surfaces of the tensile tested Sintered (DBS) segments. The striped coloured bars represent the segments impregnated with diamonds that have been heat-treated at 500°C for 20 min in $10H_2/90N_2$ atmosphere. If not otherwise marked, deposition method is PVD.

	Segment Set Code	Coating Metal	Heat Treatment	Manufacturer	Deposition Method	Diamond Size (mesh)	Diamond Type	Lost Diamond Crystals			Number of Diamond Sites					Fractured Crystals		
								Counted (L)	Change to Non-Coated	Change to Non-HT	Counted (S)	% Change to Non-Coated	% Change to Non-HT	Calculated th. No. (S_N)	% Change to S_N	Total No. Counted	Change to Non-Coated	Change to Non-HT
Tensile Test Segments - "Dog-Bone" Shaped (DBS)	DBS-2	-	-	DB	-	30/40	SYN-3	14	-	-	36	-	-	23	58.5	1	-	-
	DBS-4	-	-	DB	-	30/50	SYN-1	13	-	-	51	-	-	22	136.2	1	-	-
	DBS-11	Ti	-	DB	CVD	30/50	SYN-1	8	-5	-	40	-21.6	-	21	91.3	2	1	-
	DBS-12	Ti	HT	DB	CVD	30/50	SYN-1	2	-11	-6	40	-21.6	0.0	21	92.9	0	-1	-2
	DBS-5	Ti	-	TC	PVD	30/40	SYN-3	10	-4	-	27	-25.0	-	17	61.1	1	0	-
	DBS-6	Ti	HT	TC	PVD	30/40	SYN-3	8	-6	-2	32	-11.1	18.5	16	96.7	0	-1	-1
	DBS-13	Cr	-	TC	PVD	30/50	SYN-1	5	-8	-	30	-41.2	-	21	46.2	2	1	-
	DBS-14	Cr	HT	TC	PVD	30/50	SYN-1	10	-3	5	54	5.9	80.0	20	165.8	1	0	-1
	DBS-19	Cr	-	NDT	PC	30/50	SYN-1	6	-7	-	41	-19.6	-	20	105.7	2	1	-
	DBS-20	Cr	HT	NDT	PC	30/50	SYN-1	4	-9	-2	45	-11.8	9.8	20	125.1	2	1	0
	DBS-15	Cr(C)	-	TC	PVD	30/40	SYN-3	3	-11	-	21	-41.7	-	16	34.7	4	3	-
	DBS-16	Cr(C)	HT	TC	PVD	30/40	SYN-3	7	-7	4	35	-2.8	66.7	16	125.3	1	0	-3
	DBS-7	Ti/Cr	-	TC	PVD	30/40	SYN-3	10	-4	-	34	-5.6	-	16	113.5	2	1	-
	DBS-8	Ti/Cr	HT	TC	PVD	30/40	SYN-3	13	-1	3	38	5.6	11.8	16	135.1	2	1	0
	DBS-25	W	-	NC	CVD	35/50	SYN-1	4	-9	-	65	27.5	-	25	158.5	2	1	-
	DBS-26	W	HT	NC	CVD	35/50	SYN-1	7	-6	3	56	9.8	-13.8	26	113.4	5	4	3
	DBS-17	W	-	TC	PVD	30/50	SYN-1	10	-3	-	53	3.9	-	20	161.6	1	0	-
	DBS-18	W	HT	TC	PVD	30/50	SYN-1	11	-2	1	55	7.8	3.8	20	169.5	4	3	3
	DBS-9	W	-	TC	PVD	30/40	SYN-3	11	-3	-	42	16.7	-	16	158.4	0	-1	-
	DBS-10	W	HT	TC	PVD	30/40	SYN-3	8	-6	-3	31	-13.9	-26.2	16	93.8	2	1	2
	DBS-21	W	-	VM	PC	30/50	SYN-1	14	1	-	56	9.8	-	21	172.8	0	-1	-
	DBS-22	W	HT	VM	PC	30/50	SYN-1	7	-6	-7	44	-13.7	-21.4	20	123.7	0	-1	0
	DBS-23	Co	-	J	PC	30/40	SYN-3	0	-14	-	15	-58.3	-	15	-1.9	0	-1	-
	DBS-24	Co	HT	J	PC	30/40	SYN-3	5	-9	5	32	-11.1	113.3	15	107.0	2	1	2

Nomenclature :

HT : Diamond Heat treatment at 500°C, 20min, in $10H_2$ / $90N_2$ atmosphere Diamond Type : **SYN-1** is superior quality **SYN-3** produced by De Beers

Metal coating deposition methods : **CVD** : Chemical Vapour Deposition, **PVD** : Physical Vapour Deposition, **PC** : Powder Coating / Encapsulation

Manufacturers of Coated Diamonds : **DB** : De Beers, **NDT** : Nimbus Diamond Tool, **NC** : Norton Company, **TC** : Teer Coatings, **VM** : Van Moppes, **J** : Fuji Paudal Kabushiki Kaisha

Table 9-6 : Listing of counted and calculated values of selected observation features as resulted from the quantitative SEM analysis method applied to the fracture surfaces of the tensile tested segments.

10

Results • Part-III

"Coated-Diamond Composites with Alloy Metal-Matrices"

10.1 Introduction

This chapter presents the results of the series of experiments included in the third and final part of the experimental work of this thesis as described in Chapter 7. The work was carried out to characterise interfacial bonding and determine mechanical properties of P/M composites made of various alloy metal-matrices impregnated with coated diamonds.

10.2 Density

Measured Archimedes densities compared to the calculated theoretical density for each different metal-matrix are given in the graphs of Figure 10-1 on the next page. Results show that density variation for the diamond containing segments was small and all of them had higher densities than the corresponding blank metal-matrices. All the diamond reinforced composites exhibited densities above 96% of the theoretical apart from the two compositions, which had a high W content (MB9-10).

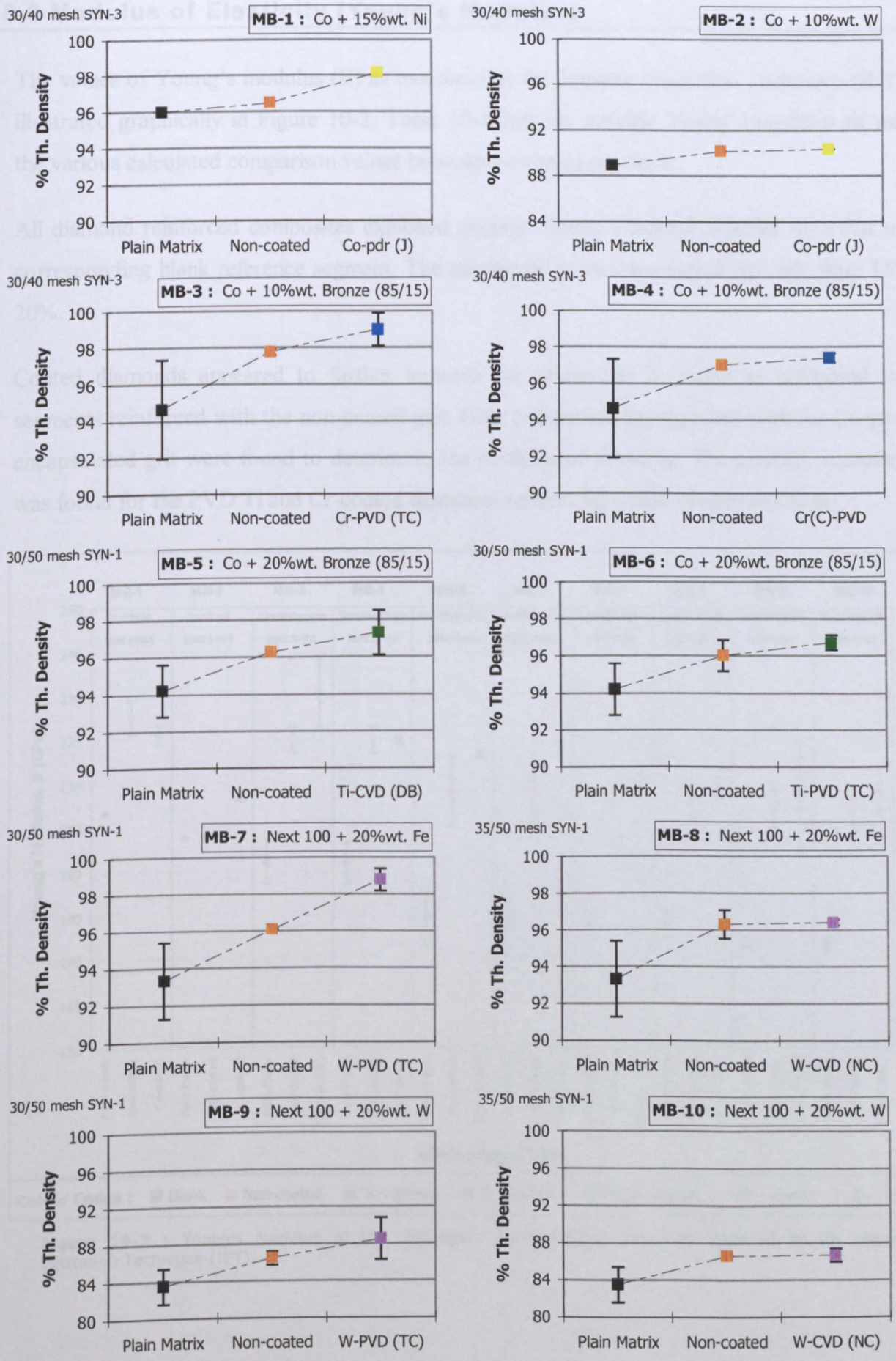

Figure 10-1 : Archimedes density of the rectangular parallelepiped segments compared to calculated theoretical density. NEXT 100 is registered trade name of Eurotungstene Poudres (France) for a pre-alloyed Cu-Fe-Co powder.

10.3 Modulus of Elasticity (Young's Modulus)

The values of Young's modulus (E) as measured by the Impulse Excitation Technique (IET) are illustrated graphically in Figure 10-2. Table 10-1 lists the average Young's modulus as well as the various calculated comparison values between the tested segments.

All diamond reinforced composites exhibited average Young's moduli superior than that of the corresponding blank reference segment. The magnitude of increase varied typically from 15% to 20%.

Coated diamonds appeared to further improve the composite E-moduli as compared to the segments reinforced with the non-coated grit. Only composites impregnated with the Co-powder encapsulated grit were found to deteriorate the modulus of elasticity. The greatest improvement was found for the PVD Ti and Cr-coated diamonds reinforcing cobalt-bronze matrices.

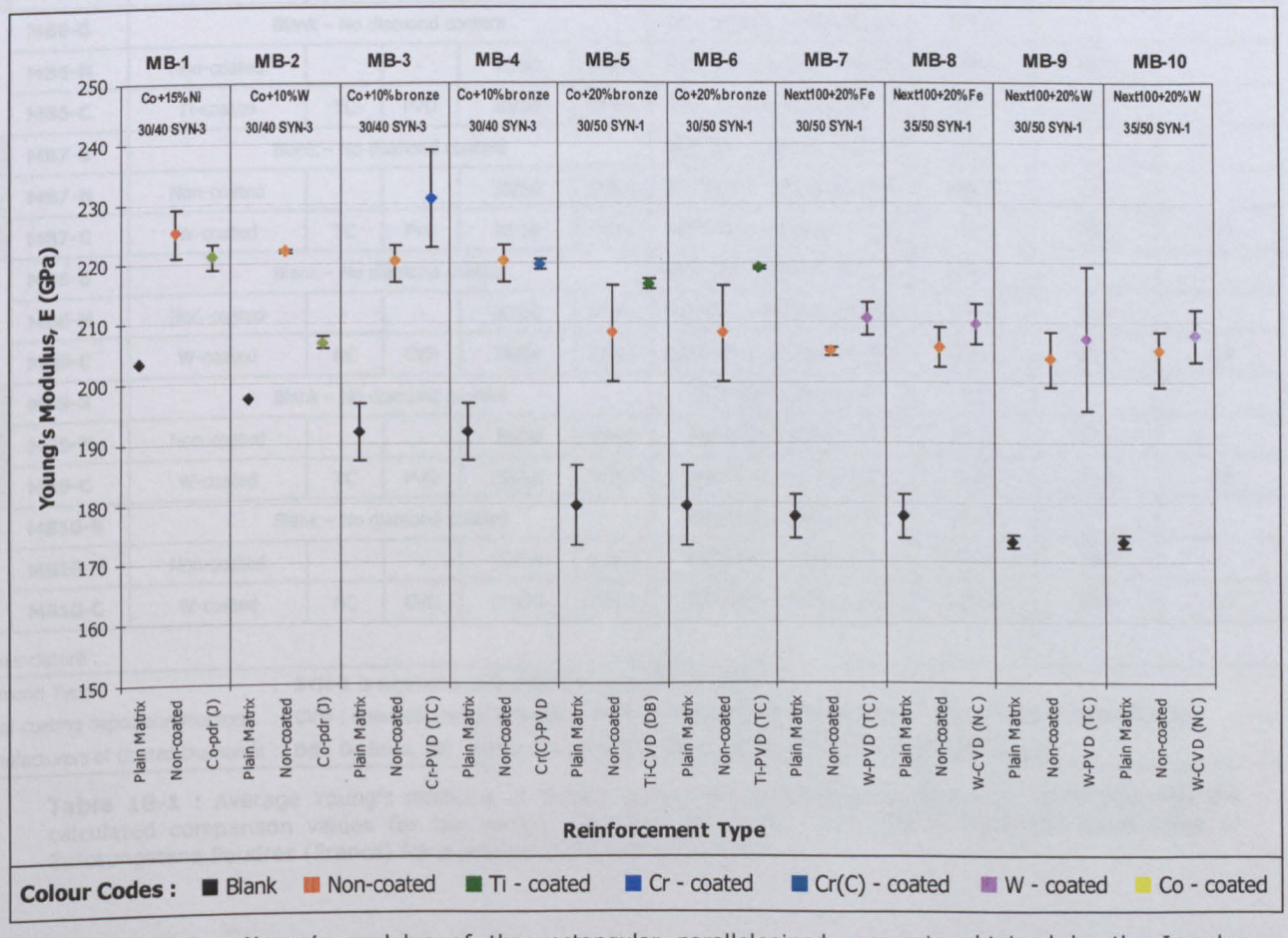

Figure 10-2 : Young's modulus of the rectangular parallelepiped segments obtained by the Impulse Excitation Technique (IET).

Segment Set Code		Diamond Condition	Manufacturer of Coating	Coating Method	Diamond Size Range (US mesh)	Diamond Type	Metal-Matrix Composition (%wt.)	Avergae E modulus (GPa)	% change to blank	% change to non-coated
MB-1	MB1-B	Blank – No diamond content					Co + 15%wt. Ni	203.5	-	-
	MB1-N	Non-coated	-	-	30/40	SYN-3	Co + 15%wt. Ni	225.1	10.6	-
	MB1-C	Co-coated	J	PC	30/40	SYN-3	Co + 15%wt. Ni	221.2	8.7	-1.7
MB-2	MB2-B	Blank – No diamond content					Co + 10%wt. W	197.5	-	-
	MB2-N	Non-coated	-	-	30/40	SYN-3	Co + 10%wt. W	222.1	12.4	-
	MB2-C	Co-coated	J	PC	30/40	SYN-3	Co + 10%wt. W	206.8	4.7	-6.9
MB-3	MB3-B	Blank – No diamond content					Co + 10%wt. bronze 85/15	192.0	-	-
	MB3-N	Non-coated	-	-	30/40	SYN-3	Co + 10%wt. bronze 85/15	220.3	14.7	-
	MB3-C	Cr-coated	TC	PVD	30/40	SYN-3	Co + 10%wt. bronze 85/15	230.7	20.2	4.7
MB-4	MB4-B	Blank – No diamond content					Co + 10%wt. bronze 85/15	192.0	-	-
	MB4-N	Non-coated	-	-	30/40	SYN-3	Co + 10%wt. bronze 85/15	220.3	14.7	-
	MB4-C	Cr(C)-coated	TC	PVD	30/40	SYN-3	Co + 10%wt. bronze 85/15	219.8	14.5	-0.2
MB-5	MB5-B	Blank – No diamond content					Co + 20%wt. bronze 85/15	179.5	-	-
	MB5-N	Non-coated	-	-	30/50	SYN-1	Co + 20%wt. bronze 85/15	208.3	16.0	-
	MB5-C	Ti-coated	DB	CVD	30/50	SYN-1	Co + 20%wt. bronze 85/15	216.4	20.5	3.9
MB-6	MB6-B	Blank – No diamond content					Co + 20%wt. bronze 85/15	179.5	-	-
	MB6-N	Non-coated	-	-	30/50	SYN-1	Co + 20%wt. bronze 85/15	208.3	16.0	-
	MB6-C	Ti-coated	TC	PVD	30/50	SYN-1	Co + 20%wt. bronze 85/15	219.3	22.1	5.3
MB-7	MB7-B	Blank – No diamond content					NEXT100 + 20%wt. Fe (CN)	177.7	-	-
	MB7-N	Non-coated	-	-	30/50	SYN-1	NEXT100 + 20%wt. Fe (CN)	205.2	15.5	-
	MB7-C	W-coated	TC	PVD	30/50	SYN-1	NEXT100 + 20%wt. Fe (CN)	210.5	18.5	2.6
MB-8	MB8-B	Blank – No diamond content					NEXT100 + 20%wt. Fe (CN)	177.7	-	-
	MB8-N	Non-coated	-	-	30/50	SYN-1	NEXT100 + 20%wt. Fe (CN)	205.9	15.9	-
	MB8-C	W-coated	NC	CVD	35/50	SYN-1	NEXT100 + 20%wt. Fe (CN)	209.7	18.0	1.8
MB-9	MB9-B	Blank – No diamond content					NEXT100 + 20%wt. W	173.5	-	-
	MB9-N	Non-coated	-	-	30/50	SYN-1	NEXT100 + 20%wt. W	203.8	17.5	-
	MB9-C	W-coated	TC	PVD	30/50	SYN-1	NEXT100 + 20%wt. W	207.1	19.4	1.6
MB-10	MB10-B	Blank – No diamond content					NEXT100 + 20%wt. W	173.5	-	-
	MB10-N	Non-coated	-	-	30/50	SYN-1	NEXT100 + 20%wt. W	205.2	18.3	-
	MB10-C	W-coated	NC	CVD	35/50	SYN-1	NEXT100 + 20%wt. W	207.8	19.8	1.2

Nomenclature :

Diamond Type : **SYN-1** is superior quality **SYN-3** produced by De Beers

Metal coating deposition methods : **CVD** : Chemical Vapour Deposition, **PVD** : Physical Vapour Deposition, **PC** : Powder Coating / Encapsulation

Manufacturers of Coated Diamonds : **DB** : De Beers, **NC** : Norton Company, **TC** : Teer Coatings, **J** : Fuji Paudal Kabushiki Kaisha

Table 10-1 : Average Young's modulus of tested rectangular parallelepiped segments. Table also lists the calculated comparison values for the various diamond conditions. NEXT 100 is registered trade name of Eurotungstene Poudres (France) for a pre-alloyed Cu-Fe-Co powder.

10.4 3-point Bending

The measured Transverse Rupture Strengths (TRS) as obtained by the 3-point bending are illustrated graphically in Figure 10-3. Table 10-2 lists the average TRS as well as the various calculated comparison values between the tested segments.

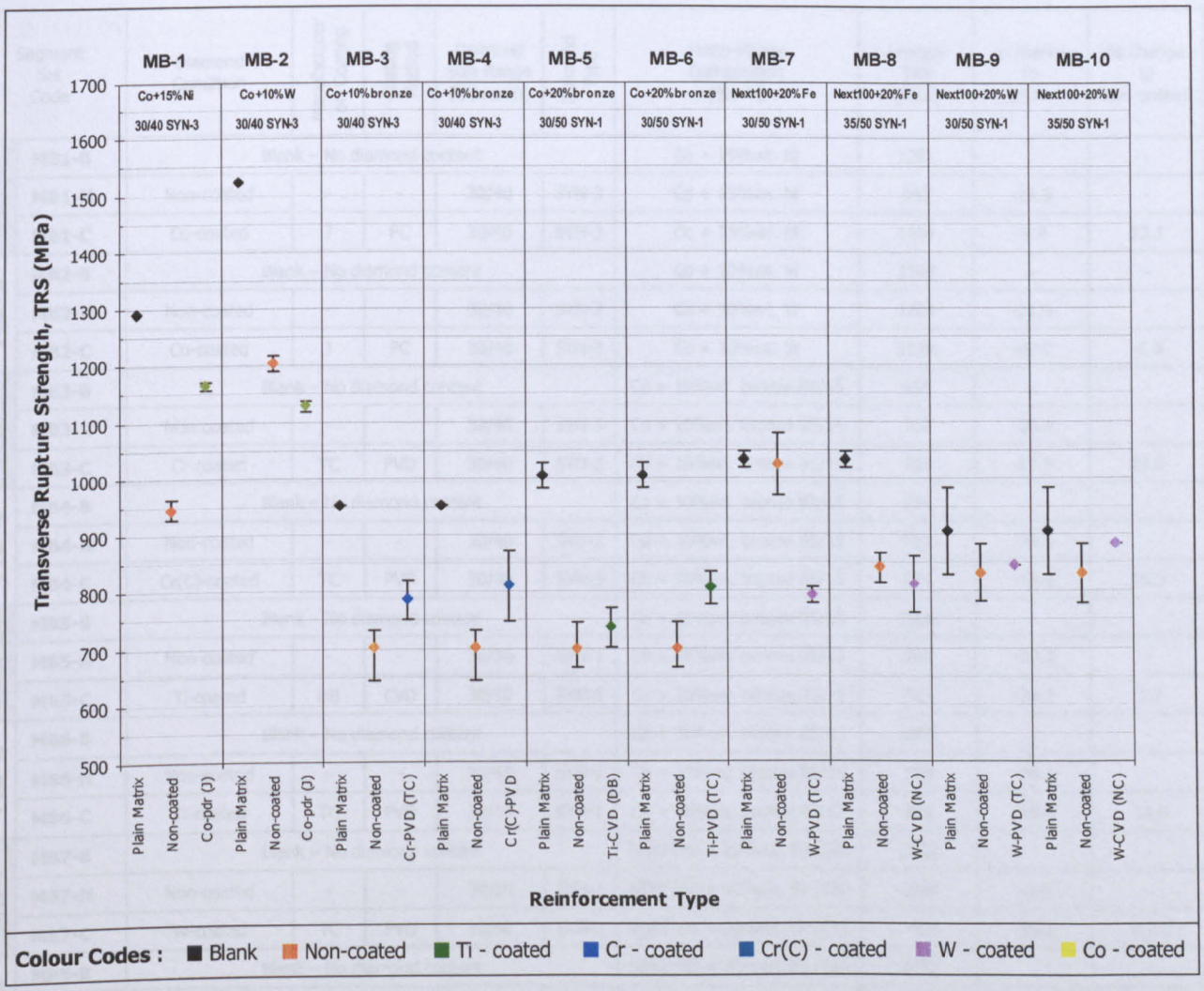

Figure 10-3 : Transverse Rupture Strength (TRS) of the rectangular parallelepiped segments obtained by the 3-point bending.

As can be seen from the results presented in Figure 10-3 and Table 10-2 all diamond impregnated composites exhibited lower bending strengths than the corresponding blank reference segments. The smallest relative decrease compared to the blank segments was found for the segments with metal-matrices containing the pre-alloyed Cu-Fe-Co powder alloyed with 20% W and impregnated with the two types of W-coated grit (MB-9, MB-10). Highest absolute TRS values were obtained for segments with the Co-Ni (MB-1) and Co-W (MB-2) alloy matrices.

Apart from two compositions, in all other cases the TRS of the segments with the coated grit was greater than that of the segments impregnated with the non-coated diamonds. Greatest improvement was measured for the Co-powder encapsulated diamonds when incorporated in the Co-Ni binder (MB-1). High levels of improvement were also found for both the PVD Ti and Cr-coated grit impregnated in the two Co-bronze alloy matrices.

Segment Set Code		Diamond Condition	Manufacturer of Coating	Coating Method	Diamond Size Range (US mesh)	Diamond Type	Metal-Matrix Composition (%wt.)	Avergae TRS (MPa)	% change to blank	% change to non-coated
MB-1	**MB1-B**	Blank – No diamond content					Co + 15%wt. Ni	1291	-	-
	MB1-N	Non-coated	-	-	30/40	SYN-3	Co + 15%wt. Ni	945	-26.8	-
	MB1-C	Co-coated	J	PC	30/40	SYN-3	Co + 15%wt. Ni	1164	-9.8	23.1
MB-2	**MB2-B**	Blank – No diamond content					Co + 10%wt. W	1524	-	-
	MB2-N	Non-coated	-	-	30/40	SYN-3	Co + 10%wt. W	1204	-21.0	-
	MB2-C	Co-coated	J	PC	30/40	SYN-3	Co + 10%wt. W	1128	-26.0	-6.3
MB-3	**MB3-B**	Blank – No diamond content					Co + 10%wt. bronze 85/15	954	-	-
	MB3-N	Non-coated	-	-	30/40	SYN-3	Co + 10%wt. bronze 85/15	702	-26.4	-
	MB3-C	Cr-coated	TC	PVD	30/40	SYN-3	Co + 10%wt. bronze 85/15	786	-17.5	12.0
MB-4	**MB4-B**	Blank – No diamond content					Co + 10%wt. bronze 85/15	954	-	-
	MB4-N	Non-coated	-	-	30/40	SYN-3	Co + 10%wt. bronze 85/15	702	-26.4	-
	MB4-C	Cr(C)-coated	TC	PVD	30/40	SYN-3	Co + 10%wt. bronze 85/15	811	-14.9	15.5
MB-5	**MB5-B**	Blank – No diamond content					Co + 20%wt. bronze 85/15	1005	-	-
	MB5-N	Non-coated	-	-	30/50	SYN-1	Co + 20%wt. bronze 85/15	700	-30.3	-
	MB5-C	Ti-coated	DB	CVD	30/50	SYN-1	Co + 20%wt. bronze 85/15	737	-26.7	5.2
MB-6	**MB6-B**	Blank – No diamond content					Co + 20%wt. bronze 85/15	1005	-	-
	MB6-N	Non-coated	-	-	30/50	SYN-1	Co + 20%wt. bronze 85/15	700	-30.3	-
	MB6-C	Ti-coated	TC	PVD	30/50	SYN-1	Co + 20%wt. bronze 85/15	805	-19.9	15.0
MB-7	**MB7-B**	Blank – No diamond content					NEXT100 + 20%wt. Fe (CN)	1032	-	-
	MB7-N	Non-coated	-	-	30/50	SYN-1	NEXT100 + 20%wt. Fe (CN)	1024	-0.8	-
	MB7-C	W-coated	TC	PVD	30/50	SYN-1	NEXT100 + 20%wt. Fe (CN)	793	-23.1	-22.5
MB-8	**MB8-B**	Blank – No diamond content					NEXT100 + 20%wt. Fe (CN)	1032	-	-
	MB8-N	Non-coated	-	-	30/50	SYN-1	NEXT100 + 20%wt. Fe (CN)	841	-18.5	-
	MB8-C	W-coated	NC	CVD	35/50	SYN-1	NEXT100 + 20%wt. Fe (CN)	812	-21.4	-3.5
MB-9	**MB9-B**	Blank – No diamond content					NEXT100 + 20%wt. W	906	-	-
	MB9-N	Non-coated	-	-	30/50	SYN-1	NEXT100 + 20%wt. W	831	-8.3	-
	MB9-C	W-coated	TC	PVD	30/50	SYN-1	NEXT100 + 20%wt. W	845	-6.8	1.7
MB-10	**MB10-B**	Blank – No diamond content					NEXT100 + 20%wt. W	906	-	-
	MB10-N	Non-coated	-	-	30/50	SYN-1	NEXT100 + 20%wt. W	831	-8.3	-
	MB10-C	W-coated	NC	CVD	35/50	SYN-1	NEXT100 + 20%wt. W	882	-2.6	6.1

Nomenclature :

Diamond Type : **SYN-1** is superior quality **SYN-3** produced by De Beers

Metal coating deposition methods : **CVD** : Chemical Vapour Deposition, **PVD** : Physical Vapour Deposition, **PC** : Powder Coating / Encapsulation

Manufacturers of Coated Diamonds : **DB** : De Beers, **NC** : Norton Company, **TC** : Teer Coatings, **J** : Fuji Paudal Kabushiki Kaisha

Table 10-2 : Average Transverse Rupture Strength (TRS) of tested rectangular parallelepiped segments. Table also lists the calculated comparison values for the various diamond conditions. NEXT 100 is registered trade name of Eurotungstene Poudres (France) for a pre-alloyed Cu-Fe-Co powder.

10.5 SEM Examination

This section presents the results of the SEM examination of the fractured surfaces produced by 3-point bending.

10.5.1 Qualitative Fracture Surface Examination

10.5.1.1 MB-1 : Co + 15%wt. Ni, Co-powder encapsulated 30/40 mesh SYN-3

10.5.1.1A Non-coated 30/40 US mesh SYN-3 Diamonds (MB1-N)

SEM inspection of the fracture surfaces of the segments with the Co + 15%wt. Ni matrix and impregnated with the 30/40 SYN-3 non-coated diamonds revealed that the abrasive crystals had been etched and that interfacial fissures had formed. The degree of etching was found to be higher for the cubic {100} faces (see Figure 10-4A).

10.5.1.1B Co-powder encapsulated (J) 30/40 US mesh SYN-3 Diamonds (MB1-C)

In contrast to the segments impregnated with the non-coated grit (MB1-N), the Co-powder encapsulated diamonds exposed to the fracture surfaces appeared to have retained an overall smooth and clean surface status with minimal signs of etching (see Figure 10-4B). Careful examination revealed a narrow dense Co-jacket surrounding each diamond. Interfacial fissures had however formed at similar widths as the segment with the non-coated grit.

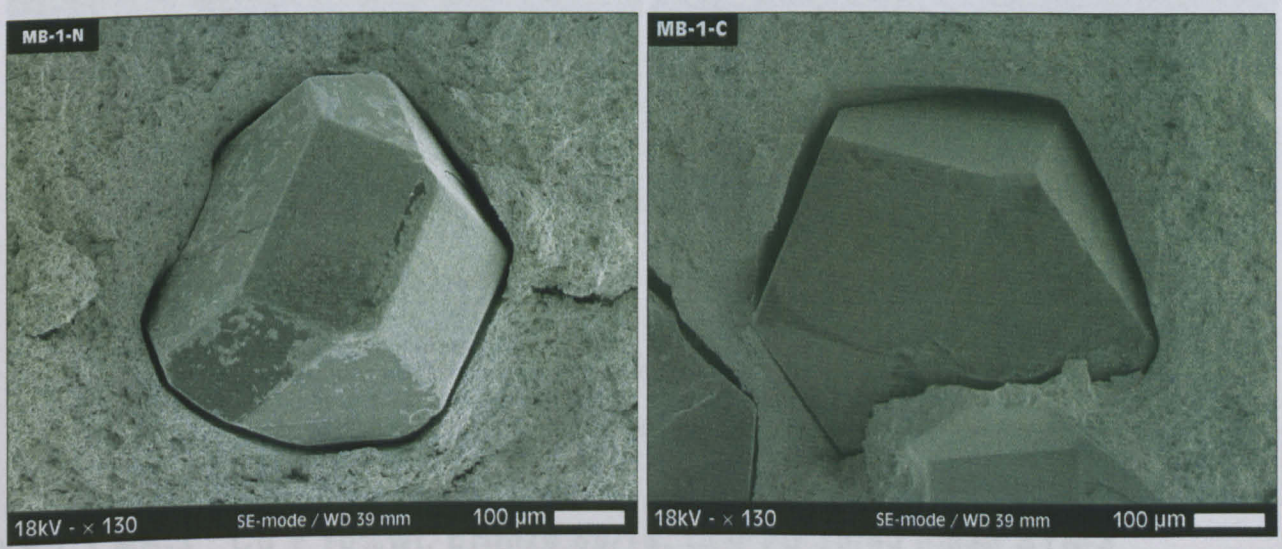

(A) Metal-Matrix : Co + 15%wt. Ni
Diamond : Non-coated 30/40 mesh SYN-3 (DB)

(B) Metal-Matrix : Co + 15%wt. Ni
Diamond : Co-encapsulated 30/40 mesh SYN-3 (J)

Figure 10-4 : SEM micrographs showing exposed non-coated and Co-powder encapsulated diamonds on 3-point bending fractures surfaces of segments with the Co + 15%wt. Ni metal-matrix produced by HP.

10.5.1.2 MB-2 : Co + 10%wt. W, Co-powder encapsulated 30/40 mesh SYN-3

10.5.1.2A Non-coated 30/40 US mesh SYN-3 Diamonds (MB2-N)

SEM inspection of the fracture surfaces of the segments with the Co + 10%wt. W matrix and impregnated with the 30/40 SYN-3 non-coated diamonds revealed that a great number of crystals had fractured (see Figure 10-5A). Diamond surfaces appeared to have reacted with the metal-matrix containing remains of both W and Co as backscattered imaging revealed.

10.5.1.2B Co-powder encapsulated (J) 30/40 US mesh SYN-3 Diamonds (MB2-C)

Interaction with the metal-matrix was considerably reduced for the Co-powder encapsulated diamonds. Metallic remains could not be identified on the exposed crystal surfaces and crystals appeared to have been slightly etched, with the cubic {100} faces being more prone to this deterioration process (Figure 10-5B). There were no macroscopically fractured diamonds found and a considerably lower number of crystals were exposed to the fracture surface compared to the segment with the non-coated grit. Developed interfacial fissures were however narrow.

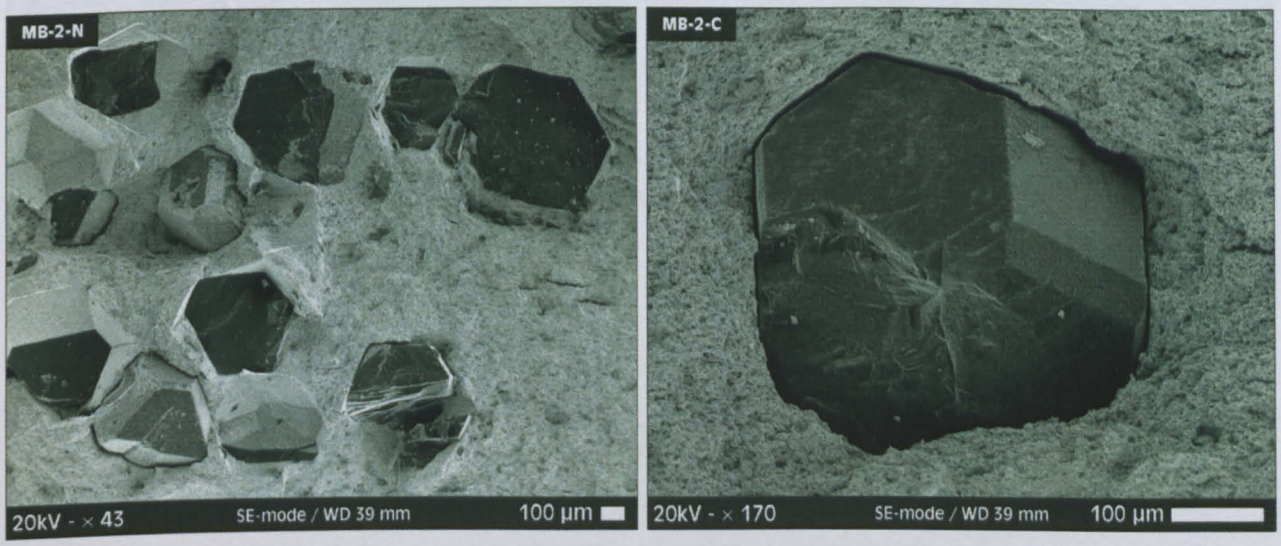

(A) Metal-Matrix : Co + 10%wt. W
Diamond : Non-coated 30/40 mesh SYN-3 (DB)

(B) Metal-Matrix : Co + 10%wt. W
Diamond : Co-encapsulated 30/40 mesh SYN-3 (J)

Figure 10-5 : SEM micrographs illustrating sections of 3-point fracture surfaces of segments with a Co + 10%wt. W matrix impregnated with non-coated and Co-powder encapsulated diamonds. **(A)** Section of the fracture surface of a segment impregnated with the non-coated grit showing the large degree of reinforcement fracture, **(B)** view of a Co-powder encapsulated diamond exposed on the fracture surface.

10.5.1.3 MB-3 : Co + 10%wt. bronze 85/15, Cr-PVD 30/40 mesh SYN-3

10.5.1.3A Non-coated 30/40 US mesh SYN-3 Diamonds (MB3-N)

Examination of the fracture surfaces of the segments with the Co + 10%wt. bronze (85Cu/15Sn) matrix and impregnated with the 30/40 SYN-3 non-coated diamonds revealed that a very small

degree of diamond etching had taken place preferentially at the cubic {100} diamond faces (see Figure 10-6A).

10.5.1.3B Cr-PVD (TC) 30/40 US mesh SYN-3 Diamonds (MB3-C)

Chromium PVD coatings were found detached from diamonds and preferentially remained in the developed pull-out craters (see Figure 10-6B). The Cr-coatings did not however retain the form of layers originally produced by the CVD, but appeared to have dissolved in the matrix. The stripped diamonds had smooth and clean surfaces retaining the edge sharpness. There were no fractured diamonds found.

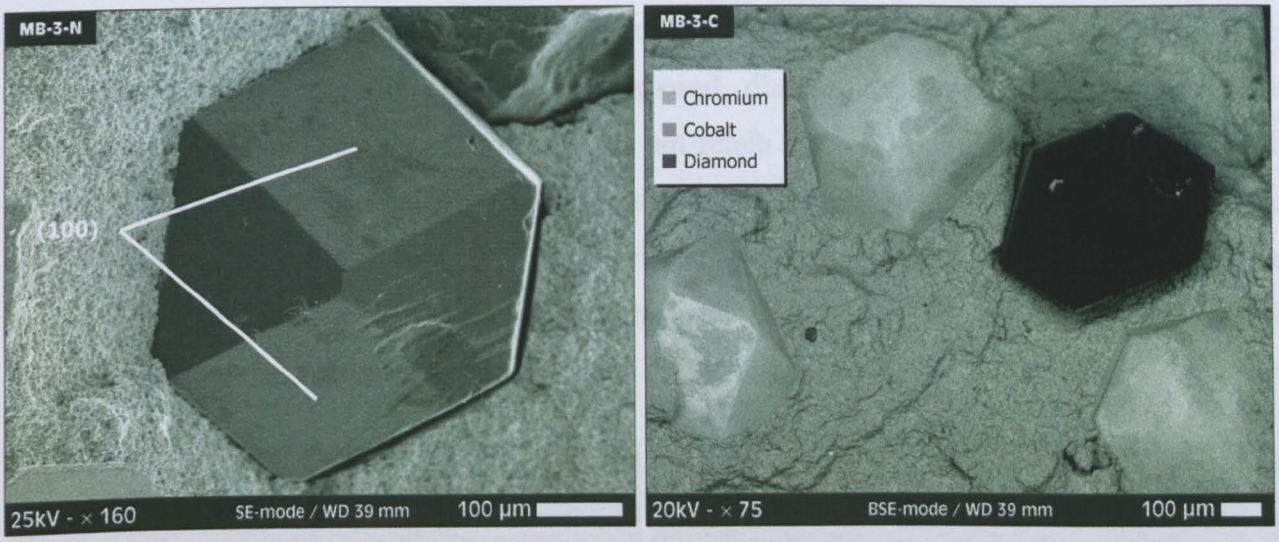

(A) Metal-Matrix : Co + 10%wt. bronze (85Cu/15Sn)
Diamond : Non-coated 30/40 mesh SYN-3 (DB)

(B) Metal-Matrix : Co + 10%wt. bronze (85Cu/15Sn)
Diamond : Cr-PVD 30/40 mesh SYN-3 (TC)

Figure 10-6 : SEM micrographs illustrating sections of 3-point fracture surfaces of segments with a Co + 10%wt. bronze matrix impregnated with non-coated and Cr-PVD-coated diamonds. **(A)** View of a non-coated diamond exposed on the fracture surface showing the slight etching of cubic (100) faces, **(B)** section of the fracture surface of a segment impregnated with the Cr-PVD-coated grit view in the BSE mode and showing Cr-coating to remain bonded to the developed pull-out craters.

10.5.1.4 MB-4 : Co + 10%wt. bronze 85/15, Cr(C)-PVD 30/40 mesh SYN-3

10.5.1.4A Non-coated 30/40 US mesh SYN-3 Diamonds (MB4-N)

Similar observations as those stated above for the MB3-N (refer to §10.5.1.3A) applied to the MB-4 segments impregnated with the non-coated grit.

10.5.1.4B Cr(C)-PVD (TC) 30/40 US mesh SYN-3 Diamonds (MB4-C)

Similar observations as those stated above for the MB3-C (refer to §10.5.1.3B) applied to the MB-4 segments reinforced with the Cr(C)-coated diamonds.

10.5.1.5 MB-5 : Co + 20%wt. bronze 85/15, Ti-CVD 30/50 mesh SYN-1

10.5.1.5A Non-coated 30/50 US mesh SYN-1 Diamonds (MB5-N)

Examination of the fracture surfaces of the segments with the Co + 20%wt. bronze (85Cu/15Sn) matrix and impregnated with the 30/50 SYN-1 non-coated diamonds revealed that practically no interaction between the diamonds and the matrix had taken place. One could possibly identify a minor degree of diamond etching on the cubic {100} diamond faces.

10.5.1.5B Ti-CVD (DB) 30/50 US mesh SYN-1 Diamonds (MB5-C)

Examination showed that the Ti-CVD coatings were preferentially detached from the diamonds and were found in the developed pull-out craters. However, there were instances where fragments of Ti-layers remained on the exposed diamond surfaces. Inspection at high magnifications showed that the Ti-coatings did not retain the form of the solid layers produced by CVD. EDAX analysis confirmed that Ti-coatings had partially dissolved in the metal-matrix and revealed the presence of oxygen at the interfacial region. There were some locations where a reaction product had formed at the interface. This interfacial product had a thickness of up to 15 microns and contained numerous cracks (Figure 10-7).

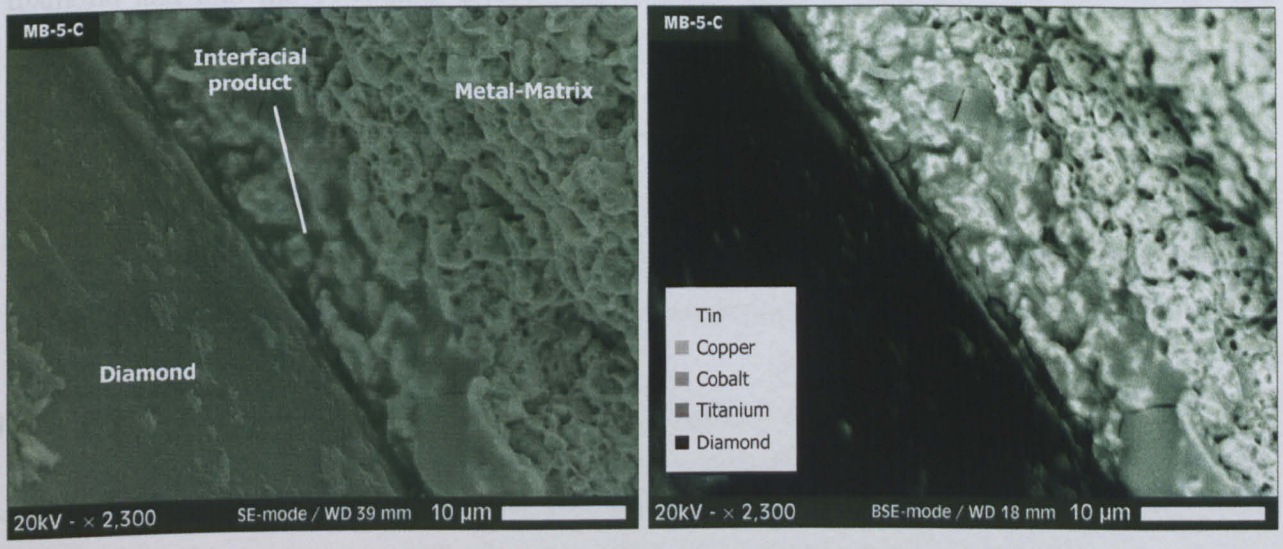

(A) Metal-Matrix : Co + 20%wt. bronze (85Cu/15Sn)
Diamond : Ti-CVD-coated 30/50 mesh SYN-1 (DB)

(B) Micrograph A viewed in BSE mode.

Figure 10-7 : SEM micrographs illustrating sections of the interfacial region of an exposed diamond in a 3-point fracture surface of segment with a Co + 20%wt. bronze matrix and impregnated with the Ti-CVD-coated diamonds. **(A)** Magnified view of the interfacial area showing the formation of a dense but cracked product, **(B)** micrograph A as viewed in the BSE mode illustrating clearly the cracks and the Ti-dissolution in the matrix.

10.5.1.6 MB-6 : Co + 20%wt. bronze 85/15, Ti-PVD 30/50 mesh SYN-1

10.5.1.6A Non-coated 30/50 US mesh SYN-1 Diamonds (MB6-N)

Similar observations to those stated above for the MB5-N (refer to §10.5.1.5A) apply for the MB-6 segments reinforced with the non-coated diamonds.

10.5.1.6B Ti-PVD (TC) 30/50 US mesh SYN-1 Diamonds (MB6-C)

Observations made for the MB6-C segment with the cobalt-bronze matrix impregnated with the Ti-PVD-coated diamonds were generally similar to those for the Ti-CVD coated diamonds. Coatings were preferentially detached from the diamonds and were found in the developed pull-out craters. Examination at high magnifications revealed that the Ti-coatings did not retain the form of the solid-dense layers produced by PVD but they seemed to have partially dissolved into the matrix. The mode of adherence of the Ti-coating layers to the metal-matrix implied that a strong bonding had been achieved (see Figure 10-8A on next page). The coating/matrix interface was not a plane of steep chemical composition change, but had been transformed into a region of gradual chemical variation. EDAX analysis confirmed the previous statement showing Ti atoms to have migrated towards the metal-matrix but also that Cu, Co and Sn had dissolved towards the diamond and into the Ti-coating layers. Additionally, EDAX revealed that tin and oxygen had segregated at the coating and the coating/matrix interfacial region. Traces of chlorine were also identified at the interfacial zone.

There were some locations at the interfacial regions where a reaction product had formed. In most of the cases, this product appeared to be thicker but also more cracked than those found for the Ti-CVD-coated diamonds as was presented in the previous section (see Figure 10-8).

10.5.1.7 MB-7 : Pre-alloyed Cu-Fe-Co + 20%wt. Fe, W-PVD 30/50 mesh SYN-1

10.5.1.7A Non-coated 30/50 US mesh SYN-1 Diamonds (MB7-N)

Examination of the fracture surfaces of the MB7-N segments revealed that the pre-alloyed Cu-Fe-Co alloyed with 20%wt. of Fe-powder metal-matrix had caused considerable etching to the non-coated diamonds. The degree of etching was found to be significantly higher for the cubic {100} faces as compared to the octahedral {111}. Etching on the cubic surfaces had the form of large cavities whereas that on the octahedral planes was rather irregular with some large sized etch trigons (Figure 10-9).

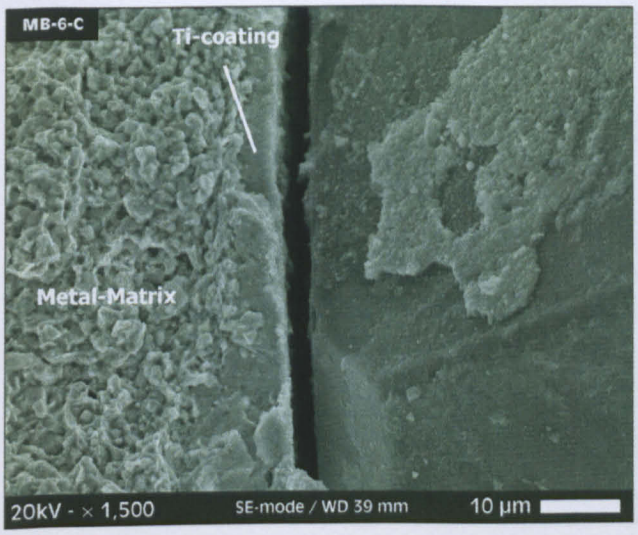

(A) Interfacial region. Excellent adherence of Ti / binder.

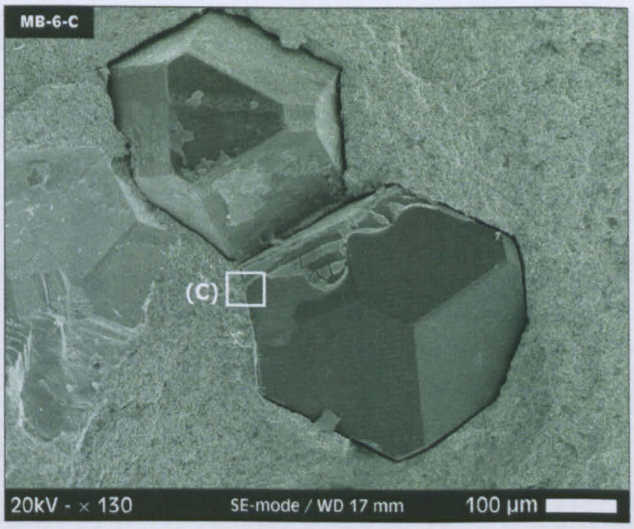

(B) Section illustrating areas of interfacial reaction.

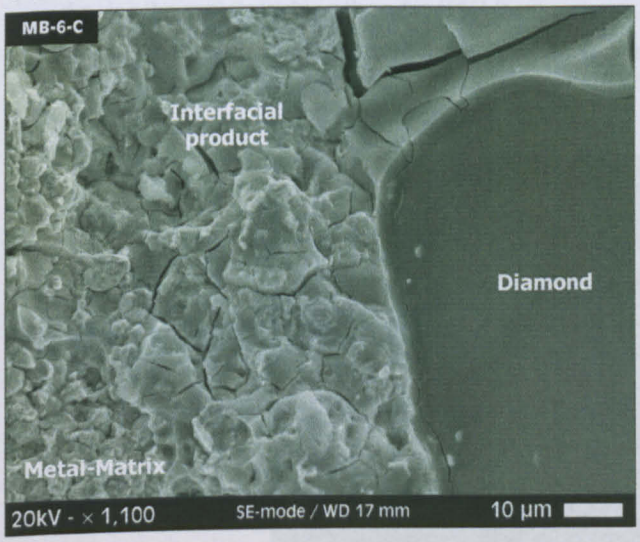

(C) Magnified view of interfacial product.

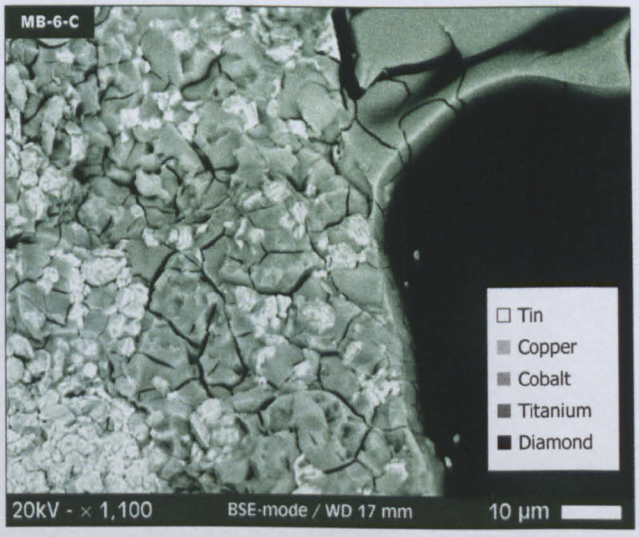

(D) Micrograph C as viewed in BSE mode.

Figure 10-8 : SEM micrographs illustrating sections of 3-point fracture surfaces of segments with a Co + 20%wt. Bronze (85Cu/15Sn) matrix impregnated with the Ti-PVD-coated diamonds (30/50 mesh SYN-1 TC).

10.5.1.7B W-PVD (TC) 30/50 US mesh SYN-1 Diamonds (MB7-C)

SEM examination revealed that the W-coatings did not retain the layered form produced by the PVD deposition but they were rather dissolved to a considerable extent by the pre-alloyed Cu-Fe-Co + 20%wt. Fe binder. Metallic islets high in tungsten were found on cubic {100} faces whereas the octahedral {111} planes remained almost free from any metal, having undergone only a small scale etching by very shallow etch features. Diamonds appeared to be very tightly enveloped by the metal-matrix and the interfacial fissures when existent were very narrow.

10.5.1.8 MB-8 : Pre-alloyed Cu-Fe-Co + 20%wt. Fe, W-CVD 35/50 mesh SYN-1

10.5.1.8A Non-coated 30/50 US mesh SYN-1 Diamonds (MB8-N)

Observations are similar to those for the MB7-N (§10.5.1.7A) (see Figure 10-10).

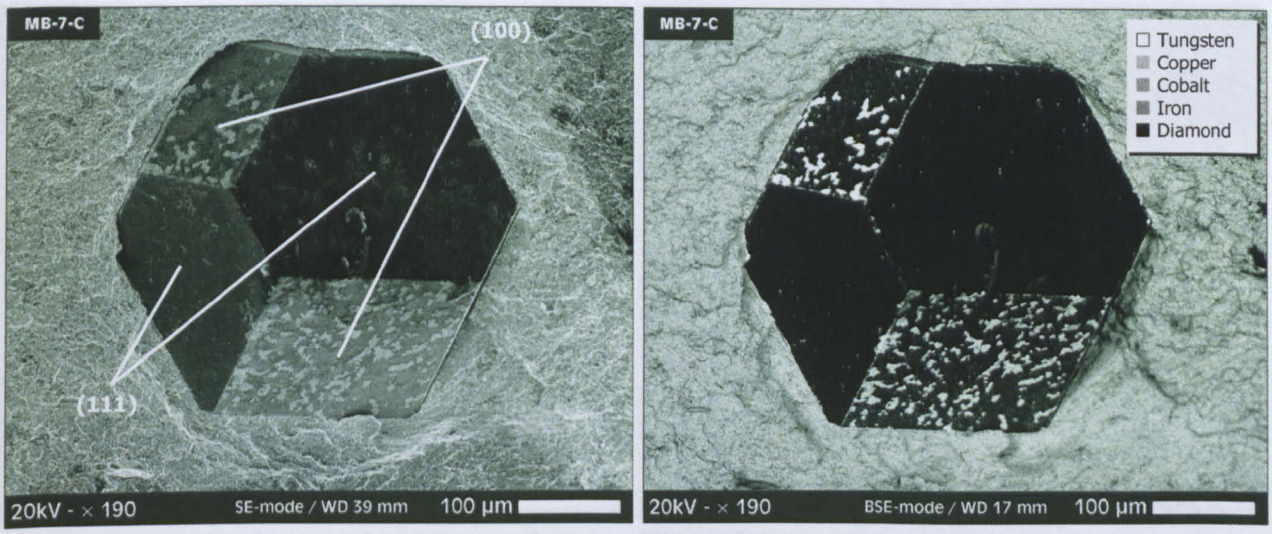

(A) View of a diamond exposed on the fracture surface showing the metallic islets on the cubic (100) faces.

(B) Micrograph A viewed in BSE mode showing islets to be tungsten rich.

Figure 10-9 : SEM micrographs illustrating an exposed diamond on the fracture surface of a segment with the pre-alloyed Cu-Fe-Co + 20%wt. Fe-powder matrix impregnated with the W-PVD-coated diamonds (TC).

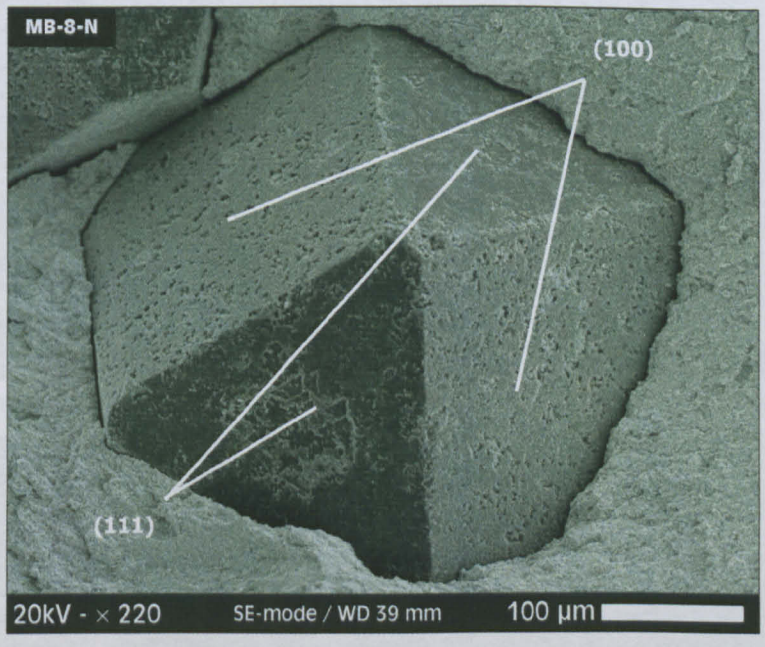

Figure 10-10 : SEM micrographs illustrating an exposed diamond on the fracture surface of a segment with the pre-alloyed Cu-Fe-Co + 20%wt. Fe-powder matrix impregnated with the non-coated diamonds. Cubic (100) faces have been etched at a higher extent compared to the octahedral (111) planes.

10.5.1.8B W-CVD (NC) 35/50 US mesh SYN-1 Diamonds (MB8-C)

The W-CVD-coated diamonds were bonded excellently to the Cu-Fe-Co (MB-8) metal-matrix. Coatings retained their original layered form produced by CVD without being consumed by dissolution as was found for the thinner W-PVD-coating presented previously (see Figure 10-11C to F on next page).

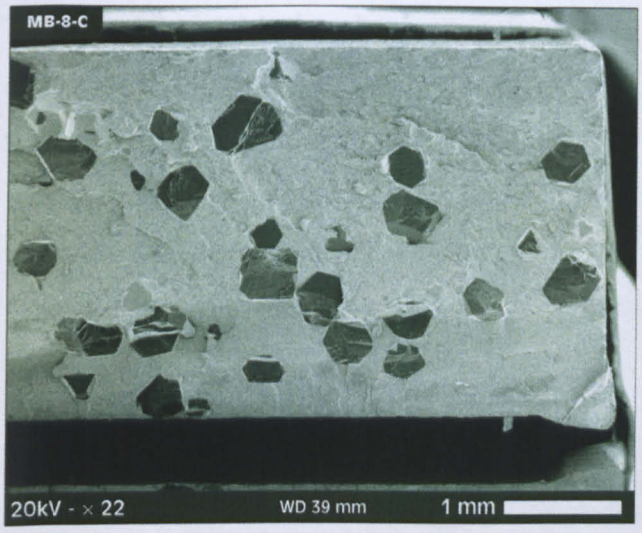

(A) View of section of the fracture surface at low magnification.

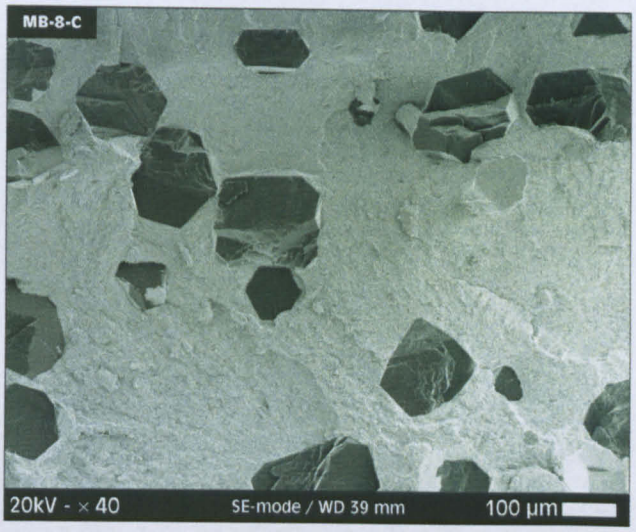

(B) Magnified section of micrograph A.

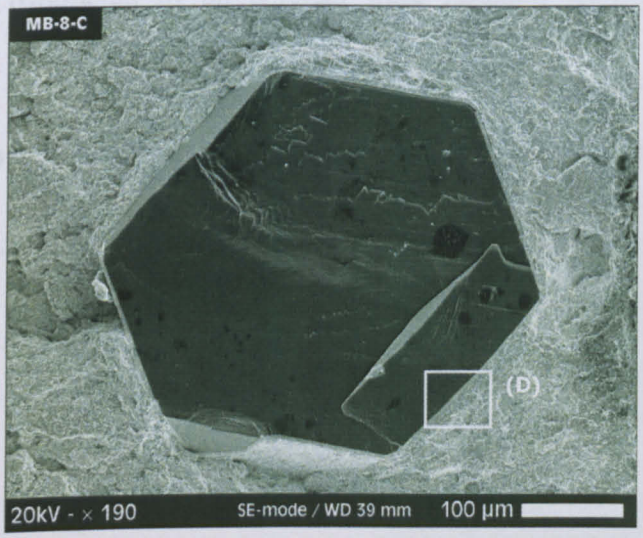

(C) Fractured diamond tightly enveloped in the W/matrix pocket.

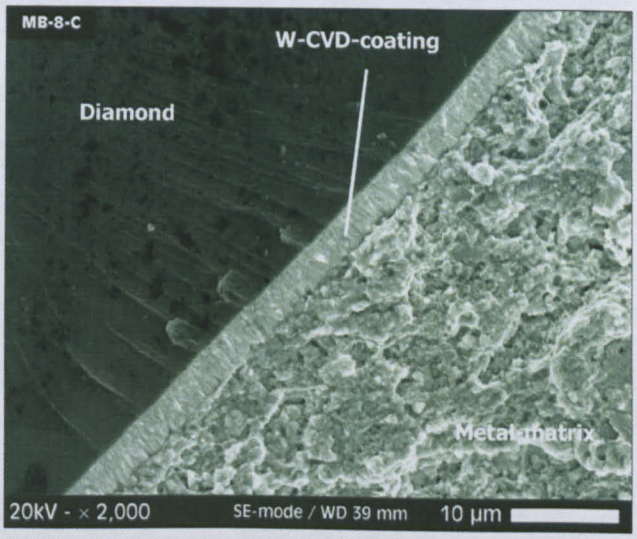

(D) Magnified view of the interfacial region.

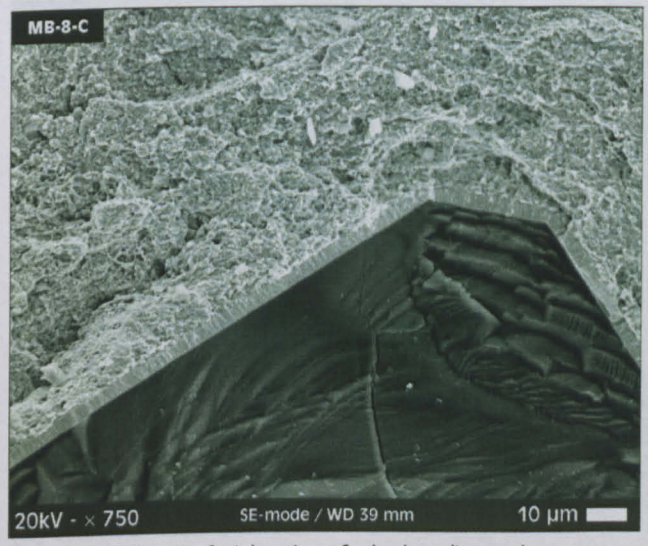

(E) View of the interfacial region of a broken diamond.

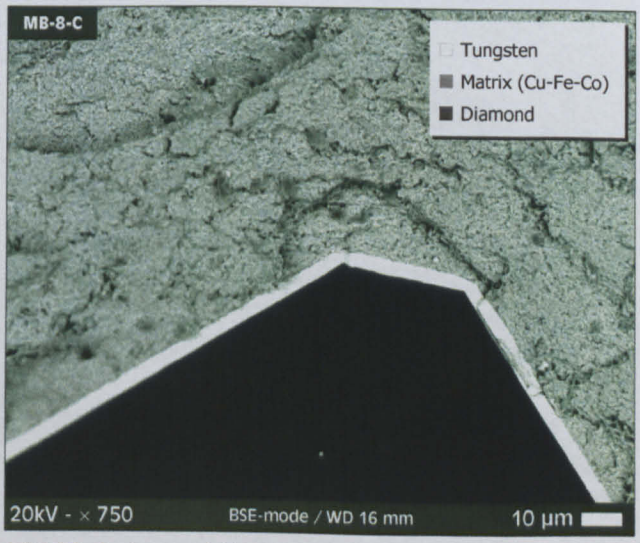

(F) BSE of micrograph E.

Figure 10-11 : SEM micrographs from the fracture surface of the segment having a pre-alloyed Cu-Fe-Co matrix alloyed with 20% Fe and impregnated with the 5 micron thick W-CVD-coated diamonds (35/50 mesh SYN-1 NC). Micrographs show that almost all of the diamonds had fractured and that the adherence of the W-coatings to both the diamond and the metal-matrix is excellent without signs of diamond etching.

EDAX analysis at points lying on a line perpendicular to the interfacial plane revealed that C-atoms had diffused into the W-coating reaching distances well within the metal-matrix. The tungsten to carbon atomic ratio in the coating (W%at./C%at.) near the coating-diamond interface was found to vary close to the value 1.5. Metallic atoms of the binder had been found to diffuse towards the diamond with Fe-atoms reaching slightly higher atomic concentrations closely followed by cobalt and then copper. EDAX analysis also revealed the segregation of oxygen at the coating/matrix interface.

However, the most significant observation for this composite was that almost all the exposed diamonds had fractured (see Figure 10-11A and B). Both the positive and negative diamond fragments of all crystals were retained on the fracture surface by the tight tungsten/matrix pockets.

10.5.1.9 MB-9 : Pre-alloyed Cu-Fe-Co + 20%wt. W, W-PVD 30/50 mesh SYN-1

10.5.1.9A Non-coated 30/50 US mesh SYN-1 Diamonds (MB9-N)

Observations were very similar to what was found for Cu-Fe-Co+20%Fe binder impregnated with the non-coated diamonds. Considerable etching of the crystals has taken place with cubic {100} faces being clearly modified to a greater extent than the octahedral {111} surfaces (Figure 10-12).

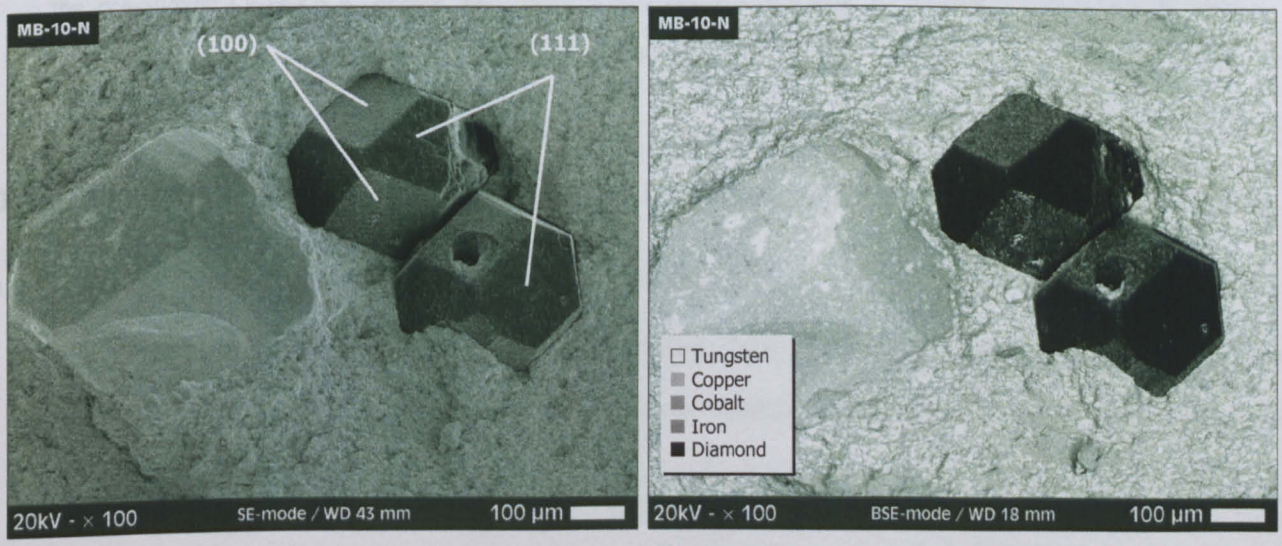

(A) Section of fracture surface.

(B) Micrograph A viewed in BSE mode.

Figure 10-12 : SEM micrographs illustrating an exposed diamond on the fracture surface of a segment with the pre-alloyed Cu-Fe-Co + 20%wt. W-powder matrix impregnated with the non-coated diamonds. Cubic (100) faces have been etched at a higher extent compared to the octahedral (111) planes.

10.5.1.9B W-PVD (TC) 30/50 US mesh SYN-1 Diamonds (MB9-C)

SEM examination of the W-alloyed Cu-Fe-Co pre-alloyed matrix showed that the interaction phenomena between the diamond crystals and the metal-matrix were similar to those found for the Fe-powder alloyed type matrix reinforced with the W-PVD-coated grit (refer to §10.5.1.7B on page 226). The W-coatings appeared to partially cover the cubic {100} and dodecahedral {110} planes whereas they were totally removed from the octahedral {111} faces (Figure 10-13). The degree of coverage of the faces by the metallic layers was considerably higher than what was found for MB7-C type segment with the Fe alloyed version of the metal-matrix.

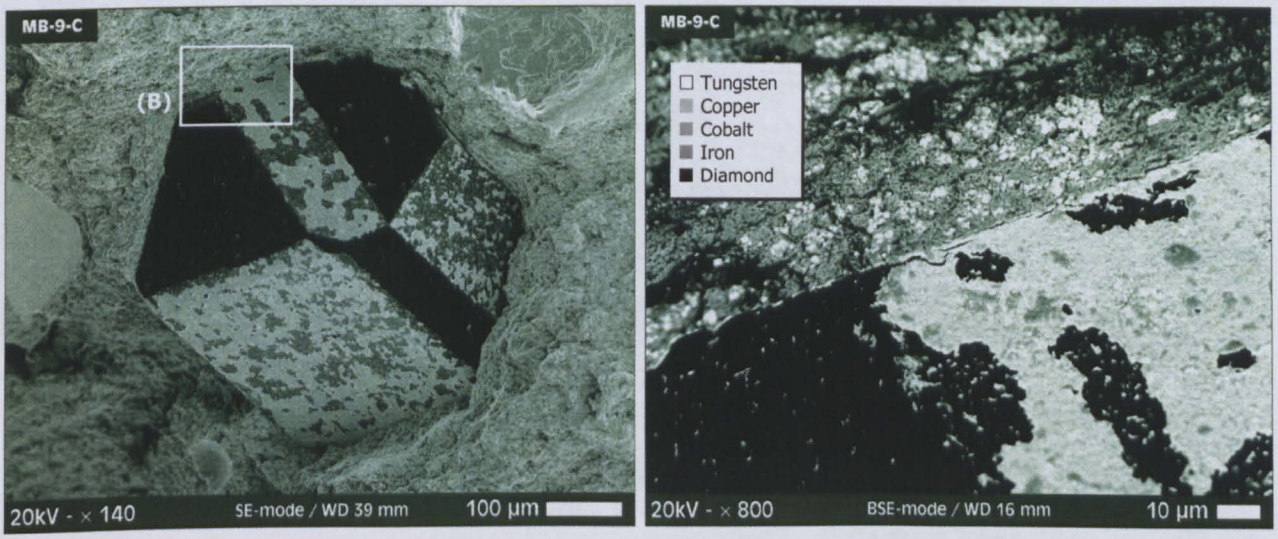

(A) Exposed diamond crystal on fracture surface. **(B)** Magnified section of micrograph A viewed in BSE mode.

Figure 10-13 : SEM micrographs illustrating an exposed diamond on the fracture surface of a segment with the pre-alloyed Cu-Fe-Co + 20%wt. Fe-powder matrix impregnated with the W-PVD-coated diamonds (TC). **(A)** View of a diamond exposed on the fracture surface showing the metallic islets on the cubic (100) and dodecahedral (110) faces, **(B)** magnified section of micrograph A viewed in BSE mode and showing the W-rich coating layers.

10.5.1.10 MB-10 : Pre-alloyed Cu-Fe-Co + 20%wt. W, W-CVD 35/50 mesh SYN-1

10.5.1.10A Non-coated 30/50 US mesh SYN-1 Diamonds (MB10-N)

Similar observations as those for the MB9-N as described above apply for the segment with the Cu-Fe-Co+20%wt. W impregnated with the non-coated 30/50 mesh SYN-1 grit (refer to §10.5.1.9A for details).

10.5.1.10B W-CVD (NC) 35/50 US mesh SYN-1 Diamonds (MB10-C)

The situation for this system was similar to the MB8-C segment with the W-CVD-coated diamonds. The W-coatings were excellently bonded to the W-alloyed Cu-Fe-Co and retained their original layered form produced by the CVD. Composite failure occurred at the W/diamond interface as indicated by the W-coating shells found attached in pull-out craters. The stripped

diamond surfaces from the W-coatings were clean and smooth without significant signs of etching. A considerable number of diamonds on the fracture surface were broken, but by no means approached the very high levels of reinforcement cracking observed for the MB-8 segments. The diamond enclosure by the metal-matrix appeared relatively tight and the interfacial fissures did not exceed in any case a value of 1 micron.

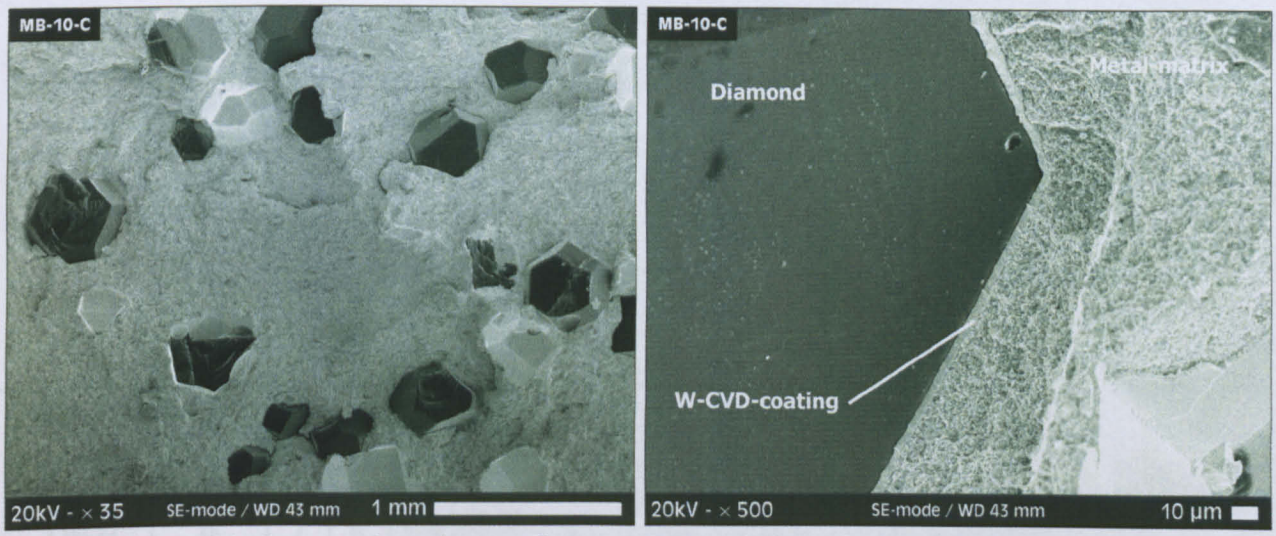

(A) View of section of the fracture surface at low magnification. **(B)** Magnified view of a section of a fractured diamond.

Figure 10-14 : SEM micrographs from the fracture surface of the segment having a pre-alloyed Cu-Fe-Co matrix alloyed with 20% W and impregnated with the 5 micron thick W-CVD-coated diamonds (35/50 mesh SYN-1 NC). Micrographs show that a large number of crystals had fractured and that the adherence of the W-coatings to the metal-matrix is excellent.

10.5.2 Quantitative Fracture Surface Examination

The graphs and tables on the following pages present some selected counted observation features as resulted from the quantitative SEM analysis method, which was applied to the examined fracture surfaces as described in Chapter 7. Interpretation of results is similarly to that carried out for the SEM results in Chapter 9 (see §9.6.2).

In the text that follows, and for any comparison being made, a composite will be considered to show "enhanced performance" if it exhibits a combination of a lower number of lost diamonds (L), a reduced number of exposed crystals at the fracture surface (S) and a high number of fractured diamonds.

Results show that in most cases the segments impregnated with the coated diamond grades exhibited lower L and S combined with greater number of fractured crystals compared to segments with non-coated diamonds. Such kind of combinations was exhibited from all segments impregnated with the various W-coated diamonds compared to the corresponding versions with the non-coated grit. The composites with the various bronze containing metal-

matrices exhibited no such clear behaviour. However, apart from the MB-6 alloy, the quantitative SEM analysis showed that for the remaining 3 alloys the segments with the coated grit were at the same levels or slightly improved compared to the non-coated versions.

The Co-powder encapsulated diamonds were found to improve performance when incorporated into the Co-Ni matrix (MB-1). However, when the same diamonds were incorporated into the Co-W alloy matrix, the Co-powder encapsulated diamonds were found to be associated with higher L and S and lower number of fractured crystals.

	Segment Set Code	Coating Metal	Manufacturer	Deposition Method	Diamond Size (mesh)	Diamond Type	Alloy Metal Matrix	Lost Diamond Crystals		Number of Diamond Sites				Fractured Crystals	
								Counted (L)	Change to Non-Coated	Counted (S)	% Change to Non-Coated	Calculated th. No. (S_N)	% Change to S_N	Total No. Counted	Change to Non-Coated
Hot-pressed (HP)	MB-1-N	Non-coated	DB	-	30/40	SYN-3	Co + 15%wt. Ni	12	-	51	-	29	74	2	-
	MB-1-C	Co	J	PC	30/40	SYN-3	Co + 15%wt. Ni	10	-2	36	-29.4	28	27	3	1
	MB-2-N	Non-coated	DB	-	30/40	SYN-3	Co + 10%wt. W	2	-	42	-	29	45	28	-
	MB-2-C	Co	J	PC	30/40	SYN-3	Co + 10%wt. W	4	2	29	-31.0	29	1	3	-25
	MB-3-N	Non-coated	DB	-	30/40	SYN-3	Co + 10%wt. bronze 85/15	2	-	60	-	28	117	8	-
	MB-3-C	Cr	TC	PVD	30/40	SYN-3	Co + 10%wt. bronze 85/15	2	0	47	-21.7	28	70	1	-7
	MB-4-N	Non-coated	DB	-	30/40	SYN-3	Co + 10%wt. bronze 85/15	2	-	60	-	28	117	8	-
	MB-4-C	Cr(C)	TC	PVD	30/40	SYN-3	Co + 10%wt. bronze 85/15	0	-2	27	-55.0	28	-2	0	-8
	MB-5-N	Non-coated	DB	-	30/50	SYN-1	Co + 20%wt. bronze 85/15	1	-	44	-	32	37	4	-
	MB-5-C	Ti	DB	CVD	30/50	SYN-1	Co + 20%wt. bronze 85/15	1	0	51	15.9	33	53	2	-2
	MB-6-N	Non-coated	DB	-	30/50	SYN-1	Co + 20%wt. bronze 85/15	1	-	44	-	32	37	4	-
	MB-6-C	Ti	TC	PVD	30/50	SYN-1	Co + 20%wt. bronze 85/15	4	3	75	70.5	33	129	8	4
	MB-7-N	Non-coated	DB	-	30/50	SYN-1	NEXT100 + 20%wt. Fe(CN)	0	-	44	-	36	23	1	-
	MB-7-C	W	TC	PVD	30/50	SYN-1	NEXT100 + 20%wt. Fe(CN)	0	0	43	-2.3	36	19	7	6
	MB-8-N	Non-coated	DB	-	30/50	SYN-1	NEXT100 + 20%wt. Fe(CN)	0	-	44	-	36	23	1	-
	MB-8-C	W	NC	CVD	35/50	SYN-1	NEXT100 + 20%wt. Fe(CN)	0	0	58	31.8	45	29	44	43
	MB-9-N	Non-coated	DB	-	30/50	SYN-1	NEXT100 + 20%wt. W	3	-	58	-	36	60	5	-
	MB-9-C	W	TC	PVD	30/50	SYN-1	NEXT100 + 20%wt. W	4	1	53	-8.6	37	44	7	2
	MB-10-N	Non-coated	DB	-	30/50	SYN-1	NEXT100 + 20%wt. W	3	-	58	-	36	60	5	-
	MB-10-C	W	NC	CVD	35/50	SYN-1	NEXT100 + 20%wt. W	0	-3	51	-12.1	45	13	13	8

Nomenclature :

Diamond Type	:	**SYN-1** is superior quality **SYN-3** produced by De Beers
Metal coating deposition methods	:	**CVD** : Chemical Vapour Deposition, **PVD** : Physical Vapour Deposition, **PC** : Powder Coating / Encapsulation
Manufacturers of Coated Diamonds	:	**DB** : De Beers, **NC** : Norton Company, **TC** : Teer Coatings, **J** : Fuji Paudal Kabushiki Kaisha
Metal Matrices	:	NEXT100 is a pre-alloyed metal matrix consisting of Cu-Fe-Co (46.2-28.6-25.2 %wt.)

Table 10-3 : Listing of selected counted observation features as resulted from the quantitative SEM analysis method applied to the fracture surfaces of the 3-point bended Hot-Pressed (HP) segments with alloy metal-matrices.

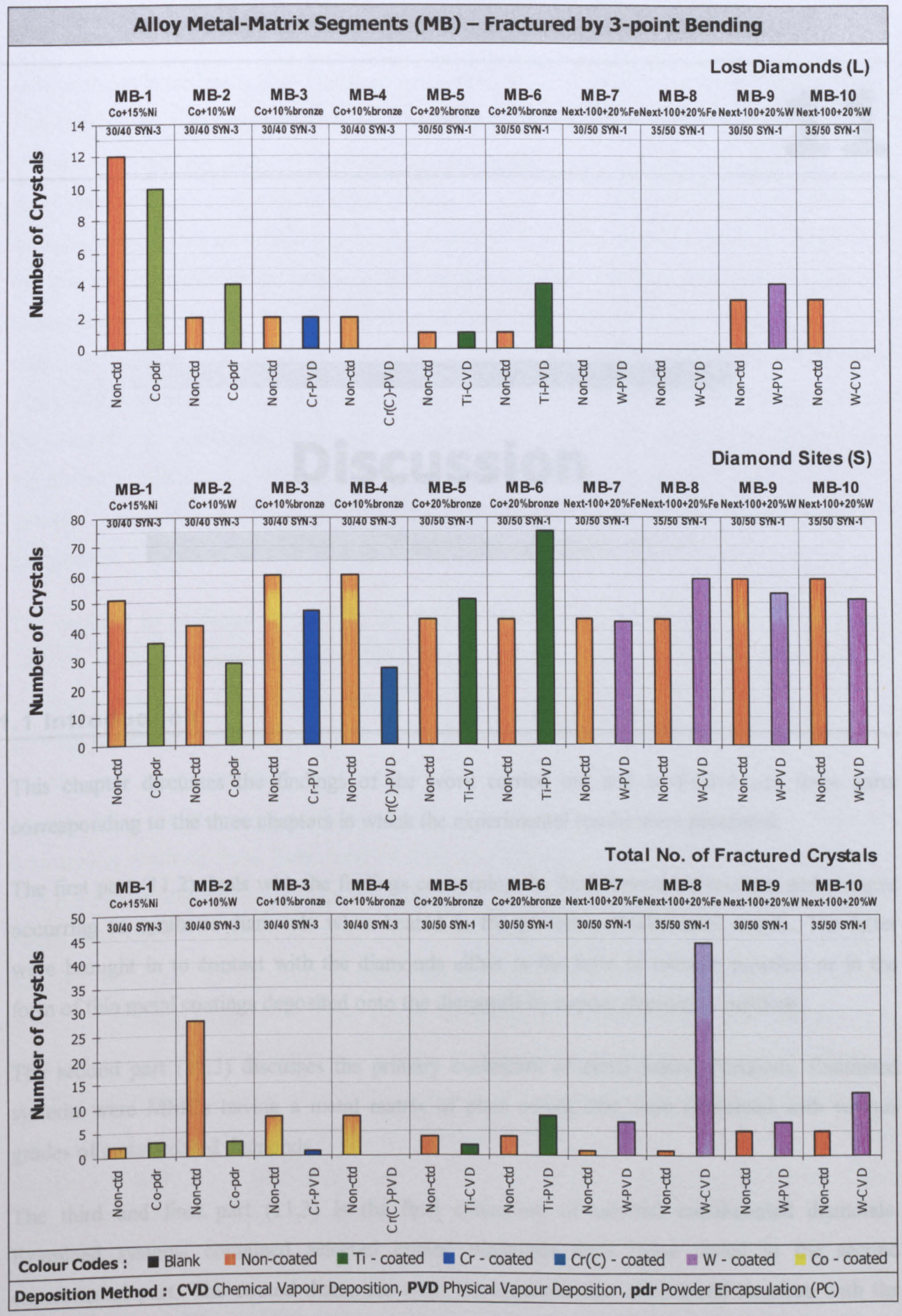

Figure 10-15 : Listing of selected counted observation features as resulted from the quantitative SEM analysis method applied to the fracture surfaces of the 3-point bended Hot-Pressed (HP) segments with alloy metal-matrices.

11

Discussion

11.1 Introduction

This chapter discusses the findings of the work carried out and is divided into three parts corresponding to the three chapters in which the experimental results were presented.

The first part (11.2) deals with the findings concerning the fundamental interactions and changes occurring to synthetic diamonds when heated in the presence of elemental metals. The latter were brought in to contact with the diamonds either in the form of metallic powders or in the form of thin metal coatings deposited onto the diamonds by vapour deposition methods.

The second part (11.3) discusses the primary evaluation of metal-coated diamonds. Examined systems were MMCs having a metal matrix of plain cobalt that were reinforced with various grades of metal-coated diamonds.

The third and final part (11.3) is the final evaluation of selected metal-coated diamonds. Examined systems contained selected coated diamonds from those tested in the second experimental part. The coated diamonds were incorporated into alloy metal matrices with the intention of formulating strong interfacial bonding at the metal-coating/binder interface.

11.2 Solid-State Interactions of Synthetic Diamonds with Metals

One problem in understanding chemical interactions between metal constituents and synthetic diamonds in real metal-bonded diamond composites, as has been addressed in previous chapters, is that commonly the diamond-metal systems are highly complex. This arises from the use of multi-metal alloy matrices, which in the majority of cases have been empirically selected by the manufacturers, based on field-testing and experience. Although from a practical point of view the true interest is to evaluate interactions of the diamonds with the alloy matrices, one must first understand the fundamental chemical phenomena that take place in the two component systems (diamond and metal) in order to determine the influence of involved parameters such as for example the chemical affinity of metal to diamond/carbon, the process temperature and time and the atmospheric conditions. Acquiring this fundamental knowledge will help in understanding the chemical interaction phenomena occurring in the complex systems and furthermore provide valuable information to future research and development for the optimisation of diamond composites.

The majority of published research in the field of metal-bonded diamond composites concerns with the study of interactions in complex systems and the determination of mechanical and wear resistance properties. Early works, mainly by Russian scientists [122, 129, 130, 132, 184, 197, 217-221], dealing with the chemical interactions in diamond-metal systems have been reported, but the vast majority of them concerned "contact angle" studies in which the metal that was brought in to contact with synthetic or natural diamonds was in the liquid state. Although information resulting from these kind of tests is extremely valuable, the studies were mainly restricted to metals and alloys with relatively low melting points because of the graphitisation of diamond at higher temperatures. Thus, high melting point and refractory metals that are of great use and importance for the diamond tools industry have only been examined when incorporated as minor alloying additions in other metals or alloys of lower melting points. Liquid phase sintering and molten-metal infiltration is used to a considerable extent in the consolidation of metal-bonded diamond composites, but the most widely used method is solid-state sintering. For these reasons, the understanding of the fundamentals of solid-state interactions in metal-diamonds systems is of great importance and it is the reason of including the series of tests presented in the first experimental section.

11.2.1 Interactions in Diamond / Metal Systems - Introduction

Transition metals can interact with diamond either by dissolving carbon or by combining with it to form carbides. Some transition metals can even be relatively inert to diamond with respect to chemical reactions. It is clear that in order for carbon atoms to be available for any sort of interaction with the metallic environment, they must first break away from the diamond structure. It has been the subject of scientific debate over the last decades, whether carbon atoms on the diamond surfaces are initially forming graphite or are directly broken away from the diamond structure. Experimental work on measurements of activation volumes for the graphitisation process has led researchers to also debate the issue of whether carbon atoms are released in groups or whether the graphitisation process involves detachment of individual atoms [7, 33].

Metals that were examined in the DRE experiment, as described analytically in Chapter 8, have been selected to be among those mostly employed either as alloy components of the matrices or as metals to form coatings on diamond crystals.

The following series of paragraphs discuss the results obtained from the DRE experiment.

11.2.2 Interactions in Diamond – Metal Powder Systems

This section examines the findings of the DRE for the systems in which the metals brought in to contact with synthetic diamonds were in the form of loose powders.

11.2.2.1 Mode of interaction between diamonds and metals

Diamond weight changes provided a primary tool for identifying the mode of interaction of the examined elemental metals to synthetic diamond crystals. Diamond weight reductions were mainly associated with loss of carbon atoms by dissolution into the metal, assuming that the atmosphere in the heating furnace was completely free from oxidising agents. On the contrary, weight gain was related to carbide formation, with metal being attached on to the diamond surface in the form of carbides.

For the plain diamond crystals heat-treated in the absence of metal, weight reductions were directly associated with surface graphitisation and oxidation of the diamond crystals, with carbon surface atoms escaping in to the environment in gaseous forms.

In respect to the above presented analysis, iron (Fe), cobalt (Co), nickel (Ni) and (Cu), which belong to the transition metals of the VIII-B and I-B groups of the periodic table of elements, were found to dissolve diamond. These metals, or their alloys, are known to catalyse the carbon dissolution and are readily used in commercial practice to synthesize diamond at high pressures (high-temperature high-pressure HPHT synthesis) in the stability region of diamond. It is thus expected that these metals will catalyse as well the reverse process of the backconversion of diamond to graphite at low pressures.

On the contrary to the above metals, chromium (Cr), molybdenum (Mo), titanium (Ti) and tungsten (W) caused the weight gain of diamond crystals indicating that reaction had taken place and metal atoms had been attached on diamond surfaces.

The behaviour of metals with respect to solubility or reactivity with carbon can be explained from the electronic structure of the metals. The ability of a transition metal to interact with carbon appears to increase with increasing number of electron vacancies in *d*-orbitals [25, 185]. Initially, an increasing number of d-vacancies is reflected as increasing solubility, which peaks at the iron group metals (see Table 11-1). Further increase of the *d*-vacancies, results in excess reaction between metal and carbon, with carbon atoms gradually losing mobility in solution and eventually tending to lock-up in the structure of the metal, forming carbides.

Metal	*d*-orbital vacancies	
Titanium (Ti)	8	↑
Tungsten (W)	6	
Chromium (Cr)	5	
Molybdenum (Mo)	5	Increasing reactivity
Iron (Fe)	4	Solubility peak
Cobalt (Co)	3	↑
Nickel (Ni)	2	
Copper (Cu)	0	Increasing solubility

Table 11-1 : *d*-orbital vacancies of transition metals.

According to the magnitude of weight changes produced to the diamonds the following ranking in decreasing order has been found (see also Figure 11-1 and Figure 11-2):

Diamond dissolution : $Fe > Co\text{-}SMS > Co\ (CoC) > Co\text{-}EF > Ni > Cu$

Carbide formation : $W > Ti > Cr > Mo$

Diamond graphitisation (oxidation) : $SYN\text{-}2 > SYN\text{-}1$

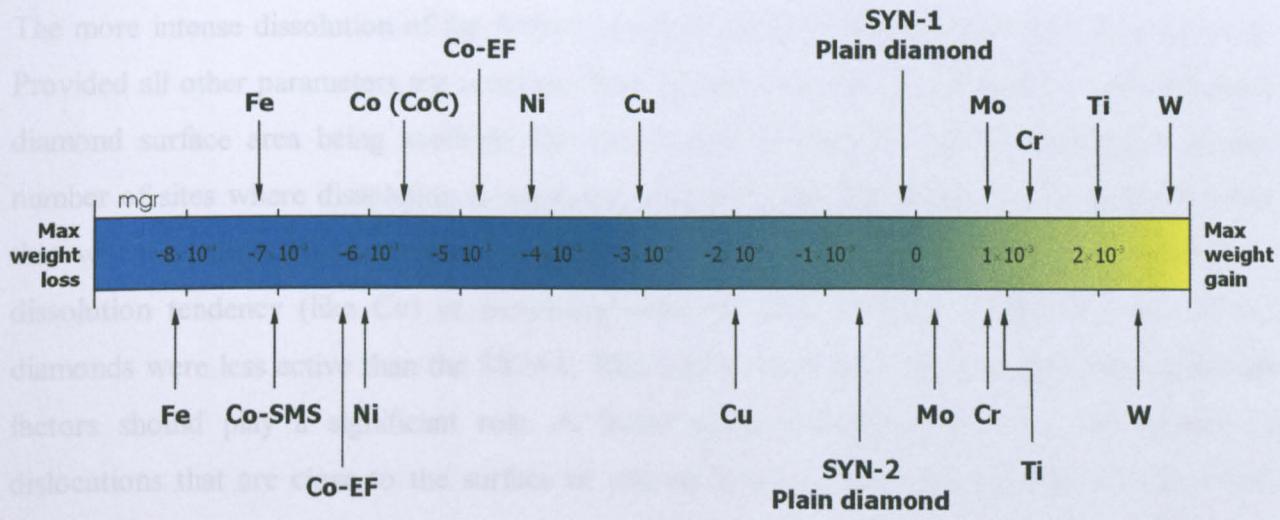

Figure 11-1 : Graphical representation of the average weight changes produced to SYN-1 (SDA100 30/40 US mesh) and to SYN-2 (MBS960 50/60 US mesh) diamonds when heat-treated with metal powders.

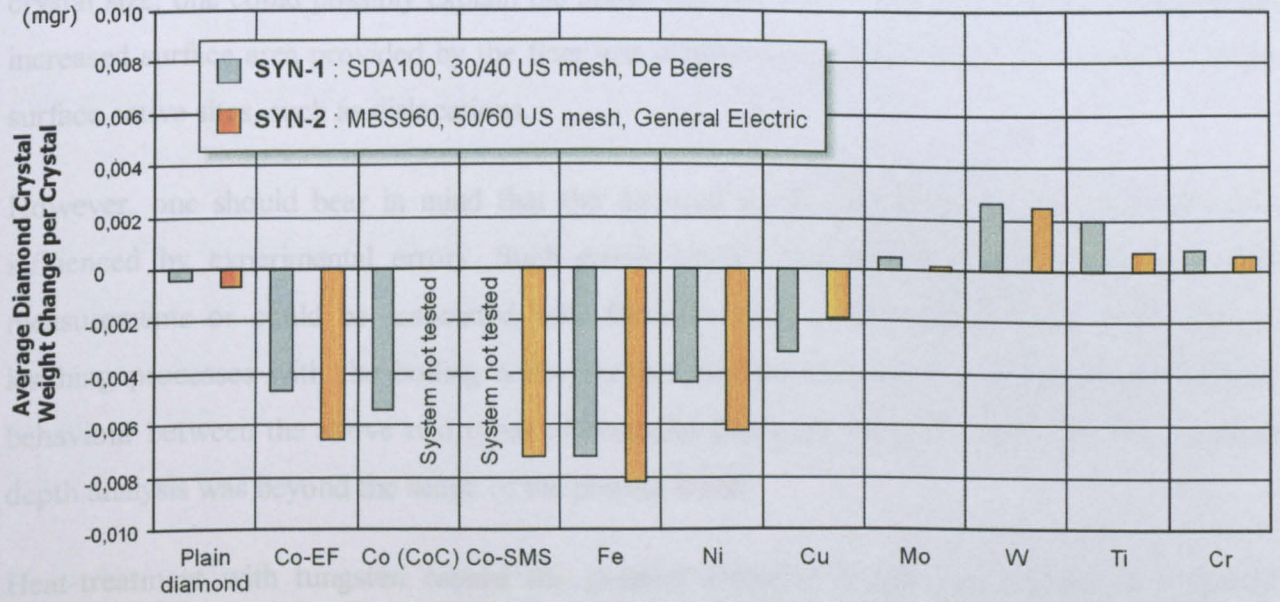

Figure 11-2 : Graphical comparison of the average crystal weight changes produced to SYN-1 (SDA100 30/40 US mesh) and to SYN-2 (MBS960 50/60 US mesh) diamonds when heat-treated with metal powders.

The mode of interaction for all the metals is in accordance with predictions based on thermodynamical and chemical data. The ranking of the metals in terms of carbon dissolution or carbide formation is in general agreement with findings of the experimental work of Tanaka *et al.* [128] and the theoretical study of Sung *et al.* [25], who have evaluated reactivity and solubility of transition metals with carbon, based on the electronic configuration of the elements.

Diamond crystal weight measurements and SEM analysis, indicated that SYN-2 crystals (MBS960 50/60 US mesh, GE) suffered from carbon dissolution to a greater extent when compared to SYN-1 diamonds (SDA100 30/40 US mesh, De Beers) and at the same time their reaction with the carbide forming elements was found to be relatively milder to that of the SYN-1 grains.

The more intense dissolution of the SYN-2 could be justified from a crystal size point of view. Provided all other parameters are constant, finer crystal mesh sizes are associated with increased diamond surface area being available for true contact to metal powders producing a greater number of sites where dissolution is nucleated. However, this approach can not explain the fact that when it comes to heat treatment with metals that are characterised by a decreasing C-dissolution tendency (like Cu) or increasing reactivity (like Mo, Cr, Ti and W), the SYN-2 diamonds were less active than the SYN-1. This controversial behaviour suggests that additional factors should play a significant role. A factor to be considered could be the number of dislocations that are close to the surface or end up at the surface of diamonds. It is now well established that dislocations meeting at the surface of diamonds are preferred sites for the reconstruction or etching of diamond [26, 222-224]. Since dislocation density increases with crystal size, one could possibly explain the above controversial behaviour by considering that the increased surface area provided by the finer grit is balanced by the considerable reduction of the surface active sites, such as dislocations.

However, one should bear in mind that the diamond weight change results could be strongly influenced by experimental errors. Such errors could originate from inaccuracies in weight measurements or could be associated with factors related to the effectiveness of the various leaching processes with the boiling acids. Further investigation into the origin of the different behaviour between the above two types of synthetic diamonds was not conducted, since such in depth analysis was beyond the scope of the present work.

Heat-treatment with tungsten caused the greatest diamond weight gain among all examined carbide forming metals. Interpreting the theoretical ranking in respect to reactivity potential, as expressed by the increasing number of *d*-orbital vacancies (see Table 11-1), one should expect titanium to be the most reacting element followed by tungsten. A reasonable explanation for this result could be credited to the different atomic weights of titanium and tungsten with the latter having an atomic weight that is approximately 4 times that of titanium. However, SEM analysis confirmed that tungsten powder had reacted at a greater degree with the synthetic diamonds and a high concentration of carbide crystallites had formed on the surfaces of the abrasive grains (see §8.3.3.7A and B). It was thus apparent that titanium powders had exhibited reduced reactivity although thermodynamically they should be favoured compared to tungsten. Reasonable explanation to this behaviour could be related to the presence of oxide layers on the surfaces of titanium powders that have inhibited their reactivity. The high number of *d*-vacancies is also responsible for the easier oxidation of titanium compared to tungsten. This is reflected in higher

degree of oxygen levels in the Ti-powders with possible oxide surface layers surrounding the powders. Since the atmosphere in the heat-treatment furnace was not particularly selected to ensure a reducing atmosphere for the Ti oxides it can be postulated that carbon atoms originating from the diamond would be initially consumed in reducing the surface oxides of titanium before reaction could take place. Due to the increased affinity of titanium for oxygen compared to tungsten, a greater amount of carbon would be needed to reduce the oxides with an immediate effect of slowing down the kinetics for titanium carbide formation. This would not only result in reduced quantity of formed carbides, but additionally there would be increased consumption of carbon originating from the diamond; the former being a factor to the measured crystal weight gain, whereas the latter being a factor contributing to the reduction of the diamond weight.

11.2.2.2 Morphological changes occurring to diamonds with heat-treatment with metals

This section contains the discussion of the findings from the microscopic examination of the retrieved diamonds as part of the DRE experiment (refer to Chapter 7).

Microscopic examination of the diamond crystals after the metal and graphite leaching processes that followed the heat-treatment with the various metal powders confirmed the results of the diamond weight change measurements. The surface morphology of the diamonds provided further evidence of the mode (dissolution or reaction) and the relative intensity to which the examined metals had interacted with the diamonds, as discussed in the previous section.

11.2.2.2A Plain diamonds

All three types of diamonds tested throughout this work (SYN-1, SYN-2 & SYN-3) were well-formed cubo-octahedral crystals. SYN-3 (type SDA75, De Beers) was found to be slightly inferior to the other two types of diamonds with respect to crystal imperfections such as cavities, incompletely grown sections etc. This was expected as SYN-3 synthetic diamonds are commercially marketed as inferior quality to SYN-1 (SDA100, De Beers).

Heating the diamonds up to 1025°C in argon was found to produce very little etching to the crystals. The two De Beers grade diamonds (SYN-1 and SYN-3) exhibited similar types of etching although to different magnitudes. The SYN-3 diamonds showed the greatest level of etching. Their octahedral planes {111} were found to be etched by parallel "positively" oriented triangular pits, known as "trigons", at a however different magnitude (see Figure 11-3). Etching of {111} surfaces of synthetic diamonds by positive trigons has been reported by numerous researchers [26, 225]. Cubic surfaces {100} had acquired a fine scale rough morphology that did

not indicate etching by some form of patterned geometry. It could be concluded, that octahedral surfaces were slightly more susceptible to etching than the cubic {100} ones.

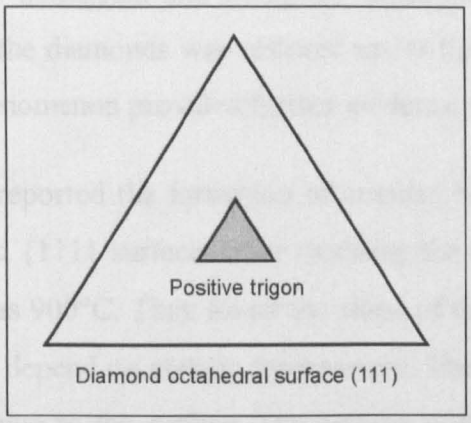

Figure 11-3 : Sketch showing positive orientation of trigons.

The General Electric diamond grade (SYN-2) showed limited signs of trigon pit formation. Their etching proceeded at a fine scale and with no distinguishable pattern.

All three types of diamonds exhibited a relatively low degree of surface modification indicating low levels of surface graphitisation. This correlated well with the nowadays well-established knowledge that in the absence of oxidising agents the onset of diamond graphitisation can be considerably delayed [33, 43]. In fact, under ultra high vacuum the graphitisation starts at temperatures of the order of 1500°C [32]. However, in the presence of oxygen graphitisation can be detected at temperatures as low as 500 – 600°C and becomes significant at temperatures above 700°C [28, 32, 226].

11.2.2.2B Diamonds heat-treated with Co-powders

Three types of cobalt powders, two fine grades (Co-EF, Co-CoC) and one of submicron size (Co-SMS), were used for the heat-treatment with the diamonds. All three types are widely used by diamond tool manufacturers.

SYN-1 (SDA100, 30/40 US mesh, De Beers) diamonds retrieved after the heating with the Co-EF grade and subsequent to chemical removal of Co appeared to have clearly undergone considerable etching. Octahedral {111} surfaces contained a large number of hexagonal and triangular well-shaped depressions formed on relatively flat and smooth diamond surface regions. Larger sized etch pits were filled with a somewhat different material that was far less smooth, contained pores and had terminal edges that were randomly etched. Openings and fissures in this material revealed that an underlying smooth and intact diamond surface existed. At the same time crystals appeared black in the optical microscope. These observations strongly

suggested that the formed material should be graphite. Subsequent leaching with chromic acid removed this material from the large pits and diamond surfaces remained flat and smooth containing only well defined hexagonal and triangular depressions (see Figure 8-13C and D). The bright yellow colour of the diamonds was restored under the light of the optical microscope (refer to Table 8-3). This phenomenon provided further evidence for the graphite formation.

De Theije *et al.* [222] have reported the formation of oriented hexagonal and positive triangular etch pits on cleaved diamond {111} surfaces after oxidising the crystals in various environments and at temperatures as high as 900°C. They found the slope of the sidewalls of the pits as well as the orientation of the pits to depend on etching temperature. The steep point bottomed pits were related to dislocations emerging to the surface. The authors postulated that hexagonal pits were developed from merging trigons that grew parallel to the surfaces at equal speeds but in different directions.

Another possible explanation for the formation of the hexagonal pits could be attributed to the known habit of epitaxial growth of graphite [0001] on diamond octahedral surfaces [25, 33, 43, 227]. However, the simplest approach could be to consider that the etch pits developed on the diamond surfaces should be the mirror image of growth steps or put in other words to be the reverse of the growth process. Visualising the diamond lattice along the octahedral <111> and cubic <100> directions, hexagonal and square geometries forming tunnels travelling along these directions are evident (see Figure 11-4A on next page).

Cubic {100} diamond surfaces showed clear signs of modification. They were almost totally covered by the graphite. After the first leaching process for the removal of cobalt, cubic {100} surfaces appeared to have acquired a relatively rough morphology (see Figure 8-15C), containing pores and numerous large sized cavities (pore sizes of the order of 1-5 microns). Similar to the octahedral surfaces, the secondary leaching process totally removed the graphite and revealed the underlying diamond cubic surfaces, with diamonds acquiring again their macroscopically visible bright yellow colour (see Table 8-3). However, the etch pattern that was revealed did not contain any hexagonal or triangular pits, but it was constructed of numerous parallel oriented truncated pyramidal depressions with either square or rectangular cross-sections (see Figures 8-13D and 8-15D). The larger in size etch pits had flat bottoms, whereas the smaller ones had square cross-sections, with bottoms ending up in a point or line edge (see Figure 11-5 on next page).

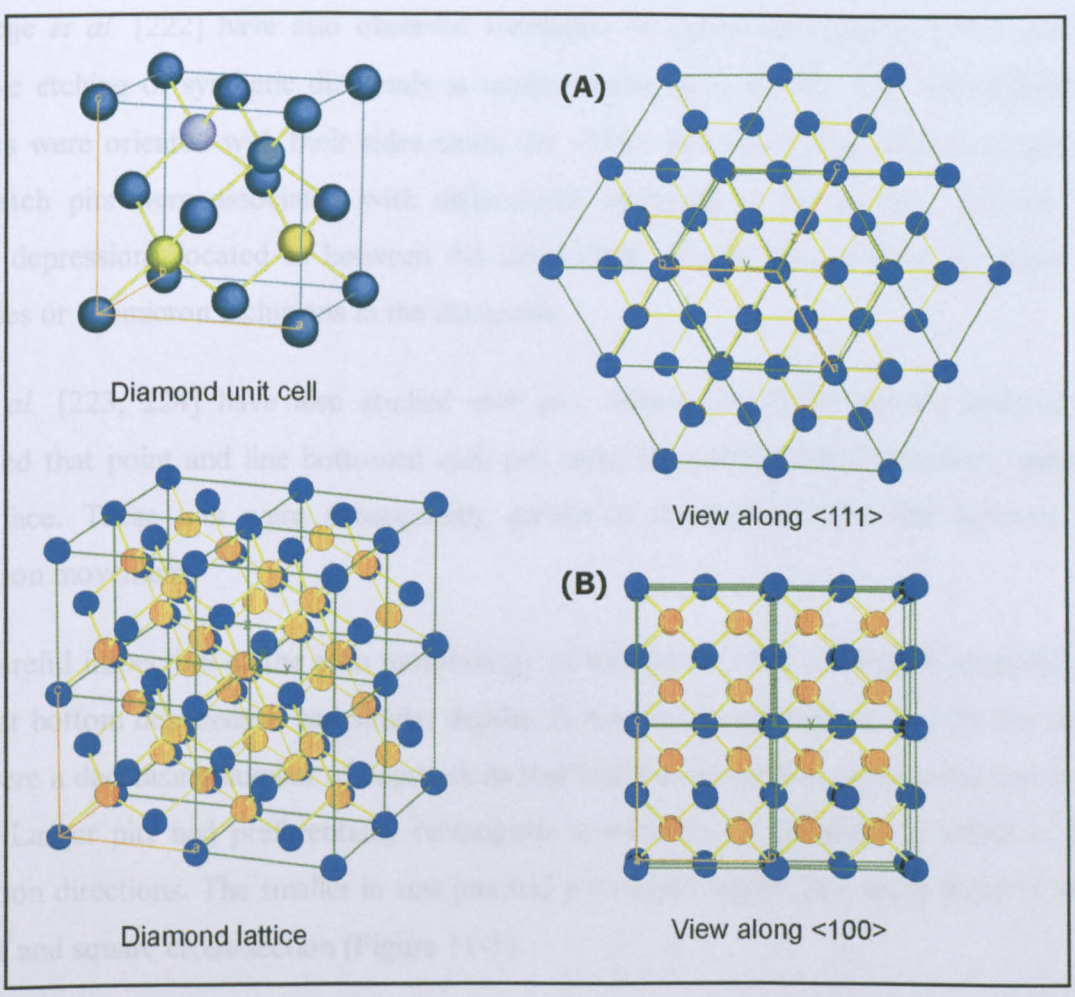

Figure 11-4 : Aspects of the diamond lattice viewed along the (A) <111> and (B) <100> directions.

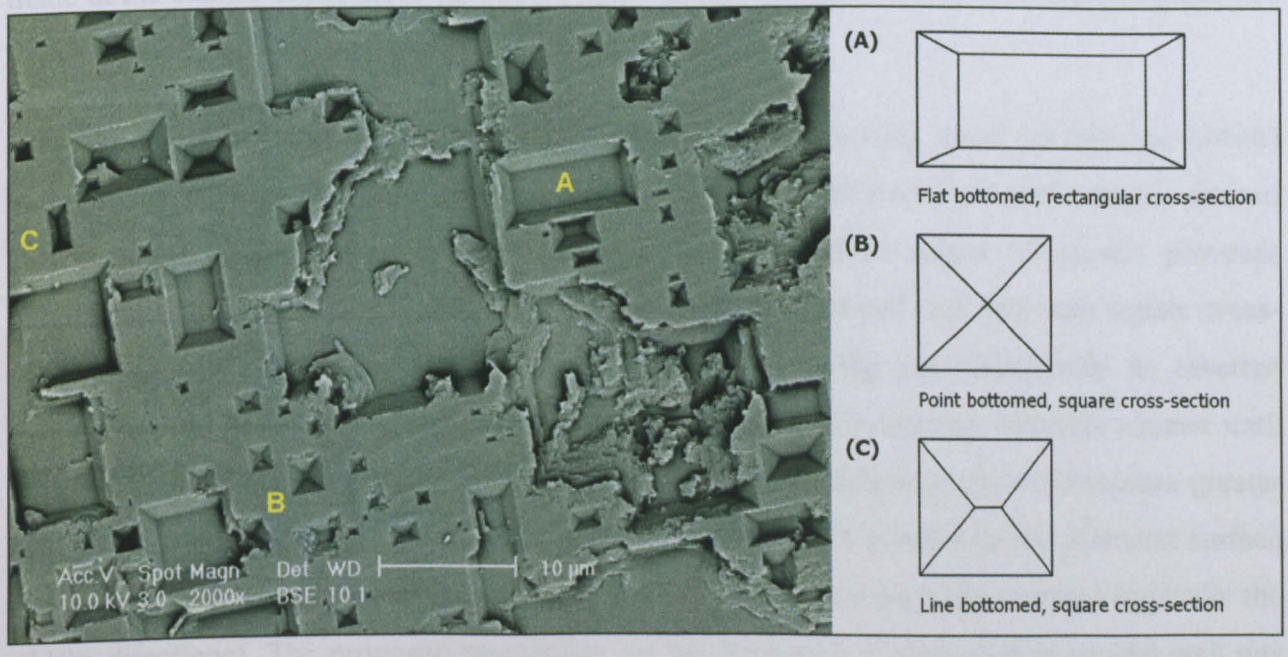

Figure 11-5 : SEM micrograph (BSE mode) showing a cubic surface of a SYN-1 diamond (SDA100 30/40 US mesh, De Beers) annealed with Co-EF powder and treated with chromic acid for graphite removal. The surface contains well defined and parallel oriented truncated etch depressions with rectangular or square cross-sections.

De Theije *et al.* [222] have also observed formation of square etch pits on {100} surfaces in oxidative etching of synthetic diamonds at temperatures up to 900°C. The well-defined square etch pits were oriented with their sides along the <110> directions. The authors suggested that larger etch pits were associated with dislocations emerging at the surface, whereas for the smaller depressions located in between the large ones, growth was credited to agglomerated impurities or submicron inclusions in the diamonds.

Yin *et al.* [223, 224] have also studied etch pits formed on HPHT grown diamonds. They suggested that point and line bottomed etch pits were associated with dislocations emerging at the surface. These pits were subsequently grown to depressions with flat bottoms due to dislocation movement.

After careful inspection of the etch morphology of the cubic {100} surfaces it appeared that all large flat bottom depressions had similar depths. It was also noted that as etch pit size increased there were a decreasing number of depressions that had a cross-section close to the geometry of a square. Larger pits had preferentially rectangular cross-sections elongated to either of the two orientation directions. The smaller in size pits had pyramidal shapes with sharp point or edge line bottoms and square cross-section (Figure 11-5).

Taking into consideration the above described observations and combined with the suggestions made in the studies of the afore mentioned authors, a mechanism for the etching/graphitisation of diamond cubic surfaces is proposed as follows.

With the effect of temperature and the presence of the C-dissolving metal (in this case cobalt) etch pits are nucleated on the diamond cubic surfaces. Etch pits nuclei are preferentially formed at the points where dislocations emerge to the surface. Initial stages of growth proceeds perpendicular to the diamond cubic surface forming point bottomed etch pits with square cross-sections. Formation of pits with such a geometry appearing macroscopically as inverted pyramids could be associated with screw dislocations. Growth continues with this manner until the pit reaches a certain depth at which the driving force for sideways growth becomes greater than that for perpendicular growth. The etch pit is then grown parallel to the diamond surface along one of the two directions to which the etch pits are macroscopically oriented (typically the <110> directions). The proposed mechanism for the formation of truncated pyramidal etch pits on diamond cubic surfaces is given schematically in Figure 11-6.

Further investigation into the origins of the etch pit shapes developed on diamond surfaces was beyond the scope of the work presented with this thesis.

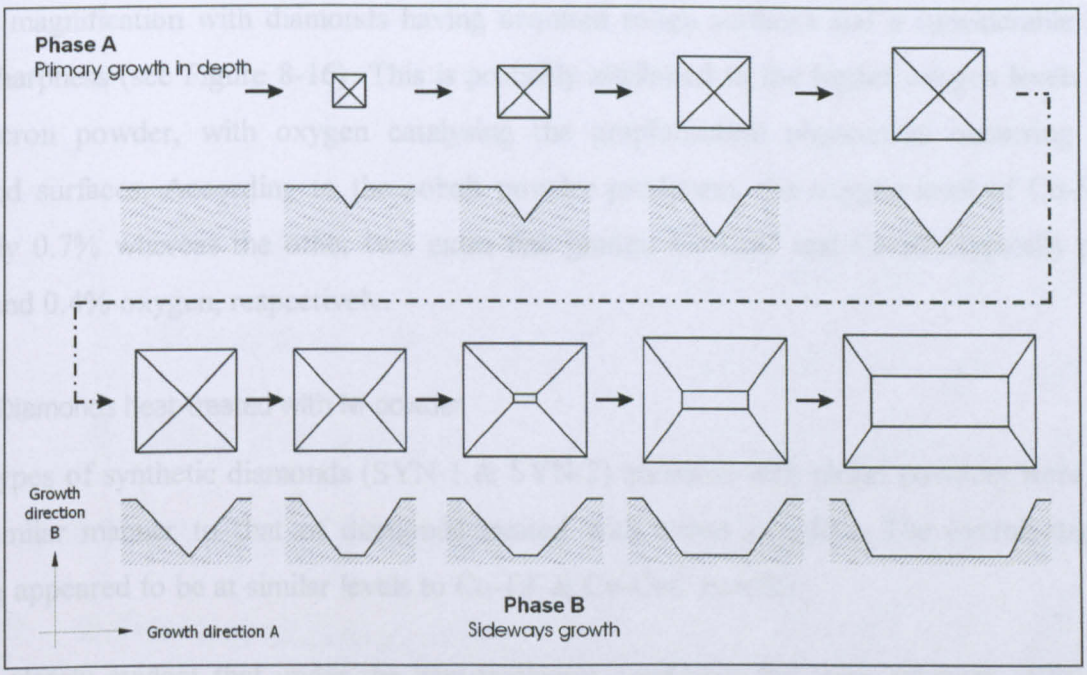

Figure 11-6 : Proposed mechanism for the formation and growth of the oriented truncated pyramidal depressions found on etched / graphitised diamond cubic {100} surfaces.

As described above, microscopic analysis after the metal leaching showed a graphite layer that covered portions of both octahedral {111} and cubic {100} surfaces (see Figures 8-13B and 8-15B and C). This indicates that carbon atoms break away from the diamond structure forming graphite and do not dissolve directly into the metal. The fact that graphite layers were found on the surfaces suggests that the rate for graphite formation was higher than the rate with which it was consumed by dissolving into cobalt. Manukyan *et al.* [114] have also addressed the possibility of development of interfacial graphite if the speed of reaction or dissolution of the graphite to the metal in contact is slower than the speed of its formation (see also §4.3, p.37). The observed phenomenon could also be the result of areas on the diamond surfaces not being in true contact with the loose cobalt powders, since the diamond powder mixture was not compacted prior to the heat treatment.

Heat-treatment of the SYN-1 diamonds with the Co (CoC) type powder produced similar type and magnitude of etching as was observed with the Co-EF grade (see Figure 8-14).

The SYN-2 (MBS960, 50/60 US mesh, General Electric) diamonds exhibited the same type of etching as that of SYN-1. However, their degree of diamond dissolution was clearly greater than that observed for the SYN-1 confirming the results obtained with the diamond crystal weight measurement experiment (see Figure 8-15A).

Greatest dissolution etching was found for the SYN-2 diamonds that had been treated with the sub-micron size cobalt powder (Co-SMS). The greater degree of etching was clearly visible even

at low magnification with diamonds having acquired rough surfaces and a considerable loss of edge sharpness (see Figure 8-16). This is probably attributed to the higher oxygen levels of this sub-micron powder, with oxygen catalysing the graphitisation phenomena occurring at the diamond surfaces. According to the cobalt powder producers, the oxygen level of Co-SMS is typically 0.7% whereas the other two extra fine grades, Co-CoC and Co-EF, typically possess 0.5% and 0.4% oxygen, respectively.

11.2.2.2C Diamonds heat-treated with Ni-powder

Both types of synthetic diamonds (SYN-1 & SYN-2) annealed with nickel powders were etched in a similar manner to that of diamonds treated with cobalt powders. The overall degree of etching appeared to be at similar levels to Co-EF & Co-CoC powder.

It was clearly evident that under the heat-treatment conditions the cubic surfaces {100} of the diamond crystals had been etched by nickel at greater levels than the octahedral {111} ones (see Figures 8-21 and 8-22). This observation contradicts the ranking found by numerous researchers who studied the oxidation and graphitisation rates of the various surfaces of synthetic diamond crystals in oxidising atmospheres or high vacuum respectively [33, 137, 228]. However, studies on the wetting of diamond surfaces by molten metals and alloys have shown the cubic surfaces to be those exhibiting the highest affinity for metals, either with the formation of carbides or with carbon dissolution [128]. Cubic surfaces were also etched at high levels when hot-pressed with various cobalt-based alloys in the study of Liao *et al.* [229]. Although not mentioned by the authors, it was clearly evident as seen in the published SEM micrographs that the diamond cubic surfaces were etched relatively more than the octahedral ones.

From examining the diamond crystal structure it follows that cubic {100} surfaces have two dangling bonds associated with each carbon atom if they are visualized as being the terminal surfaces, whereas the octahedral {111} surfaces have only one dangling bond per carbon atom (see Figure 11-7). If one considers that oxygen catalysed graphitisation would require the reaction of oxygen atoms with carbon atoms it could be postulated that the availability of two dangling bonds would be much more effective, thus explaining the observed increased reactivity of the cubic surfaces. The fact that cubic {100} diamond planes are much less dense than the octahedral {111} planes also points to the same conclusion. Furthermore, easier removal of carbon atoms from cubic {100} surfaces can be recognised from the lower abrasion resistance exhibited by these surfaces when abraded in random direction compared to the octahedral {111}.

Results of abrasion tests on diamonds have shown largest depths of cuts to be produced on the cubic {100} surfaces when abraded in random directions [230, 231].

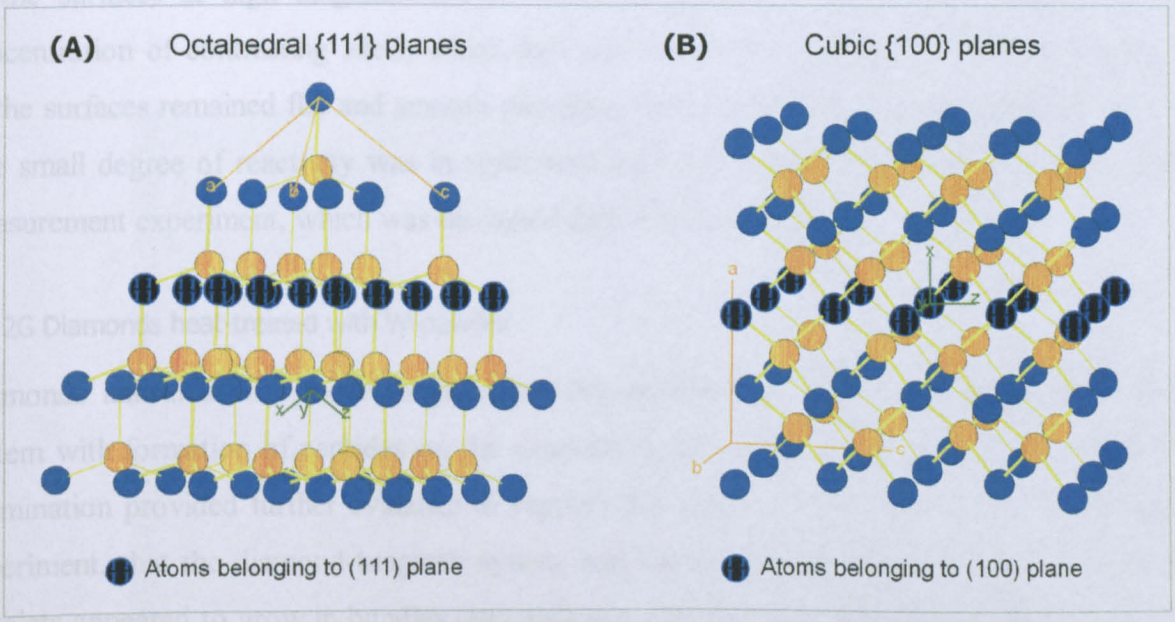

Figure 11-7 : Aspects of the diamond lattice viewed in suitable way to show the dangling bonds for the octahedral (A) and cubic planes (B).

11.2.2.2D Diamonds heat-treated with Fe-powder

Dissolution etching of both diamond types by the iron powder resulted in the formation of thick graphite layers on diamond surfaces. The degree of surface etching was much greater than all the other systems producing extended surface modification to the diamonds (see Figures 8-24A and 8-25). Crystals were considerably roughened and rounded. Careful examination of the surface topography indicated that the mechanism of etching was the same as that proposed above, with etching of {111} and {100} surfaces to have proceeded by the nucleation and growth of hexagonal and rectangular pits respectively. Because of the increased dissolution intensity of Fe, the etch pits had grown in to each other as well as perpendicularly to the planes, producing the final extensively roughened topography visible in the SEM after the graphite leaching process.

11.2.2.2E Diamonds heat-treated with Cu-powder

Copper powder produced the smallest degree of diamond dissolution from all tested metals (see Figure 8-18A). Although diamonds were annealed with copper to temperatures up to 1025°C, C-dissolution was kept to low levels and the crystals had retained their angular shape and sharp edges. Etching on the octahedral {111} surfaces had occurred with oriented shallow trigons, whereas on cubic {100} surfaces by numerous shallow pits. Similar to the cobalt systems, SYN-2 diamonds had been etched at slightly higher levels and the cubic {100} surfaces were found most susceptible to dissolution / graphitisation than the octahedral {111} ones.

11.2.2.2F Diamonds heat-treated with Mo-powder

Diamonds annealed with the molybdenum powder remained practically unaffected. Examination of the surfaces at high magnification in backscattering mode of the SEM revealed a small concentration of contrasting islets, which indicated nucleation of carbides. The remaining parts of the surfaces remained flat and smooth providing evidence that no dissolution had taken place. The small degree of reactivity was in agreement with the results of the diamond crystal weight measurement experiment, which was discussed earlier in this chapter.

11.2.2.2G Diamonds heat-treated with W-powder

Diamonds annealed with loose tungsten powder provided an excellent example of a reactive system with formation of carbides on the diamond surfaces (see Fig. 8-29 and 8-30). The SEM examination provided further evidence to support the results of the crystal weight measurement experiment, that the diamond-tungsten system was the most reactive. Carbide sub-micron sized platelets appeared to grow in bundles outwards from the diamond surface. The orientation of the platelets in each bundle appeared to be random. High magnification imaging revealed that the diamond substrate, where platelets had grown, was slightly etched compared to the flat and smooth non-reacted surfaces. This indicated that platelets had preferentially formed at the sites were etching had initially taken place. This supported the hypothesis that reactivity with diamond is possible when C-atoms are broken-out of the diamond structure. Whether graphite was formed prior to diffusion of C-atoms into the interstitial sites of the W-metal to form the carbides or whether the C-atoms were directly entering the metal upon release from the diamond structure was not possible to be identified and was beyond the scope of the present work.

The intersecting carbide platelets formed an even and almost complete coating of the surfaces of the SYN-1 diamonds. Coverage was incomplete only at the edges of the surfaces. Comparing the reactivity intensity between the two types of tested synthetic diamonds, it was clearly apparent that SYN-1 (SDA100, 30/40 US mesh, De Beers) diamonds had reacted to a greater extent than the SYN-2 (MBS960, 50/60 US mesh, General Electric). As it was explained earlier in this chapter (§11.2.2.1), this behaviour could be related to the greater number of dislocations emerging at the diamond surfaces associated with larger sized crystals. A variation in reactivity was also evident between the octahedral {111} and cubic {100} surfaces of the diamond crystals, with the latter being the more reactive (see Figure 11-8).

Graphite leaching resulted in the total removal of the carbide platelets. The uncovered diamond surfaces contained numerous shallow etch pits. These had either hexagonal or rectangular form

on the octahedral {111} and cubic {100} surfaces respectively (see Figure 11-9). This morphology of the etch pits suggests that dissolution etching takes places during the initial stages of the interaction between tungsten and diamond. The mechanism of this process could be similar to that proposed earlier in this section for the case of the diamond-cobalt system.

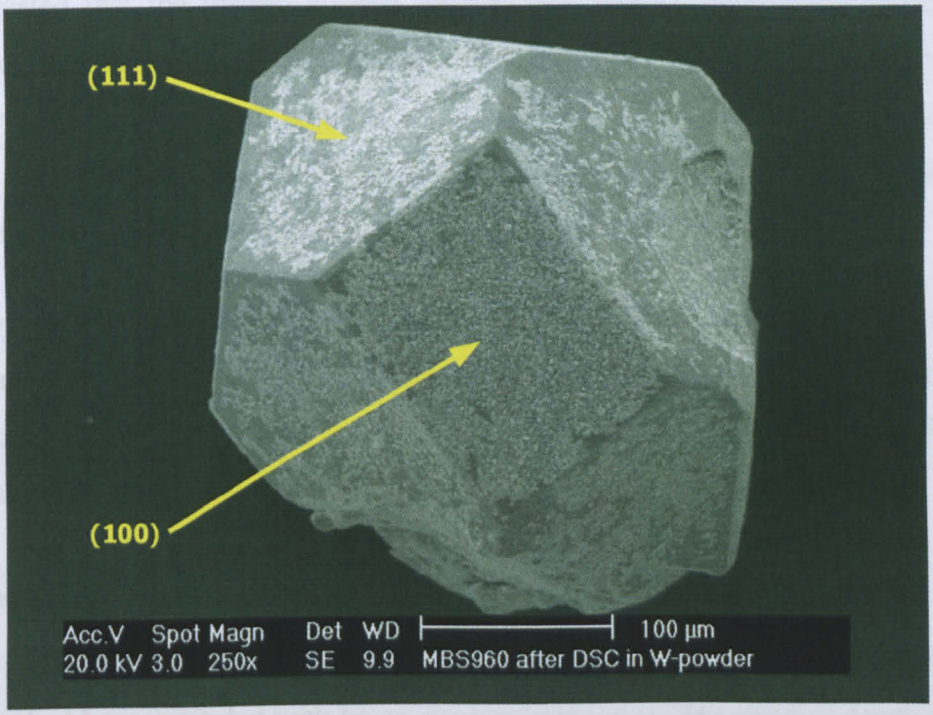

Figure 11-8 : SYN-2 type diamond crystal (MBS960, 50/60 US mesh, General Electric) retrieved after the metal leaching process that followed the annealing with the tungsten powder. The coverage of diamond surfaces with carbide platelets is higher for the cubic {100} surfaces.

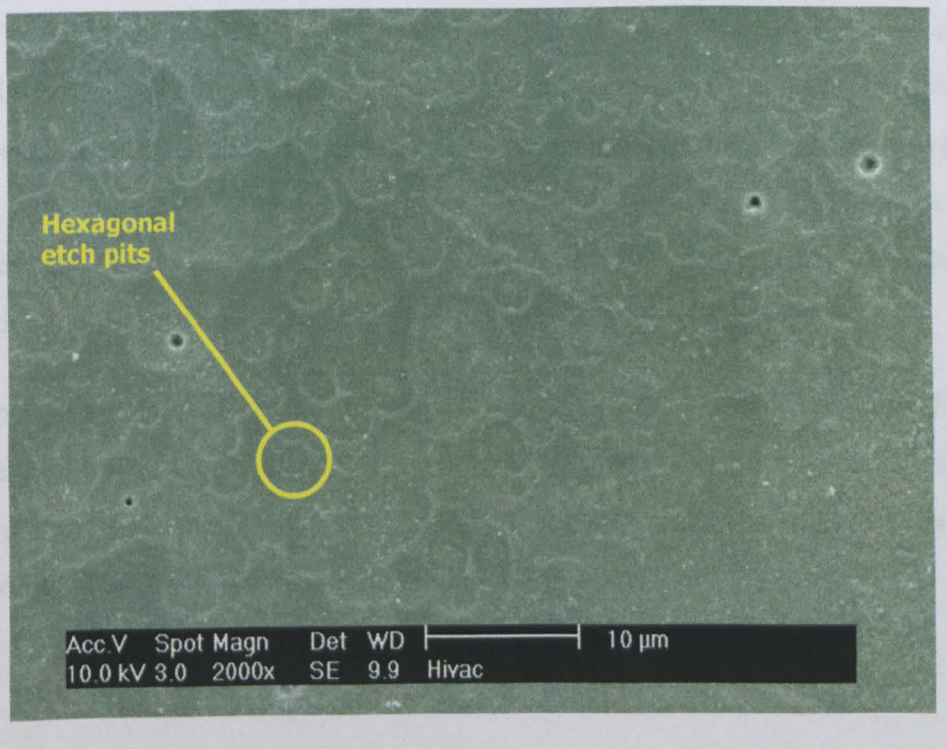

Figure 11-9 : Octahedral {111} surface of a SYN-2 diamond crystal (MBS960, 50/60 US mesh, General Electric) that had been annealed with the tungsten powder. The crystal has been subjected to two sequential leaching processes for the removal of the metal and graphite respectively. Hexagonal etch pits are clearly evident on the diamond surfaces.

11.2.2.2H Diamonds heat-treated with Ti-powder

The SEM examination confirmed that the diamond-titanium system was the second most reactive. SYN-1 crystals retrieved after the metal Ti leaching process had developed a thin coating layer (see Figure 8-33A). The fact that the coating was not dissolved during the leaching process suggested that the formed layered product was mainly composed of titanium carbide. The extensive cracking and peeling of the coating provided evidence of the brittle nature of the carbide layer. Stripped diamond surfaces were relatively smooth with only a very fine scale etching. This verified that titanium did not dissolve diamond. Etching only took place at a small degree and released carbon atoms were consumed in forming the titanium carbides.

The reactivity of the SYN-2 diamonds with the Ti-powder was greatly reduced compared to what was found for the SYN-1 diamonds (see Figure 8-34). One possible explanation for this behaviour could be related to the concentration of dislocations emerging to the diamond surfaces, as has been addressed earlier in this section.

11.2.2.2I Diamonds heat-treated with Cr-powder

Microscopic inspection revealed that a reaction product had formed on the surfaces of the SYN-1 diamonds that had been annealed with loose chromium powder. The reaction product had formed as a dense layer in the shape of a coating (see Figure 8-40). However it was extensively fractured into large pieces separated from each other with gaps of the order of 1 to 2 microns. A closer inspection of the surface morphology revealed that each piece of the coating layer could form a continuous layer if brought in contact with the neighbouring pieces. The whole pattern resembled a crazed surface. This observation suggested that a continuous coating had formed at the elevated annealing temperature and was subsequently cracked into pieces due to thermal contraction effects. The fact that the reaction product could withstand the extensive leaching process provided strong indication of chromium carbide formation.

Similar to other systems discussed previously, the cubic {100} surfaces of the diamonds exhibited the highest reactivity in terms of the degree of coverage by the chromium carbide layer. In agreement with the results of the other systems presented above, the reactivity of the SYN-2 diamonds with the Cr-powder was greatly reduced.

11.2.3 Interactions in Hot-Pressed Diamond – Metal Composites

The previous sections discussed the mode and relative intensity of the interactions between synthetic diamonds and selected metal powders. Having acquired a basic knowledge of the interactions in these systems, it became possible to examine to what extent these interaction phenomena occur when the diamond-metal systems are forced to interact under industrial conditions, which represent the real situation in which these systems are treated. The conditions and environment chosen in which to study the interactions should be a true representation of the industrial practice. For that reason it was selected to consolidate the samples by hot-pressing, which is by far the most widely employed manufacturing process.

Cold-pressed diamond-metal green compacts were consolidated with hot-pressing in graphite moulds at 850°C for 3 minutes. Because some of the refractory metals could not sinter at the above temperature, the list of metals examined was limited to those that are typically sinterable at the above selected hot-pressing conditions. The list of examined systems is given in Table 7-4 of Chapter-7.

Apart from the diamonds sintered with molybdenum, all of the other microscopically examined diamonds retrieved from the leaching baths of the consolidated samples had acquired a surface morphology that indicated considerably lower levels of dissolution etching compared to the equivalent diamond-powder metal systems as discussed previously. However, the relative ranking of the metals in terms of the etching that they produced on the diamond surfaces was in agreement with the findings presented earlier.

The reduced attack on the diamonds is attributed to the lower temperature at which the systems were exposed combined with the very short dwell time at the maximum temperature as well as with the considerably higher heating and cooling rates involved in industrial hot-pressing compared to those applied during the DSC heat-treatments. Another factor that could be responsible for the inhibited attack on the diamonds is the reducing sintering atmosphere (CO & CO_2) produced by the graphite moulds [226]. The presence of such a reducing atmosphere could decrease the amount of diamond consumed in reducing the oxides present in the metals and thus inhibit the etching processes.

Graphite had formed on the surfaces of diamonds hot-pressed with iron, nickel and cobalt as was observed in the SEM and as indicated by the black/grey colouring of the crystals under the optical microscope (see Table 8-4). Subsequent leaching of the graphite revealed the etched diamond surfaces. Hexagonal and tetragonal depressions were found on the octahedral {111}

and cubic {100} diamond surfaces respectively conforming to previous results. The size of these etch pits was considerably reduced compared to those formed during annealing of the loose powders with the diamonds in the DSC furnace under argon atmosphere. This further indicated that the process of dissolution of the diamond surfaces had remained in the primary stages. It provided evidence however that the same mechanism of dissolution etching was in effect. Similarities with the previously discussed results were also found for the relative intensity at which the various surfaces of the diamonds had been etched. It was again confirmed that under the hot-pressing conditions, the cubic {100} diamond surfaces appeared to be etched at greater levels than the octahedral {111} ones.

Diamonds sintered with copper, bronze (85/15) and molybdenum remained practically unaffected. Copper and bronze caused a very fine scale etching with only few oriented trigons visible on the octahedral {111} diamond surfaces. The relatively inert action of copper is typical at standard hot-pressing conditions [60, 188-189]. The presence on tin (Sn) has also been known to further reduce the degree of diamond etching [229, 232]. On the other hand, hot-pressing diamond with molybdenum, which is a known carbide former, produced no reaction product or any large-scale dissolution etching. High magnification imaging revealed only the formation of some small trigons on the octahedral {111} surfaces. It is apparent that with the selected hot-pressing conditions the reaction to form carbides was not favoured.

11.2.4 Interactions in Metal-Coated Diamonds

Metal-coated diamonds have been microscopically examined after metal and graphite leaching processes similarly to the diamond-metal systems previously discussed. The various types of metal-coated diamonds were examined in three states, which were:

- "as received" metal-coated crystals,
- metal-coated diamonds annealed at high temperature (1025°C) in the DSC furnace, and
- metal-coated diamonds annealed at a lower temperature of 500°C for 20 minutes in a H_2/N_2 reducing atmosphere, which is typical industrial practice.

The examination of the "as received" crystals served the need to identify the type of the deposited coatings and the possible effects of the deposition method on the diamond. The inspection of the annealed coated-diamonds aimed to detect possible diamond-metal interactions produced by the two heat-treatment methods.

11.2.4.1 Titanium coatings

Two types of vapour deposited titanium-coated diamonds were tested. Both deposition methods have resulted in the formation of dense coatings with thickness of the order of 1 micron.

11.2.4.1A Chemical-Vapour-Deposited (CVD) coating

Chemical vapour deposited titanium layers on diamonds had formed with a columnar structure, typical of CVD coatings [167]. X-ray diffraction (XRD) measurements of the "as-received" Ti-CVD-coated diamonds did not detect the formation of any titanium carbides. Metal leaching caused the total removal of the Ti-coatings confirming the XRD results and providing further evidence that the coatings were totally composed of titanium metal and that no reaction to form carbides with the diamond substrate had occurred. The stripped diamond surfaces appeared to have very limited degree of etching indicating that the crystals have not been damaged from the high temperature deposition. High magnification examination of the uncovered diamond surfaces revealed that a few small trigons had formed on octahedral {111} surfaces. These had both positive and negative orientations. The cubic {100} surfaces remained practically intact, exhibiting only a relatively very fine scale etching of no particular pattern at certain locations. Etching intensity appeared to be greater for the {111} surfaces conforming to the well-known preference of graphitisation of the octahedral surfaces compared to the cubic [33].

Annealing of the Ti-CVD coated diamonds in the DSC furnace (temperature reaching 1025°C) resulted in the coating remaining attached onto the crystals even after the treatment with boiling acids for titanium removal. This provided strong indication of titanium carbide formation. A number of authors have indicated that carbide formation of metallized diamonds takes places only after annealing [134, 170]. Carbides may start to form at temperatures as low as 300°C in high vacuum, but typically temperatures in excess of 800°C are needed to yield considerable levels of reaction [134, 172]. The coating was brittle and that was evident from its extensive cracking. Cracking is attributed to thermal contraction effects during cooling down as well as to the handling of the crystals such as leaching and sieving processes. Uncovered crystal surfaces showed negligible levels of diamond etching demonstrating the protective effect of the coating to high temperature exposure, which has been also claimed from other researchers [114].

Leaching of Ti-CVD coated grit after annealing at a lower temperature of 500°C resulted in total removal of the metallic layers indicating that carbide formation was not achieved. However, inspection of crystal surfaces at high magnification revealed the presence of small angular crystallites emerging from the diamond substrate. These crystal nuclei resisted the dissolving action of the boiling acid and were thus considered to be carbide crystals. However, their concentration and spreading over the diamond surfaces suggested reaction to have occurred locally and at limited levels. The etching of the surfaces was negligible providing evidence that the annealing did not affect the diamond.

11.2.4.1B Physical-Vapour-Deposited (PVD) coating

Observations made on titanium-coated diamonds by physical vapour deposition (PVD) were similar to those of the CVD coated grit discussed above. Reaction did not take place during deposition but occurred to a considerable extent during annealing in the DSC furnace. The reacted coating was cracked and upon subsequent leaching revealed that the underlying diamond surfaces contained a great number of carbide crystallites growing outwards from the diamonds surface. The crystallites had shapes resembling rectangular parallelepipeds. Their horizontal orientation appeared to be random whereas it was recognized that they had a tendency to be aligned perpendicularly to the diamond surface. In agreement with the CVD-coated grit, it seemed that the reactivity of octahedral {111} surfaces was greater than that exhibited by the cubic {100}. Both annealing processes caused no particular etching to the diamonds, confirming that coating offered a good protection to high temperature processing.

Comparing the two types of examined Ti-coated diamonds in terms of the degree of carbide formation on annealing finds the PVD-coating to be slightly more reactive than the CVD one.

11.2.4.2 Chromium coatings

Two types of chromium-coated diamonds have been examined. Both types of coatings were formulated by PVD on the SYN-3 grade diamonds (SDA75, 30/40 US mesh, De Beers), which is of inferior quality to the SYN-1 grade used with titanium. The first type was a standard chromium coating whereas for the second type of coating, the deposition of chromium was carried out with simultaneous deposition of carbon. The latter were termed as carbon-enriched chromium-coated diamonds and designated as "Cr(C)". The thickness of both coatings were typically of sub-micron size. However, especially for the carbon-enriched type, thickness occasionally and locally reached higher values and in some cases was up to 2 microns (Fig. 8-3).

11.2.4.2A Standard chromium PVD-coating

Metal leaching resulted in almost total removal of the Cr-coating of the "as-received" crystals. However, fractions of the coating resisted the leaching, indicating possible carbide formation. The regions where this had occurred were crystal defected areas, such as cavities and fractured corners, which were readily available for the SYN-3 diamonds (see Figure 8-42A). Considering such defected areas to be preferred sites for carbon atoms to break away from diamond structure provided a good reasoning for carbide formation. This conformed to the report of Manukyan *et al.* [117] on the ability of chromium coatings to fill surface irregularities. The authors postulated that chromium "healed" the diamond surface defects and it was for that reason lower decreases in strength due to high temperature treatment were monitored for the Cr-coated grit. Oganyan *et al.* [142] claimed that chromium was more effective at healing the diamond surfaces compared to other metals (Ti, W etc.) because of its smaller atomic radius, which enabled it to penetrate more easily confined surface defects.

Almost the entire coating remained attached onto the diamonds after the leaching process when the Cr-metalized diamonds had been annealed in the DSC furnace (see Figure 8-42B). This provided strong indication of extended chromium carbides formation. The coating was extensively fractured and cracked which were the results of the thermal contraction effects, attributed to the large mismatch in thermal expansion coefficients between diamond and chromium carbides (see Table 4-4). When annealing took place at the lower temperature of 500°C, only fractions of the coating remained bonded to the diamond after the leaching process. This gave reasons to consider carbide formation to have progressed at reduced levels with major

part of the coating to be chromium metal, which was easily removed by the leaching acid medium. The low number of carbide crystallites found on diamond surfaces after the final leaching in the chromic acid, supported the hypothesis that at the lower temperature carbides had only formed to a limited extent at certain points of the interface.

For all types of examined crystals discussed above, the diamond surfaces free from the coating were relatively smooth and flat indicating very low levels of etching, suggesting both that the deposition process did not deteriorate the diamonds but also that the formed coating protected the crystals during the annealing treatments.

The above findings are in agreement with the results of several researchers who examined chromium depositions from gaseous phases. Carbide formation has been detected during deposition of chromium from gaseous phases [120, 167-168]. Studies have shown, that upon formation of a carbide thin film at the diamond/coating interface the reaction of the outer section of the coating is controlled by the rate at which carbon atoms are released from the diamond structure and are diffused through the interfacial carbide layer. This is the reason why higher temperatures and prolonged deposition or annealing times are associated with higher carbide levels in chromium coatings as has been reported by several authors [134, 143, 172]. At the initial stages of interaction lower carbides are formed (Cr_7C_3) [143]. If conditions are such to allow sufficient diffusion of carbon atoms to occur, inner carbides are gradually saturated in carbon and transform into higher carbides (Cr_3C_2), whereas outer coating regions react to form Cr_7C_3. Chuprina *et al.* [143] reported that at temperatures of the order of 1000°C the rate of chromium carbide formation was considerably high, similarly to what was observed for the Cr-coated diamonds annealed in the DSC furnace. It is for this reason that Chattopadhyay *et al.* [120] had to reduce the deposition temperature and time in order to inhibit excess reaction and avoid the extensive cracking of the coating.

The protective function of chromium coatings in terms of oxidation resistance and in minimizing the strength decrease associated with high temperature treatment of synthetic diamonds has been identified in the several reports [136, 144].

11.2.4.2B Carbon-enriched chromium PVD-coating [Cr(C)]

Examination of "as received" Cr(C)-coated diamonds indicated that although carbon was simultaneously deposited with chromium, no carbide formation had taken place. However, on annealing in the DSC furnace extensive reaction took place, with the coatings remaining entirely on the diamond surfaces even after the leaching process (see Figures 11-10 and 8-19, 8-20). This

was attributed to the carbon content of the coating. For this coating, the availability of carbon atoms for reaction with the chromium was not dependent on diffusion from the diamond, but temperature alone was the controlling parameter. This hypothesis was supported when examining the coated diamonds that have been heat-treated at the lower temperature of 500°C. For these diamonds leaching caused almost the total removal of the coating with only a few sites of possible reaction.

The hard coating formed with the high temperature annealing in the DSC furnace contained some cracks. However, these were considerably reduced in number compared to those that had formed at the plain chromium coated grit. Subsequent removal of the hard coating revealed diamond surfaces with clear signs of reaction with the coating.

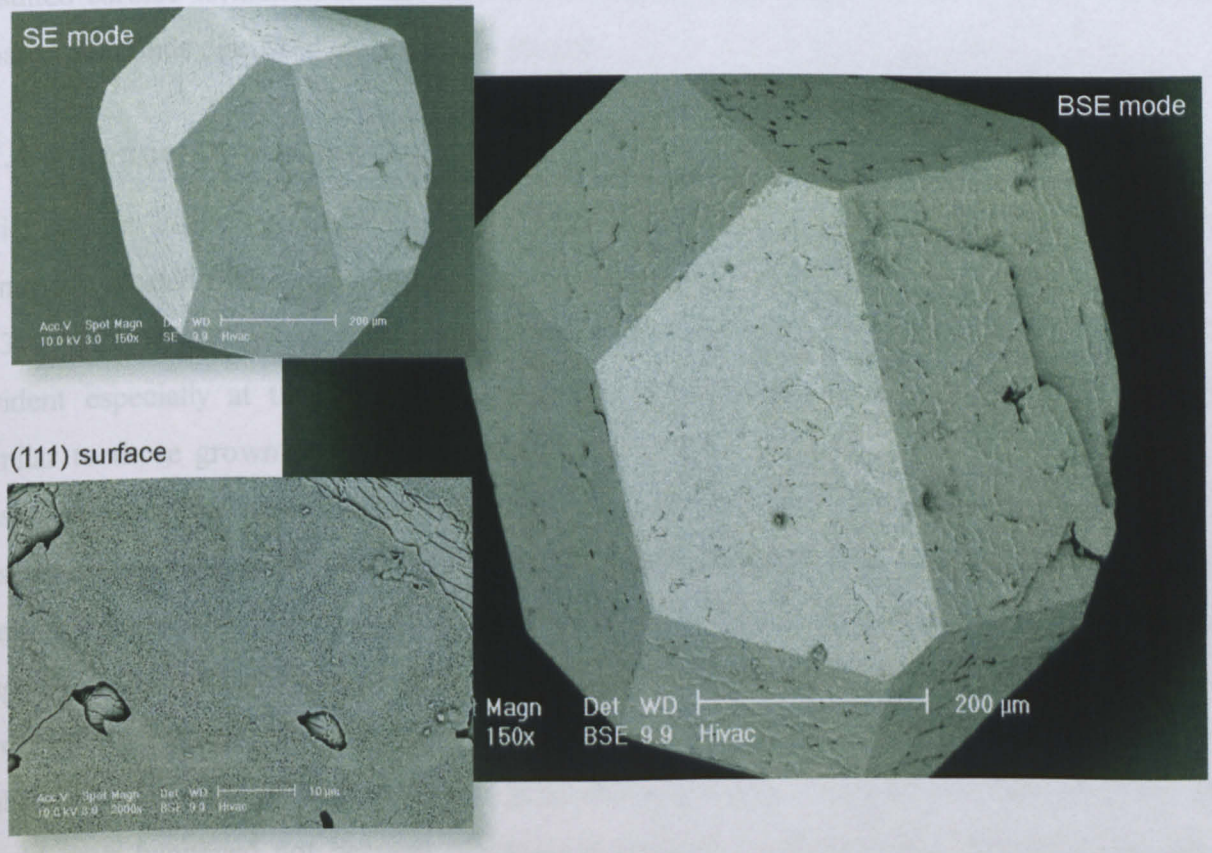

Figure 11-10 : SEM micrograph (backscattered mode) of a PVD C-enriched Cr-coated SYN-3 diamond (SDA75 30/40 US Mesh by DB) initially heat-treated in the DSC furnace and subsequently subjected to metal leaching. The coating did not dissolve by the leaching, but instead remained attached on diamond surfaces indicating strong carbide formation.

11.2.4.3 Titanium/Chromium Dual coating

The dual titanium/chromium-coated crystals were formed with simultaneous PVD deposition of the two metals on to the SYN-3 diamonds.

The dual component coating was totally removed with the leaching treatment, indicating that reactions had not been favoured. Stripped diamond surfaces showed no signs of any degradation,

providing proof that, similarly to the other PVD coatings discussed above, the deposition did not appear to have deteriorated the diamonds.

Annealing the encapsulated grit in the DSC resulted in large parts of the coating remaining attached to the diamond surfaces even after the first leaching process (see Figure 8-46), suggesting that partial reaction to form carbides had been achieved. The coating was preferentially bonded on crystal defected areas such as cavities and surface irregularities possibly associated with the easier detachment of carbon atoms from such sites as discussed earlier for the Cr-PVD-coated diamonds. Coating layers were cracked as a result of the contraction during cooling attributed to the considerable thermal expansion coefficient difference between Ti- and Cr-carbides with diamond (see Table 4-4). Heat-treatment at a lower temperature of 500°C resulted carbide formation to very limited (see Figure 8-47), similar to that found for the other coated diamonds discussed earlier in this section.

11.2.4.4 Tungsten coating

Microscopic inspection of W-coated SYN-3 diamonds after having been leached for metal removal revealed that some limited reaction had occurred during the PVD deposition (see Figure 8-31A and B). Annealing of the coated grit in the DSC promoted reactivity. This was clearly evident especially at the defected areas of the crystals where carbide platelets had formed, similar to those grown on diamonds treated with W-powder. Carbide reaction at these sites is associated with the easier detachment of carbon atoms from the diamond structure as has been discussed in previous sections. Platelets appeared to be growing outwards onto a modified diamond surface, which was associated with hexagonal patterns (see Figure 11-11). This suggested that carbides had been formed on transformed diamond surfaces, which would most probably be interfacial graphite. This hypothesis was supported by the observation that subsequent leaching with the chromic acid resulted in entire removal of these platelets. This could have happened not because of chemical removal of the carbides, but rather because of detachment of the coating due to the dissolution of the graphite substrate. However, the final leaching could not remove the reaction product from heavily defected areas, indicating that extensive reactivity had occurred locally for the reasons given previously.

Annealing at the lower temperature of 500°C resulted in limited reactivity. Parts of the coating could withstand the chemical leaching indicating some degree of carbide formation. Although it appeared highly dense, it was extensively cracked suggesting that thermal contraction effects were detrimental (see Figure 8-32B).

In all cases stripped diamond surfaces showed limited signs of surface etching providing evidence of the protective effect of the coating to high temperature treatment of diamonds.

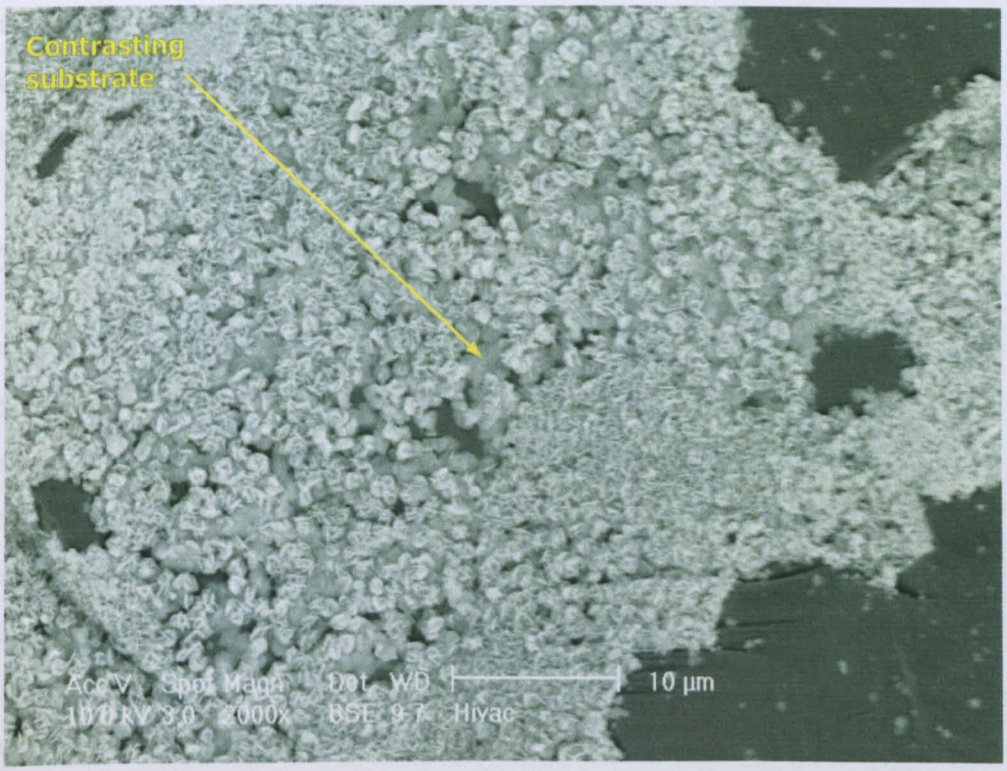

Figure 11-11 : SEM micrograph (backscattered mode) of a W-PVD-coated SYN-3 diamond (SDA75 30/40 US Mesh by DB) initially heat-treated in the DSC furnace and subsequently subjected to metal leaching. Carbide platelets have grown on a modified diamond substrate, which could be interfacial graphite.

11.3 Interfacial Bonding in Coated-Diamond reinforced Co-matrix MMCs

This section discusses the results obtained from the series of tests included in the second part of the experimental work as presented in Chapter 9. Discussion of the results is made in terms of the effect of metal-coating of diamonds on mechanical properties and interfacial bonding of composites.

11.3.1 Densification of the Coated-Diamond Composites

The obtained densities for the composites with the plain cobalt matrix were given in Figure 9-1. Furnace sintering (FS) failed to produce samples with less than 10% porosity. The container-less hot-isostatic-pressing (HIP) improved the density of previously furnace-sintered specimens to levels of the order of 93-95% of theoretical density. However, higher densities could not be achieved. This was attributed to incomplete pore closure attained with the first sintering cycle. According to solid-state sintering fundamental theory, pore closure begins at about 15% porosity and is completed at 5% residual porosity [233]. Thus, the sintered specimens subsequently subjected to HIP with densities less than 90% theoretical contained open pores. The existence of open porosity had merely or totally ruled-out the hydrostatic pressure exerted during HIP, thus minimizing the effect of pressure on the sintering stress. Under those conditions, it could be considered that the HIP acted practically as an extra furnace sintering cycle. The measured additional densification of about 5% achieved by HIP was attributed to this extended sintering cycle, but was not assisted by pressure.

The above results are in agreement with the work of Del Villar *et al.* [234]. They have studied the pressure-less/ HIP manufacturing route for 3 types of cobalt powders with different particle sizes. Their results showed that unless the cobalt powder was of ultra fine size (~0.4μm), densities in excess of 92% could not be achieved when sintering at temperatures below 1000°C, with subsequent HIP consolidation unable to produce sufficient densification.

Although pressure during hot-pressing (HP) is applied uniaxially, the constraint from the die wall introduces radial stresses. The differential stress between the axial and radial directions generates a shear state that aids particle rearrangement, the collapse of large pores, the elimination of flaws and effectively increases the particle contacts compared to HIP enhancing densification [235]. This was demonstrated with the densities obtained by hot-pressing in the present work, which were highest in all systems.

Observed variations in the measured densities of the systems were mainly attributed to the experimental error associated with the various weighing procedures in the liquid medium required by Archimedes density method. Error is also expected to have arisen from the fact that the thin metal coatings were neglected in the calculation of the theoretical densities.

11.3.2 Mechanical Properties

This section discusses the results of the mechanical property tests.

11.3.2.1 Modulus of Elasticity (Young's modulus)

The measured Young's moduli of the diamond composites with the plain cobalt matrix were given in §9.3.

The highest Young's moduli were obtained for the hot-pressed (HP) segments, followed by the hot-isostatically-pressed (HIP) and with lowest values exhibited by the pressure-less sintered (FS) specimens. This ranking followed the order found for the density as presented previously. Closely interpreting the moduli for the pressure-less (FS) and hot-isostatically (HIP) sintered segments in direct comparison with the density graphs, one can further notice the influence of porosity (see Figures 9-1 and 9-2).

The variation in E for the sintered segments did not in any case exceed 6.3% suggesting that there was no significant difference between them (see Table 9-1). The variation was slightly increased when composites were consolidated by HIP specimens, but did not go above 10%.

Hot-pressed specimens clearly demonstrated an increase in the modulus of elasticity as a result of reinforcing the cobalt matrix with diamond particles providing evidence of the beneficial effect of the shear stress state during hot-pressing. Young's moduli increases of up to about 30% were achieved. All types of coated diamonds, apart from the W-powder encapsulated grit, provided increased modulus of elasticity compared to the equivalent segments reinforced with the same type but non-coated diamond. These increases were relatively small, not exceeding 10%, but in the majority of cases being in excess of 5%.

The segments impregnated with the W-powder encapsulated diamonds (samples CD25 & CD26) were the only ones that exhibited decrease of the Young's modulus compared to the non-coated diamond reinforced reference composite. The W-powder granules were essentially diamonds encapsulated in W-powder with the aid of an organic binder. Considering that tungsten typically sinters at temperatures well above 1000°C [236], it can be postulated that inadequate

consolidation of tungsten had taken place around each diamond crystal at the hot-pressing temperature of 840°C impairing composite performance.

Highest absolute moduli values were obtained for the W-CVD coating, which had a thickness of approximately 5 microns. Highest relative increase was found for the segments containing the SYN-3 diamonds with PVD coatings of titanium (CD39 & CD40) followed by those with chromium (CD42 & CD43).

The annealing of the coated diamonds at 500°C in a H_2/N_2 atmosphere prior to consolidation did not provide a conclusive effect on the Young's modulus.

In addition to experimental measurements, Young's moduli were calculated according to 3 relatively simple models of composite mechanics, suitably adapted for the diamond composites as analytically described in Appendix-C. Good approximation of experimental results and predicted values was obtained with 2 of the models that included consideration for porosity in their calculation. These models predict modulus values of the order of 235-245 GPa if complete densification is achieved, or approximately 204-226 GPa for 5% porosity in composites impregnated with 8.75% vol. diamonds ("35" concentration). Considering that most of the hot-pressed segments had a residual porosity of the order of 4-5% and that measured Young's moduli varied in the 210-230 range, good fitting of predicted values and experimental results could be justified.

Based on chosen parameters, the best fit was achieved by calculation with Cohen and Ishai's equation [203].

11.3.2.2 Transverse Rupture Strength (TRS) in 3-point Bending

The transverse rupture strength (TRS) results from the 3-point bending test for the diamond composites with the plain cobalt matrix were given in §9.4.

In all cases, the blank references exhibited higher TRS than the diamond reinforced segments. Such behaviour is typical for particulate MMCs reinforced with non-deformable dispersoids such as the diamond composites [199]. The smallest relative decrease of composite TRS was observed for the HP segments followed by the HIP, with FS specimens showing greatest decrease for the non-corrected and porosity normalised values (Figure 9-3, Table 9-2). This ranking matches the density order and is similar to the ranking found for the Young's modulus. Correction and normalization of the measured TRS values reversed the ranking of the HIP and FS confirming the great influence of porosity (Figure 9-4, Table 9-3).

In all cases, diamond coating was found to improve the bending strength of the composites compared to the equivalent non-coated diamonds. Increases of TRS up to 40% were measured. In general, all composites impregnated with diamonds having vapour deposited metal coatings showed TRS improvements of more than 5%.

Refractory metal (W or Cr) powder diamonds granules were associated with relatively small TRS increases compared to the CVD and PVD coated diamonds. This was attributed to the inadequate sintering of the powder encapsulation as described in the previous section.

Titanium coatings were the only coating found to give slightly higher TRS values than the non-coated grit for HIP and FS segments. Although the observed difference was not significant, it could indicate that under prolonged sintering and with the lack of shear stress the interfacial interactions associated with these coatings were beneficial.

The PVD coatings of titanium (CD39, CD40) and chromium (CD42, CD43) deposited on the inferior quality diamonds (SYN-3) proved to be the most efficient for these systems. Tungsten coatings in general exhibited considerable increases of the bending strength of the HP composites. Both these results are in agreement with Young's moduli measurements.

Best results were obtained for the segments impregnated with the cobalt powder encapsulated diamonds. Considering that cobalt granules sinter with the cobalt matrix, it can be assumed that only the Co/diamond interface exists in these composites. These encapsulated diamonds have been subjected to a sintering cycle after their granulation with the Co-powder. Thus, during hot-pressing the cobalt powder surrounding each diamond, which originated from the granules, was sintered to a higher density than the bulk cobalt. The lack of a second interface and the dense nature of the metal surrounding the diamonds could effectively improve the response of the composite in bending.

Further analysis for each particular system is carried out later in this chapter.

The annealing of the coated diamonds at 500°C in a H_2/N_2 atmosphere prior to consolidation did not provide a conclusive effect on the Young's modulus.

11.3.2.3 Tensile Strength

The results of the tensile strength were analytically presented in section 9-5.

All diamond reinforced composites exhibited reduced ultimate tensile strength (UTS) and ductility compared to the plain cobalt. On the other hand, yield strength was found to be at similar levels or even exceeding that of the blank cobalt. These results clearly indicate that reinforcing with the large and rigid diamond crystals increased the elastic properties of the cobalt, but at the same time were responsible for reducing matrix plastic flow. The MMCs with non-deformable dispersed particles, as the diamond composites, are typically classified as brittle materials [199]. In such class of composites the rigid reinforcement imparts strength to the composite, but drastically lowers the ductility below that of the matrix phase alone [199]. Typically, reinforcement improves the yield stress but UTS is not always similarly affected [205]. Composite yielding is governed by the onset of matrix yielding [205]. The presence of the rigid diamond reinforcement restricts the response of the metal to loading, resulting in an uneven stress state in the matrix. This initially causes localized peak stresses that lead to micro-yielding and subsequently to global yielding. In this respect, mechanical properties of the composite depend on the size and volume concentration of reinforcement and thus on the mean free matrix separation [199].

For the majority of specimens, the composites impregnated with the coated or powder encapsulated grit exhibited improved performance in the tensile strength test compared to the segments reinforced with the equivalent non-coated diamond. This indicated that interfacial interactions attributed to the presence of the metal coating were beneficial to the composite response in tensile loading.

The annealing of the coated diamonds at 500°C in a H_2/N_2 atmosphere prior to consolidation did not provide a conclusive effect on the Young's modulus.

Results exhibited a considerable scatter, which is attributed to the influence of flaws on the surface of the "dog-bone" segments manufactured by pressure-less sintering. However, the results clearly indicated that the metal coatings had a beneficial effect on the composite tensile strength.

11.3.3 Interfacial Bonding in Coated-Diamond / Cobalt Composites

This section deals with the interfacial bonding characteristics of the examined metal-coated diamond/cobalt composites. Discussion is primarily based on the SEM examination of the fracture surfaces developed by 3-point bending and tensile testing. Analysis takes into account the SEM observations as well as the results of the quantitative fracture surface analysis method presented in 7.3.3.5. The relationship between SEM findings with mechanical test results are also included where appropriate.

11.3.3.1 Non-coated diamond systems

Examination of fracture surfaces in the SEM clearly showed, as expected, that diamonds had been dissolved by the cobalt. Etching had occurred at a relatively fine scale (see Figure 9-6) from the sintered fine cobalt powders. Diamonds in the hot-pressed segments were etched at considerably lesser extent than those consolidated with the HIP and FS routes. This clearly showed that the increased sintering temperature and time involved with the HIP and FS promoted dissolution of the diamond surfaces, as expected.

The SYN-3 type diamonds (SDA75, De Beers) were etched at slightly higher levels than the SYN-1 (SDA100, De Beers) confirming the specifications of the synthesizer of these synthetic diamonds who designates SYN-3 as an inferior quality diamond.

Hot-pressing left SYN-1 diamonds practically unaffected and SYN-3 slightly dissolved (see Figure 9-11). However, in all diamond/cobalt composites carbon dissolution had taken place. This was confirmed by the reduction of cobalt oxides in the vicinity of each diamond crystal (see Figure 11-12). Depending on diamond quality and sintering conditions the reduction zone around the diamonds increased in thickness providing additional evidence of the extent of diamond dissolution. Studies on the sintering behaviour of cobalt powders have shown that finely dispersed oxides increase the hardness of the consolidated material [85-86]. Decreasing the amount of oxides increases the ductility of the sintered cobalt [85]. It can be therefore assumed that the oxide-free zone produced around each non-coated diamond should be of increased ductility compared to the cobalt remotely from the crystals. The composite could then be realised as containing reinforcement in the form of diamonds encapsulated in a thick and ductile cobalt jacket. Such a structure is expected to provide an improvement of the mechanical performance of the composites. The above hypothesis was supported by the mechanical properties test results. The inferior quality SYN-3 type diamonds, which were more susceptible to carbon dissolution, were associated with thicker oxide-free zones. The mechanical performance of segments

impregnated with the SYN-3 diamonds was found to be slightly improved compared to the specimens reinforced with the superior quality but highly resistant to thermal etching SYN-1 type grit.

Increased surface roughening of the SYN-3 diamonds could also improve the mechanical keying of the diamonds in the cobalt [228], thus providing an additional explanation of the similarly affected mechanical performance.

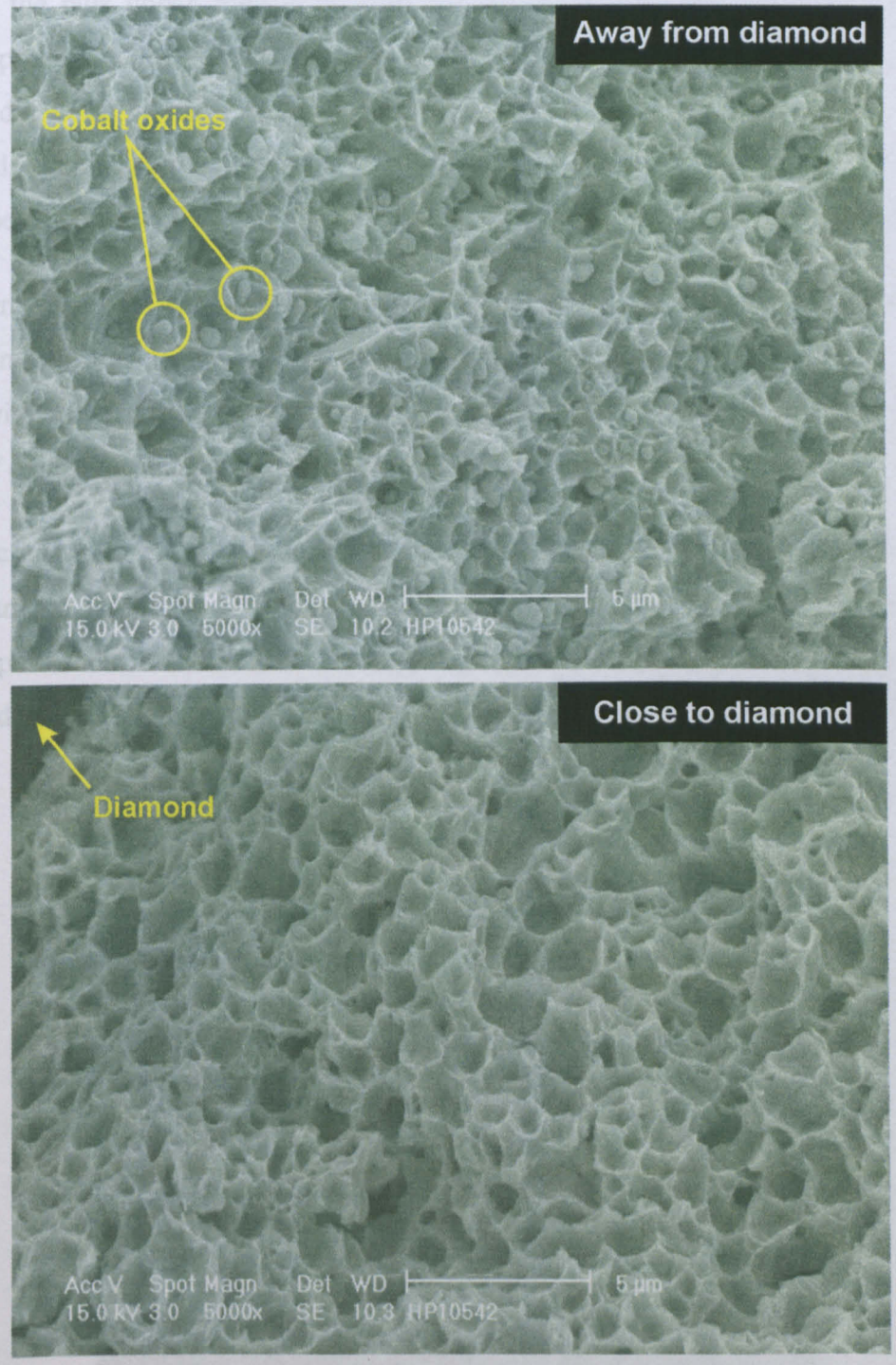

Figure 11-12 : SEM micrographs of fractured cobalt surfaces in a non-coated diamond/cobalt-matrix composite. **(A)** Cobalt in the bulk matrix, remote from the diamonds, contains finely dispersed spherical cobalt oxides. **(B)** Cobalt oxides are reduced in the vicinity of diamonds.

11.3.3.2 Co-powder encapsulated diamond systems

Interactions in composites incorporating the Co-powder granulated diamonds were similar to those that occurred with the non-coated diamonds, characterising a purely mechanical bonding.

The diamonds in the hot-pressed segments (CD-28, CD-29) showed minimal signs of dissolution etching, whereas during pressure-less sintering (DBS-23, DBS-24) they underwent relatively fine scale dissolution. The cobalt powder layer of the diamond granules appeared to be slightly denser than the bulk cobalt matrix, possibly due to the post heat-treatment that followed the granulation process. Cobalt oxides were effectively reduced around the diamonds similarly to the non-coated diamonds systems, as described in the previous paragraph (see Figure 11-13). Thus, the diamonds were essentially enclosed in a dense and more ductile cobalt jacket, which is thought to be responsible for the good mechanical properties exhibited by these composites.

The annealing of the Co-encapsulated diamonds at 500°C in a H_2/N_2 atmosphere prior to consolidation appeared to improve the mechanical performance of the composites. Considering this result with the analysis presented above, it appears that the annealing aided pre-sintering and reduction of oxides thus imparting further ductility to the cobalt jacket of the granules.

Macroscopic inspection of the fracture surfaces revealed a relatively even distribution of the Co-powder diamond granules in the segments. This certainly contributed to the improved mechanical performance and it was attributed to the close value of density of these granules to the Co-powder, thus reducing the segregation of the diamonds during mixing and cold pressing.

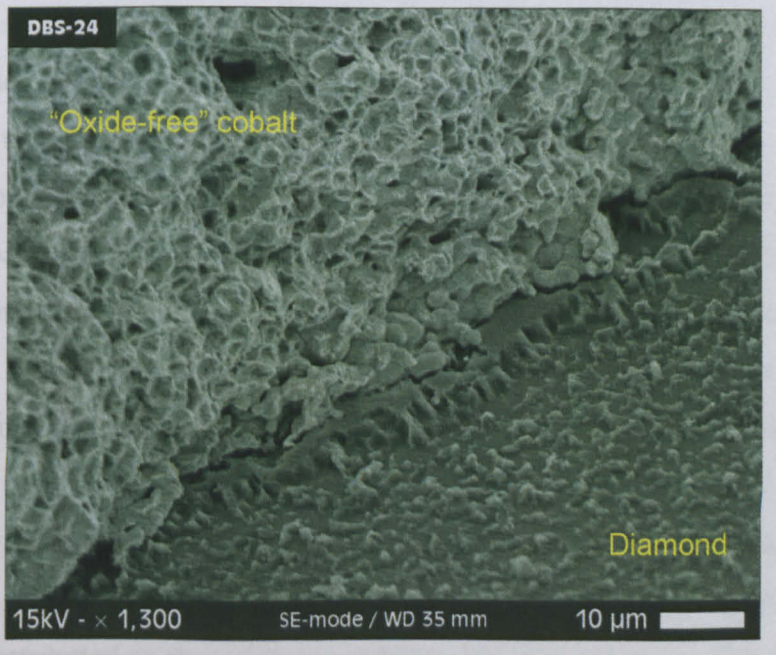

Figure 11-13 : Fracture surface detail in Co-powder encapsulated diamond / cobalt-matrix composite showing dissolution of diamond and reduction of cobalt oxides in the surrounding metal.

11.3.3.3 Ti-coated diamond systems

Examined systems included both CVD and PVD deposited titanium coated diamonds.

Reactivity in Ti-coated diamond / cobalt composites varied depending on the consolidation method and conditions and on the type of diamond crystal.

It could be distinguished, that reactivity was proportional to the tendency of the diamond to be thermally attacked at the processing conditions. This was evident when comparing the interaction features in specimens consolidated with same method but containing different types of diamond. The inferior quality diamond, the SYN-3, showed relatively higher levels of reactivity compared to equivalent SYN-1, which were much more thermally stable (see Figures 9-6 & 9-7). This was clearly evident especially when comparing segments that were consolidated at higher temperatures and longer sintering times (i.e. FS and HIP).

Hot-pressing increased the intensity of interactions between the composite constituents, despite the lower processing temperature and time compared to HIP and FS. This indicated that pressure played a significant role in enhancing the interaction phenomena. As was discussed earlier in this chapter, shear stresses during sintering improve densification. In addition, shear strains disrupt surface oxide films on particles [237]. For titanium, which is readily oxidised, disruption of surface oxide films is of great importance if reactivity should take place. It is possibly for that reason, that although processing conditions in terms of temperature and time were milder during HP the titanium coatings appeared more reactive.

Evidence of extensive reactivity was found at numerous locations in the interfacial regions exposed at the fractured surfaces. Even for systems that showed high levels of interactions, reaction was not uniform over the entire length of the visible interfaces. It appeared that reactivity was favoured at certain locations, very often around diamond crystal corners. The phenomenon was particularly apparent for the hot-pressed systems. EDAX analysis revealed that oxygen atomic concentrations were particularly high at the interfacial region. These facts indicated that the Ti-coated diamond cobalt matrix composites behaved as a pseudo-Class I composite, exhibiting primarily a mutual non-reactivity between the composite constituents attributed to oxide film barrier on titanium coating (refer to §5.4). Rupture of the oxide film was particularly efficient under hot-pressing providing enhanced reactivity as discussed above. The observed limited reactivity in the pressure-less sintered (FS) and hot-isostatic-pressed segments could be primarily attributed to the enhanced diffusion through the oxide film favoured under the higher processing temperatures and longer sintering times associated with these consolidation

routes. In addition partial reduction of the oxides by the N_2/H_2 reducing atmosphere could also have taken place.

The examination of the interfacial regions as exposed on fracture surfaces showed that in these composites reaction between the constituents could be essentially realised to have taken place at fractions of the interface. Studies on other Class-I reactive MMCs have shown that thin or discontinuous reaction products appear to inhibit interfacial sliding and apparently increase the elastic modulus [238-239]. However, in systems prone to progressive interfacial reactions there is evidence that the interface becomes the preferred site for cracking, both in-plane and through-thickness relative to the layer. The mechanical properties of the various Ti-coated diamond impregnated segments appeared to be in agreement with the above considerations. Young's modulus and TRS of the pressure-less sintered and HIP composites, which exhibited limited reactivity, were found to be at similar levels or slightly improved compared to the composites containing the equivalent non-coated grit. For the hot-pressed systems in which interactions were favoured, mechanical performance was further enhanced. Thick reaction product layers with extensive in plane and through thickness cracking were found at several interfacial locations (see Figures 9-15C and D). However, they were not associated with deteriorated composite performance. In fact they were related with enhanced mechanical properties as demonstrated by segments with the Ti-PVD coated diamonds (CD39, CD40).

Diffusion of carbon originating from the diamonds through the coating towards the cobalt matrix was limited. This was evident by the presence of spherical cobalt oxides close to the Ti/Co interface. Diamond surfaces were in general not particularly etched indicating that the Ti-coating provided good protection of the diamonds from the Co-matrix. In locations where reactivity was achieved, metal remains were found inside each etch pit on diamond surfaces (see Figure 9-24). This provided further support to the proposed mechanism on the reactivity of diamond to metals as presented in Part-I of the discussion presented earlier in this chapter. Thus, it was evident that reaction of diamond to metal was only possible upon release of carbon atoms from the diamond structure, which initially takes place inside each etch pit.

Fracture surface analysis revealed that the failure path primarily involved detachment of the diamond/titanium interface, although there were locations where fracture had also travelled through the Ti/Co interface. In the majority of cases, Ti-coating was found to preferentially bond and remain attached to the cobalt binder (Figure 11-14). Pull-out craters contained almost intact the Ti-coating jackets. The Co-Ti phase diagram can in some extent predict the bonding of Ti-coating to the cobalt-matrix. According to this phase diagram, titanium exhibits a considerable

solubility in cobalt (Figure 11-15). At the hot-pressing temperature of 840°C, the phase diagram predicts that practically only diffusion of Ti-atoms into the cobalt occurs and that solid-solutions of cobalt FCC (αCo) with up to approximately 9 at% Ti are formed.

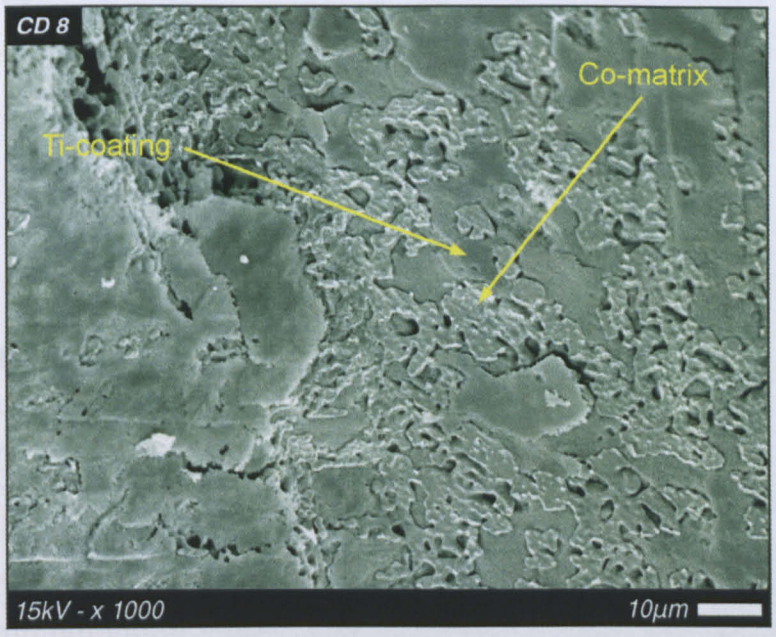

Figure 11-14 : Aspect of the walls of a diamond pull-out crater in a Ti-PVD-coated diamond reinforced cobalt composite, showing the adherence of the Ti to the Co-binder.

On sintering and HIPing at 970°C, the solubility of Ti in Co further increases to levels of the order of 12 at% (Figure 11-15). However, at this temperature Co becomes considerably soluble in BCC titanium (βTi). Due to the increased sintering time involved with the FS and HIP routes it is expected that equilibrium conditions will be approached much more than in the case of HP. Under such conditions of increased mutual solubility, thin Ti-coating layers could totally dissolve. Chen *et al* [94] in their patent address the problem of Ti-coating dissolution by the binder especially for coatings with sub-micron thickness. Furthermore, the much slower cooling rate could involve precipitation of Ti-Co intermetallics as predicted by the phase diagram. Considering the possible presence of intermetallics at the interfacial region, interfacial brittleness may be associated with the inferior mechanical properties of the sintered segments.

For the majority of the exposed diamonds, the cubic surfaces {100} appeared to have interacted with the metallic environment to a greater extent than the octahedral {111} ones (see Figure 9-9A). This observation is in agreement with the findings of the DRE experiment as discussed in Part-I (§11.2) of this chapter.

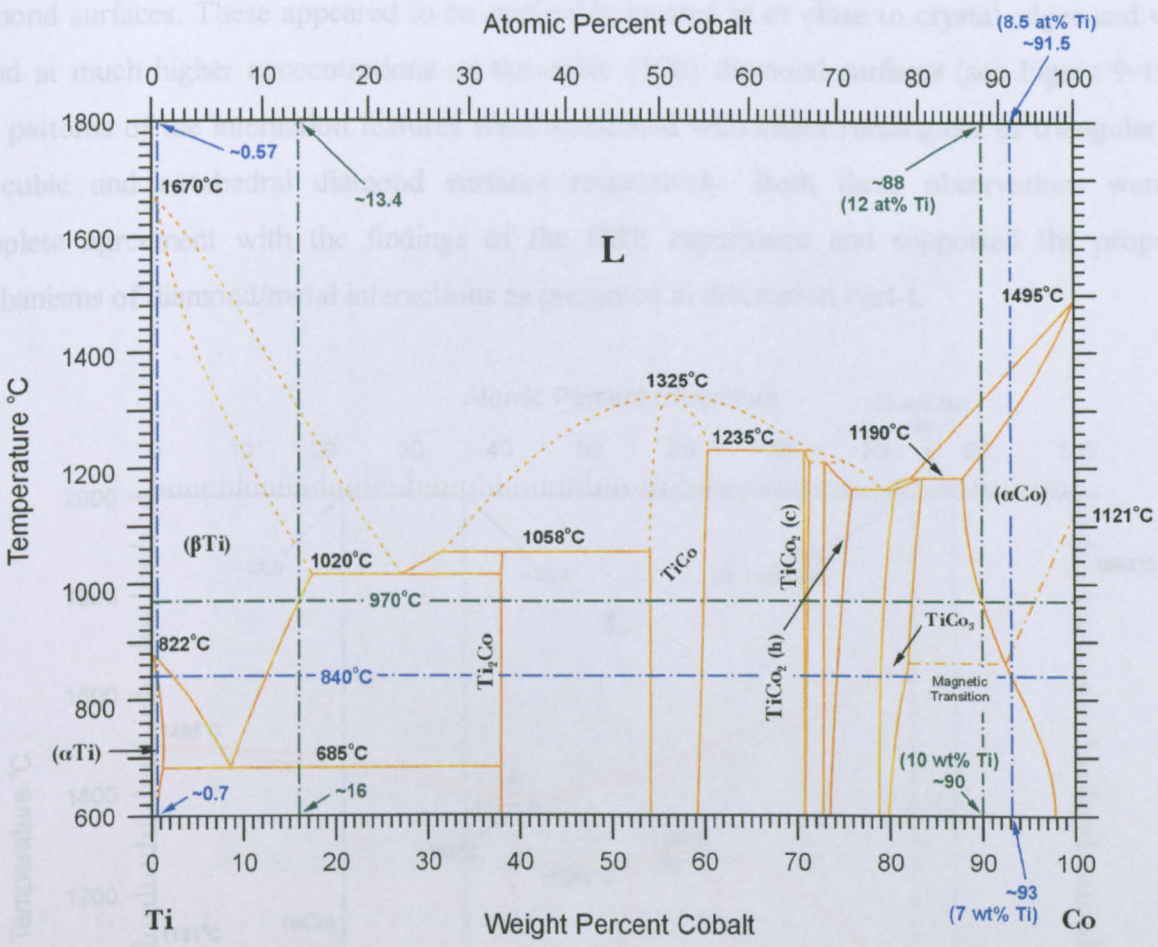

Figure 11-15 : Titanium-cobalt phase diagram [240]. Maximum weight and atomic solubility values in solid-solutions are shown for the hot-pressing and pressure-less sintering temperatures (840°C and 970°C respectively).

11.3.3.4 Cr-coated diamond systems

This section discusses the results from the examination of systems with Cr-coated diamonds, in which the coating was in the form of a continuous layer. The Cr-coatings were deposited by PVD on both SYN-1 and SYN-3 diamonds.

Composites impregnated with the Cr-PVD-coated diamonds that were consolidated by either the pressure-less sintering or HIPing showed a clear preference for the Cr-coatings to remain attached onto the Co-matrix in the developed pull-out cavities. The diamond/chromium interface was the weakest and thus was the preferred path for failure under 3-point bending. The bonding of the chromium coating to cobalt is not surprising at the processing temperature of 970°C considering the mutual high solubility of each metal atom in each other, as predicted thermodynamically from the Co-Cr phase diagram (Figure 11-16). Interaction of the diamonds with the metallic environment was kept at low levels providing further evidence that Cr-carbide formation was not favoured and that the Cr-coating provided good protection from the cobalt. Limited isolated areas with signs of either etching or reactivity were found occasionally on

diamond surfaces. These appeared to be preferably located at or close to crystal edges and were found at much higher concentrations on the cubic {100} diamond surfaces (see Figure 9-10B). The patterns of the interaction features were associated with either rectangular or triangular pits on cubic and octahedral diamond surfaces respectively. Both these observations were in complete agreement with the findings of the DRE experiment and supported the proposed mechanisms of diamond/metal interactions as presented in discussion Part-I.

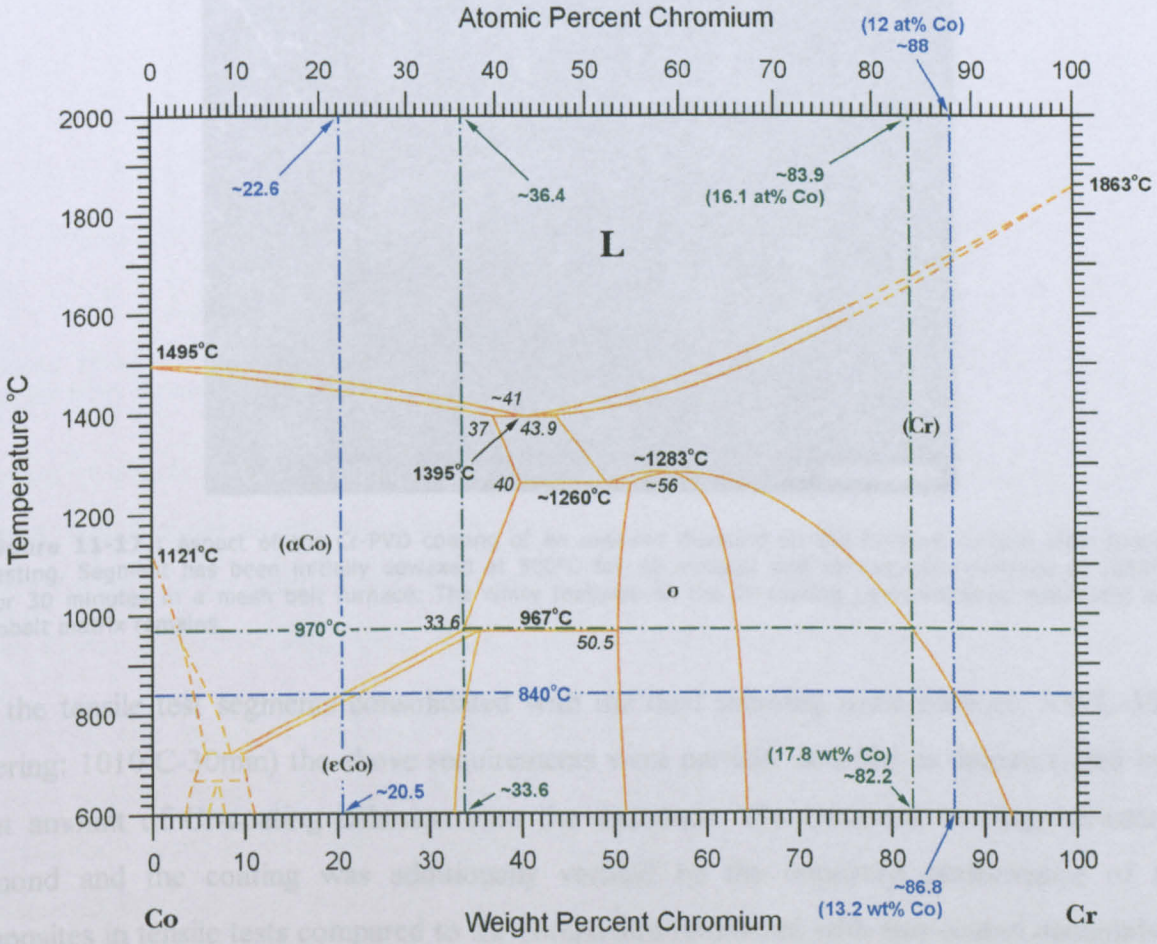

Figure 11-16 : Cobalt-chromium phase diagram [240]. Maximum weight and atomic solubility values in solid-solutions are shown for the hot-pressing and pressure-less sintering temperatures (840°C and 970°C respectively).

Sintering at a higher temperature of 1010°C for 30 minutes, in order to consolidate the tensile test specimens, completely altered the bonding characteristics in the composites. The bonding strength of the diamond/chromium interface increased. Diamonds revealed at the fracture surfaces retained almost entirely the Cr-coating jacket (see Figure 9-25). Composite failure in tension primarily occurred at the Cr/Co interface towards the Co side. Cobalt remains were readily found of the Cr-coating (Figure 11-16).

Naidich *et al.* [97, 115, 140] in a series of studies have established that Cr-coatings on diamond can achieve the highest normal adhesion strength compared to other carbide forming metals

(refer also to §4.6.2, Figures 4-17 & 4-18). The authors reported that the adhesion strength of Cr-coatings to diamond starts to built-up only at temperatures in excess of 900°C and for heating times greater than 30 minutes. Maximum strength was achieved at approximately 1000°C with the diamonds held at temperature for approximately 1 hour.

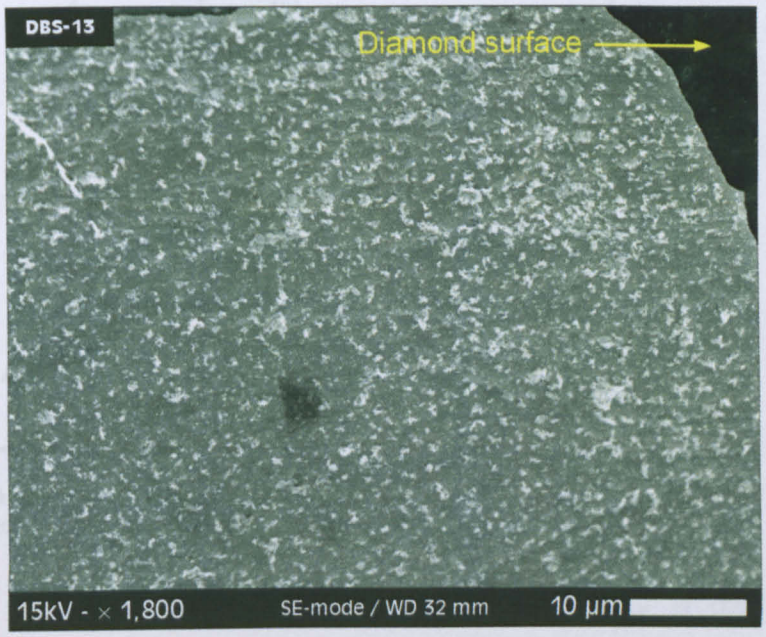

Figure 11-17 : Aspect of the Cr-PVD coating of an exposed diamond on the fracture surface after tensile testing. Segment has been initially dewaxed at 500°C for 30 minutes and subsequently sintered at 1010°C for 30 minutes in a mesh belt furnace. The white features on the Cr-coating (grey coloured substrate) are cobalt matrix remains.

For the tensile test segments consolidated with the dual sintering route (dewax: 500°C-30min, sintering: 1010°C-30min) the above requirements were partially satisfied as demonstrated by the great amount of Cr-coating adhesion onto the diamonds. The enhanced bonding between the diamond and the coating was additionally verified by the improved performance of these composites in tensile tests compared to the composites reinforced with non-coated diamonds (see Table 9-4).

Examination of the fracture surfaces of hot-pressed segments revealed that a very good bonding of the Cr-PVD coatings with the cobalt matrix had been achieved. This indicated that the diamond / Cr-coating was the weakest interface.

The reaction product zones were preferentially formed at crystal edges and corners and where the diamond concentration parallel to the hot-pressing direction was high (Figure 11-18), similar to what was found for the Ti-coatings as discussed in the previous paragraph. These observations indicate that interactions between the composite constituents were promoted at locations of high stress. At such locations oxide films on metal were disrupted permitting atom diffusion and enhanced sintering as has been discussed earlier.

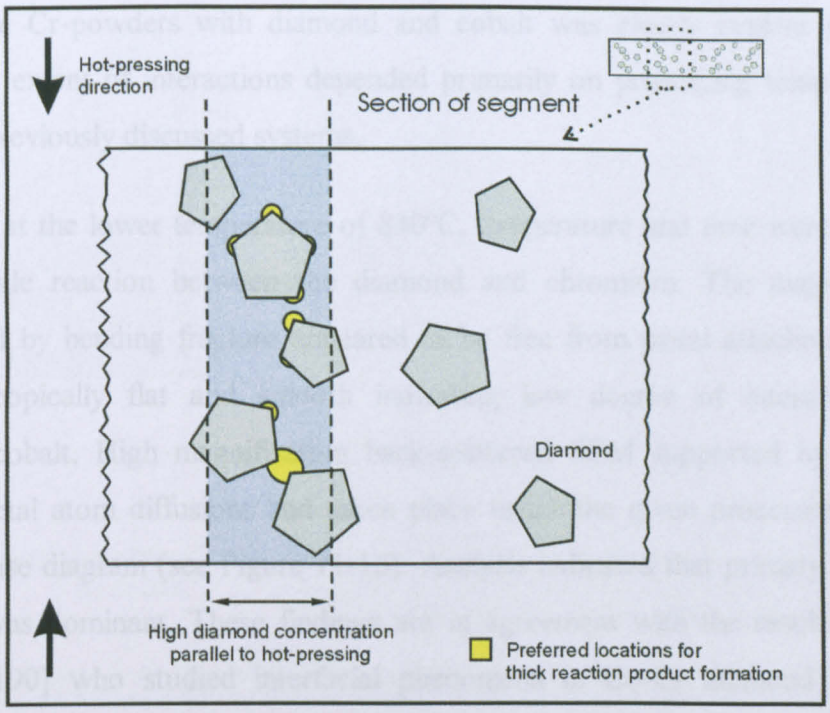

Figure 11-18 : Sketch of a segment section showing the sites where thick reaction product zones had preferentially formed in hot-pressed Cr-PVD-coated diamond impregnated composites.

Reaction products were comparatively thicker than those formed in the Ti-coated diamond systems, which could be attributed to the higher levels of mutual solubility of Co and Cr in each other. Cracking of the reaction products was evident, but occurred at a lower level than in the Ti-coated diamond systems, suggesting that the toughness of the interfacial product was greater.

Apart from the locations indicated above, enhanced reactivity was also related with larger diamond crystal size. This observation is in agreement with the findings of the DRE experiments. Larger crystals are associated with a higher concentration of dislocations emerging to diamond surfaces that eventually provide a higher number of available sites for diamond dissolution processes.

The beneficial effect of the interfacial bonding attributed to the Cr-coating was shown by the higher Young's moduli and the TRS values of the composites compared to those with the non-coated grit. Greater improvements were achieved for the inferior quality diamonds (SYN-3) possibly due to their higher degree of surface dissolution under processing conditions.

11.3.3.5 Cr-powder encapsulated diamond systems

There were two types of composites impregnated with the Cr-powder encapsulated diamonds that were tested and examined. One type was the bending segments hot-pressed at 840°C and the second type were the "dog-bone" shaped specimens for the tensile test that were consolidated by the double step sintering route with a maximum temperature of 1010°C.

Reactivity of the Cr-powders with diamond and cobalt was clearly evident in both types of composites. The extent of interactions depended primarily on processing temperature and time similarly to the previously discussed systems.

On hot-pressing at the lower temperature of 840°C, temperature and time were not sufficient to initiate large scale reaction between the diamond and chromium. The majority of diamond surfaces exposed by bending fracture appeared to be free from metal attachments and were in general macroscopically flat and smooth indicating low degree of interactions with both chromium and cobalt. High magnification back-scattered SEM supported by EDAX analysis revealed that metal atom diffusions had taken place under the given processing conditions, in-line with the phase diagram (see Figure 11-16). Analysis indicated that primary Cr diffusion into the Co-matrix was dominant. These findings are in agreement with the results of the work of Akyüz *et al.* [190] who studied interfacial phenomena in Co-Cr diamond composites with varying contents of Cr. The authors concluded that under standard hot-pressing conditions inter-diffusion between metal constituents takes place, but the diffusion of Co into Cr is limited, thus creating Kirkendall voids in the latter.

Some limited signs of diamond reaction with the metallic surroundings were evident. Chromium bridges strongly adhering to both the metallic environment as well as to the diamond surface were found at certain points of the diamond/metal interface (see Figure 9-17E and F). The Cr-powders were much larger in size than the cobalt imposing problems of densification at the areas of high Cr-powder concentrations. However, small improvements in Young's modulus and TRS where measured compared to the composites with the non-coated diamonds (see Tables 9-1 & 9-2), possibly associated with the bonding achieved by the Cr-bridges.

Examination of the fracture surfaces of the tensile segments showed clearly the effect of the higher sintering temperature and longer time. Interactions between the composite constituents were greatly promoted. Large rounded etch pits had formed on diamond surfaces at the points of contact of the chromium powders with the diamond (see Figure 9-26). At the centre of each depression a knoll of metal was found to strongly adhere onto diamond. The C/Cr atomic ratio of these metal knolls, as found by EDAX analysis, suggests possible formation of higher chromium carbides. The diamond surfaces that were not in contact with chromium powder were heavily dissolved by the cobalt-matrix (see Figure 11-19 on next page). The diamond surface in between closely spaced etch pits created by chromium was relatively flat and smooth, providing evidence that cobalt did not access these areas.

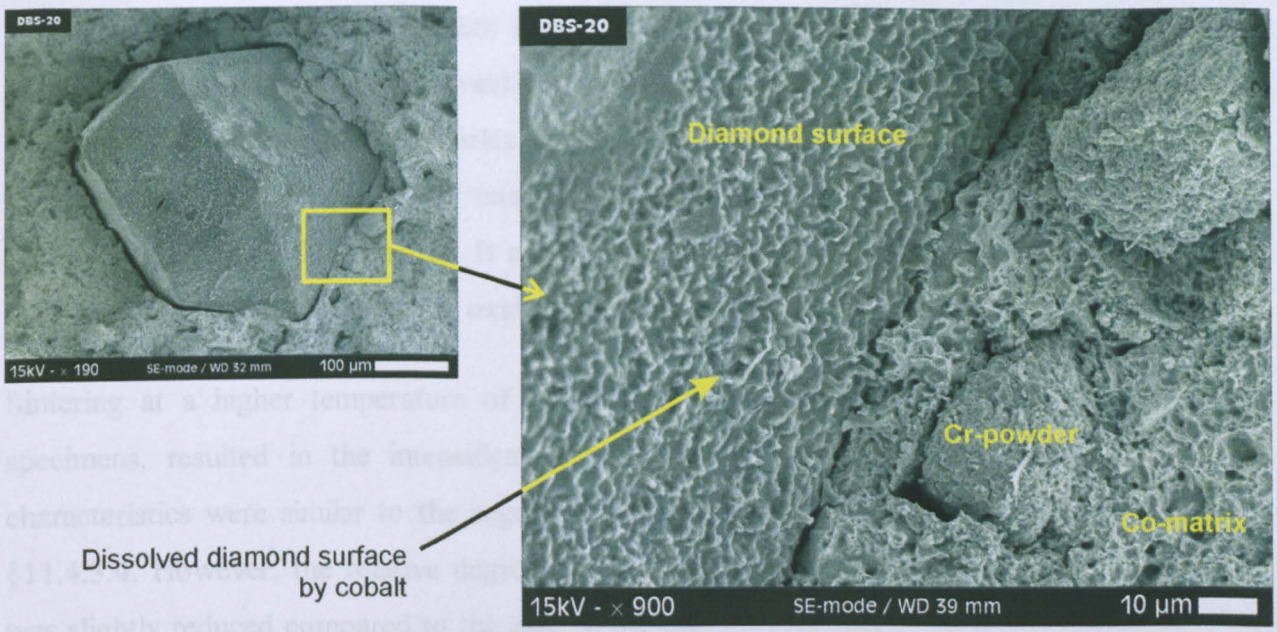

Figure 11-19 : Aspect of an interfacial region exposed on the fracture surface by the tensile test in a segment consisting of cobalt reinforced with Cr-powder encapsulated diamonds. The SEM micrograph on the right shows the extensive diamond dissolution by the Co-matrix at the areas where chromium powders did not contact the crystals.

The bonding characteristics as described above for the sintered segments were also shown by the very good combination of values for the parameters calculated with the quantitative SEM analysis of the fractured surfaces. Composites combined a decreased number of lost crystals (L) and diamond sites (S_N) with an increased number of fractured crystals, which according to the composite materials theory indicates enhanced interfacial bonding (refer to Table 9-6). The tensile strength of the composites was among the highest measured providing evidence to support the above analysis.

11.3.3.6 Carbon-enriched Chromium-coated diamond systems

The interfacial characteristics in the composites impregnated with the Cr(C)-PVD-coated diamonds were very similar to those of the Cr-PVD-coated grit.

In sintered segments the coating preferentially adhered to the cobalt matrix similar to the Cr-PVD-coatings as discussed earlier. The diamonds appeared to be unaffected by the contact with the coating and the very few surface etch features indicated minimal interactions with the metallic environment. This observation suggests that chromium preferentially consumed the free carbon that was co-deposited during PVD. It can be further postulated that these carbon atoms as being freely available were the first to react at first rather than carbon atoms originating from the diamond. As has been shown and discussed in previous sections, if carbon atoms from the diamonds should be available for reaction, they should first break out of the diamond structure, which is an additional step in the process.

Cobalt spherical oxides were present in the bulk matrix. However, examination of the fracture surfaces at high magnifications revealed a thick cobalt zone surrounding each diamond crystal that was free from any oxide particles. In the case of the composites impregnated with the Cr-PVD-coated diamonds the Cr/Co interfacial regions contained the spherical oxides in typical concentrations of the bulk matrix. It can be thus concluded that it is the free carbon from the Cr(C) coating that had reduced the oxides in the cobalt matrix.

Sintering at a higher temperature of 1010°C for 30 minutes, to consolidate the tensile test specimens, resulted in the intensification of the interaction phenomena. Interfacial bonding characteristics were similar to the segments with the Cr-PVD-coated diamonds as described in §11.4.3.4. However, the relative degree of interaction of the diamond surface with the coating was slightly reduced compared to the case of the pure Cr-coatings and this was attributed to the presence of the free carbon. The tensile strength of the composites was considerably improved compared to the equivalent segments with the non-coated grit (see Table 9-4). However, it was slightly reduced compared to the segments with the plain Cr-coated diamonds, which could be interpreted as demonstrating the slightly reduced reactivity because of the presence of the free carbon.

Examination of the fracture surfaces of hot-pressed segments revealed that the coatings preferentially remained attached onto the diamond surfaces. Diffusion of Cr into the cobalt matrix appeared to have been limited. Since this was not the case for the segments with the plain Cr-coated diamonds, it could be postulated that this change in the behaviour of chromium could be associated to its reactivity with the free carbon. If that was the case, it could be postulated that carbides had formed in the coating increasing its stiffness and thus creating a rigid jacket enclosing the diamonds. This jacket could withstand the bending stresses. This hypothesis is supported from the results of the DRE for the Cr(C)-coated diamonds heat-treated in the DSC furnace (see §11.2.4.2B on page 256). It was there shown that a hard and stiff highly carbidized coating had formed during annealing.

Young's modulus and TRS were slightly inferior to that of the equivalent segments with the plain Cr-PVD-coated diamonds, but they were considerably improved compared to the composites with the non-coated grit.

11.3.3.7 Ti/Cr-coated diamond systems

This section discusses the interfacial bonding in composites reinforced with diamonds having a composite coating, which had been formed by co-deposition of titanium and chromium by PVD.

The Ti/Cr-coatings appeared to preferably adhere to the cobalt matrix rather than the diamond when the composite consolidation was made by pressure-less sintering or HIPing. This is in-line with what was found for the specimens impregnated with both the Ti- and Cr-coated diamonds and is attributed to the diffusion of the metal atoms in each other as has been discussed in the corresponding paragraphs.

Sintering at a higher temperature of 1010°C for 30 minutes, to consolidate the tensile test specimens, enhanced the interaction phenomena. Diamonds exposed to the fracture surfaces retained their Ti/Cr-coating to a large extent. This indicated that the diamond/coating bonding strength had been favoured under the processing conditions. This was mainly attributed to the Cr content of the coating, which at the given processing conditions exhibits relatively strong bonding to the diamond, as was discussed in §11.4.3.4. Evidence of the reaction of the diamond with the various metals constituents, as metal fragments adhered to diamond etch pits, were readily available (see Figure 9-28).

The tensile strength of the composites impregnated with the Ti/Cr-coated diamonds was slightly improved compared to the equivalent segments with the non-coated grit. This performance lies in between the very high tensile strength of segments with plain Cr-coated diamonds and the poor strength of Ti-coated grit, demonstrating the mixed behaviour of the Ti/Cr-coatings.

The interfacial bonding characteristics for the composites that were hot-pressed was similar to those found for the Ti- and Cr-coated systems. Their TRS values were found to be at intermediate levels between the higher values associated with the Cr-coated diamonds and the lower values of the Ti-coated diamonds.

11.3.3.8 W-coated diamond systems

This section discusses the results from the examination of systems with W-coated diamonds, for which the coating was in the form of a continuous layer. The W-coatings were deposited by either CVD or PVD on both SYN-1 and SYN-3 diamonds.

On sintering (FS) and hot-isostatic pressing (HIP) cobalt powder containing the W-coated crystals extensive reactivity at the interfacial regions around the diamonds was evident. Interactions between the composite constituents were more intense than any of the other systems previously discussed for the FS and HIP consolidation routes. This result is in agreement with the findings of the DRE, in which tungsten was found to be the most reactive metal to the synthetic diamonds.

Examination of crystals exposed by the bending fracture revealed that almost every etch pit on the diamond surfaces contained a metal fragment (see Figure 9-12B). Etch pit geometries on octahedral {111} surfaces could be identified as hexagonal or triangular. Etching on the cubic {100} surfaces was more intense producing a highly roughened topography on which rectangular pits were hardly distinguished. The portions of the diamond surfaces that remained smooth and flat contained no metal. These observations were completely in agreement with the findings of the DRE as concerning the shape of the etch pits and the higher reactivity of {100} surfaces over the {111}. Furthermore, these observations supported the proposed mechanism on diamond/metal interaction, which involves an initial stage of carbon atoms breaking away from the diamond structure with the aid of a metal catalyst. Carbon atoms upon release are available to react. It is thus expected that reaction should take place at the origins of carbon atoms nucleation, which are the etch pits.

Layers of the PVD deposited tungsten coatings could not be identified. This strongly indicated that the thin W-PVD coatings, that typically had a thickness of approx. 0.5 μm, had been consumed. It is obvious that some of the tungsten had reacted with the diamond as discussed in the previous paragraph, however in order to explain the complete loss of W-coating continuity a considerable amount of tungsten must have been dissolved into cobalt. This was confirmed by EDAX analysis as well as by back-scattered SEM. Tungsten was shown to have dissolved in the surrounding cobalt binder over considerable distances. The preference for dissolution of tungsten into cobalt rather than the opposite is also predicted from the Co-W phase diagram (Figure 11-20).

The fact that W-PVD-coatings dissolved and had lost continuity made diamond surfaces directly accessible to the cobalt binder. This was evident by the high degree of diamond dissolution etching, which is not expected in a pure tungsten/diamond system as has been shown with the DRE. At the areas of direct contact of the cobalt with the diamond surfaces, dissolution of the latter would be catalysed. This would have increased the amount of carbon atoms released from the diamond structure. The high reactivity observed in the sintered and HIP composites with the W-PVD coated diamonds could be associated with the high carbon atom availability originating from the catalysed dissolution of diamond by cobalt. The carbon availability was also confirmed by the fact that there were no cobalt spherical oxides found in the vicinity of the diamonds.

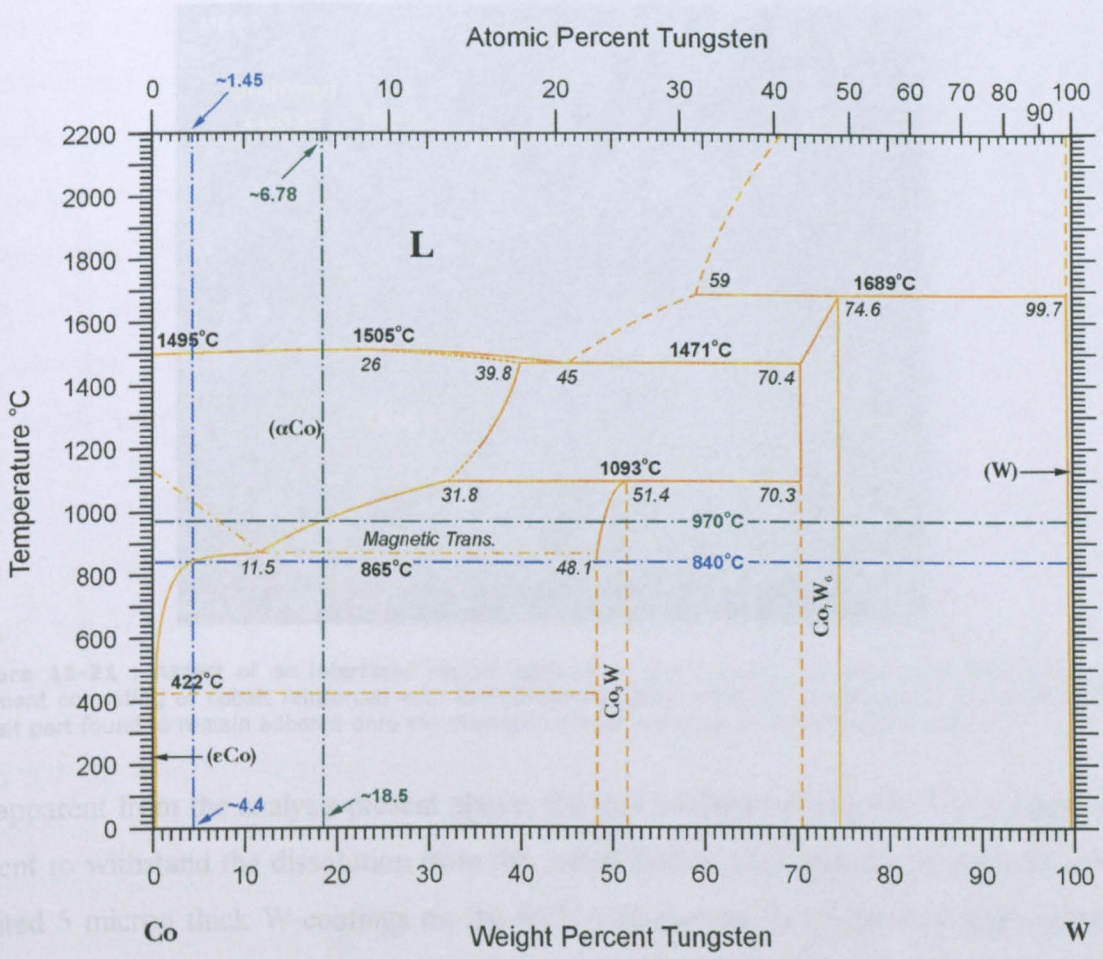

Figure 11-20 : Cobalt-tungsten phase diagram [240]. Maximum weight and atomic W solubility in cobalt are shown for the hot-pressing and pressure-less sintering temperatures (840°C and 970°C respectively).

Sintering of the segments containing the W-PVD-coated diamonds at a higher temperature of 1010°C in order to consolidate the "dog-bone" specimens for the tensile test resulted in intensification of the interaction phenomena discussed above. Flat and smooth areas on diamonds were not found indicating that there were no surfaces remaining non-reacted. The thin tungsten coatings had been dissolved. Attachment of metal fragments onto the diamond surfaces had occurred in a similar manner as described above. However, in this case the amount and the size of the metal parts were considerably increased suggesting that a very strong interfacial bonding had been achieved (see 9-30B). In some instances there were even large sintered parts of the matrix, which were found to strongly adhere onto diamond surfaces (see Figure 11-21).

The achieved interfacial bonding was also shown by the very good combination of values for the parameters calculated with the quantitative SEM analysis of the fractured surfaces. Composites exhibited a decreased number of lost crystals (L) and diamond sites (S_N) combined with an increased number of fractured crystals (refer to Table 9-6). The usage of the W-PVD-coated diamonds was found to be beneficial for the segment ultimate tensile strength and yield strength as compared with the reference specimens impregnated with the non-coated diamond grade.

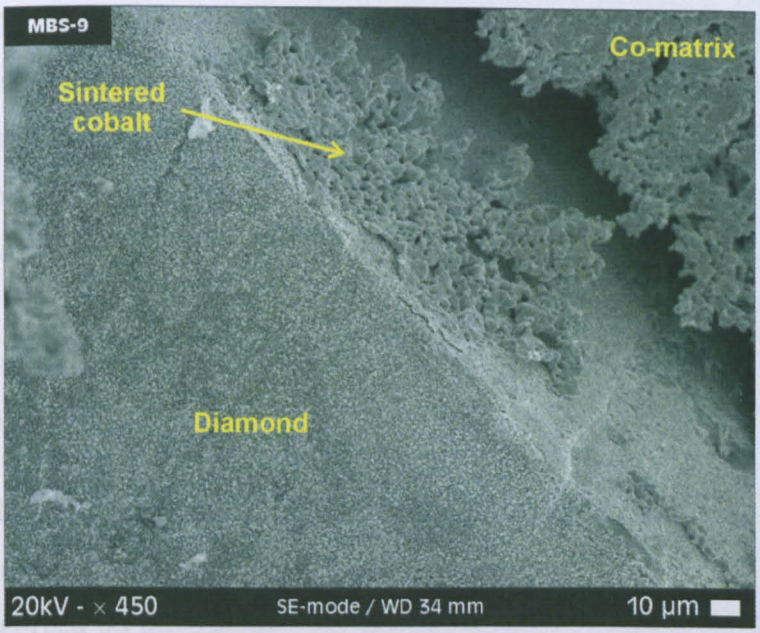

Figure 11-21 : Aspect of an interfacial region exposed on the fracture surface by the tensile test in a segment consisting of cobalt reinforced with W-PVD-coated 30/40 mesh SYN-3 diamonds. The large sintered cobalt part found to remain adhered onto the diamond surface indicates strong interfacial bonding.

As is apparent from the analysis present above, the low thickness of the W-PVD coating was not sufficient to withstand the dissolution from the cobalt matrix. This was not the case for the CVD deposited 5 micron thick W-coatings on the SYN-1 diamonds. In composites impregnated with these diamonds, the integrity and continuity of the W-CVD coating was not affected under the high temperature and prolonged sintering, which was required to produced the tensile test specimens (samples DBS-25 & DBS-26).

On subjecting the segment to tensile fracture, the W-CVD coatings appeared to preferentially adhere to the cobalt matrix rather than the diamond surfaces indicating that the diamond/tungsten interface was the weakest (see Figure 9-29B). There were however some limited number of diamonds for which the failure occurred at the W/Co interface (see Figure 9-29A).

Diamond surfaces stripped from the W-CVD coating appeared to be relatively smooth and flat with very few shallow etch features suggesting that they had undergone a minimal dissolution. This provided evidence of the protective effect of the thick W-coating against the cobalt and oxygen in contrast to what was found for the thin W-PVD coatings.

Apart from a few very small crystallites on the diamond surfaces, no other features suggested the formation of tungsten carbide platelets similar to those formed under the DRE experiment. There are two possible explanations for this phenomenon. The first could be associated with the protective sealing of the crystals by the thick and dense W-CVD coating, which kept oxygen present in the cobalt away from the diamond surfaces. Thus, in the absence of oxygen, catalysed

graphitisation of the diamonds had been avoided. The crystals could withstand the high temperature processing without back-converting into graphite which could then react with the tungsten to form carbide. On the other hand, a sealing effect was not achieved by the W-PVD coatings, due to their low thickness and the coating discontinuity that was frequently observed in the "as-received" coated diamonds. For the diamond/W-powder systems examined in the DRE, oxygen could have originated from oxide films on the surface of the tungsten powders, which upon reduction could have catalysed the graphitisation of the diamonds, thus subsequently enhancing the reactivity.

The second possible explanation for the observed limited reactivity of the diamonds could be attributed to the presence of hydrogen in the sintering atmosphere. It has been reported that hydrogen can be absorbed on the diamond surfaces either preventing the reaction with the metals or even disrupting already formed diamond-metal bonds [115, 241].

A very strong and firm bonding between the W-CVD coating and the Co-matrix had been achieved (see Figure 9-29B & D). At some locations of the W/Co interfacial zone a relatively thick reaction product had formed, which was extended into the cobalt side indicating tungsten diffusion into cobalt. EDAX analysis at points across the interfacial zone confirmed tungsten migration into the neighbour cobalt matrix. The formed reaction product zones did not suffer from reduced toughness since they did not contain any cracks as it has been seen with the previously examined systems.

The W-CVD coating seemed to function as a tight metal sheath, both mechanically enclosing the diamonds as well as chemically protecting them. The quantitative SEM analysis on the developed fracture surfaces showed composites to possess a combination of parameter values* indicative of enhanced interfacial characteristics that permitted effective matrix to reinforcement load transfer (refer to Table 9-6).

The tensile strength of the composites reinforced with the W-CVD coated diamonds was considerably improved compared to the reference segments incorporating the equivalent non-coated grit, which supported the analysis presented in the previous paragraphs.

Examination of the fracture surfaces of hot-pressed (HP) segments revealed that both the PVD and CVD W-coatings preferentially remained attached onto the diamond surfaces (see Figure 9-18A, B and 9-19C). Although the temperature and time of hot-pressing were considerably lower

* According to composite materials mechanics, interfacial bonding with enhanced composite mechanical properties is associated with low number of diamond sites on the fracture surface (S_N), low number of lost diamonds (L) and a high number of fracture crystals.

than that of pressure-less sintering, considerable chemical interactions between the composite constituents had taken place. Enhanced densification and chemical interactions were attributed to the stress state developed during hot-pressing as has been discussed earlier for the other coated diamond systems. Diffusion of tungsten into the cobalt matrix was evident by EDAX analysis and back-scattered SEM.

In contrast to sintered segments, layers of the W-PVD coatings could be found in the hot-pressed segments. This indicated that dissolution of the W-PVD coating into the matrix was not as extensive as in the case of sintering discussed above.

Cobalt spherical oxides were found in the Co-matrix close to the interface of the W-CVD coated diamonds. This confirmed that carbon diffusion through the thick W-CVD layers was limited. For the thinner W-PVD coatings oxide concentration around the W/Co interface was found to be reduced compared to the amount of oxides in the bulk Co-matrix, suggesting that some carbon diffusion from the diamond had taken place.

The surfaces of CVD coated diamonds appeared relatively smooth and flat indicating minimal interaction with the tungsten as was found for the sintered segments. However, diamonds having the thinner PVD coatings appeared to be slightly etched suggesting that some activity of the diamonds with the metals had occurred. This was further confirmed by the small crystallites found inside trigon etch pits (see Figure 9-19C). EDAX analysis indicated these to be W-carbide crystallites.

The W-coatings were found to effectively envelope the diamonds in the cobalt binder as indicated by the increased number of broken crystals found on the fracture surfaces (refer to Table 9-5). The improved Young's moduli also demonstrated the beneficial effect of the W-coated diamonds, as measured with the impulse excitation technique (refer to Table 9-1). The positive effect of the W-coating for the hot-pressed segments was further apparent with the TRS in 3-point bending. Increases of the order of 14 to 27% compared to the reference segments with the non-coated grit were measured.

11.3.3.9 W-powder encapsulated diamond systems

The segments that were impregnated with the W-powder diamond granules were consolidated with either pressure-less sintering at 1010°C for 30 minutes or with hot-pressing at 840°C.

Examination of the fracture surfaces of sintered segments revealed that extensive reactivity between the diamond and the metal constituents had taken place. This was clearly evident by the

large number of metal remains found bonded onto the diamond surfaces (see Figure 9-31). High magnification SEM coupled with EDAX analysis showed that tungsten was concentrated inside etch pit cavities formed on diamond surfaces (see Figure 9-32). The high W/C ratio suggested formation of tungsten carbides. The reacted W metal was found only inside the etch pits whereas the non-reacted diamond surfaces remained relatively smooth and free from attached metal. This observation supported the proposed mechanism of diamond / metal interactions as presented in the discussion Part-I. Sintered cobalt fragments were also found to adhere onto diamond surfaces providing further evidence of the achieved interfacial bonding.

The amount of metal found to adhere onto diamond was higher for the cubic {100} than the octahedral {111} diamond surfaces in agreement with the findings of the DRE and to other diamond/metal systems as discussed in numerous cases earlier in this chapter.

The increased UTS and yield strength compared to the segments incorporating the non-coated grit provided further evidence of the achieved interfacial bonding revealed by the SEM analysis (see Table 9-4). The UTS values achieved by the segments were among the highest measured.

Interfacial bonding in the hot-pressed segment was of a similar type to that described above. However, the amount of metal found to adhere onto exposed diamonds surfaces was considerably reduced compared to the sintered segments indicating a lower intensity of the reactions, which is expected considering the much lower processing temperature and shorter heating time. For many of the diamonds, cracking followed the boundary of the W-granules. Cracking was slightly displaced towards the tungsten side. This suggested that the interfacial strength at the W/Co boundary had not reached the levels achieved in other W-coated systems previously discussed.

In areas where the W-powder zone that surrounded the diamond crystals was thick, the sintering of the tungsten was poor. The strength of the interfacial regions at such sites was expected to be low. It is probably for that reason that the measured Young's moduli were lower than the reference segments with the non-coated grit. However, the bonding achieved at other interfacial sites as evident by the SEM examination appeared to counteract the effect of the poorly sintered tungsten regions with TRS in 3-point bending to show improvements in the order of 13 to 15%.

11.4 Interfacial Bonding in Coated-Diamond reinforced Alloy-matrix MMCs

This section discusses the results obtained from the series of tests included in the third and last part of the experimental work as presented in Chapter 10. Results are examined in a similar manner to the preceding Part-II. Initially the discussion deals with the effect of metal coating of diamonds on the mechanical properties of the composites and then interfacial bonding in each system is examined in detail.

11.4.1 Densification of the Coated-Diamond Composites

The obtained densities for the various systems were given in Figure 10-1.

Results showed that the segments impregnated with the coated-diamonds had either similar or higher densities than the reference segments containing the non-coated grit. This indicated that there was no added porosity effect associated with the usage of coated grit.

11.4.2 Mechanical Properties

This section discusses the results of the mechanical property tests.

11.4.2.1 Modulus of Elasticity (Young's modulus)

The measured Young's moduli of the diamond composites with alloy metal-matrices were given in §10.3.

Incorporation of diamonds into the alloy metal-matrix resulted the increase of the modulus of elasticity. This provided evidence that some degree of interfacial continuity between the alloy matrix and diamonds that could provide effective load transfer had been achieved. Apart from the two systems with the Co-powder encapsulated diamonds (MB-1 & MB-2), all other coated diamonds showed improved Young's modulus compared to the reference segments with the non-coated grit. The Co-powder encapsulated diamonds were the only diamonds coated with non-carbide forming metal and were the only ones to show reduced modulus compared to the reference segments impregnated with the non-coated grit. This indicated that the presence of carbide forming metal in the form of a coating at the interfacial region between the alloy metal-matrix and the diamond reinforcement was beneficial to the composite Young's modulus.

Further analysis for each particular system is carried out later in this chapter.

11.4.2.2 Transverse Rupture Strength (TRS) in 3-point Bending

The transverse rupture strength (TRS) results from the 3-point bending test for the diamond composites with the plain cobalt matrix were given in §10.4.

The blank references exhibited higher TRS than the diamond reinforced segments. As has been addressed earlier in this chapter (refer to §11.3.2.2 on page 262), such behaviour is typical for particulate MMCs reinforced with non-deformable dispersions [199].

Apart from three compositions (MB-2, MB-7 & MB-8), in all other cases the TRS values of the segments with the coated grit were greater than that for the segments with the equivalent non-coated diamonds.

The bending strength of each individual system will be analytically discussed in the next section, which deals with the interfacial bonding in the composites.

11.4.3 Interfacial Bonding in Coated-Diamond / Alloy-Metal Matrix Composites

This section deals with the interfacial bonding characteristics of the various metal-coated diamond /cobalt composites. Discussion is based on the SEM examination of the fracture surfaces developed by 3-point bending. Analysis takes into account the SEM observations as well as the results of the quantitative fracture surface analysis method presented in 7.3.3.5. Relations of SEM findings with mechanical test results are also included where appropriate.

11.4.3.1 MB-1 : Co + 15%wt. Ni, Co-powder encapsulated 30/40 mesh SYN-3

The SEM examination revealed that both the Co-powder encapsulated diamonds as well as the plain non-coated diamonds were held purely mechanically in the Co+15%wt. Ni binder. There were no metallic remains found on the diamonds and wide interfacial fissures had formed around the diamond crystals. This was not surprising since both cobalt and nickel are metals that primarily dissolve carbon as has been discussed earlier in this chapter.

The plain crystals appeared to have been etched by the binder to a greater extent than the Co-powder diamond granules. Increased dissolution was also clearly evident for the cubic {100} surfaces in agreement with the findings of the DRE.

Quantitative SEM analysis on the fracture surfaces developed by 3-point bending revealed that the segments with the Co-powder granules possessed a slightly better combination of values of

measured parameters indicating enhanced reinforcement compared to the specimens with the non-coated grit. Improvement was found regarding the TRS in 3-point bending with the Co-powder encapsulated diamonds to giving an improvement of the order of 23%.

11.4.3.2 MB-2 : Co + 10%wt. W, Co-powder encapsulated 30/40 mesh SYN-3

The Co + 10%wt. W is a typical situation of a matrix that follows the principle of incorporating a small alloying addition of a carbide forming metal, such as tungsten, in a relative inert binder such as cobalt.

The signs of interfacial reactions between the tungsten and diamond were clearly evident on the surfaces of diamonds exposed to the fracture surfaces. Numerous parts of the metal matrix were found to strongly adhere onto diamond surfaces. EDAX analysis performed on such features revealed that these were tungsten rich, providing strong indications of tungsten carbide formation at the diamond / metal interface. A considerable number of diamonds, which corresponded to approximately 67% of the exposed crystals, had been fractured (see Table 10-3). As has been addressed previously in this thesis, based on principle mechanics of particulate MMCs an increased number of fractured diamonds is associated with a high interfacial bonding strength that exceeds the inherent strength or cleavage of the crystals. This is a strong indication of enhanced chemical bonding, which is directly related with diamond retention during the service life of the diamond tool.

When the Co-powder diamond granules were incorporated into the same binder, diamond surfaces exposed at the fracture surfaces were free from any metallic remains. It was clearly evident that the Co-powder jacket had restricted access of the tungsten to the diamond surfaces and thus reactions to form stable carbides were inhibited. The enveloping of the diamond by the metal-matrix was primarily characterized as mechanical rather than chemical.

The fact that interfacial reactions between diamonds and tungsten were restricted with the use of the Co-powder encapsulated diamonds was also demonstrated by the results of the quantitative SEM analysis of the fracture surfaces as well as by the measured mechanical properties. The segments impregnated with the non-coated grit showed a lower number of lost diamonds and much higher number of fractured diamond (approx. 10 times more) than the segments incorporating the Co-powder diamond granules (see Table 10-3). In addition, the Young's modulus and TRS values were about 6 to 7% greater for the segments impregnated with the non-coated diamonds (see Tables 10-1 and 10-2).

11.4.3.3 MB-3 : Co + 10%wt. bronze 85/15, Cr-PVD 30/40 mesh SYN-3

The SEM examination revealed that non-coated diamonds had undergone only a limited degree of dissolution etching by the cobalt/bronze binder and there were no signs of any metal remains on the diamond surfaces. The bonding of the diamonds to the metal-matrix was purely of a mechanical nature. The alloying with bronze had transformed cobalt into an almost inert binder. Only on the cubic {100} diamond surfaces was some limited degree of dissolution etching detected (see Figure 10-6A). This behaviour of the metal-matrix towards diamond was expected. The relatively inert activity of copper (Cu) and bronze (Cu_{85}/Sn_{15}) was also demonstrated with the DRE (refer to §11.3.3). Numerous researchers have reported the very low wetting and poor adhesion of copper, tin and bronze to diamond [128, 130, 217, 242]. Even small alloying additions of tin can transform matrices such as cobalt into almost an inert binder [229, 232].

With the incorporation of the Cr-PVD-coated diamonds into the cobalt/bronze matrix interfacial reactivity was clearly evident. There were several signs of reactivity of diamonds with chromium. However, reactivity of the chromium with diamond was not the dominating phenomenon. As was demonstrated in Part-II of this chapter (§11.3.3.4), chromium coatings were found to be particularly reactive to diamond at higher temperatures in the vicinity of 1000°C. It was thus considered that the employed hot-pressing temperature of 850°C was insufficient to yield the required amount of chromium/diamond reactivity to turn this interface into the strongest one. However, consolidation conditions were found sufficient to cause the thin Cr-coatings to adhere to the binder. Chromium coatings were preferentially found at the walls of the diamond pull-out craters similarly to the segments with the pure cobalt matrix discussed in Part-II. EDAX analysis revealed chromium to have been dissolved into the metal-matrix to a considerable degree.

The use of the Cr-PVD-coatings was found to be beneficial in terms of superior mechanical properties of the segments into which such diamonds were impregnated. Young's modulus was improved by 5% whereas the TRS increased by 12% relative to the segment with the non-coated grit.

11.4.3.4 MB-4 : Co + 10%wt. bronze 85/15, Cr(C)-PVD 30/40 mesh SYN-3

The MB-4 systems shared the same metal-matrix as the MB-3 discussed in the previous paragraph, but the cobalt/bronze matrix was reinforced with the carbon-enriched Cr-PVD-coated grit.

The SEM examination revealed similar interfacial characteristics to those described for the MB-3 system. The Cr(C) coatings remained preferentially bonded to the metal-matrix and had been dissolved to a considerable extent. The signs of reactions at the diamond surfaces were limited. This was mainly attributed to the relatively low hot-pressing temperature of 850°C, which is typically not sufficient for chromium carbide formation as has been discussed earlier in this chapter.

The segments impregnated with the Cr(C)-coated diamonds exhibited a very low number of diamond sites at the fracture surface, which according to particulate MMC theory should indicate that fracture preferentially occurred within the bulk of the matrix rather than the interfacial regions. The segments with the Cr(C)-coated grit showed an increase in TRS of the order of 15.5% that was the highest measured.

11.4.3.5 MB-5 : Co + 20%wt. bronze 85/15, Ti-CVD 30/50 mesh SYN-1

The cobalt alloyed with 20%wt. bronze was found to be almost entirely inert to the non-coated diamonds similarly to what was found for the MB-3 and MB-4 systems with the 10%wt. bronze additions. On incorporating the Ti-CVD-coated diamonds into the cobalt/bronze matrix interfacial activity was apparent. Titanium coatings had partially dissolved into the matrix, but there were many small parts of the coating that remained strongly adhered onto the exposed diamond surfaces indicating possible titanium carbide formation (Figure 11-22).

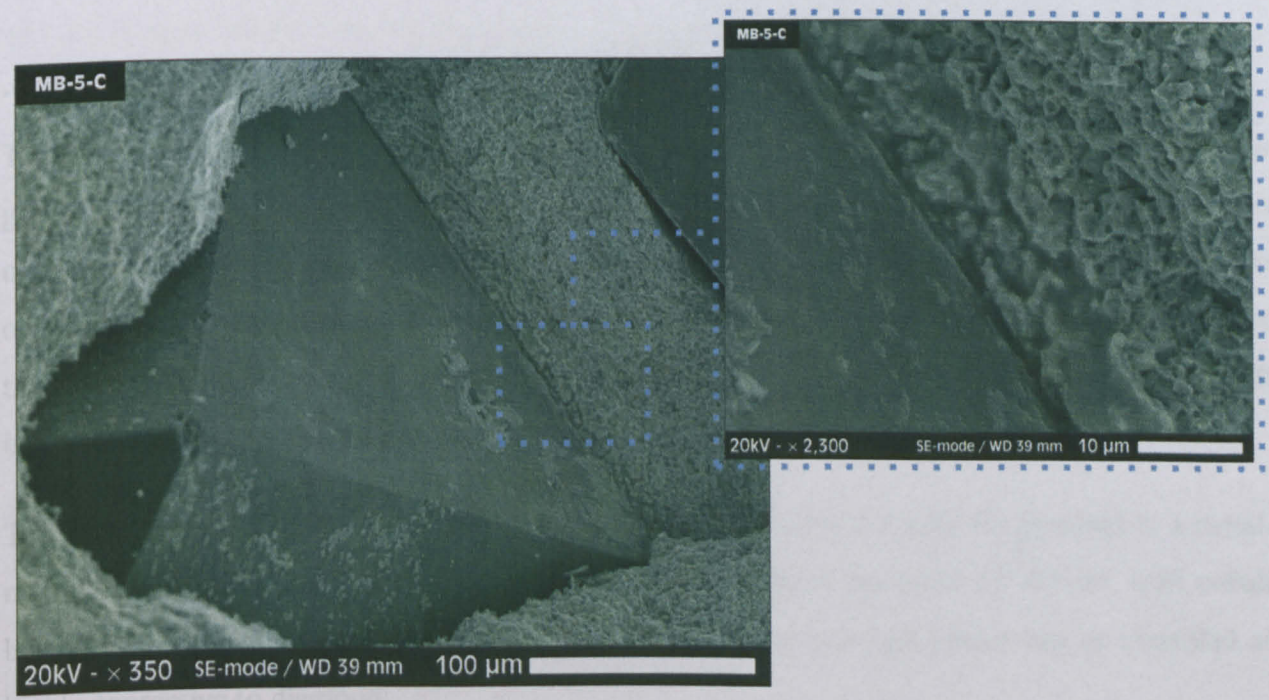

Figure 11-22 : Aspect of a Ti-CVD-coated diamond in a Co + 20% bronze 85/15 matrix. The micrograph on the left shows Ti-coating remains strongly adhered on the exposed diamond surfaces. The micrograph on the top right is a magnified view of an interfacial region showing the formed reaction product zone.

At numerous locations along the interface a dense reaction product had formed (see Figures 10-7 & 11-22). It was typically of the order of 10 micron thick and contained a few cracks starting from the diamond surfaces and arranged perpendicularly to them. This reaction product contained considerably fewer number of cracks compared to the segments with the pure cobalt binder as examined in Part-II. The presence of the Ti-CVD-coating was found to be beneficial for the measured mechanical properties of the hot-pressed segments (see Tables 10-1 & 10-2).

11.4.3.6 MB-6 : Co + 20%wt. bronze 85/15, Ti-PVD 30/50 mesh SYN-1

The MB-6 systems shared the same metal-matrix as the MB-5 discussed in the previous paragraph, but the Ti-coated diamonds incorporated into the cobalt/bronze matrix were deposited by PVD instead of CVD.

The SEM examination revealed that interfacial phenomena were similar to those described for the MB-5 systems with the Ti-CVD-coated grit. It could be however noted, that reactivity of the Ti-PVD coatings with both the binder and the diamonds appeared to be slightly enhanced compared to the Ti-CVD coatings discussed in the previous paragraph (see Figure 10-8).

The average Young's modulus of segments impregnated with the Ti-PVD-coated diamonds was found to be approximately 5% greater than the modulus of the specimens with the non-coated grit. The improvement in TRS was found to be of the order of 15% providing further indication of the beneficial effect of the interfacial reactivity attributed to the presence of the Ti-coating.

11.4.3.7 MB-7 : Pre-alloyed Cu-Fe-Co + 20%wt. Fe, W-PVD 30/50 mesh SYN-1

The pre-alloyed Cu-Fe-Co powder* used as a base to formulate the MB-7 belongs to a new generation of pre-alloyed powders specially designed for diamonds tools. This powder as well as other similar type pre-alloyed powders from various manufacturers are claimed to yield similar or improved performance in sawing or drilling applications. Their evolution mainly arose from the need to minimize cobalt consumption for diamond tool production cost reduction since cobalt is a considerably expensive metal.

The incorporation of 20%wt. of iron powder into the pre-alloyed Cu-Fe-Co resulted in a metal-matrix rich in iron. EDAX analysis showed iron levels to be at the order of 40%wt. with cobalt being at 21-23%wt. and copper being the balance. Such an iron rich binder can be classified as highly aggressive to diamond.

* The pre-alloyed Cu-Fe-Co is traded with the name "NEXT-100".

The SEM analysis of fracture surfaces of segments impregnated with the non-coated grit revealed that the diamonds had been dissolved to a considerable extent demonstrating the aggressiveness of the Cu-Fe-Co metal-matrix. The morphology of the diamond surfaces were very similar to that produced when diamonds were heated in pure iron powder as has been found with the DRE (refer to 11.2.2.2D on page 247). This provided evidence of the dominant effect of the iron content.

The cubic {100} diamond surfaces were clearly dissolved to a greater extent than the octahedral {111} surfaces in complete agreement with the findings of the DRE (see Figure 10-10).

Incorporating the W-PVD-coated diamonds into the Cu-Fe-Co matrix resulted in totally different type of interactions as revealed by the SEM examination of the fracture surfaces. The W-PVD-coatings appeared to partially dissolve into the matrix, but seemed to effectively protect the diamonds from dissolution by the aggressive matrix. The octahedral {111} surfaces were free from any signs of the coating and were only slightly etched, indicating that their bonding with tungsten was weak. On the contrary, the cubic {100} diamond surfaces retained a great part of the W-coating in the form of relatively small irregularly shaped islets (see Figure 10-9). This clearly indicated that tungsten had reacted with the diamond cubic {100} surfaces. The preference of tungsten to react only with the cubic surfaces could be associated with the availability of carbon originating from the diamond. As has been shown by the results of the DRE, the cubic {100} diamond surfaces are more reactive than the octahedral {111} surfaces and this is more pronounced in the presence of carbon dissolving metals such as Fe and Co.

The interfacial bonding achieved by the W-PVD-coated diamonds was also confirmed by the greater number of broken crystals counted on the fracture surfaces compared to the segments with the non-coated grit. The improvement of the Young's modulus was in line with the observed chemical bonding.

Although reactivity was clearly evident, the segments impregnated with the W-coated grit exhibited reduced TRS in 3-point bending. One could possibly attribute this behaviour to defects in the segments, such as for example surface flaws created by diamond crystals emerging to the external surfaces of the segments. However, the variance between the measured TRS was not particularly broad to justify this explanation. The lower TRS could be related to composite toughness reduction attributed to limited internal stress relaxation. The presence of rigid reinforcements in a MMC, such as diamonds, strongly bonded at the interfacial region can

impose increased constraint and plastic flow to the metal-matrix, which may result in reduced toughness [243].

11.4.3.8 MB-8 : Pre-alloyed Cu-Fe-Co + 20%wt. Fe, W-CVD 35/50 mesh SYN-1

The MB-8 systems shared the same metal-matrix as the MB-7 discussed in the previous paragraph, but in this case it was the thick W-CVD-coated diamonds incorporated into the Cu-Fe-Co matrix instead of the thin PVD W-coated grit.

The SEM examination revealed that the thick tungsten CVD coatings did not suffer from dissolution into the Cu-Fe-Co binder. The 5 microns thick W-coatings were bonded excellently to both the diamond and metal-matrix (see Figures 10-11C and D).

Apart from one crystal, all diamonds exposed at the fracture surfaces had fractured or cleaved. This is almost the ideal example for the case of a particulate MMC in which strong interfacial bonding results in reinforcement cracking.

The Young's modulus was found to be slightly higher than the modulus of the segments with the non-coated grit. Similarly to the case with the PVD W-coated diamonds, the TRS of the segments impregnated with the CVD W-coated grit was found slightly reduced compared to that for the non-coated crystals. Considering the clearly evident strong interfacial bonding, it was apparent that the lower bending strength was the effect of reduced composite toughness as discussed in the previous paragraph.

11.4.3.9 MB-9 : Pre-alloyed Cu-Fe-Co + 20%wt. W, W-PVD 30/50 mesh SYN-1

The MB-9 belongs to the category of binders in which a carbide forming metal is added as an alloying addition into a non-reactive base metal or alloy. In the case of the MB-9 binder, the base was Cu-Fe-Co alloy and tungsten was the alloying addition.

Examination of the fractured surfaces of segments impregnated with non-coated diamonds revealed that the dissolution etching processes were reduced compared to the case of non-coated diamonds hot-pressed in the Fe-rich Cu-Fe-Co binder (MB-7 and MB-8 systems). This was attributed to the reduced iron content combined with the presence of tungsten. Inspecting the condition of exposed diamond surfaces made apparent that there was a clear difference in the activity between the cubic {100} and octahedral {111} diamond surfaces. The octahedral {111} surfaces had been etched at a relatively lower degree and macroscopically appeared to have remained fairly inert considering the aggressiveness of the metallic environment. This was

attributed to the combined effect of the presence of tungsten as well as to the high resistance of octahedral diamond surfaces to dissolution or reaction as has been found with the DRE. On the contrary, cubic {100} diamond surfaces had clearly undergone substantial dissolution by the metal-matrix (see Figure 10-12), in agreement with the increased reactivity of these surfaces compared to the octahedral as has been addressed numerous times already for many systems previously discussed in this chapter. Reactivity of the cubic surfaces with tungsten was found to be limited. There were only a few points where W-rich metal remains were found adhered onto the exposed diamond surfaces.

Incorporating the W-PVD-coated diamonds into the W-alloyed Cu-Fe-Co matrix resulted in totally different type of interactions as revealed by the SEM examination of the fracture surfaces. Similarly to the segments impregnated with non-coated grit, the difference in the reactivity between the cubic {100} and octahedral {111} diamond surfaces was clearly apparent. The thin W-coating appeared almost entirely dissolved from the octahedral surfaces. There were, however, small angular crystallites emerging from the diamond surfaces that indicated a small degree of carbide formation. On the contrary, the cubic surfaces had retained the majority of the W-coating providing clear evidence of increased reactivity. The behaviour of both the cubic and octahedral surfaces conformed to their relative reactivity evolved by the DRE and as was addressed for the MB-7 system previously discussed.

The greater number of broken crystals and lower number of diamond sites counted on the fracture surfaces compared to the segments with the non-coated grit confirmed the interfacial bonding achieved by the W-PVD-coated diamonds.

The small improvements in Young's modulus and TRS were in line with the observed chemical bonding. Considering that strong bonding was achieved only for the cubic surfaces one could assume the composites as being of a mixed type interfacial bonding. It could be assumed that the strongly bonded cubic surfaces constrained the matrix plastic flow and acted towards composite toughness reduction, whereas the weakly bonded octahedral surfaces having the opposite effect, with the net effect being the slight increase of the TRS.

11.4.3.10 MB-10 : Pre-alloyed Cu-Fe-Co + 20%wt. W, W-CVD 35/50 mesh SYN-1

The MB-10 systems shared the same metal-matrix as the MB-9 discussed in the previous paragraph, but in this case it was the thick W-CVD-coated diamonds incorporated into the W-alloyed Cu-Fe-Co matrix instead of the thin PVD W-coated grit.

The SEM examination revealed that interfacial bonding was very similar to the case of the Fe-rich Cu-Fe-Co matrix impregnated with the thick tungsten CVD coatings (MB-8 system). The thick W-CVD coatings did not suffer from dissolution into the binder. For most of the diamonds the thick W-coatings were bonded excellently to both the diamond and metal-matrix (see Figures 10-14B).

The interfacial bonding was also demonstrated by the results of the quantitative SEM analysis of the fractured surfaces. The segments impregnated with the W-CVD-coated diamonds exhibited a reduced number of lost crystals and diamond sites, combined with an increased number of broken diamonds (see Table 10-3).

Improvements of the measured mechanical properties provided further evidence of the beneficial effect from impregnating the Cu-Fe-Co-W matrix with the W-CVD-coated diamonds.

11.5 Summary

The summary that follows provides an overview of the main points evolved in discussing the results. The summary is laid out in three sections in accordance with the way in which both the results and the discussion were presented.

11.5.1 Part-I: Fundamental Study of Diamond-Metal Reactivity

In the absence of oxidising agents and metal, the synthetic crystals could withstand the heat treatments associated with the DRE with little graphitisation. Annealing of synthetic diamonds with loose elemental powders showed some of the metals to catalyse the diamond graphitisation and promote dissolution of carbon into the metal, whereas others reacted to form carbides. The relative ranking of the tested metals in decreasing order was found as follows:

$$\textit{Diamond dissolution: } Fe > Co\text{-}SMS > Co\ (CoC) > Co\text{-}EF > Ni > Cu$$

$$\textit{Carbide formation: } W > Ti > Cr > Mo$$

The tendency of metals to dissolve or react with diamond and the ranking found corresponded well with the electronic structure of the metals and depended on their *d*-orbital vacancies. The only discrepancy was the relative ranking between W and Ti, which was associated with the increased oxidation of the powders of the latter.

The SYN-2 type diamonds (MBS960, 50/60 mesh, General Electric) were found to be prone to increased dissolution compared to the SYN-1 type grit (SDA100, 30/40 mesh, De Beers), which was associated with the increased surface area available for these finer crystals. In addition, SYN-2 diamonds exhibited reduced reactivity, which was related to the density of dislocations emerging to crystal surfaces.

Dissolution of the crystals occurred in the form of oriented hexagonal or triangular pits on the octahedral {111} diamond surfaces, whereas on the cubic {100} surfaces etch pits had the form of oriented rectangular depressions. These patterns were suggested to originate because of the geometrical characteristics of the diamond lattice. The cubic {100} diamond surfaces were found to be more reactive than the octahedral {111} surfaces.

High magnification SEM revealed that reactions to form carbides occurred at the etched diamond surface sites. The results suggested that graphitisation is a necessary step in order for diamond surfaces to react with the metals.

The results of the diamond crystals weight change measurement and the observations from the SEM examination were in complete agreement.

The interaction phenomena between diamond and metals for systems hot-pressed under standard industrial conditions were in accordance to the previous findings for the metal powder systems. The intensity of interactions was however considerably reduced mainly due to the milder processing conditions.

Examination of metal-coated diamonds subjected to the DRE showed that the diamond crystals had not been affected by the deposition treatment as far as it concerned the status of their surfaces.

Some limited signs of reaction between metal and diamond during deposition were evident only for the Cr and W PVD-coated diamonds. On annealing the coated diamonds to temperatures up to 1025°C, coatings reacted with the diamond substrate at variable levels. The relative intensity of these reactions conformed to the ranking found for the diamond-metal powder systems. A particularly high level of reaction was evident for the Cr(C)-coatings, which was attributed to the presence of the free carbon that was co-deposited during formation of this composite coating. Heat-treatment at the lower temperature of 500°C resulted in limited reactivity of the coatings to the diamonds. Reactivity was found to be greater for the inferior quality SYN-3 diamonds (SDA75, De Beers) and to be particularly favoured at crystal defected areas.

Diamond surfaces inspected after the various heat-treatments did not show signs of degradation.

11.5.2 Part-II: Characterisation of Coated-Diamond / Co-matrix MMCs

Consolidation of the composites with the plain cobalt matrix was made with various methods.

The pressure-less sintered segments exhibited the lowest densities followed by the hot-isostatically pressed. Highest segment densities were achieved by hot-pressing.

The influence of density was clearly apparent to the mechanical performance of the sintered and HIP segments. The variation of the measured mechanical properties in these segments was relatively small and did not evolve any significant effect of the metal coating. Significant improvements of mechanical properties due to the use of coated diamonds were only measured for hot-pressed segments and for segments consolidated with the highest utilized sintering temperature of 1010°C.

Heat-treatment of the coated diamonds at 500°C prior to segment consolidation was not found to have a particular beneficial effect.

Three simple models for predicting the modulus of elasticity of MMCs were employed for calculating the Young's modulus. Close approximation between calculated and actual values was found only of the two models that included consideration for porosity.

In the absence of a carbide-forming metal-coating, cobalt attacked the diamonds by catalysing their dissolution. The intensity by which cobalt attacked the diamonds increased for higher consolidation temperatures and longer sintering times. For all production routes, the bonding of the diamonds in cobalt was purely a mechanical type of enveloping. Highest densification and best mechanical properties were achieved with hot-pressing the non-coated diamonds in the cobalt. In general, the mechanical properties of segments with the non-coated diamonds were quite good considering the purely mechanical type of bonding. This was attributed to the reduction of cobalt oxides in the vicinity of the diamonds, which created ductile cobalt zones around the diamonds. Segments incorporating the SYN-3 (SDA75, De Beers) type of synthetic diamonds showed slightly better mechanical properties than segments with the SYN-1 (SDA100, De Beers), despite being of inferior quality. This behaviour was attributed to the greater thermal attack of the SYN-3 diamond by cobalt, which caused greater levels of dissolution, thus producing thicker ductile cobalt zones around each crystal.

The interaction phenomena in segments impregnated with the Co-powder encapsulated diamonds were very similar to those observed in the segments with the non-coated grit. The primary difference was that in this case, the cobalt powder of the granules was sintered at slightly greater levels than the bulk matrix. This resulted in a tough and ductile jacket around each diamond that aided mechanical properties. The fact that the thick cobalt/diamond granules had similar density to the granulated cobalt powder, resulted in minimising the diamond segregation during the cold-press die filling. Thus, diamonds in the segments were found to be relatively evenly spread reducing the risks of excessive local stresses.

Reactivity in composites with Ti-coated diamonds was very much dependent on consolidation conditions. Reaction of the Ti coating with both the diamonds and cobalt was favoured during the consolidation of the tensile test specimens (1010°C, 30min) and during hot-pressing (840°C, 3 min). The activity of Ti-coating observed with hot-pressing was attributed to the rupture of titanium oxide films. This was particularly efficiently achieved at certain interfacial locations, which were assumed as sites of high stress state. Thick reaction products were found to form at

such locations. Reactivity of diamond surfaces with the titanium was found to nucleate and grow from within etch pits. This confirmed the findings of the DRE and supported the proposed mechanism for diamond/metal interaction. Furthermore, cubic {100} diamond surfaces exhibited an increased activity in complete agreement with the findings of the DRE. However, in general the Ti-coatings offered protection to the diamonds against dissolution by the cobalt. The obtained degree of reactivity was found to be sufficient to cause improvement in mechanical properties. For hot-pressed segments there was a distinct enhancement of the Young's modulus and TRS in 3-point bending of the order of 4.0-9.5% and 5-20% respectively. Segments incorporating the SYN-3 diamonds exhibited greater improvements in mechanical properties, which was suggested to be related to their lower thermal stability as addressed above.

Consolidation conditions were also critical for segments incorporating the Cr-PVD-coated diamonds. For sintering temperatures below 1000°C the bonding strength of chromium to diamond did not exceed the strength of the Cr/Co interfacial bonding. Reactivity of chromium to diamond was only evident in defected areas or locations of high stress state for the same reasons as addressed for the Ti-coatings. Reactions were favoured on cubic {100} surfaces and were associated with the attachment of chromium inside diamond etch pits conforming to the findings of the DRE. For the hot-pressed segments the obtained degree of reactivity was sufficient to yield improvements of the order of 3-9% in elasticity modulus and 10-28% for the TRS in 3-point bending. Sintering above 1000°C resulted in the abundant reactivity of the Cr-coating with the diamonds and the cobalt matrix, with clearly evident beneficial effects on the tensile properties. Improvements of the order of 22-35% and 27-28% were measured for the ultimate tensile strength and yield strength compared to the composites impregnated with non-coated grit.

The critical influence of temperature on chromium to diamond reaction as addressed above was also demonstrated with the segments impregnated with the Cr-powder encapsulated diamonds. On hot-pressing the Cr-powder diamond granules with cobalt at 840°C only limited reactivity was evident. Diffusion of chromium into cobalt was the dominating phenomenon. Only small improvements of Young's modulus and TRS were measured that were mainly attributed to poor sintering of the chromium powders around the diamond crystals. Consolidating the segments at a temperature in excess of 1000°C intensified the reactions between the Cr-powders and diamonds. Reactions took place at the points of true contact between the Cr-powders and diamond surfaces. The fractions of the diamond surfaces not in direct contact with Cr-powder had been dissolved by cobalt. The tensile properties of the segments were considerably improved by orders of 32-42% and 24-31% for the UTS and yield strength respectively.

The presence of free carbon in carbon-enriched Cr-PVD-coated diamonds limited its reactivity to both the diamond and cobalt relative to the standard Cr-PVD-coatings. On pressure-less sintering and hot-isostatic pressing the Cr(C)-coatings were preferentially bonded to cobalt. The free carbon of the coating provided extra protection to the diamond, which remained practically unaffected, and at the same time reduced the cobalt oxides in the vicinity of the diamonds. On hot-pressing, the Cr(C)-coating remained attached onto diamonds instead of the cobalt, without however showing considerable signs of reaction with the latter. This was attributed to the increased stiffness of the coating because of chromium carbide formation in the coating attributed to the free carbon. The reaction of chromium with the free carbon together with the relatively low temperature and short duration of hot-pressing were assumed to be responsible for the poor adhesion of these coatings to the cobalt matrix. On sintering at 1010°C considerable reactivity of the Cr(C)-coating to both the diamonds and the cobalt was evident. However, the intensity of these interactions was reduced compared to the standard Cr-PVD-coatings because of the free carbon. The limited reactivity of the Cr(C)-coating was also demonstrated by the relatively smaller improvements in the mechanical properties compared to segments impregnated with the standard Cr-PVD-coated grit. The Young's modulus and TRS of hot-pressed segments were improved by approximately 6-7% and 17-24% respectively. The UTS and yield strength of high temperature sintered segments increased by about 12-17% and 18-21% respectively compared to the values measured for segments with non-coated diamonds.

The interfacial phenomena in segments incorporating the diamonds with the composite Ti/Cr PVD coatings were in line with the phenomena observed for the standard Ti- and Cr-coated diamonds. Similarly, the mechanical properties of the segments lay in between those of the standard Ti- and Cr-coated diamonds.

The W-coated diamonds appeared to be the most reactive in agreement with the DRE. There were two types of W-coated diamonds examined, a thin PVD and a 5 micron thick CVD. The thin PVD coating was found to react with diamond but was also incapable of resisting dissolution into the cobalt with the immediate result being the direct exposure of diamond surfaces to cobalt. Tungsten reaction with diamond was nucleated inside etch pits conforming to the findings of the DRE. At higher sintering temperatures the reactions were intensified. The increased number of fractured crystals counted on fractured surfaces confirmed interfacial bonding. The use of the W-PVD-coated diamonds was found to be beneficial for UTS and yield strength in tension with improvements of up to 14% and 23% respectively. Similarly,

improvements of the order of 3.0-7.5% and 14-27% were measured for the Young's modulus and TRS of the hot-pressed segments.

The thicker W-CVD coatings could withstand the dissolution by cobalt without losing their continuity. They therefore offered maximum protection of the diamonds against catalysed graphitisation by cobalt and oxidising agents. The W-CVD-coatings preferentially bonded to the cobalt matrix. There were however interfacial locations where additional bonding to the diamond had been achieved. In general the reaction with diamond was limited compared to the PVD-coatings and was attributed to the effective sealing of the diamond surfaces from oxygen and cobalt. The W-CVD-coatings functioned as a tight metal sheath that proved to be quite beneficial for segment mechanical performance. Tensile properties were considerably improved even from the W-PVD-coated diamonds, with UTS and yield strengths increases reaching levels of the order of 19-35% and 10-23% respectively. The Young's modulus and TRS for the hot-pressed segments were found to be increased by about 5.5-8.0% and 17-26% compared to segments impregnated with non-coated grit.

Finally, reactivity in segments impregnated with the W-powder encapsulated diamonds clearly depended on consolidation temperature. On hot-pressing at 840°C the interaction of the tungsten powders with both the diamond and cobalt exhibited reduced intensity. The poor sintering of the tungsten at that temperature was reflected by reduction of Young's modulus compared to the non-coated diamond reference segments. The bending strength was found to be improved by 13-15%. However, on consolidating the segments by sintering at 1010°C resulted in extensive reactivity. Metal remains were abundantly found on diamonds attached on the etch pits with the cubic {100} diamond surfaces exhibiting highest interaction activity in complete agreement with the results of the DRE. The tensile properties of the segments were considerably improved by orders of 23-34% and 4.5-6% for the UTS and yield strength respectively.

11.5.3 Part-III: Characterisation of Coated-Diamond / Alloy-matrix MMCs

Consolidation of the composites with the alloyed metal-matrices was by hot-pressing. The densities of the coated diamond reinforced segments were either of similar levels or higher than the non-coated impregnated reference samples. This demonstrated that there was no added porosity effect associated with the usage of coated grit. Young's modulus was found increased for all composites incorporating coated diamonds in which the coating metal was a metal belonging to carbide forming elements.

The discussion of the results of the examined systems is summarised as follows.

The Co+15%wt. Ni binder (MB-1) held both the Co-powder encapsulated as well as the non-coated diamonds purely mechanically. Diamond dissolution was the dominant interfacial phenomenon with diamond surfaces demonstrating variable degrees of interactions in complete agreement with the findings of the DRE. Quantitative SEM analysis indicated the use of the Co-powder diamond granules to be slightly beneficial, confirming the observed 23% increase in composite TRS associated with these abrasives.

The Co+10%wt. W (MB-2) was a chemically reactive binder in terms of carbide formation activity. This was clearly demonstrated by the signs of reactivity on non-coated diamond surfaces, which indicated formation of interfacial tungsten carbides. Approximately 67% of the crystals on the fracture plane were found broken providing strong evidence of enhanced interfacial bonding. The incorporation of Co-powder encapsulated grit into the MB-2 binder resulted in restricting access of tungsten to the diamond surface, with a direct effect being the retardation of reactivity. This was found to reduce interfacial bonding as demonstrated by the quantitative SEM results and the reduction in both the composite modulus and TRS.

In contrary to the effect of alloying with tungsten seen for the MB-2 binder, the addition of 10% 85/15 bronze into cobalt transformed the latter into a relative inert metal-matrix (MB-3). The interfacial bonding of non-coated diamonds in this binder was purely of a mechanical nature with very limited levels of carbon dissolution being evident. The incorporation of Cr-PVD-coated diamonds into the MB-3 binder resulted in both signs of reactions of chromium to diamond but also diffusion bonding of the chromium to the metal-matrix. The latter was the dominating interfacial phenomenon. The incorporation of the Cr-PVD-coated grit into the MB-3 binder was found to increase composite Young's modulus and TRS by 5 and 12% respectively. Similar type of interfacial phenomena occurred when the Cr(C)-PVD-coated diamonds were incorporated into the same metal-matrix (MB-4 system). TRS increases of the order of 15% were measured for the segment impregnated with the Cr(C)-coated diamonds compared to the reference segment with the non-coated grit.

The interfacial bonding and mechanical properties were also studied for composites (MB-5 and MB-6 systems) having a Co-based binder in which the bronze (85/15) alloying addition was increased to 20%. These binders were almost completely inert with respect to interaction with the non-coated diamonds resulting in purely mechanical gripping of these abrasive crystals. Two types of Ti-coated diamonds were incorporated into this binder, a CVD (MB-5) and a PVD (MB-

6). The Ti-coatings were found to promote interfacial interactions with both the diamond and the metal-matrix. In contrast to the chromium coatings discussed above, the reactivity of the Ti-coatings to the diamonds occurred at considerable levels, which resulted in parts of the coating being strongly adherent to the diamond surfaces. The intensity of the interfacial reactions to both the diamond and the matrix was found slightly increased for the PVD coatings. This was also demonstrated by measured mechanical properties. The Young's modulus and TRS were found to increase by 4% and 5.3% for the CVD-coated diamonds, and by 5.2 and 15% for the PVD-coated diamonds respectively.

The remaining systems examined involved binders based on a Cu-Fe-Co alloy formulated from pre-alloyed powders, which was alloyed with 20%wt. of either Fe (MB-7 & MB-8) or W (MB-9 and MB-10).

Adding 20%wt. Fe in the above Cu-Fe-Co resulted in the formulation of a very aggressive matrix in terms of diamond dissolution potential. This was clearly evident on the surfaces of non-coated diamonds, which were heavily etched by the binder. The mode of dissolution conformed to the previous findings of the DRE. The surface morphology of the non-coated diamonds resembled the patterns found in the diamond / Fe-powder systems providing evidence that the effect of the high iron content was characterising the chemical activity of the binder. The W-coating was found to provide very efficient protection to the diamonds from the aggressive binder. Tungsten was found to be readily dissolving into the metal matrix and in the case of the thin W-PVD-coated diamonds the coating did not withstand this dissolution action and lost continuity. Diamond surfaces were made accessible to the binder and evidence of catalysed dissolution were visible on diamond surfaces. This however, promoted reactivity to form carbides due to the increased release of carbon atoms from the diamond surfaces, which was particularly apparent on the diamond cubic {100} surfaces. In contrast to the PVD-coatings, the thick W-CVD coatings did not suffer from loss of continuity and provided excellent protection of the diamonds from the binder. The W-CVD-coated diamonds appeared to operate ideally with this binder and apart from one diamond all other crystals found on the fractured surfaces were broken, indicating a very strong encapsulation of the diamonds by the W-CVD jackets. The Young's modulus of segments impregnated with the W-coated grit was found to increase relatively to the segments with the non-coated grit. However, the TRS showed reductions, which were associated with reductions of matrix toughness due to increased matrix constraint and plastic flow imposed by the presence of the rigid diamond crystals.

In contrast to the previous systems (MB-7 & MB-8), adding 20%wt. W in the Cu-Fe-Co alloy resulted in reducing the aggressiveness of the binder and increasing the potential for carbide formation reactions. Dissolution etching was efficiently retarded by the presence of the W-alloying addition. Octahedral {111} surfaces of non-coated diamonds were practically intact with the binder and only the cubic {100} surfaces showed clear signs of interactions with the binder. This different behaviour of the diamond surfaces was in agreement with previous findings. Evidence of carbide formation was provided by small crystallites emerging from the diamond {100} surfaces. The difference between activities of diamond surfaces was more pronounced for the W-PVD-coated crystals. Tungsten dissolved into the matrix, but on the cubic surfaces the W-layers appeared to remain to great extents indicating that reactivity of the coating with the diamond had taken place. The thicker W-CVD coating did not suffer from dissolution and achieved bonding to both the diamond and the metal-matrix. Composites impregnated with both types of W-coated grit showed improved mechanical properties and better combination of counted features in the quantitative SEM analysis compared to the non-coated grit.

12

Conclusions

12.1 Introduction

This chapter lists the main conclusions drawn from the investigation into the interfacial bonding in diamond MMCs reinforced with metal-coated diamonds.

The conclusions from the study on the fundamental chemical interaction phenomena occurring between synthetic diamonds and elemental metals are listed first (§12.2), followed by conclusions drawn from examining interfacial bonding and mechanical properties of coated-diamond reinforced MMCs (§12.3).

12.2 Interactions between Synthetic Diamonds and – Elemental Metals

The fundamental study into the chemical phenomena taking place in simple two component systems made of synthetic diamonds and elemental metals has shown the following:

Synthetic diamonds – loose metal powder systems:

- In the absence of oxidising agents and metal, all tested non-coated synthetic diamonds showed limited graphitisation during the high temperature heating, which reached 1025°C.

- Metals of the VIII-B and I-B group of periodic table of elements catalysed the dissolution of carbon from the diamond into the metal. On the contrary, tested metals belonging to the IV-B and VI-B groups preferentially reacted with diamonds to form carbides.

- Under the selected testing conditions, the relative ranking in decreasing order of tested metals in terms of dissolution activity towards diamond was shown to be: Fe > Co > Ni > Cu.

- Under the selected testing conditions, the relative ranking in decreasing order of tested metals in terms of intensity of carbide formation was shown to be: W > Ti > Cr > Mo.

- The SYN-2 type diamonds (MBS960, 50/60 US mesh) dissolved more aggressively and additionally reacted less favourably than the SYN-1 type crystals (SDA100, 30/40 US mesh).

- Dissolution of octahedral {111} diamond surfaces took place in the form of hexagonal or triangular pits, which were oriented parallel to each other. On the other hand, dissolution of cubic {100} diamond surfaces proceeded with the nucleation and growth of rectangular parallelepiped depressions.

- The cubic {100} diamond surfaces were found more reactive than the octahedral {111} ones.

- Reaction occurred at the etched features on diamond surfaces, indicating that graphitisation of the diamond surface is the necessary step for diamond surfaces to react with the metals. Carbides were found in the form of platelets emerging in random directions from the diamond surfaces.

Hot-pressed synthetic diamonds and metal powders:

- The mode of interaction of metals when hot-pressed under standard industrial conditions is the same as that exhibited with the loose metal powder systems. The intensity of these interactions is however considerably reduced reflecting the lower temperature and shorter heating durations involved with hot-pressing.

Metal coated diamond systems:

- Some limited degree of carbide formation, to have taken place during the coating deposition, was only detected for the Cr-PVD and W-PVD-coated diamonds. All other tested coatings showed no carbide formation during the vapour deposition.

- Strong reactivity between the diamonds and the metal coatings took place with annealing to 1025°C in argon atmosphere. The PVD coatings of Cr, carbon enriched Cr [Cr(C)] and W appeared to exhibit the highest reactivity.

- Annealing of the coated grit at 500°C in H_2/N_2 caused limited reactivity.

- Reactivity was promoted at crystals defected areas such as cavities, etch pits and other surface irregularities. The SYN-3 diamonds (SDA75), which represented the least thermally resistant diamond grade from all tested synthetic diamonds, exhibited the highest reactivity with the metal coating.

- The metal coating offered superior protection from oxidation and graphitisation of the diamonds during both the vapour deposition and the subsequent heat-treatments.

12.3 Interfacial Bonding & Mechanical Properties of Coated-Diamond reinforced MMCs

The work carried out in order to examine the effect of metal coatings deposited on to diamonds as regarding the interfacial bonding and mechanical properties of diamond reinforced MMCs has shown the following:

- From the three manufacturing routes employed, the pressure-less sintering (FS) and hot-isostatic-pressing produced composites with relatively high levels of porosity. Interfacial reactivity in those systems was evident, but its effect on composite properties was not possible to be identified since mechanical properties were greatly influenced by the high levels of porosity.

- Hot-pressing (HP) yielded the highest composite densities, at relative lower temperatures and shortest processing times, conditions that ensured minimal chemical interactions between composite constituents.

- Composites impregnated with the vapour deposited coated diamonds provided increased Young's modulus compared to the equivalent segments impregnated with non-coated diamonds. Increases of the order of 5 to 10% were typically monitored.

- Good prediction of calculated composite modulus to the experimentally measured values was obtained with the relative simple models of Cohen-Ishai [203] and Halpin-Tsai [202] that included consideration for composite porosity.

- Composites impregnated with the coated or powder encapsulated diamonds typically exhibited improved bending strength compared to segments reinforced with non-coated grit. Increases of up to 40% were measured. In some cases, for systems showing clearly strong interfacial bonding, reduced TRS values were seen. This was attributed to the well bonded rigid diamond crystals imposing constraint plastic flow to the matrix.

- Most of the composites incorporating the coated diamonds and consolidated by sintering at the temperature above 1000°C exhibited improved tensile properties than the equivalent reference segments with the non-coated grit.

- The "as sintered" rough external surfaces of the diamond-reinforced segments influenced their tensile properties and relatively large scatter of results was evident.

- The diamond/cobalt systems, which included the non-coated diamonds as well as the Co-powder encapsulated grit reinforcing a pure Co-matrix, showed relatively high mechanical properties although interfacial bonding was identified to be purely of mechanical nature. This was attributed to thick ductile cobalt zones surrounding the crystals, which originated from the reduction of cobalt oxides at the vicinity of the diamonds.

- The stress state imposed by hot-pressing proved beneficial to densification and rupturing of oxide layers on metal coatings. Reactivity was enhanced at the interfacial regions of high stress state, which were identified to be related to areas in the composites where the concentration of diamond crystals parallel to the hot-pressing direction was increased.

- Thick reaction products were occasionally formed at interfacial regions in composites impregnated with coated diamonds. These reaction products showed variable degrees of cracking depending on the coating metals as were visible on fracture surfaces. However, they were not associated with reduced mechanical properties. In fact such reaction product zones were found to be beneficial for the composite performance.

- Reaction on the diamond surfaces took place at the locations were prior dissolution of the diamond had occurred, in agreement to the findings of the fundamental reactivity tests.

- The cubic {100} diamond surfaces were found to be more reactive than the octahedral {111} surfaces, conforming to the finding of the Diamond Reactivity Experiment (DRE).

- Variable levels of diffusion of atoms from the coating into the metal matrix were observed. For some systems and for diamonds with thin coatings, the dissolution of the coating from the

binder resulted in loss of coating continuity. This was particularly evident with the thin W-PVD-coated diamonds.

- For systems in which either the coating was partially peeled-off or was dissolved by the binder, the diamond surfaces had been made accessible to the metal-matrix, resulting locally the catalysed dissolution of the diamond surfaces. This proved to promote carbide formation with the remaining coating that retained contact with the crystal.

- Coating thickness was shown to be a critical parameter to avoid loss of coating continuity in binders readily dissolving the coating metal. Diamonds enclosed by continuous coating layers were effectively protected by dissolution even when introduced into very aggressive binders. This was clearly demonstrated by the 5 microns thick W-CVD coatings, which provided excellent protection to the diamonds from oxidation and graphitisation in Co-matrices as well as in a highly aggressive Fe-rich binder.

- Thick coatings appeared to provide a supplementary mechanical strengthening of diamond retention in addition to the chemical bonding effect.

- The consolidation temperature was found critical with respect to the intensity of the interfacial reactions. At the employed temperatures below 1000°C, the coating/matrix interfaces appeared to be the strongest. For sintering above 1000°C, the reactivity of the various coatings to the diamond increased drastically and in many cases the diamond/coating interface proved to be the strongest.

- Encapsulation of diamond with carbide former powders promoted interfacial reactivity, but suffered from reduced sintering at the zones around the diamonds, especially when consolidation was made by low temperature hot-pressing. Sintering at higher temperatures improved this situation, but increased the attack of the diamonds at the locations were the binder accessed the diamond surfaces.

- The proposed quantitative fracture surface analysis method proved to be a powerful tool for evaluating interfacial bonding in diamond composites when combined which standard qualitative SEM analysis.

13

Future Work

As an outcome of the experimental work carried out during the course of this research, and the results obtained, there have been several areas identified where there is scope for further investigation.

Reactivity of carbide forming metals with synthetic diamond was found to strongly depend on temperature and time. The influence of these two parameters should be studied in more detail in order to establish the minimum required conditions for achieving interfacial reactivity. These kinetic studies should cover the complete range of temperatures of practical importance for diamond reinforced MMCs consolidation. Such investigation could be performed with both loose metal-powder/diamond systems as well as with metal-coated crystals, similarly to what was done in this work. Furthermore, it could be of interest to determine the effect of heat treatment atmosphere on metal/diamond reactivity. Test atmospheres could involve various levels of vacuum or CO/CO_2 reducing atmospheres, which are typically employed.

It still remains an issue to find a technique to prepare samples and to study qualitatively and in detail the formed products across diamond crystal/metal interfaces. Possible candidate techniques could be X-ray photoelectron spectroscopy (XPS) and transition electron microscopy (TEM).

The achievement of interfacial bonding with the use of metal-coated diamonds was shown to be associated with increased number of broken crystals found at the fracture surfaces. Provided that the strength of diamond crystals remains unaffected by the coating deposition and subsequent heat-treatment, such phenomenon indicates achievement of strong interfacial bonding. The status of the diamond surfaces observed for the coated diamonds after the deposition and the heat-treatments indicated that the crystals had undergone very limited attack by the contact with the carbide forming metals. However, heating diamonds at high temperatures may cause variable degree of reduction in crystal toughness due to internal stresses arising from local graphitisation around metallic inclusions. Possible deterioration of crystal toughness due to both coating deposition and subsequent heat-treatment was not determined in this work. It could be of interest to determine at which extent such crystal toughness reduction may occur and how this would influence the performance of the diamond MMCs. The relative toughness of the diamonds could be determined by a standardised method such as the *"friability test"* (see §2.3.3.2 p.12 and §4.6.1 p.66) after each high temperature treatment of the crystals.

Further work could also be carried out in assessing the strength of adhesion of the deposited metal coatings on diamond crystals. This could be achieved either by directly measuring the tensile or shear force required to separate the coating from the diamond or indirectly by determining the weight loss caused by coating peeling-off after ball milling the coated crystals.

Hot-pressing was demonstrated to be the most appropriate method for achieving composite densification and improved mechanical properties at relative low temperatures and short heating durations, thus affirming its wide acceptance for diamond MMCs consolidation by the industry. The results showed that the onset of reactivity between synthetic diamonds and carbide forming metals and the strengthening of the diamond/coating interface to occur at relative higher temperatures and longer heating times compared to the standard hot-pressing conditions. Since coating of the diamonds was proved to provide efficient protection from catalysed surface graphitisation and dissolution by the binder, it could be interesting to investigate possible hot-pressing at higher temperatures and longer times sufficient to allow adequate chemical interactions at the diamond/coating interface. In other words, it should be examined the possibility of incorporating the required post-deposition heat-treatment of coated diamonds into the hot-pressing cycle. The hot-pressing temperatures and times to be selected should be based on the findings of previous studies on diamond/metal reactivity kinetics as proposed above.

Coating thickness was found to be a critical parameter in order to maintain coating continuity in binders readily dissolving the coating metal. Composite mechanical properties and examination of fracture surfaces also indicated that increased coating thickness appeared to have a supplementary mechanical effect in strengthening the enveloping of the crystals by the metal-matrix. For the above two reasons it is justified that the effect of coating thickness on diamond retention and composite mechanical properties should be studied much more extensively than what it was done in this work. Thickness to be studied could range from 5 to 20 microns or even higher, if such were feasible to be deposited at acceptable temperatures and durations not detrimental to diamond crystal strength.

Mechanical property results showed a significant scatter for some of the tested composite systems. It was believed that this was mainly attributed to the fact that the testing was conducted to specimens with external rough surfaces as produced by hot-pressing or sintering and which may have contained protruding diamond crystals and even small cracks. It is envisaged that the scatter in results can be reduced and thus improve the validity of results by testing segments with polished external surfaces. Test specimens enabling polishing of their external surfaces should not contain diamonds close to the surfaces. Preparation of such samples could be achieved by initially filling the cold-pressing die with a portion of metal-matrix powder, then add the powder mixture containing the diamonds and finally adding again a portion of metal-matrix powder, thus creating a "sandwich" structure.

In this work assessment of interfacial bonding was made by means of determination of diamond MMCs mechanical properties and SEM analysis. Although these employed methods were believed to be sufficient to characterise interfacial bonding it could be interesting to combine the obtained results with supplementary actual wear tests. The wear test to be employed should offer testing in as much as possible controlled conditions in terms of work piece properties and process variables such as applied pressure, feeding rate, cutting depth, coolant, removal of debris etc. At the same time it should be possible to examine the gradually worn surfaces of the diamond impregnated segments by means of optical microscopy (OM) and scanning electron microscopy (SEM) in order to identify the mode of diamond crystal breakdown sequence, the crystal protrusion height and to determine the number of pull-out sites associated with the use of both coated and non-coated diamonds. It is envisaged that the above requirements can only be satisfied in laboratory scale test apparatus with a device that would offer continuous monitoring of process parameters and enable ease and quick mounting and dismounting of the test segments from the wear test arrangement.

Further work can be carried out in assessing the effect of coating diamonds with other carbide forming metals not examined in this work, such as Mo, V, Hf etc.

Finally, future studies could also expand the field of examination into the technology of multi-layered coated diamonds. In that case, and in order to limit the variety of systems to be examined, a small number of metal-matrices could be selected as the base to formulate the diamond impregnated composites to be tested. The examined multi-layered coated diamonds could be then selected to have an inner layer being of a carbide forming metal exhibiting the highest adhesion strength to diamond as determined from preliminary studies as suggested earlier in this chapter. Investigation could then focus on determining the optimum number, type and thickness of intermediate coating layers in order to establish compatibility with the chosen metal-matrices and enhanced composite mechanical properties. Techniques and methods for evaluation could be among those employed in this work as well as others proposed above.

PAGE

NUMBERING

AS ORIGINAL

A

A.1 Selection Criteria of Diamond Segment Parameters

The following figure illustrates in a graphical manner the choice of segment parameters as a function of some general workpiece parameters according to the general segment-designing rule presented in §3.4.2.

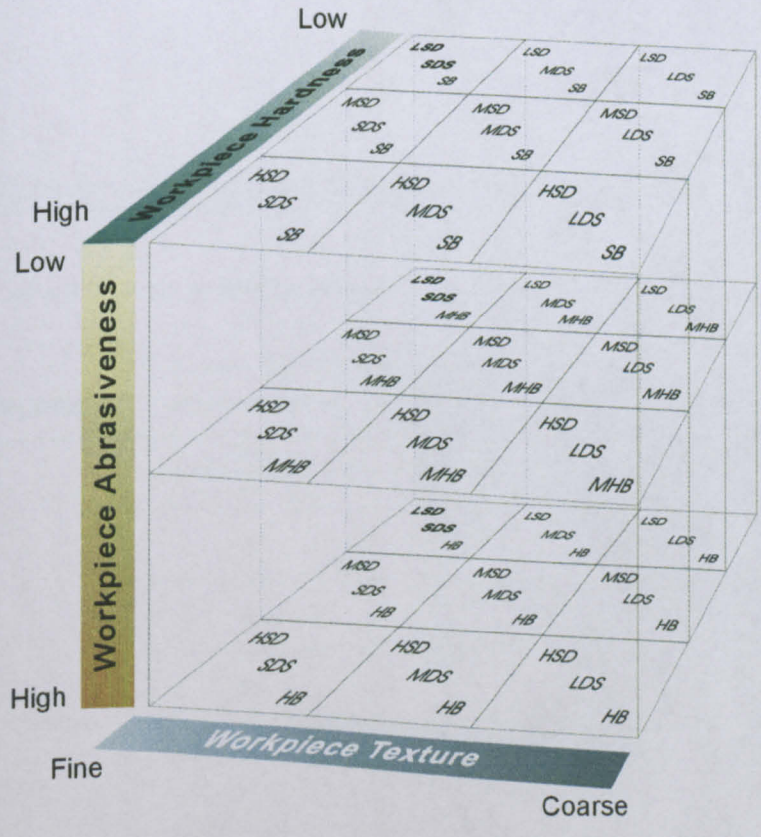

Diamond Strength

LSD :	Low Strength Diamond
MSD :	Medium Strength Diamond
HSD :	High Strength Diamond

Diamond Size

SDS :	Small Diamond Size
MDS :	Medium Size Diamond
LDS :	Large Size Diamond

Bond

SB :	Soft Bond
MHB :	Medium Hard Bond
HB :	Hard Bond

Figure A-1 : Choice of some of the segment's parameters according to the properties of the workpiece.

A.2 Diamond Sizes – FEPA standards

The following table gives the relationship between diamond sizes in mesh and metric designation according to the FEPA standards.

US Mesh	Aperture Size (µm)	Particles Per Carat (PPC) *
20	841	150
25	707	250
30	595	440
35	500	720
40	420	1380
45	354	2650
50	297	5000
60	250	8300
70	210	14000
80	177	23000

US Mesh Size Range		FEPA equivalent	
20/25	20/30	D851	D852
25/30		D711	
30/35	30/40	D601	D602
35/40		D501	
40/45	40/50	D426	D427
45/50		D356	
50/60		D301	
60/70		D251	
70/80		D213	

* PPC for cubo-octahedral crystals

Table A-1 : Diamond sizes and FEPA standard equivalents [244].

B

Wetting and solubility data

B.1 Data on wetting of diamond and graphite

Table B-1 : Data on wetting of graphite by liquid metals and alloys.

Graphite	Liquid Metal or Alloy	Temperatures (°C)	Contact Angle θ (degrees)	Work of Adhesion W_a (erg/cm^2)	Bonding Strength (MPa)	Reference
Elements inert to carbon	Ag	980	136	255		[185, 197]
	Bi	800	136	94		[185, 197]
	Cu	1100	140	316		[185, 197]
		1500	142	20		[197]
	Ga	100	139	180		[197]
		1000	137	170		[197]
	Ge	1000	139	100		[197]
		1100	148	98		[185]
	In	800	143	106		[185, 197]
	Pb	800	138	96		[185]
		800	138	75		[197]
	Sb	900	140	84		[185, 197]
	Sn	900	156	45		[185]
		1000	149	65		[197]
		1100	150	70		[197]

Table continues on next page

Continued from previous page

Graphite	Liquid Metal or Alloy	Temperatures (°C)	Contact Angle θ (degrees)	Work of Adhesion Wa (erg/cm^2)	Bonding Strength (MPa)	Reference
Transition metals and alloys	Ag + 0.1% Ti	1000	85	990		[197]
	Ag + 1% Ti	1000	7	1810		[197]
	Ce	1090	13	1530		[197]
	Co	1500	48	3200		[197]
		1550	68	2556		[185]
	Co + 15.5 C	1550	120			[197]
	Cu + 5% Co	1300	138	335-338		[185, 197]
	Cu + 0.6% Cr	1150	84	1380		[197]
	Cu + 5% Cr	1200	18	2595		[185]
	Cu + 6% Cr	1150	1150	40		[197]
	Cu + 10% Cr	1200	5	2640		[185]
	Cu + 10.2% Cr	1250	0	2620		[197]
Transition metals and alloys	Cu + 5% Nb	1200	71	1763		[185]
	Cu + 5% Ni	1300	140	307		[185]
	Cu + 10% Ni	1500	139	310		[197]
	Cu + 20% No	1500	134	375		[197]
	Cu + 24% Mn	1200	70	1780		[197]
	Cu + 6.3% Ti	1150	30	2450		[197]
	Cu + 10% Ti	1150	0	2660-2680		[185, 197]
	Cu + 5% V	1200	53	2130		[185]
	Cu + 6.2% V	1200	60	660		[197]
	(Cu + 9.3Ni) + 6.2 V	1200	50	2490		[197]
	(Cu + 9.3Ni) + 7 Nb	1200	40	2390		[197]
	(79Cu + 21Ni) + Mo	1400	100	950		[197]
	(51Cu + 39Ni +10Si) + W	1420	61	1800		[197]
	Fe	1550	50	3040-3340		[185, 197]
	Fe + 15.7 C	1550	107			[197]
	Fe + 32 V	1550	35			[197]
	Fe + 53 V	1550	0			[197]
	La	900	45	1220		[197]
	Nb	1000	10	1185		[197]
	Ni	1500	45	2985		[197]
		1550	57	2704		[185]
	Ni + 13 C	1550	115			[197]
	Pb + C	1560	116			[197]
	Pd	1560	44-48	2138-2500		[185, 197]
	Pr	920	20	1310		[197]
	Pt	1800	87	1830		[197]
	Sn + 0.9% Ti	1150	76	560		[197]
	Sn + 7% Ti	1150	5	900		[197]
	Ti	1800	0	2920		[197]
Elements forming covalent bonds with carbon	Al	800	157	68		[185]
		1000	151			[197]
		1100	142			[197]
		1200	38	1523		[185]
	Si	1450	0	1720		[185]

Table B-2 : Data on wetting of diamond by liquid metals and alloys.

Diamond	Liquid Metal or Alloy	Temperatures (°C)	Contact Angle θ (degrees)	Work of Adhesion Wa (erg/cm²)	Bonding Strength (MPa)	Reference
Elements inert to carbon	Ag	1000	120	450		[197]
	Au	1100	151	120		[197]
		1150	150	120		[197]
	Cu	1100	155	127		[185]
		1100	145	235		[197]
		1150	146	235		[197]
	Ge	1000	136	115		[197]
		1100	131	145		[197]
		1200	113	390		[197]
	In	400	156	45		[197]
		500	152	60		[197]
		1000	142	100		[197]
	Pb	1000	110	265		[197]
	Sb	900	120	180		[197]
	Sn	900	125	195		[197]
		1000	125	190		[197]
		1100	125	150		[197]
		1150	124	185		[197]
Transition metals and Alloys	Ag + 0.1% Ti	1000	45	1555		[197]
	Ag + 0.45% Ti	1000	5	1815		[197]
	Au + 5% Ta	1150	30	2200		[197]
	Cu + 0.37% Cr	1150	37	2390		[197]
	Cu + 4.5% Cr	1200	40	2349		[185]
	Cu + 5% Cr	1200	26	2527		[185]
	Cu + 6% Cr	1150	0	2660		[197]
	Cu + 5% Ti	1150	0	2680		[185]
	Cu + 12.8% Ti	1150	0	2660		[197]
	Cu + 5.1% Sn + 1.07% Ti	1150	121		0	[132]
	Cu + 10% Sn + 1.07% Ti	1150	7-15		17	[132]
	Cu + 10% Sn + 2.1% Ti	1150	120		≈ 0	[132]
	Cu + 10% Sn + 4.9% Ti	1150	8		≈ 0	[132]
	Cu + 10% Sn + 10.4% Ti	1150	22		0	[132]
	Cu + 10% Sn + 15.4% Ti	1150	6		0	[132]
	Cu + 15% Sn + 1.07% Ti	1150	121-123		0-26	[132]
	Cu + 20% Sn + 1.07% Ti	1150	11-32		25	[132]
	Cu + 20% Sn + 2.1% Ti	≈ 950	10-140		121-746	[132]
	Cu + 20% Sn + 2.1% Ti	≈ 1000	6-149		26-457	[132]
		≈ 1050	5-12		18-72	[132]
		≈ 1150	6		3-67	[132]
	Cu + 20% Sn + 10% Ti	900	15-49		74-165	[132]
		≈ 960	24-29		30-344	[132]
		1000	5-60		49-111	[132]
	Cu + 29.9% Sn + 1.07% Ti	1150	7-9		-	[132]
	Cu + 40% Sn + 1.07% Ti	1150	10		20	[132]
	Sn + 0.5% Ti	1150	38	855		[197]
	Sn + 2.5% Ti	1150	22	865		[197]
Elements forming covalent bonds with carbon	Al	800	150			[197]
		900	145			[197]
		1000	75			[197]
	Cu + 5% B	1150	36			[197]
	Cu + 10% Si	1200	70			[197]
	Cu + 40% Si	1200	24			[197]
	Ni + 40% Si	1200	47			[197]

B.2 Ellingham diagrams for carbides

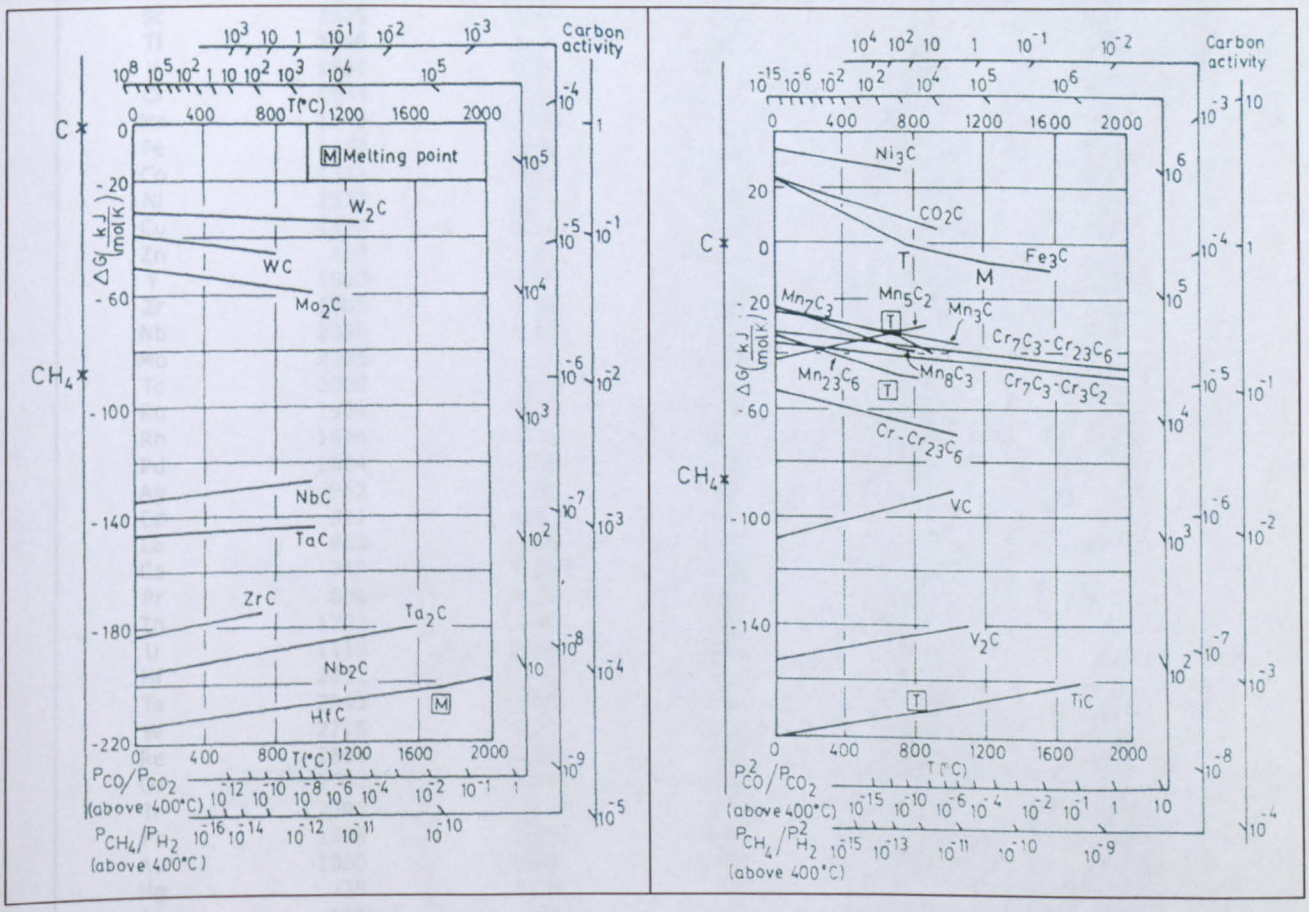

Figure B-1 : Ellingham diagrams for carbides [245].

B.3 Carbon Solubility of Elements

Eutectic solubilities of carbon in solid and liquid metals are listed in Table B-3 along with their corresponding eutectic temperatures. In order to compare the listed values of solubilities at a certain temperature (e.g. 1000°C) the "effective solubility" has been also estimated and included. The so-called "effective solubility" is obtained by interpolation or extrapolation of eutectic solubilities. Effective solubilities of carbon in transition metals are highest when transition metals possess about an equal amount of valence electrons and vacancies in their *d*-orbitals.

Table B-3 lists the effective solubilities for molten transition metals as given in Table B-3 in accordance with their *d*-vacancies.

Element	Eutectic Temperature (°C)	Solid (atom %)		Liquid (atom %)	
		Eutectic	Effective (1000°C)	Eutectic	Effective (1000°C)
Sc	1579	2.20	1.39	1.11	0.71
Ti	1648	3.10	1.88	1.96	1.19
V	1650	4.30	2.61	15.00	9.10
Cr	1534	0.30	0.20	13.90	9.07
Mn	1243	11.00	8.85	11.10	8.91
Fe	1153	9.10	7.89	16.90	14.70
Co	1321	4.50	3.41	11.90	9.01
Ni	1327	2.70	2.03	6.93	5.22
Cu	1110	0.04	0.04	4.00	3.60
Zn	420	0.01	0.02	1.00	2.38
Y	1560	7.00	4.49	6.96	4.46
Zr	1805	1.50	0.83	2.96	1.64
Nb	2339	5.70	2.44	10.50	4.51
Mo	2205	1.10	0.50	17.00	7.71
Tc	2000	4.00	2.00	20.20	10.10
Ru	1924	3.00	1.56	13.40	6.95
Rh	1694	1.50	0.89	15.50	9.16
Pd	1504	9.00	5.98	20.30	13.50
Ag	962	0.01	0.01	0	0
Cd	321	0.01	0.03	0	0
La	806	3.40	4.22	20.60	25.60
Ce	740	5.00	6.76	0	0
Pr	800	8.00	10.00	10.60	13.20
Th	1707	3.50	2.05	12.00	7.02
U	1119	0.02	0.02	1.95	1.74
Hf	2231	0	0	6.95	3.11
Ta	2843	7.00	2.46	23.50	8.27
W	2715	1.20	0.44	22.90	8.42
Re	2505	11.00	4.39	17.00	6.77
Os	2732	2.50	0.92	17.50	6.40
Ir	2296	3.10	1.35	20.70	8.99
Pt	1705	3.00	1.76	16.50	9.66
Au	1050	0.01	0.01	4.70	4.48
Hg	-39	0	0	0	0
Li	165	0	0	1.17	7.06
B	2075	0	0	1.35	0.65
Si	1404	0	0	1.16	0.83
Ge	2500	0	0	0	0
Pb	1170	0	0	0.41	0.35
Pu	640	0	0	0	0

Table B-3 : Carbon solubilities (atom%) of elements. Solid eutectic solubility denotes the maximum carbon solubility in the liquid phase that is in equilibrium with the liquid phase at the eutectic point. Liquid eutectic solubility denotes the carbon content at eutectic composition. Effective solubility at 1000°C is obtained by multiplying the eutectic solubility by $1000/T_{eutectic}$ [25].

3d - period	C (atom %)	*4d* - period	C (atom %)	*5d* - period	C (atom %)
Sc	0.7	Y	4.5	La	25.6
Ti	1.2	Zr	1.6	Hf	3.1
V	9.1	Nb	4.5	Ta	8.3
Cr	9.1	Mo	7.7	W	8.4
Mn	8.9	Tc	10.1	Re	6.8
Fe	14.7	Ru	7.0	Os	6.4
Co	9.0	Rh	9.2	Ir	9.0
Ni	5.2	Pd	13.5	Pt	9.7
Cu	3.6	Ag	0	Au	4.5
Zn	2.4	Cd	0	Hg	0

Table B-4 : Effective solubilities of carbon in molten transition metals [25].

The unusual high effective solubility of La is due to the extrapolation from its melting point (806°C) to 1000°C. The unexpected value for Pd can be explained by alterations occurring at its electronic state when carbon atoms are in the vicinity of Pd [25].

C

Models of Composite Mechanics

C.1 Models for Young's modulus prediction

This appendix presents some models on composite mechanics to predict the Young's modulus of particulate composites. Calculation of the E-modulus for the diamond composites and comparison with experimentally obtained values of the Young's modulus is also been included.

C.2 Hashin and Shtrikman Equation

According to Hashin and Shtrikman [201], the modulus of a particulate metal-matrix composite in which the reinforcement has a spherical shape and does not deform falls within the following bounds:

$$E_{LB} \leq E_C \leq E_{UB} \qquad \textbf{(C-1)}$$

where, E_C is the Young's modulus of the composite and E_{LB} and E_{UB} are the lower and upper bounds of the modulus. According to the authors, the latter are given by the following expressions :

$$E_{LB} = \frac{9 \cdot A \cdot B}{3 \cdot A + B} \qquad \textbf{(C-2)}$$

where :

$$A = \left[K_m + \frac{V_p}{\frac{1}{K_p - K_m} + \frac{3 \cdot V_m}{3 \cdot K_m + 4 \cdot G_m}} \right] \quad and \quad B = \left[G_m + \frac{V_p}{\frac{1}{G_p - G_m} + \frac{6}{5} \cdot \frac{V_m \cdot (K_m + 2 \cdot G_m)}{G_m \cdot (3 \cdot K_m + 4 \cdot G_m)}} \right] \qquad \textbf{(C-3)}$$

and,

$$E_{UB} = \frac{9 \cdot A' \cdot B'}{3 \cdot A' + B'} \qquad \textbf{(C-4)}$$

where :

$$A' = \left[K_p + \frac{V_m}{\frac{1}{K_m - K_p} + \frac{3 \cdot V_p}{3 \cdot K_p + 4 \cdot G_p}} \right] \qquad B' = \left[G_p + \frac{V_m}{\frac{1}{G_m - G_p} + \frac{6}{5} \cdot \frac{V_p \cdot (K_p + 2 \cdot G_p)}{G_p \cdot (3 \cdot K_p + 4 \cdot G_p)}} \right] \qquad \textbf{(C-5)}$$

Symbols G and K denote shear and bulk modulus respectively, whereas V is the volume fraction. The subscripts m and p denote the matrix and particle respectively. Apparently, $V_m=1-V_p$.

The model predicts that when the ratio $m=E_p/E_m$ is small, i.e. $0.5<m<3$, the separation between the upper and lower bounds is relatively small enough to obtain an estimate within about 10% of the true modulus value, provided that there are nor cracks or voids present. For composites with m ratios out of this range, the accuracy of estimation drops dramatically.

Upper and lower bounds predictions of Young's modulus for diamond reinforced composites with a plain cobalt matrix was calculated according to Hashin and Shtrikman equation. Shear and bulk modulus values were taken from literature.

Calculation is shown in the following graph (Figure C-1). The experimentally obtained values of Young's modulus for the non-reinforced specimens (blank specimens) as well as for those reinforced with 8.75% vol. (35 concentration) of SYN-3, 30/40 US mesh diamonds are included into the plot to aid the comparison of predicted and measured values.

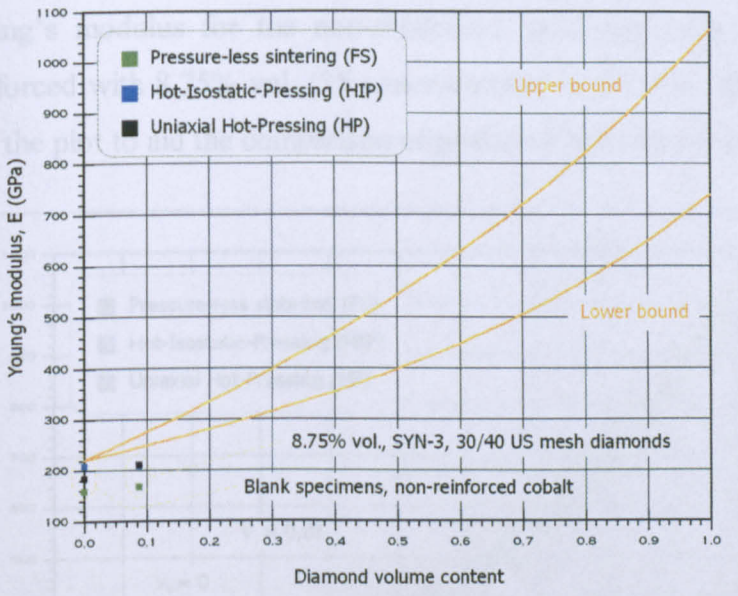

Calculation values:

Diamond

Shear modulus G_p = 455 GPa

Bulk modulus K_p = 542 GPa

Cobalt matrix

Shear modulus G_m = 85 GPa

Bulk modulus K_m = 180 GPa

Figure C-1 : Young's modulus calculation according to Hashin and Shtrikman equation [201]. Experimentally obtained values of the modulus for non-reinforced as well as diamond reinforced cobalt manufacture with the 3 different routes are also included.

As seen from the Figure C-1, calculation with Hashin and Shtrikman equation overestimates the modulus values. This could be attributed to the large m ratio associated with the diamond composites ($m=E_p/E_m$ = *1050 GPa / 211 GPa = 4.98*), which exceeds the set limit of $0.5<m<3$ as discussed in previous paragraph and thus is claimed to result inaccurate predictions. However, the main factor for observed overestimation is believed to be related to the porosity of the composites, which the model does not take into account.

C.3 Cohen and Ishai Equation

Cohen and Ishai [203] have suggested the following equation to predict modulus of two-phase particulate composites taking into consideration the existence of voids in the material:

$$E_C = E_m \cdot \left(1 - V_V^{2/3}\right) \cdot \left[1 + \frac{V_p}{\frac{m}{m + V_V^{2/3} - 1} - V_p^{1/3}}\right] \qquad \textbf{(C-6)}$$

where, E_C and E_m is the Young's modulus of the composite and metal-matrix respectively, m is the ratio of the E-moduli of reinforcement and matrix ($m=E_p/E_m$), Vp is the volume fraction of the reinforcement particles and V_V is the volume fraction of voids in the composites, such as porosity.

Calculation is shown in the following graph (Figure C-2). The experimentally obtained values of Young's modulus for the non-reinforced specimens (blank specimens) as well as for those reinforced with 8.75% vol. (35 concentration) of SYN-3, 30/40 US mesh diamonds are included into the plot to aid the comparison of predicted and measured values.

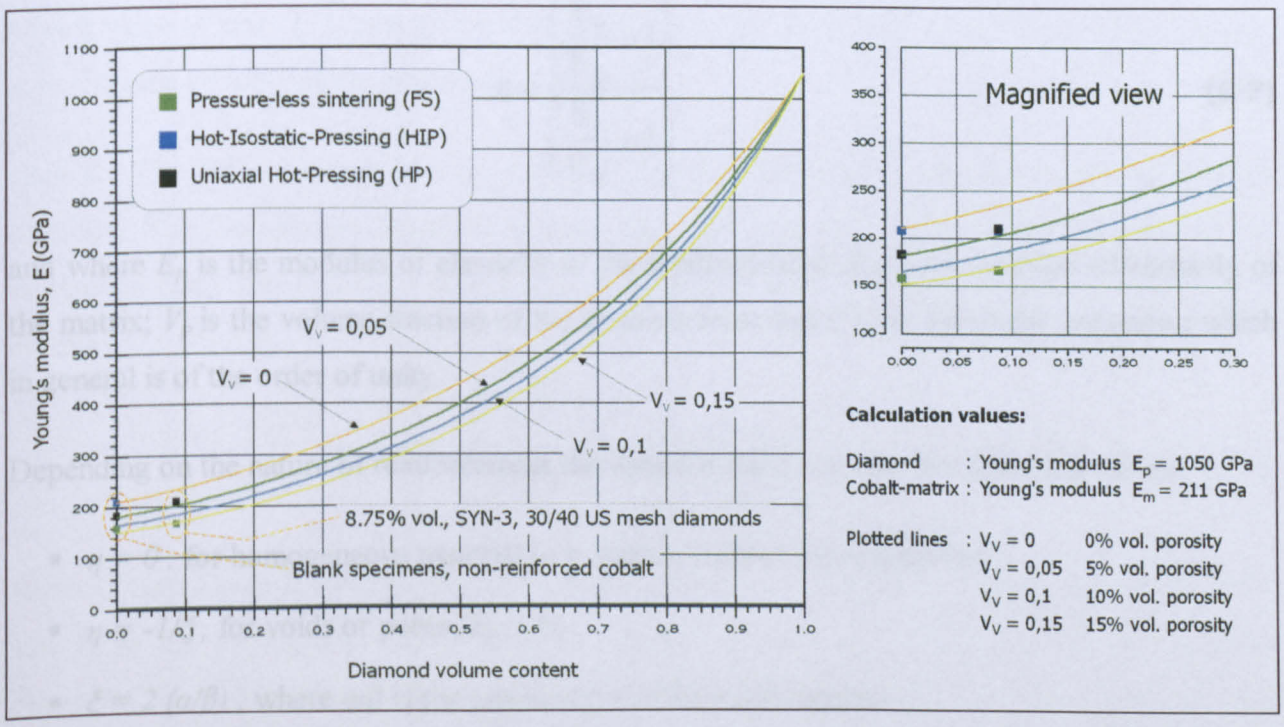

Figure C-2 : Young's modulus calculation according to Cohen and Ishai equation [203]. Experimentally obtained values of the modulus for non-reinforced as well as diamond reinforced cobalt manufacture with the 3 different routes are also included.

As seen from the Figure C-2, the Cohen and Ishai equation results in a fairly good prediction of the obtained Young's modulus values, by taking into consideration the porosity of the composite structure.

C.4 Tsai-Halpin equation

The so-called *Tsai-Halpin equation* is an equation for calculating the modulus of elasticity of composite materials derived from the analysis presented by Tsai and Hahn [246] and Halpin [202, 247]. The model takes into consideration loading condition and reinforcement geometry. Although it is a semi-empirically derived equation it is widely employed in composite materials mechanics, because it provides a fast calculation and it has given very good approximations to both experimental data and values obtained by other more rigorous models such as the Eshelby method [200].

The Tsai-Halpin equation is given by the following expression:

$$E_C = E_m \cdot \frac{(1+\xi \cdot \eta \cdot V_p)}{(1-\eta \cdot V_p)} \quad \textbf{(C-6)}$$

where:

$$\eta = \frac{\left(\frac{E_p}{E_m} - 1\right)}{\left(\frac{E_p}{E_m} + \xi\right)} \quad \textbf{(C-7)}$$

and where E_p is the modulus of elasticity of the reinforcement; E_m is the modulus of elasticity of the matrix; V_p is the volume fraction of the reinforcement and ξ is an adjustable parameter which in general is of the order of unity.

Depending on the nature of reinforcement the values η and ξ can take the following values:

- $\eta = 0$, for homogeneous material (e.g. matrix without reinforcement)
- $\eta = -1/\xi$, for voids or pores $(E_p = 0)$
- $\xi = 2\,(\alpha/\beta)$, where α/β is the aspect ratio of the reinforcement

It is possible to employ the model for calculating the modulus of elasticity of a composite structure containing more than one types of reinforcement. If however the composite is composed by only one type of reinforcement it can be assumed that the pores in the structure consist a second type of reinforcement (i.e. a "pseudo-reinforcement"). Thus, it is feasible to obtain an estimate of the Young's modulus by taking into account the porosity of the composite. For the case of diamond composites, which typically contain residual porosity, the calculation will include the following steps:

Step A : The composite is considered to be composed of the metal matrix "reinforced" with the pores. The modulus of elasticity of this composite structure, which is termed as "effective-matrix", is computed with the Tsai-Halpin equation as follows:

$$E_{\text{Effective-Matrix}} = E_m \cdot \frac{(1+\xi \cdot \eta \cdot V_v)}{(1-\eta \cdot V_v)} \quad \textbf{(C-8)}$$

where, $E_{Effective\text{-}Matrix}$ is the modulus of elasticity of the composite structure of metal-matrix and pores; E_m is the modulus of elasticity of the metal-matrix and V_V is the volume fraction of the pores.

Assuming that pores have attained a spherical shape in the composite, the aspect ratio α/β will have a value of unity *(1)*, thus giving $\xi = 2\ (\alpha/\beta) = 2$. For pores or voids, the factor η is given by $\eta = -1/\xi$ (see above), which results in $\eta = -0.5$.

Step B : The "effective-matrix" consists the matrix of the composite reinforced with the diamond particles. The Tsai-Halpin equation is employed once again to compute the modulus of the composite with the "effective-matrix" modulus as computed in step-A used as the matrix modulus:

$$E_{Composite} = E_{Effective-Matrix} \cdot \frac{\left(1 + \xi' \cdot \eta' \cdot V_p\right)}{\left(1 - \eta' \cdot V_p\right)} \qquad \textbf{(C-9)}$$

where, $E_{Effective\text{-}Matrix}$ is the modulus of elasticity of the "effective-matrix" as calculated in step-A and V_p is the volume fraction of diamonds in the composite. Considering that the synthetic diamonds are well-formed cubo-octahedral crystals the aspect ratio α/β will have a value of unity *(1)*, giving $\xi' = 2\ (\alpha/\beta) = 2$. The η' factor is then computed from the following equation similarly to equation C-7:

$$\eta' = \frac{\left(\frac{E_p}{E_{Effective-matrix}} - 1\right)}{\left(\frac{E_p}{E_{Effective-matrix}} + \xi'\right)} \qquad \textbf{(C-10)}$$

Calculation of the Young's modulus for the diamond composites according to the above-presented Tsai-Halpin approach is shown graphically in the following graph (Figure C-3).

Calculation has been made for *various levels of* porosity as illustrated in the figure. The plot corresponding to 0% porosity (V_V=0) represents the result obtained with the standard usage of Tsai-Halpin equation that does not involve two-step calculation ($E_{Effective\text{-}matrix}$=$E_m$).

The experimentally obtained values of Young's modulus for the non-reinforced specimens (blank specimens) as well as for those reinforced with 8.75% vol. (35 concentration) of SYN-3, 30/40 US mesh diamonds are included into the plot to aid the comparison of predicted and measured values.

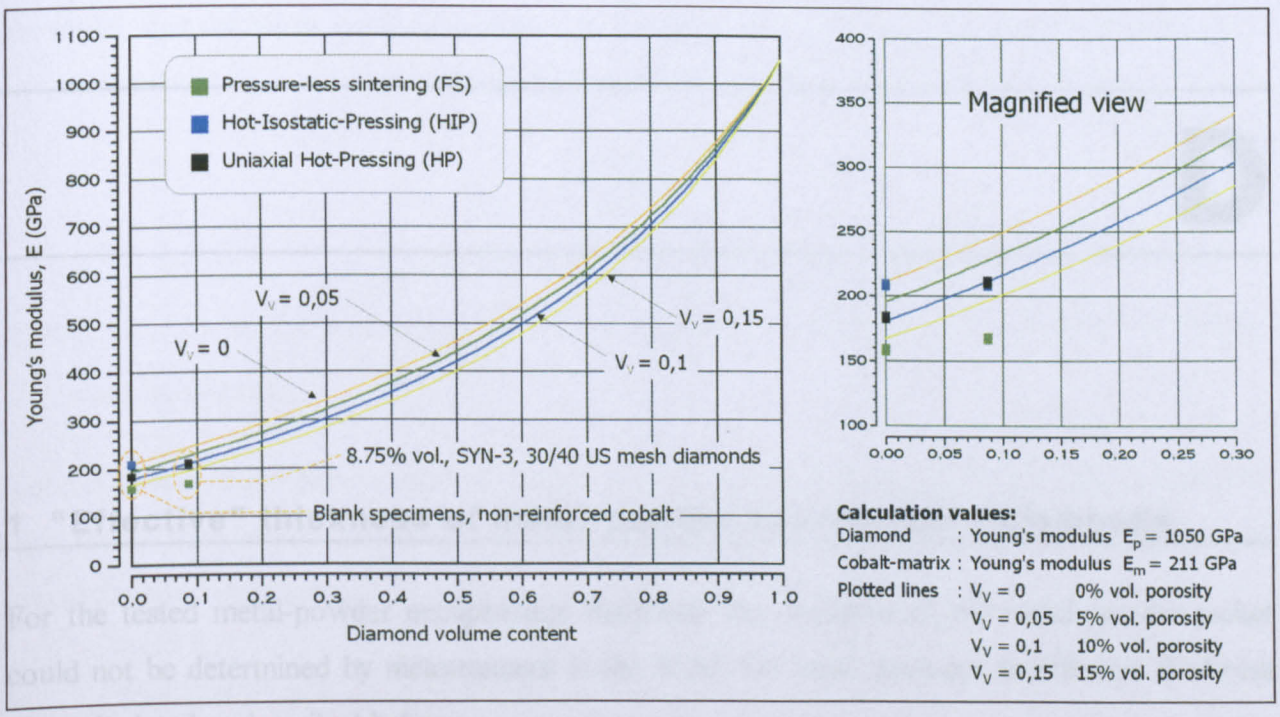

Figure C-3 : Graphical representation of Young's modulus calculation results for the diamond composites according to Tsai-Halpin equation [202, 246-247]. Calculation assumes 2 types of inclusions in the composites, firstly the pores and secondly the diamond reinforcement. Experimentally obtained values of the modulus for non-reinforced as well as diamond reinforced cobalt manufacture with the 3 different routes are also illustrated.

As seen from the Figure C-3, the calculation with the Tsai-Halpin equation as described in detailed above resulted in a slight overestimate of the obtained Young's modulus values compared to measured values. Most closely predicted values were those for the hot-pressed specimens.

D

D.1 "Effective" thickness of metal-powder encapsulated-diamonds

For the tested metal-powder encapsulated diamonds the thickness of the metal-powder jacket could not be determined by measurement in the SEM. For these granules an effective thickness was calculated as described below.

The model on which the following calculation is based on, assumes that the metal-powder capsule had formed a dense and evenly thick layer enclosing the crystals and considers diamonds to possess a simple spherical shape rather the true cubo-octahedral form. Figure D-1 illustrates the described model.

According to the assumed model it can be written:

$$V_{CD} = \frac{4}{3} \cdot \pi \cdot R_{CD}^3 \Rightarrow R_{CD} = \sqrt[3]{\frac{3}{4\pi} \cdot V_{CD}}$$

$$V_D = \frac{4}{3} \cdot \pi \cdot R_D^3 \Rightarrow R_D = \sqrt[3]{\frac{3}{4\pi} \cdot V_D} \qquad \textbf{Eq. D-1}$$

where, V_{CD} is the volume of the encapsulated diamond, V_D is the volume of the diamond, R_{CD} is the radius of the encapsulated diamond, and R_D is the radius of the diamond.

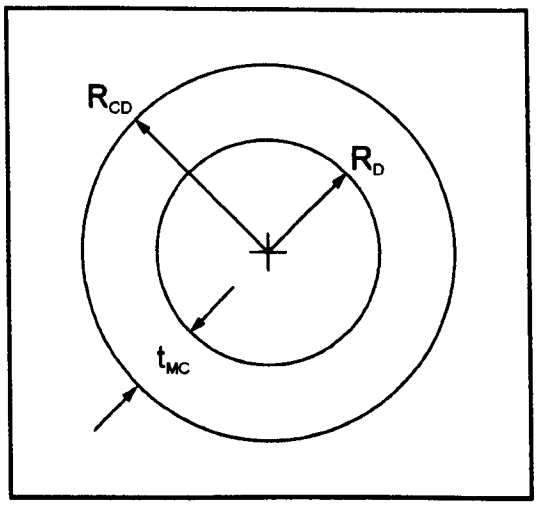

Figure D-1 : The assumed metal-powder encapsulated diamond geometry.

The thickness of the metal capsule (t_{MC}) is given as :

$$t_{MC} = R_{CD} - R_D = \sqrt[3]{\frac{3}{4\pi} \cdot V_{CD}} - \sqrt[3]{\frac{3}{4\pi} \cdot V_D} \qquad \textbf{Eq. D-2}$$

Assuming that the mean value of diamond US mesh size would represent the average diameter of the encapsulated diamond population, it can be written that:

$$R_D = \frac{\overline{d_{US\ mesh}}}{2} \qquad \textbf{Eq. D-3}$$

where, $\overline{d_{US\ mesh}}$ is the mean diameter of the diamonds based on the US mesh size range, expressed in microns.

The "*diamond factor content (α)*" is known from the manufacturers of the granulated diamonds. This factor describes the percentage of the total weight of the coated grit that corresponds to the actual diamond mass content of the granule. The following equations apply:

$$\left.\begin{aligned} \rho_{MC} &= \frac{m_{MC}}{V_{MC}} = \frac{\alpha \cdot m_{CD}}{V_{MC}} \\ \rho_D &= \frac{m_D}{V_D} = \frac{(1-\alpha)\cdot m_{CD}}{V_{MC}} \end{aligned}\right\} \Rightarrow \quad \frac{\rho_{MC}}{\rho_D} = \frac{\alpha \cdot V_D}{(1-\alpha)\cdot V_{MC}} \Rightarrow V_{MC} = \frac{\alpha \cdot \rho_D \cdot V_D}{(1-\alpha)\cdot \rho_{MC}} \qquad \textbf{Eq. D-4}$$

where, ρ_{MC} is the density of the metal coating, ρ_D is the density of the diamond and V_{MC} is the volume of the metal coating.

From the coated diamond geometry it follows that:

$$V_{CD} = V_{MC} + V_D \qquad \textbf{Eq. D-5}$$

Combining Equations D-4 and D-5 results in:

$$V_{CD} = \frac{\alpha \cdot \rho_D + (1-\alpha)\cdot \rho_{MC}}{(1-\alpha)\cdot \rho_{MC}} \cdot V_D \qquad \textbf{Eq. D-6}$$

Substituting D-3 and D-6 into equation D-2 gives:

$$t_{MC} = \sqrt[3]{\frac{3}{4\pi}\cdot V_{CD}} - R_D = \sqrt[3]{\frac{3}{4\pi}\cdot\frac{\alpha \cdot \rho_D + (1-\alpha)\cdot \rho_{MC}}{(1-\alpha)\cdot \rho_{MC}}\cdot V_D} - \frac{\overline{d_{US\ mesh}}}{2} \qquad \textbf{Eq. D-7}$$

Additionally the volume of the diamond V_D can be written as:

$$V_D = \frac{4}{3}\pi \cdot \left(\frac{\overline{d_{US\ mesh}}}{2}\right)^3 \qquad \textbf{Eq. D-8}$$

Substituting D-8 into equation D-7 gives the formula for calculating the coating thickness:

$$t_{MC} = \frac{\overline{d_{US\,mesh}}}{2} \cdot \left(\sqrt[3]{\frac{\alpha \cdot \rho_D + (1-\alpha) \cdot \rho_{MC}}{(1-\alpha) \cdot \rho_{MC}}} - 1 \right) \qquad \textbf{Eq. D-9}$$

The following Table lists the metal coating thickness as computed according to Equation D-9 for the various metal-powder encapsulated diamonds employed in this thesis.

Diamond Condition	Manufacturer	Diamond Size Range	Mean Diameter $\overline{d_{US\,mesh}}$ (microns)	Actual Diamond Content in Encapsulated Crystals (α %wt.)	Calculated Thickness of Metal Capsule (microns)
Cr - coated (PC)	NDT	30/50 (US mesh) 297/595 μm	446	65 %	53.6
W - coated (PC)	VM	30/50 (US mesh) 297/595 μm	446	48.1 %	11.9
Co - coated (PC)	J	30/40 (US mesh) 420/595 μm	507.5	37 %	18.4

Table D-1 : Calculated average thickness of the metal jacket of the metal-powder encapsulated diamonds. (Manufacturer codes: NDT-Nimbus Diamond Tools, VM-Van Moppes, J-Fuji Paudal Kabushiki Kaisha). Densities used for the calculations: 3.52 g·cm^{-3} for diamond, 19.25 g·cm^{-3} for tungsten, 8.832 g·cm^{-3} for cobalt and 7.19 g·cm^{-3} for chromium [248].

D.2 Metal leaching procedure

Table D-2 gives the acid solutions, which were used for leaching the various metals from the diamond surfaces as part of the DRE experiment.

Metal - Alloy	Acid	Approx. Time Required	Time actually allowed
Cobalt (Co)	HNO_3 – boiling	20 min	1 h
Iron (Fe)	HNO_3 : HCl at approx. ratio 1:3 – boiling	30 min	> 1h
Copper (Cu)	HNO_3 : HCl at approx. ratio 1:3 – boiling	30 min	> 1h
Bronze 85/15	HNO_3 : HCl at approx. ratio 1:3 – boiling	30 min	> 1h
Nickel (Ni)	HNO_3 : HCl at approx. ratio 3:1 – boiling	30 min	> 1h
Tungsten (W)	HNO_3 : HCl at approx. ratio 1:2 – boiling	30 min	> 1h
Titanium (Ti)	Concentrated HCl - boiling	30 min	> 1h
Chromium (Cr)	Conc. HCl – boiling, or conc. H_2SO_4 - boiling	30 min	> 1h
Molybdenum (Mo)	Conc. HCl – boiling, or mixed HNO_3 : HCl - boiling	40 min	> 1h

Table D-2 : List of acid solutions used for the various metal leaching procedures employed with the DRE.

D.3 Graphite leaching procedure

Graphite removal was achieved by treating the previously metal leached diamonds in a hot chromic acid bath.

The chromic acid was prepared by mixing 3 parts by volume of 85% orthophosphoric acid and 1 part by volume of sulphuric acid. For every litre of the above mixture, 200 grams of potassium dichromate were added. These relative proportions were scaled down if less quantity of the chromic acid was required. The mixture was stirred and allowed to settle for approximately 10 minutes. The chromic acid was then poured into a beaker and the remaining sludge was appropriately disposed. Approximately 50 ml of the chromic acid and the diamonds to be leached were placed in a beaker and were heated on a hot plate under a fume cupboard. As heating up the chromic acid and the diamonds foam develops on the surface of the liquid. Initially this foam is orange and gradually turns into a greenish colour. Subsequently, the foam died away and white fumes were coming off the liquid. This was the sign for the onset of graphite dissolution. The time required for complete dissolution of the graphite was in the order of few minutes but depended on the amount of graphite on the diamonds. Since prolonged treatment of the diamonds in the chromic acid does not cause any damage to them, a minimum time of 30 minutes was allowed to ensure complete removal of graphite.

The liquid was left to cool down before water was added. Diamonds were then retrieved by pouring the liquid through a sieving arrangement comprised of a 250 and a 150 micron sieves, with the former being on the top. The diamonds were carefully retrieved from the sieves, washed with diluted water and methanol, and were then finally dried.

The used chromic acid was disposed into a waste beaker and it was then neutralised by adding NaOH.

D.4 Segment density measurement

Density is defined as the quotient of the mass by volume. In practice density is measured by the direct determination of the mass and volume of the sample. Mass is determined by weighting the sample in a balance of high accuracy while the volume of a sample with a simple geometry can be calculated from its dimensions. However, if the shape is complex, like in the case of the diamond impregnated segments which had relatively irregular surfaces with diamond crystals occasionally protruding, volume of the segment had to be determined by the utilisation of Archimedes principle.

D.4.1 Density Measurement (Archimedes Principle)

The Archimedes technique for obtaining density for a porous material requires a series of weight determinations. The segments were first weighted dry in air (W_{air}), then weighted again after fluid impregnation ($W_{impregnated}$) and finally weighted while immersed in a liquid of high density ($W_{immersed}$). A wire was used to suspend the segments in the liquid bath and its weight was measured in the liquid too (W_{wire}). The density of the segment was calculated from the weight determinations as follows (all weights in grams):

$$\rho = \frac{W_{air} \cdot \rho_{liquid}}{W_{impregnated} - (W_{immersed} - W_{wire})} \qquad \textbf{Eq. D-10}$$

Flutec PP11 ($C_{14}F_{14}$), which has a density of 2.03 gr/cm^3 at 25°C was used as the liquid for both the impregnation and immersion.

D.4.2 Theoretical density

The theoretical density of the diamond-impregnated segments was calculated according to their diamond content and the composition of the matrix.

References

[1] Heinz W. F., "Diamonds, diamond bits, reaming shells, core barrels" in Diamond Drilling Handbook, SADA, 1st Edition, Sigma Press, South Africa, 1985, pp.27-136.

[2] Luo S. Y., "Characteristics of diamond sawblade wear in sawing", *International Journal of Machine Tools & Manufacture*, (1996), **36** [6], pp.661-672.

[3] Vander Sande J. V., Uhlmann D. R. and Akeson A., "Improved diamond tool life through the use of coated diamonds", Superabrasives '85 Conference, Chicago, Illinois, (1985) MR85-308.

[4] Clark T. J., "Superbrasives and ultrahard tool materials" in ASM Handbook, Vol. 2, Properties and selection: Nonferrous alloys and special-purpose materials, (1991), pp.1008-1018.

[5] Antony T. R., "Methods of diamond making" in Diamond and Diamond-Like Films and Coatings, Edited by Clausing *et al.*, Plenum Press, New York, (1991), pp.555-577.

[6] Bundy F. P., "Direct conversion of graphite to diamond in static pressure apparatus", *The Journal of Chemical Physics*, (1963), **38** [3], pp.631-643.

[7] Bundy F. P., Bovenkerk H. P., Strong H. M. and Wentorf Jr. R. H., "Diamond-graphite equilibrium line from growth and graphitisation of diamond", *The Journal of Chemical Physics*, (1961), **35** [2], pp.383-391.

[8] Wilks E. and Wilks J., Properties and Applications of Diamond, Butterworth-Heinemann Ltd., Oxford, (1991), pp.8-17.

[9] Antony T. R., "Inclusions in diamond with solubility changes and phase transformations", *Diamond and Related Materials*, (1999), **8**, pp.78-88.

[10] Bundy F. P., Bassett W. A., Weathers M. S., Hemley R. J., Mao H. K. and Goncharov A. F., "Pressure-temperature phase and transformation diagram for carbon; updated through 1994 – review article", *Carbon*, (1996), **34** [2], pp.141-153.

[11] *ibid* [8], p.21.

[12] Wentorf R. H., De Vries R. C. and Bundy F. P., "Sintered superhard materials", *Science*, (1980), **208**, pp.873-880.

[13] *ibid* [8], p.28-29.

[14] Pierson H. O., "Structure and properties of diamond and diamond polytypes", in Handbook of Carbon, Graphite, Diamond and Fullerenes – Properties, Processing and Applications, Noyes Publications, New Jersey, (1993), pp.244-277.

[15] Pierson H. O., "Graphite structure and properties", in Handbook of Carbon, Graphite, Diamond and Fullerenes – Properties, Processing and Applications, Noyes Publications, New Jersey, (1993), pp.43-69.

[16] Gardinier C. F., "Physical properties of superabrasives", *American Ceramic Society Bulletin*, (1998), **67** [6], pp.1006-1009.

[17] Wilks E. and Wilks J., "The morphology of diamond" in Properties and Applications of Diamond, Butterworth-Heinemann Ltd., Oxford, (1991), pp.108-144.

[18] Field J. E., "Cleavage, fracture and tensile strength of diamond" in Properties and Growth of Diamond, Edited by Gordon Davies, INSPEC, London, (1994), pp.36-51.

[19] Field J. E., "Hardness, plasticity and shear strength of diamond" in Properties and Growth of Diamond, Edited by Gordon Davies, INSPEC, London, (1994), pp.52-56.

[20] Brookes C. A., in The Properties of Natural and Synthetic Diamond, Edited by J. E. Field, Academic Press, London, (1979), pp.383-402.

[21] Wilks E. and Wilks J., "Strength and fracture" in Properties and Applications of Diamond, Butterworth-Heinemann Ltd., Oxford, (1991), pp.177-213.

[22] Bullen G. J., "The effect of temperature and matrix on the strength of synthetic diamond", *Industrial Diamond Review*, (1975), **35**, pp.363-365.

[23] Bakon A., "Structure and properties: A study of the changes occurring in diamond powders on heating", *Soviet Journal of Superhard Materials (Sverkhtverdye Materialy)*, (1983), **5** [6], pp.23-26.

[24] Novikov N. V., Shul'zhenko A. A., Nikitin Yu. I., Katsai M. Ya., Uman S. M., Mel'nik V. I. and Yakimenko V. D., "Heat resistant, high strength synthetic diamond grits", *Soviet Journal of Superhard Materials (Sverkhtverdye Materialy)*, (1984), **6** [5], pp.33-35.

[25] Sung C. M. and Tai M. F., "Reactivities of transition metals with carbon: Implications to the mechanism of diamond synthesis under high pressure", *International Journal of Refractory Metals & Hard Materials*, (1997), **15** [4], pp.237-256.

[26] Theije de F. K., Roy O., Laag van der N. J. and Enckevort van W. J. P., "Oxidative etching of diamond", *Diamond and Related Materials*, (2000), **9** [3], pp.929-934.

[27] Evans S., "Reactivity of diamond surfaces" in Properties and Growth of Diamond, Edited by Gordon Davies, INSPEC, London, (1994), pp.64-67.

[28] Wilks E. and Wilks J., "Wear and surface characteristics" in Properties and Applications of Diamond, Butterworth-Heinemann Ltd., Oxford, (1991), pp.337-378.

[29] Ikawa N. and Tanaka T., "Thermal aspects of wear of diamond grain in grinding", *Annals of the C.I.R.P.*, (1971), **19**, pp.153-157.

[30] Thornton A. G. and Wilks J., "Tool wear and solid state reactions during machining", *Wear*, (1979), **53** [1], pp.165-187.

[31] Thornton A. G. and Wilks J., "The wear of diamond tools turning mild-steel", *Wear*, (1980), **65** [1], pp.67-74.

[32] Evans S., "Graphitisation of diamond surfaces" in Properties and Growth of Diamond, Edited by Gordon Davies, INSPEC, London, (1994), pp.68-69.

[33] Evans T., "Changes produced by high temperature treatment of diamond", in The Properties of Diamond, (1979), Edited by J. E. Field, Academic Press, London, pp.403-424.

[34] Evans T. and Phaal C., "The kinetics of the diamond-oxygen reaction", in the Proceedings of the Fifth Biennial Conference on Carbon, The Pennsylvania State University, Pergamon Press, Oxford, (1962), pp.147-153.

[35] van Enckevort W. J. P., "Etching of diamond", in The Properties of Diamond, (1979), Edited by J. E. Field, Academic Press, London, pp.301-308.

[36] van Enckevort W. J. P., "The effect of crystallographic orientation on the optical anisotropy of graphite layers on diamond surfaces", *Journal of Applied Crystallography*, (1987), **20** [1], pp.11-15.

[37] Evans S. and Ney M. R., "Cobalt-catalysed graphitisation of diamond studied by X-ray photoelectron spectroscopy", *Journal of Hard Materials*, (1990), **1** [3], pp.169-180.

[38] Clifton P. H. and Evans S., "XPS studies of diamond/transition-metal interfaces", *Industrial Diamond Review*, (1995), [1], pp.26-31.

[39] Bullen G. J., "Choosing the best grit for the job", *Industrial Diamond Review*, (1982), **42** [488], pp.7-13.

[40] Rabinkin A., "Diamond interaction with various metals and alloys under different environmental conditions", in Proceedings of High Pressure in Research and Industry, 8th AIRAPT Conference, 19th EHPRG Conference, Uppsala, Sweden, (1981), pp.17-22.

[41] Evans T. and James P. F., "A study of the transformation of diamond to graphite", *Proceedings of the Royal Society of London*, (1964), **A277**, pp.260-269.

[42] Davies G. and Evans T., "Graphitisation of diamond at zero pressure and at high pressure", *Proceedings of the Royal Society of London*, (1972), **A328**, pp.413-427.

[43] Fedoseev D. V., Vnukov S. P., Bukhovets V. L. and Anikin B. A., "Surface graphitisation of diamond at high temperatures", Surface and Coatings Technology, (1986), **28**, pp.207-214.

[44] Przyklenk K., "Diamond impregnated tools - uses and production", *Industrial Diamond Review*, (1993), [4], pp.192-195.

[45] Konstanty J., "The materials science of stone sawing", *Industrial Diamond Review*, (1991), [1], pp.27-31.

[46] Chalkley J. R. and Thomas D. M., "The tribological aspects of metal-bonded diamond grinding wheels", *Powder Metallurgy*, (1969), **12** [24], pp.582-597.

[47] Pryzklenk K. and Stockl J., "Diamond tool manufacture on pressure sintering presses", *Industrial Diamond Review*, (1995), [1], pp.15-17.

[48] Dwan J. D., "Production of diamond impregnated cutting tools", *Powder Metallurgy*, (1998), **41** [2], pp.84-86.

[49] Lenel F. V., Powder Metallurgy – Principles and Applications, Metal Powder Industries Federation, Priceton, New Jersey, (1980), pp.492-493.

[50] Igharo M., "Nimbus Diamond Tool and Machine Co. Ltd. (Company Profile)", *Powder Metallurgy*, (1991), **34** [3], pp.152-154.

[51] Gutmanas E. Y., Rabinkin A. and Roitberg M., "On cold sintering of metal-bonded diamond composites", *Materials Science and Engineering*, (1980), **45**, pp.269-275.

[52] Gutmanas E. Y., "Cold sintering under high pressure – Mechanisms and application", *Powder Metallurgy International*, (1983), **15** [3], 129-131.

[53] Novikov N. V., Maistrenko, Trefilov V. I. and Kovtun V., "Structire & properties of shock-wave sintered diamond composites", *Industrial Diamond Review*, (1993), [5], pp.278-281.

[54] Padukov K. L., Levashov E. A., Kost A. G. and Borovinskaya I. P., "SHS – A new fabrication method", *Industrial Diamond Review*, (1992), [5], pp.255-256.

[55] Padyukov K. L. and Levashov E. A., "Self-propagating high-temperature synthesis: A new method for the production of diamond-containing materials", *Diamond and Related Materials*, **2** [1], pp.207-210.

[56] Manukyan N. V., Apoyan G. S., Kasyan V. L. and Egoyan I.Z., "Structure and properties of extruded abrasive-metal composites", *Soviet Powder Metallurgy & Metal Ceramics*, (1988), **26** [10], pp.826-828.

[57] Manukyan N. V., Agbalyan S. G., Egoyan I.Z. and Oganyan A. P., "Extrusion behaviour of diamond metal composites", *Soviet Powder Metallurgy & Metal Ceramics*, (1991), **29** [10], pp.772-775.

[58] Wright D. N., and Wapler H., "Investigations and prediction of diamond wear when sawing", *Annals of the C.I.R.P.*, (1986), **35** [1], pp.239-244.

[59] Wright D. N., Wilson S. M., Brown W. F. and Ovens U., "Segment wear on diamond impregnated mining bits", *Industrial Diamond Review*, (1990), [5], pp.248-252.

[60] Raal F. A., "The importance of bonding to diamond surfaces in industrial application", *Industrial Diamond Review*, (1968), **28**, pp.495-497.

[61] Clyne T. W. and Withers P. J., An Introduction to Metal Matrix Composites, Edited by Davis E. A. and Ward I. M., Cambridge University Press, Cambridge, (1993), pp.117-123.

[62] Zhou Y., Funkenbusch P. D. and Quesnel D. J., "Stress distributions at the abrasive - matrix interface during tool wear in bound abrasive grinding - a finite element analysis", *Wear*, (1997), **209**, pp.247-254.

[63] De Chalus P. A., "Metal powders for optimum grain retention", *Industrial Diamond Review*, (1994), [4], pp.170-172.

[64] Toenshoff H. K. and Asche J., "Wear of metal-bond diamond tools in the machining of stone", *Industrial Diamond Review*, (1997), [1], pp.7-13.

[65] Aleksandrov V. A., Levin M. D. and Mechnik V. A., "Determination of the volume of fractured material acting on a segment of diamond disk tool", *Soviet Journal of Superhard Materials*, (1986), **8**, pp.42-47.

[66] Birle J. D., McEachron R. W. and Ratterman E., "Classification of the sawability of portland cement concretes containing various aggregates", *GE Superabrasives Report*, (1995).

[67] Birle J. D. and Ratterman E., "An approximate ranking of the sawability of hard building stones based on laboratory tests", *GE Superabrasives Report*, (1986).

[68] Luo S. Y., "Investigation of the worn surfaces of diamond sawblades in sawing granite", *Journal of Materials Processing Technology*, (1997), **70**, pp.1-8.

[69] "Metallurgy of diamond tools", *Industrial Diamond Review*, (1985), [5], pp.248-250.

[70] Stasyuk L. F., Bogatyreva G. P. and Kushtalova I. P., "Effect of diamond quality on the wear of composites", *Soviet Journal of Superhard Materials*, (1986), **8** [5], pp.58-61.

[71] Hutchings I. M., Tribology, Arnold, London, (1992), pp.144-146.

[72] Tanaka T. and Isono Y., "Influence of metal constituents to the characteristics and grinding abilities of metal bonded diamond wheel", *Journal of Materials Processing Technology*, (1997), **63** [1-3], pp.175-180.

[73] Schatt W. and Wieter K. P., Powder Metallurgy – Processing and Materials, European Powder Metallurgy Association, Liveseys Ltd., Shrewsbury, UK, (1997), pp.96-99.

[74] "The future of diamond characterization", *GE Superabrasives Brochure*, (1993).

[75] Bridwell H. C. and Appl F. C., "A study of "free cutting" with diamond saws", *Industrial Diamond Review*, (1974), **34**, pp.51-53.

[76] Igharo M. and Russell J., "Development of diamond impregnated cutting tools", *Surface Engineering*, (1994), **10** [1], pp.52-55.

[77] Bailey M. W. and Bullen G. J., "Sawing in the stone and civil engineering industries", *Industrial Diamond Review*, (1979), pp.56-60.

[78] Bullen G. J. and Brown W. F., "Drilling high tensile steel reinforced concrete", *Industrial Diamond Review*, (1984), [1], pp.11-16.

[79] Thakur B. N., "Role of metal powders in manufacturing diamond tools", Superabrasives '85 Conference, Chicago, Illinois, (1985) MR85-307.

[80] Vukoman J. and Sreto T., "Characterization of fine metal powder binders for diamond tools", *International Journal of Materials & Product Technology*, (1990), **8**, pp.430-439.

[81] Chepeleva V. P., Delevi V. G., Kizikov E. D., Trunevich L. V. and Cherepenina E. S., "Structure Formation in a titanium-nickel alloy of eutectic composition", *Soviet Powder Metallurgy & Metal Ceramics*, (1984), **23** [1], 63-67.

[82] Konstanty J. and Bunsch A., "Hot pressing of cobalt powders", *Powder Metallurgy*, (1991), **34** [3], pp.195-198.

[83] Aronsson B., "Cobalt in hard materials products - A survey with emphasis on recent research and development", Cobalt '93 Conference, The Cobalt Development Institute, (1993).

[84] Betteridge W., Cobalt and its Alloys, John Wiley & Sons, (1982), pp.41-42.

[85] Konstanty J., Bunsch A. and Cias A., "Factors affecting hardness and ductility of Hot-Pressed cobalt powders", *Powder Metallurgy International*, (1991), **23** [6], pp.354-356.

[86] Akyuz D. A., Streit P., Hofmann H. and Peersman J., "Hot-pressing behaviour of fine cobalt powders", in 2nd International Conference on PM Diamond Tools '97, Montreux, (1997), pp.63-75.

[87] Sakka Y., "Sintering characteristics of cobalt ultrafine powders", *Journal of the Less-Common Metals*, (1991), **168**, pp.277-287.

[88] Bonneau M., "Mechanical properties of special ternary alloy bonds compared with cobalt bonds", in 2nd International Conference on PM Diamond Tools '97, Montreux, (1997), pp.120-125.

[89] Gille G., Bredthauer J., Gries B., Mende B. and Heinrich W., "Advanced and new grades of WC and binder powder - their properties and application", *International Journal of Refractory Metals & Hard Materials*, (2000), **18** [2], pp.87-102.

[90] "Cobalite – Pre-alloyed fine metal matrix powders for diamond tools", Union Miniere Brochure.

[91] "Next", Eurotungstene Metal Powders Brochure, (1998).

[92] Swennen B., "Cobalt nad nickel in the workplace-update on scientific facts, legislation and implementations", in 2nd International Conference on PM Diamond Tools '97, Montreux, (1997), pp.50-61.

[93] Chen S. H. and Hansen J. S., "Diamond having multiple coatings, methods for their manufacture and use of same", *European Patent*, EPA 0 467 404, (1992).

[94] Chen S. H. and Sung C. M., "Chemically bonded superabrasive grit", *US Patent*, US5062865, (1991).

[95] Hsieh Y. Z. and Lin S. T., "Diamond tool bits with iron alloys as the binding matrices", *Materials Chemistry and Physics*, (2001), **72** [2], pp.121-125.

[96] Wang C. Y., Wei X., Tang Z. L. and Pan Z. C., "The role of coolant in granite sawing", *Industrial Diamond Review*, (1995), [4], 156-160.

[97] Naidich Yu. V., Umanskii V. P. and Lavrinenko I. A., "Metal and alloy bond strengths to diamond", *Industrial Diamond Review*, (1984), [6], pp.327-331.

[98] Hughes F., Diamond Grinding of Metals, De Beers Industrial Diamond Division (Pty) Ltd., (1978), pp.3-25.

[99] Hughes F. H., "Metal coated synthetic diamonds embedded in a synthetic resinous matrix bond", *US Patent*, 3902873, (1975).

[100] Lindstrom O. and Lundblad E., "Metal-coated diamonds in synthetic resin bonded grinding wheels", *US Patent*, 3904391, (1975).

[101] Roy A. R. and Van Schalkwyk J. D., "Method of producing coated abrasive particles", *US Patent*, 3923476, (1975).

[102] Lindstrom O. B., "Agglomerates of metal-coated diamonds in a continuous synthetic resinous phase", *US Patent*, 3955324, (1976).

[103] Lindstrom O. and Lundblad E., "Method for preparing diamonds for use with grinding wheels", *US Patent*, 3957461, (1976).

[104] Farkas P., "A method of coating diamond particles", *US Patent*, 3650714, (1972).

[105] Caveney R. J., "Metal-coated diamonds in a metal alloy matrix", *US Patent*, 3879901, (1975).

[106] Nicholas M. G., Scott P. M. and Dewar B. I., "Method for metal coating diamonds so as to improve the interfacial bond strength", *US Patent*, 3924031, (1975).

[107] Caveney R. J., "Diamond particle having a composite coating of titanium and a metal layer", *US Patent*, 3929432, (1975).

[108] Lee M., Szala L. E. and Hibbs Jr. L. E., "Modifying the surface of diamond particles", *US Patent*, 4063907, (1977).

[109] Wilder A. G. and Bridwell H. C., "Abrasive particles encapsulated with a metal envelope of allotriomorphic dentrites", US Patent, 3871840, (1975).

[110] Pipkin N. J., "Metal coating of abrasive particles", *US Patent*, 4399167, (1983).

[111] Chen S H. and Sung C. M., "Multiple Metal Coated Superabrasive Grit and Methods for their Manufacture", *US Patent*, 5024680, (1991).

[112] Horton R. M., Anthon R. A. and Hoggins J. T., "Multilayer coated abrasive element for bonding to a backing", *US Patent*, 5049164, (1991).

[113] McEachron R., Connors E. J. and Slutz D. E., "Multi-layer metal coated diamond abrasives with an electolessly deposited metal layer", *US Patent*, 5232469, (1993).

[114] Manoukian N. and Samvelian R., "Prospective method and technique for diamond coating", in 2nd International Conference on PM Diamond Tools '97, Montreux, (1997), pp. 76-87.

[115] Naidich Yu. V., "The diamond powder with metal-coating particles for diamond-metal composites and tool", in Powder Metallurgy '94 – Hard Materials, (1994), [1], pp.267-274.

[116] Oki T., Fukuta Y., Hisada E. and Aoki S., "Coated abrasive grains and a manufacturing method therefore", *US Patent*, 5090969, (1992).

[117] Manukyan N. V., Agbalyan S. G., Oganyan A. P., Oganyan A. A. and Serobyan D. M., "Cladding diamond powders by thernodiffusion saturation - (II) The structure and properties of metallized diamond powders", *Soviet Powder Metallurgy & Metal Ceramics*, (1989), **28** [7], pp.532-535.

[118] Naidich Yu. V., Volk G. P. and Lavrinenko I. A., "Infiltration of metal-coated diamond powders by molten metal", *Soviet Powder Metallurgy & Metal Ceramics*, (1981), **20** [9], pp.610-612.

[119] Chattopadhyay A. K., and Hintermann H. E., "On improved bonding of TiC-coated CBN grits in nickel-based alloys", *Annals of the C.I.R.P.*, (1993), **42** [1], pp.413-416.

[120] Chattopadhyay A. K., and Hintermann H. E., "On surface modification of superabrasive grits by CVD of chromium", *Annals of the C.I.R.P.*, (1992), **41** [1], pp.381-385.

[121] Manukyan N. V., Oganyan A. P. and Apoyan G. S., "Thermodiffusional application of iron coatings to diamond powders", *Soviet Journal of Superhard Materials*, (1984), **6** [5], pp.45-48.

[122] Manukyan N. V., Agbalyan S. G., Oganyan A. P., Oganyan A. A. and Serobyan D. M., "Cladding diamond powders by thermodiffusion saturation - (I) Kinetics of the formation of metallic coatings on the surface of diamond", *Soviet Powder Metallurgy & Metal Ceramics*, (1989), **28** [6], pp.464-467.

[123] Zaitsev A. G., Duda T. M. and Prudnikov E. L., "Influence of metallization on serviceability of wheels with oriented grains", *Soviet Journal of Superhard Materials*, (1983), **5** [2], pp.22-29.

[124] Duda T. M., Tkach V. N. and Bogatyreva G. P., "Characteristics of the formation of chemical coatings on diamonds", *Soviet Journal of Superhard Materials*, (1985), **7** [5], pp.39-43.

[125] Bakon A. and Szymanski A., "The antioxidation coating of diamond and the strengthening of ceramic grinding tools with a glass-ceramic layer as part of the bonding material", *Materials Science and Engineering*, **41**, (1979), pp.281-288.

[126] Toth L. E., "General properties, preparation, and characterization", in Transition Metal Carbides and Nitrides, Academic Press Inc., London, (1971), p.1-28.

[127] Seal M., "A review of methods of bonding or making electrical contacts to diamond", *Industrial Diamond Review*, (1969), **29**, pp.408-412.

[128] Tanaka T., Ikawa N. and Tsuwa H., "Affinity of diamond for metals, *Annals of the C.I.R.P.*, (1981), **30** [1], pp.241-245.

[129] Scott P. M. and Nicholas M., "The wetting and bonding of diamonds by copper-base binary alloys", *Journal of Materials Science*, (1975), **10**, pp.1833-1840.

[130] Naidich Y. V. and Kolesnichenko G. A., "Investigation of the wetting of diamond and graphite by molten metals and alloys - III Wetting of diamond crystals", *Soviet Powder Metallurgy & Metal Ceramics*, (1964), pp.191-195.

[131] van Enckevort W. J. P., "Bonding of diamond", in The Properties of Diamond, (1979), Edited by J. E. Field, Academic Press, London, pp.309-315.

[132] Evens D., Nicholas M. and Scott P. M., "The wetting and bonding of diamonds by copper-tin-titanium alloys", *Industrial Diamond Review*, (1977), pp.306-309.

[133] Perry S. S., McGinnis S. P. and Somorjai G. A., "Adhesion at diamond-metal interfaces : a chemical composition perspective", *Journal of Adhesion Science Technology*, (1995), **9** [6], pp.711-724.

[134] Novikov N. V. and Bondar I. V., "Interaction of carbon material with metallized coating", *Surface and Coatings Technology*, (1991), **46** [3], pp.301-305.

[135] Chuprina V. G., "Physicochemical interaction and structure development during the formation of metal gas-transfer coatings on diamond (review) – 1. Kinetics", *Soviet Powder Metallurgy & Metal Ceramics*, (1992), **32** [7], pp.578-583.

[136] Grishachev V. F., Maslov V. P., Prilutskii E. V. and Semenov-Kozbar A. A., "Oxidation of diamonds with diffusive coatings of transition-metal carbides", *Soviet Journal of Superhard Materials*, (1984), **6** [2], pp.38-41.

[137] Oki T., Fukuta Y., Hisada E. and Shimakami S., "Thermal resistance of chromium-carbide coated diamond particles", *Metallurgical Review of MMIJ*, (1991), **3** [1], pp.64-79.

[138] Haruna K., Maeta H., Ohashi K. and Koike T., "Thermal expansion coefficient of synthetic diamond single crystal at low temperatures", *Japanese Journal of Applied Physics*, (1992), **31** [8], pp.2527-2529.

[139] Cai O., "Encapsulated diamond : remarks and technical notes", *Diamante Applicazioni & Tecnologia*", (1996), pp.62-72.

[140] Naidich Yu. V., Umanskii V. P. and Lavrinenko I. A., "A study of diamond to metal adhesive strength", *Soviet Journal of Superhard Materials*, (1984), **6** [6], pp.25-30.

[141] Oganyan A. P., "Metallization of diamond powders with adhesion-active metals - II. A structural analysis of metallized diamond powders", *Soviet Powder Metallurgy & Metal Ceramics*, (1991), **30** [11], pp.909-910.

[142] Oganyan A. P., "Metallizing of diamond powders with adhesion-active metals - 1. Deposition of refractory-metals from a gas-phase", *Soviet Powder Metallurgy & Metal Ceramics*, (1992), **30** [9], pp.743-747.

[143] Chuprina V. G., Umanskii V. P., Lavrinenko I. A. and Naidich Yu. V., "X-Ray diffraction investigation of chromium coatings on diamond", *Soviet Powder Metallurgy & Metal Ceramics*, (1980), **19** [6], pp.432-435.

[144] Naidich Yu. V., Chashnik V. M., Lavrinenko I. A., Volk G. P. and Gnitetskii O. A., "Formation and some properties of chromium and chrome-nickel coatings applied to diamonds by gas-phase method", *Soviet Powder Metallurgy & Metal Ceramics*, (1987), **26** [8], pp.645-649.

[145] Chuprina V. G., "Physicochemical interaction and structure formation under formation of metallic gas-transport coatings on the diamond (review) - II. Mechanism", *Soviet Powder Metallurgy & Metal Ceramics*, (1992), **31** [8], pp.687-692.

[146] Nicholas M. G., Scott P. M. and Dewar B. I., "Method of producing nickel coated diamond particles", *US Patent*, 4062660, (1977).

[147] Chuprina V. G., Volk G. P. and Lavrinenko I. A., "Radiographic study of the formation of molybdenum coatings on diamonds", *Soviet Powder Metallurgy & Metal Ceramics*, (1986), **25** [11], pp.911-914.

[148] Chuprina V. G. and Volk G. P., "Special features of formation of molybdenum coatings on diamond with the spatial-distribution of reagents", *Soviet Powder Metallurgy & Metal Ceramics*, (1998), **27** [4], pp.311-314.

[149] Volk G. P., Lavrinenko I. A., Chuprina V. G. and Naidich Y. V., "Kinetics and mechanism of formation of molybdenum coatings applied to diamond by reactive deposition in a finely divided metallizing agent", *Soviet Powder Metallurgy & Metal Ceramics*, (1984), **23** [2], pp.129-132.

[150] Shapoval V. I., Kushkhov Kh. B., Malyshev V. V., Vesna V. T. and Maslov V. P., "Deposition of molybdenum carbide on the surface of diamonds by electrolysis of ionic melts", *Soviet Powder Metallurgy & Metal Ceramics*, (1986), **25** [7], pp.567-569.

[151] Duda T. M., "Interaction at diamond-coating-bond interfaces", *Soviet Journal of Superhard Materials*, (1986), **8** [5], pp.38-41.

[152] Brauninger G. and Hayden S. C., "MBS* -960 Cr2 and MBS*-960 Ti2 : Chromium- and Titanium-coated manufactured diamonds for sawing and drilling applications", *GE Superabrasives Report* GES95-1093, (1995).

[153] Chuprina V. G. and Shurkhal V. V., "An X-Ray diffraction study of the process of formation of vanadium coatings on diamond", *Soviet Powder Metallurgy & Metal Ceramics*, (1987), **26** [3], pp.269-272.

[154] Chuprina V. G., Shalya I. M. and Shurkhal V. V., "Formation of chromium-copper coatings on the diamond", *Powder Metallurgy and Metal Ceramics*, (1993), **32** [9-10], pp.794-798.

[155] Grishachev V. F., Maslov V. P., Prilutskii E. V. and Semenov-Kobzar A. A., "Oxidation resistance of diamonds with molybdenum disilicide coatings", *Soviet Powder Metallurgy & Metal Ceramics*, (1984), **23** [1], pp.60-62.

[156] Chuprina V. G., Shalya I. M. and Umanskii V. P., "Oxidation of nickel-molybdenum coatings on diamond", *Soviet Powder Metallurgy & Metal Ceramics*, (1991), **30** [4], pp.308-312.

[157] Chuprina V. G., Shalya I. M. and Shurkhal V. V., "Specific features of obtaining molybdenum-nickel coatings on diamonds", *Soviet Powder Metallurgy & Metal Ceramics*, (1993), **31** [6], pp.479-484.

[158] Chuprina V. G. and Shurkhal V. V., "An X-Ray diffraction study on molybdenum coating formed on diamond in the presence of nickel", *Soviet Powder Metallurgy & Metal Ceramics*, (1989), **27** [11], pp.917-921.

[159] Chuprina V. G., Knyazeva I. A., Lavrinenko I. A. and Naidich Y. V., "X-Ray diffraction investigation of Ni-Mn-Sn-Ti coatings applied to diamond", *Soviet Powder Metallurgy & Metal Ceramics*, (1984), **23** [1], pp.38-41.

[160] Matarrese R. R., "Dual-coated diamond pellets and saw blade segments made therewith", *US Patent*, 5143523, (1992).

[161] Kimura K., "Method for forming metal-coated abrasive grain granules", *US Patent*, 4770907, (1988).

[162] Lin Z. and Queeney R. A., "Fracture resistance of diamond-reinforced hot pressed Cu/Ni powders", *Powder Metallurgy International*, (1986), **18** [2], pp.76-78.

[163] Yu J., Cheng B., Ye X. and Liu Z., "Study on surface of diamond particle by chemical Cu-cladding and its application in diamond wheel", *Journal Wuhan University of Technology*, (1996), **11** [3], pp.28-35.

[164] Pierson H. O., "Chemical vapor deposition of nonsemiconductor materials", in ASM Handbook-Vol. 5, 10th Edition, (1994), pp.510-516.

[165] Blocher J. M. Jr., "Chemical vapor deposition", in ASM Handbook-Vol. 4, 9th Edition, (1991), pp.381-386

[166] Zarnoch K. and Iacovangelo C. D., "Tungsten metallization of CVD diamond", *US Patent*, 5346719, (1994).

[167] Hanni W. and Hintermann H. E., "Chemical vapour deposition of chromium", *Thin Solid Films*, (1977), **40**, pp.107-114.

[168] Vesna V. T., Grishachev V. F., Maslov V. P., Sabko V. E. and Shcherbakova L. E., "Deposition of chromium coatings on diamonds from a gaseous phase", *Soviet Powder Metallurgy & Metal Ceramics*, (1982), **21** [4], pp.292-294.

[169] Rigney D. V., "Vacuum coating", in ASM Handbook-Vol. 4, 9th Edition, (1991), pp.387-411.

[170] Chuprina V. G., Umanskii V. P. and Lavrinenko I. A., "X-Ray study of the process of formation of titanium coatings on diamond", *Soviet Progress in Chemistry*, (1983), **49**, [4], pp.16-19.

[171] Thornton J. A. and Muenz W. D., "Sputtering", in ASM Handbook-Vol. 4, 9th Edition, (1991), pp.412-416.

[172] Zhu Y., Wang L., Yao W. and Cao L., "The interface diffusion and reaction between Cr layer and diamond particle during metallization", *Applied Surface Science*, (2001), **171** [1-2], pp.143-150.

[173] Chistyakov E. M., Polupan B. I., Pipkevich G. Y. and Zeberin A. G., "Metal Coating of Superhard Materials Powders using a Magnetron Sprayer", *Soviet Journal of Superhard Materials*, (1985), **7** [1], pp.42-44.

[174] Kume S., Suzuki K., Yoshida H., Sakakibara S., Yamada Y., Fuyuki T., Akiyama S., Yamamoto M., Nakagawa H. and Kanetake N., "Ultrahigh pressure hot isostatic pressing of TiN-coated diamond/TiN/alumina composites under thermodynamically unstable condition for diamonds", *International Journal of Refractory Metals & Hard Materials*, (2001), **19** [1], pp.17-22.

[175] St. Pierre P. D., "Refractory metal oxide coated abrasives and grinding wheels made therefrom", *US Patent*, 4951427, (1990).

[176] Porter D. A. and Easterling K. E., "Crystal interfaces and microstructure", in Phase Transformations in Metals and Alloys", 2nd Edition, Chapman & Hall, London, (1993), pp.110-184.

[177] Askeland D. R., "Atom movement in materials", in The Science and Engineering of Materials, 3rd SI Edition, Chapman & Hall, London, (1996), pp.111-137.

[178] Metcalfe A. G., "Introduction and review", in Interfaces in Metal-Matrix Composites, Edited by Arthur G. Metcalfe, Academic Press Inc., London, (1972), pp.1-30.

[179] Metcalfe A. G., "Physical chemical aspects of the interface", in Interfaces in Metal-Matrix Composites, Edited by Arthur G. Metcalfe, Academic Press Inc., London, (1972), pp.65-123.

[180] Clyne T. W. and Withers P. J., An introduction to composite materials, 2nd Edition, Edited by D. R. Clarke, S. Suresh and I. M. Ward, Cambridge University Press, Cambridge, (1996), pp.137-138.

[181] Clyne T. W. and Withers P. J., "The interfacial region", in An Introduction to Metal Matrix Composites, Edited by E. A. Davis and I. M. Ward, Cambridge University Press, Cambridge, (1993), pp.166-217.

[182] Ebert L. J. and Wright P. K., "Mechanical aspects of the interface", in Interfaces in Metal-Matrix Composites, Edited by Arthur G. Metcalfe, Academic Press Inc., London, (1972), pp.31-64.

[183] Bronshtein D. Kh., Delevi V. G., Simkin E. S. and Tsypin N. V., "Reaction of diamond with hard metals during the shaping of composite materials", *Soviet Powder Metallurgy & Metal Ceramics*, (1981), [9], pp.629-631.

[184] Naidich Yu. V. and Kolesnichenko G. A., "Investigation of the wetting of diamond and graphite by molten metals and alloys - V. Carbide-formation kinetics at the graphite/metallic melt interface", *Soviet Powder Metallurgy & Metal Ceramics*, (1968), [2], pp.139-141.

[185] Naidich Y. V. and Kolesnichenko, "Investigation of the wetting of graphite and diamond by liquid metals and alloys", *Poroshkovaya Metallurgiya*, (1961), **1** [6], pp.55-60.

[186] Molinari A., Marchetti F., Gialanella S, Scardi P., and Tiziani A., "Study of the diamond-matrix interface in hot-pressed cobalt-based tools", *Materials Science and Engineering*, (1990), **A130**, pp.257-262.

[187] Levin E. and Gutmanas E.Y., "Solid-state bonding of diamond to Nichrome and Co-20% W alloys", *Journal of Materials Science Letters*, (1990), **9** [6], pp.726-730.

[188] Dewar B., Nicholas M. and Scott P. M., "The solid phase bonding of copper, nickel and some of their alloys to diamonds", *Journal of Materials Science*, (1976), **11**, pp.1083-1090.

[189] Lin Z. and Queeney R. A., "Interface bonding in a diamond/metal matrix composite", in Proceedings of the 1988 International Powder Metallurgy Conference, Orlando, FL, USA, (1988), **20**, pp.443-450.

[190] Akyuz D. A. and Hofmann H., "Interface Aspects in Cobalt-based Diamond Cutting Tool Segments", in Proceedings of the 1998 Powder Metallurgy World Congress & Exhibition, Granada, Spain, (1988), **4**, pp.158-163.

[191] Pereyaslov V. P., Primak L. P., Voloshin M. N., Gordienko V. P. and Kolomiets V. P., "Diamond tool based on titanium", *Soviet Journal of Superhard Materials*, (1987), **9** [2], pp.34-37.

[192] Xu Z. Y. and Lin Z. D., "Bonding Mechanisms of Diamonds", *Modern Developments in Powder Metallurgy*, (1985), **17**, pp.273-288.

[193] Kushtalova I. P., Stasyuk L. F. and Kizikov E. D., "Development of a diamond containing material with a tungsten-free matrix for dressing tools", *Soviet Journal of Superhard Materials*, (1986), **8** [1], pp.48-51.

[194] Stasyuk L. F. and Kushtalova I. P., "Rules of formation of diamond-containing materials with a metal carbide matrix at high-pressures", *Soviet Powder Metallurgy & Metal Ceramics*, (1987), **26** [4], pp.309-312.

[195] Schuster J. C., "Physical chemistry of ceramic-metal interface formation", *Transactions of JWRI (Journal of Welding Research Institute)*, (1994), **23** [2], pp.143-147.

[196] Ruhle M., "Structure and chemistry of metal/ceramic interfaces", in Fundamentals of Metal-Matrix Composites, Edited by S. Suresh, A. Mortensen and A. Needleman, Butterworth-Heinemann, (1993), pp.81-108.

[197] Naidich Y. V., "The wettability of solids by liquid metals", *Progress in Surface and Membrane Science*, (1981), **14**, pp.353-485.

[198] *ibid* [181], pp.7-10.

[199] Krock R. H., " Inorganic particulate composites", in Modern Composite Materials, Edited by L. J. Broutman and R. H. Krock, Addison-Wesley Publishing Co., (1967), pp.455-478.

[200] Clyne T. W. and Withers P. J., "Basic composite mechanics", in An Introduction to Metal Matrix Composites, Edited by E. A. Davis and I. M. Ward, Cambridge University Press, Cambridge, (1993), pp.12-43.

[201] Hashin Z. and Shtrikman S., "On some variational principles in elasticity and their application to the theory of two-phase materials", *Armed Services Technical Information Agency Report*, AD 265-817, ONR Contract No. NOnr 551(42), (1961).

[202] Halpin J. C. and Tsai S. W., "Environmental factors in composite design", *Airforce Materials Laboratory*, AFML-TR-67-423, (1967).

[203] Lange F. F., "Fracture of brittle matrix, particulate composites", in Interfaces in Metal-Matrix Composites, Edited by Arthur G. Metcalfe, Academic Press Inc., London, (1972), pp.1-44.

[204] Clyne T. W. and Withers P. J., "The Eshelby approach to modelling composites", in An Introduction to Metal Matrix Composites, Edited by E. A. Davis and I. M. Ward, Cambridge University Press, Cambridge, (1993), pp.44-70.

[205] Clyne T. W. and Withers P. J., "Plastic deformation", in An Introduction to Metal Matrix Composites, Edited by E. A. Davis and I. M. Ward, Cambridge University Press, Cambridge, (1993), pp.71-116.

[206] *ibid* [181], pp.230-234.

[207] *ibid* [181], p.258.

[208] Novikov N. V., Tsypin N. V., Maistrenko A. L. and Vovchanvskii I. F., "Diamond-containing composite materials based on hard alloys", *Soviet Journal of Superhard Materials*, (1983), **5** [2], pp.1-5.

[209] Bronshtein D. K., Maistrenko A. L., Simkin E. S. and Tsypin N. V., "Strength of diamond-containing composite-material based on tungsten carbide hard alloy", *Soviet Powder Metallurgy & Metal Ceramics*, (1991), **29** [9], pp.720-724.

[210] Majstrenko A. L., "Strength and fracture of composite diamond-bearing tool materials", *Advances in Fracture Research*, Fracture `84 - Proceedings of the 6th International Conference on Fracture, New Delhi, India, (1984), **4**, pp.3021-3028.

[211] Heritage K., Frisby C. and Wolfenden A., "Impulse excitation technique for dynamic flexural measurements at moderate temperature", *Review of Scientific Instruments*, (1988), **59** [6], pp.973-974.

[212] Spinner S. and Tefft W. E., "A method for determining mechanical resonance frequencies and for calculating elastic moduli from these frequencies", *Proceedings of the ASTM*, (1961), **61**, pp.1221-1238.

[213] *ibid* [84], p.24.

[214] BS EN 23327, "Determination of transverse rupture strength", (1993).

[215] Thümmler F. and Oberacker R., An Introduction to Powder Metallurgy, Edited by I. Jenkins and J. V. Wood, The Institute of Materials, London, (1993), pp.255-258.

[216] Ghosh P. K., Prasad P. R. and Ray S., "Effect of porosity on the strength of particulate composites", *Zeitschrift für Metallkunde*, (1984), **75** [12], pp.934-937.

[217] Naidich Y. V. and Kolesnichenko G. A., "Investigation of the wetting of diamond and graphite by molten metals and alloys - IV. Influence of temperature on the adhesion of metals inert to carbon", *Soviet Powder Metallurgy & Metal Ceramics*, (1966), pp.156-158.

[218] Delevi V. G., Knyazeva I. A., Lavrinenko I. A. and Naidich Yu. V., "Composition and structure formation at the contact interface between carbon and an Ni-Mn-Sn-Ti alloy", *Soviet Powder Metallurgy & Metal Ceramics*, (1984), **23** [9], pp.697-701.

[219] Naidich Y. V. and Kolesnichenko G. A., "Study of the wetting of diamond and graphite by liquid metals - II. Angles of contact and adhesion between Tin-Titanium and Copper-Tin-Titanium alloys and the graphite surface", *Soviet Powder Metallurgy & Metal Ceramics*, (1963), pp.35-38.

[220] Naidich Y. V., Perevertailo V. M. and Zabuga V. V., "Surface and adhesion properties of Ni-Mn-Ga melts in contact with graphite", *Soviet Powder Metallurgy & Metal Ceramics*, (1988), **27** [4], pp.319-325.

[221] Naidich Y. V., Perevertailo V. M. and Loginova O. B., "Effect of degree of wettability of diamond grains by metal melts on the form of grain growth", *Soviet Journal of Superhard Materials*, (1989), **11** [6], pp.1-5.

[222] de Theije F. K., van Veenendaal E., van Enckevort W. J. P. and Vlieg E., "Oxidative etching of cleaved synthetic diamond {111} surfaces", *Surface Science*, (2001), **492** [1-2], pp.91-105.

[223] Yin L. W., Li M. S., Sun D. S., Hao Z. Y. Li F. Z. and Yao Z. Y., "Observation of etch pits and defects in diamond single crystals under high temperature - high pressure", *Materials Science and Engineering*, (2001), **A315** [1-2], pp.108-112.

[224] Yin L. W., Li M. S., Cui J.-J., Sun D. S. and Hao Z. Y., "Frank dislocation loops related to vacancies in HPHT as-grown synthetic diamond single crystals.", *Scripta Materialia*, (2001), **45** [1], pp.13-17.

[225] Wang Y. M., Wong K. W., Lee S. T., Nishitani-Gamo M., Sakaguchi I., Loh K. P. and Ando T., "Recent studies on diamond surfaces", *Diamond and Related Materials*, (2000), [9], pp.1582-1590.

[226] Young B., "The graphitisation of diamond during the manufacture of diamond tools", *Industrial Diamond Review*, (1966), pp.483-488.

[227] Narayan J., Nelson M., oktyabrsky S. and Jagannadham K., "Diamond deposition on 3d transition metals and their alloys", *Materials Science and Engineering*, (1996), **B38** [1-2], pp.46-52.

[228] Tokura H. and Yoshikawa M., "Heat treatment of diamond grains for bonding strength improvement", *Journal of Materials Science*, (1989), **24**, pp.2231-2238.

[229] Liao Y. S. and Luo S. Y., "Effects of matrix characteristics on diamond composites", *Journal of Materials Science*, (1993), **28** [5], pp.1245-1251.

[230] *ibid* [8], p.236-239.

[231] Field J. E., "Wear and Abrasion of Diamond Surfaces" in Properties and Growth of Diamond, Edited by Gordon Davies, INSPEC, London, (1994), pp.73-75.

[232] Luo S. Y. and Liao Y. S., "Observations of fracture surfaces of sintered diamond composites", *Key Engineering Materials*, (1995), **108-110**, pp.449-456.

[233] German R. M., Sintering Theory and Practice, John Wiley & Sons Inc., (1996), p.111.

[234] Villar del M., Echeberria J., Iturriza I. and Castro F., "Sintering/HIPing of cobalt powders for diamond tools", in Proceedings of the 1998 Powder Metallurgy World Congress & Exhibition, Granada, Spain, (1988), **4**, pp.475-480.

[235] *ibid* [233], pp.320-326.

[236] *ibid* [233], p.173.

[237] *ibid* [233], p.330.

[238] *ibid* [61], p.195.

[239] Tressler R. E., "Interfaces in oxide reinforced metals", in Interfaces in Metal-Matrix Composites, Edited by Arthur G. Metcalfe, Academic Press Inc., London, (1972), pp.285-328.

[240] ASM Handbook, Vol. 3, Alloy Phase Diagrams, (1992).

[241] Pepper S. V., "Transformation of the diamond (110) surface", *Journal of Vacuum Science & Technology*, (1982), **20** [2], pp.213-216.

[242] Nogi K., Okada Y., Ogino K. and Iwamoto N., "Wettability of diamond by liquid pure metals", *Materials Transactions JIM*, (1994), **35** [3], pp.156-160.

[243] Olster E. F. and Jones R. C., "Effect on interface on fracture", in Interfaces in Metal-Matrix Composites, Edited by Arthur G. Metcalfe, Academic Press Inc., London, (1972), pp.245-284.

[244] Holz R. and Sauren J., Grinding Handbook – Grinding with diamond and CBN, Ernst Winter & Son, Vulkan-Verlag, Essen.

[245] Coltters R. G., "Thermodynamics of binary metallic carbides: A review", *Materials Science and Engineering*, (1985), **76**, pp.1-50.

[246] Tsai S. W. and Hahn H. T., Introduction to Composite Materials, Technomic Publishing Company, Pennsylvania, (1980), pp.379-430.

[247] Halpin J. C., Primer on Composite Materials: Analysis, Technomic Publishing Company, Pennsylvania, (1984), pp.130-142.

[248] Askeland D. R., The Science and Engineering of Materials, 3rd SI Edition, Chapman & Hall, London, (1996), pp.830-831.